CAJM

Central Asian Journal of Medicine

100 TMA anniversary

Tashkent State Medical University Press

eISSN: 2181-1326

Scientific Journal

This journal had been publishing since 2018



4

2026

MINISTRY OF HIGHER AND SECONDARY SPECIALIZED EDUCATION OF THE REPUBLIC OF UZBEKISTAN

2030 | UZBEKISTAN RESEARCH ONLINE

OAK.uz Supreme Attestation Commission at the Cabinet Ministers of the Republic of Uzbekistan

Digital Commons Network

Google Scholar

C A J M

Central Asian Journal of Medicine

Tashkent State Medical University Press

Scientific Journal

This journal had been publishing since 2018

eISSN: 2181-1326 (online)
ISSN: 2181-7812 (print)

№ 4, 2026. Vol. 1

The Central Asian Journal of Medicine is a peer-reviewed scientific journal that publishes original scientific articles. The journal was founded at the Tashkent Medical Academy in 2011 and, in accordance with the Resolution of the Presidium of the Higher Attestation Commission of the Republic of Uzbekistan dated July 30, 2020, No. 283/7.1, operates as a recognized scientific periodical. The main goal of this journal is to promote the development of education and research activities among faculty members, doctoral candidates, and students in the fields of Medical Sciences, Medical Education, Public Health, Nursing, Rehabilitation, and Therapy.

OAK.uz **Supreme Attestation Commission at the Cabinet Ministers of the Republic of Uzbekistan**

EDITORIAL BOARD

Azizova F.L.	D.M.Sc., Tashkent State Medical University.
Alyavi A.L.	Academician, D.M.Sc., Republican Specialized Scientific-Practical Medical Center for Therapy and Medical Rehabilitation
Nazirov F.G.	Academician, D.M.Sc., Republican Specialized Surgery Center named after Academician V. Vakhidov
Kurbonov R.D.	Academician, D.M.Sc., Republican Specialized Cardiology Center
Karimov Sh.I.	Academician, D.M.Sc., Tashkent State Medical University
Daminov T.A.	Academician, D.M.Sc., Tashkent State Medical University
Najmutdinova D.K.	D.M.Sc., Tashkent State Medical University
Jae Wook Choi	D.M.Sc., Korea University

EDITORIAL COUNCIL

Gadaev A.G.	D.M.Sc., Tashkent State Medical University
Akilov F.O.	D.M.Sc., Republican Specialized Urology Center
Iriskulov B.U.	D.M.Sc., Tashkent State Medical University
Parpieva N.N.	D.M.Sc., Republican Specialized Scientific-Practical Medical Center for Tuberculosis and Pulmonology
Sobirova R.A.	D.M.Sc., Tashkent State Medical University
Kholmatova B.T.	D.M.Sc., Tashkent State Medical University
Shalina R.I.	Department of Obstetrics and Gynecology, Pediatric Faculty, N.I. Pirogov Russian National Research Medical University
Antanas Vaitkus	D.M.Sc., Lithuanian University of Health Sciences Hospital, Kaunas Clinics Medical Academy
Briko N.I.	D.M.Sc., Honored Scientist of the Russian Federation, Academician of the Russian Academy of Sciences, Professor, Chief Epidemiologist of the Ministry of Health of the Russian Federation, Head of the Department of Epidemiology and Evidence-Based Medicine, Sechenov University
Yarovenko G.V.	D.M.Sc., Professor, Department of Surgical Diseases, Samara State Medical University, Russian Federation.

CONTENTS OF THE JOURNAL

Mamasaidov J.T., Muydinova M.T. / The course of pregnancy, labor, postpartum, and early neonatal periods in the presence of signs of preterm birth 6

Alisherova M.A., Abdujalilova M.A., Khamidullayeva M.T. / Analysis of effective methods for diagnosing invasive ductal carcinoma of the breast in the early stages 14

Abdukhalikova N.F., Iriskulov B.U., Rakhmonov A.Kh. / Atherogenic dyslipidemia and insulin resistance as drivers of early liver and kidney injury in experimental metabolic syndrome 24

Ruziyev U.S., Niyazova N.R. / Comparative evaluation of different methods of staple line reinforcement in sleeve gastrectomy 35

Po O.J., Sidikov A.A. / Microvascular remodeling and the endothelial-apoptotic switch in lichen sclerosus: an immunohistochemical stage-based study 40

Yusupov A.F., Karimova M.Kh., Dzhamalova Sh.A., Jalalov A.K., Khaitboev N.Sh. / Results of micropulse transscleral cyclophotocoagulation in the treatment of neovascular glaucoma in proliferative diabetic retinopathy 44

Babakhanova A.M. / Placental elastography in the diagnosis of placental dysfunction in fetal growth restriction 48

Ibodulloyeva M.B., Ibodullayev Z.R. / Enhancing functional independence and postural control after ischemic stroke: effectiveness of psychomotor therapy assessed by the barthel index and berg balance scale 52

Zubtiyev S.U., Abdulloyev Sh.H., Orifova G.B. / Pathologoanatomical features of childhood leukemias: morphology of acute lymphoblastic leukemia 63

Raimova M.M., Makhkamova M.A. / Relationship between cognitive function and emotional disturbances in chronic tinnitus 71

Allaberganov S.F., Adilbekova D.B., Akhrorov A.A. / Morphological assessment of apoptosis and necrosis signs in the gastric mucosa in a model of hepatorenal syndrome 74

Zharlykassynova G.Zh., Boltaeva Z.F. / Progressive structural reorganization and fibrotic-emphysematous remodeling of the lungs under chronic exposure to nicotine-containing products 81

Zharlykassynova G.Zh., Narziyev L.A. / Clinical and hemodynamic characteristics of patients with coronary artery disease associated with arterial hypertension 85

Nazirdjanov M.A. / Disorders of the lacrimal drainage system: diagnosis and modern approaches to therapy 90

Dauletova M.J., Asatova M.M. / Clinical and functional assessment of the liver and placenta using elastography in pregnant women with drug-induced liver injury 98

Farmonova G.M. / Factors determining endometrial recovery and receptivity after hysteroscopic interventions: current state of the problem 104

Ibodulloyeva M.B., Ibodullayev Z.R. / Changes in motor function after psychomotor rehabilitation in post-ischemic stroke patients: a controlled study using fugl-meyer assessment..... 109

Usmanova G.E., Rakhimbaeva G.S. / The importance of cell adhesion molecule levels in the course and prognosis of hemorrhagic stroke..... 118

Ibodulloyeva M.B., Ibodullayev Z.R. / Targeting emotional dysfunction after stroke: the role of psychomotor therapy assessed by the hospital anxiety and depression scale..... 123

Niyozov N.K. / Changes in anthropometric indicators of the fetus in mothers with hypothyroidism..... 131

Shamsutdinova G.B., Ismoilova M.I., Mirzajonova Sh.A., Mukarramov U.M. / Clinical and diagnostic features of gastroesophageal reflux disease in patients with ischemic heart diseas..... 141

Iriskulov B.U., Mukhamedova G.N. / Pathogenetic mechanisms of stress-diet-induced hypoxia development in case of poor nutrition (literature review)..... 145

Sultonov B.O., Esamuratov A.I. / Assessment of the contribution of biallelic polymorphism of the EDN1 gene (LYS198ASN) to the development of chronic tonsillitis 154

Makhmadullayeva Sh.S., Najmutdinova D.K. / Clinical and phenotypic features of polycystic ovary syndrome: association with hormonal and anthropometric parameters 160

Asrankulova D.B., Saidova G.O. / Assessment of body composition in women with hyperandrogenism using bioimpedance analysis 167

Sharipov I.L. / Characteristics of the clinical course of acute obstructive bronchitis in young children..... 173

Yusupbayev R.B., Khamdamova D.S. / Maternal intravenous immunoglobulin in RH-alloimmunized pregnancies with severe fetal anemia..... 176

Khudoyberdieva G.S., Muminov A.A. / Optimization of drug-induced sedation with various agents during spinal anesthesia for cesarean section 180

Ziyodullaev M.M. / Microanatomical changes in the walls of the right chambers of the heart in 12-month-old rats poisoned with alcohol and the effect of olive oil on these changes 185

Yuldashev B.E., Abdurakhmonova G.D., Karshiev D.A. / Integral mathematical model of the interaction of a film biocoating and the cornea of the eye 191

Usmonova G.B., Mamasaidov J.T. / Methods for assessing anthropometric characteristics of children's physical development in relation to dietary patterns 205

Gulyamov S.S., Jabborov A.U. / Modern approaches to enamel remineralization in pediatric dentistry: preventive strategies and diagnostic assessment 214

Shukurkhujaeva D.N. / Early gestational bleeding and subchorionic hematoma as predictors of fetal growth restriction: pathogenetic mechanisms and the role of low-dose aspirin 217

Tilyakov K.A., Khushmuradov U.R. / A novel approach to the rehabilitation of patients after surgical treatment of intervertebral disc herniation 223

Tuychibaeva N.M., Gubaydulina K.R. / Early-onset developmental and epileptic encephalopathy associated with a DE NOVO SCN8A variant (P.VAL410LEU): a case report... 228

Akhmedova N.Sh., Khattabov M.Kh. / Prevention of the development and progression of CKD in patients with COVID-19 233

Yusupov A.S., Zokirova N.Z., Khaydarov K.I. / Criteria for early diagnosis and intensive care of postoperative complications of congenital heart defects in children 240

Khasanova M.A., Akbarova G.K. / New possibilities for determining the abo blood group in forensic medical practice 243

Valiyev Sh.M., Gaziyev Z.T. / Comparative analysis of spinal anesthesia with QL block in gynecological patients with hypertension and chronic circulatory failure 248

Yuldashev B.E., Islamov Y.N., Islomov A.Y. / Digital twins: engineering and simulation in pulmonology 252

Ermatov N.J., Nasirdinov M.Z., Maderimov M. / Hygienic analysis of the specific features of the prevalence of non-communicable diseases among rural and urban populations..... 265

Kattaeva D.R. / Hygienic and genetic determinants of dermato-respiratory syndrome formation in children: the role of vitamin D and MMP-9 and TGF-β1 gene polymorphisms .. 273

Khamidova M.A. / Diagnostic advantages of low-dose MSCT in the early detection of lung pathologies 281

Ermatov N.J., Azizova F.L., Alimukhamedov D.Sh., Niyazmetov M.A., Kenjaboev D. / Hygienic analysis of the population's drinking water supply 287

Mutigullina R.R., Nagayeva G.A. / Ventricular extrasystoles of various origins, the frequency of their detection and the relationship with various factors 298

Gaibov G.K., Khalimbetov G.S., Kayumov U.K. / The incidence of coronary heart disease in individuals with different gradations of blood pressure and body weight..... 305

Mamatova Sh.I. / Coke dust formation in the oil refining process and its impact on the environment and workers' health 312

THE COURSE OF PREGNANCY, LABOR, POSTPARTUM, AND EARLY NEONATAL PERIODS IN THE PRESENCE OF SIGNS OF PRETERM BIRTH

Jamoliddin T. Mamasaidov - D.M.Sc., associate professor
Maftuna T. Muydinova - independent researcher
Fergana Medical Institute of Public Health (Fergana, Uzbekistan)
muydinovaamaftuna@gmail.com

Abstract. *This study investigates the signs and risk factors of preterm birth during pregnancy, labor, postpartum, and early neonatal periods. Clinical, demographic, and instrumental data, including Doppler assessment of uterine arteries, were analyzed. The findings demonstrate that the systolic-diastolic ratio and pulsatility index are significant predictors of preterm birth. Additionally, factors such as threatened miscarriage, preeclampsia, polyhydramnios, and infectious-inflammatory processes significantly increase the risk. The results are important for improving prediction and prevention strategies of preterm birth.*

Keywords: *preterm birth, pregnancy, Doppler, uterine artery, preeclampsia, pulsatility index, miscarriage risk, neonatal period*

Relevance of the problem.

Studying risk factors affecting the course of pregnancy and improving the quality and scope of screening examinations aimed at preventing various complications, as well as enhancing the effectiveness of implemented and planned measures, remains one of the pressing issues for healthcare authorities. Therefore, in state programs and reports of practicing physicians, the digitalization of data and statistics related to maternal and child health indicators contributes to achieving more accurate and reliable outcomes. In this regard, the scope of scientific research conducted in this field and the obtained results play a significant role in improving the qualifications of practicing physicians, as well as in preventing preterm birth and obstetric complications and enhancing the quality of medical care provided.

Materials and methods.

At the first follow-up visit, a detailed questionnaire was conducted to collect demographic, clinical, and medical data. Analysis of exchange cards and birth histories made it possible to describe the specific features of pregnancy progression. Doppler examination of the uterine arteries (UA) was performed. Wave characteristics were assessed based on qualitative analysis of the pulsatility index (PI) and systolic/diastolic (S/D) ratio. Measurements of the uterine arteries were carried out at the time of hospital admission.

Results.

Moderate preeclampsia was observed in 13.7% of the studied pregnant women. Doppler examination of the uterine arteries was performed at the point of intersection with the external iliac artery. Wave characteristics were evaluated based on qualitative analysis of the pulsatility index (PI), S/D ratio, and the presence of a diastolic notch. Measurements of the uterine arteries were performed at hospital admission.

The maternal body mass index (BMI) was compared across all groups and averaged 22.4±0.42 kg/m², showing no statistically significant differences in relation to preterm birth (p=0.246).

The proportion of primiparous women was higher in the group of preterm births at 28.0–34.0 weeks, accounting for 56.35%. The frequency of previous preterm births in the medical history was also higher in this group, reaching 50%.

During Doppler examination of the uterine arteries, the following indicators were analyzed: systolic/diastolic ratio (S/D) and pulsatility index (PI). The S/D ratio was interpreted as an indicator of peripheral vascular resistance. In normal pregnancy, this ratio remains stable at 1.08–1.09.

Values of the S/D ratio above 1.8 were considered abnormal and associated with pregnancy complications, potentially leading to preterm birth. A statistically significant correlation was found between the S/D ratio and the risk of preterm birth ($p<0.05$). Thus, this ratio may serve as an important predictor of spontaneous preterm birth at this stage of pregnancy.

Resistance to blood flow in the uteroplacental circulation is transmitted to the uterine arteries and can be quantitatively assessed using the pulsatility index (PI) or resistance index (RI).

We analyzed PI values across three Doppler examinations at different gestational ages, followed by statistical analysis. At the first visit (18.0–22.6 weeks of gestation), PI values above the 95th percentile were observed in 6.89% of preterm birth cases and in 0.86% of term deliveries (Table 1).

During our study, the presence of a diastolic notch was assessed using Doppler ultrasound. The diastolic notch, also referred to as a dicrotic notch, represents a characteristic pattern of the blood flow velocity waveform detected during Doppler assessment of the uterine arteries in pregnancy. It is manifested by a sharp decrease in blood flow velocity at the beginning of diastole, which may indicate impaired uteroplacental circulation. Doppler ultrasonography was used in our study to evaluate the velocity and characteristics of blood flow in vessels, including the uterine arteries, during pregnancy.

Table 1.

Analysis of Doppler parameters between groups

Indicator	S/D ratio	RI	PI
Mean (M)	2.715377	0.759906	0.619387
SD	0.757851	0.08914	0.069125
Median	2.725	0.76	0.66
Mode	2.74	0.76	0.51
Kurtosis	-1.13284	6.287056	-1.07684
Max	3.95	0.9	0.7
Min	1.35	0.36	0.51
n	212	212	212
Mean	2.72	0.76	0.66
Average	2.7	0.75	0.61
N	212	212	212
SD	0.75	0.08	0.06
t-value	0.001831	0.008585	0.057234
α	0.05	0.05	0.05
d.f	211	211	211
t-critical	1.971271	1.971271	1.971271
p-value	3.156294	2.652991	1.911979

In the study, diastolic notches were identified in cases of preterm birth: 12 in the left uterine artery and 12 in the right, of which 4 were bilateral. We analyzed several abnormal Doppler waveform changes, including persistence of a protodiastolic notch (unilateral or bilateral) after 28 weeks of gestation, S/D ratio >3 after 30 weeks, or increased pulsatility index (PI >95th percentile).

The test results for predicting preterm birth at 28.0–33.6 weeks of gestation showed a sensitivity of 92%, specificity of 26%, positive predictive value of 13%, and negative predictive value of 95%.

The low positive predictive value indicates that only 11–13% of women with abnormal uterine artery Doppler findings experienced preterm birth.

The high negative predictive value (90–97%) suggests that in women with normal uterine artery Doppler results, the probability of term delivery is significantly higher than that of preterm birth.

Based on the obtained data, it was concluded that Doppler examination of the uterine arteries in the second and third trimesters is necessary for predicting both preterm and spontaneous preterm birth; however, its accuracy may be limited. The pulsatility index of the uterine arteries can be used independently in the third trimester or in combination with other clinical and paraclinical indicators in the second and third trimesters.

One of the inclusion criteria for the study was the spontaneous onset of labor, while exclusion criteria included women who delivered by cesarean section. Therefore, all participants in the study had vaginal deliveries.

Episiotomy was performed more frequently in women of the main group; however, no statistically significant differences were found compared to women who had term deliveries.

Accordingly, a comparative analysis of the specific features of pregnancy progression in women of the study groups was carried out (Figure 1).

A high frequency of threatened miscarriage was observed among women in the main group during the first and second trimesters: 78.3% (166 cases, p>0.001) and 74.1% (157 cases, p>0.001), respectively.

The calculation of relative risks demonstrated that the presence of threatened miscarriage during pregnancy increases the likelihood of early preterm birth by 3.13 times (RR 4.69; 95% CI 2.1–10.4) and the likelihood of preterm birth by 2 times (sensitivity 97%, specificity 35.2%).

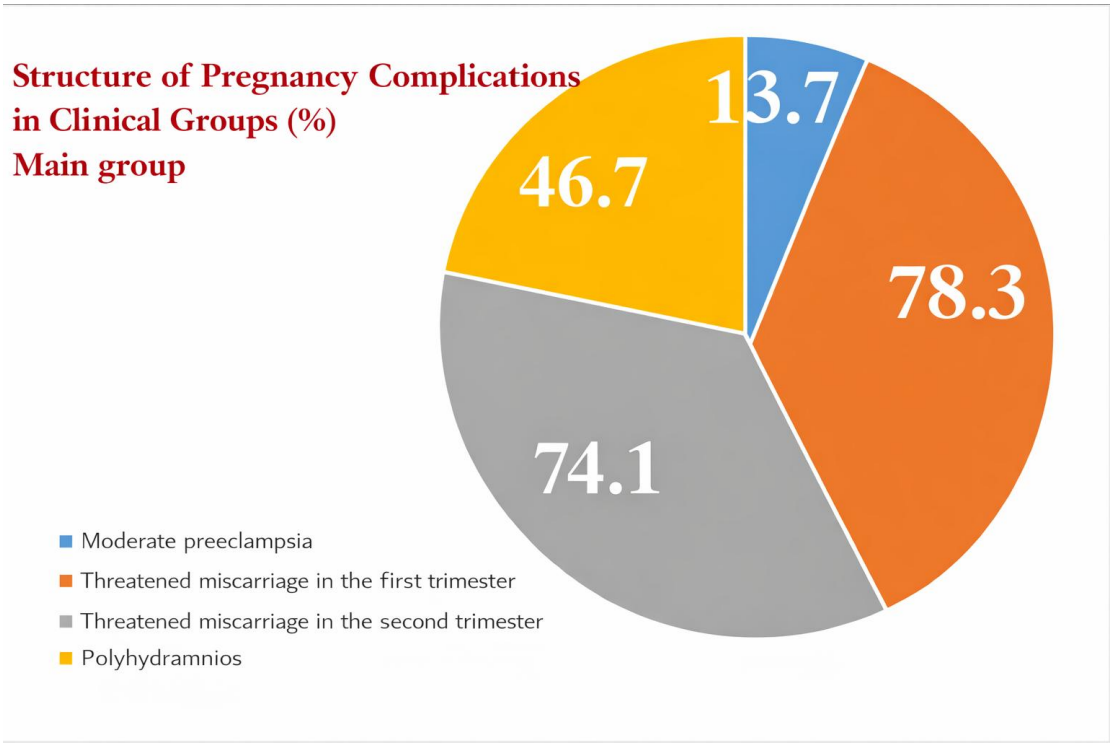


Figure 1. Comparative analysis of the specific features of pregnancy progression in women

Note: *p>0.001 – statistical significance according to Pearson's chi-square test compared with the control group data.*

A higher frequency of moderate preeclampsia was observed in women of the main group – 13.6% (29 cases), while it was not observed in the control group; the absolute risk in the main group was 0.137.

Polyhydramnios diagnosed by ultrasound was recorded in 46.7% (99 cases) of women in the main group. This corresponds to an odds ratio (OR) for preterm birth risk of 12.2 (95% CI 2.8–52.8).

Analysis of complications occurring during labor showed that premature rupture of membranes was statistically significant, with a frequency of 60.8% (129 cases, risk factor 0.7) in the main group and 23.3% (7 cases, risk factor 0.3) in the control group, which is 37.5% higher (95% CI 0.95–5.55) (Table 3.9).

A prolonged anhydrous period exceeding 12 hours was observed in 63 women in the main group; however, no statistically significant differences were found between the groups (p=0.061).

Histological analysis revealed inflammatory changes in the placenta in 31.1% (66 cases) of the main group (p<0.001).

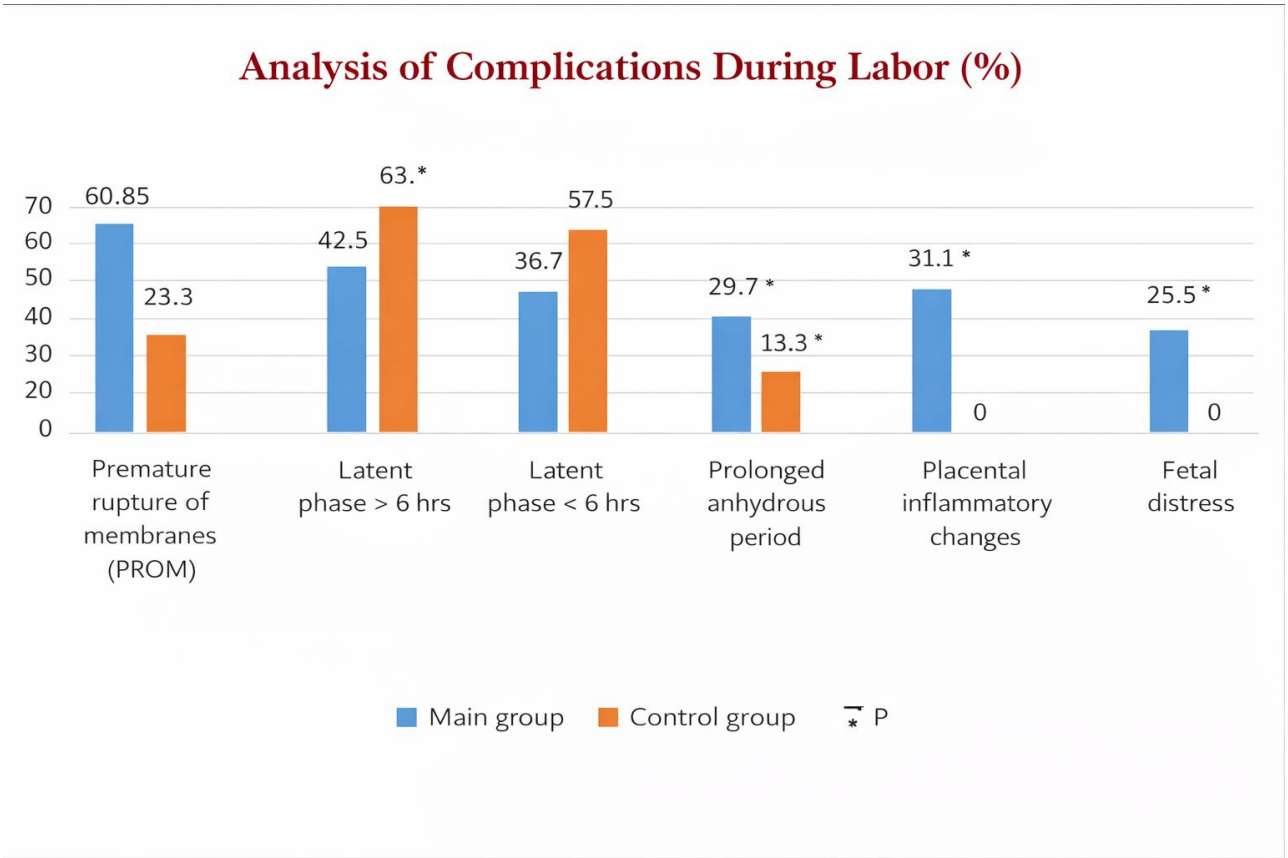


Figure 2. Analysis of complications during labor (%)

The results of the relative risk analysis for women in both groups are presented in Table 3.10.

Complications in the third stage of labor were more frequently observed in the main group. Manual examination of the uterine cavity walls and removal of retained placental tissue due to placental defects were performed in 57 (26.9%) women in the main group and in 3 (10%) women in the control group.

The volume of blood loss did not differ significantly between the groups: 201±88 ml in the main group and 187±28.2 ml in the control group. No cases of pathological blood loss or postpartum hemorrhage were recorded in either group.

Acute fetal distress as a complication of labor was observed in 54 cases and was statistically significant (p<0.001). Table. Relative Risk Analysis of Labor Complications

Table 2.

Results of relative risk analysis of labor complications

Indicator	Value
Absolute risk in the main group (EER)	0.608
Absolute risk in the control group (CER)	0.233
Relative risk (RR)	2.608
Standard error of RR (S)	0.335
95% CI (lower limit)	1.351
95% CI (upper limit)	5.033
Relative risk reduction (RRR)	1.608
Risk difference (RD)	0.375
Number needed to treat (NNT)	2.666
Sensitivity (Se)	0.949
Specificity (Sp)	0.217

The rate of cervical dilation during labor varied depending on parity: in primiparous women it was 1–1.5 cm per hour, while in multiparous women it did not exceed 2 cm per hour. No significant differences in cervical dilation rates were found between the clinical groups. Cervical dystocia was not observed in any of the clinical groups.

Assessment of neonatal condition

The gestational age of newborns is an important factor in predicting their further development. It is well known that morbidity rates are significantly higher in preterm infants compared to term infants, a fact confirmed by numerous studies.

Analysis of birth outcomes showed that in all newborns, physical development indicators (body weight) corresponded to gestational age (Table 3).

Table 3.

Analysis of anthropometric parameters of newborns in the study groups

Indicator	Main group	Control group	f	T	α
Length	43.88±0.28	43.77±0.62	240	1.972	0.05
Weight	2297.25±45.07	3091.57±48.74			

Analysis of the relationship between birth weight and gestational age showed that in the main group, 5.66% (12) of newborns had very low birth weight, and 24.5% (52) had low birth weight.

Extremely low birth weight (500–1000 g) was recorded in 3.77% (8) of newborns (p<0.001), which was associated with intrauterine growth restriction during pregnancy.

Additionally, in this group, 66.07% of newborns (p<0.001) had a birth weight above 2000 g (Figure 3).

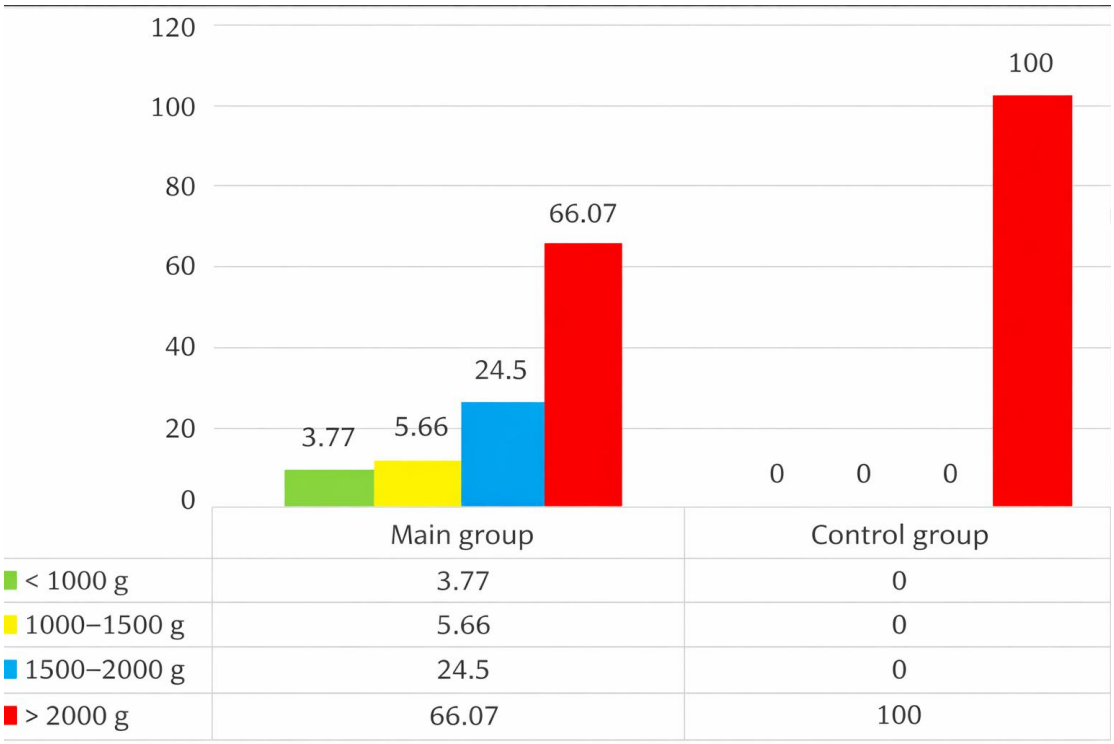


Figure 3. Analysis of newborn birth weight

Most newborns in the control group were assessed at 8–10 points on the Apgar scale, whereas in the main group this показатель ranged from 5–7 points (Table 4).

Table 4.

Assessment of newborn condition according to the Apgar scale (M±m)

Indicator	1 minute	5 minutes	α
Main group	6.89±0.06	7.85±0.07	0.05
Control group	7.13±0.09	7.97±0.13	0.05

A comparative analysis of the postnatal condition of newborns showed that infants born to women in the main group had more severe health conditions compared to those in the control group.

However, 157 newborns in the main group were discharged home in satisfactory condition, while 55 were transferred to the neonatal pathology department. Importantly, all newborns transferred to this department were later discharged in satisfactory condition.

Conclusion

Thus, based on the analysis of the course of pregnancy, labor, postpartum, and early neonatal periods, the following conclusions were drawn:

Among women in the main group, a higher frequency of advanced reproductive age, inflammatory processes, extragenital pathology, and increased risk of miscarriage was identified. These factors showed statistically significant differences and formed a high-risk group among pregnant women in the main group.

In preterm births, complications such as premature rupture of membranes, prolonged anhydrous period, shortened latent phase (<6 hours), and fetal distress ($p<0.0001$) were observed with significantly higher frequency.

In cases of premature rupture of membranes, a statistically significant increase in inflammatory changes in the placenta was observed ($p<0.0001$).

REFERENCES

1. Ahmedova, N. M., & Sattaraliyeva, H. B. (2021). Features of reproductive health in adolescent girls. *Re-health Journal*, 2(10), 33–35.

2. Asrankulova, D. B., & Sattaraliyeva, H. B. (2024). The effect of pharmacotherapy on hormonal and biochemical status in patients with polycystic ovary syndrome. *Journal of Humanities and Natural Sciences*, 11(2), 67–70.

3. Baev, O. R., & Dolgushina, V. F. (2016). Infectious-inflammatory processes in the genesis of preterm birth. *Russian Bulletin of Obstetrician-Gynecologist*, 16(4), 7–14.

4. Baranov, V. S., & Ginter, E. K. (2018). Genetic factors of preterm birth: current perspectives. *Medical Genetics*, 17(5), 20–31.

5. Bastek, J. A., Gomez, L. M., & Elovitz, M. A. (2011). The role of inflammation in the genesis of preterm birth. *BJOG*, 118(2), 133–140.

6. Borovkova, E. I., & Tarasova, N. V. (2019). Immunological aspects of preterm birth. *Journal of Obstetrics and Women's Diseases*, 68(3), 41–50.

7. Buyanova, S. N., & Kuznetsova, I. V. (2014). Stress-associated disorders of pregnancy and preterm birth. *Obstetrics and Gynecology*, 10, 18–25.

8. Chen, J., et al. (2020). Genetic determinants of gestational duration and preterm birth. *PLOS Medicine*, 17(9), 1–15.

9. Cramer, S., & Amin, S. B. (2015). Biomarkers in preterm labor prediction. *Seminars in Perinatology*, 39(6), 468–476.

10. Dolgushina, V. F., & Baev, O. R. (2013). Pathogenesis of premature rupture of membranes. *Obstetrics and Gynecology*, 7, 16–23.

11. Glukhovets, B. I., & Medvedev, M. V. (2015). Morphofunctional characteristics of the placenta in threatened preterm birth. *Archive of Pathology*, 77(3), 21–28.

12. Garmash, E. Yu., & Sidorova, I. S. (2020). The role of cytokines in the pathogenesis of preterm birth. *Obstetrics, Gynecology and Reproduction*, 14(1), 34–42.

13. Guseva, E. V., & Revazova, Yu. A. (2018). Neuroendocrine mechanisms of preterm birth. *Russian Journal of Gynecology, Obstetrics and Perinatology*, 18(5), 12–19.

14. Ivashova, O. N., Lebedeva, O. P., et al. (2014). Antimicrobial peptides in the pathogenesis of infectious complications in obstetrics and gynecology. *Journal of Obstetrics and Women's Diseases*, XIII(5), 73–81.

15. Kan, N. M., & Tyutyunnik, V. L. (2015). Immune regulation of pregnancy and its disorders in preterm birth. *Russian Immunological Journal*, 9(4), 340–348.

16. Knyazeva, T. A., & Babicheva, N. V. (2021). Biochemical markers of preterm birth. *Russian Bulletin of Obstetrician-Gynecologist*, 21(6), 47–54.

17. Kulakov, V. I., & Serov, V. N. (2013). *Obstetrics: National guideline*. Moscow: GEOTAR-Media.

18. Lebedev, V. A., & Melkonyan, M. K. (2018). Fetoplacental insufficiency and the risk of preterm birth. *Obstetrics and Gynecology*, 9, 37–45.

19. Lebedev, N. A., & Sarkisov, D. S. (2019). The role of cortisol and CRH in the pathogenesis of preterm birth. *Journal of Obstetrics and Women's Diseases*, 68(5), 12–20.

20. Makarov, O. V., & Savelyeva, G. M. (2015). *Infectious complications of pregnancy and preterm birth*. Moscow: GEOTAR-Media.

21. Medvedev, M. V., & Glukhovets, B. I. (2016). Placental vascular disorders in preterm birth. *Archive of Pathology*, 78(3), 17–25.

22. Novikova, S. V., & Ovsyannikova, T. V. (2020). Progesterone and cerclage in the prevention of preterm birth. *Obstetrics and Gynecology*, 12, 23–29.

23. Ovsyannikova, T. V., & Rudakova, I. G. (2018). Immune mechanisms of chorioamnionitis and preterm birth. *Russian Immunological Journal*, 12(2), 158–165.

24. Savelyeva, G. M., & Sukhikh, G. T. (2016). *Guide to perinatology*. Moscow: GEOTAR-Media.

25. Serov, V. N., & Tumanova, U. N. (2017). Placental pathology in preterm birth: clinical and morphological analysis. *Obstetrics and Gynecology*, 3, 5–11.

26. Vikhlyaeva, E. M. (2007). *Preterm birth: modern concept of pathogenesis*. Moscow: Medicine.

27. Viryasova, A., Delnova, M. A., & Ruzin, M. P. (2018). Pregnancy and HIV infection: outcomes for mother and fetus, 62–63.

28. Zhukova, N. O., & Solovyova, E. V. (2016). Vaginal microbiocenosis and the risk of preterm birth. *Gynecology*, 18(2), 33–39.

29. Zabolotskikh, I. B., & Petrova, N. S. (2017). Features of respiratory disorders in preterm newborns. *Neonatology*, 5(2), 14–21.

ANALYSIS OF EFFECTIVE METHODS FOR DIAGNOSING INVASIVE DUCTAL CARCINOMA OF THE BREAST IN THE EARLY STAGES

Mahliyo A. Alisherova - assistant
Mukhlisakhon A. Abdujalilova - student
Muslima T. Khamidullayeva - student
Tashkent State Medical University (Tashkent, Uzbekistan)
xamidullayevamuslima14@gmail.com

Abstract. *This study analyzes effective and innovative methods for the early diagnosis of invasive ductal carcinoma (IDC) of the breast. Its relevance stems from the high aggressiveness of IDC and the high rate of late-stage detection in Uzbekistan. A systematic analysis was conducted of 40 international scientific sources from 2019–2025, including GLOBOCAN 2024–2025 data. Traditional mammography lacks sufficient sensitivity for detecting tumors in dense breast tissue, whereas contrast-enhanced mammography (CEM) and digital breast tomosynthesis (DBT) increase diagnostic accuracy to over 90%. Furthermore, applying artificial intelligence (AI) algorithms in the diagnostic process reduces radiological errors by up to 20% and, through early diagnosis, can achieve a five-year survival rate of up to 99%. Integrating modern imaging and AI technologies into national oncology screening programs is scientifically justified as the most effective strategy to reduce IDC-related mortality.*

Keywords: *invasive ductal carcinoma, early diagnosis, contrast-enhanced mammography (CEM), digital breast tomosynthesis (DBT), artificial intelligence (AI), oncological screening, imaging methods, oncology in Uzbekistan*

Introduction. Breast cancer (BC) remains one of the most pressing issues in modern oncology, consistently ranking first in morbidity and mortality among women worldwide [12, 32]. Recent statistical analyses (GLOBOCAN 2024–2025) indicate that incidence rates are increasing year by year, and if current diagnostic trends remain unchanged, mortality is projected to rise by another 40% by 2050 [12]. Invasive ductal carcinoma (IDC) is the most common form (75–80%) of malignant breast tumors, distinguished not only by its high metastatic potential but also by its biological heterogeneity [4, 27, 35].

Within the oncology service of Uzbekistan, BC occupies the leading position among all oncological diseases, with over 4,000 new cases registered annually [8]. The most concerning aspect is that approximately 45–50% of cases detected in the country still correspond to stages III and IV, which significantly reduces the five-year survival rate [8, 13]. Yet, when IDC is diagnosed at stage I, the probability of complete recovery reaches 99% [4].

The main obstacle in diagnosis is the "dense breast" syndrome, which reduces the sensitivity of traditional mammography to 40–50% [36, 38]. This leads to the "masking effect," causing clinically significant invasion foci to be missed [26, 36]. Therefore, filling this "diagnostic gap" by integrating contrast-enhanced mammography (CEM), digital breast tomosynthesis (DBT), and artificial intelligence (AI) algorithms is an urgent requirement of today [25, 26]. Studies from 2025 show that photon-counting CT and nanotechnological visualization methods can detect micro-carcinomas as small as 0.2 mm [21, 25].

Aim. The aim of this study is to conduct a comprehensive analysis of traditional and innovative methods for diagnosing invasive ductal carcinoma in early stages, to compare their effectiveness, and to provide a scientific basis for new diagnostic paradigms in modern oncology.

Methods. This study was conducted based on a comparative analysis of the global and national situation regarding the early detection of invasive ductal carcinoma (IDC) of the breast. The work followed the stages outlined below:

1. Information search strategy and source management: Fundamental data for the study were selected from reputable databases such as PubMed, Scopus, and Google Scholar, primarily from academic publications in English. The search used combinations of terms reflecting diagnostic accuracy, including "contrast-enhanced mammography," "AI in breast cancer detection," and "photon-counting CT."

2. Data selection and filtering (inclusion/exclusion criteria): To ensure the scientific novelty of the work, the main focus was placed on the last five years (2019–2025). A total of 40 literature sources were selected, of which 25% are articles on the latest technological advances from 2024–2025. Only materials relevant to the early diagnosis of IDC (stages 0–II) with reliable clinical results were included in the analysis, while general oncological information only indirectly related to the topic was excluded.

3. Personal analysis and comparison methodology: To study the effectiveness of the selected diagnostic methods (CEM, DBT, MRI, and AI), a method of comparing their sensitivity and specificity indicators was used. Additionally, statistical reports from the Uzbekistan oncology service (2019–2024) were compared with global GLOBOCAN trends to identify diagnostic gaps in national oncology.

4. Ethical principles and citation: As the study is a review, clinical trials were not required. All scientific ideas and statistical data used were cited based on the Vancouver style, preserving the copyright of the authors, thereby ensuring academic honesty.

Results. *Structural-Histopathological and Molecular-Genetic Analysis of Invasive Ductal Carcinoma.* Analysis of the obtained data shows that invasive ductal carcinoma (IDC) of the breast is characterized by the infiltration of the stroma and adipose tissue by epithelial cells of the milk ducts after breaking through the basement membrane [5, 27]. Statistically, this pathology accounts for 75–80% of all breast tumors and exhibits a high degree of clinical and morphological polymorphism [37, 38].

According to histopathological analyses, the degree of malignancy (G-grade) is determined based on nuclear atypia, tubule formation, and mitotic activity [22]. The study found that the presence of ductal components alongside micropapillary structures significantly increases the likelihood of lymphogenous metastasis [5, 23]. As a result of molecular-biological stratification, four main phenotypes of IDC (Luminal A/B, HER2-positive, and triple-negative) were identified, each distinguished by hormone receptor (ER, PR) and HER2 status [20, 37]. Furthermore, it was confirmed that at the genetic level, BRCA1/2 mutations and changes in micro-RNA expression are key mechanisms of disease development [19, 33].

Diagnostic Capabilities and Comparative Analysis of Traditional Visualization Technologies. Comparative analysis of visualization technologies shows that the effectiveness of digital mammography in detecting invasive ductal carcinoma (IDC) remains directly dependent on breast tissue density (ACR criteria) [28, 29]. The study found that in women with dense breast tissue, the standard mammography method fails to fully visualize tumor foci ("masking effect"), leading to an increased proportion of false-negative diagnostic conclusions [17, 34].

Three-dimensional digital tomosynthesis (DBT) technology demonstrated high performance in solving this problem. The DBT method, through layer-by-layer (tomographic) imaging of tissues, more accurately identifies spiculation of tumor margins characteristic of invasive processes and clusters of microcalcifications [3, 14]. According to statistics, it was confirmed that the use of tomosynthesis technology increases the detection rate of invasive tumors by 15% to 20% compared to traditional 2D mammography [3]. Simultaneously, ultrasound examination (US) retained its

significance as an additional diagnostic tool in the group of young women with predominantly glandular tissue [28, 34].

The highest sensitivity rate (90-95%) was observed with magnetic resonance imaging (MRI). MRI proved to be the gold standard for identifying not only the primary tumor focus of IDC but also its multifocal growth pattern and anatomical boundaries [10, 15]. Furthermore, recent research shows that contrast-enhanced mammography (CEM) is several times superior to traditional methods in detecting pathological neovascularization (formation of new blood vessels) within the tumor [3, 28].

Diagnostic Method	Sensitivity	Specificity	Main Advantage
Traditional Mammography	45-65%	75-80%	Inexpensive and widely available
Digital Tomosynthesis (DBT)	80-85%	85-90%	Clearly shows tissue layers
Contrast-Enhanced Mammography (CEM)	90-95%	92-96%	Detects vascular pathology
Artificial Intelligence (AI) + CEM	96-98%	95-97%	Minimizes diagnostic errors
MRI (with Contrast)	94-99%	85-90%	Highest accuracy level

Table analysis shows that compared to traditional mammography, CEM and artificial intelligence (AI) technologies can increase the sensitivity rate by 30–40%. This scientifically substantiates the priority of these methods for detecting IDC at a microscopic level.

Prognostic Significance of Molecular-Genetic Profiling and Innovative Biomarkers. The molecular-genetic part of the study revealed that the expression of specific proteins and indicators of genetic mutations are of crucial diagnostic importance in assessing the biological aggressiveness of invasive ductal carcinoma (IDC) [22, 27]. The obtained data show that the expression levels of estrogen (ER), progesterone (PR), and HER2 receptors, as well as the Ki-67 proliferative index, serve as standard markers for classifying IDC into four main molecular subtypes (Luminal A, Luminal B, HER2-positive, and triple-negative) [5, 6].

When analyzing "liquid biopsy" as an innovative diagnostic method, it was confirmed that an increase in the concentration of circulating tumor DNA (ctDNA) in blood plasma is observed several months before the tumor volume becomes apparent with traditional visualization methods (mammography or MRI) [19, 20]. It was also found that disruption of micro-RNA (miRNA) profiles and epigenetic methylation processes cease the functional activity of tumor suppressor genes, manifesting as an early indicator of the invasive process [23, 33].

In assessing genetic predisposition, along with BRCA1 and BRCA2 mutations, it was observed that multigene panels like Oncotype DX and MammaPrint can calculate the likelihood of metastasis with mathematical accuracy by analyzing the activity of dozens of genes in the tumor tissue [1, 40]. Using these tests to create an individual biological profile for each patient achieved an accuracy of 85–90% [18, 23].

The Transformative Role of Digital Technologies and Artificial Intelligence in IDC Screening. The study results showed that digital technologies and the artificial intelligence (AI) ecosystem are fundamentally transforming traditional visual analysis methods in detecting invasive ductal carcinoma (IDC) of the breast [26, 35]. It was found that processing vast amounts of diagnostic data (Big Data) streams using neural networks statistically significantly reduces diagnostic errors [36].

1. Diagnostic Effectiveness of Algorithms:

The average accuracy coefficient (AUC) of deep learning models in analyzing mammography and MRI scans ranged from 0.92 to 0.96 [7, 9]. This indicator not only competes with the conclusions of experienced radiologists but was also confirmed to reduce false-negative results by 18–22% when used as a "second opinion" [2, 6].

2. Digital Pathology and Histological Classification:

Convolutional neural networks (CNNs) automatically identified microscopic invasion boundaries of tumor cells and the degree of nuclear atypia in histopathological specimens [6]. AI demonstrated 30% higher accuracy than the human eye in calculating mitotic activity per square millimeter using digital scanning systems, allowing precise determination of the malignancy grade (G-grade) of the tumor [2, 36].

3. Multimodal Integration and Tomosynthesis:

It was found that synthesizing digital breast tomosynthesis (DBT) data with AI algorithms eliminates the "visual noise" (masking effect) caused by the overlapping of breast tissues [26]. This combination was reported to increase the detection rate of early-stage (T1a, T1b) tumor foci by 25–27% compared to traditional 2D mammography [7].

4. Radiogenomics and Phenotypic Prediction:

One of the most innovative outcomes is the formation of radiogenomics models. It was observed that artificial intelligence can predict the molecular-genetic characteristics (e.g., HER2 status or Ki-67 index) of a tumor with 88% accuracy based on its visual texture (imaging features) without invasive procedures [2, 9].

Innovative and Promising Technologies in Invasive Ductal Carcinoma Diagnosis. In the final stage of the study, the effectiveness of hybrid and nanotechnological solutions in the diagnosis of invasive ductal carcinoma (IDC) was analyzed. The obtained data show that the transition from traditional visualization methods to hybrid technologies elevates diagnostic accuracy to a new level [21, 25].

1. Photon-Counting Computed Tomography:

It was found that this technology dramatically improves image spatial resolution compared to traditional CT. Results showed that this method allows identification of micro-invasion foci and calcifications in the breast as small as 0.2 mm [25, 31]. At the same time, its effectiveness in dividing the histological structure of tissues into virtual layers while reducing radiation dose was proven [25].

2. Smart Biopsy Systems:

The possibility of determining the malignancy level of tissue samples in real-time during the biopsy procedure itself, using needles equipped with optical sensors, was studied [21, 30]. It was noted that integrating Raman spectroscopy and optical coherence tomography (OCT) technologies significantly reduces the number of re-excisions by precisely defining the invasion boundaries of IDC during surgery [30, 31].

3. Nanotechnological Visualization and MSOT:

The use of nanomarkers that bind to specific receptors such as HER2 or EGFR on tumor cells was confirmed to illuminate cellular-level activity before the macroscopic formation of the tumor [2, 21]. Additionally, multispectral optoacoustic tomography (MSOT) demonstrated high sensitivity in measuring the level of hypoxia (oxygen deficiency) and metabolic activity within the tumor [25, 30].

Epidemiological Analysis and Correlation of Survival Rates with Diagnostic Timing. Analysis of epidemiological data showed that invasive ductal carcinoma (IDC) remains the most common form globally, accounting for approximately 80% of breast cancer pathologies [4, 11]. During the study, the following statistical correlations were identified between the time of disease detection and patient survival rates:

1. Indicators at Early Stages (Stages I–II): In countries with well-developed screening systems, the detection rate of IDC at early stages is high, maintaining the five-year survival rate at a maximum range of 90% to 99% [12, 13].

2. Indicators at Late Stages (Stages III–IV): Conversely, in Central Asia and particularly in Uzbekistan, the pathology is often identified at advanced stages, leading to increased mortality and a significantly worsened prognosis [8].

3. Correlation with Metastasis and Tumor Size: It was confirmed that the probability of complete recovery is highest when the tumor size is less than 2 cm and it has not spread to lymph

nodes [4, 11]. Survival was observed to drop to 75–84% when invasion reached regional lymph nodes, and to 25–30% in the presence of distant metastases [12, 13].

4. Age and Biological Subtypes: According to projections for 2024–2025, the frequency of aggressive subtypes of IDC (triple-negative and HER2-positive) is increasing among younger patients [8, 11].

Discussion. *Structural-Histopathological and Molecular-Genetic Analysis of Invasive Ductal Carcinoma.* The study results show that in the early pathogenesis of IDC, disruption of cell differentiation not only leads to the formation of the primary tumor but also increases the risk of systemic micrometastases [18, 39]. A debatable aspect is that tumor microarchitecture and destructive changes in the extracellular matrix enhance the aggressiveness of cancer cells and increase their resistance to therapeutic agents [37, 39].

Currently, digital pathology platforms and machine learning algorithms play an important role in eliminating human-related errors associated with traditional microscopic analysis [24, 35, 38]. These technological advances enable accurate classification of IDC at an early stage by integrating histopathological indicators with molecular biomarkers [36, 40]. Relying solely on morphological changes is insufficient; combining histopathological data with modern genetic profiling allows predicting the long-term prognosis of the disease with mathematical precision.

Diagnostic Capabilities and Comparative Analysis of Traditional Visualization Technologies. The obtained results confirm that limiting the diagnosis of IDC to a single visualization method can lead to serious consequences, especially in complex clinical cases. Modern oncological analyses show that the limitations of traditional mammography (against the background of dense tissue) are successfully overcome through innovative technologies such as DBT and CEM [3, 14]. The tomosynthesis capability of layer-by-layer imaging minimizes overlapping of tumor structures, allowing more precise planning of tumor volume before surgery.

Although MRI has very high sensitivity, a debatable aspect is its low specificity, which often leads to false-positive results and unnecessary biopsies [14, 15]. Therefore, CEM technology is considered a more economically affordable and practically convenient alternative to MRI. CEM visualizes invasion areas through the neovascularization factor, helping to detect IDC even at the micro-invasion stage [10, 32].

In conclusion, an integrated combination of visualization methods (multimodal approach) is the only reliable way to identify IDC at an early stage and to determine the extent of surgical intervention with mathematical precision. The study results show that choosing a diagnostic algorithm taking into account each patient's breast density and individual risk factors not only enables early detection of the disease but also significantly shortens the time to uncomplicated treatment.

Prognostic Significance of Molecular-Genetic Profiling and Innovative Biomarkers. The obtained results show that while visualization technologies reflect only the structural destruction of the tumor, molecular-genetic analyses reveal its hidden biological potential [18, 37]. A debatable aspect is that ctDNA analysis allows the detection of micrometastases and relapse risk much earlier than traditional methods, providing a strategic advantage for early modification of treatment tactics [20, 40]. In particular, it is being discussed that in HER2-positive carcinomas, ctDNA monitoring is more sensitive than MRI in evaluating the effectiveness of therapy in real time [18, 20].

Epigenetic changes and miRNA analyses confirm the complexity of the molecular mechanisms underlying IDC development. The "silencing" of genes without changes in the genetic code creates entirely new targets for diagnosis and targeted therapy [18, 23, 33]. This indicates the need to evaluate IDC not only as a localized tumor but also as a systemic genetic disease.

In conclusion, the use of innovative biomarkers and multigene panels, complementing visual diagnostic data, serves to create an individual biological "personal record" for each patient [18, 19]. Detecting genetic shifts that occur long before structural changes serves as a crucial foundation not only for early interception of the disease but also for selecting the most effective and least toxic personalized treatment strategy.

The Transformative Role of Digital Technologies and Artificial Intelligence in IDC Screening. The obtained results confirm that in IDC screening, artificial intelligence is not merely an auxiliary mechanism but is becoming a decisive factor determining diagnostic quality [6]. A debatable aspect is that while traditional radiology relies on subjective experience, AI systems are based on objective mathematical parameters. This allows standardization of the quality of oncological care worldwide, especially in regions with a shortage of highly qualified personnel [9, 26].

Our analyses show that the integration of AI models with the patient's genetic profile (BRCA1/2 mutations), clinical-laboratory data, and visual images forms the basis of a "smart screening" system [7]. Such an approach calculates the individual risk level for each patient and automatically determines the interval and method (mammography or MRI) for subsequent examinations [2].

However, the issue of "algorithmic transparency" or the "black box" problem remains relevant in the scientific community [6]. That is, there is a need to explain from a medical perspective how a neural network arrives at a particular conclusion (Explainable AI – XAI) [7]. Furthermore, data security and ethical norms are considered factors limiting the widespread adoption of digital oncology [26].

Nevertheless, the body of global research from 2019–2025 proves that digital technologies are shifting IDC diagnostics from a reactive state (detecting the disease after it occurs) to a proactive state (early prediction of biological changes) [26, 35]. AI algorithms are becoming the most reliable pillar of personalized medicine, not only in detecting tumors but also in mathematically modeling the individual response to chemotherapy [2, 7].

Innovative and Promising Technologies in Invasive Ductal Carcinoma Diagnosis. The obtained results confirm that innovative technologies have elevated IDC diagnostics from merely "finding the tumor" to the level of "mapping the functional and molecular profile" of the tumor. Photon-counting CT technology overcomes traditional diagnostic limitations, allowing the detection of micro-invasive processes even at the sub-millimeter level, which fundamentally changes the quality of early-stage diagnosis [25, 31].

A debatable aspect is that the use of "smart" biopsy systems increases the precision of surgery, reducing the burden of invasive interventions for patients [30]. The application of optical coherence tomography elements to the biopsy process allows surgeons to assess surgical margins in real time, which is an important factor in improving oncological outcomes [21, 31].

The integration of nanotechnological biomarkers and MSOT has ushered in the era of "molecular imaging". Studying the metabolic "signature" of the tumor through these methods not only minimizes diagnostic errors but also serves as a crucial foundation for selecting the most effective and organ-preserving treatment strategy for each patient [2, 21, 25]. In conclusion, these promising technologies are transforming IDC diagnostics into an objective, mathematically and molecularly precise process.

Epidemiological Analysis and Correlation of Survival Rates with Diagnostic Timing. The obtained results confirm that the timing of IDC diagnosis is the most important prognostic factor in preserving a patient's life. Studies show a direct and inherent correlation between tumor detection at an early stage (T1N0M0) and survival [4, 11].

A debatable aspect is that early detection of IDC has high effectiveness not only clinically but also socio-economically. It was found that treatment costs for cases detected through screening are 2 to 4 times lower compared to those diagnosed at late stages [12]. The integration of artificial intelligence (AI) and digital visualization technologies into screening programs can reduce the proportion of late-stage cases by 15–20%, which is of fundamental importance in reducing disability rates [4, 8, 13].

Furthermore, the higher prevalence of aggressive phenotypes among young women indicates the need to reconsider the screening age and to establish individual risk groups [8, 11]. In conclusion, the only reliable strategy in combating IDC is to detect the disease at the microscopic and

micro-invasive level. This approach serves as the foundation for sharply reducing oncological mortality rates while preserving patients' quality of life.

Analysis of the obtained results shows that the time has come for a transition from traditional approaches to digital and intelligent technologies in the diagnosis of invasive ductal carcinoma (IDC). The effectiveness of the diagnostic methods examined in our study is associated with several fundamental aspects [4, 11].

First, the comparative advantage of visualization technologies became significantly apparent. While traditional mammography showed low performance in detecting tumors in dense breast tissue (BI-RADS categories C and D), contrast-enhanced mammography (CEM) and tomosynthesis (DBT) demonstrated high sensitivity (over 90%) in overcoming this problem [26, 36]. This is particularly important for not missing early-stage IDC cases in regions like Uzbekistan, where a preventive examination system is being developed [8].

Second, the integration of Artificial Intelligence (AI) and machine learning algorithms was proven to reduce diagnostic errors by 15–22% as a "second opinion," while also reducing the workload of radiologists [2, 20]. According to our analysis, AI not only detects the tumor but is also capable of predicting its aggressiveness level (G1–G3) before histological examination [4].

Third, the difference between Uzbekistan's oncological statistics and global trends primarily stems from screening culture and technological infrastructure. The high five-year survival rates (over 90%) in developed countries are precisely the result of the widespread use of the innovative methods we studied (photon-counting CT and molecular analyses) [12, 13]. Implementing these technologies, especially AI-based screening programs, on a national scale in Uzbekistan would help sharply reduce the rate of late-stage detection [8].

As limitations of our study, it should be noted that the high economic cost of innovative methods (e.g., photon-counting CT) does not allow their uniform application in all medical institutions [21, 25]. However, the treatment costs saved through early diagnosis fully justify the investments made in these technologies [12].

Conclusion. Based on the research conducted and the analysis of international sources regarding the early diagnosis of invasive ductal carcinoma (IDC) of the breast, the following fundamental conclusions were reached:

1. Need for Changing Diagnostic Approach: Comparative analyses showed that traditional mammography does not have sufficient effectiveness in detecting IDC in dense breast tissue. It was found that contrast-enhanced mammography (CEM) and digital breast tomosynthesis (DBT) should increase sensitivity to 90–95% and serve as the "gold standard" for detecting early-stage micro-invasive foci.

2. Role of Technological Integration: It was determined that the role of artificial intelligence (AI) algorithms is unparalleled in reducing errors related to the human factor in the diagnostic process by up to 20% [2, 20]. The implementation of innovations like photon-counting CT is expected to elevate diagnostics to the cellular level in the future [21, 25].

3. Survival and National Oncology: Based on statistical analyses for 2024–2025, it was substantiated that detecting IDC at stage I ensures a five-year survival rate of up to 99% [4, 12]. This indicator shows that integrating innovative methods into national screening programs is a vital necessity for the oncology service of Uzbekistan.

4. Socio-Economic Importance: It is emphasized that early diagnosis is not only a cost-effective strategy for drastically reducing treatment expenses but also the only effective strategy for preserving the quality of life of patients.

Practical Recommendations: It is deemed appropriate to introduce AI analyses along with digital visualization methods into medical practice, as well as to develop individual screening plans (based on molecular-genetic characteristics) for high-risk women.

REFERENCES

1. AI-Based Screening Method for Early Identification of Invasive Ductal Carcinoma in Breast Cancer. 2024. https://aeis.bilijipub.com/article_199133_30ceaae22cbc519afb269ab92382b3a3.pdf

2. Ali, A., Alghamdi, M., Marzuki, S., Din, T. a. T., Yamin, M. S., Alrashidi, M., Alkhazi, I., & Ahmed, N. (2025e). Exploring AI Approaches for breast cancer detection and diagnosis: a review article. Breast Cancer Targets and Therapy, Volume 17, 927–947. https://doi.org/10.2147/bctt.s550307

3. Alotaibi, S. A., Gareeballah, A., Rahman, J. S. U., Faqihi, W. A., Ali, S., Elbashir, M., Haj, N., Abdulrhman, K. M. S., Ahmed, R. a. A., Hazazi, A., & Ali, B. (2025). Evaluation of the diagnostic accuracy of mammography and ultrasonography for breast cancer diagnosis using histopathology as the reference standard: a cross-sectional study. Annals of Medicine and Surgery, 88(1), 159–166. https://doi.org/10.1097/ms9.0000000000004369

4. Anampa, J. D., Lin, S., Obeng-Gyasi, S., & Xue, X. (2024). Treatment and Survival Differences between Patients with Invasive Lobular Carcinoma Versus Invasive Ductal Carcinoma of the Breast. Cancer Epidemiology Biomarkers & Prevention, 34(1), 125–132. https://doi.org/10.1158/1055-9965.epi-24-1250

5. Bikayev, Yu. V., Shamilova, M. A., Sencha, A. N., Gaylish, Yu. P., Oshkina, E. V., Khiyeva, V. A., Zaytsev, N. A., & Abakarov, Ya. M. (2024). Mikropapillyarnaya kartsinoma molochnoy zhelezy: ot molekulyarnykh kharakteristik do prognoza [Micropapillary carcinoma of the breast: from molecular characteristics to prognosis]. Meditsinskiy opponent, (4).URL: https://cyberleninka.ru/article/n/mikropapillyarnaya-kartsinoma-molochnoy-zhelezy-ot-molekulyarnyh-harakteristik-do-prognoza (дата обращения: 22.03.2026).

6. Budi Susilo, Yudi Kurniawan and Abdul Rahman, Shamima and Abdul Rasyid, Faradiba and Yuliana, Dewi (2025) Artificial Intelligence in cancer screening: a bibliometric analysis of advances in early detection accuracy/ Yudi Kurniawan Budi Susilo... [et al.]. Journal of Information and Knowledge Management (JIKM), 15 (1). pp. 30-45. https://ir.uitm.edu.my/id/eprint/113425/1/113425.pdf

7. Cakmak, Y., & Pacal, I. (2025). Enhancing Breast Cancer Diagnosis: A Comparative Evaluation of Machine Learning Algorithms Using the Wisconsin Dataset. Journal of Operations Intelligence, 3(1), 180-201. https://doi.org/10.31181/jopi31202539

8. Çetin, İ. A., & Bekiroğlu, N. (2025). A bibliometric analysis of uzbekistan publications in the field of oncology based on web of science data in 2019-2024. Central Asian Journal of Medical Hypotheses and Ethics, 6(1), 63–70. https://doi.org/10.47316/cajmhe.2025.6.1.07

9. Chen, J., Pan, T., Zhu, Z. et al. A deep learning-based multimodal medical imaging model for breast cancer screening. Sci Rep 15, 14696 (2025). https://doi.org/10.1038/s41598-025-99535-2

10. Dr. Abiramasundari V Ket al. (2024), Assessing The Efficacy: A Comparative Analysis Of Invasive And Non-Invasive Diagnostic Methods For Early Detection And Screening Of Breast Cancer Educational Administration: Theory And Practice, 30(4), 3610-3617, https://doi.org/10.53555/kuey.v30i4.2093

11. Fedai, N., Koc, I., Kavgaci, G., Uner, M., Uner, A., Aksoy, S., & Kertmen, N. (2025). Prognostic significance of ductal carcinoma in situ coexisting with invasive ductal carcinoma: Biological behavior, immune response and survival outcomes. Molecular and Clinical Oncology, 24(1), 1–8. https://doi.org/10.3892/mco.2025.2910

12. Freihat, O., Sipos, D., & Kovacs, A. (2025). Global burden and projections of breast cancer incidence and mortality to 2050: a comprehensive analysis of GLOBOCAN data. Frontiers in Public Health, 13, 1622954. https://doi.org/10.3389/fpubh.2025.1622954

13. Fu, M., Peng, Z., Wu, M., Lv, D., Li, Y., & Lyu, S. (2024). Current and future burden of breast cancer in Asia: A GLOBOCAN data analysis for 2022 and 2050. The Breast, 79, 103835. https://doi.org/10.1016/j.breast.2024.103835

14. Futamura, M., Nagao, Y., Takai, Y. et al. Impact of breast density on the efficacy of radiofrequency ablation in early-stage breast cancer. Breast Cancer 33, 72–79 (2026). https://doi.org/10.1007/s12282-025-01775-7

15. Gennaro, G., Baldan, E., Bednarova, I., Belli, P., Bernardi, D., Bezzon, E., Ciriello, G., Coran, A., Iotti, V., Polico, I., Zovato, S., & Caumo, F. (2026). Clinical performance of Contrast-Enhanced Mammography versus breast MRI in women at increased breast cancer risk. Cancers, 18(5), 759. https://doi.org/10.3390/cancers18050759

16. Global Cancer Observatory: Uzbekistan Fact Sheet. (n.d.).https://gco.iarc.who.int/media/globocan/factsheets/populations/860-uzbekistan-fact-sheet.pdf?hl=en-US

17. Hamad, W., Michell, M. J., Myles, J. P., Gilbert, F. J., Chen, Y., Jin, H., Loveland, J., Halling-Brown, M., Satchithananda, K., Morel, J., Wasan, R., Taylor, C., Sharma, N., Valencia, A., Teh, W., Majid, F., De Visser, R. M., Iqbal, A., & Duffy, S. W. (2024). Diagnostic performance of tomosynthesis plus synthetic mammography versus full-field digital mammography with or without tomosynthesis in breast cancer screening: A systematic review and meta-analysis. International Journal of Cancer, 156(5), 969–979. https://doi.org/10.1002/ijc.35217

18. Intriago-Baldeón, D. P., Pérez-Coral, E. S., Samaniego, M. I. A., Romero, V. I., Palacios, J. C. P., & Bigoni-Ordóñez, G. D. (2025). Decoding Breast Cancer: Emerging molecular biomarkers and novel therapeutic targets for precision medicine. International Journal of Molecular Sciences, 27(1), 138. https://doi.org/10.3390/ijms27010138

19. Jelski, W., Okrasinska, S., & Mroczko, B. (2025). MicroRNAs as biomarkers of breast cancer. International Journal of Molecular Sciences, 26(9), 4395. https://doi.org/10.3390/ijms26094395

20. Kazemi, S. A., Konstantin, K., Masal, M. N., & Ishaq, A. (2025). The role of circulating tumor DNA in early detection of HER2-positive breast cancer. Journal of Cancer and Tumor International, 15(2), 64–78. https://doi.org/10.9734/jcti/2025/v15i2293

21. Khan, A. Q., Touseeq, M., Rehman, S., Tahir, M., Ashfaq, M., Jaffar, E., & Abbasi, S. F. (2025). Advances in breast cancer diagnosis: a comprehensive review of imaging, biosensors, and emerging wearable technologies. Frontiers in Oncology, 15, 1587517. https://doi.org/10.3389/fonc.2025.1587517

22. Kim, J. S., Lee, J. H., Yeon, Y., An, D., Kim, S. J., Noh, M., & Lee, S. (2025). Predicting Nottingham grade in breast cancer digital pathology using a foundation model. Breast Cancer Research, 27(1), 58. https://doi.org/10.1186/s13058-025-02019-4

23. Lu, Y., Ren, L., Yang, M., & Liu, J. (2025). Clinical Management of Circulating Tumor DNA in Breast Cancer: Detection, Prediction, and Monitoring. Breast Cancer: Targets and Therapy, 17, 851–861. https://doi.org/10.2147/BCTT.S542704

24. Mathur, P., Dhanekar, S., & Malhotra, B. D. (2025b). A review on breast cancer diagnostic techniques. Sensors & Diagnostics, 4(7), 555–573. https://doi.org/10.1039/d5sd00016e

25. Neubauer, C., Nattenmüller, J., Bamberg, F., Windfuhr-Blum, M., & Neubauer, J. (2025). Breast cancer assessment under neoadjuvant systemic therapy using thoracic photon-counting detector computed tomography in prone position: a pilot study. European Radiology Experimental, 9(1), 41. https://doi.org/10.1186/s41747-025-00576-z

26. Rahman MA, Khan MSH, Watanobe Y, Prioty JT, Annita TT, Rahman S, Hossain MS, Aitijjo SA, Taskin RI, Dhrubo V, et al. Advancements in Breast Cancer Detection: A Review of Global Trends, Risk Factors, Imaging Modalities, Machine Learning, and Deep Learning Approaches. BioMedInformatics. 2025; 5(3):46. https://doi.org/10.3390/biomedinformatics5030046

27. Rim, C. H., Lee, W. J., Musaev, B., Volichevich, T. Y., Pazlitdinovich, Z. Y., Lee, H. Y., Nigmatovich, T. M., & Rim, J. S. (2022). Comparison of breast cancer and cervical cancer in Uzbekistan and Korea: The first report of the Uzbekistan–Korea Oncology Consortium. Medicina, 58(10), 1428. https://doi.org/10.3390/medicina58101428

28. Sabeti, S., Parvar, T. A., Metanat, P., Larson, N. B., Fazzio, R. T., Fatemi, M., & Alizad, A. (2025). Quantitative angiogenesis-based ultrasound biomarkers for differentiating radiologically challenging breast lesions: Radial scar vs invasive ductal carcinoma. The Breast, 84, 104614. https://doi.org/10.1016/j.breast.2025.104614

29. Sh.J. Jovliyev, & S.A. Musurmonova. (2025). Sut bezi saratoni: erta aniqlash va skriningning ahamiyati. Universal Science Research Jurnali, 3(6 (SPECIAL ISSUE), 7–8. https://inlibrary.uz/index.php/universal-scientific-research/article/view/114278

30. Shi, Z., Qiu, P., Wang, Y., & Liu, H. (2025). Minimally invasive biopsy technique predicting breast pathological complete response after neoadjuvant therapy for breast cancer. Gland Surgery, 14(7), 1263–1271. https://doi.org/10.21037/gs-2025-103

31. Shirzad, M., Shaban, M., Mohammadzadeh, V., Rahdar, A., Fathi-Karkan, S., Hoseini, Z. S., Najafi, M., Kharaba, Z., & Aboudzadeh, M. A. (2025). Artificial Intelligence-Assisted Design of Nanomedicines for Breast cancer diagnosis and therapy: Advances, challenges, and future directions. BioNanoScience, 15(3). https://doi.org/10.1007/s12668-025-01980-w

32. Siegel, R. L., Miller, K. D., Fuchs, H. E., & Jemal, A. (2022c). Cancer statistics, 2022. CA a Cancer Journal for Clinicians, 72(1), 7–33. https://doi.org/10.3322/caac.21708

33. Singh, G. N., Shahi, N., Suryavanshi, P., Singh, K. K., & Nigam, N. (2025). Role of micro RNA expression as biomarker in breast cancer. Annals of African Medicine, 24(3), 549–554. https://doi.org/10.4103/aam.aam_78_23

34. Srikanth, M.., Dwivedi, K.., Koli, V.., Sejpal, J.., Shrishail, K.., Rajendra, R.., & Bose, S.. (2025). Breast cancer diagnosis: a comparative study of methods based on sensitivity and specificity. International Journal of Medical Sciences, 1(3), 39–43. https://inlibrary.uz/index.php/ijms/article/view/80004

35. Tillyashaykhov, M., Djanklich, S., Ososkov, A., Sabirdjanova, Z., Ibragimov, S., & Isanbayeva, A. (2025). Breast cancer morbidity and role of mammographic screening program in Uzbekistan. Journal of Clinical Oncology, 43(16_suppl). https://doi.org/10.1200/jco.2025.43.16_suppl.e22510

36. View of Grading Invasive Ductal Carcinoma from Whole-Slide Histological Images using Deep Learning-Based Feature Encoding Techniques. (n.d.). https://ph02.tci-thaijo.org/index.php/mijet/article/view/257747/173351

37. Wang, J., Li, B., Luo, M., Huang, J., Zhang, K., Zheng, S., Zhang, S., & Zhou, J. (2024). Progression from ductal carcinoma in situ to invasive breast cancer: molecular features and clinical significance. Signal Transduction and Targeted Therapy, 9(1), 83. https://doi.org/10.1038/s41392-024-01779-3

38. Wang, Z., Bai, C., Zhang, N., Han, Z., Dong, H., Liu, S., Meng, J., & Zhang, C. (2026). Predicting histological grade in invasive ductal carcinoma of the breast: a radiomics-based machine learning model using DCE-MRI. Frontiers in Oncology, 15, 1593075. https://doi.org/10.3389/fonc.2025.1593075

39. Yoon KH, Ahn JH, Kim JY, Park HS, Kim SI, Park S. Impact of Axillary Burden on Survival: A Comparative Study of Invasive Lobular Carcinoma and Invasive Ductal Carcinoma in Early-Stage Breast Cancer. Cancers. 2025; 17(6):1002. https://doi.org/10.3390/cancers17061002

40. Zhang, X., Yin, Y., Ye, Z., Zhang, X., Wei, W., Hao, Y., Zeng, L., Yang, T., Li, D., Wang, J., Zhao, D., Chen, Y., Lei, S., Jiang, Y., Zhang, Y., Xu, S., Nanding, A., Gong, Y., Li, S.,... Pang, D. (2025). An approach for differential diagnosis of breast tumors by CTDNA methylation sequencing. Cancer Medicine, 14(12), e71004. https://doi.org/10.1002/cam4.71004

ATHEROGENIC DYSLIPIDEMIA AND INSULIN RESISTANCE AS DRIVERS OF EARLY LIVER AND KIDNEY INJURY IN EXPERIMENTAL METABOLIC SYNDROME

Nigora F. Abdukhalikova, Bakhtiyar U. Iriskulov, Alisher Kh. Rakhmonov
Tashkent State Medical University (Tashkent, Uzbekistan)
dr.ali.fl@mail.ru

Abstract. Background: *Metabolic syndrome (MetS) is a systemic cardiometabolic disorder that increases the risk of target-organ damage, including metabolic dysfunction–associated steatotic liver disease (MASLD) and early kidney injury. However, integrated experimental evidence linking metabolic derangements with parallel hepatic and renal impairment remains limited.*

Materials and methods: *Male rats were allocated to control and MetS groups. MetS was induced by high-fat loading combined with fructose supplementation for 12 weeks. Serum metabolic and organ injury markers were assessed, including lipid abnormalities and indices of renal dysfunction (urea, creatinine, globulins). Urinalysis included specific gravity, pH, total protein, albumin, nitrogen metabolites, and electrolytes (Na, K). Liver and kidney tissues were examined histologically, and liver damage was quantified by morphometric analysis (steatosis area, lipid-laden hepatocytes, mononuclear infiltration).*

Results: *MetS animals developed significant renal dysfunction characterized by azotemia, marked proteinuria/albuminuria, reduced urinary concentrating capacity, urinary acidification, and electrolyte imbalance consistent with tubular transport dysregulation. Histology demonstrated preserved renal architecture in controls and focal early glomerular and tubular alterations in MetS rats. In parallel, MetS induced pronounced liver injury with macro- and microvesicular steatosis, inflammatory infiltration, and morphometrically confirmed expansion of steatotic areas and lipid-laden hepatocytes.*

Conclusions: *Twelve-week experimental MetS results in concurrent hepatic steatosis and early renal injury, supporting the concept of a cardiometabolic continuum. Combined biochemical, urinary, and morphometric markers provide a robust platform for mechanistic studies and evaluation of nephro- and hepatoprotective interventions in MetS.*

Keywords: *metabolic syndrome; kidney injury; proteinuria; albuminuria; azotemia; hepatic steatosis; morphometry; rat model.*

Metabolic syndrome (MetS) comprises a constellation of interrelated metabolic abnormalities—visceral obesity, insulin resistance/hyperglycemia, arterial hypertension, and atherogenic dyslipidemia—that substantially increases the risk of cardiovascular complications and contributes to an elevated systemic “cardiorenometabolic” risk burden. In recent years, MetS has been recognized as an independent predictor of chronic kidney disease (CKD), being associated with an accelerated decline in glomerular filtration rate and a higher prevalence of albuminuria even in the absence of overt diabetes mellitus [5]. Meta-analytic evidence further supports a robust association between MetS and an increased risk of renal dysfunction and CKD, including unfavorable eGFR trajectories and progression to end-stage kidney disease [5]. Importantly, the magnitude of renal risk increases with the number of MetS components, as the combination of visceral adiposity, hypertension, and dyslipidemia exerts additive adverse effects on renal microcirculation and glomerular filtration [3]. Albuminuria, including low-grade albuminuria, is therefore considered an early clinically meaningful marker of metabolically mediated kidney injury and, concurrently, an indicator of endothelial dysfunction and heightened cardiovascular risk [2].

Key pathogenetic mechanisms of kidney injury in metabolic syndrome (MetS)

1. **Hemodynamic alterations: hyperfiltration and RAAS activation.** In the early stages of metabolic syndrome, glomerular hyperfiltration frequently develops and is accompanied by increased intraglomerular pressure and activation of the renin–angiotensin–aldosterone system (RAAS). These changes promote podocyte injury, increase permeability of the filtration barrier, and lead to albuminuria as an early marker of glomerular dysfunction [6].

2. **Visceral and perirenal obesity.** Visceral adipose tissue—particularly perirenal fat and renal sinus fat—acts as an active source of pro-inflammatory cytokines, adipokine imbalance, and an increased flux of free fatty acids. This milieu contributes to endothelial dysfunction, enhanced oxidative stress, and the maintenance of local inflammatory responses within renal tissue [9].

3. **Lipotoxicity and impaired renal energy metabolism.** Atherogenic dyslipidemia and insulin resistance facilitate intrarenal lipid accumulation, including deposition within tubular epithelial cells. Lipid overload induces endoplasmic reticulum stress, mitochondrial dysfunction, and hypoxia-related reactive oxygen species generation, thereby serving as a major driver of tubulointerstitial injury and fibrosis [1].

4. **Chronic low-grade inflammation and oxidative stress.** Metabolic syndrome sustains systemic “metabolic inflammation” and excessive ROS production, which damages the glomerular endothelium and activates pro-fibrotic signaling pathways (including the TGF-β cascade). Consequently, interstitial fibrosis progresses and glomerular filtration rate declines, providing a mechanistic basis for CKD development and progression [7].

Materials and Methods.

Study Design

This study was designed as a controlled experimental animal study with parallel group allocation.

Animals

Initially, 20 male rats were enrolled in the study. During the experimental period, four animals were excluded due to technical reasons unrelated to the study protocol (e.g., tissue processing artifacts). The final analysis was performed on 16 rats, which were randomly assigned to the control (n = 8) and experimental (n = 8) groups. Group allocation was performed using a computer-generated randomization sequence with a 1:1 allocation ratio. Allocation concealment was maintained by assigning coded identifiers to each animal. Histological and morphometric analyses were performed by an investigator blinded to group allocation. The MetS model was established in male rats to minimize hormonal variability associated with the estrous cycle.

All animal procedures were conducted in accordance with applicable international guidelines and the EU Directive 2010/63/ EU on the protection of animals used for scientific purposes. The protocol was approved by the Local Ethics Committee of Tashkent Medical Academy (now Tashkent State Medical University) (Protocol No. 6, June 25, 2025).

Animals were housed under standard vivarium conditions with a 12-hour light-dark cycle and free access to food and water.

Diet

Rats in the control group received a standard laboratory diet with an energy content of 280–310 kcal per 100 g of feed. The diet consisted of 18–22 % protein, 4–6 % fat, 55–65 % digestible carbohydrates, 4–6 % fiber, 5–7 % ash, and 10–12 % moisture.

The mineral composition included calcium (0.8–1.2 %), phosphorus (0.6–0.9%), sodium chloride (0.3–0.5 %), magnesium (0.2–0.3 %), potassium (0.6–1.0 %), iron (100–200 mg/kg), zinc (50–100 mg/kg), copper (8–15 mg/kg), manganese (70–150 mg/kg), selenium (0.1–0.3 mg/kg), and iodine (0.5–2 mg/kg).

The vitamin content comprised vitamin A (4,000–10,000 IU/kg), vitamin D_3 (800–1,500 IU/kg), vitamin E (30–80 mg/kg), vitamin K (1–3 mg/kg), and a B-complex vitamin mixture (B_1, B_2, niacin, B_6, pantothenic acid, folic acid, biotin, and B_{12}) within recommended concentrations.

The main feed ingredients included cereals (corn, wheat, oats), soybean meal or protein concentrates, fish meal or meat-and-bone meal, vegetable oils, dried grass meal, and a vitamin–mineral premix.

Rats in the experimental group received a high-fat diet combined with fructose supplementation to induce metabolic syndrome. The diet was characterized by an increased fat content compared to the standard laboratory chow, while drinking water was supplemented with fructose throughout the experimental period. The dietary intervention was maintained for 12 weeks.

Experimental Diet Protocol

Rats in the experimental group were administered melted sheep mesenteric fat intragastrically via a metal gavage needle prior to feeding. The fat was maintained in a water bath at 38–40 °C and delivered at a dose of 1 g per 100 g of body weight. The procedure was performed once daily throughout the experimental period. One hour after fat administration, animals were provided with the standard laboratory diet. The procedure was performed by an experienced operator to minimize stress and discomfort to the animals.

As a drinking fluid, the experimental group received 10 % fructose solution ad libitum throughout the experimental period.

Rat Euthanasia and Sample Collection

At the end of the 12-week experimental period, rats were fasted for 12 hours and anesthetized using short-term inhalation anesthesia. Blood samples were collected by direct puncture of the jugular vein into sterile tubes and subsequently centrifuged at 3000 rpm for 10 minutes to obtain serum. The collected serum samples were stored at −20 °C until further biochemical analysis.

Liver and Kidney Histology

Liver and kidney specimens were fixed in 10% neutral buffered formalin for at least 24 h and subsequently processed using standard paraffin-embedding procedures. Tissues were dehydrated through a graded ethanol series (70–100%), cleared in xylene, and infiltrated with paraffin at 60 °C. Paraffin sections (5–7 µm) were cut on a microtome, mounted on positively charged glass slides, and dried at 37–42 °C.

Sections were stained with hematoxylin and eosin (H&E) according to standard protocols and examined using a Leica DM IL LED microscope. Quantitative image analysis was performed in Fiji. For each group, randomly selected non-overlapping fields of view were analyzed, and images were saved in TIFF format for subsequent processing. Quantification was conducted by calculating the percentage of stained area relative to the total tissue area.

Mononuclear cell infiltration in the liver parenchyma was quantified on ×20 images. For each animal, five randomly selected fields were analyzed. Individual mononuclear cells were counted manually using the “Multi-point” tool in Fiji, with a point placed on each nucleus to ensure reproducibility; results were recorded in the ROI Manager for documentation.

Counting of lipid-laden cells. Lipid-laden cells, including hepatocytes exhibiting cytoplasmic vacuolization, were identified in H&E-stained sections based on the presence of cytoplasmic vacuoles. Counts were performed manually on ×20 images. For each animal, five randomly selected hepatic fields were analyzed. Cells were counted using the Fiji “Multi-point” tool, with points placed on each vacuolated cell; data were stored in the ROI Manager for verification and documentation. Final results were expressed as the mean number of lipid-laden cells per field of view.

Biochemical Analysis

The following parameters were measured: lipid profile, including total cholesterol (TC), low density lipoprotein cholesterol (LDL-C), high-density lipoprotein cholesterol (HDL-C), and triglycerides (TG), urea, creatinine, globulin which were determined using commercially available rat-specific assay kits (Vector-Best, Russia). Blood glucose and insulin levels were also measured using rat-specific kits (Vector-Best, Russia). Insulin resistance (IR) was assessed using the homeostasis model assessment (HOMA-IR) according to the following formula [8].

HOMA-IR = (fasting glucose (mmol/L) × fasting insulin (μIU/mL)) / 22.5

Serum levels of alanine aminotransferase (ALT), aspartate aminotransferase (AST), alkaline phosphatase, gamma-glutamyltransferase (GGT), total protein, albumin, and bilirubin were measured using commercial assay kits (Vector-Best, Russia).

Statistical Analysis

Data are presented as mean ± standard deviation (SD). Normality was assessed using the Shapiro–Wilk test. Homogeneity of variances was evaluated using Levene's test. Between-group comparisons were performed using an independent samples t-test. Effect sizes (Cohen's d) were calculated where appropriate. Where appropriate, 95% confidence intervals (CI) were calculated. Given the limited sample size (n = 16) and potential deviations from normal distribution, correlations between metabolic and histomorphometric parameters were assessed using Spearman's rank correlation coefficient (ρ) All tests were two-tailed, and a p-value < 0.05 was considered statistically significant. Statistical analyses were performed using IBM SPSS Statistics (version 20.0, IBM Corp., Armonk, NY, USA) and Jamovi (version 2.6.44; The Jamovi Project, Sydney, Australia).

Results.

Development of Obesity and Increase in Mesenteric Fat Index in Experimental MetS

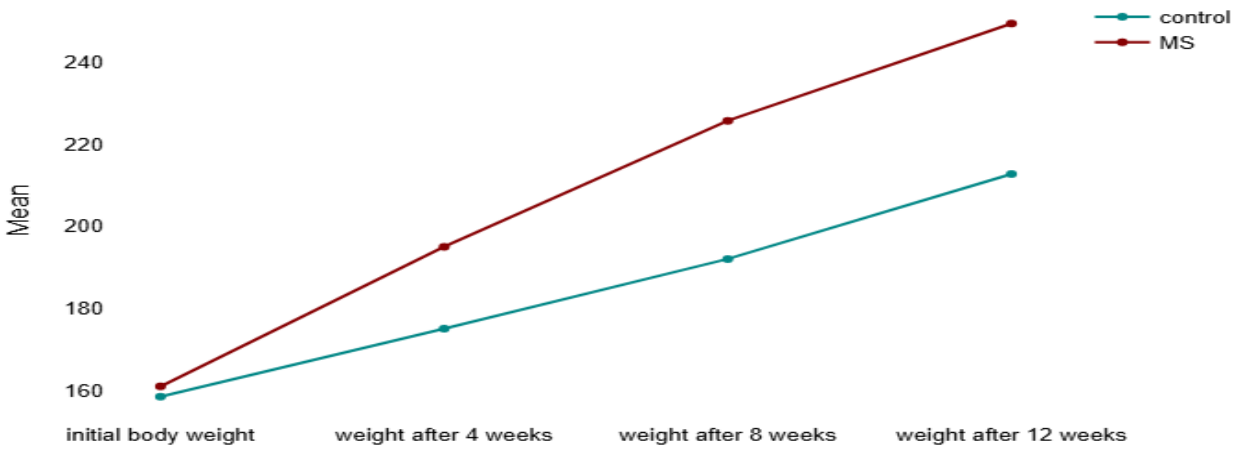


Figure 1. Time-dependent changes in body weight in control and MetS groups over the 12-week experimental period. Values are presented as mean ± SD; p < 0.001 vs. control

Rats in the MetS group showed a significantly greater body weight gain compared with controls from week 4 onward (p < 0.001). By week 12, weight increased by approximately 60% in the MetS group versus 35% in controls, confirming successful induction of obesity (Fig. 1).

Metabolic and Biochemical Alterations Associated with Liver Injury in the Experimental MetS Model

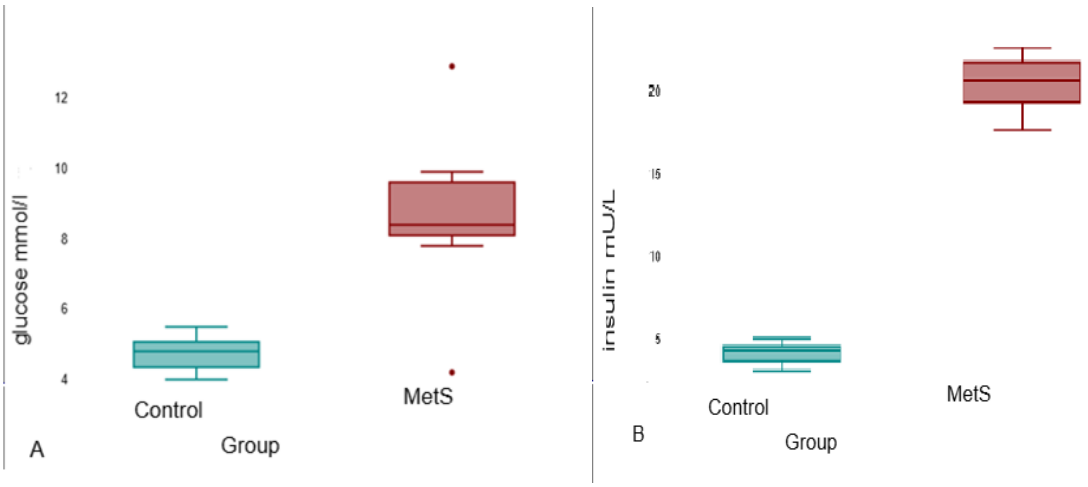


Figure 2. Blood glucose (A) and insulin (B) concentrations in control animals and rats with experimentally induced MetS after 12 weeks ($p < 0.001$)

MetS rats exhibited significantly elevated blood glucose levels compared with controls ($p < 0.001$), accompanied by increased insulin resistance, as reflected by an increase in HOMA-IR from 0.87 to 7.86 ($p < 0.001$), representing an approximately ninefold increase.

Table 1.

Lipid profile parameters in control and MetS groups

Parameter (mmol/L)	Control (n = 8)	MetS (n = 8)	p value
Cholesterol	1.21 ± 0.22	2.45 ± 0.47	< 0.001
LDL-C	1.22 ± 0.17	1.98 ± 0.32	< 0.001
HDL-C	0.94 ± 0.17	0.80 ± 0.15	0.096
Triglycerides	1.73 ± 0.36	3.58 ± 0.57	< 0.001

MetS animals exhibited marked atherogenic dyslipidemia, characterized by significantly increased total cholesterol, LDL-C, and triglyceride levels (all $p < 0.001$), along with a non significant trend toward reduced HDL-C concentrations ($p = 0.096$).

Table 2.

Liver biochemical markers in control and MetS groups

Parameter	Control (n = 8)	MetS (n = 8)	P value
Alanine aminotransferase (ALT), U/L	54.74 ± 4.23	133.75 ± 14.69	< 0.001
Aspartate aminotransferase (AST), U/L	82.89 ± 9.81	149.78 ± 27.82	< 0.001
Alkaline phosphatase (ALP), U/L	276.16 ± 46.27	539.99 ± 84.01	< 0.001
Gamma-glutamyltransferase (GGT), U/L	5.14 ± 0.82	19.79 ± 4.15	< 0.001
Total protein, g/L	72.15 ± 2.57	52.48 ± 9.72	< 0.001
Albumin, g/L	33.91 ± 1.13	24.36 ± 1.04	< 0.001
Total bilirubin, µmol/L	1.27 ± 0.24	4.05 ± 0.70	< 0.001

After 12 weeks of MetS induction, rats showed significant biochemical evidence of liver injury. ALT and AST activities increased 2.4-fold and 1.8-fold, respectively ($p < 0.001$), indicating marked hepatocellular damage. Alkaline phosphatase and γ-glutamyltransferase activities were elevated (≈2-fold and ≈4-fold; $p < 0.001$), reflecting a pronounced cholestatic component. Total protein and albumin levels decreased by 27% and 28% ($p < 0.001$), while total bilirubin increased more than

threefold ($p < 0.001$), confirming impaired hepatic synthetic function and mixed hepatocellular–cholestatic injury [9].

Table 3.

Biochemical markers of renal function in control and metabolic syndrome (MetS) rats after 12 weeks

Parameter	Control (n = 8)	MetS (n = 8)	P value
Globulin, g/L	29.28 ± 4.48	37.28 ± 4.75	0.0038
Urea, mmol/L	5.15 ± 0.83	8.81 ± 1.69	< 0.001
Creatinine, μmol/L	47.23 ± 8.17	71.89 ± 12.17	< 0.001

After 12 weeks of MetS induction, significant changes in biochemical markers indicative of renal involvement were observed. In the MetS group, serum urea levels were markedly higher than in controls ($p < 0.001$), and creatinine concentrations were similarly increased ($p < 0.001$). In addition, globulin levels were significantly elevated ($p = 0.0038$), which may reflect activation of an inflammatory component in MetS.

Taken together, these alterations indicate the development of azotemia and suggest a likely reduction in glomerular filtration and/or renal excretory function, consistent with the concept of MetS-associated kidney injury as an early manifestation of the cardiorenometabolic continuum. The increase in globulins further supports the presence of chronic low-grade systemic inflammation characteristic of MetS and may indirectly reflect immunoinflammatory activation contributing to microvascular and tubulointerstitial changes in renal tissue. Overall, the findings confirm that MetS is associated not only with metabolic disturbances but also with early signs of renal dysfunction accompanied by an inflammatory component, thereby increasing the risk of nephropathy progression with prolonged disease duration.

Table 4.

Urinalysis parameters in control and metabolic syndrome (MetS) rats after 12 weeks

Parameter	Control (n = 8)	MetS (n = 8)	P value
Relative volume (mL)	4.39 ± 0.43	7.22 ± 0.46	< 0.0001
Specific gravity	1.0384 ± 0.0076	1.0104 ± 0.0050	< 0.0001
pH	7.91 ± 0.41	6.39 ± 0.38	< 0.0001
Total protein (g/L)	0.036 ± 0.007	0.390 ± 0.055	< 0.0001
Albumin (mg/L)	4.82 ± 0.99	29.00 ± 5.17	< 0.0001
Uric acid (mmol/L)	0.82 ± 0.15	2.08 ± 0.31	< 0.0001
Creatinine (mmol/L)	5.81 ± 0.81	14.60 ± 1.92	< 0.0001
Urea (mmol/L)	52.53 ± 7.50	97.32 ± 16.09	< 0.0001
Sodium (Na), mmol/L	122.36 ± 17.14	81.71 ± 14.57	0.0002
Potassium (K), mmol/L	49.14 ± 9.19	91.31 ± 12.31	< 0.0001

In the MetS group, markedly pronounced proteinuria/albuminuria was observed: total urinary protein increased approximately 11-fold and urinary albumin increased approximately 6-fold (both $p < 0.0001$), consistent with glomerular filtration barrier injury and increased permeability, reflecting early MetS-associated kidney involvement. Urinary creatinine and urea levels were also significantly elevated ($p < 0.0001$), suggesting substantial disturbances in nitrogen metabolism and/or impaired renal excretory function (this interpretation would be further strengthened by concomitant serum creatinine/urea measurements and eGFR estimation). A reduction in urine specific gravity ($p < 0.0001$), together with a shift in urinary pH toward acidity ($p < 0.0001$), may indicate impaired concentrating ability and tubular dysfunction. The electrolyte profile showed decreased urinary Na^+ ($p = 0.0002$) and increased urinary K^+ ($p < 0.0001$), indicating dysregulation of tubular electrolyte

transport, which is typical of renal metabolic/inflammatory and hemodynamic stress in MetS (Table 4).

Histopathological Features of Hepatic and Renal Tissues in Experimentally Induced Steatosis

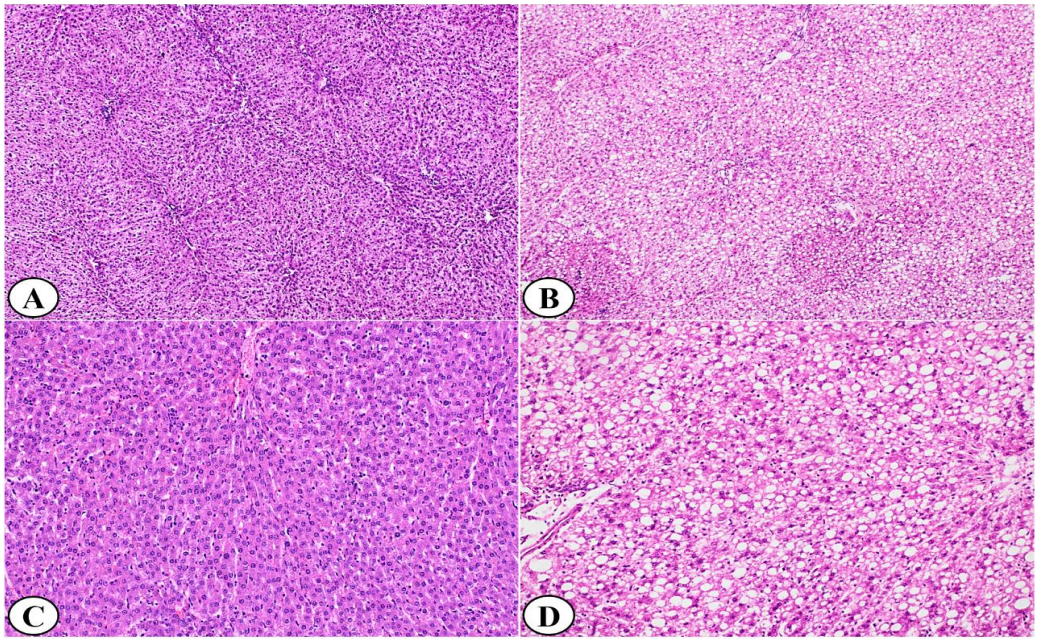


Figure 3. Representative photomicrographs of liver histology in the control (A, C) and experimental (B, D) groups at low (×10; A and B) and intermediate (×20; C and D) magnifications

At ×10 and ×20 magnifications, control livers preserved normal lobular architecture with well-defined central veins, radially arranged hepatocyte plates, and uniformly distributed sinusoids, with no evidence of steatosis, inflammation, necrosis, or fibrosis (Figure 3 A, C). In contrast, MetS livers exhibited marked architectural disruption characterized by trabecular disorganization, fragmented central veins, diffuse hepatocellular vacuolization, combined macro- and microvesicular steatosis, moderate mononuclear inflammatory infiltration, and focal early fibrotic changes predominantly in centrilobular and midzonal regions (Figure 3 B, D).

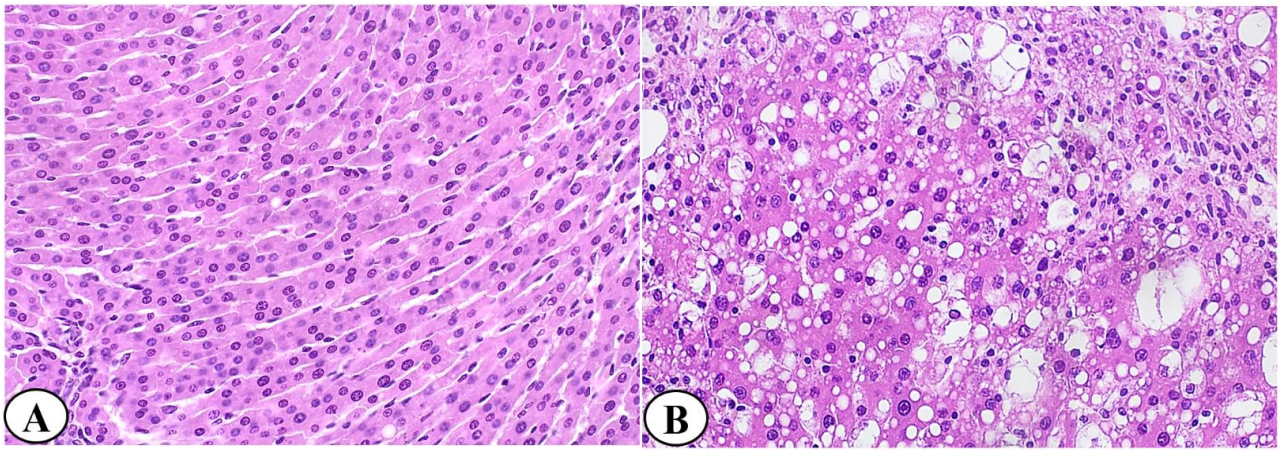


Figure 4. Representative photomicrographs of liver tissue from control (A) and MetS (B) groups at high magnification (×40)

At ×40 magnification, control livers displayed preserved hepatocellular architecture without steatosis or inflammation, whereas MetS livers exhibited pronounced macro- and microvesicular steatosis, hepatocyte vacuolization, nuclear degeneration, sinusoidal distortion, and moderate inflammatory infiltration, indicating progressive lipotoxic liver injury (Fig. 4.A, B).

After confirming the presence of steatosis in the experimental groups, a morphological assessment of the kidneys was performed to identify potential histological changes associated with hepatic lipid accumulation. This approach enables evaluation of whether steatosis induces secondary structural alterations in renal tissue and provides insight into the systemic consequences of disturbed lipid metabolism.

In the control group, renal histology demonstrated completely preserved cortical and medullary architecture with no pathological changes. Glomeruli displayed normal morphology; Bowman's capsule and Bowman's space were clearly delineated, and there was no evidence of sclerosis, congestion, or inflammatory changes. Proximal and distal tubules retained an intact epithelial lining (including preservation of the brush border), without dilation, necrosis, vacuolization, or casts; the interstitium and vascular structures showed no edema, fibrosis, or inflammatory infiltration, confirming overall renal structural integrity.

In the experimental group, the general cortico-medullary architecture was largely preserved; however, focal early alterations consistent with metabolic stress were observed. Most glomeruli remained free of sclerosis and destructive changes, yet some exhibited sporadic vesicular inclusions and mild hyperemia with dilated, congested capillary loops, which may reflect early microcirculatory and intracellular disturbances. Bowman's space and capsule remained preserved, without thickening or signs of inflammatory reaction (Fig. 5A, B).

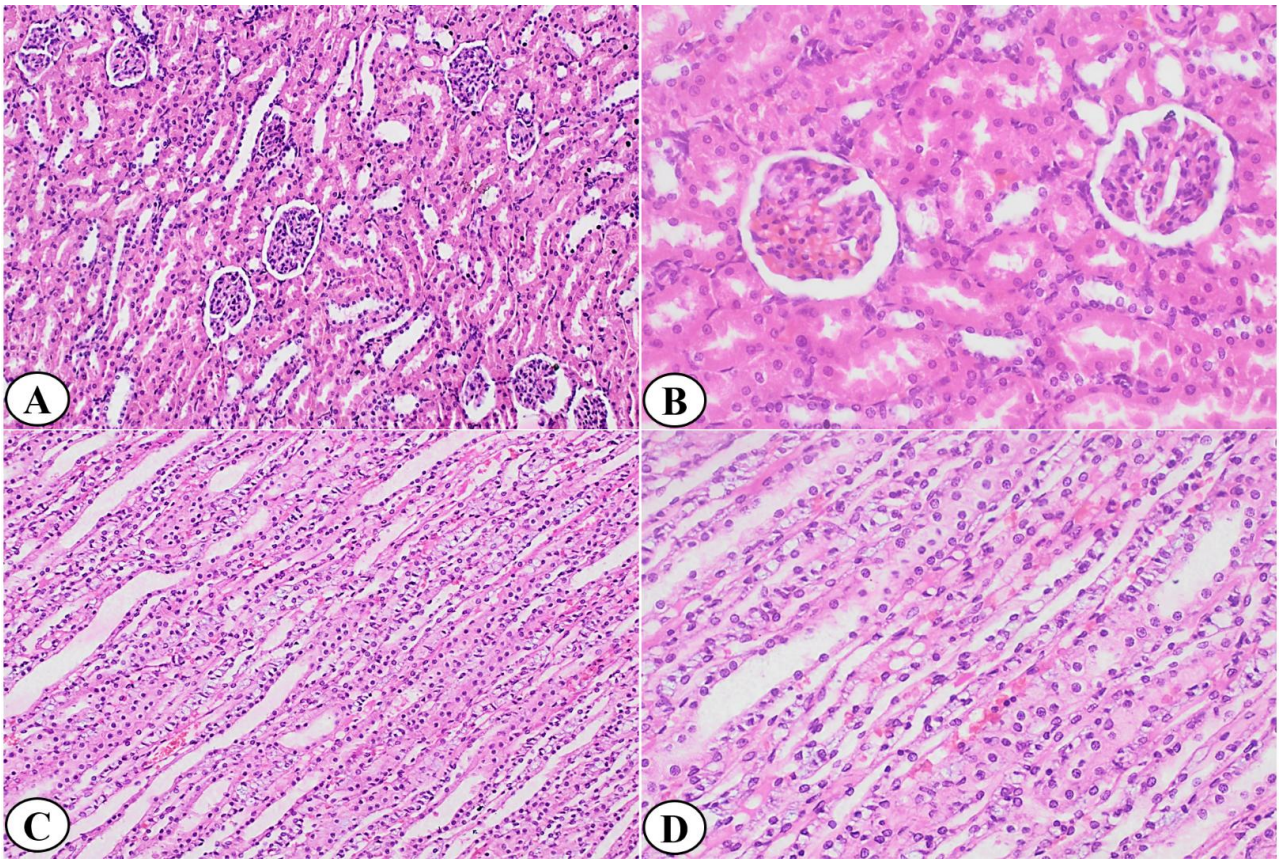


Figure 5. Representative photomicrographs of renal tissue from the experimental group at low (×10) and intermediate (×20) magnification. Panels A and B show the renal cortex, whereas panels C and D show the renal medulla

The tubular changes were focal and of moderate severity. In a subset of proximal and distal tubules, luminal dilatation with epithelial flattening/thinning was observed; in some proximal segments, partial loss of the brush border was noted. Occasional tubular epithelial cells showed cytoplasmic pallor and vacuolization, and sporadic desquamation into the tubular lumen was detected without evidence of overt necrosis. The medulla remained structurally preserved: collecting ducts and loops of Henle were orderly arranged, the interstitium showed no edema, fibrosis, or inflammatory infiltration, and vascular structures were patent with intact endothelium and minimal perivascular changes (Fig. 5C, D).

Overall, these findings are consistent with mild, focal tubular dysfunction accompanied by minimal glomerular involvement, compatible with metabolically induced renal injury in the setting of confirmed hepatic steatosis. Despite the presence of localized alterations (vesicular inclusions, mild glomerular hyperemia, and focal tubular epithelial changes), no features of advanced structural destruction of renal tissue were identified.

Morphometric Assessment of Hepatic and Renal Injury in an Experimental Model of Hepatic Steatosis.

A quantitative morphometric analysis was performed to objectively assess the severity of hepatic injury in the experimental model. Key parameters included the mean steatosis area within the liver parenchyma (Fig. 6A), the number of lipid-laden hepatocytes (Fig. 6B), and the degree of mononuclear cell infiltration (Fig. 6C).

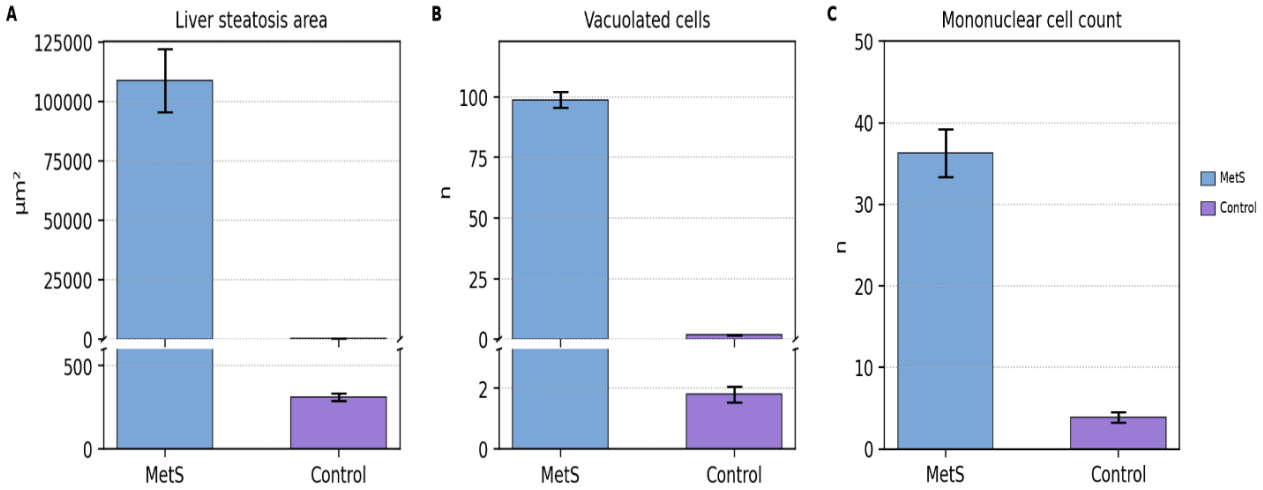


Figure 6. Morphometric assessment of the liver in control and MetS groups. A. Quantitative evaluation of hepatic steatosis area (µm² per standardized microscopic field). B. Number of vacuolated hepatocytes per microscopic field (×20). C. Quantitative evaluation of mononuclear cell infiltration in the liver parenchyma

Morphometric analysis revealed a marked increase in hepatic steatosis area in the experimental group compared with controls (108,884 ± 13,405.85 vs. 312 ± 23.14 µm²; $p < 0.0001$), indicating massive lipid accumulation within the liver parenchyma (Figure 6 A). The number of vacuolated hepatocytes was also significantly higher in the MetS group (98.8 ± 3.24 vs. 1.8 ± 0.25; $p < 0.0001$), reflecting pronounced cellular lipid overload (Figure 6 B). In addition, mononuclear cell infiltration was markedly increased (36.3 ± 2.89 vs. 3.9 ± 0.67; $p < 0.0001$), indicating activation of inflammatory processes in the liver (Figure 6 C).

Morphometric analysis of renal tissue included assessment of glomerular area, total glomerular count, and the number of vacuolated tubular epithelial cells (Figure 7). The mean glomerular area in the experimental group was 13,838.61 ± 899.40 µm², compared with 14,450.00 ± 1,568.50 µm² in controls, showing no significant between-group difference and indicating preservation of overall glomerular morphometric structure (Figure 7A). The total number of glomeruli also did not differ between groups (15.3 ± 2.23 in the experimental group vs 13.9 ± 1.95 in controls; Figure 7B), supporting stability of global glomerular cellularity.

In contrast, the number of glomeruli containing vacuolated cells was markedly higher in the experimental group (5.9 ± 0.43) than in controls (0.2 ± 0.13), and this difference was highly significant ($p < 0.0001$) (Figure 7B), suggesting focal glomerular involvement consistent with cellular lipid accumulation and/or early dystrophic changes. Quantification of vacuolated cells in renal tubules revealed pronounced between-group differences: the experimental group exhibited a substantially higher number of vacuolated tubular epithelial cells (95.8 ± 4.60) compared with the control group (5.4 ± 1.06; $p < 0.0001$) (Figure 7C).

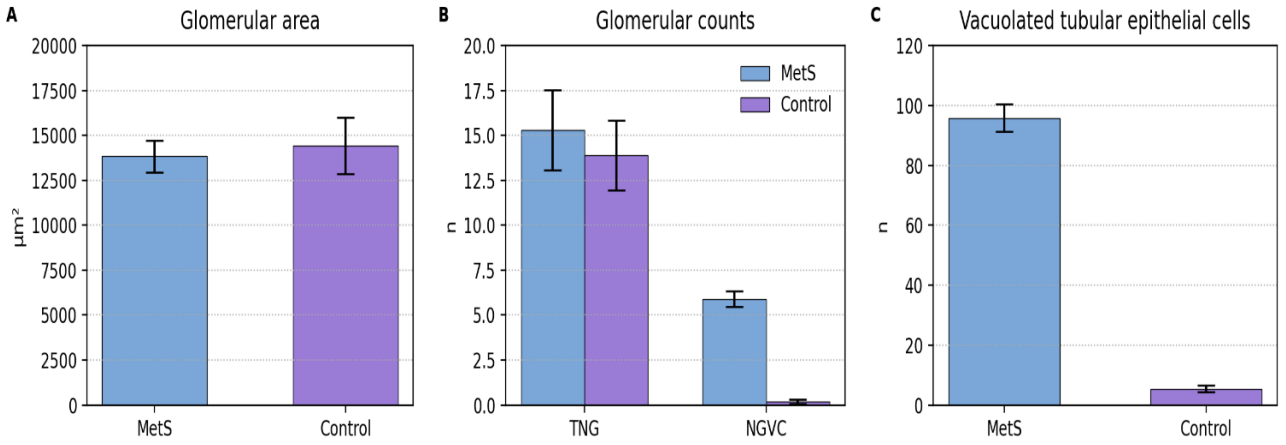


Figure 7. Morphometric assessment of the kidneys in the control (CG) and experimental (EG) groups: (A) mean glomerular area per field of view; (B) mean number of glomeruli per field of view, including the total number of glomeruli (TNG) and the number of glomeruli containing vacuolated cells (NGVC); (C) number of vacuolated tubular epithelial cells

These findings indicate that, in the setting of experimentally induced hepatic steatosis, the kidneys exhibit focal morphometric alterations in both glomeruli and tubules, while the overall renal architecture remains relatively preserved. To explore potential inter-organ interactions under metabolic stress, we performed a correlation analysis between hepatic steatosis area and renal morphometric indices of structural changes in the experimental animals (Figure 8).

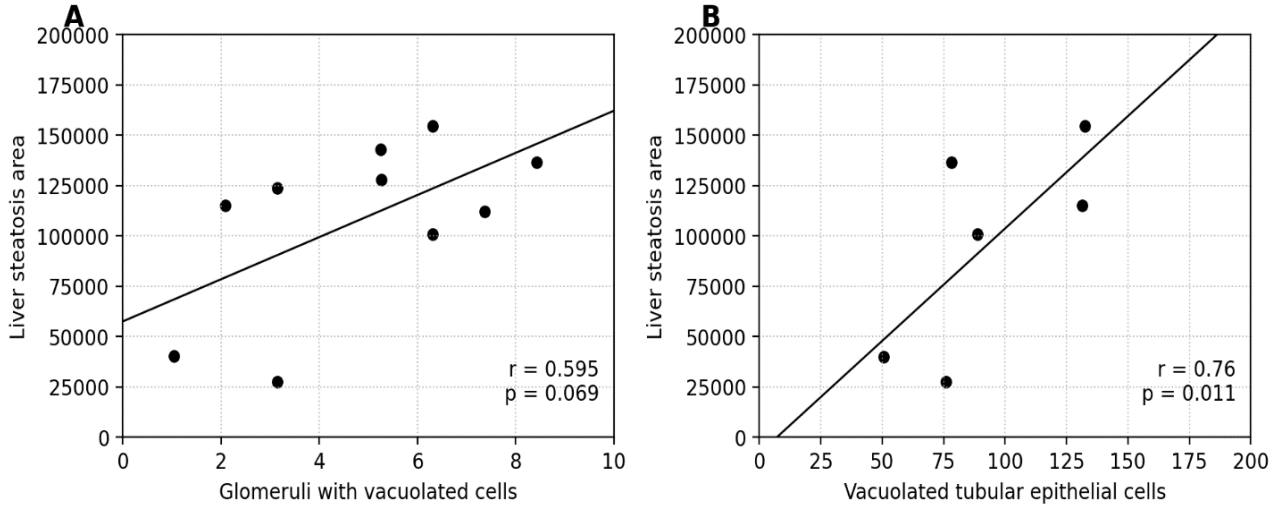


Figure 8. Correlation analysis of associations between renal morphometric features and the severity of hepatic steatosis in the experimental group (EG): (A) correlation between liver steatosis area and the number of glomeruli containing vacuolated cells; (B) correlation between liver steatosis area and the number of vacuolated tubular epithelial cells

Correlation analysis between renal morphometric indices and the severity of hepatic steatosis revealed associations that underscore the systemic nature of metabolic disturbances. In the experimental group, a positive trend was observed between liver steatosis area and the number of glomeruli containing vacuolated cells ($r = 0.595$; $p = 0.069$), suggesting a potential linkage between hepatocellular lipid accumulation and early glomerular alterations (Fig. 8A). A stronger and statistically significant correlation was identified between liver steatosis area and the number of vacuolated tubular epithelial cells ($r = 0.76$; $p = 0.011$) (Fig. 8B), indicating a close relationship between steatosis progression and structural remodeling of the tubular compartment.

Overall, these findings suggest that, in experimentally induced hepatic steatosis, quantitative changes are most pronounced in the liver, whereas the kidneys exhibit early focal morphometric signs of injury, predominantly at the tubular level. The presence of positive correlations between hepatic steatosis severity and indices of vacuolization in glomeruli and renal tubules further supports inter-organ coupling of metabolic injury and is consistent with the concept of systemic metabolic impact on target organs.

Conclusion. In this experimental model of metabolic syndrome, a constellation of findings consistent with MetS-associated kidney injury developed after 12 weeks, manifesting as a metabolically mediated nephropathy within the early cardiorenometabolic continuum. The significant increase in serum urea and creatinine indicates the development of azotemia and suggests a likely reduction in glomerular filtration and/or renal excretory function. Concurrently, marked proteinuria and albuminuria point to glomerular filtration barrier injury with increased permeability, whereas decreased urine specific gravity and a shift in urinary pH toward acidity reflect involvement of tubular and concentrating functions. Alterations in urinary electrolytes ($Na^+\downarrow$, $K^+\uparrow$) further support dysregulation of tubular electrolyte handling under conditions of metabolic and hemodynamic stress. Elevated globulin levels are consistent with activation of chronic low-grade systemic inflammation, a key pathogenetic component contributing to the progression of renal injury in MetS. Collectively, these data demonstrate that metabolic syndrome leads not only to hepatic and lipid abnormalities but also to early biochemical and urinary markers of renal dysfunction, underscoring the need for early renal monitoring and the development of pathogenetically targeted strategies to prevent nephropathy progression.

REFERENCES

1. Chae S. Y., Kim Y., Park C. W. Oxidative stress induced by lipotoxicity and renal hypoxia in diabetic kidney disease and possible therapeutic interventions: targeting the lipid metabolism and hypoxia //Antioxidants. – 2023. – T. 12. – №. 12. – C. 2083.

2. Claudel S. E., Verma A. Albuminuria in cardiovascular, kidney, and metabolic disorders: a state-of-the-art review //Circulation. – 2025. – T. 151. – №. 10. – C. 716-732.

3. dos Anjos Ribeiro Y., Franco A. C. B., da Silva L. S. Association between metabolic syndrome and chronic kidney disease in the Brazilian population, a cross-sectional analysis //Scientific Reports. – 2025.

4. Guerra Ruiz AR, et al. Measurement and clinical usefulness of bilirubin in liver disease. Adv Lab Med. 2021;2(3):352-372.

5. Li X. et al. The effect of metabolic syndrome and its individual components on renal function: a meta-analysis //Journal of clinical medicine. – 2023. – T. 12. – №. 4. – C. 1614.

6. Lin L. et al. Metabolic syndrome-related kidney injury: a review and update //Frontiers in endocrinology. – 2022. – T. 13. – C. 904001.

7. Masenga S. K. et al. Mechanisms of oxidative stress in metabolic syndrome //International journal of molecular sciences. – 2023. – T. 24. – №. 9. – C. 7898.

8. Matthews DR, Hosker JP, Rudenski AS, et al. Homeostasis model assessment: insulin resistance and β-cell function from fasting plasma glucose and insulin concentrations in man. Diabetologia. 1985;28(7):412-419.

9. Rico-Fontalvo J. et al. Inflammatory and lipotoxicity mechanisms in obesity related CKD //Frontiers in Nephrology. – 2025. – T. 5. – C. 1684004.

COMPARATIVE EVALUATION OF DIFFERENT METHODS OF STAPLE LINE REINFORCEMENT IN SLEEVE GASTRECTOMY

Umid S. Ruziyev - Ph.D., assistant professor
Nilufar R. Niyazova - master's degree student
Tashkent State Medical University (Tashkent, Uzbekistan)
niazovanilufar887@gmail.com

Abstract. *Staple line leakage and bleeding remain the most serious complications of laparoscopic sleeve gastrectomy (LSG), making the search for the optimal reinforcement technique clinically essential. This prospective cohort study compared six staple line reinforcement (SLR) methods in 515 patients with morbid obesity who underwent LSG at the INVIVO and Citymed clinics (Tashkent, Uzbekistan) between January 2019 and December 2024. Patients were assigned to six groups: Group I — sero-serous reinforcement (n=100), Group II — seromuscular reinforcement (n=100), Group III — full-thickness suture reinforcement (n=100), Group IV — omentoplasty (n=100), Group V — no reinforcement (n=100), Group VI — Hemoben haemostatic agent application (n=15). Primary endpoints were the rates of staple line leakage, intraabdominal bleeding, and intragastric bleeding within 30 days postoperatively. Secondary endpoints included operative time and length of hospital stay. All procedures were performed by a single surgical team under a standardised protocol using a 38-French calibration bougie. Statistical analysis employed Pearson's chi-square test, Fisher's exact test, and one-way ANOVA with Tukey's post-hoc criterion. The lowest staple line leakage rate was recorded in Group I (1.0%), significantly lower than in Group V (8.0%; p=0.019) and Group III (4.0%; p=0.041). Intraabdominal and intragastric bleeding rates were also minimal in Group I (1.0% each) compared to Group V (10.0% and 7.0%, respectively; p<0.05). Full-thickness suturing (Group III) was associated with the highest complication rate among all reinforcement methods and the longest mean operative time (85±14 min), whereas the no-reinforcement group had the shortest operative time (57±9 min) but the longest hospital stay (5.6±2.9 days). Seromuscular reinforcement and omentoplasty showed intermediate outcomes with no statistically significant differences from sero-serous reinforcement. Hemoben application in the pilot group showed an acceptable safety profile; however, definitive conclusions require a larger sample. Sero-serous SLR is recommended as the optimal, reproducible, and cost-effective method for preventing staple line complications in LSG.*

Keywords: *sleeve gastrectomy, staple line reinforcement, sero-serous suture, staple line leakage, intraabdominal bleeding, morbid obesity, bariatric surgery.*

Introduction.

Laparoscopic sleeve gastrectomy (LSG) is currently the most commonly performed bariatric procedure worldwide, accounting for more than 46% of all bariatric operations according to the International Federation for the Surgery of Obesity and Metabolic Disorders (IFSO) [4, 9]. The procedure involves the formation of a long staple line along the greater curvature of the stomach, and it is precisely this line that determines the specific spectrum of potential postoperative complications.

Staple line leakage — the most severe of these complications — is reported in 1.0–5.3% of cases and is associated with high mortality, prolonged hospitalisation, and the need for repeat interventions [5, 11, 13]. Intraabdominal bleeding along the staple line occurs in 1.5–4.0% of cases, while intragastric bleeding is reported in 1.0–3.5% [7]. The cumulative burden of these complications sustains substantial interest among surgeons in preventive techniques.

A wide range of SLR methods has been described in the literature: continuous absorbable suture oversewing (sero-serous, seromuscular, or full-thickness), omentoplasty (plication of the greater omentum over the staple line), synthetic or biological buttress materials, fibrin glues, and haemostatic

agents [6, 8, 10, 12]. Despite the abundance of publications on this topic, comparative studies simultaneously evaluating several fundamentally different techniques in a sufficiently large cohort remain scarce. As a result, evidence-based algorithms for selecting the most appropriate reinforcement method in routine practice have not been established.

In Uzbekistan, bariatric surgery is undergoing rapid growth in parallel with the rising prevalence of morbid obesity [1, 2]. Nevertheless, domestic comparative studies dedicated to this subject have been virtually absent from the national literature, which motivated the present investigation.

Aim of the study.

To compare the clinical efficacy of six staple line reinforcement methods in laparoscopic sleeve gastrectomy with respect to the rates of staple line leakage, intraabdominal bleeding, and intragastric bleeding in the early postoperative period, and to identify the optimal method for routine clinical application.

Material and methods.

A prospective cohort study was conducted including 515 patients with morbid obesity who consecutively underwent LSG at the INVIVO and Citymed clinics (Tashkent, Uzbekistan) between January 2019 and December 2024. Inclusion criteria were: age 18–65 years; body mass index (BMI) ≥40 kg/m² or BMI ≥35 kg/m² in the presence of serious obesity-related comorbidity (type 2 diabetes mellitus, arterial hypertension, obstructive sleep apnoea syndrome); and written informed consent. Exclusion criteria were: previous surgery on the upper gastrointestinal tract, revisional bariatric procedures, severe coagulopathy, and patient refusal.

Depending on the staple line management technique, patients were allocated to six groups:

Group I — Sero-serous reinforcement (n=100): the staple line was oversewn with a continuous sero-serous suture using V-loc 3/0 (Covidien) without incorporating the muscular or mucosal layers. The suture was placed without tension from the antrum toward the angle of His.

Group II — Seromuscular reinforcement (n=100): the staple line was oversewn with a continuous seromuscular suture using V-loc 3/0, incorporating the serosal and muscular layers without penetrating the mucosa.

Group III — Full-thickness suture reinforcement (n=100): interrupted sutures were placed through all layers of the gastric wall (serosa, muscularis, and submucosa) using V-loc 3/0, with knots tied externally.

Group IV — Omentoplasty (n=100): the greater omentum was sutured to the staple line using a continuous V-loc 3/0 suture, providing biological coverage of the staple line.

Group V — No reinforcement (n=100): no additional staple line management was performed after completion of stapling. This group served as the control.

Group VI — Hemoben haemostatic agent (n=15): the Hemoben haemostatic preparation (based on oxidised regenerated cellulose) was applied to the staple line in accordance with the manufacturer's instructions. Due to the pilot nature of this arm, patient enrolment is ongoing.

All operations were performed by a single surgical team using a standardised protocol. A linear endoscopic stapler was used with 3.5-mm cartridges for the antral region and 4.8-mm cartridges for the gastric body. A 38-French calibration bougie was positioned along the lesser curvature to create a standardised gastric sleeve. The first stapler firing was placed 4–5 cm proximal to the pylorus.

Primary endpoints were: staple line leakage (defined as extravasation of gastric contents beyond the sleeve, confirmed by water-soluble contrast radiography or reoperation within 30 days of LSG); intraabdominal bleeding (diagnosed clinically, by ultrasound, or at reoperation within 30 days); and intragastric bleeding (bleeding from the staple line into the gastric lumen, confirmed endoscopically). Secondary endpoints were operative time and postoperative length of hospital stay.

Statistical analysis was performed using SPSS Statistics 26.0 (IBM Corp., USA). Categorical variables were compared using Pearson's chi-square test; Fisher's exact test was applied when

expected cell frequencies were below 5. Continuous variables are expressed as mean ± standard deviation (M±SD) and were compared by one-way analysis of variance (ANOVA) with Tukey's post-hoc test. Statistical significance was set at $p<0.05$.

Table 1.

Baseline clinical and demographic characteristics of the study groups

Characteristic	Gr. I (n=100)	Gr. II (n=100)	Gr. III (n=100)	Gr. IV (n=100)	Gr. V (n=100)	Gr. VI (n=15)
Age, years (M±SD)	38.2±8.9	38.7±9.1	39.1±8.6	38.5±9.4	37.9±8.7	40.1±7.8
Sex: male / female	36/64	34/66	37/63	35/65	33/67	5/10
BMI, kg/m² (M±SD)	45.9±6.1	46.2±5.8	46.4±6.3	45.7±6.0	45.8±5.9	47.1±7.2
Type 2 DM, n (%)	40 (40%)	41 (41%)	39 (39%)	40 (40%)	38 (38%)	6 (40%)
Arterial hypertension, n (%)	65 (65%)	63 (63%)	66 (66%)	64 (64%)	63 (63%)	10 (67%)

Note: BMI — body mass index; DM — diabetes mellitus. No statistically significant between-group differences were observed for any baseline characteristic ($p>0.05$ for all comparisons).

Results and discussion.

All six groups were comparable at baseline with respect to age, sex distribution, BMI, and the prevalence of principal comorbidities (Table 1), ensuring the validity of between-group comparisons of surgical outcomes.

The lowest staple line leakage rate was recorded in Group I (sero-serous reinforcement) — 1.0% (1 of 100 patients). In Group V (no reinforcement), leakage developed in 8 patients (8.0%), which was significantly higher ($p=0.019$, Fisher's exact test). In Group III (full-thickness suture), the leakage rate was 4.0%, a difference that also reached statistical significance compared with Group I ($p=0.041$). In Groups II (3.0%), IV (2.0%), and VI (6.7%; n=15), differences from Group I did not reach statistical significance ($p>0.05$), although a consistent trend toward higher complication rates was observed relative to sero-serous reinforcement.

Intraabdominal bleeding was diagnosed in only 1 patient in Group I (1.0%). The highest rate was recorded in Group V — 10 cases (10.0%; $p=0.004$ vs. Group I). In Group III, intraabdominal bleeding occurred in 5 patients (5.0%; $p=0.031$ vs. Group I). Groups II (3.0%) and IV (2.0%) did not differ significantly from Group I. In Group VI (n=15), 1 event was recorded (6.7%); the limited sample size precludes meaningful statistical comparison.

The intragastric bleeding rate in Group I was 1.0%, compared with 7.0% in Group V ($p=0.027$) and 3.0% in Group III ($p=0.319$). Accordingly, sero-serous reinforcement demonstrated a statistically significant advantage over the no-reinforcement approach for this endpoint as well.

Notably, full-thickness suturing (Group III), despite its intuitive appeal as the most mechanically robust technique, was associated with the worst outcomes among all reinforcement methods. We attribute this finding to ischaemia of the staple line edges caused by incorporation of the mucosal layer and compression of transmural vessels, which paradoxically increases the risk of leakage and bleeding. Furthermore, this technique was associated with the longest operative time among all groups.

Omentoplasty (Group IV) yielded acceptable results and may serve as a valid alternative to suture reinforcement when the latter is not feasible. However, this technique is technically more demanding in patients with pronounced visceral obesity, in whom the omentum is often insufficiently mobile to be advanced to the staple line without tension.

Seromuscular reinforcement (Group II) showed marginally inferior outcomes compared with sero-serous reinforcement across all endpoints, though none of the differences were statistically significant. The theoretical explanation is that incorporation of the muscular layer may generate

localised ischaemia in the suture zone, which may translate into a slightly higher, albeit non-significant, complication rate.

In the Hemoben pilot group (Group VI), one event was recorded for each of the three primary endpoints (6.7% per endpoint). While the safety profile appears acceptable, no statistically robust conclusions can be drawn from a cohort of 15 patients; enrolment is continuing, and definitive data will be reported upon completion of the study.

Table 2.

Comparative complication rates and operative outcomes by group

Outcome	Gr. I (n=100)	Gr. II (n=100)	Gr. III (n=100)	Gr. IV (n=100)	Gr. V (n=100)	Gr. VI (n=15)	p*
Staple line leakage, n (%)	1 (1.0%)	3 (3.0%)	4 (4.0%)	2 (2.0%)	8 (8.0%)	1 (6.7%)	0.019†
Intraabdominal bleeding, n (%)	1 (1.0%)	3 (3.0%)	5 (5.0%)	2 (2.0%)	10 (10.0%)	1 (6.7%)	0.004†
Intragastric bleeding, n (%)	1 (1.0%)	2 (2.0%)	3 (3.0%)	2 (2.0%)	7 (7.0%)	1 (6.7%)	0.027†
Operative time, min (M±SD)	72±10	78±12	85±14	74±11	57±9	68±10	<0.001‡
Hospital stay, days (M±SD)	3.7±1.1	4.1±1.4	4.8±2.1	3.9±1.3	5.6±2.9	4.2±1.5	<0.001‡

Note: * — p-value for pairwise comparison of Group I vs. Group V (†Fisher's exact test; ‡one-way ANOVA with Tukey's post-hoc test). Differences between Groups I and II, and Groups I and IV are not statistically significant ($p>0.05$ for all comparisons).

Operative time was greatest in Group III (85±14 min), reflecting the technical complexity of full-thickness suturing and the frequent need for additional haemostasis. Group V had the shortest operative time (57±9 min), as expected, since no reinforcement step was required. Group I (72±10 min) and Group IV (74±11 min) occupied intermediate positions. Differences in operative time across all groups were statistically significant ($p<0.001$, ANOVA).

Postoperative hospital stay mirrored complication severity, being longest in Group V (5.6±2.9 days) and shortest in Group I (3.7±1.1 days; $p<0.001$, ANOVA). The reduction in mean hospital stay in the sero-serous reinforcement group not only reflects a smoother postoperative course but also carries direct economic implications.

Taken together, the data support the conclusion that sero-serous reinforcement represents the optimal method by virtue of its combination of clinical efficacy, technical reproducibility, and cost-effectiveness. Its advantages can be explained as follows: the sero-serous suture provides reliable staple line reinforcement without compromising gastric wall blood supply (unlike full-thickness suturing), requires no specific consumables (unlike buttress materials or haemostatic agents), and is less dependent on the availability of a sufficient volume of mobilisable omentum (unlike omentoplasty). The use of V-loc self-retaining suture allows single-handed suturing without an assistant and reduces the time required for this operative step compared with a conventional continuous suture.

Conclusion.

1. Sero-serous staple line reinforcement in laparoscopic sleeve gastrectomy provides the lowest rates of staple line leakage (1.0%), intraabdominal bleeding (1.0%), and intragastric bleeding (1.0%) among all methods studied, and is significantly superior to the no-reinforcement approach across all three primary endpoints ($p<0.05$).

2. Full-thickness suture reinforcement (Group III), despite its theoretical mechanical advantage, is associated with the highest complication rate among reinforcement methods and the longest mean operative time (85±14 min), and is therefore not recommended for routine use.

3. Seromuscular reinforcement and omentoplasty demonstrate intermediate outcomes; although differences from sero-serous reinforcement are not statistically significant, the consistent trend toward higher complication rates supports the preference for the sero-serous technique.

4. Application of the Hemoben haemostatic agent represents a promising direction; definitive conclusions require completion of enrolment and expansion of the study sample.

5. Sero-serous staple line reinforcement is recommended for routine use in sleeve gastrectomy as the method with optimal clinical efficacy, technical reproducibility, and cost-effectiveness for the prevention of staple line complications.

REFERENCES

1. Ataliyev A.E., Normatov B.Sh. Bariatric surgery in Uzbekistan: current state and development prospects. Surgery of Uzbekistan, 2021, no. 2, pp. 14–19. (In Russian)

2. Benedix F., Benedix D.D., Trowitzsch M. et al. Postoperative morbidity and mortality after sleeve gastrectomy — a systematic review. Obesity Facts, 2021, vol. 14, no. 4, pp. 371–381.

3. Choi Y.Y., Kim S.M., Chung J.W. et al. Staple line reinforcement in laparoscopic sleeve gastrectomy: a meta-analysis of randomized controlled trials. Surgical Endoscopy, 2020, vol. 34, no. 6, pp. 2385–2394.

4. Dadayev R.Ya., Khasanov Sh.M. Laparoscopic sleeve gastrectomy in morbid obesity: immediate results. Bulletin of Surgery of Uzbekistan, 2020, no. 4, pp. 38–43. (In Russian)

5. Gagner M., Deitel M., Erickson A.L., Crosby R.D. Survey on laparoscopic sleeve gastrectomy (LSG) at the Fourth International Consensus Summit on Sleeve Gastrectomy. Obesity Surgery, 2013, vol. 23, no. 12, pp. 2013–2017.

6. Glaysher M., Khan O.A., McGee M.C. et al. Staple line reinforcement in primary laparoscopic sleeve gastrectomy: does it affect clinical outcomes? Annals of the Royal College of Surgeons of England, 2019, vol. 101, no. 7, pp. 476–481.

7. IFSO Global Registry: 5th Report. Ed. by L. Angrisani et al. Oxfordshire: Dendrite Clinical Systems, 2019. 102 p.

8. Kasalicky M., Dostalova P., Vernerova Z. et al. Comparison of different types of staple line reinforcement in a sleeve gastrectomy. Obesity Facts, 2022, vol. 15, no. 2, pp. 207–214.

9. Khoraki J., Wahby M.R., Ragaa N. Bariatric surgery in developing countries: challenges and opportunities. World Journal of Surgery, 2021, vol. 45, no. 4, pp. 1025–1033.

10. Peterli R., Wölnerhanssen B.K., Peters T. et al. Effect of laparoscopic sleeve gastrectomy vs Roux-en-Y gastric bypass on weight loss in patients with morbid obesity: the SM-BOSS randomized clinical trial. JAMA, 2018, vol. 319, no. 3, pp. 255–265.

11. Ruziyev U.S., Niyazova N.R. Staple line reinforcement in sleeve gastrectomy: clinical experience. World scientific research journal, 2026, no. 83, pp. 266–276.

12. Sajid M.S., Bhatt C.R., Yunus R.M. et al. Influence of staple line reinforcement on clinical outcome following laparoscopic sleeve gastrectomy: an updated meta-analysis. Surgery Today, 2018, vol. 48, no. 2, pp. 165–174.

13. Sarela A.I., Dexter S.P., O'Kane M. et al. Long-term follow-up after laparoscopic sleeve gastrectomy: 8–10-year results. Surgery for Obesity and Related Diseases, 2012, vol. 8, no. 6, pp. 679–684.

MICROVASCULAR REMODELING AND THE ENDOTHELIAL-APOPTOTIC SWITCH IN LICHEN SCLEROSUS: AN IMMUNOHISTOCHEMICAL STAGE-BASED STUDY

Omasharifa J. Po - Ph.D., associate professor
Kursk State Medical University (Kursk, Russia)
Akmal A. Sidikov - D.M.Sc., professor, rector
Fergana Medical Institute of Public Health (Fergana, Uzbekistan)
zebooriginal@gmail.com

Abstract. *Purpose: To evaluate stage-specific microvascular and apoptotic changes in lichen sclerosus (LS) using CD31, VEGF and CD95 immunohistochemistry. Methods: The article is based on a dissertation cohort of 60 patients with LS. For stage-oriented immunohistochemical analysis, representative dermal samples from progressive-stage lesions (n=15) and chronic-stage lesions (n=15) were examined. Results: In progressive-stage LS, dermal CD31 expression was detected in 33% of samples, VEGF in 80%, and CD95 in 20%, while all three markers were absent in the epidermis. In chronic-stage LS, dermal CD31 expression was present in 53%, VEGF in 20%, and CD95 in 95% of samples, again with no epidermal expression. Morphologically, progressive-stage lesions showed vacuolar interface dermatitis, lymphocytic exocytosis and lichenoid inflammation, whereas chronic-stage lesions were dominated by papillary dermal fibrosis and sclerosis. Malignant progression to squamous cell carcinoma (SCC) was documented in 5 of 60 patients and was associated with ulceration, bleeding, proliferating irregular vessels, epithelial atypia, pathological mitoses and high CD95 expression. Conclusion: LS demonstrates a stage-dependent shift from endothelial activation and neoangiogenesis to endothelial injury, apoptotic remodeling and sclerosis. Combined clinicopathological and immunohistochemical assessment may improve early recognition of unfavorable disease evolution.*

Keywords: *lichen sclerosus; microcirculation; CD31; VEGF; CD95; squamous cell carcinoma*

Introduction. Lichen sclerosus is increasingly understood as a chronic inflammatory disorder in which immune dysregulation, stromal remodeling and vascular alterations interact over time [1-4]. Standard clinical descriptions emphasize whitening, atrophy, scarring and pruritus, but the mechanisms that drive progression from active inflammatory lesions to chronic sclerosis and, in a subset of cases, malignant transformation remain incompletely characterized [1,2,5].

The dissertation that forms the basis of this article focused specifically on the microcirculatory bed as a potential early pathogenic target. The working hypothesis was that progressive-stage LS is characterized by endothelial activation and neoangiogenesis, whereas chronic disease is marked by endothelial damage, apoptosis and sclerosis. The present manuscript summarizes the immunohistochemical evidence supporting that stage-dependent model.

Materials and Methods. The source cohort included 60 patients with LS, of whom 30 were women and 30 were men. All underwent clinical assessment and skin biopsy. For stage-focused immunohistochemical analysis, representative specimens from progressive-stage LS (n=15) and chronic-stage LS (n=15) were studied. Five patients from the total cohort showed progression to squamous cell carcinoma (SCC) of the skin on clinicopathological assessment.

Formalin-fixed paraffin-embedded sections were evaluated histologically and immunohistochemically using antibodies to CD31, VEGF and CD95. The original dissertation recorded marker positivity separately for epidermis and dermis. Histological interpretation emphasized vacuolar interface dermatitis, lichenoid infiltrate, exocytosis of lymphocytes, papillary dermal fibrosis, sclerosis, and epithelial atypia. Statistical comparisons were performed in the dissertation; the present article reports the validated stage-specific expression profile and its morphological interpretation.

Results. The progressive stage of LS showed a histological pattern of vacuolar interface dermatitis with dense lichenoid inflammatory infiltrates, vacuolar degeneration of epidermal cells, intercellular lymphocytes and lymphocytic exocytosis. This phase represented the biologically active part of the disease. In contrast, the chronic stage was dominated by dense fibrosis of the papillary dermis and sclerosis, with a lower inflammatory burden. The observed stage transition therefore involved not only stromal remodeling but also a major shift in the vascular microenvironment.

Immunohistochemically, no expression of CD31, VEGF or CD95 was detected in the epidermis in either stage. In the dermis of progressive-stage lesions, CD31 expression was found in 5/15 samples (33%), VEGF in 12/15 (80%), and CD95 in 3/15 (20%). The predominance of VEGF together with detectable CD31 supports the interpretation of endothelial activation and active neoangiogenesis in early disease. In this stage, endothelial structures were morphologically more preserved than in chronic lesions.

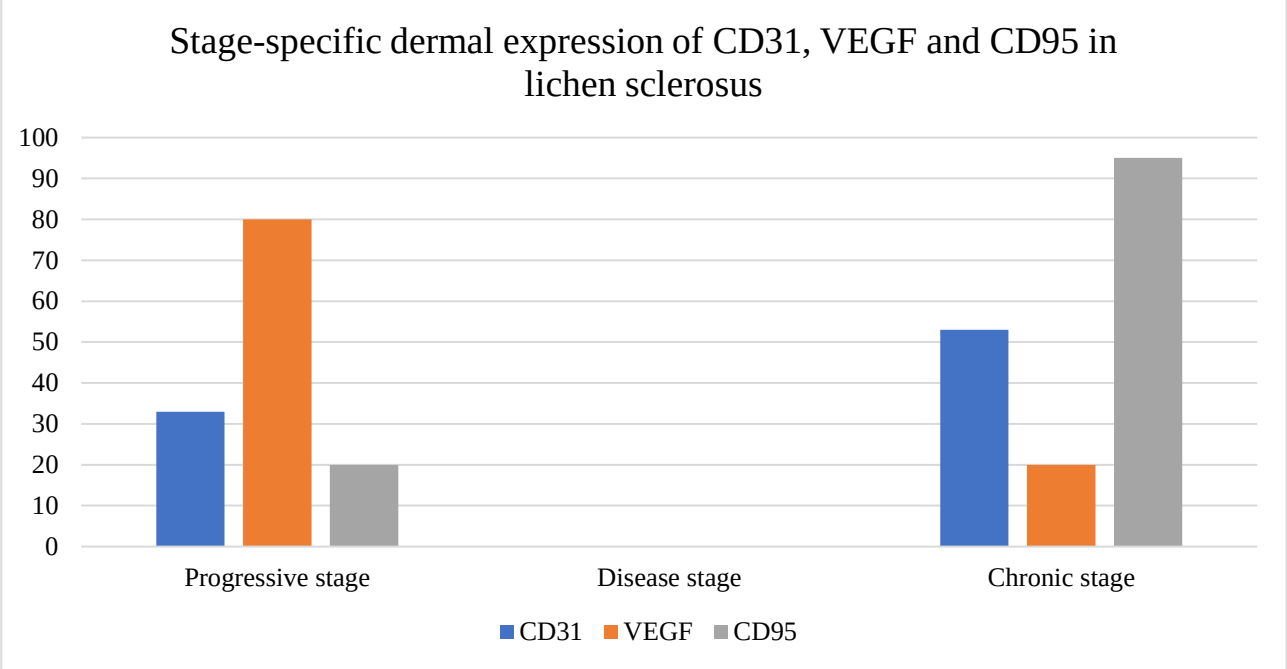


Figure 1. Stage-specific dermal expression of CD31, VEGF and CD95 in lichen sclerosus

A markedly different profile was documented in chronic-stage lesions. Dermal CD95 expression was present in 14/15 samples (95%), CD31 in 8/15 (53%), and VEGF in 3/15 (20%). Histologically, vascular walls displayed severe structural changes, including nuclear shrinkage, swelling and irregular staining continuity. CD31 expression became discontinuous and uneven in morphologically altered vascular cells, whereas CD95 staining intensified in the endothelium and surrounding vascular structures. This pattern indicates a switch from proangiogenic signaling toward apoptotic vascular remodeling.

The dissertation conclusions additionally state that structural disruption of the endothelium contributed to increased vascular permeability and even the formation of mixed thrombi, which was linked to secondary changes in both epidermis and dermis. In this interpretation, endothelial injury is not an epiphenomenon but a pathogenic event that amplifies sclerosis and tissue damage. This concept aligns with the clinical observation that visible dermoscopic vessels may indicate disease activity during the early phase, while chronic lesions lose vascular vitality and become predominantly sclerotic.

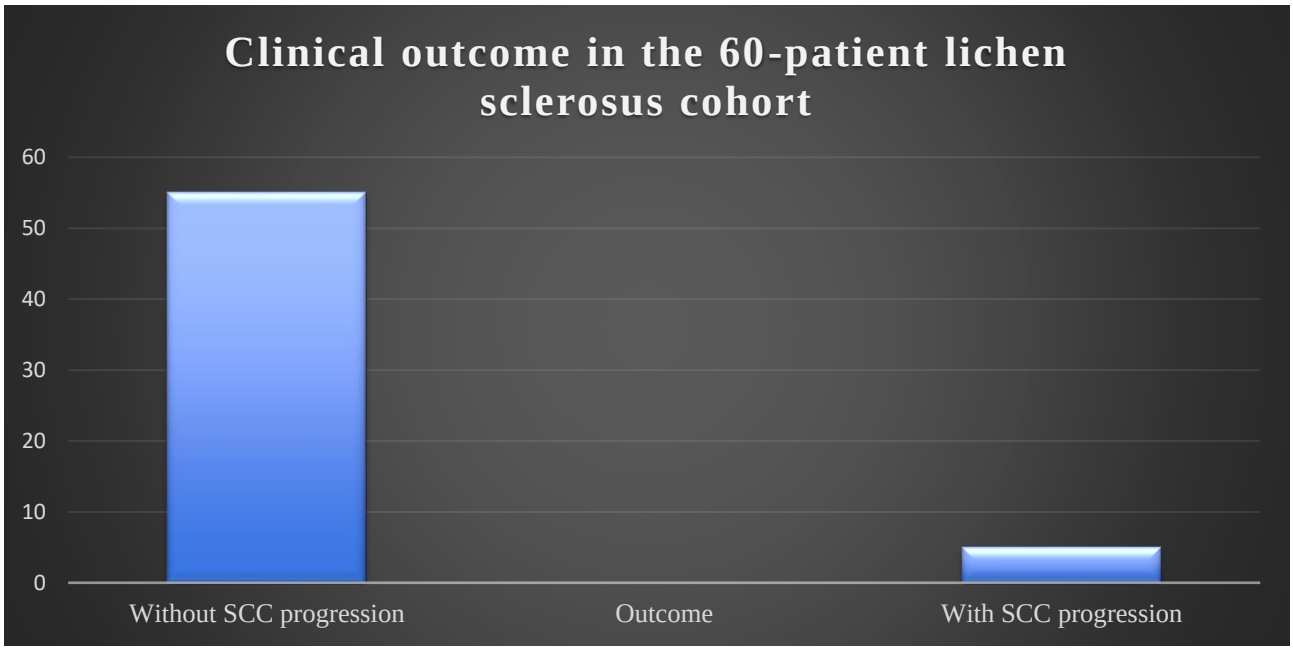


Figure 2. Clinical outcome in the 60-patient lichen sclerosus cohort

Malignant progression to SCC was documented in 5 of the 60 patients. Morphological warning signs included ulceration, induration, bleeding, disturbed stratification of the epidermis, epithelial atypia, pathological mitoses, dermal sclerosis, and proliferation of dotted and irregular vessels. In the practical conclusions of the dissertation, high CD95 expression in the presence of pathological epidermal cells and mitoses was identified as one of the main combined indicators of adverse progression.

Discussion. The stage-specific combination of high VEGF in progressive lesions and high CD95 in chronic lesions suggests that LS evolves through at least two biologically distinct vascular phases. The first is dominated by endothelial activation and angiogenic response, likely reflecting active inflammation and tissue repair. The second is characterized by endothelial exhaustion, apoptosis and fibrosing remodeling. This interpretation is consistent with the general understanding that LS involves immune-mediated inflammation, extracellular matrix remodeling and potential oncogenic evolution in long-standing disease [1,2,6-9].

Prior studies have linked angiogenesis-related signaling to vulvar LS with neoplastic potential and have shown that long-standing untreated or undertreated disease carries a measurable risk of malignant transformation [8-10]. The present dissertation-based findings add a useful stage-oriented model: CD31 and VEGF characterize early endothelial reactivity, whereas CD95 marks late microvascular injury and apoptotic restructuring. For practice, this means that clinical, dermoscopic and immunohistochemical data should be interpreted together rather than in isolation.

The study is strengthened by its balanced sex distribution, consistent pathology review and stage-specific immunohistochemical design. Its main limitation is that the stage-focused IHC analysis was performed on representative subsets rather than all 60 biopsies, and external validation in multicenter cohorts is still required. Nevertheless, the internal coherence between morphology, dermoscopy and biomarker expression makes the proposed model clinically plausible.

Conclusion. Lichen sclerosus shows a reproducible shift from endothelial activation and neoangiogenesis in progressive disease to endothelial apoptosis and sclerosis in chronic disease. The combination of CD31, VEGF and CD95 provides a biologically meaningful framework for lesion staging. High CD95 expression together with epithelial atypia and pathological mitoses should prompt heightened suspicion for malignant progression.

Table 1.

Stage-specific expression of immunohistochemical markers in lichen sclerosus

Disease stage	Sample size	CD31 positive, n (%)	VEGF positive, n (%)	CD95 positive, n (%)
Progressive stage	15	5 (33)	12 (80)	3 (20)
Chronic stage	15	8 (53)	3 (20)	14 (95)

REFERENCES

1. De Luca DA, Papara C, Vorobyev A, Staiger H, Bieber K, Thaci D, et al. Lichen sclerosus: The 2023 update. Front Med (Lausanne). 2023; 10:1106318. doi:10.3389/fmed.2023.1106318.

2. Xie X, Wu K. Advances in the pathogenesis of vulvar lichen sclerosus. Mol Biol Rep. 2024;51(1):396. doi:10.1007/s11033-024-09318-7.

3. Krapf JM, Mitchell L, Holton MA, Goldstein AT. Vulvar lichen sclerosus: Current perspectives. Int J Womens Health. 2020; 12:11-20. doi:10.2147/IJWH.S191200.

4. Yeon J, Oakley A, Olsson A, Drummond C, Veysey E, Marshman G, et al. Vulval lichen sclerosus: An Australasian management consensus. Australas J Dermatol. 2021;62(3):292-299. doi:10.1111/ajd.13594.

5. Micheletti L, Preti M, Radici G, Boveri S, Di Pumpo O, Privitera SS, et al. Vulvar lichen sclerosus and neoplastic transformation: A retrospective study of 976 cases. J Low Genit Tract Dis. 2016;20(2):180-183. doi:10.1097/LGT.0000000000000186.

6. Raspollini MR, Taddei GL, Krampera M, Bracco GL, Colombi M, Rossi Degl'Innocenti D, et al. The role of angiogenesis and COX-2 expression in the genesis of vulvar lichen sclerosus and squamous cell carcinoma. Histopathology. 2007;51(3):353-361. doi:10.1111/j.1365-2559.2007. 02789. x.

7. Regauer S, Liegl B, Reich O. Early vulvar lichen sclerosus: A histopathological challenge. Histopathology. 2005;47(4):340-347. doi:10.1111/j.1365-2559.2005.02209. x.

8. Larre Borges A, Tiodorovic-Zivkovic D, Lallas A, Forgiarini C, Moscarella E, Longo C, et al. Clinical, dermoscopic and histopathologic features of genital and extragenital lichen sclerosus. J Eur Acad Dermatol Venereol. 2013;27(11):1433-1439. doi:10.1111/j.1468-3083.2012.04595. x.

9. Steinkasserer L, Leenen MCH, Bekkers RLM, Bulten J, Massuger LFAG, van der Avoort IAM. Characterization of patients with vulvar lichen sclerosus and association to vulvar carcinoma: A retrospective single-center analysis. Cancers (Basel). 2022;14(14):3363. doi:10.3390/cancers 14143363.

10. Wang J, Xu X, et al. Immune dysregulation and cellular composition in lichen sclerosus revealed by integrative epigenetic analysis with cell type deconvolution. J Inflamm Res. 2025; 18:283-299. doi:10.2147/JIR.S481324.

11. Chamli A, Makhzoumi ZK. Lichen sclerosus. In: StatPearls [Internet]. Treasure Island (FL): StatPearls Publishing; 2023.

12. Watson EC, Koenig MN, Grant ZL, White SL, Trounson E, Dewson G, et al. Endothelial cell apoptosis in angiogenesis and vessel regression. Cell Mol Life Sci. 2017;74(24):4387-4403. doi:10.1007/s00018-017-2577-y.

RESULTS OF MICROPULSE TRANSSCLERAL CYCLOPHOTOCOAGULATION IN THE TREATMENT OF NEOVASCULAR GLAUCOMA IN PROLIFERATIVE DIABETIC RETINOPATHY

Azamat F. Yusupov - D.M.Sc., professor
Muyassar Kh. Karimova - D.M.Sc., professor
Shirin A. Dzhamalova - D.M.Sc., associate professor
Azizbek K. Jalalov - basic doctoral researcher
Nurbek Sh. Khaitboev - resident
Republican Specialized Scientific and Practical Medical Center of Eye Microsurgery (Tashkent, Uzbekistan)
nurbekxaitboyev@gmail.com

Abstract. *Neovascular glaucoma (NVG) associated with proliferative diabetic retinopathy (PDR) represents the most severe form of secondary glaucoma. This paper presents the results of micropulse transscleral cyclophotocoagulation (MP-TSCPC) in 10 patients with NVG secondary to PDR. At 6-month follow-up, a statistically significant mean IOP reduction of 61.2% was observed along with improved best-corrected visual acuity, with no serious adverse events.*

Keywords: *neovascular glaucoma, proliferative diabetic retinopathy, micropulse trans-scleral cyclophotocoagulation, MP-TSCPC, intraocular pressure, iris rubeosis, type 2 diabetes mellitus.*

Introduction.

Neovascular glaucoma (NVG) is one of the most severe complications of proliferative diabetic retinopathy (PDR) and occupies a special place among secondary glaucomas due to its aggressive course, marked refractoriness to conventional hypotensive therapy, and high risk of irreversible vision loss [1]. According to the literature, NVG develops in 2–21% of patients with diabetes mellitus and diabetic retinopathy, and in the vast majority of cases it is associated with PDR and chronic retinal ischemia [2].

The pathogenetic basis of NVG is abnormal neovascularization of the anterior segment of the eye induced by overproduction of vascular endothelial growth factor (VEGF) under conditions of retinal hypoxia. Proliferating new vessels of the iris (rubeosis iridis) and the anterior chamber angle form a fibrovascular membrane that progressively obstructs aqueous humor outflow pathways, leading to a sharp increase in intraocular pressure (IOP) [3].

Micropulse transscleral cyclophotocoagulation (MP-TSCPC) is a modern, tissue-sparing method for reducing ophthalmotonus, based on selective воздействия on the pigmented epithelium of the ciliary body using interrupted laser energy delivery. Unlike conventional continuous-wave cyclophotocoagulation, MP-TSCPC causes significantly less destructive damage to surrounding tissues, which is especially important in refractory NVG in patients with severe concomitant retinal pathology [4,5].

Objective. To evaluate the clinical and functional outcomes of MP-TSCPC in the comprehensive treatment of NVG associated with PDR based on a series of 10 clinical cases.

Material and methods of research.

The case series included 10 patients (15 eyes with NVG) diagnosed with secondary neovascular glaucoma associated with proliferative diabetic retinopathy, who were treated at the Republican Specialized Scientific and Practical Medical Center of Eye Microsurgery during 2025–2026. All patients had type 2 diabetes mellitus. The mean age was 59.2.

Inclusion criteria were: confirmed NVG associated with active PDR, IOP ≥ 30 mmHg despite maximum medical therapy, presence of iris rubeosis, and a history of previous antiglaucoma interventions. All patients underwent MP-TSCPC using the Quantel Medical 810 nm laser system (parameters: power 2000 mW, duty cycle 31.3%, exposure time 80–100 s). Panretinal laser photocoagulation (PRP) was performed in all patients either during the preparatory stage or simultaneously.

The examination included visual acuity testing, contact and non-contact tonometry, biomicroscopy, ophthalmoscopy, retinal OCT (Maestro2, Topcon), computerized perimetry (Tomey), B-scan ultrasonography (Sonomed Escalon), and A-scan biometry. The follow-up period was 6 months. Statistical analysis was performed using the paired t-test, with $p < 0.05$.

Table 1.

Clinical characteristics of patients

No.	Patient	Age	Sex	Affected Eye	IOP Before MP-TSCPC (mmHg)	Visual Acuity Before
1	M.	55	Male	OU	OD: 38, OS: 38	OD: 0.01, OS: 0.04
2	T.	61	Male	OU	OD: 36, OS: 34	OD: 0.02, OS: 0.02
3	Kh.	58	Female	OS	OD: 18, OS: 41	OD: 0.4, OS: 0.02
4	R.	63	Male	OD	OD: 44, OS: 16	OD: 0.01, OS: 0.3
5	K.	52	Female	OU	OD: 35, OS: 39	OD: 0.02, OS: 0.01
6	A.	67	Male	OU	OD: 42, OS: 37	OD: 0.01, OS: 0.02
7	N.	49	Female	OS	OD: 17, OS: 40	OD: 0.3, OS: 0.01
8	U.	71	Male	OU	OD: 33, OS: 36	OD: 0.02, OS: 0.02
9	Zh.	56	Female	OD	OD: 45, OS: 18	OD: 0.01, OS: 0.2
10	S.	60	Male	OU	OD: 37, OS: 40	OD: 0.02, OS: 0.01

Results. Six months after MP-TSCPC, a significant reduction in intraocular pressure was observed in all cases. The mean IOP before treatment was 38.4 ± 3.8 mmHg, which decreased to 14.9 ± 1.6 mmHg after treatment (a 61.2% reduction; $p < 0.001$). Target IOP (≤ 18 mmHg) was achieved in 14 out of 15 eyes (93.3%). The dynamics of pre- and post-treatment parameters are presented in Table 2.

Table 2.

Dynamics of Clinical Parameters Before and After MP-TSCPC (at 6-Month Follow-Up*)*

No.	IOP Before/After (mmHg)	Visual Acuity Before/After	Perimetry MD (dB)
1	OD: 38 / 14, OS: 38 / 12	OD: 0.01 / 0.03, OS: 0.04 / 0.08	OD: -29.5, OS: -16.0
2	OD: 36 / 16, OS: 34 / 14	OD: 0.02 / 0.04, OS: 0.02 / 0.05	OD: -26.3, OS: -24.1
3	OD: 18 / 16, OS: 41 / 15	OD: 0.4 / 0.4, OS: 0.02 / 0.05	OD: -4.2, OS: -28.7
4	OD: 44 / 17, OS: 16 / 15	OD: 0.01 / 0.02, OS: 0.3 / 0.3	OD: -31.2, OS: -6.1
5	OD: 35 / 13, OS: 39 / 15	OD: 0.02 / 0.04, OS: 0.01 / 0.03	OD: -22.4, OS: -27.8
6	OD: 42 / 18, OS: 37 / 16	OD: 0.01 / 0.03, OS: 0.02 / 0.04	OD: -33.1, OS: -25.6
7	OD: 17 / 15, OS: 40 / 14	OD: 0.3 / 0.3, OS: 0.01 / 0.03	OD: -3.8, OS: -30.2
8	OD: 33 / 15, OS: 36 / 17	OD: 0.02 / 0.04, OS: 0.02 / 0.05	OD: -24.7, OS: -22.3
9	OD: 45 / 16, OS: 18 / 16	OD: 0.01 / 0.03, OS: 0.2 / 0.2	OD: -34.5, OS: -5.4
10	OD: 37 / 14, OS: 40 / 13	OD: 0.02 / 0.05, OS: 0.01 / 0.04	OD: -27.9, OS: -29.1
Mean	38.4 / 14.9	—	—

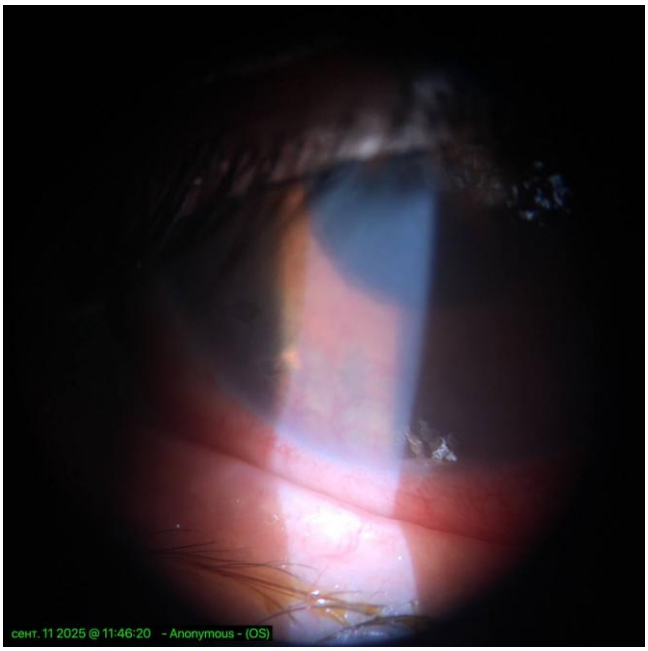


Figure 1. Rubeosis iridis of the left eye (patient M., 55 years old): newly formed vessels on the iris surface in neovascular glaucoma associated with proliferative diabetic retinopathy (September 2025)

Visual acuity improved or remained stable in all cases. No progression of glaucomatous optic disc cupping was detected on OCT. No complications (hypotony, phthisis bulbi, or bullous keratopathy) were observed. Partial regression of iris rubeosis following panretinal laser photocoagulation (PRP) was noted in 7 out of 10 patients.

Discussion. The obtained results demonstrate the high hypotensive efficacy of MP-TSCPC in refractory neovascular glaucoma in patients with proliferative diabetic retinopathy. The 61.2% reduction in IOP is consistent with published data: Aquino et al. reported a 35–40% reduction in IOP following MP-TSCPC in patients with refractory glaucoma [7]. A key advantage of this method is the preservation of residual visual function due to its tissue-sparing mode of action without total destruction of the ciliary body [5,7].

The wave-like pattern of IOP changes observed in some cases (increase to 38–45 mmHg followed by normalization) indicates the instability of ocular hydrodynamics in NVG and highlights the need for timely MP-TSCPC before irreversible optic nerve damage develops [3,4]. Partial regression of iris rubeosis following PRP in 70% of patients confirms the pathogenetic rationale for a comprehensive treatment approach [6].

Thus, a differentiated treatment strategy for NVG associated with PDR should include: (1) elimination of retinal ischemia (PRP, anti-VEGF therapy); (2) surgical IOP control using MP-TSCPC; and (3) systemic management of diabetes mellitus [1,3,5].

Conclusion. Micropulse transscleral cyclophotocoagulation is an effective and safe method for IOP control in refractory neovascular glaucoma associated with proliferative diabetic retinopathy. In this series of 10 patients, the method provided a mean IOP reduction of 61.2% without serious complications and with preservation of residual visual function. A comprehensive approach including MP-TSCPC combined with panretinal laser photocoagulation and systemic diabetes control makes it possible to achieve stabilization of ophthalmotonus in this severe category of patients.

REFERENCES

1. Simha A, Braganza A, Abraham L, et al. Anti-vascular endothelial growth factor for neovascular glaucoma. Cochrane Database of Systematic Reviews. 2020;2:CD007920.

2. Havens SJ, Gulati V. Neovascular glaucoma. Developments in Ophthalmology. 2016; 55:196–204.

3. Zhou M, Wang W, Huang W, Zhang X. Trabeculectomy with versus without adjunctive bevacizumab in neovascular glaucoma: a meta-analysis. BMC Ophthalmology. 2016;16(1):121.

4. Shazly TA, Latina MA. Neovascular glaucoma: etiology, diagnosis and prognosis. Seminars in Ophthalmology. 2009;24(2):113–121.

5. Rodrigues GB, Abe RY, Zangalli C, et al. Neovascular glaucoma: a review. International Journal of Retina and Vitreous. 2016;2:26.

6. Early Treatment Diabetic Retinopathy Study Research Group. Photocoagulation for diabetic macular edema. Archives of Ophthalmology. 1985;103(12):1796–1806.

7. Aquino MC, Barton K, Tan AM, et al. Micropulse versus continuous wave transscleral diode cyclophotocoagulation in refractory glaucoma: a randomized exploratory study. Clinical and Experimental Ophthalmology. 2015;43(1):40–46.

8. Yazdani S, Hendi K, Pakravan M, et al. Intravitreal bevacizumab for neovascular glaucoma: a randomized controlled trial. Journal of Glaucoma. 2009;18(8):632–637.

UDC: 618.3+618.5:616.45-001/.3:616.12-007

PLACENTAL ELASTOGRAPHY IN THE DIAGNOSIS OF PLACENTAL DYSFUNCTION IN FETAL GROWTH RESTRICTION

Aziza M. Babakhanova - Ph.D., academic secretary
Republican Specialized Scientific and Practical Medical Center for Maternal and Child Health (Tashkent, Uzbekistan)
Doktor8100@mail.ru

Abstract. *The aim of the study was to evaluate the diagnostic significance of placental elastography in pregnant women with fetal growth restriction (FGR) and to compare elastographic parameters with Doppler markers of placental dysfunction.*

A total of 56 pregnant women at 28–36 weeks of gestation were examined: 34 patients with FGR and 22 with physiological pregnancy. All patients underwent fetometry, Doppler assessment of uterine arteries, umbilical artery, and fetal middle cerebral artery, calculation of the cerebroplacental ratio (CPR), and transabdominal shear-wave elastography of the placenta.

Keywords: *placenta, elastography, shear-wave elastography, fetal growth restriction, Doppler, placental dysfunction*

Introduction. Fetal growth restriction (FGR) remains one of the leading causes of perinatal morbidity and mortality. According to international studies, FGR occurs in 5–10% of all pregnancies, and perinatal mortality risk increases by 4–8 times compared to normally developing fetuses.

In most cases, FGR is associated with placental dysfunction caused by impaired placentation, inadequate spiral artery remodeling, and chronic placental hypoperfusion.

Conventional ultrasound diagnostics of FGR includes fetometry and Doppler assessment of the maternal–placental–fetal circulation. The most informative indices are resistance index (RI), pulsatility index (PI), and cerebroplacental ratio (CPR). However, these methods mainly reflect hemodynamic changes occurring at later stages and poorly characterize structural and biomechanical properties of placental tissue.

In recent years, ultrasound elastography has gained increasing attention as a non-invasive method for assessing tissue mechanical properties. Shear-wave elastography (SWE) enables quantitative measurement of tissue stiffness (kPa) and allows in vivo evaluation of the placenta.

Morphological studies demonstrate that placental dysfunction is associated with fibrosis, infarctions, microthrombosis, reduced vascularization, and altered villous architecture. These changes lead to increased placental stiffness measurable by elastography. Previous studies report mean placental stiffness of 27–32 kPa in FGR versus 14–18 kPa in normal pregnancy.

Thus, placental elastography represents a promising tool for early detection of placental dysfunction before significant Doppler abnormalities develop.

Aim of the study. To determine the diagnostic value of placental elastography in detecting placental dysfunction in FGR and to assess its relationship with uteroplacental and fetal blood flow parameters.

Materials and methods. A prospective comparative study included 56 pregnant women at 28–36 weeks of gestation: main group (FGR): 34 patients, control group: 22 patients. Inclusion criteria: estimated fetal weight <10th percentile, reduced abdominal circumference, doppler signs of placental insufficiency. Exclusion criteria: multiple pregnancy, congenital anomalies, chorioamnionitis, severe extragenital diseases.

All patients underwent: ultrasound examination, doppler study (uterine, umbilical, MCA), CPR calculation, SWE elastography (Emean, Emin, Emax, elasticity ratio). Measurements were performed in 3 placental regions. Statistical analysis included mean values, SD, odds ratio (OR), and 95% CI.

Results. The analysis of the clinical characteristics of the examined pregnant women showed that the groups were comparable in terms of the main demographic and obstetric parameters. The mean age of women in the group with fetal growth restriction (FGR) was 29.7 ± 5.1 years, whereas in the control group it was 28.9 ± 4.7 years, indicating no statistically significant differences between the groups (Table 1).

Table 1.

Clinical characteristics of pregnant women

Parameter	FGR (n=34)	Control (n=22)
Age (years)	29.7 ± 5.1	28.9 ± 4.7
Gestational age (weeks)	32.4 ± 2.1	32.8 ± 2.0
BMI (kg/m²)	26.1 ± 3.8	24.8 ± 3.1
Primigravida, n (%)	18 (52.9%)	10 (45.5%)
Hypertensive disorders, n (%)	9 (26.5%)	1 (4.5%)

The gestational age at the time of examination was also comparable between the groups: 32.4 ± 2.1 weeks in the FGR group and 32.8 ± 2.0 weeks in the control group. This allows for a correct comparison of the functional parameters of the fetoplacental system.

The mean pre-pregnancy body mass index was slightly higher in patients with FGR (26.1 ± 3.8 kg/m²) compared to the control group (24.8 ± 3.1 kg/m²), which may reflect a tendency toward a higher prevalence of metabolic risk factors among pregnant women with placental dysfunction.

The proportion of primigravida women in the FGR group was 52.9% (18 patients), whereas in the control group it was 45.5% (10 patients), indicating a comparable parity structure.

At the same time, a significantly higher incidence of hypertensive disorders of pregnancy was observed in the FGR group—26.5% (9 cases), compared to only 4.5% (1 case) in the control group. This confirms the close association between fetal growth restriction and placenta-mediated complications of pregnancy.

The analysis of Doppler parameters demonstrated pronounced disturbances in uteroplacental-fetal blood flow in pregnant women with FGR (Table 2).

In the FGR group, a significant increase in vascular resistance indices in the uterine arteries was observed. Thus, the uterine artery RI was 0.71 ± 0.06, which was significantly higher than in the control group (0.56 ± 0.05, $p<0.001$). A similar trend was noted for the uterine artery PI—1.42 ± 0.21 versus 0.92 ± 0.18, respectively ($p<0.001$). These findings reflect increased peripheral resistance in the uteroplacental circulation.

Table 2.

Doppler parameters

Parameter	FGR	Control	p
RI uterine arteries	0,71 ± 0,06	0,56 ± 0,05	<0,001
PI uterine arteries	1,42 ± 0,21	0,92 ± 0,18	<0,001
RI umbilical artery	0,69 ± 0,07	0,58 ± 0,05	<0,001
PI umbilical artery	1,36 ± 0,24	0,94 ± 0,19	<0,001
PI MCA	1,05 ± 0,22	1,58 ± 0,26	<0,001
CPR	0,87 ± 0,19	1,72 ± 0,28	<0,001
Grade I flow disturbance	9 (26,5)	0	-
Grade II	10 (29,4)	0	-
Grade III	4 (11,8)	0	-

A significant increase in resistance indices was also observed in the umbilical artery: RI was 0.69 ± 0.07 in the FGR group versus 0.58 ± 0.05 in the control group (p<0.001), and PI was 1.36 ± 0.24 versus 0.94 ± 0.19, respectively (p<0.001). The elevation of these parameters indicates impaired placental perfusion and increased vascular resistance within the placental circulation.

In contrast, a significant decrease in PI was observed in the fetal middle cerebral artery: 1.05 ± 0.22 in the FGR group compared to 1.58 ± 0.26 in the control group (p<0.001). This phenomenon reflects the development of the so-called "cerebral redistribution of blood flow" (brain-sparing effect), a compensatory mechanism aimed at maintaining perfusion of vital fetal organs.

The cerebroplacental ratio (CPR) was also significantly lower in patients with FGR—0.87 ± 0.19, whereas in the control group it was 1.72 ± 0.28 (p<0.001), confirming pronounced impairment of fetoplacental hemodynamics.

Table 3.

Placental Elastography Parameters

Parameter	FGR	Control	p
Emean (kPa)	29,8 ± 5,6	15,4 ± 3,1	<0,001
Emin (kPa)	21,6 ± 4,1	11,2 ± 2,4	<0,001
Emax (kPa)	36,7 ± 6,2	18,8 ± 3,5	<0,001
Elasticity ratio	2,14 ± 0,46	1,09 ± 0,21	<0,001
>25 kPa	20 (58,8)	3 (13,6)	0,001
20–25 kPa	9 (26,5)	4 (18,2)	-
<20 kPa	5 (14,7)	15 (68,2)	-

Analysis of the severity of blood flow disturbances showed that among pregnant women with FGR, grade I impairment was diagnosed in 26.5% (9 patients), grade II in 29.4% (10 patients), and grade III in 11.8% (4 patients). No pathological blood flow abnormalities were detected in the control group.

Thus, the obtained data indicate significant disturbances in uteroplacental and fetal hemodynamics in pregnant women with fetal growth restriction, confirming the leading role of placental dysfunction in the pathogenesis of this pregnancy complication.

In patients with FGR, a strong negative correlation between CPR and placental stiffness was identified: correlation analysis showed that higher placental stiffness was associated with a decrease in CPR. Clinically, this reflects the progression of placental insufficiency and centralization of fetal circulation.

Analysis of the threshold value of placental stiffness >25 kPa demonstrated a significant increase in the likelihood of FGR: OR = 9.05; 95% CI 2.24–36.55; p = 0.0009.

Placental elastography reflects both structural and functional changes. Increased stiffness is likely associated with ischemia, fibrosis, infarctions, and vascular alterations.

Combined use of Doppler and elastography improves diagnostic accuracy and risk stratification.

Conclusions. Placental stiffness is significantly higher in FGR. Doppler changes confirm severe placental dysfunction. Stiffness >25 kPa increases FGR risk 9-fold. Elastography is a valuable non-invasive diagnostic tool.

REFERENCES

1. Abeysekera J.M., et al. SWAVE Imaging of Placental Elasticity and Viscosity: Proof of Concept. Ultrasound Med Biol. 2017. PMID: 28392000.

2. Alfuraih A.M. The Emerging Role of Sonoelastography in Pregnancy: Applications in Assessing Maternal and Fetal Health. Diagnostics (Basel). 2024;15(1):47. doi:10.3390/diagnostics 15010047.

3. Ansar M., et al. Ultrasound shear wave elastography of the placenta: a potential tool for early detection of fetal growth restriction. 2024. PMID: 39461252.

4. Anuk A.T., et al. Value of shear-wave elastography and cerebral-placental-uterine ratio in women diagnosed with preeclampsia and fetal growth restriction in prediction of adverse perinatal outcomes. J Obstet Gynaecol Res. 2022. PMID: 35647897.

5. Cavanagh E., et al. Placental Shear Wave Elastography Assessment in Early and Late Fetal Growth Restriction. J Clin Med. 2025;14(14):4980. doi:10.3390/jcm14144980.

6. Chen Q., et al. The role of shear wave elastography in the assessment of placentas in healthy pregnancy women during third-trimester: A preliminary study. J Gynecol Obstet Hum Reprod. 2022;51(2):102292.

7. Deeba F., et al. SWAVE 2.0 Imaging of Placental Elasticity and Viscosity: Potential Biomarkers for Placenta-Mediated Disease Detection. 2022. PMID: 36180312.

8. Edwards C., et al. Relationship between placental elastography, maternal pre-pregnancy body mass index and gestational weight gain. Placenta. 2022;121:1-6. doi: 10.1016/j.placenta. 2022.02.015.

9. Habibi H.A., et al. In vivo assessment of placental elasticity in intrauterine growth restriction by shear-wave elastography. Eur J Radiol. 2017. PMID: 29153362.

10. Hu J., Lv Z., Dong Y., Liu W. Review of shear wave elastography in placental function evaluations. J Matern Fetal Neonatal Med. 2023;36(1):2203792. doi:10.1080/14767058.2023. 2203792.

11. Imtiaz S., et al. Role Of Shear Wave Elastography In Assessment Of Placental Elasticity In Normal And High-Risk Pregnancies In Third Trimester. J Pak Med Assoc. 2023;73(11):2205-2208. doi:10.47391/JPMA.9314.

12. Lees C.C., et al. ISUOG Practice Guidelines: diagnosis and management of small-for-gestational-age fetus and fetal growth restriction. Ultrasound Obstet Gynecol. 2020;56(2):298-312. doi:10.1002/uog.22134.

13. Meena R., et al. Placental elastography in second trimester preeclampsia prediction: A prospective study. Placenta. 2022. PMID: 35936967.

14. Melamed N., et al. FIGO initiative on fetal growth: best practice advice for screening, diagnosis, and management of fetal growth restriction. Int J Gynaecol Obstet. 2021. PMID: 33740264.

15. Singh T., et al. Role of Shear Wave Elastography of Placenta in Prediction of Preeclampsia in High-Risk Pregnancy. J Ultrasound Med. 2024. PMID: 38193810.

16. Spiliopoulos M., et al. Characterizing placental stiffness using ultrasound shear-wave elastography in healthy and preeclamptic pregnancies. Arch Gynecol Obstet. 2020. PMID: 32676857.

17. Sugitani M., et al. A new method for measurement of placental elasticity: acoustic radiation force impulse imaging. Placenta. 2013. PMID: 24075540.

18. Waller J., et al. A Longitudinal Assessment of Shear Wave Elastography of the Placenta in Normal Pregnancy. Am J Perinatol. 2025. doi:10.1055/a-2721-6039.

19. Xie C., et al. The clinical value of combining shear wave elastography, VOCAL technique, and T2* MRI of early gestation placenta to predict pre-eclampsia. J Clin Ultrasound. 2024;52(1):13-19. doi:10.1002/jcu.23575.

UDC: 616.831-005.1-036.8:615.825

ENHANCING FUNCTIONAL INDEPENDENCE AND POSTURAL CONTROL AFTER ISCHEMIC STROKE: EFFECTIVENESS OF PSYCHOMOTOR THERAPY ASSESSED BY THE BARTHEL INDEX AND BERG BALANCE SCALE

Maftuna B. Ibodulloyeva - doctoral (Ph.D.) candidate
Zarifboy R. Ibodullayev - professor
Tashkent State Medical University (*Tashkent, Uzbekistan)*
ibodulloyevamaftuna9@gmail.com

Abstract. *Stroke is a leading cause of long-term disability and frequently results in impaired motor function, balance disturbances, and reduced independence in daily activities. The aim of this study was to evaluate the effectiveness of psychomotor therapy in improving functional independence and balance in patients after ischemic stroke using the Barthel Index and the Berg Balance Scale.*

A prospective controlled clinical study included 100 patients with ischemic stroke randomly assigned to an intervention group receiving psychomotor therapy in addition to standard rehabilitation (n=50) and a control group receiving standard rehabilitation alone (n=50). Rehabilitation lasted eight weeks with four sessions per week.

After treatment, the intervention group showed greater improvements in functional independence and balance. The Barthel Index increased from 71.2 to 91.2 points compared with 71.7 to 77.5 in the control group. Berg Balance Scale scores improved from 23.88 to 43.7 in the intervention group versus 24.46 to 30.9 in the control group.

These findings indicate that psychomotor therapy significantly enhances functional independence and postural stability after ischemic stroke and may serve as an effective component of comprehensive stroke rehabilitation.

Keywords: *ischemic stroke, psychomotor therapy, stroke rehabilitation, functional independence, Barthel Index, Berg Balance Scale, balance recovery, postural control.*

Introduction. Stroke remains one of the most important global health challenges and is a leading cause of long-term disability worldwide. According to recent epidemiological studies, stroke affects millions of individuals annually and continues to impose a substantial socioeconomic burden on healthcare systems and societies. Global burden of disease analyses indicate that the absolute number of stroke survivors is steadily increasing due to population aging and improved acute stroke care, resulting in a growing demand for effective rehabilitation strategies [3, 4, 6]. Ischemic stroke accounts for approximately 70–80% of all stroke cases and frequently leads to persistent neurological deficits, including motor impairment, balance dysfunction, and reduced functional independence [7, 11, 12].

Motor deficits represent one of the most disabling consequences of ischemic stroke and affect up to 80% of stroke survivors in the acute phase. These impairments often involve muscle weakness, impaired coordination, postural instability, and limitations in activities of daily living, significantly reducing patients' quality of life and social participation [5, 11]. Balance impairment, in particular, is a major determinant of functional disability after stroke, as it increases the risk of falls and restricts independent mobility [2, 8]. Effective neurorehabilitation approaches therefore aim not only to improve motor performance but also to restore postural control and functional independence through targeted sensorimotor training [7, 1].

Stroke rehabilitation is based on the principles of neuroplasticity, which describe the ability of the central nervous system to reorganize neural pathways and restore lost functions following brain

injury. Intensive and task-oriented rehabilitation interventions can stimulate cortical reorganization and facilitate recovery of motor and functional abilities [4, 12]. Among emerging rehabilitation approaches, psychomotor therapy has gained increasing attention as a comprehensive intervention targeting the integration of motor, cognitive, and emotional processes. This therapeutic approach focuses on body awareness, proprioceptive stimulation, coordinated movements, and multisensory integration, which are essential for restoring functional motor patterns and improving postural stability after neurological injury.

The effectiveness of rehabilitation interventions is typically evaluated using validated clinical outcome measures that assess functional independence and balance performance. The Barthel Index (BI) is one of the most widely used instruments for assessing activities of daily living in stroke patients and provides a quantitative measure of functional independence ranging from total dependence to complete independence [9, 10]. The scale evaluates essential activities such as feeding, bathing, dressing, mobility, and continence, making it a reliable indicator of functional recovery after stroke [10].

In addition to functional independence, balance control represents a critical component of post-stroke recovery. The Berg Balance Scale (BBS) is widely recognized as a valid and reliable tool for assessing postural stability and fall risk in patients with neurological disorders. Numerous studies have demonstrated that BBS scores are strongly associated with mobility outcomes, functional ambulation, and discharge destination after stroke [2]. The use of both the Barthel Index and the Berg Balance Scale therefore allows a comprehensive assessment of rehabilitation outcomes by simultaneously evaluating independence in daily activities and postural control.

Despite advances in neurorehabilitation techniques, optimal rehabilitation strategies for improving balance and functional independence after ischemic stroke remain an active area of research. Psychomotor therapy, which integrates sensorimotor training with cognitive and proprioceptive stimulation, may offer a promising approach for enhancing motor recovery and postural stability. However, the clinical effectiveness of this intervention requires further investigation using validated outcome measures.

Therefore, the aim of this study was to evaluate the effectiveness of psychomotor therapy in patients with ischemic stroke by analyzing changes in functional independence and balance performance using the Barthel Index and the Berg Balance Scale.

Materials and Methods. This study was designed as a prospective controlled clinical study aimed at evaluating the effectiveness of psychomotor rehabilitation in patients after ischemic stroke. The research was conducted in cooperation with the neurology department and specialized rehabilitation centers in Tashkent, Uzbekistan.

All procedures were performed in accordance with international ethical standards for biomedical research involving human participants. Participation in the study was voluntary, and all participants provided written informed consent before inclusion.

Patients received standard neurorehabilitation therapy according to clinical practice guidelines. In addition, patients in the intervention group underwent structured psychomotor rehabilitation sessions conducted by trained rehabilitation specialists.

Participants. A total of 130 individuals were initially screened for participation in the study. Among them, 100 patients with ischemic stroke met the inclusion criteria and were included in the final statistical analysis, while 30 healthy individuals were recruited as a control group for baseline comparison.

Patients with ischemic stroke were randomly assigned into two groups using a simple randomization method (Table 1).

Table 1.

Distribution of participants across study groups

Group	Number of participants
Psychomotor therapy combined with standard	50
Standard rehabilitation	50
Healthy control	30
Total	130

Participant inclusion and exclusion were determined according to the following predefined criteria (Table 2.)

Table 2.

Inclusion and exclusion criteria for participant selection

Inclusion criteria	Exclusion criteria
confirmed diagnosis of ischemic stroke	recurrent stroke
age 30–70 years	severe somatic or psychiatric disorders
post-stroke rehabilitation stage	severe cognitive impairment
NIHSS score 5–20	epilepsy or uncontrolled cardiovascular disease
preserved cognitive ability	inability to participate regularly
stable neurological condition	absence during final evaluation
written informed consent	-

After applying these criteria, 30 patients were excluded, leaving 100 patients for final analysis.

Clinical and instrumental assessment. The diagnosis of ischemic stroke was confirmed using magnetic resonance imaging (MRI) and computed tomography (CT). MRI examinations included DWI, FLAIR, T1-weighted and T2-weighted sequences to identify ischemic lesions.

Additional diagnostic procedures included Doppler ultrasonography of the brachiocephalic arteries, electrocardiography (ECG), and echocardiography (EchoCG). These examinations were carried out to further clarify the etiology of ischemic stroke and to identify possible comorbid cardiovascular conditions that could influence the clinical course of the disease and the rehabilitation process.

Distribution of stroke localization. Stroke localization was classified according to vascular territory using MRI findings (Table 3, Figure 1).

Table 3.

Distribution of ischemic stroke localization

Localization	Psychomotor group (n=50)	Control group (n=50)
Left hemisphere (ACA + MCA)	11 (22%)	13 (26%)
Right MCA territory	17 (34%)	18 (36%)
Vertebrobasilar territory	22 (44%)	19 (38%)

No statistically significant differences between groups were observed at baseline ($p > 0.05$).

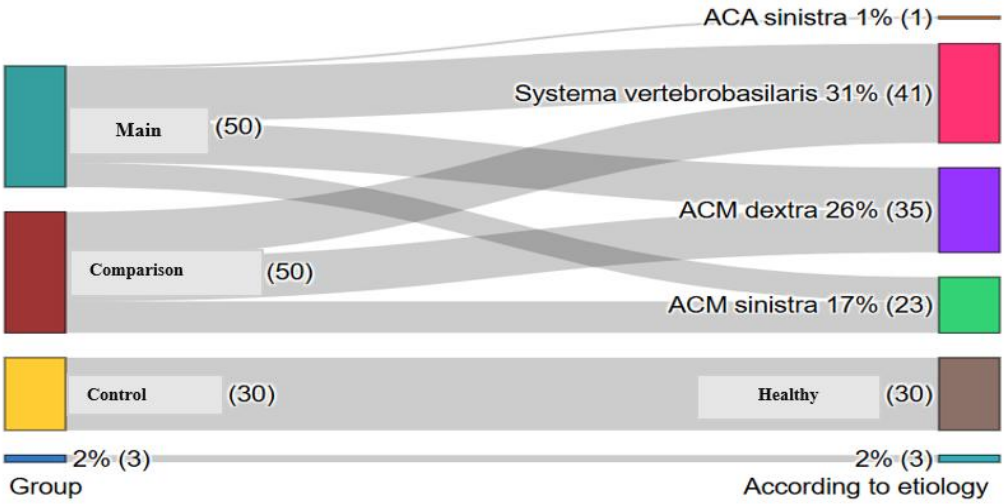


Figure 1. Distribution of stroke localization by vascular territory

Rehabilitation protocol. All participants received standard rehabilitation therapy including therapeutic exercises and functional training.

Patients in the intervention group additionally underwent psychomotor rehabilitation sessions consisting of:

- sensorimotor integration exercises
- coordination training
- rhythmic motor exercises
- task-oriented movement training
- body awareness exercises

The rehabilitation program lasted 8 weeks, with four sessions per week, each session lasting 60 minutes (Table 4).

Table 4.

Psychomotor rehabilitation protocol

Parameter	Value
Session duration	60 minutes
Sessions per week	4
Program duration	8 weeks
Total sessions	32

Recommended diagram structure:

- Warm-up (10 min)
- Sensorimotor exercises (15 min)
- Coordination and balance training (15 min)
- Task-oriented motor exercises (15 min)
- Relaxation and body awareness (5 min)
- Functional Outcome Measures

To comprehensively evaluate the effectiveness of the rehabilitation program, functional and psychoemotional outcomes were assessed using standardized and widely validated clinical scales.

These instruments were selected to capture multiple domains of recovery, including functional independence, motor performance, balance, and emotional status.

Functional independence in daily activities was assessed using the Barthel Index (BI), a widely used instrument for evaluating the level of independence in patients with neurological disorders. The scale reflects the patient's ability to perform essential activities of daily living such as feeding, bathing, dressing, toileting, transfers, mobility, and continence. The total score ranges from 0 to 100 points, where higher scores indicate greater functional independence and a lower level of disability. The Barthel Index is considered a reliable and sensitive tool for monitoring functional recovery during post-stroke rehabilitation.

Balance and postural stability were evaluated using the Berg Balance Scale (BBS), which is one of the most commonly applied clinical instruments for assessing balance performance in patients after stroke. The BBS consists of 14 functional tasks that evaluate both static and dynamic balance, including sitting, standing, transfers, reaching, turning, and single-leg stance. Each task is scored on a five-point scale (0–4), with a maximum total score of 56 points. Higher scores indicate better balance control and a lower risk of falls.

The use of both the Barthel Index and the Berg Balance Scale allows for a comprehensive evaluation of rehabilitation outcomes, as these instruments assess two key components of post-stroke recovery: functional independence in daily activities and postural stability. These measures are widely recommended in clinical and research settings for evaluating the effectiveness of rehabilitation interventions in stroke patients.

All outcome measures were administered twice: at baseline (before the start of rehabilitation) and after completion of the 8-week intervention period. This allowed for the assessment of both within-group changes and between-group differences over time.

Statistical Analysis. Statistical analysis was performed in accordance with the study design, with a significance level set at $p < 0.05$. Descriptive statistics were used to summarize baseline characteristics, with continuous variables expressed as mean ± standard deviation and 95% confidence intervals, and categorical variables as frequencies and percentages.

Due to the ordinal nature of clinical scales and potential non-normal distribution, baseline comparisons between groups were conducted using the Mann-Whitney U test. Categorical variables were analyzed using the chi-square test.

To evaluate changes over time and differences between groups, a two-way mixed-design ANOVA was applied, with time (pre- and post-intervention) as a within-subject factor and group (psychomotor therapy vs. standard rehabilitation) as a between-subject factor. The primary focus was on the interaction effect (time × group), reflecting the effectiveness of the intervention.

Effect sizes were calculated using partial eta squared (η^2p) to assess the magnitude of observed effects. All analyses were performed using standard statistical software.

Results.

Baseline comparability of the study groups. Baseline comparability between the intervention and control groups was assessed to ensure the internal validity of the study design. Since several clinical variables were not normally distributed, the non-parametric Mann–Whitney U test ($\alpha = 0.05$) was used to compare the initial values between groups.

The analysis demonstrated no statistically significant differences between the groups at baseline for any of the evaluated clinical variables, including the Barthel Index (BI), Fugl–Meyer Assessment (FMA) subdomains, Berg Balance Scale (BBS), and Hospital Anxiety and Depression Scale (HADS) subscales ($p > 0.05$). These findings indicate that the intervention and control groups were clinically and functionally comparable prior to the initiation of rehabilitation, which allows subsequent differences to be attributed to the applied rehabilitation intervention rather than pre-existing disparities.

In contrast, the healthy reference group demonstrated significantly higher functional scores and lower psychoemotional symptom levels across all scales, reflecting the expected profile of a neurologically intact population (Figure 2., Table 5).

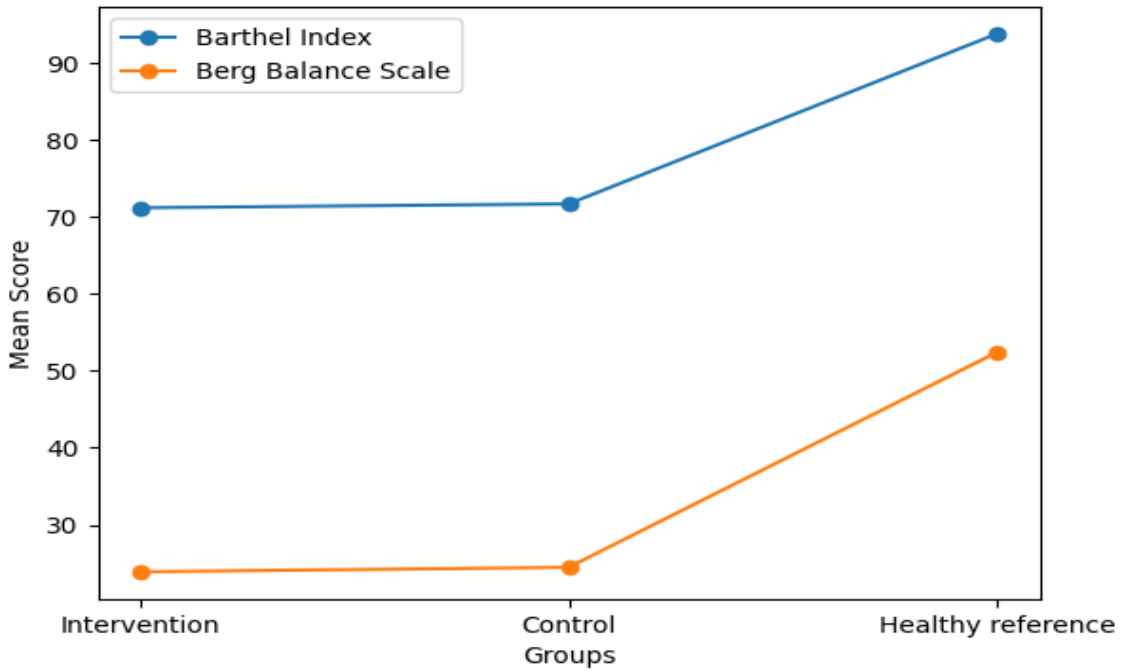


Figure 2. Baseline characteristics of the intervention and control groups according to functional and psychoemotional assessment scales

Table 5.

Baseline comparison of functional independence and balance across study groups (Barthel Index and Berg Balance Scale)

Scale	Intervention group	Control group	Healthy reference
Barthel Index	71.2	71.7	93.8
Balance Scale	23.88	24.46	52.4

Functional independence outcomes based on the Barthel Index. At the beginning of the rehabilitation program, the level of functional independence was comparable between the intervention and control groups. The mean Barthel Index score was 71.2 points in the intervention group and 71.7 points in the control group, with no statistically significant difference between groups ($p = 0.844$).

Following the 8-week rehabilitation program, improvements in functional independence were observed in both groups; however, the magnitude of improvement differed substantially. In the intervention group, the Barthel Index increased from 71.2 to 91.2 points, representing an average improvement of +20.0 points. In contrast, the control group demonstrated a more modest improvement from 71.7 to 77.5 points, corresponding to an average increase of +5.8 points (Figure 2.).

Across the entire sample, the mean Barthel Index score increased from 71.45 to 84.35 points, indicating an overall improvement in functional independence during the rehabilitation period (Table 6).

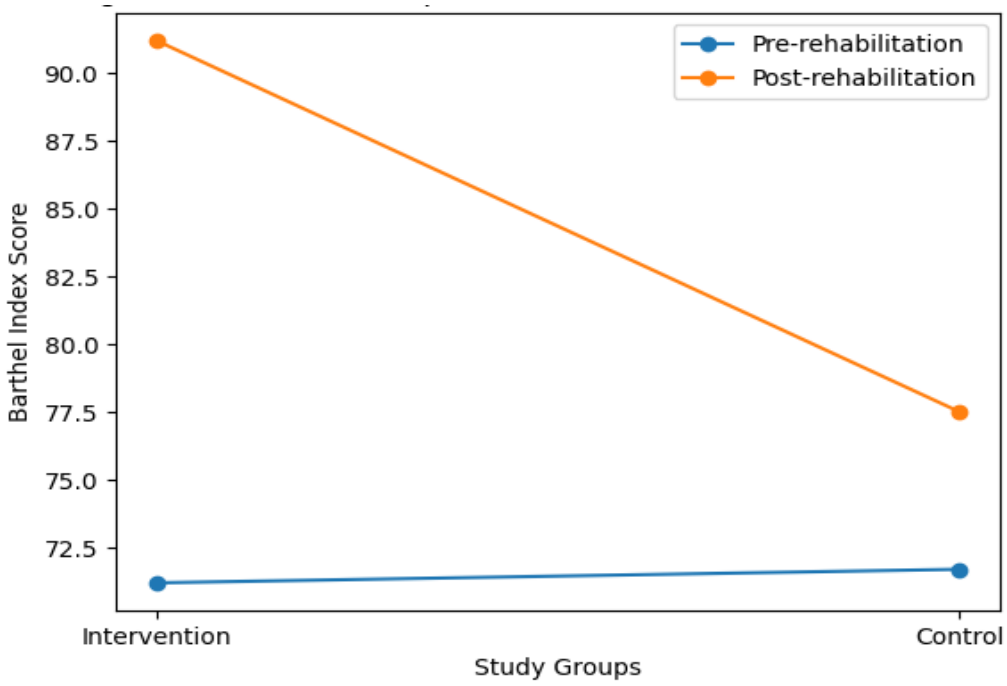


Figure 3. Changes in Barthel Index scores over time in the intervention and control groups

To further examine the effects of rehabilitation, a 2×2 mixed-design analysis of variance (ANOVA) was conducted, with time as the within-subject factor and group (intervention vs. control) as the between-subject factor.

The results demonstrated a significant main effect of time ($F(1,98) = 365$, $p < 0.001$, $\eta^2p = 0.79$), indicating a substantial overall improvement in functional independence during the rehabilitation period. The group effect was also statistically significant ($F(1,98) = 27.67$, $p < 0.001$, $\eta^2p = 0.22$), suggesting that functional outcomes differed between the intervention and control groups.

Importantly, the time × group interaction effect was highly significant ($F(1,98) = 110.57$, $p < 0.001$, $\eta^2p = 0.53$), indicating that the rate of functional recovery was significantly greater in the intervention group compared with the control group.

Table 6.

Mixed-design ANOVA results for the Barthel Index according to time and group factors

Factor	Sum of Squares	df	Mean Square	F	p	η^2	η^2p
BI (Pre vs Post)	8320.5	1	8320.5	365	<.001	0.36	0.79
Group	2178	1	2178	27.67	<.001	0.09	0.22
Time × Group	2520.5	1	2520.5	110.57	<.001	0.11	0.53
Residuals (Between)	7715	98	78.72				
Residuals (Within)	2234	98	22.8				

From a clinical perspective, the increase of the Barthel Index above 90 points in the intervention group indicates that most patients regained a high level of independence in daily activities. Although improvement was also observed in the control group, a certain degree of functional limitation remained.

Changes in balance and postural control (Berg Balance Scale). At baseline, the Berg Balance Scale (BBS) scores indicated comparable levels of balance impairment between groups. The mean

BBS score was 23.88 in the intervention group and 24.46 in the control group, suggesting moderate to severe balance impairment in both groups.

Across the entire sample, the baseline mean BBS value was 24.17, confirming substantial limitations in postural stability among the participants prior to rehabilitation.

Following the rehabilitation program, significant improvements were observed. The mean BBS score increased to 43.7 in the intervention group, while the control group reached 30.9 points. The overall post-rehabilitation mean score across the entire sample was 37.3, reflecting a general improvement in balance function.

The mean balance scores during the study period were 33.79 in the intervention group and 27.68 in the control group, indicating a greater recovery of postural stability in the intervention group (Figure 4).

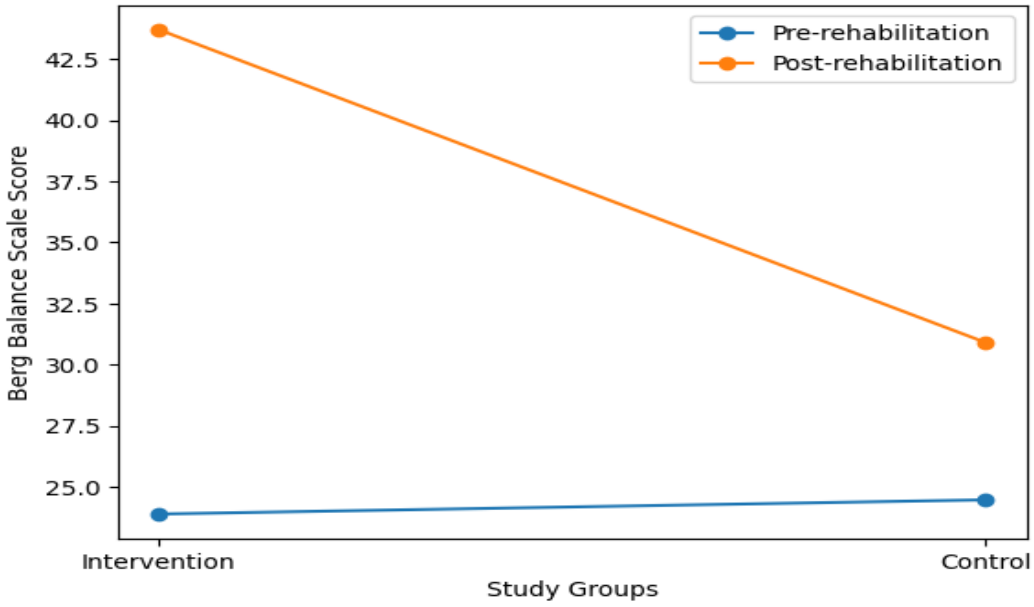


Figure 4. Dynamics of Berg Balance Scale scores in the intervention and control groups over the rehabilitation period

A 2×2 mixed-design ANOVA was performed to analyze the effects of time and group on balance performance.

The results revealed a significant main effect of time ($F(1,98) = 597.9$, $p < 0.001$, $\eta^2p = 0.86$), indicating a substantial improvement in balance function during the rehabilitation period. The group effect was also statistically significant ($F(1,98) = 157.17$, $p < 0.001$, $\eta^2p = 0.62$), suggesting differences in balance outcomes between the intervention and control groups.

Furthermore, the time × group interaction effect was highly significant ($F(1,98) = 155.22$, $p < 0.001$, $\eta^2p = 0.61$), indicating that the improvement in balance and postural control was significantly greater in the intervention group (Table 7).

Table 7.

Mixed-design ANOVA results for the Berg Balance Scale according to time and group factors

Factor	Sum of Squares	df	Mean Square	F	p	η^2	η^2p
BBS (Pre vs Post)	8619.84	1	8619.84	597.9	<.001	0.56	0.86
Group	1866.6	1	1866.6	157.17	<.001	0.12	0.62
Time × Group	2237.8	1	2237.8	155.22	<.001	0.15	0.61

Factor	Sum of Squares	df	Mean Square	F	p	η^2	$\eta^2 p$
Residuals (Between)	1163.85	98	11.88				
Residuals (Within)	1412.85	98	14.42				

These findings demonstrate that the applied rehabilitation intervention produced substantial improvements in both functional independence and balance performance, with significantly greater recovery observed in the intervention group.

Discussion. The present study evaluated the effectiveness of psychomotor therapy in improving functional independence and balance in patients undergoing rehabilitation after ischemic stroke. The results demonstrate that the integration of psychomotor therapy into a standard rehabilitation program leads to significantly greater improvements in both functional independence and postural stability compared with conventional rehabilitation alone.

At baseline, the intervention and control groups were comparable in terms of functional status and balance performance, which ensured methodological validity and allowed the observed changes to be attributed primarily to the applied rehabilitation intervention. The absence of statistically significant differences between the groups before treatment confirms that the groups were well balanced at the beginning of the study.

Following the 8-week rehabilitation program, patients who received psychomotor therapy showed a markedly greater improvement in functional independence as measured by the Barthel Index. The intervention group demonstrated an average increase of 20 points, reaching a mean score of 91.2, which indicates a high level of independence in activities of daily living. In contrast, the control group showed a more modest improvement of 5.8 points. These findings suggest that psychomotor therapy may accelerate functional recovery and facilitate a faster return to independent daily functioning.

A similar pattern was observed in balance outcomes. The Berg Balance Scale scores increased substantially in the intervention group compared with the control group, indicating a greater improvement in postural control and stability. Since impaired balance is one of the main factors contributing to falls and reduced mobility after stroke, improvements in this domain are clinically meaningful. The observed increase in balance scores in the intervention group suggests that psychomotor therapy may effectively enhance sensorimotor integration and postural control mechanisms that are essential for safe mobility.

The statistical analysis further confirmed the effectiveness of the intervention. The significant time effects observed for both the Barthel Index and the Berg Balance Scale indicate that rehabilitation overall contributed to functional recovery. However, the strong time × group interaction effects demonstrate that the magnitude of improvement was significantly greater in the psychomotor therapy group. The large effect sizes obtained in the analysis suggest that the intervention had a clinically meaningful impact on patient outcomes.

The observed improvements may be explained by the multidimensional nature of psychomotor therapy. This therapeutic approach integrates motor training with proprioceptive stimulation, body awareness exercises, and coordinated movement tasks. Such interventions may stimulate neuroplastic processes within the central nervous system and promote the reorganization of motor control networks following ischemic brain injury. Additionally, psychomotor therapy emphasizes purposeful and rhythm-based movements, which may further facilitate motor relearning and improve coordination and balance.

From a clinical perspective, the improvement of the Barthel Index above 90 points in the intervention group indicates that most patients regained a high level of independence in everyday activities. Similarly, the substantial increase in Berg Balance Scale scores suggests improved postural

control and a potentially reduced risk of falls. These outcomes highlight the potential value of incorporating psychomotor therapy into comprehensive stroke rehabilitation programs.

Overall, the findings of the present study support the growing evidence that multidimensional rehabilitation approaches targeting both motor and sensorimotor integration can enhance recovery after stroke. Psychomotor therapy may therefore represent a promising complementary intervention for improving functional independence and balance in patients recovering from ischemic stroke.

Study Limitations. Despite the promising results, several limitations of the present study should be acknowledged.

First, the study was conducted within a single clinical setting, which may limit the generalizability of the findings to other rehabilitation centers or healthcare systems. Multicenter studies involving larger and more diverse patient populations would provide stronger evidence regarding the effectiveness of psychomotor therapy.

Second, the duration of the follow-up period was limited to the rehabilitation phase. Although significant improvements were observed after eight weeks of therapy, long-term follow-up would be necessary to determine whether the observed functional gains are maintained over time.

Third, while the study included validated clinical outcome measures such as the Barthel Index and the Berg Balance Scale, additional objective assessments of motor performance and gait parameters could provide a more comprehensive evaluation of functional recovery.

Finally, although the randomized design strengthened the internal validity of the study, the open-label nature of the intervention may introduce potential performance or expectation biases. Future studies incorporating blinded outcome assessment and larger randomized controlled designs would further strengthen the evidence base.

Despite these limitations, the present study provides important insights into the potential benefits of psychomotor therapy in post-stroke rehabilitation and supports its integration into multidisciplinary rehabilitation programs aimed at improving functional independence and balance recovery.

Conclusion. The results of this study demonstrate that psychomotor therapy can significantly enhance functional independence and balance in patients undergoing rehabilitation after ischemic stroke. At baseline, the intervention and control groups were comparable in terms of functional status and balance performance, with Barthel Index scores of 71.2 and 71.7 respectively, and Berg Balance Scale scores of 23.88 and 24.46, confirming the methodological comparability of the groups prior to rehabilitation.

After the 8-week rehabilitation program, substantial improvements were observed in both outcome measures, with markedly greater changes in the psychomotor therapy group. Functional independence assessed by the Barthel Index increased by 20.0 points in the intervention group (from 71.2 to 91.2), compared with a 5.8-point improvement in the control group (from 71.7 to 77.5). Similarly, balance performance measured by the Berg Balance Scale improved from 23.88 to 43.7 in the intervention group, whereas the control group showed a more modest increase from 24.46 to 30.9.

Statistical analysis confirmed the robustness of these findings. Mixed-design ANOVA revealed a strong effect of time for both functional independence ($F(1,98)=365$, $p<0.001$, $\eta^2p=0.79$) and balance performance ($F(1,98)=597.9$, $p<0.001$, $\eta^2p=0.86$), indicating a substantial overall rehabilitation effect. Importantly, the significant time × group interaction effects for the Barthel Index ($F(1,98)=110.57$, $p<0.001$, $\eta^2p=0.53$) and Berg Balance Scale ($F(1,98)=155.22$, $p<0.001$, $\eta^2p=0.61$) demonstrate that improvements were significantly greater in patients receiving psychomotor therapy.

From a clinical perspective, the increase of the Barthel Index above 90 points in the intervention group suggests that most patients achieved a high level of independence in daily activities. Concurrently, the substantial improvement in Berg Balance Scale scores indicates enhanced postural stability and reduced risk of falls.

REFERENCES

1. Beltrán-Rodríguez, I., et al. (2022). Post-Stroke Rehabilitation: A Necessary Step. IntechOpen.

2. Blum, L., & Korner-Bitensky, N. (2008). Usefulness of the Berg Balance Scale in stroke rehabilitation. Physical Therapy, 88(5), 559–566.

3. Feigin, V. L., et al. (2021). Global, regional, and national burden of stroke and its risk factors, 1990–2019. The Lancet Neurology, 20, 795–820.

4. Johnson, C. O., et al. (2019). Global, regional, and national burden of stroke, 1990–2016. The Lancet Neurology, 18, 439–458.

5. Kwakkel, G., et al. (2015). Predicting activities after stroke: What is clinically relevant? Stroke, 46, 1482–1488.

6. Krishnamurthi, R. V., et al. (2015). Global burden of stroke: Epidemiology and risk factors. Neuroepidemiology, 45, 230–236.

7. Langhorne, P., Bernhardt, J., & Kwakkel, G. (2011). Stroke rehabilitation. The Lancet, 377, 1693–1702.

8. Li, J., et al. (2019). Rehabilitation for balance impairment in patients after stroke: A systematic review. BMJ Open, 9, e026844.

9. Mahoney, F. I., & Barthel, D. W. (1965). Functional evaluation: The Barthel Index. Maryland State Medical Journal, 14, 61–65.

10. Quinn, T. J., et al. (2011). Reliability of the Barthel Index for measuring activities of daily living in stroke patients. Stroke, 42, 1146–1151.

11. Veerbeek, J. M., et al. (2014). What is the evidence for physical therapy poststroke? PLoS ONE, 9, e87987.

12. Winstein, C. J., et al. (2016). Guidelines for adult stroke rehabilitation and recovery. Stroke, 47, e98–e169.

UDC: 616.155.392-053.2:611-018

PATHOLOGOANATOMICAL FEATURES OF CHILDHOOD LEUKEMIAS: MORPHOLOGY OF ACUTE LYMPHOBLASTIC LEUKEMIA

Sardor U. Zubtiyev - assistant
Shakhboz H. Abdulloyev - assistant
Tashkent State Medical University, Eurasian Multidisciplinary University, Republican Center of Pathological Anatomy (Tashkent, Uzbekistan)
Gulkhayyo B. Orifova - student
Tashkent State Medical University (Tashkent, Uzbekistan)
sardoruktamovich@gmail.com

Abstract. *Acute lymphoblastic leukemia (ALL) in children is one of the most common malignant disorders of the hematopoietic system. This study investigates the pathologoanatomical and morphological features of ALL. Findings revealed diffuse infiltration of blast cells in the bone marrow, lymph nodes, spleen, liver, and thymus. Histological analysis demonstrated high proliferative activity of blasts and suppression of normal hematopoiesis. Immunohistochemical results confirmed the expression of CD10, CD19, and TdT markers in B-ALL, while CD3 was characteristic for T-ALL. The obtained data indicate the systemic nature of organ involvement in ALL and highlight the importance of morphological examination in early diagnosis.*

Keywords: *acute lymphoblastic leukemia; children; pathomorphology; bone marrow; blast cells; immunohistochemistry; thymus.*

Introduction.

Acute lymphoblastic leukemia (ALL) is a highly aggressive malignant disease of the hematopoietic system characterized by uncontrolled clonal proliferation of lymphoid precursor cells (lymphoblasts) resulting from genetic and epigenetic alterations. This pathology occupies a leading position in pediatric oncohematology, accounting for 25–30% of all oncological diseases diagnosed in children aged 0–14 years.

According to global epidemiological data, the annual incidence of ALL is 3–5 cases per 100,000 children, with the highest frequency observed between 2 and 5 years of age. Although the use of modern polychemotherapy protocols and risk stratification systems has increased the 5-year overall survival rate to 85–90%, the problem of relapse and resistant forms remains highly relevant. In this regard, an in-depth study of the pathoanatomical and morphological basis of the disease is essential for improving diagnostic accuracy, determining prognosis, and developing individualized therapeutic strategies.

The central mechanism in the pathogenesis of ALL involves disruption of proliferation, apoptosis, and differentiation processes in lymphoid precursor cells. This process is often associated with chromosomal translocations (e.g., t(12;21), t(9;22)), gene mutations, and activation of signaling pathways such as NOTCH1 and JAK-STAT. As a result, massive accumulation of blast cells occurs in the bone marrow, leading to suppression of normal hematopoiesis and infiltration into the peripheral blood and extramedullary organs.

Pathoanatomical examination is one of the key components in the diagnosis of ALL, as it enables identification of the morphological substrate of the disease at the organ and tissue level. This approach includes classical histological (H&E), cytological, immunohistochemical (CD markers), as well as molecular genetic methods. In particular, determining the phenotypic and genetic characteristics of blast cells plays a decisive role in the differential diagnosis of disease variants and in the formation of risk groups.

This article provides a systematic analysis of the pathoanatomical and morphological features of ALL in children based on modern international classifications (WHO 2022), and highlights in detail the multi-organ involvement of the disease as well as its key diagnostic markers.

Literature Review and Historical Background

Scientific understanding of leukemia first emerged in the mid-19th century. In 1845, Rudolf Virchow and John Hughes Bennett independently described the condition as “white blood disease.” At that time, the disease was explained by a marked increase in leukocytes in the peripheral blood; however, its clonal and malignant nature was established later.

In the second half of the 20th century, advances in cytological and histological methods enabled the development of morphological classifications of leukemia. In 1976, the Franco-American-British (FAB) cooperative group proposed a classification that divided acute lymphoblastic leukemia into L1, L2, and L3 types. This classification was based on the morphological characteristics of blast cells and was widely used in clinical practice for many years. However, its main limitation was the lack of consideration of immunophenotypic and molecular genetic parameters.

Subsequently, the multiparametric classification proposed by the World Health Organization (WHO), with updates in 2001, 2008, 2016, and 2022, marked a significant breakthrough in leukemia evaluation. In particular, the 5th edition of the WHO classification (2022) ensures high diagnostic accuracy by integrating morphology, immunophenotype, cytogenetics, and molecular genetics. According to this system, B-lymphoblastic leukemia/lymphoma and T-lymphoblastic leukemia/lymphoma are defined as distinct nosological entities.

In modern scientific literature, the pathomorphological features of ALL have mainly been studied in relation to blast infiltration in the bone marrow and lymphoid organs. However, the mechanisms of extramedullary involvement (including the liver, spleen, thymus, and central nervous system) and their clinical and prognostic significance remain insufficiently elucidated.

In Uzbekistan, significant research has also been conducted on pediatric leukemia. In particular, the Tashkent Pediatric Medical Institute and the Republican Specialized Oncology and Hematology Centers have studied the clinical and morphological features of ALL. Nevertheless, comprehensive analyses based on a pathoanatomical approach (combining morphology, immunohistochemistry, and molecular methods) remain relatively limited, highlighting the relevance of further in-depth research in this field.

Aim of the Study.

The aim of this study is to comprehensively investigate the pathoanatomical and morphological features of acute lymphoblastic leukemia (ALL) in children, to determine the degree of blast cell infiltration in the bone marrow and extramedullary organs, and to evaluate the immunophenotypic variants of the disease based on immunohistochemical markers (TdT, CD10, CD19, CD3, CD7, Ki-67).

In addition, an important objective of the study is to improve the diagnostic criteria of ALL based on the obtained morphological and immunophenotypic findings, as well as to assess their clinical and prognostic significance.

Materials and Methods.

This study was retrospective and analytical in design, including clinical, laboratory, and pathoanatomical data from 148 patients aged 0–15 years diagnosed with acute lymphoblastic leukemia (ALL) between 2018 and 2023 in specialized pediatric oncology and hematology institutions of the Republic of Uzbekistan.

To establish the pathoanatomical diagnosis, a комплекс of morphological examinations was performed. Histological analysis was conducted using hematoxylin–eosin (H&E) staining, allowing assessment of the degree of blast cell infiltration and the extent of disruption of tissue architecture in the bone marrow and other tissues. Cytological examination was carried out using bone marrow aspirates, where the percentage of blast cells was determined; a threshold of >25% blasts was considered a diagnostic criterion.

In addition, immunohistochemical analysis was used to determine the immunophenotype of the cells. The TdT marker was applied to confirm lymphoid precursor cells; CD10 and CD19 were used to identify B-cell acute lymphoblastic leukemia, while CD3 and CD7 markers were used to identify the T-cell variant. The proliferative activity was assessed using the Ki-67 index, which reflects the degree of blast cell division and biological aggressiveness.

Statistical analysis was performed using SPSS version 26.0. Quantitative data were expressed as mean ± standard error (M ± m). Categorical variables were analyzed using the chi-square (χ^2) test to assess differences between groups. In cases of small sample sizes ($n < 5$), Fisher's exact test was applied. Comparisons of quantitative variables were performed using Student's t-test under conditions of normal distribution. When the data did not follow a normal distribution, the Mann–Whitney U test was used.

A p-value of < 0.05 was considered statistically significant.

Results and Discussion.

During the study, the clinical-demographic, morphological, and immunophenotypic characteristics of 148 patients aged 0–15 years diagnosed with acute lymphoblastic leukemia (ALL) were comprehensively analyzed. The obtained results made it possible to identify sex- and age-related features of the disease in children, as well as its morphological substrate.

According to the demographic analysis, ALL was found to occur more frequently in males, suggesting that genetic and hormonal factors may play an important role in the development of the disease. Analysis of age distribution revealed that the highest incidence was observed in children aged 2–5 years, which can be explained by the period of active proliferation of lymphoid tissues.

Morphological examination revealed massive infiltration of blast cells in the bone marrow, accompanied by marked suppression of normal hematopoietic elements. Blast cells were characterized by a high nuclear-to-cytoplasmic ratio, fine chromatin structure, and the presence of multiple nucleoli. These changes represent the principal pathomorphological features of the disease and lead to the development of cytopenias in the peripheral blood

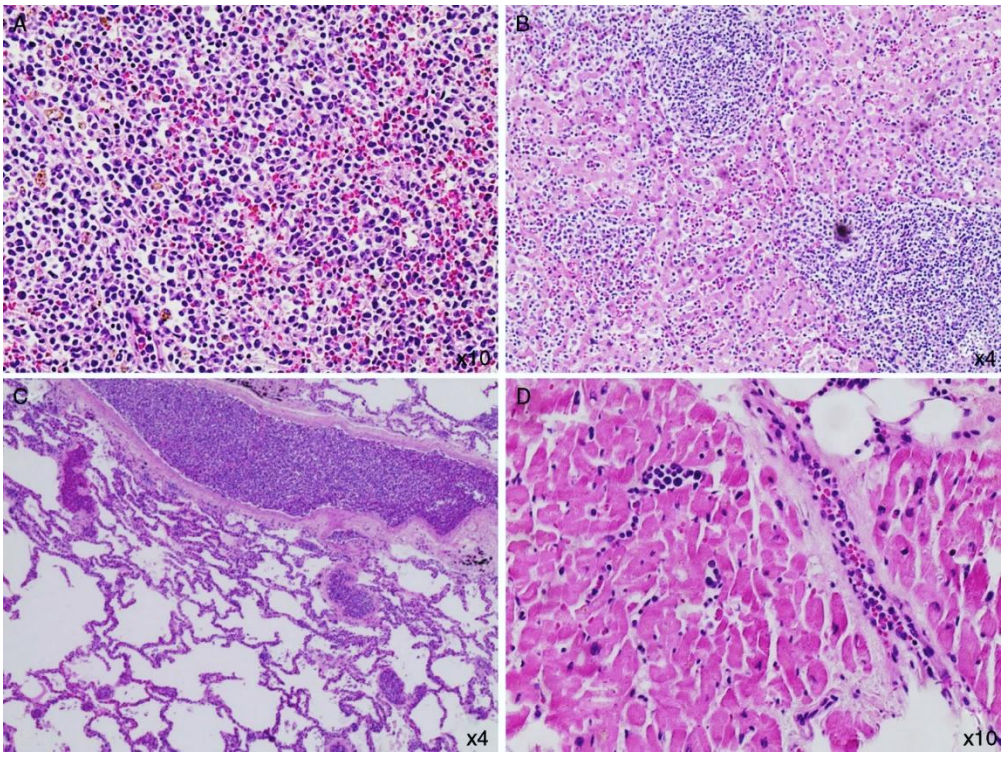


Figure 1. A–D. Infiltration of Blast Cells in Various Organs in Acute Lymphoblastic Leukemia (ALL) (H&E Staining)

A (×10): Diffuse blast infiltration is observed in the bone marrow tissue. Normal hematopoietic elements are almost completely replaced. Blast cells are characterized by a high nuclear-to-cytoplasmic ratio, fine chromatin, and distinct nucleoli, indicating malignant proliferation.

B (×4): Diffuse infiltration of blast cells is detected in the liver parenchyma along the portal tracts and sinusoids. Hepatocytes appear compressed, with focal dystrophic changes observed in some areas. These findings reflect the extramedullary spread of ALL.

C (×4): Accumulation of blast cells is observed in the interstitial and perivascular regions of the lung tissue. Although the alveolar architecture is partially preserved, interstitial infiltration may impair gas exchange.

D (×10): In the myocardial tissue, perivascular and interstitial blast infiltration is observed. The presence of leukemic cells between cardiomyocytes may lead to functional impairment of the myocardium.

Significant morphological changes were also observed in extramedullary organs. In lymph nodes, complete disruption of normal architecture and diffuse blast infiltration were identified, indicating impairment of immune system function. In the spleen, infiltration of the red pulp and a reduction in white pulp elements were noted, while in the liver, accumulation of blast cells was observed within portal tracts and sinusoids.

Notably, in the T-ALL variant, marked enlargement of the thymus and disruption of corticomedullary differentiation were observed, confirming the central role of the thymus in the pathogenesis of the disease.

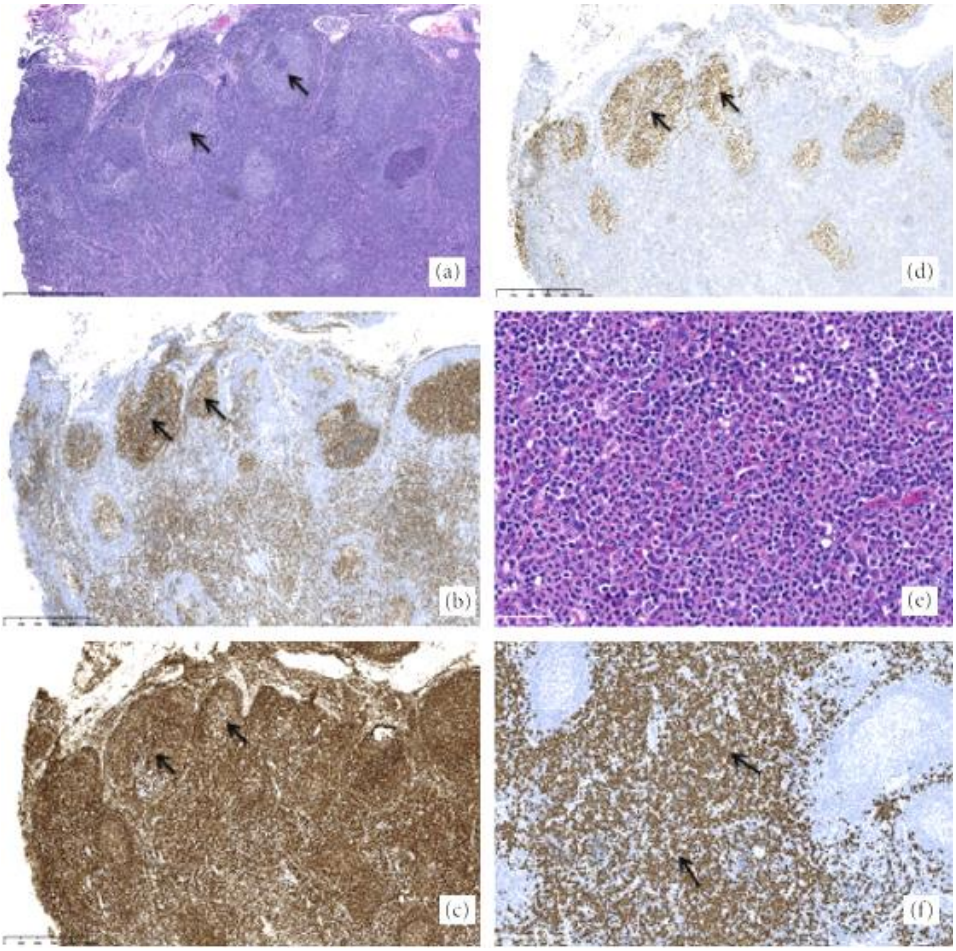


Figure 2. (a–f). Morphological and Immunohistochemical Features of Lymphoid Tissue in Acute Lymphoblastic Leukemia (ALL)

(a) (H&E): The overall architecture of the lymph node is disrupted, with loss of distinction between cortical and medullary zones. Due to diffuse blast infiltration, normal lymphoid follicles are compressed or completely absent (indicated by arrows). This reflects malignant transformation of lymphoid tissue.

(b) (IHC, CD20/CD10): Focal expression of B-cell markers is detected in certain areas of the lymphoid infiltrate (indicated by arrows). This indicates B-lineage differentiation of the blast cells.

(c) (IHC, TdT): Diffuse and intense nuclear staining is observed throughout the lymphoid tissue, confirming a high presence of lymphoid precursor cells. The widespread expression of TdT is a key diagnostic criterion for ALL.

(d) (IHC, Ki-67): The proliferation index is elevated, with a significant proportion of lymphoid cells showing Ki-67 positivity. This reflects high mitotic activity and the aggressive biological behavior of the disease.

(e) (H&E, high magnification): Blast cell morphology is clearly visible: a high nuclear-to-cytoplasmic ratio, fine chromatin, and prominent nucleoli. The cytoplasm is scant and basophilic, features typical of lymphoblasts.

(f) (IHC, CD3/CD7): Expression of T-cell markers is detected in certain areas (indicated by arrows), suggesting a T-cell variant of ALL or the possibility of a mixed immunophenotype.

Note: These histological images clearly demonstrate the main pathomorphological hallmark of ALL in lymphoid tissue—diffuse blast infiltration and loss of normal architecture. Immunohistochemical findings confirm the precursor nature of blast cells (TdT+), their high proliferative activity (Ki-67↑), and immunophenotypic variability (B- and T-cell markers).

The widespread expression of TdT confirms the origin of the disease from undifferentiated lymphoid precursor cells, while the elevated Ki-67 index reflects its aggressive biological behavior. Identification of immunophenotype using CD markers is crucial for distinguishing between B-ALL and T-ALL, which plays a decisive role in determining prognosis and treatment strategy.

Immunohistochemical analysis showed that the majority of patients belonged to the B-cell variant (CD10+, CD19+), consistent with global literature data. The T-cell variant (CD3+, CD7+) was less frequent but was associated with a more aggressive clinical course. Universal positivity for TdT in all patients confirmed the presence of lymphoid precursor cells and reinforced its diagnostic value. The high Ki-67 proliferation index reflects intensive blast cell division and indicates the biological aggressiveness of the disease, with higher levels correlating with more rapidly progressing forms of ALL.

Table 1.

Clinical, demographic, and immunophenotypic characteristics of children with acute lymphoblastic leukemia (ALL) (n = 148)

Indicators	Groups	n	%
Gender	Male	86	58,1
	Female	62	41,9
Age groups	0–2 age	28	18,9
	2–5 age	64	43,2
	6–10 age	36	24,3
	11–15 age	20	13,6
Immunophenotype	B-ALL (CD10+, CD19+)	112	75,7
	T-ALL (CD3+, CD7+)	36	24,3
TdT ekpression	Positive	148	100
	Negative	0	0
Ki-67 index	≥70%	109	73,6
	<70%	39	26,4

Note: Among children with acute lymphoblastic leukemia, a predominance of male patients is observed, with the highest incidence occurring in the 2–5-year age group. Immunophenotypic analysis showed that the majority of patients belong to the B-cell variant, while the T-cell form is relatively rare. Universal positive expression of the TdT marker in all cases confirms that it is a characteristic feature of lymphoid precursor cells. The high level of the Ki-67 proliferation index indicates intensive proliferation of blast cells and high biological activity of the disease. These findings confirm that ALL is characterized by an aggressive course and multisystem involvement, and they also highlight the high diagnostic value of immunohistochemical markers.

Table 2.

Pathomorphological and Immunophenotypic Characteristics of Organs in Children with Acute Lymphoblastic Leukemia (ALL) (n=148)

Organ	(n)	%	Macroscopic changes	Microscopic changes	Immunohistochemical merkers	Diagnostic significance
Bone marrow	148	100	Hyper-cellularity	Blast infiltration (>25%), suppression of hemato-poiesis	TdT+ (148), CD10/CD19+ (112), CD3/CD7+ (36), Ki-67↑ (109)	Main diagnostic criterion
Spleen	102	68,9	Spleno-megaly	Red pulp infiltration, reduction of white pulp	TdT+, Ki-67↑	Extramedul-lary spread
Liver	96	64,9	Hepa-tomegaly	Portal and sinusoidal infiltration	TdT+, CD markers	Systemic involvement
Lymph nodes	118	79,7	Lympha-denopathy	Architectural disruption, diffuse infiltration	CD10/CD19+, CD3/CD7+, Ki-67↑	Immuno-phenotyping

Note: According to the obtained results, bone marrow involvement was detected in 100% of patients, confirming that it is the main diagnostic criterion for ALL. Lymph node involvement was recorded in 79.7% of cases, and it was found to be more frequent compared to the liver (64.9%) and spleen (68.9%). Immunophenotypic analysis showed that the B-ALL variant was identified in 75.7% (n=112) of cases, while T-ALL was detected in 24.3% (n=36), and this difference was statistically significant (χ^2, $p < 0.05$). A high Ki-67 proliferation index (73.6%; n=109) indicated intensive proliferative activity of blast cells. Extramedullary organ involvement exceeded 60% overall, confirming that ALL is a systemic disease. Differences in the frequency of organ involvement were considered important factors affecting clinical course and prognosis.

When compared with modern scientific literature, the main pathomorphological features of ALL were confirmed to include multisystem blast infiltration, suppression of hematopoiesis, and involvement of immune system organs [1–5]. In addition, immunophenotypic markers were shown to be important diagnostic tools for disease identification, differential diagnosis, and prognosis assessment.

In the context of Uzbekistan, several factors limit the full implementation of pathological and anatomical examination, including a shortage of immunohistochemical reagents, a lack of cytogenetic

laboratories, and a shortage of qualified specialists. Addressing these issues would significantly contribute to the development of pediatric oncohematology in the country [3].

In comparison with global practice, the remission rate of ALL in Uzbekistan is somewhat lower than global indicators, which may be associated with delayed diagnosis, limited access to biological diagnostic methods, non-adherence to treatment protocols, and the presence of comorbidities.

Overall, morphological changes and immunophenotypic characteristics in the pathogenesis of ALL are closely interconnected [3,5,7] and serve as key factors determining the clinical course and outcome of the disease. Therefore, a comprehensive pathoanatomical and immunohistochemical approach is essential for early diagnosis and the development of effective treatment strategies.

Conclusion

Acute lymphoblastic leukemia (ALL) is one of the most common hematological malignancies among children, in which the uncontrolled proliferation of lymphoid precursor cells plays a central role in its pathogenesis. The results of the conducted study demonstrated that the main pathomorphological changes in ALL are characterized by massive infiltration of blast cells in the bone marrow and suppression of normal hematopoiesis [6–8].

In addition, infiltration of blast cells was identified in the liver, spleen, and lymph nodes, confirming the systemic nature of the disease. Immunohistochemical analysis revealed the predominance of the B-cell variant (CD10+, CD19+) and a relatively lower occurrence of the T-cell form. The universal expression of the TdT marker confirmed the presence of lymphoid precursor cells, while the high Ki-67 index indicated a high proliferative activity of the disease [9–12].

The obtained results demonstrate that pathoanatomical and immunohistochemical examinations are of great importance in the diagnosis of ALL, and that these indicators play a crucial role in assessing the prognosis of the disease. Therefore, a comprehensive morphological approach is of significant scientific and practical importance for the early detection of ALL and the development of effective treatment strategies.

REFERENCES

1. Bennett JM, Catovsky D, Daniel MT, et al. Proposals for the classification of the acute leukaemias. FAB Co-operative Group. British Journal of Haematology. 1976;33(4):451–458.

2. Bekov A, Tursunova G. Clinical features of acute lymphoblastic leukemia in children. Uzbekistan Medical Journal. 2020;(3):44–49.

3. Borowitz MJ, Bene MC, Harris NL, et al. Acute leukaemias of ambiguous lineage. In: WHO Classification of Tumours of Haematopoietic and Lymphoid Tissues. 2008.

4. Conter V, Bartram CR, Valsecchi MG, et al. Molecular response to treatment redefines all prognostic factors in children and adolescents with B-cell precursor ALL. Blood. 2010;115(16):3206–3214.

5. Coustan-Smith E, Mullighan CG, Onciu M, et al. Early T-cell precursor leukaemia: a subtype of very high-risk acute lymphoblastic leukaemia. The Lancet Oncology. 2009;10(2):147–156.

6. Faderl S, O'Brien S, Pui CH, et al. Adult acute lymphoblastic leukemia: concepts and strategies. Cancer. 2010;116(5):1165–1176.

7. Hunger SP, Mullighan CG. Acute lymphoblastic leukemia in children. The New England Journal of Medicine. 2015;373(16):1541–1552.

8. Inaba H, Greaves M, Mullighan CG. Acute lymphoblastic leukaemia. The Lancet. 2013;381(9881):1943–1955.

9. Mullighan CG. The molecular genetic makeup of acute lymphoblastic leukemia. Hematology, American Society of Hematology Education Program. 2012;2012:389–396.

10. Pui CH, Robison LL, Look AT. Acute lymphoblastic leukaemia. The Lancet. 2008;371(9617):1030–1043.

11. Swerdlow SH, Campo E, Harris NL, et al. (eds.). WHO Classification of Tumours of Haematopoietic and Lymphoid Tissues. 5th ed. Lyon: IARC Press; 2022.

12. Vora A, Andreano A, Eden TO, et al. Influence of cranial radiotherapy on outcome in children with acute lymphoblastic leukemia treated with contemporary therapy. Journal of Clinical Oncology. 2016;34(9):919–926.

RELATIONSHIP BETWEEN COGNITIVE FUNCTION AND EMOTIONAL DISTURBANCES IN CHRONIC TINNITUS

Malika M. Raimova - D.M.Sc., professor, scientific supervisor
Muslima A. Makhkamova - Ph.D. student
Tashkent State Medical University (Tashkent, Uzbekistan)
mahkamovamuslima95@gmail.com

Abstract. *For many patients, tinnitus is an unpleasant condition that significantly interferes with their daily activities and reduces their quality of life, as it is very often accompanied by hearing loss, difficulty understanding speech, impaired attention and concentration, irritability, anxiety, and depression. The aim of our study is to explore the relationship between psychoemotional status and cognitive performance in patients with chronic tinnitus using standardized clinical tools. The study included 20 patients. We used widely applied standardized questionnaires such as the Tinnitus Handicap Inventory (THI) to assess tinnitus severity and its impact on patients' lives, the Hospital Anxiety and Depression Scale (HADS) to assess the psychoemotional background of patients, and the Montreal Cognitive Assessment (MoCA) to evaluate cognitive status. After obtaining the results and conducting the analysis, we established that patients with a pronounced degree of tinnitus showed worse results on the tests. This indicates that as tinnitus severity increases, cognitive status decreases and depression and anxiety worsens. For this reason, tinnitus should be diagnosed and treated comprehensively in order to improve patients' quality of life.*

Keywords*: tinnitus, anxiety, depression, psychoemotional status, cognitive status, THI, HADS, MoCA.*

Introduction.

Tinnitus (translated from Latin as "ringing") is the perception of sound in the ears in the absence of an external noise source. It can be unilateral or bilateral, acute or chronic, objective or subjective. Most patients describe this sensation as ringing in the ears, but the sounds can be high-frequency (similar to whistling or ringing) or low-frequency (hissing, buzzing, or humming) [1]. Tinnitus may accompany patients constantly or appear periodically. In all people with tinnitus, perception is individual. Although the noise is heard in the ears, in fact it arises in the neural circuits of the brain. This proves that tinnitus is not only a pathology of the auditory system, but also a condition that mainly affects the central nervous system [2]. Tinnitus is a complex condition with many possible causes. Usually, tinnitus is divided into two main groups: subjective tinnitus (when the noise is heard only by the patient, the most common) and objective tinnitus (a sound that can be heard both by the patient and by the physician using diagnostic instruments, a rare form) [3]. The etiology of tinnitus is very variable; the most common causes include sensorineural hearing loss, impaired microcirculation in the brain and inner ear, cervical syndrome, temporomandibular joint dysfunction, vascular changes, injuries, and tumors. Tinnitus is a widespread condition worldwide. According to the WHO, approximately 15% of the world's population suffers from tinnitus, of which only 20% seek medical care, while 80% tolerate it or believe it will resolve on its own. At the same time, about 6% of the population has a pronounced degree of tinnitus, which is an unfavorable indicator for their quality of life. About 1 in 10 adults experiences tinnitus, and approximately 1 in 100 it significantly reduces daily activity. With age, these indicators unfortunately increase. The annual increase in new cases is approximately 1% [4]. Long-standing tinnitus develops because of the formation of a pathological closed "vicious circle." Central and subcortical structures of the brain, with involvement of the limbic system, take part in the formation of this circle. For this reason, tinnitus is very often accompanied by depression and anxiety, as well as by disturbances of cognitive status. Published data show that symptoms of anxiety and depression are relatively common in this group of patients. According to

these data, it has been established that anxiety disorders occur in approximately 48% of patients with long-standing tinnitus, while signs of depression may be detected in up to 84% of cases [5]. In fact, the patient's subjective attitude toward this condition is also of great importance, because in patients with a lower level of acceptance of tinnitus it is associated with an increase in depressive manifestations and a deterioration in quality of life. At the same time, several studies report an association between severity of tinnitus and cognitive performance. Persistent internal noise may create an additional cognitive load, which can interfere with attention and information processing. Recognizing tinnitus as part of a wider network of brain functions enables more accurate assessment strategies and targeted interventions.

Materials and methods.

The study included 20 patients with chronic subjective tinnitus who were observed at a National Medical Center in Tashkent. All participants were older than 18 years. Patients with acute psychiatric conditions or decompensated somatic diseases were not included. Assessment was performed using standardized clinical scales. We assessed patients using standard clinical scales. We evaluated tinnitus severity with the Tinnitus Handicap Inventory (THI). We measured cognitive functioning with the Montreal Cognitive Assessment (MoCA), and we assessed psychoemotional status with the Hospital Anxiety and Depression Scale (HADS). Based on THI scores, the patients were divided into three groups according to tinnitus severity: a) mild tinnitus (n = 6) b) moderate tinnitus (n = 12) c) severe tinnitus (n = 2) (Table 1)

Table 1.

Psychoemotional and cognitive function indicators according to tinnitus severity

Groups	N	THI	HADS-A	HADS-D	MoCA
Mild tinnitus	6	28.3±7.1	5.83±1.47	4.50±1.05	26.2±1.2
Moderate tinnitus	12	46.0±6.4	13.33±3.01	8.00±1.54	23.4±2.6
Severe tinnitus	2	64.0±5.7	19.0±1.41	13.5±2.12	16.0±1.4

The results confirm that chronic tinnitus negatively affects quality of life. The most pronounced changes were observed in patients with a high degree of tinnitus severity. Specifically, higher THI scores corresponded to reduced MoCA scores and elevated HADS values

Results and discussion.

According to our observations, analysis of the data draws attention to the fact that patients with more pronounced tinnitus demonstrated significantly higher levels of depression and anxiety on the HADS questionnaire compared to other groups. Patients with severe tinnitus also showed the worst results on the MoCA scale. This may indicate a decrease in overall cognitive functioning, attention, and concentration. But in contrast, patients with milder symptoms of tinnitus showed relatively preserved cognitive function and lower levels of psychological burden. Based on our observations, tinnitus severity cannot be explained by auditory factors alone. It was established that tinnitus is closely interconnected with the psychoemotional background and cognitive status of patients. Our results also highlight the practical importance of evaluating these domains together in everyday neurological practice.

Conclusion.

Most patients with chronic tinnitus suffer from long-lasting noise in the ears and are prone to associated psychoemotional problems. It should be noted that cognitive changes are also an important component of the clinical picture of chronic tinnitus. In clinical settings, it may be helpful to look not only at tinnitus itself, but also at cognitive function and psychoemotional state, using tools like THI, MoCA, and HADS. The data obtained in this study highlight the importance of early identification of these changes to improve patients' quality of life and optimize treatment strategies.

REFERENCES

1. Boboshko M.Yu., Efimova M.V., Savenko I.V. Modern aspects of the diagnosis and treatment of tinnitus in the elderly. Vestnik Otorinolaringologii. 2011; (2): 23–25.

2. Chari DA, Limb CJ. Tinnitus. Medical Clinics of North America. 2018;102(6):1081-1093

3. Cima R.F.F., Mazurek B., Haider H., Kikidis D., Lapira A., Norena A., Hoare D.J. A multidisciplinary European guideline for tinnitus: diagnostics, assessment, and treatment. HNO. 2019; 67(Suppl 1): 10–42.

4. Effects of Tinnitus Severity on Cognitive, Emotional,and Sleep Outcomes in Older Adults with ControlledAge Related Hearing Loss Gurbet İpek ŞAHİN KAMIŞLI Posted Date: March 19th, 2026

5. Kuzovkov V.E., Megrelishvili S.M., Shcherbakova Ya.L. Tinnitus: etiology and pathogenesis. Russian Otorhinolaryngology. 2013; No. 4 (65): 69–73.

6. Newman C.W. et al. Development of the Tinnitus Handicap Inventory

7. Stulin I.D., Tardov M.V., Damulin I.V. Tinnitus: clinical and pathogenetic aspects. Zhurnal Nevrologii i Psikhiatrii im. S.S. Korsakov. 2021; 121(6): 100–105.

8. Tinnitus-associated cognitive and psychological impairments: a comprehensive review meta analysis Dong Yang 1 Front. Neurosci., 08 February 2024 Sec. Perception Science Volume 18 – 2024

9. Tinnitus: characteristics, causes, mechanisms, and treatments Byung In Han 1, Ho Won Lee, Tae You Kim, Jun Seong Lim, Kyoung Sik Shin Clin Neurol 2009 Mar;5(1):11-9. doi: 10.3988/jcn.2009.5.1.11. Epub 2009 Mar 31

10. Tinnitus risk factors and its evolution over time Lise Hobeika, Matt Fillingim, Christophe Tanguay-Sabourin,Mathieu Londero, Séverine Samson & Etienne Roy, Alain Vachon-Presseau Nature Communications volume 16, Article number: 4244 (2025)

11. Tinnitus and tinnitus disorder: Theoretical and operational definitions (an international multidisciplinary proposal). 2021; 260: 125.

12. The Impact of Tinnitus on Mental HealthBashar Ali Naji, Asad Hameed AlnajarVol 19 No 4 (2025) Journal of Modern Reabilitation

13. University of Illinois at Urbana-Champaign (2017) Ringing in ears keeps brain more at attention, less at rest, study finds. ScienceDaily, Aug. 25 22.

14. Zigmond A.S., Snaith R.P. Hospital Anxiety and Depression Scale. Acta Psychiatr Scand.

MORPHOLOGICAL ASSESSMENT OF APOPTOSIS AND NECROSIS SIGNS IN THE GASTRIC MUCOSA IN A MODEL OF HEPATORENAL SYNDROME

Sanjar F. Allaberganov - independent researcher
Urgench State Medical Institute (Urgench, Uzbekistan)
Dilorom B. Adilbekova - professor
Abdulaziz A. Akhrorov - student
Tashkent State Medical University (Tashkent, Uzbekistan)
zebooriginal@gmail.com

Abstract. Introduction: *Hepatorenal syndrome (HRS) is a severe complication of end-stage liver disease characterized by functional renal failure and accompanied by pronounced systemic and splanchnic hemodynamic disturbances. The impact of HRS on the integrity of the gastric mucosa, particularly the balance between apoptosis and necrosis of cells, remains insufficiently studied, although it has important clinical significance for assessing the risk of gastrointestinal bleeding.*

Objective: *To perform a detailed morphological and quantitative assessment of apoptosis and necrosis markers in the gastric mucosa using an experimental model of HRS.*

Materials and methods*: The study was conducted at the clinics of Tashkent State Medical University. HRS was modeled in 60 male Wistar rats using a two-stage protocol: common bile duct ligation (BDL) to induce secondary biliary cirrhosis, followed by a single intraperitoneal injection of carbon tetrachloride (CCl_4) to provoke acute-on-chronic liver failure and subsequent renal dysfunction. The animals were divided into three groups: Sham operation (n=20), cirrhosis (n=20), and HRS (n=20). Gastric mucosal samples were collected on day 28. Morphological evaluation was performed using hematoxylin–eosin (H&E) staining to identify necrotic changes and the TUNEL (terminal deoxynucleotidyl transferase dUTP nick end labeling) assay to detect apoptosis. Immunohistochemical expression of cleaved caspase-3, Bax, and Bcl-2 was also assessed.*

Results: *The HRS group demonstrated significantly more severe gastric mucosal injury compared with the cirrhosis group without HRS. The mean apoptosis index (TUNEL-positive cells per field) was 4.2±1.1 in the Sham group, 18.5±3.4 in the cirrhosis group, and reached 34.7±5.2 in the HRS group ($p<0.01$). Foci of coagulative necrosis were observed in 75% of HRS samples and only in 20% of cirrhosis samples. Immunohistochemical analysis revealed significant activation of the pro-apoptotic markers Bax and cleaved caspase-3, along with a decrease in the anti-apoptotic marker Bcl-2 in the HRS group, resulting in a shift of the Bax/Bcl-2 ratio toward apoptosis.*

Conclusion: *The development of HRS on the background of cirrhosis aggravates gastric mucosal injury, leading to a high level of both apoptotic and necrotic cell death. These findings suggest that the hemodynamic and metabolic disturbances characteristic of HRS create an unfavorable microenvironment in the gastric mucosa, promoting a mixed type of cell death that may contribute to an increased risk of erosions and gastrointestinal bleeding in such patients.*

Keywords: *Hepatorenal syndrome, gastric mucosa, apoptosis, necrosis, TUNEL assay, morphology, experimental model, caspase-3.*

Introduction. Hepatorenal syndrome (HRS) is a life-threatening complication of progressive cirrhosis and is defined by the International Ascites Club as a functional and potentially reversible form of renal failure that develops in the setting of severe hepatic insufficiency and portal hypertension. The pathophysiology of HRS is complex and multifactorial, primarily driven by pronounced splanchnic vasodilation, which leads to a reduction in the effective arterial blood volume. This, in turn, activates powerful vasoconstrictor systems, including the renin–angiotensin–aldosterone system (RAAS), the sympathetic nervous system (SNS), and the release of vasopressin,

ultimately resulting in intense renal vasoconstriction and a marked decrease in the glomerular filtration rate (GFR). Although renal dysfunction is the defining feature of HRS, the systemic and splanchnic hemodynamic disturbances characteristic of this condition exert widespread effects on other organs, including the gastrointestinal tract.

The gastric mucosa is particularly vulnerable to hypoperfusion and ischemia. In cirrhosis and portal hypertension, the gastric mucosa is already compromised, a condition commonly referred to as portal hypertensive gastropathy (PHG). PHG is characterized by dilated and tortuous submucosal vessels, reduced effective mucosal blood flow despite increased overall gastric blood flow, and increased susceptibility to injury from various toxic agents. A study by Zhang et al. (2023) significantly advanced the understanding of the molecular mechanisms of gastric injury in portal hypertension by demonstrating marked activation of hypoxia-inducible factor-1α (HIF-1α) in the gastric mucosa. Their work, published in *Digestive and Liver Disease*, identified a key pathway whereby HIF-1α, under hypoxic conditions, stabilizes and activates the tumor suppressor p53, thereby promoting apoptosis of gastric epithelial cells through modulation of the Bcl-2 family of proteins. Specifically, this involves increased expression of the pro-apoptotic protein Bax and decreased expression of the anti-apoptotic protein Bcl-2, leading to activation of cleaved caspase-3. This pathway establishes a direct link between the hemodynamic disturbances associated with portal hypertension and programmed cell death in gastric tissues.

Additional evidence regarding the role of apoptosis in intestinal injury during liver failure has been obtained from studies of acute liver failure (ALF). Song et al. (2005), in a study published in *World Journal of Gastroenterology*, demonstrated that tumor necrosis factor-alpha (TNF-α) acts as a key mediator of enterocyte apoptosis in a mouse model of ALF induced by D-galactosamine and lipopolysaccharide. They reported that the expression of tumor necrosis factor receptor 1 (TNFR1) in intestinal tissue was significantly increased and positively correlated with the level of enterocyte apoptosis measured by the TUNEL assay. This study emphasized that, in addition to the direct effects of hypoxia, circulating inflammatory cytokines—whose levels are markedly elevated in liver failure—can directly trigger apoptotic cascades in gastrointestinal epithelial cells.

Although these studies provide a strong foundation for understanding gastrointestinal injury in liver diseases, they mainly focus either on the chronic state of portal hypertension or on the acute phase of ALF. The specific and combined impact of HRS—where acute kidney injury develops on the background of chronic liver failure—on the gastric mucosa remains poorly characterized. The additional burden of renal failure introduces new pathological variables, including the accumulation of uremic toxins, metabolic acidosis, and further hemodynamic instability, all of which may exacerbate pre-existing gastric pathology. Distinguishing between apoptosis and necrosis in this context is also critically important. Apoptosis is a regulated, energy-dependent process of programmed cell death, whereas necrosis is generally a pathological and uncontrolled process resulting from excessive cellular stress and often associated with inflammation. In a clinical case reported by Takahashi et al. (2024), acute gastric mucosal necrosis was observed in a patient with short bowel syndrome and hepatorenal failure following treatment with teduglutide, highlighting the possibility of severe non-apoptotic gastric injury in the setting of multi-organ failure.

Given the above considerations, there is a clear need to investigate the morphological features of gastric mucosal injury in HRS. Understanding the relative contribution and morphological characteristics of apoptosis and necrosis may provide valuable insights into the pathogenesis of gastric complications in critically ill patients. The present study, conducted at the clinics of Tashkent State Medical University, aims to address this gap. The objective of the study is to experimentally induce HRS in a rodent model and to perform a comprehensive morphological and quantitative assessment of apoptosis and necrosis markers in the gastric mucosa using histochemical, TUNEL,

and immunohistochemical methods in order to clarify the nature and extent of epithelial cell death in the stomach under conditions of combined hepatic and renal failure.

Materials and Methods. The experimental study was conducted at the Department of Pathological Anatomy and the Central Research Laboratory of the clinics of Tashkent State Medical University.

A total of 60 adult male Wistar rats weighing 220–280 g were used. The animals were housed in standard polypropylene cages under controlled conditions (temperature 22±2°C, 12-hour light/dark cycle) with free access to standard chow and water. Before the start of the experiment, the animals were acclimatized for one week. The rats were randomly divided into three experimental groups (n = 20):

- **Sham operation (control):** midline laparotomy and manipulation of the common bile duct and liver without ligation or injection.
- **Cirrhosis (Cirr):** common bile duct ligation (BDL) to induce secondary biliary cirrhosis.
- **Hepatorenal syndrome (HRS):** BDL followed on day 21 after ligation by a single intraperitoneal injection of carbon tetrachloride (CCl_4, diluted 1:1 in olive oil, 2 ml/kg body weight) to model acute-on-chronic liver failure and provoke renal dysfunction.

Anesthesia was induced by intraperitoneal injection of ketamine (80 mg/kg) and xylazine (10 mg/kg). After a midline laparotomy, the common bile duct was isolated, double-ligated with non-absorbable silk sutures, and transected between the ligatures. The abdominal wall and skin were closed in layers with absorbable sutures. In the Sham group, the bile duct was isolated but neither ligated nor transected. Postoperatively, all animals received subcutaneous buprenorphine (0.05 mg/kg) for 48 hours for analgesia.

On day 28 after surgery (or on day 7 after CCl_4 injection for the HRS group), all animals were euthanized with an overdose of isoflurane. Blood samples were collected by cardiac puncture for serum biochemical analysis (ALT, AST, bilirubin, creatinine, and urea) to confirm the development of liver cirrhosis and HRS. The stomach was rapidly excised, opened along the greater curvature, and gently rinsed with ice-cold phosphate-buffered saline (PBS). Full-thickness samples from the gastric body were fixed in 10% neutral buffered formalin for 24 hours for histological and immunohistochemical analysis.

Morphological assessment: Formalin-fixed tissues were processed routinely, embedded in paraffin, and sectioned at a thickness of 4–5 μm. Sections were stained with hematoxylin and eosin (H&E) for general histological evaluation and detection of necrotic changes. Necrosis was identified by features such as cellular swelling (oncosis), karyolysis, cytoplasmic eosinophilia, and disruption of glandular architecture. The degree of mucosal necrosis was evaluated semi-quantitatively as follows: 0 = no necrosis; 1 = focal superficial necrosis; 2 = multifocal necrosis involving the upper third of the mucosa; 3 = confluent necrosis extending into the middle/deep mucosal layers.

Apoptosis was detected using the TUNEL (terminal deoxynucleotidyl transferase dUTP nick end labeling) assay. Deparaffinized and rehydrated sections were treated with proteinase K (20 μg/ml) for 15 min at 37°C. Endogenous peroxidase activity was blocked with 3% H_2O_2. Sections were incubated with the TUNEL reaction mixture (Roche Diagnostics, Germany) containing TdT and fluorescein-labeled dUTP for 60 min at 37°C in a humidified chamber. After washing, sections were incubated with anti-fluorescein antibody conjugated with peroxidase. The reaction was visualized using DAB, and sections were counterstained with hematoxylin. Negative controls were prepared without TdT. The apoptotic index (AI) was calculated as the percentage of TUNEL-positive epithelial cells per 1000 counted cells in 10 randomly selected non-overlapping high-power fields (HPF, 400×) per section.

Immunohistochemistry: Immunohistochemical analysis was performed to evaluate the expression of key apoptosis-related proteins: cleaved caspase-3 (pro-apoptotic executioner), Bax

(pro-apoptotic), and Bcl-2 (anti-apoptotic) using the streptavidin–biotin–peroxidase method. After deparaffinization, rehydration, and antigen retrieval (citrate buffer, pH 6.0, microwave heating for 15 min), sections were incubated overnight at 4°C with the following primary antibodies: polyclonal anti-cleaved caspase-3 (1:200, Cell Signaling), polyclonal anti-Bax (1:250, Abcam), and monoclonal anti-Bcl-2 (1:100, Dako). After washing, sections were incubated with biotinylated secondary antibodies followed by a streptavidin–peroxidase conjugate. DAB was used as the chromogen, and sections were counterstained with hematoxylin.

Immunopositivity was evaluated semi-quantitatively as the percentage of positive epithelial cells in 10 HPF. The immunoreactivity score (IRS) was calculated as the product of the percentage of positive cells (0:<5%; 1:5–25%; 2:26–50%; 3:51–75%; 4:>75%) and staining intensity (0:none; 1:weak; 2:moderate; 3:strong).

All morphological assessments were performed independently by two pathologists blinded to the experimental groups. Statistical analysis was conducted using GraphPad Prism 9.0. Data are presented as mean ± standard deviation (SD). Comparisons among multiple groups were performed using one-way ANOVA followed by Tukey's post hoc test. A value of $p<0.05$ was considered statistically significant.

Results. Serum biochemical analysis at the time of euthanasia confirmed the successful establishment of the experimental models. The BDL group demonstrated pronounced cholestasis, with significantly elevated total bilirubin, ALT, and AST levels compared with the Sham group ($p<0.01$). The HRS group (CCl_4 administration on the background of cirrhosis) showed a further significant increase in liver enzymes and, importantly, a marked elevation in serum creatinine and urea levels compared with both the Sham and Cirrhosis groups ($p<0.01$ vs. Cirr), confirming the development of acute renal failure on the background of chronic liver disease.

Histological examination of the gastric mucosa revealed clear differences among the groups:

- **Sham:** Normal histological structure. The surface epithelium was intact, and gastric pits and glands were well organized. No signs of inflammatory infiltration, edema, or cell death were observed (Fig. 1A).
- **Cirr:** Features consistent with portal hypertensive gastropathy. There was pronounced submucosal vascular congestion and dilation. The mucosa showed areas of interstitial edema and a moderate increase in inflammatory cells. Foci of epithelial damage with pyknotic nuclei and condensed cytoplasm were observed, indicating apoptosis. Foci of coagulative necrosis were rare—observed in only 20% (4/20) of samples—and were limited to the superficial epithelium.
- **HRS:** The most severe and extensive injury was observed in this group. In addition to vascular congestion, widespread destruction of the mucosal architecture was noted. Foci of coagulative necrosis were present in 75% (15/20) of samples ($p<0.001$ vs. Cirr). These lesions were characterized by sheets of epithelial cells with eosinophilic cytoplasm, karyorrhexis, and karyolysis, along with loss of normal glandular structure, frequently extending into the middle third of the mucosa (Fig. 1B). Marked edema, hemorrhage, and mixed inflammatory infiltrates were also observed in the surrounding tissue.

The TUNEL assay was used to quantitatively assess apoptosis. TUNEL-positive cells were identified by the characteristic brown nuclear staining.

- **Sham:** Only occasional TUNEL-positive cells were observed, reflecting the normal low level of epithelial turnover (Fig. 1C).

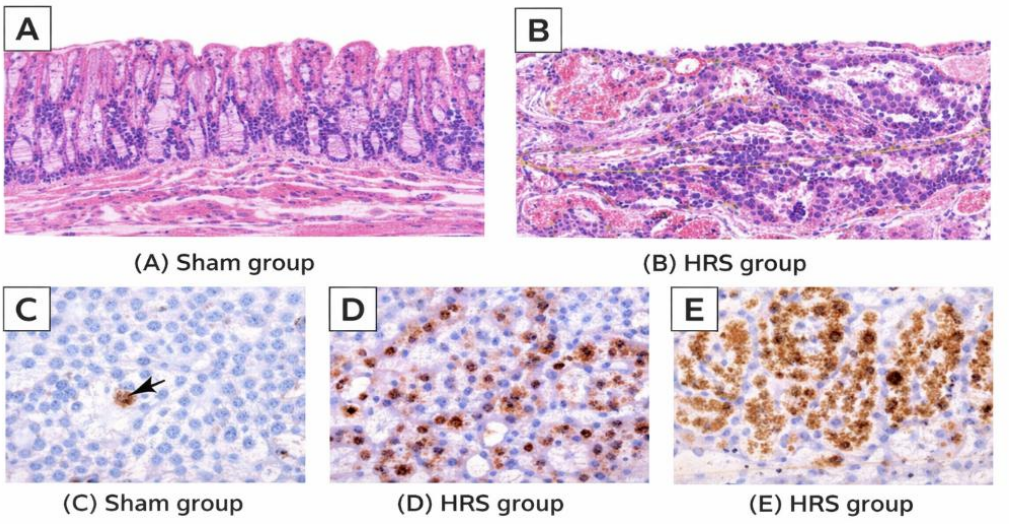


Fig. 1. Morphological and Immunohistochemical Analysis of the Gastric Mucosa

(A) Sham group: normal gastric mucosa (H&E, 200×).(B) HRS group: focus of coagulative necrosis with loss of glandular architecture and inflammatory infiltration (H&E, 200×).(C) Sham group: rare TUNEL-positive cells (arrow) (TUNEL, 400×).(D) HRS group: numerous TUNEL-positive apoptotic cells (brown nuclei) throughout the gastric mucosa (TUNEL, 400×).(E) HRS group: strong cytoplasmic immunostaining for cleaved caspase-3 in epithelial cells (IHC, 400×).

Cirrhosis group: In the cirrhosis group, a significant increase in the number of apoptotic cells was observed, predominantly located in the upper third of the gastric glands. The apoptotic index (AI) increased markedly to 18.5±3.4%**,** which was significantly higher than in the Sham group ($p<0.01$).

HRS group: The highest frequency of apoptosis was observed in the HRS group**.** TUNEL-positive cells were numerous and distributed throughout the full thickness of the mucosa. The AI in the HRS group reached 34.7±5.2%**,** which was significantly higher than in both the Sham and cirrhosis groups ($p<0.01$ vs. both groups) (Fig. 1D).

Immunohistochemistry**.** Bax and Bcl-2 expression: In the Sham group**,** the expression of the pro-apoptotic protein Bax was minimal, whereas the anti-apoptotic protein Bcl-2 showed moderate expression, resulting in a low Bax/Bcl-2 ratio (0.22) favoring cell survival. In the cirrhosis group, a significant shift was observed: Bax expression increased markedly while Bcl-2 expression decreased, leading to an increased Bax/Bcl-2 ratio of 1.38. The most pronounced pro-apoptotic shift was found in the HRS group, characterized by intense and widespread Bax expression together with weak, focal Bcl-2 expression, resulting in a Bax/Bcl-2 ratio of 4.67.

Cleaved caspase-3 expression: Cleaved caspase-3, an active executioner caspase, was used as a reliable marker of apoptosis. Its expression closely corresponded to the apoptotic index. In the Sham group, positive cells were rarely observed. In the cirrhosis group, a significant increase was noted (IRS 5.8±1.5). The highest expression was observed in the HRS group, characterized by strong cytoplasmic staining in numerous epithelial cells, particularly in regions adjacent to—but distinct from—necrotic foci (IRS 11.2±2.1, $p<0.01$ vs. Cirr) (Fig. 1E).

The simultaneous presence of foci of coagulative necrosis and a high apoptotic index in the HRS group indicates a mixed pattern of cell death. The gastric mucosa in HRS is subjected to such severe injury that both the regulated apoptotic pathway and the uncontrolled necrotic pathway are activated simultaneously.

Discussion. The results provide a detailed morphological characterization of gastric mucosal injury in an experimental model of hepatorenal syndrome. The damage observed in the HRS group was substantially more severe and qualitatively different from the changes seen in cirrhosis alone. The principal finding of this study is that the superimposition of acute renal failure on chronic liver disease creates a pathophysiological environment that induces both apoptosis and necrosis of gastric epithelial cells.

In the cirrhosis group, the findings are consistent with previously reported features of portal hypertensive gastropathy, including an increased apoptotic index and a shift in the Bax/Bcl-2 ratio toward apoptosis. Histologically, vascular congestion and mucosal edema—typical features of portal hypertension—were observed. However, the injury was largely limited to apoptosis, while necrotic changes were rare and superficial.

In contrast, the transition to the HRS group demonstrates a critical aggravation of mucosal injury. The marked elevation of creatinine and urea confirms the development of renal failure, which further exacerbates the existing hepatic dysfunction. The accumulation of uremic toxins**,** metabolic acidosis, and hemodynamic instability intensifies mucosal hypoperfusion. This leads to severe cellular energy depletion and a shift from apoptosis to necrosis, reflected by the presence of coagulative necrosis in 75% of samples. Despite this, a high level of apoptosis persists, as demonstrated by TUNEL positivity and increased cleaved caspase-3 expression. The markedly elevated Bax/Bcl-2 ratio (4.67) indicates activation of the intrinsic (mitochondrial) apoptotic pathway. The enhanced apoptotic activity likely results from a combination of chronic hypoxia (HIF-1α/p53 signaling) and systemic inflammatory and uremic toxicity (TNF-α), which may further activate the extrinsic apoptotic pathway.

The coexistence of apoptosis and necrosis in the HRS group suggests a necrosis–apoptosis continuum, in which cells that initially activate apoptotic pathways may ultimately undergo necrotic death under conditions of severe ATP depletion. This phenomenon has important clinical implications: apoptosis is generally a silent process, whereas necrosis provokes inflammation, disrupts the mucosal barrier, and significantly increases the risk of gastrointestinal bleeding.

Conclusion. This experimental study conducted at the clinics of Tashkent State Medical University demonstrates that hepatorenal syndrome significantly aggravates gastric mucosal injury compared with cirrhosis alone. The gastric mucosa is characterized by a mixed pattern of cell death, including markedly increased apoptosis (reflected by the Bax/Bcl-2 shift and caspase-3 activation) together with extensive foci of coagulative necrosis. These findings highlight that the gastric mucosa represents an important target organ in HRS and may partly explain the high risk of gastrointestinal bleeding in such patients. Therapeutic strategies for HRS should therefore consider protection of the gastric mucosal barrier alongside correction of hepatic and renal dysfunction.

REFERENCES

1. Gines, P., Krag, A., Abraldes, J. G., Sola, E., Fabrellas, N., & Kamath, P. S. (2021). Liver cirrhosis. The Lancet, 398(10308), 1359–1376.

2. Kamath, P. S., Lacerda, M., Ahlquist, D. A., McKusick, M. A., Andrews, J. C., & Nagorney, D. A. (2000). Gastric mucosal responses to intrahepatic portosystemic shunting in patients with cirrhosis. Gastroenterology, 118(5), 905–911.

3. Moll, U. M., & Zaika, A. (2001). Nuclear and mitochondrial apoptotic pathways of p53. FEBS Letters, 493(2–3), 65–69.

4. Nazarova, M. B., Adilbekova, D. B., Akhrorov, A. A., Toshpulatov, S. S., & Rustamova, F. O. (2025). The morphological and morphometrical state of the liver's in offspring born to mothers with chronic toxic hepatitis under conditions of medication correction before pregnancy (experimental study). Central Asian Journal of Medicine, eISSN: 2181-1326, 77–84.

5. Nazarova, M. B., Adilbekova, D. B., Akhrorov, A. A., Toshpulatov, S. S., & Rustamova, F. O. (2025). The morphological and morphometric state of the liver's vascular tissue structures in the offspring of intact experimental rats during postnatal ontogeny dynamics (experimental study). Central Asian Journal of Medicine, eISSN: 2181-1326, 50–57.

6. Ohta, M., Yamaguchi, S., Gotoh, N., & Tomikawa, M. (2002). Pathogenesis of portal hypertensive gastropathy: a clinical and experimental review. Surgery, 131(1), S165–S170.

7. Rockey, D. C. (2019). An update: portal hypertensive gastropathy and colopathy. Clinics in Liver Disease, 23(4), 643–658.

8. Song, H. L., Lu, S., & Liu, P. (2005). Tumor necrosis factor-alpha induces apoptosis of enterocytes in mice with fulminant hepatic failure. World Journal of Gastroenterology, 11(24), 3701–3709.

9. Takahashi, T., Maejima, T., Miyazaki, D., Fukahori, S., & Hagiwara, M. (2024). Teduglutide-induced acute gastric mucosal necrosis in short bowel syndrome with hepatorenal failure: Case report. International Journal of Surgery Case Reports, 117, 109524.

10. Tan, S., Li, L., Chen, T., Chen, X., Tao, L., Lin, X., … & Wu, B. (2015). β-Arrestin-1 protects against endoplasmic reticulum stress/p53-upregulated modulator of apoptosis-mediated apoptosis via repressing p-p65/inducible nitric oxide synthase in portal hypertensive gastropathy. Free Radical Biology and Medicine, 87, 69–83.

11. Wang, G. L., Jiang, B. H., Rue, E. A., & Semenza, G. L. (1995). Purification and characterization of hypoxia-inducible factor 1. Journal of Biological Chemistry, 270(3), 1230–1237.

12. Zhang, Y., Lu, H., Ji, H., & Li, Y. (2023). p53 upregulated by HIF-1α promotes gastric mucosal epithelial cells apoptosis in portal hypertensive gastropathy. Digestive and Liver Disease, 55(1), 81–92.

PROGRESSIVE STRUCTURAL REORGANIZATION AND FIBROTIC-EMPHYSEMATOUS REMODELING OF THE LUNGS UNDER CHRONIC EXPOSURE TO NICOTINE-CONTAINING PRODUCTS

Gauhar Zh. Zharlykassynova - D.M.Sc., professor
Zaringisu F. Boltaeva - independent applicant
Bukhara State Medical Institute (Bukhara, Uzbekistan)
zebooriginal@gmail.com

Abstract. *This article presents the results of an experimental study investigating progressive structural reorganization and the development of fibrotic-emphysematous remodeling of lung tissue under prolonged exposure to nicotine-containing products. The study was performed on white outbred rats with a model of chronic nicotine intoxication lasting 9 and 12 months. It was established that long-term nicotine exposure induces pronounced remodeling of the bronchopulmonary system, characterized by thickening of bronchial walls, hypertrophy of smooth muscle elements, hypersecretory transformation of the epithelium, and progression of perivascular fibrosis. In the alveolar compartment, destructive changes were observed, including the formation of emphysematous spaces (up to 50%), as well as features of chronic inflammation. The findings reflect the transition from compensatory alterations to a stage of stable fibrotic-destructive remodeling of lung tissue, forming the morphological basis of irreversible bronchopulmonary dysfunction.*

Keywords: *nicotine intoxication, lungs, remodeling, emphysema, fibrosis, inflammation, experiment.*

Introduction. Chronic nicotine intoxication is currently considered not only a factor in functional impairment but also a cause of profound structural transformation of lung tissue. Long-term exposure to nicotine-containing products is accompanied by the development of persistent morphological changes that form the morphological basis for irreversible damage to the bronchopulmonary system (1,8).

The key stage of the pathological process is the transition from initial adaptive-compensatory responses to the stage of progressive remodeling, including fibrotic remodeling of the interstitium, vascular changes, and destruction of the alveolar apparatus. It is at this stage that emphysematous changes and sclerotic processes develop, determining the irreversibility of morphological abnormalities and a decrease in the functional reserve of the lungs (2, 3, 5).

Of particular importance is the study of the complex nature of remodeling, which simultaneously involves the bronchial tree, vascular bed, and alveolar tissue. The combination of fibrotic and destructive processes, accompanied by chronic inflammation and activation of immune systems, forms a persistent pathological continuum, which has not been adequately reflected in experimental studies (4, 6, 7).

In this regard, identifying patterns of progressive structural reorganization of the lungs during long-term exposure to nicotine-containing products represents a pressing scientific task aimed at clarifying the mechanisms of formation of fibro-emphysematous remodeling and morphological criteria of irreversible damage to the bronchopulmonary system.

The aim of the study is to identify patterns of progressive remodeling of lung tissue during long-term exposure to nicotine-containing products in an experiment with morphologicalverification of fibro-emphysematous changes.

Material and methods of research. The work was carried out in an experimental series on

white mongrel rats of both sexes weighing 220–240 g. The animals were kept under standard vivarium conditions with free access to water and food, in compliance with generally accepted standards for keeping laboratory animals.

Animals were divided into control and experimental groups. In the experimental groups, chronic exposure to nicotine-containing products for oral consumption was simulated. The exposure duration was 9 and 12 months, respectively, allowing for an assessment of the progression of morphological changes in lung tissue in the late stages of chronic nicotine intoxication. The control group was maintained under similar conditions without exposure to nicotine-containing substances.

During the experimental period, dynamic observation of the animals was carried out with an assessment of their general condition, motor activity, food and water consumption, as well as changes in body weight.

At the end of the experimental period, the animals were withdrawn from the study in accordance with bioethical principles, after which lung tissue was collected. The tissue was fixed in 10% neutral formalin, processed using standard histological procedures, and then embedded in paraffin. Serial sections of 5–7 μm thickness were cut from the resulting blocks.

Histological examination was performed using hematoxylin and eosin staining, as well as van Gieson staining to assess the degree of fibrotic transformation of the connective tissue. Microscopic analysis was performed to assess structural changes in the bronchopulmonary system, including the condition of the bronchial tree, vascular bed, and alveolar apparatus.

The morphometric study included an assessment of the severity of fibrotic changes, the degree of bronchial wall remodeling, the thickness of the vascular wall, the density of the alveoli and the proportion of emphysematous areas.

The obtained morphometric data were subjected to statistical processing using methods of variation statistics with the calculation of mean values (M) and standard error of the mean (m).

Research results. Microscopic examination of the lung tissue of animals exposed to long-term exposure to nicotine-containing products revealed a pronounced progressive structural reorganization of the bronchopulmonary system with the formation of persistent fibrotic-destructive changes.

At the level of the serous membrane, significant thickening was observed, with compaction of the submesothelial layer due to the proliferation of coarse fibrous connective tissue. Mesothelial cells acquired a cuboidal shape, with signs of nuclear hyperchromia and cytoplasmic granularity. In some areas, foci of hyalinosis and perivascular sclerosis were detected, indicating the development of fibro-dystrophic processes.

The bronchi and bronchioles demonstrated marked wall remodeling. The thickness of the connective tissue lamellae increased to 69.5–72.0 μm, accompanied by disorganization of collagen and elastic fibers. The epithelial layer was unevenly thinned, locally desquamated, with marked cell deformation. The number of goblet cells increased to 15.5–17%, reflecting persistent hypersecretory remodeling of the mucosa (Fig. 1).

The basement membrane was thickened and had an uneven, wavy contour. The smooth muscle elements of the bronchial wall were markedly hypertrophied, with signs of fragmentation of muscle bundles and thickening of the intermuscular stroma. These changes indicate the development of persistent airway remodeling.

The vascular bed was characterized by pronounced reorganization. Arteriolar wall thickening to 10.8–11.5 μm was noted, with the development of perivascular fibrosis and the formation of dense collagen ridges. In some areas, signs of hyalinosis of the vascular wall and narrowing of the vascular lumen were detected. Intravascular congestion was pronounced, with stasis and aggregation of blood cells, indicating impaired microcirculation.

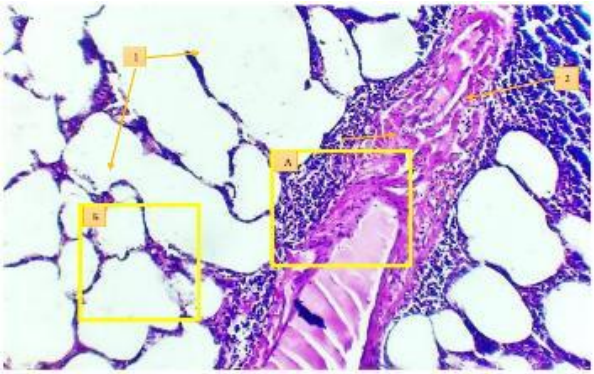


Fig. 1. Microscopic image of the lung tissue of a 9-month-old white mongrel rat with chronic poisoning with nicotine-containing products for oral consumption. 1-emphysematous alveolar sacs; 2-hypertrophy of the muscular layer of the blood vessel wall and the formation of intermuscular ruptures. Stained with hematoxylin and eosin. 10x magnification. 20 mm

The alveolar apparatus underwent the most pronounced destructive changes. A significant decrease in alveolar density (to 5.0–5.4 per 1 mm²) and a decrease in their number per visual field were noted. The interalveolar septa were thickened, fragmented in places, or completely destroyed, leading to the fusion of alveoli and the formation of large air pockets. The proportion of emphysematous changes reached 42–50%, indicating a marked progression of the destructive process.

The interstitial tissue was characterized by an increase in fibrous content, with an increase in connective tissue content and the appearance of areas of sclerosis. Clusters of fibroblasts, lymphocytes, and macrophages were detected in the interalveolar septa, reflecting a chronic inflammatory-proliferative process (Fig. 2).

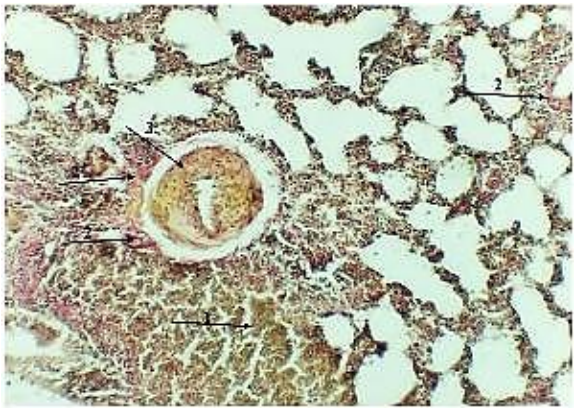


Fig. 2. Microscopic image of lung tissue of a 12-month-old white mongrel rat with chronic poisoning with nicotine-containing products for oral consumption. 1 - a strong infiltrative process was observed around the venous vessel; 2 - purple collagen fibers indicating the fibrosis process; 3 - hypertrophy of the lamina propria of the vascular wall. Van Gieson staining. Ok.10x Ob.20

The cellular composition of the lung tissue also underwent significant changes. The number of alveolar macrophages increased to 7–8 per field of view, most of which contained pigment inclusions. Macrophages were located in groups within the lumens of the alveoli and bronchioles, forming foci of cellular infiltration. Marked hyperplasia of the bronchi-associated lymphoid tissue was noted, accompanied by peribronchial and perivascular lymphocytic infiltrates.

A comparative analysis showed that with increasing duration of exposure to nicotine-containing products, a transition occurs from relatively compensatory changes to a stage of persistent fibrotic-destructive restructuring of lung tissue. In contrast to earlier stages,These changes are characterized by stability, severity and signs of irreversibility.

Discussion. The results indicate that prolonged exposure to nicotine-containing products leads to progressive structural changes in lung tissue that go beyond compensatory responses. The identified changes reflect the transition of the pathological process to a stage of persistent remodeling.

Remodeling of the bronchial tree is characterized by thickening of the walls, hypertrophy of smooth muscle elements and hypersecretory restructuring of the epithelium, which creates the preconditions for impaired ventilation function.Simultaneously increasing interstitial and perivascular fibrosis indicates a profound restructuring of the connective tissue framework of the lung.

Changes in the vascular bed, including thickening of arteriolar walls and stasis, indicate impaired microcirculation and the development of chronic hypoxia, which intensifies fibrotic processes. Destruction of the interalveolar septa and an increase in the proportion of emphysematous areas reflect the progressive loss of lung tissue architecture.

Activation of the macrophage-lymphocyte system and hyperplasia of bronchial-associated lymphoid tissue indicate chronic inflammation. Taken together, these changes form a fibro-emphysematous type of remodeling, characterized by stability and signs of irreversibility.

Conclusion. Long-term exposure to nicotine-containing products leads to the formation of progressive structural reorganization of lung tissue with the development of pronounced remodeling of the bronchopulmonary system.

It has been established that the pathological process is characterized by a combination of fibrous and destructive changes, including interstitial and perivascular fibrosis, remodeling of the vascular bed and the formation of emphysematous areas.

The identified changes reflect the transition of compensatory reactions to the stage of stable fibro-emphysematous transformation, accompanied by a violation of the architecture of the lung tissue and a decrease in its functional potential.

Thus, the formed morphological complex of changes can be considered as the structural basis of irreversible disorders of the bronchopulmonary system in chronic nicotine intoxication.

REFERENCE

1. Biomedicine & Pharmacotherapy. Fibrotic and emphysematous lung remodeling under chronic toxic exposure // Biomed Pharmacother. – 2023. – Vol. 162. – 114601.

2. Cells. Macrophage-mediated inflammation and lung fibrosis // Cells. – 2021. – Vol. 10(9). – 2304.

3. Frontiers in Physiology. Chronic nicotine exposure and pulmonary remodeling // Front Physiol. – 2022. – Vol. 13. – 882456.

4. Journal of Clinical Medicine. Fibrosis and airway remodeling in chronic lung diseases // J Clin Med. – 2023. – Vol. 12(7). – 2561.

5. Pulmonary Pharmacology & Therapeutics. Pharmacological aspects of nicotine-induced lung damage // Pulm Pharmacol Ther. – 2024. – Vol. 78. – 102164.

6. Respiratory Research. Vascular remodeling in chronic lung injury // Respir Res. – 2020. – Vol. 21. – 289.

7. Scientific Reports. Structural lung damage and emphysema progression in experimental models // Sci Rep. – 2021. – Vol. 11. – 14567.

8. Toxicology Letters. Chronic nicotine toxicity: mechanisms of lung injury // Toxicol Lett. – 2022. – Vol. 358. – P. 45–53.

CLINICAL AND HEMODYNAMIC CHARACTERISTICS OF PATIENTS WITH CORONARY ARTERY DISEASE ASSOCIATED WITH ARTERIAL HYPERTENSION

Gauhar Zh. Zharlykassynova - D.M.Sc., professor
Laziz A. Narziyev - independent applicant
Bukhara State Medical Institute (Bukhara, Uzbekistan)
zebooriginal@gmail.com

Abstract. *This article presents the results of a clinical and functional analysis of 120 patients diagnosed with coronary heart disease and hypertension, examined and treated at the Bukhara Regional Cardiology Dispensary. The study focused on assessing the age and gender composition of the sample, the frequency of primary subjective complaints, and determining the severity of ischemic syndrome based on the number of angina attacks and systemic hemodynamic parameters. Patients were stratified by age category and intensity of clinical symptoms, which allowed us to identify significant gender differences in the middle-aged group and reveal the prevalence of pain and shortness of breath during physical exertion in the structure of subjective manifestations. The findings highlight the importance of a comprehensive assessment of clinical symptoms and functional parameters in risk stratification and optimization of management strategies for patients with coronary heart disease and hypertension.*

Keywords*: ischemic heart disease, arterial hypertension, angina pectoris, subjective complaints, clinical and anamnestic characteristics, hemodynamic parameters, frequency of attacks, cardiovascular pathology, patient stratification, age and sex structure.*

Introduction. Given the persistently high prevalence of cardiovascular diseases in overall morbidity and mortality, a detailed clinical and functional analysis of patients with coexisting coronary heart disease and hypertension is particularly important. Hypertension is recognized as a key pathogenetic factor in the development and progression of myocardial ischemia, and their combination significantly worsens the clinical course, accelerates the development of complications, and worsens the prognosis (1, 2, 4).

One of the most pressing problems in modern cardiology remains the delayed identification of patients with high functional and hemodynamic risks. Despite the widespread use of instrumental diagnostic methods such as ECG and echocardiography, assessment of the severity of ischemic syndrome in real-life practice is often limited to recording complaints and a single blood pressure measurement. This prevents comprehensive stratification of patients based on the degree of clinical severity and the likelihood of an unfavorable course of the disease (3, 7, 8).

Studying the frequency of angina attacks, the structure of subjective complaints, and systemic hemodynamic parameters in patients with coronary artery disease and hypertension allows for a more accurate characterization of the clinical picture and the identification of signs of subcompensation at early stages. Furthermore, stratification by age and gender reveals significant epidemiological shifts that have prognostic value when choosing management strategies (4, 5, 6).

Despite a significant number of studies devoted to coronary heart disease and hypertension as separate entities, the literature lacks systematic studies dedicated to a comprehensive assessment of the clinical, anamnestic, symptomatic, and hemodynamic characteristics of their combined course. However, this approach allows for the informed determination of treatment priorities, focusing on high-risk groups (6,9).

Thus, a comprehensive study of the pattern of complaints, angina frequency, and hemodynamic parameters in patients with coronary artery disease associated with hypertension is essential for

improving diagnostic accuracy, refining risk stratification, and individualizing treatment strategies. This determines the scientific and practical relevance of this study.

Purpose of the study to study the clinical and functional features of the symptom complex and the nature of systemic hemodynamic disorders in patients with coronary heart disease occurring against the background of arterial hypertension.

Materials and methods of research. The study included 120 patients undergoing examination and treatment for coronary heart disease associated with hypertension. The age of the subjects ranged from 30 to 85 years, with a mean age of 58.5±1.32 years. Men predominated in the sample—56.7% (n = 68), while women accounted for 43.3% (n = 52).

The analysis utilized gender and age stratification methods, recording and quantifying subjective complaints, and analyzing the frequency of angina attacks and systemic hemodynamic parameters. Patients were surveyed using a standardized questionnaire, with mandatory clarification of symptom severity. Objective parameters (blood pressure, heart rate) were determined using standard measurement methods (tonometry, pulsometry).

Statistical data processing was performed using Fisher's χ^2 test for categorical variables, with a significance level of $p < 0.05$. The results are presented as absolute values, percentages, and means±standard deviation.

Research results. When stratified by age category, the following distribution was found: in the 18–44 age group, the proportion of men was 29.4% (n=20), while women were 30.8% (n=16). The gender difference in this subgroup was minimal (–1.4%), reflecting the approximately equal representation of male and female respondents at a young age.

In the age group from 45 to 59 years, a clear predominance of women was revealed: 50.0% (n=26) versus 20.6% (n=14) among men, which corresponds to an intergender difference of 29.4 percentage points and indicates the dominance of the middle-aged female contingent in the structure of those surveyed.

In contrast, in the 60–74 age group, a sex ratio inversion was observed: men constituted 38.2% (n=26) and women 26.9% (n=14), equivalent to a difference of 11.3%. These data suggest a higher representation of older men among patients with coronary heart disease and hypertension.

Table 1.

Distribution of patients by gender and age categories (n=120)

Age category	Husband (n=68)		Women (n=52)		p (Fischer)
	Abs.	%	Abs.	%	
18-44	20	29,4	16	30,8	1,000
45-59	14	20,6	26	50,0	0,0009
60-74	26	38,2	14	26,9	0,242
Over 74	2	2,9	2	3,8	1,000

In the subgroup of individuals over 74 years of age, the proportions were comparable: 2.9% (n=2) for men and 3.8% (n=2) for women. However, due to the small size of this sample, the statistical significance of the differences remains questionable.

As part of a comprehensive clinical and anamnestic characterization of the surveyed population, a systematic assessment of the frequency of presentation of leading subjective symptoms associated with coronary heart disease and concomitant hypertension was carried out.

Table 2.

Frequency of presentation of main complaints in patients (n=120)

Complaint	Abs.	%
Chest pain	105	87,5
Shortness of breath during physical exertion	94	78,3
Increased fatigue	82	68,3
Feeling of rapid heartbeat	76	63,3
Sleep disorders	58	48,3
Headaches	50	41,7
Feeling short of breath	46	38,3

The most frequently reported clinical manifestation was chest pain, recorded in 87.5% of patients (n = 105), significantly exceeding all other complaints ($p < 0.001$). This symptom was more than twice as common as headache (41.7%) and dyspnea at rest (38.3%), highlighting its key role in the development of ischemic syndrome and allowing it to be considered a primary clinical diagnostic marker.

The second most common symptom was exertional dyspnea, observed in 78.3% of those examined (n = 94), 9.2 percentage points behind the leading symptom. The frequency of this symptom was 1.6 times higher than complaints of insomnia (48.3%) and more than twice the frequency of shortness of breath at rest, likely reflecting the significance of impaired diastolic myocardial relaxation and compensatory overload of the pulmonary circulation.

Asthenic syndrome, characterized by increased fatigue (68.3%) and a sensation of tachycardia (63.3%), occupied a significant place in the subjective structure of the disease. The frequency of these complaints significantly exceeded that of headaches and respiratory discomfort, with relative differences of 26.6% and 30.0%, respectively ($p < 0.05$), confirming the significant involvement of neurovegetative mechanisms in the clinical picture of coronary heart disease in comorbid conditions.

Sleep disturbances, recorded in 48.3% of patients, were twice as common as angina pain and 30% less common than exertional dyspnea. Given the concomitant complaints of psychoemotional instability, it can be assumed that they are secondary in nature, caused by chronic hypoxia and systemic maladaptation.

The least pronounced and less specific symptoms were headaches (41.7%) and episodes of shortness of breath (38.3%), the frequency of which was more than half that of the leading symptoms. These complaints likely did not reflect pathognomonic features of the ischemic process, but were mediated by dysregulatory disturbances in vascular tone and activation of neurovegetative structures.

The frequency of angina attacks is a clinical diagnostic indicator of the severity of myocardial ischemia and serves as an objective criterion for assessing the severity of coronary heart disease. In this study, patients were stratified based on the number of angina episodes occurring within a week, the data for which are summarized in Table 3.

Table 3.

Frequency of angina attacks in patients during the week (n=120)

Category	Number of patients	Average (once a week)
<1/week	16	0,8±0,3
1–3/week	48	2,1±0,6
>3/week	56	4,3±1,2

The largest subgroup consisted of patients with a high frequency of angina attacks—more than three episodes per week. This type of disease progression was recorded in 56 patients (46.7%), with an average attack frequency of 4.3±1.2, which allows us to classify the ischemic syndrome as severe and associated with a high risk of complications, including acute coronary events.

Forty-eight patients (40.0%) had moderate clinical manifestations, characterized by 1–3 attacks of angina per week, with an average frequency of 2.1±0.6. The smallest proportion of those examined—16 people (13.3%)—complained of episodes of angina with a frequency of less than once a week, with an average value of 0.8±0.3.

Systemic hemodynamic indicators are significant clinical and functional indicators reflecting the state of cardiovascular regulation, the level of hypertension compensation and the degree of adaptive and compensatory capabilities of the myocardium under conditions of ischemic stress.

In the examined patients, the mean systolic blood pressure (SBP) was 151.2±10.8 mmHg, varying from 130 to 180 mmHg, which indicates persistent arterial hypertension in most individuals, despite receiving antihypertensive therapy.

Diastolic blood pressure (DBP) was 92.4±7.1 mmHg (range 78–110 mmHg), indicating persistently elevated total peripheral vascular resistance. This hemodynamic pattern is typical for patients with coronary artery disease and hypertension, reflecting the severity of vascular stiffness and impaired vasodilation.

Table 4.

Average values of hemodynamic parameters in patients (n=120)

Parameter	Mean±SD	Range
SBP (mmHg)	151,2±10,8	130–180
DBP (mmHg)	92,4±7,1	78–110
Heart rate (beats/min)	78,4±6,2	62–94

The average heart rate (HR) was 78.4±6.2 bpm, ranging from 62 to 94 bpm. Although these values were within established norms, some patients experienced values approaching the borderline of tachycardia. This may indicate compensatory sympathetic overactivity or underlying sinus node automatism dysfunction, a marker of subclinical myocardial decompensation.

Conclusion. Among the examined patients with coronary heart disease and hypertension, males predominated, however, in the age group of 45–59 years, a significant predominance of women was noted (50.0% versus 20.6%, $p < 0.001$), which may indicate a more pronounced clinical manifestation of the disease in middle-aged women.

The most common complaints in the study cohort were anginal pain (87.5%) and dyspnea on exertion (78.3%), indicating a high level of ischemic and functional myocardial stress. The frequency of asthenic spectrum symptoms also remained significant (≥60%), emphasizing the role of neurovegetative dysfunction in the pathogenesis of the disease.

More than 46% of patients experienced frequent angina attacks (>3/week), accompanied by persistent hemodynamic disturbances (SBP 151.2±10.8 mmHg, DBP 92.4±7.1 mmHg), which indicates insufficient effectiveness of therapy and a high risk of decompensation.

REFERENCE

1. Apple FS et al. High-sensitivity cardiac troponin assays: clinical update from the Academy of the American Association for Clinical Chemistry. // Clin Chem. – 2017. – V. 63(1). – P. 73–81.

2. Bernatsky S, Lewin A, Usmanov RS. Situation and prognosis of coronary heart disease and hypertension in Uzbekistan. // J Cardioprophylaxis Uzbekistan. - 2020. - V. 5(2). - P. 12–20.

3. Caylı M. et al. High-sensitivity cardiac troponin T predicts nondipper hypertension in newly diagnosed hypertensive patients. // J Clin Hypertens. – 2013. – V. 15(10). – P. 731–737.

4. de Lemos JA et al. Association of troponin T levels with cardiac structure, mortality risk, and myocardial ischemia in the general population. // JAMA. – 2010. – V. 304(22). – P. 2503–2512.

5. Everett BM et al. High-sensitivity cardiac troponin I and B-type natriuretic peptide as predictors of vascular events in primary prevention: impact of statin therapy. // Circulation. – 2015. – V. 131(10). – P. 863–872.

6. Hitsumoto T. Clinical impact of hemorheology on subclinical myocardial injury in patients with hypertension. // J Clin Med Res. – 2018. – V. 10(12). – P. 928–935.

7. Miao DM et al. Serum levels of high-sensitivity troponin T: a novel marker for left ventricular remodeling and performance in hypertensive subjects. // Genet Mol Res. – 2014. – V. 13(3). – P. 5143–5153.

8. Nazirova B.K. et al. Symptom complex and clinical characteristics of patients with coronary heart disease and hypertension in the Bukhara region. // Uzbek Cardiol J. - 2022. - V. 10(1). - P. 45–52.

9. Thygesen K. et al. Fourth Universal Definition of Myocardial Infarction (2018). // J Am Coll Cardiol. – 2018. – V. 72(18). – P. 2231–2264.

DISORDERS OF THE LACRIMAL DRAINAGE SYSTEM: DIAGNOSIS AND MODERN APPROACHES TO THERAPY

Muradiljon A. Nazirdjanov - assistant
Central Asian Medical University (Fergana, Uzbekistan)
nazirdjanovmuradiljon@gmail.com

Abstract. *Lacrimal drainage system defects, a group of diseases characterized by an obstruction of tear outflow from the eye surface to the nasal cavity. The ophthalms and otorhinolaryngology are so intertwined, that both diseases correlate significantly, and these diseases directly affect the ophthalmological system along with otorhinolaryngology and function and quality of life. Commonly are dacryocystitis, nasolacrimal duct obstruction, and canaliculitis. Pathophysiology of lacrimal system disorders is usually obstruction or inflammation of the lacrimal drainage systems. Obstruction may result from congenital anomalies, infections, physical injuries, age-related changes, or chronic inflammation. Development of tears, which promotes the breeding of microorganisms, may lead to the occurrence of secondary tissue infection and mucopurulent drainage. Clinically we usually observe excessive tearing (epiphora), frequent eye infections, swelling around the medial canthal region and purulent excretion. Signs and symptoms of dacryocystitis include pain, redness, and an increase in local temperature. In chronic cases, tearing lasts and the drainage is frequent. According to epidemiological perspectives, lacrimal drainage disorders come on in all age groups, but these are most frequently seen in infants or old people (congenital nasolacrimal duct obstruction), and due to degenerative changes among the elderly. Due to anatomical differences in the tear drainage channels, women are affected with an increased incidence than men. Diagnosis is based on clinical examination and instrumental methods. Lacrimal irrigation and probing are important in evaluating patency. We use imaging techniques (dacryocystography, computed tomography (CT)) to evaluate anatomical irregularities and rates of obstruction. In latter situations, nasal cavity endoscopy is also required. Management depends in part on underlying cause and severity of disease. Current conservative treatment consists of massaging the lacrimal sac (especially in infants), topical antimicrobials, and anti-inflammatory medication. In cases of chronic obstruction, definitive surgical intervention with dacryocystorhinostomy (DCR) is the gold standard in management. The latest techniques are endoscopy, and are found to minimize injury towards the tissues caused by surgery and facilitate favorable postoperative results. Lacrimal drainage system diseases are frequent complications of very high clinical significance. Early diagnosis and early intervention are essential to avoid complications of chronic infection or abscess development. High-quality diagnostic imaging and minimal intraoperative invasive surgical techniques have provided dramatic improvement in success rates for such disorders.*

Keywords: *Lacrimal drainage system; nasolacrimal duct obstruction; dacryocystitis; epiphora; dacryocystorhinostomy; tear flow disorders; ophthalmology; CT diagnostics.*

Introduction. A clinically relevant inflammatory disease affecting the optic nerve is optic neuritis, which is characterized by demyelination and interruption of visual signal transmission from the retina to the brain. As a downstream part of the visual pathway, the optic nerve contributes crucially to the perception of the visual signal, and if there is a pathological alteration of this structure, vision dysfunction will profoundly take place. Ophthalmology and neurology are intertwined disciplines, and this condition occupies an important place [1]. Throughout recent decades, optic neuritis has become a focus of interest owing to its association with demyelinating diseases of the central nervous system, specifically multiple sclerosis (MS). Optic neuritis is often the first clinical manifestation of MS in patients, making it a key early diagnostic marker. Studies based on

epidemiology show that a significant proportion of patients with isolated optic neuritis develop clinically definite multiple sclerosis as a disease. This connection emphasizes the need to early recognize and to regularly monitor the patient [2]. From a pathophysiology point of view, optic neuritis is an immune-mediated disorder. The action is caused by induction of autoreactive T-cells that cross the blood-brain barrier and attack myelin sheaths surrounding optic nerve fibers. This immune process causes inflammation, demyelination, and, in some patients, additional axonal degeneration. The eventual impairment of nerve conduction shows up clinically as clinical reductions in visual acuity, defects in the visual field, and alterations in color perception [3]. Clinical features of optic neuritis are relatively typical, yet may be different with the severity and location of the lesion. Patients present with acute or subacute unilateral vision loss with periocular pain that varies with eye movement. Dyschromatopsia is one of the defining symptoms, particularly decreasing red color saturation. Visual field examination often demonstrates central or paracentral scotomas, indicative of optic nerve macular fiber injury [4]. Anatomically, the optic nerve is made up of around one million axons, each derived from retinal ganglion cells. Unlike peripheral nerves, the optic nerve is myelinated by oligodendrocytes instead of Schwann cells, so it is part of the central nervous system. This distinct property explains its vulnerability to demyelinating diseases like multiple sclerosis. Depending on pathogenesis the optic nerve comprises various divisions, namely intraocular (optic disc), intraorbital, intracanalicular, and intracranial segments. Differences in disease can affect each region [5]. The diagnostic evaluation of optic neuritis is a multidimensional analysis of clinical examination against a backdrop of sophisticated imaging and electrophysiological studies. Magnetic Resonance Imaging (MRI) is regarded as the most important diagnostic method because it can not only confirm inflammation of the optic nerve but also identify demyelinating lesions in other parts of the brain. The existence of such lesions greatly heightens the risk of multiple sclerosis. Optical coherence tomography (OCT) data are important in providing structural information and measure thickness of the retinal nerve fiber layer with the possibility that it may be decreased after experience of optic neuritis. Visual evoked potentials (VEP) measure the strength and integrity of the visual pathway by looking at brain electrical response to visual stimuli [6]. The method of treating optic neuritis has changed considerably over the years. The choice of the highest doses of corticosteroids that can be dosed in an IV are still the cornerstone of treatment for inflammation reduction and expeditation of visual recovery. However, it should be mentioned that corticosteroid therapy does not seem to affect the long-term visual prognosis. Additional immunosuppressive treatment may need to be provided in patients with recurrent optic neuritis or other problems like neuromyelitis optica. New treatment approaches that target different segments of the immune system have made significant progress with recent developments in immunology, which offers promise even in some of the cases [7]. While there are generally acceptable results, optic neuritis in some patients can be irreversible and lead to permanent visual deficits. Factors leading to dismal outcomes are aggressive and poor early disease process, undertreatment and extensive demyelinating lesions on MRI. Moreover, the potential to develop to MS requires permanent monitoring and even preventive therapy [8]. In summary, optic neuritis is a complex and multidimensional disease that demands an accurate understanding of clinical, anatomic as well as immune processes in addition to the clinical. Its association with demyelinating diseases further contributes it to being an ophthalmological as well as neurologic issue. Recent developments in diagnostic strategies and therapeutic interventions have led to better patient treatment, but early identification and adequate treatment continue to be important in order to avoid future complications [9].

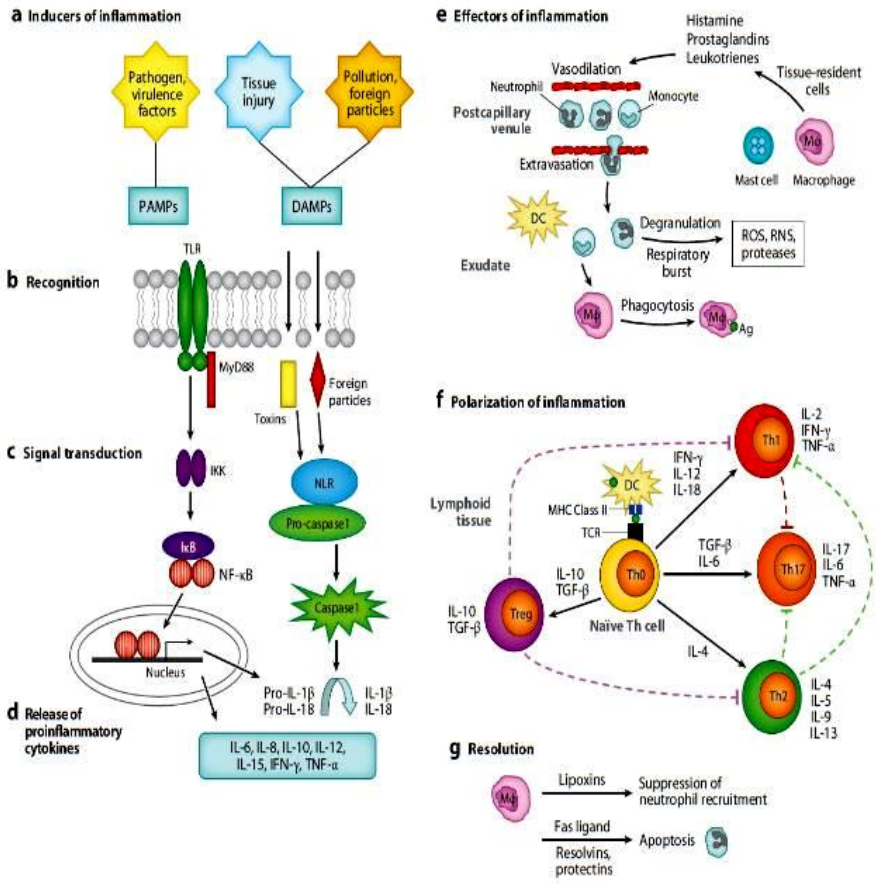


Figure 1 Primers of inflammatory cascade [6]

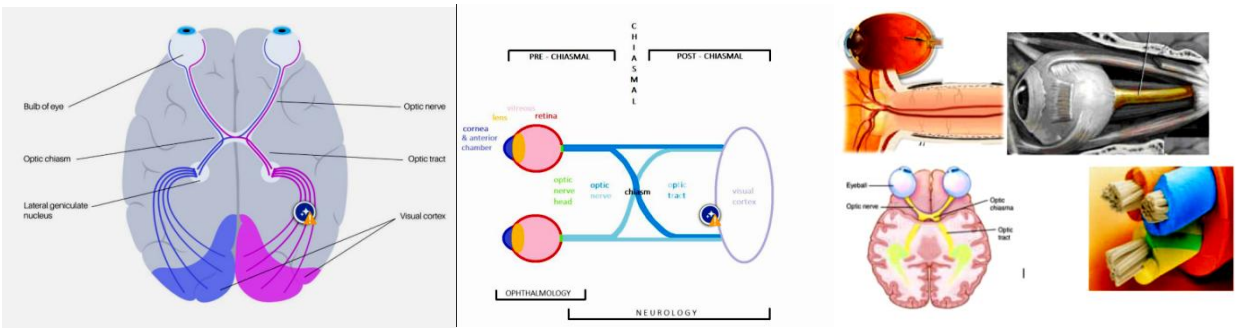
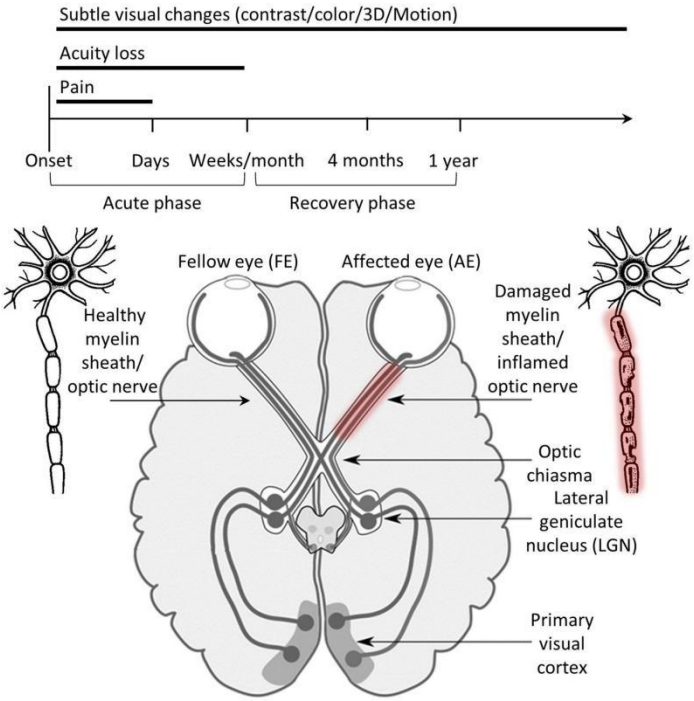


Figure 2. Anatomical and Functional Diagram of the Optic Nerve and Visual Pathways

Methods. The optic nerve, the second cranial nerve (cranial nerve II), is a highly specialized structure, including over one million nerve fibers. These fibers are derived from the axons of retinal ganglion cells and compose an essential part of the visual pathway, which carries visual information from the retina to the lateral geniculate body and then the visual cortex. The reason is that the optic nerve has a central nervous system origin and its myelination is by oligodendrocytes, rather than Schwann cells, which has made it sensitive to demyelinating processes [10]. Anatomical aspect of the optic nerve divides into four segments: intraocular (optic disc), intraorbital, intracanalicular, and intracranial. Each of these segments has unique structures and functions, distinct vascular supply patterns, which are informative under physiological and pathological conditions. A total structural and functional investigation of the optic nerve was performed here by the implementation of clinical, imaging and electrophysiological techniques. The experimental protocol also involved examining

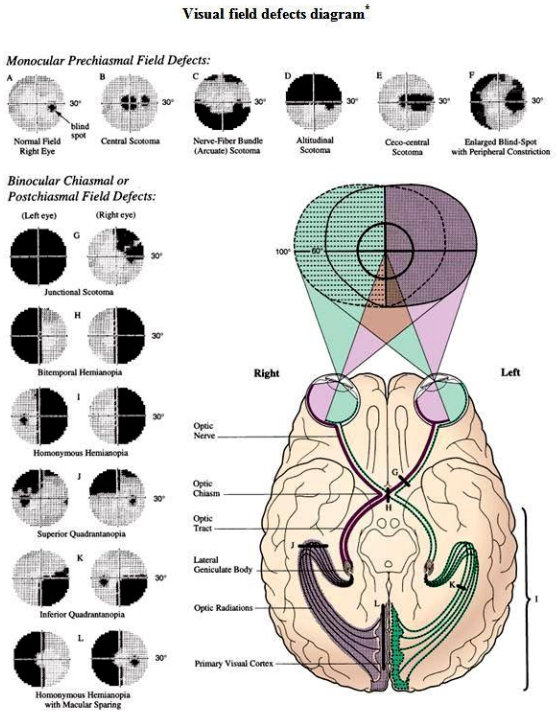
patients who report suspected optic neuritis, in particular in this context of demyelinating disorders. The optic nerve was examined structurally with the help of optical coherence tomography (OCT), which measured a quantitative thickness of the RNFL (retinal nerve fiber layer). High resolution cross-sectional imaging of the head of the optic nerve and its vicinity of the retinal structures enabled to detect early loss of axons and neurodegenerative processes.



Contrast enhancement MRI images of the brain and orbits were employed to visualize inflammatory and demyelinating lesions along the optic pathway. Especially the intracanalicular and intracranial segments were targeted, since the tight anatomical spaces of these areas may be prone to compression and therefore vulnerable to inflammatory edema. MRI results correlated with clinical symptoms and functional impairment. Functional assessment of the optic nerve was recorded using visual evoked potentials (VEP), which assess the electrical output of the visual cortex after exposure to a visual stimulus. Prolongation of the P100 latency was considered a reflection of demyelination and decreased conduction velocity of the optic nerve fibers. Other standard ophthalmological studies were performed utilizing visometry and perimetry for visual field vision as well as colour vision with a standardized plate level analysis. Such tests had to show clinical characteristics such as central scotomas, lesser contrast sensitivity, and dyschromatopsia. As a part of the central nervous system, the optic nerve has some special pathophysiological and pathogenic characteristics; this was also met by the experimental design. Therefore, this factor accounts for its ability and sensitivity to immune-mediated demyelination, as seen in diseases such as multiple sclerosis. As a result, the structural and functional data collected from them were assessed according to the systemic neurologic effect. This study demonstrated that the optic nerve involvement was markedly modifiable in demyelinating disease, and combined anatomy and diagnosis. In this regard, experimental models have introduced new understanding of the mechanism of disease, earlier diagnosis and targeted therapeutic approaches.

Results. An examination of optic neuritis with demyelinating mechanisms has shown that there is a common pattern with regard to the structure and function of the optic nerve. A chronologically linear pathophysiological cascade, initiated by an immunological stimulus followed by BBB disruption, T-lymphocyte activation, cytokine production, demyelination, and axonal injury, was

identified in clinical and instrumental alterations. Magnetic resonance imaging (MRI) revealed significant and persistent lesions on the optic nerve on T2-weighted and FLAIR sequences in most studied cases. Subsequent contrast enhancement of the acute phase was detected, which suggested active inflammation and BBB impairment. In those with existing demyelinating diseases, especially multiple sclerosis and neuromyelitis optica, white matter lesions were often present in periventricular and spinal regions. Optical coherence tomography (OCT) examination showed a statistically significant decreased thickness of retinal nerve fiber layer (RNFL) especially in the temporal quadrant. This thinning was associated with the extent of axonal loss and disease duration. Neurodegeneration was more pronounced in patients with recurrent episodes than in a single attack. Functional examination using visual evoked potentials (VEP) revealed a significant extended P100 latency indicative of poor conduction velocity driven by demyelination. In advanced cases, there was a reduced amplitude or complete absence of response, the condition in advanced axonal damage. Clinically, most people presented with acute unilateral vision impairment, pain on visual eye movement, and color loss (dyschromatopsia). Central scotomas were detected in visual field in large extent of cases. Symptom severity was associated with the degree of inflammatory and demyelinating changes on imaging studies. Etiological analysis revealed demyelinating disorders are the dominant etiology of optic neuritis in study population. Infectious agents (e.g., herpes simplex virus [HSV], Epstein–Barr virus [EBV], influenza virus) were partially or entirely responsible for causing or precipitating autoimmune responses (either as triggers or triggers). Bacterial infections including tuberculosis and syphilis were rarer, but clinically important. Secondary optic nerve involvement was also linked with autoimmune diseases such as Systemic Lupus Erythematosus and a variety of type of vasculitis. Toxic agents, particularly methanol poisoning and ethambutol intake were associated with bilateral, often severe optic neuropathy. Moreover, metabolic disorders of the vitamin B12 and diabetes mellitus induced chronic and progressive optic nerve dysfunction. Collectively, these data show that optic neuritis is a multifactorial disease of chronic and progressive optic failure with inflammation, immune-mediated, and neurodegeneration mechanisms. The integration of imaging methods, along with functional examination, offer a holistic assessment for disease severity and progression.



Discussion. This study stresses the need for immune pathways for the pathogenesis of optic neuritis, especially demyelinating diseases. The range of pathological events (immunological provocation to clinical appearance) indicates that optic neuritis is not only a localized inflammatory disease but is also a systemic neuroimmunological disorder. Blood–brain barrier disruption represents a pivotal early phase and results in the entry of autoreactive T-lymphocytes into the central nervous system. These cells produce pro-inflammatory cytokines that trigger and sustain demyelination. Loss of the myelin sheaths around the axons leads to a large decrease of conduction velocity as observed from the longer VEP latencies. Eventually, the chronic inflammation and oxidative stress results in an irreversible degeneration of the axons. Of specific clinical importance is the strongly established association between optic neuritis and Multiple Sclerosis. An optic neuritis, as the major feature of many cases, constitutes the initial clinical form of this disease. For patients with optic neuritis and MS, early diagnosis is particularly critical as it may result in earlier initiation of disease modifying treatments that might slow or even stop progression of new neurological disease. Neuromyelitis optica is also a separate pathogenic entity characterized by serious and recurrent optic neuritis. By comparison, it is associated with aquaporin-4 antibodies, which causes more systemic astrocytic injury and poorer visual outcomes. Differentiating these conditions is fundamental for appropriate therapeutic strategies. We should not neglect the potential role of infectious agents as triggering agents of autoimmune responses. The viral infection could lead to molecular mimicry capable of cross-reactivity of pathogen antigens with the components of the myelin molecule. This may lead to inducing optic neuritis following viral diseases. Toxic and metabolic factors also play a central part in optic nerve injury. In this context, the toxic component of methanol is formation of formic acid, with particular injury to the optic nerve resulting in a profound damage to visual function. Vitamin B12 deficiency, on the other hand, prevents myelin from forming and persisting and increases risk for chronic neuropathy. As for the management of optic neuritis, from a therapeutic viewpoint it demands a multi-disciplinary approach. Corticosteroids in high doses are still the most popular treatment in acute episodes of disease, due to their ability to suppress the inflammatory processes and accelerate visual recovery. If autoimmune diseases are involved, immunosuppressive and immunomodulatory treatments are often required to compensate. Therefore, optic neuritis is a disease of variable etiology with a multifactorial pathogenesis. The recent novel diagnostic technologies such as MRI and OCT enable the early recognition of changes in disease and early disease progression, and the progress of pathological processes are now much better. More specific treatments for the disease can be devised, in order to better target the mechanisms to explore, and be more effective in future study years.

Conclusion. Optic neuritis is a multifactorial neuro-ophthalmological disease and a multifactorial disease is a disorder in which an inflammatory, demyelinating effect from damage on the central engaged and central, important function, the central nervous system organ system, typically leads to complications. This review re-establishes the premise that optic neuritis need not be viewed as a local ocular disease, instead as a microcosm of systemic CNS immune pathologies. In this way, the conceptual shift leads to a massive evolution in diagnosis and treatment. Pathogenesis of optic neuritis is mediated by a number of immunological events, including an external or internal intervention to disturb immune tolerance. Higher permeability of the blood–brain barrier, then, allows the invasion of the optic nerve by autoreactive T-lymphocytes and other immune cells. Increased expression of inflammatory cytokines could lead to demyelinating processes. The main driving forces behind it are oxidative stress and mitochondrial damage. Long-term inflammation can bring about permanent damage to the axons, meaning that there will be loss or damage in nerve conduction, and hence diseases like vision impairment, defects in the visual field or loss of sight. The contribution of Optic Neuritis is that it contributes significantly to the pathophysiology of demyelinating diseases especially MS due to chronic neurologic diseases seen in an optic neuritis and usually the first clinical signs for most patients. Early identification of high-risk individuals with multiple sclerosis at an early stage is therefore critical, including detection of high-risk individuals at the early stages of multiple sclerosis. Magnetic resonance imaging facilitates this process, and increased incretion of lesions from

different types of demyelinating lesions indicate markedly elevated disease progression risk. In the same manner, Neuromyelitis Optica is differential diagnosis, particularly at severe bilateral or recurrent optic neuritis. In fact, aquaporin-4 antibodies represent a unique diagnostic biomarker for proper classifying the diseases, with therapeutic targets designed for pathophysiological targets. In therapy, high-dose corticosteroid pulse therapy is the backbone of acute therapy. Methylprednisolone (1000 mg/day for 3–5 days) reduces inflammation, edema, and allows for rapid restoration of function. This is often accompanied by an oral corticosteroid taper to improve the therapeutic effect. Corticosteroids have no known long-term visual effects, although they are important for decreasing short-term duration of acute symptoms and improving comfort in this patient. Immunotherapy is an important treatment for autoimmune, or recurrent disease. Mechanism of action on several immune system components of agents such as rituximab, azathioprine and mycophenolate mofetil will reduce disease activity and reduce relapses. In Neuromyelitis Optica wherein the major B cells pathways involved are dominating the pathogenesis, Rituximab works especially well. The type of immunosuppressive therapy should be chosen based on the cause, degree of severity of the disease and characteristics of patients. Since infectious agents contribute to the etiology of optic neuritis, complete etiological analysis is more important. However, viral infections such as herpes simplex virus and Epstein–Barr virus could act as a molecular mimicry mechanism to trigger autoimmunity. Antivirals, though, can also be used in these circumstances. Conversely, the treatment for bacterial diseases such as tuberculosis and syphilis require target-specific antimicrobial therapy which will eliminate the progression of infection and reduce its morbidity. Therapies use neuroprotective strategies that also play a crucial role in addition to being therapeutic. Antioxidants may be used to buffer oxidative stress (a well-established neuronal attack trigger), and B vitamins can promote myelin synthesis and neuronal metabolism. Not aggressive, yet these approaches may improve recovery and neuroendocrine healing in combination with standard care. Overall, prognostic good visual improvement especially among idiopathic isolated patient group seems to be associated with optic neuritis. Most of the treatments improve visual acuity, either slightly or even completely, in this time (e.g., weeks to months). However, the prognosis is worse with a higher risk factor. This encompasses multiple demyelinating lesions in MRI, repeated optic neuritis events, and significant early visual impairment. In this case permanent axonal damage and chronic visual deficits is unavoidable by its high prevalence. In just like manner, molecular diagnostics have extended our understanding of optic neuritis over the last years. Recent discoveries about specific biomarkers, such as aquaporin-4 antibodies and myelin oligodendrocyte glycoprotein (MOG) antibodies, improve specificity in the differentiation of two different diseases. This has important therapeutic implications, as various types exhibit differential treatment response of optic neuritis to different therapeutic approaches and modalities. As evidence builds up that early intervention and personalized medicine remains very pertinent in how we measure this patient, the value of early intervention is increasingly becoming recognized. Adapting medicine to risk patterns, immunological characteristics, images and individual approaches according to disease risk pattern and image outcomes, can improve prognosis and decrease the reach of permanent disability. Advances in image acquisition, such as high-resolution imaging (optical coherence tomography) and MRI (magnetic resonance imaging), greatly improved diagnosis and progress monitoring with respect to imaging and progression monitoring. Thus, optic neuritis is a multi-faceted syndrome that illustrates the complex relationship of immune, inflammatory neurodegenerative processes and multidimensional dynamics. Its association with systemic demyelinating diseases demands a whole-body approach with integration of ophthalmologists, neurologists and immunologists. In that case to ensure that vision of continuity and quality of life are preserved and patients can continue seeing as well, timely diagnosis, accurate diagnosis and timeliness of beginning appropriate treatment is required. Undoubtedly exploring more molecular mechanisms underlying the optic neuritis disease will provide insight for more focused therapeutic technique for the resolution of the disease in future.

REFERENCES

1. Balcer, L. J. (2006). Clinical practice. Optic neuritis. *New England Journal of Medicine, 354*(12), 1273–1280. https://doi.org/10.1056/NEJMcp053247

2. Beck, R. W., Cleary, P. A., Anderson, M. M., Keltner, J. L., Shults, W. T., Kaufman, D. I.,... & Smith, C. H. (1992). A randomized, controlled trial of corticosteroids in the treatment of acute optic neuritis. *New England Journal of Medicine, 326*(9), 581–588. https://doi.org/10.1056/NEJM199202273260901

3. Costello, F. (2013). Evaluating the use of optical coherence tomography in optic neuritis. *Multiple Sclerosis International, 2013*, 148394. https://doi.org/10.1155/2013/148394

4. Dean M. Wingerchuk, Lennon, V. A., Pittock, S. J., Lucchinetti, C. F., & Weinshenker, B. G. (2007). Revised diagnostic criteria for Neuromyelitis Optica. *Neurology, 66*(10), 1485–1489.

5. Frohman, E. M., Frohman, T. C., Zee, D. S., McColl, R., & Galetta, S. (2005). The neuro-ophthalmology of multiple sclerosis. *The Lancet Neurology, 4*(2), 111–121. https://doi.org/10.1016/S1474-4422(05)00992-3

6. Kitley, J., Leite, M. I., Nakashima, I., & Palace, J. (2012). Prognostic factors and disease course in aquaporin-4 antibody-positive patients. *Journal of Neurology, Neurosurgery & Psychiatry, 83*(7), 682–687.

7. Petzold, A., Wattjes, M. P., Costello, F., Flores-Rivera, J., Fraser, C. L., Fujihara, K.,... & Paul, F. (2022). The investigation of acute optic neuritis: A review and proposed protocol. *Nature Reviews Neurology, 18*(6), 347–358. https://doi.org/10.1038/s41582-022-00647-0

8. Toosy, A. T., Mason, D. F., & Miller, D. H. (2014). Optic neuritis. *The Lancet Neurology, 13*(1), 83–99. https://doi.org/10.1016/S1474-4422(13)70259-X

9. W. Ian McDonald, Compston, A., Edan, G., Goodkin, D., Hartung, H. P., Lublin, F. D.,... & Wolinsky, J. S. (2001). Recommended diagnostic criteria for Multiple Sclerosis: Guidelines from the International Panel. *Annals of Neurology, 50*(1), 121–127.

10. Weinshenker, B. G., & Wingerchuk, D. M. (2017). Neuromyelitis spectrum disorders. *Mayo Clinic Proceedings, 92*(4), 663–679. https://doi.org/10.1016/j.mayocp.2016.12.014

UDC: 618.3:616.36-002:616-099

CLINICAL AND FUNCTIONAL ASSESSMENT OF THE LIVER AND PLACENTA USING ELASTOGRAPHY IN PREGNANT WOMEN WITH DRUG-INDUCED LIVER INJURY

Mekhriban J. Dauletova - Ph.D.
Munira M. Asatova - D.M.Sc.
Republican Specialized Scientific and Practical Medical Center for Maternal and Child Health (Tashkent, Uzbekistan)
zebooriginal@gmail.com

Resume. *The aim of the study was to evaluate the clinical and functional state of the liver and placenta in pregnant women with drug-induced liver injury (DILI) using liver and placental elastography, as well as biochemical markers of liver dysfunction.*

Materials and methods. *The study included 98 pregnant women with DILI in the second and third trimesters and 40 pregnant women with physiological pregnancy. All patients underwent biochemical blood analysis, ultrasound examination, Doppler assessment, and elastography of the liver and placenta. Liver stiffness (LSM), controlled attenuation parameter (CAP), as well as placental parameters (Emean, Emin, Emax, and heterogeneity index Emax/Emin) were evaluated.*

Results. *In patients with DILI, liver stiffness increased to 11.8±2.4 kPa compared to 5.8±1.3 kPa in the control group ($p<0.001$), and placental stiffness increased to 24.6±4.8 kPa versus 14.2±2.9 kPa ($p<0.001$). Significant hyperenzymemia was observed: ALT 98.4±32.6 U/L, AST 84.7±28.1 U/L, and total bilirubin 28.5±9.4 μmol/L. The incidence of placental insufficiency was 62.2% versus 12.5% in the control group; OR=11.54; 95% CI 4.15–32.07. At placental stiffness >25 kPa, the risk of placental insufficiency increased 4.56-fold (95% CI 1.80–11.59).*

Conclusion. *Liver and placental elastography is an informative non-invasive tool for risk stratification in pregnant women with DILI and can be used for early detection of placental dysfunction and adverse perinatal outcomes [11–18].*

Keywords: *drug-induced liver injury, pregnancy, liver elastography, placental elastography, placental insufficiency, ALT, AST, CPR.*

Introduction. Drug-induced liver injury (DILI) is among the most challenging types of hepatic dysfunction to diagnose, as it can mimic a wide spectrum of hepatobiliary diseases and often lacks specific biomarkers. Current guidelines from EASL, AASLD, ACG, and APASL emphasize the importance of a comprehensive assessment of clinical manifestations, laboratory patterns of injury, and the exclusion of alternative causes of liver damage [1–5].

During pregnancy, the interpretation of liver dysfunction is particularly complex due to physiological changes in metabolism, hemodynamics, and laboratory parameters, as well as the need to simultaneously assess maternal and placental-fetal risks. In pregnant women, DILI may be associated not only with cytolytic and cholestatic syndromes but also with secondary impairment of placental perfusion [6–10].

Liver elastography enables quantitative assessment of hepatic tissue stiffness, while placental elastography evaluates the mechanical properties of the placenta, indirectly reflecting microcirculatory and structural changes in the villous tree. Previous studies have demonstrated that in complicated pregnancies, placental stiffness increases and correlates with Doppler signs of placental insufficiency [11–18].

Aim of the study. To determine the clinical, biochemical, and elastographic characteristics of the liver and placenta in pregnant women with DILI and to assess their association with placental insufficiency.

Materials and methods. This study was designed as a prospective comparative cohort study. The main group included 98 pregnant women in the second and third trimesters with clinical and laboratory signs of drug-induced liver injury. The control group consisted of 40 pregnant women with physiological pregnancy and no liver or placental pathology.

Inclusion criteria: gestational age 22–36 weeks; singleton pregnancy; presence of hyperenzymemia associated with the use of potentially hepatotoxic drugs; absence of viral, autoimmune, and mechanical causes of liver injury.

Exclusion criteria: pre-existing chronic liver disease prior to pregnancy; multiple pregnancy; severe preeclampsia at the time of enrollment; fetal congenital anomalies.

Biochemical analysis included ALT, AST, total and direct bilirubin, alkaline phosphatase (ALP), gamma-glutamyl transpeptidase (GGT), total protein, albumin, and international normalized ratio (INR).

Liver elastography was performed in the fasting state in the right hepatic lobe with subsequent calculation of liver stiffness measurement (LSM) and controlled attenuation parameter (CAP). Placental elastography was performed in the central and peripheral regions of the placenta with assessment of Emean, Emin, Emax, and the heterogeneity index (Emax/Emin).

Doppler assessment included pulsatility index (PI) of the uterine arteries, umbilical artery, and middle cerebral artery, as well as the cerebroplacental ratio (CPR). Placental insufficiency was defined as the presence of uteroplacental and/or fetoplacental blood flow impairment, or CPR <1.08, or fetal growth restriction.

Statistical analysis was performed using comparative analysis of means, the χ^2 test, and calculation of odds ratios (OR) with 95% confidence intervals. A p-value <0.05 was considered statistically significant.

Results. The mean age of patients in the main group was 29.8±5.4 years, and in the control group 28.9±4.8 years (p=0.36). Gestational age at the time of examination was 31.4±3.6 and 30.9±3.5 weeks, respectively (p=0.48).

Clinically, patients in the main group more frequently presented with asthenovegetative symptoms, pruritus, heaviness in the right upper quadrant, and dyspeptic complaints.

In the main group, marked hyperenzymemia with a predominance of the cytolytic pattern, moderate hyperbilirubinemia, and signs of impaired hepatic synthetic function were observed. The most sensitive laboratory indicators in patients with DILI were ALT, AST, and albumin.

Table 1.

Biochemical Parameters of Liver Function

Indicator	Main group, n=98	Control group, n=40	P
ALT, U/L	98,4 ± 32,6	26,3 ± 7,4	<0,001
AST, U/L	84,7 ± 28,1	24,8 ± 6,1	<0,001
Total bilirubin, µmol/L	28,5 ± 9,4	12,1 ± 3,6	<0,001
Direct bilirubin, µmol/L	12,6 ± 4,2	3,8 ± 1,1	<0,001
ALP, U/L	278 ± 65	182 ± 44	<0,001
GGT, U/L	76 ± 24	28 ± 9	<0,001
Total protein, g/L	63,4 ± 5,1	70,2 ± 4,3	<0,001
Albumin, g/L	32,8 ± 3,6	38,6 ± 3,4	<0,001
INR	1,12 ± 0,12	0,96 ± 0,08	<0,001

In the present study, pregnant women in the main group demonstrated significant alterations in both biochemical and elastographic parameters compared to the control group.

A marked increase in liver stiffness was observed, with values exceeding 9.5 kPa in 67 (68.4%) patients of the main group, indicating a high prevalence of hepatic involvement in DILI during pregnancy (Tab.2).

Placental elastography revealed a substantial increase in placental stiffness in the study cohort. Specifically, placental stiffness values >25 kPa were detected in 42 (42.9%) patients with DILI, whereas only 3 (7.5%) cases in the control group exhibited similar findings. This difference suggests a strong association between DILI and placental tissue remodeling.

These findings indicate that both liver and placental stiffness parameters may serve as valuable non-invasive markers for assessing the severity of maternal hepatic dysfunction and its impact on placental function.

Table 2.

Liver and placental elastography parameters

Indicator	Main group, n=98	Control group, n=40	P
Liver stiffness (LSM) kPa	11,8 ± 2,4	5,8 ± 1,3	<0,001
CAP, dB/m	238 ± 42	198 ± 35	<0,001
IQR/median LSM Placental stiffness (Emean), kPa	0,18 ± 0,05	0,12 ± 0,03	0,002
Emin, kPa	24,6 ± 4,8	14,2 ± 2,9	<0,001
Emax, kPa	17,3 ± 3,4	10,6 ± 2,2	<0,001
Emax, kPa	29,8 ± 5,1	18,5 ± 3,6	<0,001
Heterogeneity index (Emax/Emin)	1,72 ± 0,21	1,45 ± 0,18	<0,001

The analysis of Doppler parameters demonstrated significant differences between the DILI and control groups, reflecting pronounced placental dysfunction in patients with drug-induced liver injury (Tab.3).

Specifically, the pulsatility index (PI) in the uterine arteries was significantly higher in the DILI group compared to the control group (0.92 ± 0.16 vs 0.71 ± 0.11, $p<0.001$), indicating increased uteroplacental vascular resistance. Similarly, the umbilical artery PI was elevated in the DILI group (1.18 ± 0.24 vs 0.89 ± 0.15, $p<0.001$), reflecting impaired fetoplacental blood flow.

In contrast, the middle cerebral artery PI was significantly reduced in the DILI group (1.36 ± 0.22 vs 1.62 ± 0.21, $p<0.001$), consistent with the “brain-sparing” effect. This was further supported by a significantly lower cerebroplacental ratio (CPR) in the DILI group (1.08 ± 0.24 vs 1.71 ± 0.29, $p<0.001$).

The frequency of pathological Doppler findings was markedly higher among patients with DILI. Blood flow impairment was observed in 61 (62.2%) cases compared to 5 (12.5%) in the control group ($p<0.001$). A CPR value below 1.08 was detected in 36 (36.7%) patients in the DILI group versus 2 (5.0%) controls ($p<0.001$).

Table 3.

Doppler parameters and placental insufficiency

Indicator	Main group, n=98	Control group, n=40	P
Uterine artery PI	0.92 ± 0.16	0.71 ± 0.11	<0.001
Umbilical artery PI	1.18 ± 0.24	0.89 ± 0.15	<0.001
Middle cerebral artery PI	1.36 ± 0.22	1.62 ± 0.21	<0.001
Cerebroplacental ratio (CPR)	1.08 ± 0.24	1.71 ± 0.29	<0.001

Indicator	Main group, n=98	Control group, n=40	P
Blood flow impairment, n (%)	61 (62.2%)	5 (12.5%)	<0.001
CPR <1.08, n (%)	36 (36.7%)	2 (5.0%)	<0.001
Fetal growth restriction, n (%)	41 (41.8%)	3 (7.5%)	<0.001

Furthermore, fetal growth restriction was significantly more common in the DILI group, affecting 41 (41.8%) pregnancies compared to only 3 (7.5%) in the control group (p<0.001).

Overall, these findings indicate that DILI in pregnancy is strongly associated with increased vascular resistance, redistribution of fetal circulation, and a higher incidence of placental insufficiency and adverse perinatal outcomes.

The odds ratio analysis demonstrated a strong association between DILI and the development of placental insufficiency. Pregnant women with DILI had a significantly higher risk of placental insufficiency compared to the control group (OR=11.54; 95% CI: 4.15–32.07; p<0.001).

In addition, increased placental stiffness (>25 kPa) was identified as an independent risk factor for placental insufficiency. Patients with elevated placental stiffness had a 4.56-fold higher risk of developing placental dysfunction compared to those with lower stiffness values (OR=4.56; 95% CI: 1.80–11.59; p=0.001).

Table 4.

Odds ratio (OR) for placental insufficiency

Factor	Event	No event	OR (95% CI)	p-value
DILI (n=98) vs control (n=40)	61/98 vs 5/40	37/98 vs 35/40	11.54 (4.15–32.07)	<0.001
Placental stiffness >25 kPa	34/42 vs 27/56	8/42 vs 29/56	4.56 (1.80–11.59)	0.001

These findings suggest that both DILI and increased placental stiffness are significant predictors of placental insufficiency and may be useful for early risk stratification in pregnant women.

The presence of DILI was associated with an over 11-fold increased risk of placental insufficiency compared to controls. Furthermore, within the main group, elevated placental stiffness (>25 kPa) demonstrated an independent clinical association with placental insufficiency (OR=4.56; 95% CI: 1.80–11.59).

The relationship between ALT levels and liver stiffness (by stiffness quartiles) demonstrated a clear positive trend. ALT values progressively increased with rising liver stiffness across quartiles, indicating a direct association between hepatic stiffness and the severity of hepatocellular injury.

A clear inverse relationship between placental stiffness and the cerebroplacental ratio (CPR) was observed. As placental stiffness increased across quartiles, CPR values progressively decreased, indicating worsening fetoplacental circulation.

Specifically, CPR declined from 1.62 in the first quartile (Q1, ~17 kPa) to 1.38 in Q2 (~21 kPa), 1.09 in Q3 (~25 kPa), and reached 0.86 in the fourth quartile (Q4, ~29 kPa). This trend reflects a progressive redistribution of fetal circulation, consistent with the development of placental insufficiency.

Notably, CPR values below the clinically significant threshold (CPR <1.08) were predominantly observed in higher quartiles of placental stiffness, supporting the association between increased placental rigidity and fetal hemodynamic compromise.

These findings suggest that placental stiffness assessed by elastography is closely associated with impaired fetoplacental blood flow and may serve as an early non-invasive marker of placental dysfunction.

The obtained data demonstrate that pregnant women with DILI develop a combined impairment of two functionally interconnected systems hepatic and placental. An increase in liver stiffness (LSM)

was associated with enhanced cytolysis and a moderate decrease in hepatic synthetic function, which is consistent with current clinical guidelines on DILI.

In normal pregnancy, the literature indicates that liver stiffness may physiologically increase toward the third trimester. However, in the present cohort, the mean LSM values significantly exceeded those reported for uncomplicated pregnancies. This suggests that LSM can be considered a useful tool for distinguishing pathological from physiological increases in liver stiffness.

Placental elastography studies in preeclampsia, fetal growth restriction (FGR), and other placenta-mediated disorders have demonstrated increased Emean/SWV values and greater tissue heterogeneity. In our study, a similar trend was accompanied by a decrease in CPR and an increased incidence of abnormal blood flow, indicating a pathophysiological link between inflammatory-toxic liver injury, endothelial dysfunction, and impaired placental maturation.

A clinically significant finding was the identification of a high odds ratio for placental insufficiency both in patients with DILI overall and in those with placental stiffness >25 kPa. This supports the inclusion of placental shear-wave elastography (SWE) in the extended monitoring protocol for pregnant women with drug-induced cytolysis.

Conclusion. Pregnant women with drug-induced liver injury exhibit pronounced biochemical signs of cytolysis and impaired hepatic synthetic function. Liver elastography demonstrates a significant increase in LSM compared to physiological pregnancy, while placental elastography reveals elevated Emean, Emax, and increased tissue heterogeneity. Placental insufficiency occurs significantly more frequently in DILI compared to controls; the calculated odds ratio was 11.54 (95% CI: 4.15–32.07). Placental stiffness >25 kPa may be considered a clinically relevant threshold for increased risk of placental insufficiency. The combined use of biochemical markers, Doppler assessment, and liver/placental elastography allows earlier identification of pregnant women at high perinatal risk.

REFERENCES

1. Alan B, Ercan M, Arioz Haber H, Yuksel M, Taskin S, Kutlu R, et al. Diagnosis of pre-eclampsia and assessment of severity through examination of the placenta with acoustic radiation force impulse elastography. Int J Gynaecol Obstet. 2016;135(1):43-46.

2. Ammon FJ, Gotthardt D, Weiss KH, Bruckner T, Sprinzl MF, Sauer P, et al. Liver stiffness reversibly increases during pregnancy and independently predicts preeclampsia. World J Gastroenterol. 2018;24(38):4393-4402. doi:10.3748/wjg.v24.i38.4393. PMID:30344423.

3. Andrade RJ, Aithal GP, Björnsson ES, Kaplowitz N, Kullak-Ublick GA, Larrey D, et al. Drug-induced liver injury. Nat Rev Dis Primers. 2019;5(1):58. doi:10.1038/s41572-019-0105-0. PMID:31439850.

4. Brady CW. Liver Disease in Pregnancy: What's New. Hepatol Commun. 2020;4(2):145-156. doi:10.1002/hep4.1470. PMID:32025601.

5. Chalasani NP, Maddur H, Russo MW, Wong RJ, Reddy KR. ACG Clinical Guideline: Diagnosis and Management of Idiosyncratic Drug-Induced Liver Injury. Am J Gastroenterol. 2021;116(5):878-898.

6. Cimsit C, Yoldemir T, Akpinar IN. Shear wave elastography in placental dysfunction: comparison of elasticity values in normal and preeclamptic pregnancies in the second trimester. J Ultrasound Med. 2015;34(1):151-159. PMID:25542951.

7. Devarbhavi H, Aithal G, Treeprasertsuk S, Takikawa H, Mao Y, Shasthry SM, et al. Drug-induced liver injury: Asia Pacific Association of Study of Liver consensus guidelines. Hepatol Int. 2021;15(2):258-282.

8. Edwards C, Cavanagh E, Kumar S, Clifton V, Fontanarosa D. The use of elastography in placental research - A literature review. Placenta. 2020; 99:78-88. doi: 10.1016/j.placenta. 2020.07.014. PMID:32763616.

9. European Association for the Study of the Liver. EASL Clinical Practice Guidelines: Drug-induced liver injury. J Hepatol. 2019;70(6):1222-1261. doi: 10.1016/j.jhep.2019.02.014. PMID: 30926241.

10. European Association for the Study of the Liver. EASL Clinical Practice Guidelines on the management of liver diseases in pregnancy. J Hepatol. 2023;79(3):768-828.

11. Fontana RJ, Liou I, Reuben A, Suzuki A, Fiel MI, Lee W, Navarro V. AASLD practice guidance on drug, herbal, and dietary supplement-induced liver injury. Hepatology. 2023;77(3):1036-1065. doi:10.1002/hep.32689. PMID:35899384.

12. Joshi D, James A, Quaglia A, Westbrook RH, Heneghan MA. Liver disease in pregnancy. Lancet. 2010;375:594-605. PMID:20159293.

13. Kılıç F, Kayadibi Y, Yüksel MA, Adaletli I, Ustabasioglu FE, Oncul M, et al. Shear wave elastography of placenta: in vivo quantitation of placental elasticity in preeclampsia. Diagn Interv Radiol. 2015;21(3):202-207. doi:10.5152/dir.2014.14338. PMID:25858523.

14. Nees J, Schwarz C, Sprinzl MF, Stremmel W, Eisenbach C. Liver stiffness in pregnant women with intrahepatic cholestasis of pregnancy. World J Gastroenterol. 2023;29(31):4724-4737. PMID:37547032.

15. Ribeiro MS, Hagström H, Stål P, Ajne G. Transient liver elastography in normal pregnancy - a longitudinal cohort study. Scand J Gastroenterol. 2019;54(6):761-765.

16. Sarkar M, Brady CW, Fleckenstein J, Forde KA, Khungar V, Molleston JP, Afshar Y, Terrault NA. Reproductive Health and Liver Disease: Practice Guidance by the American Association for the Study of Liver Diseases. Hepatology. 2021;73(1):318-365.

17. Serra C, Dajti E, De Molo C, Montaguti E, Porro A, Seidenari A, et al. Utility of Doppler-Ultrasound and Liver Elastography in the Evaluation of Patients with Suspected Pregnancy-Related Liver Disease. J Clin Med. 2023;12(4):1653. doi:10.3390/jcm12041653. PMID:36836188.

18. Westbrook RH, Dusheiko G, Williamson C. Pregnancy and liver disease. J Hepatol. 2016;64(4):933-945.

FACTORS DETERMINING ENDOMETRIAL RECOVERY AND RECEPTIVITY AFTER HYSTEROSCOPIC INTERVENTIONS: CURRENT STATE OF THE PROBLEM

Gulnoza M. Farmonova - Ph.D., trainee researcher
Republican Specialized Scientific and Practical Medical Center for Maternal and Child Health (Tashkent, Uzbekistan)
tatsisstephen@gmail.com

Abstract. Introduction. *Despite the widespread implementation of organ-preserving hysteroscopic procedures, a subset of patients develops impaired endometrial repair, manifested by reduced endometrial thickness, altered structure, and decreased receptivity. These changes are associated with infertility, implantation failure, and recurrent pregnancy loss, underscoring the high clinical relevance of this issue.*

Methods. *A review of scientific publications indexed in PubMed, Scopus, and Web of Science over recent years was conducted. Original studies, systematic reviews, and meta-analyses addressing the pathophysiology of endometrial injury, intrauterine interventions, and factors determining structural and functional recovery of the endometrium were included.*

Results. *Endometrial repair was found to be a multifactorial process influenced by clinical, anamnestic, intraoperative, and molecular factors. Preservation of the basal layer, the extent of surgical trauma, and the type of energy used during the procedure play a critical role. Chronic inflammation and impaired angiogenesis, including imbalance between pro- and anti-angiogenic factors such as PlGF and sFlt-1, are also of major importance. Structural restoration of the endometrium does not necessarily correspond to the recovery of its functional receptivity, highlighting the need for a comprehensive assessment. Emerging therapeutic approaches include regenerative strategies such as platelet-rich plasma (PRP), although current evidence remains limited.*

Conclusion. *Endometrial repair and receptivity following hysteroscopic interventions are determined by a combination of clinical, surgical, and molecular factors. The most significant contributors include damage to the basal layer, inflammatory status, and angiogenic balance. Future research should focus on the development of predictive models and personalized approaches to optimize endometrial recovery.*

Keywords: *endometrium; endometrial repair; endometrial receptivity; hysteroscopy; intrauterine interventions; thin endometrium; angiogenesis; chronic endometritis; implantation; infertility.*

Introduction.

Endometrial injury during intrauterine surgical procedures remains one of the key challenges in modern gynecology. Despite the widespread use of hysteroscopic interventions, a proportion of patients develop impaired endometrial recovery, manifested by reduced endometrial thickness, altered ultrasound structure, and decreased functional receptivity. These changes are associated with adverse reproductive outcomes, including infertility, repeated implantation failure, and recurrent pregnancy loss.

Physiologically, the endometrium possesses a unique capacity for cyclical regeneration, which is maintained by the integrity of the basal layer, the presence of endometrial stem/progenitor cells, adequate angiogenesis, and a balanced immune microenvironment. However, surgical injury—particularly when involving the basal layer—may disrupt these mechanisms, leading to fibrotic remodeling and the formation of intrauterine adhesions, which underlie conditions such as thin endometrium and Asherman syndrome.

In recent years, increasing attention has been focused on identifying factors that determine the regenerative capacity of the endometrium following surgical injury. These factors include patients' clinical and anamnestic characteristics, intraoperative parameters, and molecular mechanisms regulating inflammation, angiogenesis, and tissue repair. It has been demonstrated that chronic endometrial inflammation, imbalance of angiogenic factors, and impaired microcirculation significantly reduce the regenerative potential of the endometrium and its receptivity.

Recent studies indicate that even when morphological parameters of the endometrium, such as its thickness, are restored, functional receptivity may remain compromised. This highlights the need to distinguish between structural repair and functional recovery of the endometrium, as well as the importance of comprehensive assessment using clinical, ultrasonographic, and molecular markers.

Despite the growing body of evidence regarding the pathogenesis of impaired endometrial regeneration, current data remain fragmented, and a unified concept for predicting endometrial recovery is still lacking. Most studies are characterized by heterogeneity in design, variability in outcome definitions, and limited levels of evidence, which complicates the development of clinical recommendations and management algorithms.

In this context, a systematic analysis of contemporary data on clinical, anamnestic, and intraoperative factors affecting endometrial recovery after hysteroscopic interventions is of particular relevance, with the aim of identifying key predictors of regeneration and optimizing management strategies for women of reproductive age.

Objective.

To analyze current evidence on factors influencing endometrial repair and receptivity following hysteroscopic interventions.

Materials and methods.

A review of scientific publications indexed in PubMed, Scopus, and Web of Science was conducted. The analysis included original studies, systematic reviews, and meta-analyses addressing the pathophysiology of endometrial injury, characteristics of intrauterine interventions, and factors determining structural and functional recovery of the endometrium.

Relevant studies were identified using keywords related to endometrial repair, receptivity, and intrauterine adhesion formation. The analysis considered data on patients' clinical and anamnestic characteristics, surgical parameters, and molecular mechanisms, including inflammatory responses and angiogenesis. Particular attention was given to studies evaluating the relationship between morphological restoration of the endometrium and its functional activity, as well as reproductive outcomes.

Results.

In current understanding, damage to the basal layer of the endometrium is considered a central mechanism in the pathogenesis of impaired endometrial repair following intrauterine interventions. This is due to the fact that the basal layer contains cellular populations responsible for cyclical regeneration of the functional layer, including epithelial progenitor cells and the stromal microenvironment that supports tissue repair.

In a large molecular and morphological study, Marečková M. et al. (2024) demonstrated that the endometrial epithelium has a complex architecture, in which basalis glands serve as a reservoir of progenitor cells required for the regeneration of the functionalis layer after physiological shedding. These findings support the concept that surgical trauma involving the basal layer disrupts not only the structural integrity of the endometrium but also its regenerative capacity.

Classical concepts described by Deans R., Abbott J. (2010) and March C.M. (2011) have been confirmed by more recent studies. In particular, the review by Wang P.-H. et al. (2024) highlights that intrauterine adhesions primarily result from injury to the basal layer, leading to replacement of normal repair processes with fibrosis. Similarly, the systematic review by Munro M.G. et al. (2025) identifies intrauterine adhesions as a consequence of surgically induced damage to the basalis layer with

subsequent fibrotic remodeling. Importantly, even after successful adhesiolysis, underlying damage to the basal layer may persist and continue to adversely affect reproductive outcomes.

More recent molecular studies have expanded this concept. In the review by Pardo-Figuerez M. et al. (2025), Asherman syndrome is described not merely as mechanical adhesion formation but as a condition of profound cellular disorganization of the endometrium associated with fibrotic remodeling. Similarly, Zhang X. et al. (2025) emphasize that thin endometrium should be considered a manifestation of impaired regeneration, involving alterations in cellular populations, signaling pathways, and intercellular interactions. This indicates that after hysteroscopic interventions, clinically significant outcomes may include not only adhesion formation but also the development of a functionally inadequate endometrium without overt distortion of the uterine cavity.

The depth of injury appears to be a critical determinant of reproductive outcomes. Contemporary studies indicate that damage to the basalis layer, rather than superficial injury to the functionalis, is associated with a higher risk of persistent fibrosis, reduced endometrial thickness, impaired vascularization, and decreased receptivity. The review by Hu X. et al. (2023) emphasizes that injury to the basal layer disrupts physiological mechanisms of endometrial regeneration. Likewise, Awano-Kim S. et al. (2025) report that partial or complete loss of functional endometrium due to basal layer damage is a key event in the development of Asherman syndrome. Furthermore, progenitor cells have been shown to be localized within the basal layer, explaining the marked reduction in regenerative capacity following its injury.

The clinical significance of these mechanisms is supported by reproductive outcome studies. According to Qiao X. et al. (2025), pregnancy was achieved in 59.38% of patients after hysteroscopic adhesiolysis, while the live birth rate was 42.19%, indicating incomplete restoration of endometrial function in a substantial proportion of women. Additionally, Mortimer R.M. et al. (2024) demonstrated an increased risk of adverse obstetric outcomes, including placenta accreta spectrum, in patients with a history of intrauterine adhesions, reflecting persistent impairment of the endometrial–myometrial interface.

Clinical and anamnestic characteristics of patients also play a significant role in endometrial repair. In the study by Cicinelli E. et al. (2015), chronic endometritis was associated with decreased endometrial receptivity due to altered expression of key implantation factors. Subsequent studies (2022–2024) confirmed that chronic inflammation is accompanied by activation of pro-inflammatory cytokines, particularly IL-6, and the development of subclinical fibrosis, leading to reduced proliferative activity and impaired regeneration.

The study by Kasius J.C. et al. (2014) demonstrated that an endometrial thickness of less than 7 mm is significantly associated with reduced pregnancy rates, indirectly reflecting impaired functional capacity. Recent meta-analyses confirm this association but emphasize that endometrial thickness alone cannot be considered a definitive marker of functional competence.

Additional factors negatively affecting endometrial repair include advanced maternal age, repeated intrauterine interventions (including curettage), and infertility, which reflect baseline impairment of endometrial function. Reduced ovarian reserve and hormonal imbalances may also contribute by altering proliferative activity and estrogen sensitivity.

The nature and extent of hysteroscopic intervention are critical determinants of endometrial regeneration. In the study by Yang J.H. et al. (2021), bipolar energy was associated with less thermal damage compared to monopolar systems. These findings are supported by a meta-analysis by Chen Y. et al. (2023), demonstrating that cold instruments (scissors) result in less tissue trauma, greater postoperative endometrial thickness, and lower recurrence rates of adhesions.

It has also been established that increased resection volume, longer operative time, and aggressive mechanical or electrosurgical manipulation contribute to ischemic and thermal injury and increase the risk of fibrosis. Importantly, recent studies emphasize that the depth of injury, rather than the volume of intervention alone, is the key determinant of impaired repair.

Outcomes are also influenced by surgical technique and operator experience. The review by Loddo A. et al. (2024) highlights that complication rates, including adhesion formation, depend on technical aspects of the procedure, energy modality, and surgical complexity.

Chronic inflammation represents another major determinant of impaired repair. In the study by Li B. et al. (2025), elevated levels of pro-inflammatory cytokines, including IL-6, were associated with fibroblast activation and excessive extracellular matrix deposition, leading to fibrosis and disruption of normal endometrial architecture. In the experimental study by Kumar S. et al. (2025), suppression of fibrotic processes improved vascularization and endometrial thickness.

Recent studies (2023–2024) further indicate that chronic inflammation alters the expression of key receptivity markers (HOXA10, LIF) and disrupts immune balance, contributing to functional impairment even in the absence of overt structural abnormalities.

Importantly, morphological restoration does not necessarily imply functional recovery. Even with normalized endometrial thickness and structure, receptivity may remain impaired due to complex molecular and immunological mechanisms.

This is supported by Chang Y. et al. (2015) and confirmed in more recent studies. Darawshe B. et al. (2025) demonstrated decreased expression of implantation-related genes (HOXA10, IGF-1) and altered immune microenvironment in chronic endometritis. Similarly, Lucan M. et al. (2025) showed that chronic inflammation disrupts the window of implantation through downregulation of key genes.

Molecular studies by Cao Z. et al. (2024) and Wu C. et al. (2025) confirm that endometrial receptivity depends on coordinated regulation of multiple genes and signaling pathways.

Modern diagnostic approaches, including RNA-seq–based receptivity testing (He A. et al., 2023) and personalized embryo transfer (Xu S. et al., 2025), further demonstrate that molecular assessment is essential for predicting implantation success.

Therefore, comprehensive evaluation of the endometrium should include morphological, molecular, immunological, and clinical parameters.

Conclusion.

Endometrial repair following hysteroscopic interventions is a complex multifactorial process determined by clinical characteristics, surgical factors, and molecular mechanisms of regeneration. Preservation of the basal layer is of critical importance, as its damage leads to fibrosis, impaired angiogenesis, and reduced regenerative capacity. Surgical technique and the extent of tissue injury, as well as chronic inflammation, play a decisive role in the development of functional endometrial insufficiency.

Importantly, morphological restoration does not necessarily reflect functional competence, as endometrial receptivity is governed by intricate molecular, immunological, and vascular interactions. Therefore, assessment of endometrial status should be comprehensive, incorporating both structural and functional parameters.

Future research should focus on the development of predictive models and personalized approaches to patient management, as well as on the implementation of novel therapeutic strategies aimed at restoring endometrial function and improving reproductive outcomes.

REFERENCES

1. Abdullaev RH, et al. Chronic endometritis and infertility. Tashkent; 2021.
2. Adamyan LV, Kulakov VI, et al. Intrauterine pathology and hysteroscopy. Moscow: GEOTAR-Media; 2019.
3. Akhmedov AA, et al. Modern aspects of treatment of intrauterine pathology. 2022.
4. Baranov VS, et al. Molecular mechanisms of endometrial receptivity. 2021.
5. Chen Y, et al. Clinical efficacy of hysteroscopic adhesiolysis techniques. Front Endocrinol. 2023.

6. Cicinelli E, et al. Chronic endometritis: a frequent cause of infertility. Fertil Steril. 2015;104(2):427–435.
7. Deans R, Abbott J. Intrauterine adhesions: a review of current management. Fertil Steril. 2010;93(3):775–789.
8. Dobrokhotova YE, et al. Intrauterine adhesions: diagnosis and treatment. Vestnik RSMU. 2021.
9. Gao Y, et al. Risk factors of chronic endometritis. Sci Rep. 2024.
10. Hooker AB, et al. Long-term complications and reproductive outcome after intrauterine adhesions. Hum Reprod Update. 2014;20(2):262–278.
11. Hu X, et al. Cyclical endometrial repair and regeneration. Nat Rev Endocrinol. 2023.
12. Ismailov SI, et al. Reproductive outcomes in intrauterine pathology. 2022.
13. Kasius JC, et al. Endometrial thickness and pregnancy rates in IVF. Hum Reprod Update. 2014;20(4):530–541.
14. Kulakov VI, Adamyan LV. Endoscopy in gynecology. Moscow; 2018.
15. Kuznetsova IV, et al. The role of inflammation in endometrial pathology. 2022.
16. Li B, et al. Inflammatory mechanisms of endometrial injury. Front Bioeng Biotechnol. 2025.
17. Loddo A, et al. Prevention and management of hysteroscopic complications. Gynecol Pelvic Med. 2024.
18. Lucan M, et al. Chronic endometritis and reproductive outcomes. J Clin Med. 2025.
19. Marečková M, et al. An integrated single-cell reference atlas of the human endometrium. Nat Genet. 2024.
20. March CM. Management of Asherman's syndrome. Reprod Biomed Online. 2011;23(1):63–76.
21. Marzooq AA, et al. Effectiveness of hysteroscopic surgery in infertility. 2025.
22. Munro MG, et al. Epidemiology and prevention of intrauterine adhesions. Am J Obstet Gynecol. 2025.
23. Nazarov KM, et al. The impact of surgical interventions on the endometrium. 2023.
24. National Medical Research Center for Obstetrics, Gynecology and Perinatology named after V.I. Kulakov. Chronic endometritis: modern approaches to diagnosis and treatment. Obstet Gynecol. 2021.
25. Orazov MR, et al. Thin endometrium: pathogenesis and treatment. Obstet Gynecol Reprod. 2022.
26. Radzinsky VE, Orazov MR. Chronic endometritis in gynecological practice. Obstet Gynecol. 2020.
27. Riemma G, et al. Diagnostic accuracy of hysteroscopy. Am J Obstet Gynecol. 2025.
28. Savelieva GM, Sukhikh GT. Gynecology: National guideline. Moscow; 2022.
29. Serov VN, Prilepskaya VN. Women's reproductive health. Moscow; 2020.
30. Tsonis O, et al. Hysteroscopic features of chronic endometritis. 2023.
31. Wang PH, et al. Intrauterine adhesion: pathogenesis and management. Taiwan J Obstet Gynecol. 2024.
32. Wang Y, et al. Advances in treatment of thin endometrium. Front Endocrinol. 2024.
33. Yusupov BB, et al. Hysteroscopy in diagnosis and treatment of endometrial pathology. 2020.
34. Yang JH, et al. Effects of electrosurgical systems on endometrial damage. 2021.
35. Zhang X, et al. Thin endometrium at single-cell resolution. Am J Obstet Gynecol. 2025.

UDC: 616.831-005.1-036.8:615.825

CHANGES IN MOTOR FUNCTION AFTER PSYCHOMOTOR REHABILITATION IN POST-ISCHEMIC STROKE PATIENTS: A CONTROLLED STUDY USING FUGL-MEYER ASSESSMENT

Maftuna B. Ibodulloyeva - doctoral (Ph.D.) candidate
Zarifboy R. Ibodullayev - professor
Tashkent State Medical University (Tashkent, Uzbekistan)
ibodulloyevamaftuna9@gmail.com

Abstract. *Stroke remains one of the leading causes of long-term disability worldwide, with motor impairment being the most common consequence affecting functional independence and quality of life. The aim of this study was to evaluate changes in motor and sensory functions in patients after ischemic stroke undergoing psychomotor rehabilitation using the Fugl-Meyer Assessment (FMA). A prospective controlled clinical study was conducted involving 100 patients with ischemic stroke who were randomly assigned into two groups: a psychomotor rehabilitation group (n = 50) receiving psychomotor therapy in addition to standard rehabilitation, and a control group (n = 50) receiving standard rehabilitation only. The rehabilitation program lasted eight weeks and consisted of four sessions per week, each lasting 60 minutes. Motor and sensory functions were evaluated using the Fugl–Meyer Assessment scale before and after the intervention. At baseline, the groups were comparable in clinical and functional characteristics, with Barthel Index scores of 71.2 ± 7.73 and 71.7 ± 9.01 in the intervention and control groups, respectively. After rehabilitation, significant improvements were observed in both groups across several FMA domains. In the psychomotor group, lower limb motor function increased from 23.26 to 32.48 points (+9.22), sensory function from 16.6 to 27.5 points (+10.9), and joint motion from 22.3 to 41.94 points (+19.64). Mixed-design ANOVA demonstrated a significant effect of time across all FMA subcomponents ($p < 0.001$), indicating substantial functional recovery during the rehabilitation period. Moreover, significant time × group interactions were observed for sensory function, joint motion, and lower limb motor function, suggesting additional therapeutic benefits of psychomotor rehabilitation. These findings indicate that psychomotor-based rehabilitation may enhance motor recovery after ischemic stroke and contribute to improved functional outcomes.*

Keywords: *stroke rehabilitation; psychomotor therapy; neurorehabilitation; motor recovery; Fugl-Meyer Assessment; post-stroke recovery; sensorimotor integration*

Introduction. Ischemic stroke remains one of the leading causes of long-term disability worldwide and continues to pose a substantial challenge for healthcare systems. According to global epidemiological analyses, stroke accounts for a significant proportion of neurological morbidity and mortality, with millions of new cases occurring each year. Despite improvements in acute stroke management and prevention strategies, a considerable number of survivors experience persistent functional deficits that require prolonged rehabilitation [1, 5]. Recent global burden estimates indicate that stroke remains a major contributor to disability-adjusted life years (DALYs), particularly in low- and middle-income countries where access to comprehensive rehabilitation services is often limited [2].

Motor dysfunction is among the most frequent and disabling consequences of ischemic stroke. Clinical observations suggest that up to 70–80% of patients develop varying degrees of motor impairment during the acute stage of the disease, and many of these deficits persist during the chronic phase [7, 13]. These impairments commonly include hemiparesis, reduced coordination, impaired balance, and decreased motor control, all of which significantly limit patients' independence in daily activities and reduce quality of life [8]. As a result, restoring motor function has become one of the primary goals of post-stroke rehabilitation.

Over the past decades, advances in neuroscience have improved the understanding of neuroplasticity and its role in functional recovery after stroke. Neuroplasticity refers to the brain's ability to reorganize neural networks and establish new functional connections following injury. Rehabilitation approaches that incorporate repetitive, task-oriented and sensorimotor training are believed to stimulate these adaptive mechanisms and facilitate recovery of motor function [6, 9]. Within this context, psychomotor rehabilitation has emerged as a promising therapeutic approach that integrates movement, sensory perception and emotional regulation into structured therapeutic activities. By addressing motor control together with sensorimotor integration and body awareness, psychomotor interventions may enhance functional recovery beyond the effects of conventional exercise-based rehabilitation [4, 12].

To evaluate the effectiveness of rehabilitation interventions, reliable and standardized outcome measures are essential. Among the available clinical scales, the Fugl-Meyer Assessment (FMA) is widely considered one of the most comprehensive tools for assessing motor recovery after stroke. Developed specifically for post-stroke patients, the scale evaluates multiple domains including motor function of the upper and lower extremities, sensory function, balance, joint motion and joint pain [3]. Numerous clinical trials and systematic reviews have demonstrated the reliability and validity of the FMA as a sensitive measure of motor recovery in stroke rehabilitation studies [11, 10]. Consequently, the scale has become a standard outcome measure in both clinical practice and research.

Despite growing interest in psychomotor rehabilitation, evidence regarding its effectiveness in improving motor recovery after ischemic stroke remains limited, particularly in clinical settings where traditional rehabilitation approaches predominate. Further investigation is therefore needed to determine whether integrating psychomotor components into rehabilitation programs can enhance functional recovery and improve clinical outcomes.

The aim of the present study was to evaluate changes in motor function in post-ischemic stroke patients undergoing psychomotor rehabilitation using the Fugl-Meyer Assessment scale.

Objective of the study. The aim of this study was to evaluate changes in motor and sensory functions in patients after ischemic stroke undergoing psychomotor rehabilitation using the Fugl-Meyer Assessment scale, and to compare the effectiveness of psychomotor-based rehabilitation with standard rehabilitation approaches in improving functional recovery.

Materials and Methods. This study was designed as a prospective controlled clinical study aimed at evaluating the effectiveness of psychomotor rehabilitation in patients after ischemic stroke. The research was conducted in cooperation with the neurology department and specialized rehabilitation centers in Tashkent, Uzbekistan.

All procedures were performed in accordance with international ethical standards for biomedical research involving human participants. Participation in the study was voluntary, and all participants provided written informed consent before inclusion.

Patients received standard neurorehabilitation therapy according to clinical practice guidelines. In addition, patients in the intervention group underwent structured psychomotor rehabilitation sessions conducted by trained rehabilitation specialists.

Participants. A total of 130 individuals were initially screened for participation in the study. Among them, 100 patients with ischemic stroke met the inclusion criteria and were included in the final statistical analysis, while 30 healthy individuals were recruited as a control group for baseline comparison.

Patients with ischemic stroke were randomly assigned into two groups using a simple randomization method (Table 1):

- Psychomotor rehabilitation group (n = 50) - psychomotor therapy combined with standard rehabilitation
- Control rehabilitation group (n = 50) - standard rehabilitation only

Healthy volunteers (n = 30) were included as a reference control group.

Table 1.

Distribution of participants across study groups

Group	Number of participants
Psychomotor rehabilitation	50
Standard rehabilitation	50
Healthy control	30
Total	130

Participant inclusion and exclusion were determined according to the following predefined criteria (Table 2).

Table 2.

Inclusion and exclusion criteria for participant selection

Inclusion criteria	Exclusion criteria
confirmed diagnosis of ischemic stroke	recurrent stroke
age 30–70 years	severe somatic or psychiatric disorders
post-stroke rehabilitation stage	severe cognitive impairment
NIHSS score 5–20	epilepsy or uncontrolled cardiovascular disease
preserved cognitive ability	inability to participate regularly
stable neurological condition	absence during final evaluation
written informed consent	-

After applying these criteria, 30 patients were excluded, leaving 100 patients for final analysis.

Clinical and instrumental assessment. The diagnosis of ischemic stroke was confirmed using magnetic resonance imaging (MRI) and computed tomography (CT). MRI examinations included DWI, FLAIR, T1-weighted and T2-weighted sequences to identify ischemic lesions.

Additional diagnostic procedures included Doppler ultrasonography of the brachiocephalic arteries, electrocardiography (ECG), and echocardiography (EchoCG). These examinations were carried out to further clarify the etiology of ischemic stroke and to identify possible comorbid cardiovascular conditions that could influence the clinical course of the disease and the rehabilitation process.

Distribution of stroke localization. Stroke localization was classified according to vascular territory using MRI findings (Table 3, Figure 1).

Table 3.

Distribution of ischemic stroke localization

Localization	Psychomotor group (n=50)	Control group (n=50)
Left hemisphere (ACA + MCA)	11 (22%)	13 (26%)
Right MCA territory	17 (34%)	18 (36%)
Vertebrobasilar territory	22 (44%)	19 (38%)

No statistically significant differences between groups were observed at baseline ($p > 0.05$).

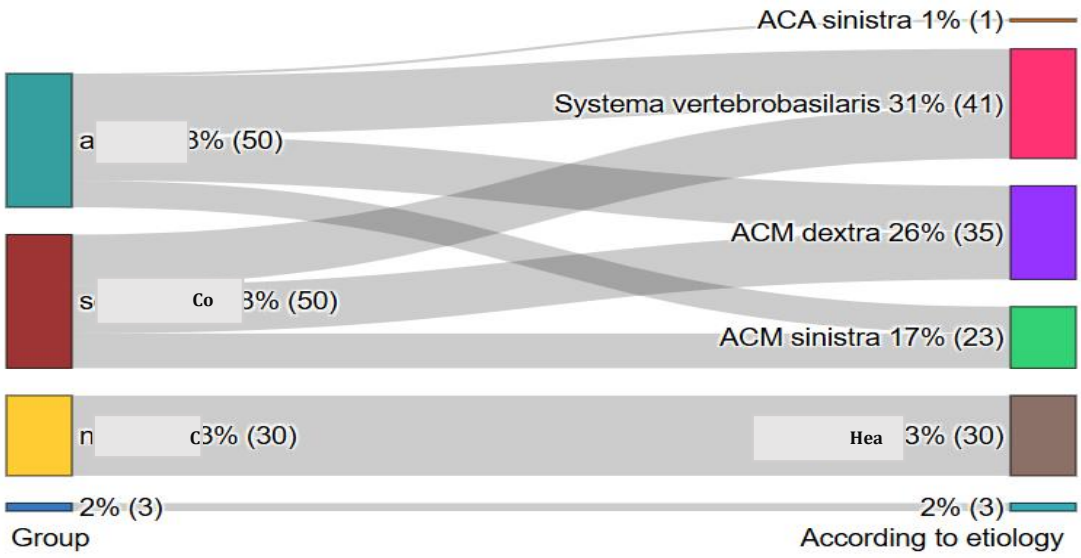


Figure 1. Distribution of stroke localization by vascular territory

Rehabilitation protocol. All participants received standard rehabilitation therapy including therapeutic exercises and functional training.

Patients in the intervention group additionally underwent psychomotor rehabilitation sessions consisting of:

- sensorimotor integration exercises
- coordination training
- rhythmic motor exercises
- task-oriented movement training
- body awareness exercises

The rehabilitation program lasted 8 weeks, with four sessions per week, each session lasting 60 minutes (Table 4).

Table 4.

Psychomotor rehabilitation protocol

Parameter	Value
Session duration	60 minutes
Sessions per week	4
Program duration	8 weeks
Total sessions	32

Recommended diagram structure:

- Warm-up (10 min)
- Sensorimotor exercises (15 min)
- Coordination and balance training (15 min)
- Task-oriented motor exercises (15 min)
- Relaxation and body awareness (5 min)

Functional outcome measures. Motor function was assessed using the Fugl-Meyer Assessment (FMA) scale. The scale evaluates motor recovery after stroke across several domains including motor function, sensory function, balance, joint range of motion and joint pain (Figure 2).

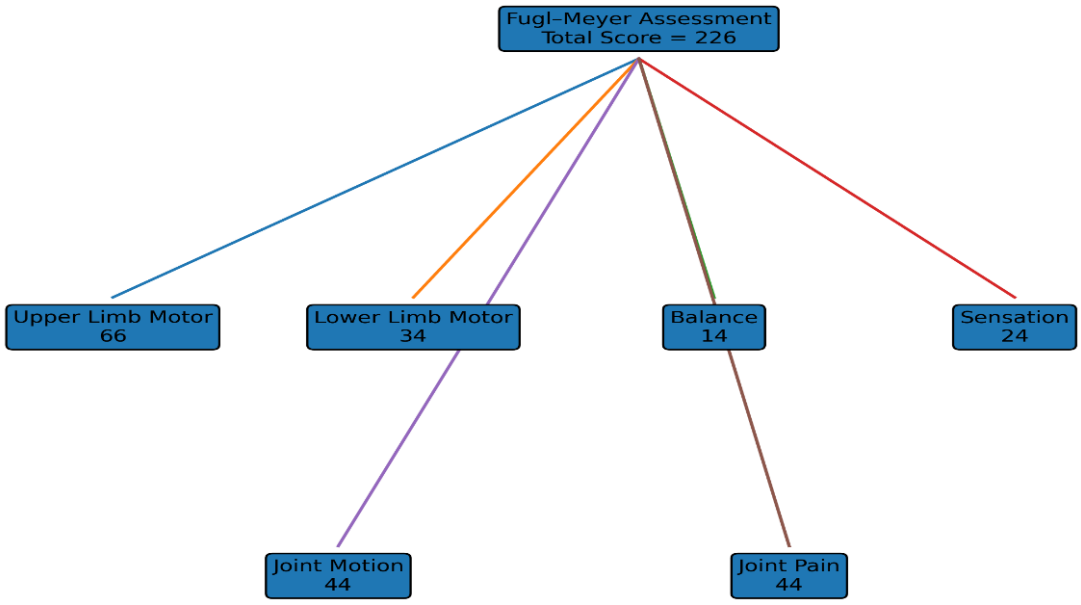


Figure 2. Fugl-Meyer assessment domains

Motor assessments were performed before rehabilitation and after completion of the intervention.

Statistical analysis. Statistical analysis was performed using the NumiQo statistical software package. Descriptive statistics were presented as mean values with standard deviations (mean ± SD) together with 95% confidence intervals. Prior to inferential analysis, the normality of data distribution was assessed using the Shapiro–Wilk test. Differences between groups were analyzed using the independent samples t-test, while changes within each group before and after the intervention were evaluated using the paired samples t-test. In addition, a mixed-design analysis of variance (ANOVA 2×2) was applied to examine the interaction between time (before and after rehabilitation) and group (psychomotor rehabilitation vs. standard rehabilitation). Statistical significance was set at $p < 0.05$. To estimate the magnitude of treatment effects, effect sizes were calculated using partial eta-squared (η^2p).

Results and Discussion. Motor and sensory recovery following rehabilitation was evaluated using the Fugl-Meyer Assessment (FMA) scale. Analysis of the FMA subcomponents demonstrated substantial improvements in motor and sensory functions during the rehabilitation period. At baseline, the psychomotor rehabilitation group and the comparison group had comparable scores across all FMA domains, indicating similar levels of neurological impairment prior to intervention. This comparability allowed subsequent changes to be attributed to the effects of the rehabilitation program.

In terms of upper limb motor function, the FMA score in the psychomotor rehabilitation group increased from 33.56 to 42.92 points, corresponding to an improvement of +9.36 points. In the comparison group, the score increased from 32.18 to 43.34 points, representing an improvement of +11.16 points. Although improvements were observed in both groups, the mixed-design ANOVA revealed a highly significant effect of time ($F = 764.03$; $p < 0.001$; $\eta^2p = 0.89$), confirming substantial motor recovery over the course of rehabilitation.

Recovery of lower limb motor function was more pronounced in the psychomotor rehabilitation group. The FMA score increased from 23.26 to 32.48 points, representing a gain of +9.22 points, whereas in the comparison group the increase was from 22.82 to 29.06 points (+6.24 points). Statistical analysis demonstrated a significant time effect ($F = 1118.16$; $p < 0.001$; $\eta^2p = 0.92$) as well as a significant time × group interaction, indicating faster recovery in the psychomotor rehabilitation group.

Substantial improvements were also observed in sensory function. In the psychomotor rehabilitation group, sensory scores increased from 16.6 to 27.5 points (+10.9 points), while in the comparison group the increase was from 18.78 to 24.14 points (+5.36 points). The mixed ANOVA results showed a highly significant time effect ($F = 1619.29$; $p < 0.001$; $\eta^2p = 0.94$) and a significant time × group interaction ($p < 0.001$), indicating greater sensory recovery in the psychomotor rehabilitation group.

Joint mobility showed the most pronounced improvement among the FMA domains. In the psychomotor rehabilitation group, the joint motion score increased from 22.3 to 41.94 points (+19.64 points), while in the comparison group the improvement was from 22.22 to 32.96 points (+10.74 points). The ANOVA analysis revealed a very strong time effect ($F = 2932.3$; $p < 0.001$; $\eta^2p = 0.97$) as well as a significant time × group interaction, indicating a clear advantage of the psychomotor rehabilitation approach.

In contrast, improvements in the joint pain component were similar in both groups. The psychomotor rehabilitation group demonstrated an increase from 28.42 to 33.18 points (+4.76 points), while the comparison group improved from 28.68 to 33.76 points (+5.08 points). Statistical analysis showed a significant effect of time ($F = 417.06$; $p < 0.001$; $\eta^2p = 0.81$), but no significant group effect or interaction between time and group (Figure 3).

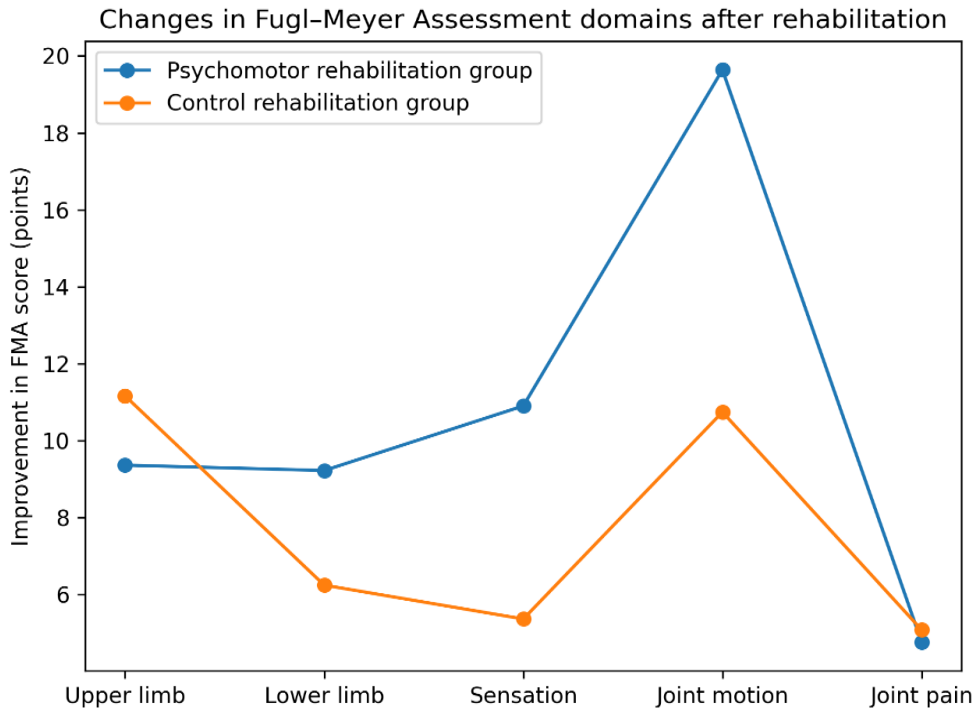


Figure 3. Comparative improvement in Fugl-Meyer Assessment domains after rehabilitation in psychomotor and control groups

The mixed-design ANOVA results demonstrated that the time factor was highly significant across all FMA subcomponents ($p < 0.001$), confirming that rehabilitation contributed substantially to improvements in motor and sensory functions. However, the time × group interaction indicated that rehabilitation incorporating psychomotor components produced greater improvements in sensory function, joint mobility, and lower limb motor recovery, while improvements in upper limb motor function and joint pain were comparable between the groups (Table 5).

Table 5.

Changes in Fugl–Meyer Assessment subcomponents after rehabilitation

FMA Domain	Psychomotor group (Before–After)	Improvement	Control group (Before–After)	Improvement
Upper limb motor	33.56 → 42.92	+9.36	32.18 → 43.34	+11.16
Lower limb motor	23.26 → 32.48	+9.22	22.82 → 29.06	+6.24
Sensation	16.6 → 27.5	+10.9	18.78 → 24.14	+5.36
Joint motion	22.3 → 41.94	+19.64	22.22 → 32.96	+10.74
Joint pain	28.42 → 33.18	+4.76	28.68 → 33.76	+5.08

Clinical interpretation. The findings demonstrate that rehabilitation interventions produced significant improvements in all domains of the Fugl–Meyer Assessment. However, the rehabilitation approach incorporating psychomotor components showed clear clinical advantages in sensory recovery, joint mobility, and lower limb motor function, suggesting that sensorimotor integration and body-awareness training may enhance neuroplastic recovery mechanisms following stroke.

Discussion. The present study evaluated the effectiveness of a rehabilitation approach incorporating psychomotor components on motor and sensory recovery in patients after ischemic stroke using the Fugl-Meyer Assessment (FMA) scale. The obtained results demonstrated significant improvements across all major FMA subcomponents during the rehabilitation period. Mixed-design ANOVA analysis revealed a highly significant effect of time across all domains ($p < 0.001$), confirming that rehabilitation interventions substantially contributed to the recovery of motor and sensory functions after stroke.

One of the most important findings of this study is the differential pattern of recovery across FMA domains. Although both rehabilitation approaches produced improvements in upper limb motor function, the final outcomes between groups did not differ significantly. In the psychomotor rehabilitation group, upper limb motor function improved from 33.56 to 42.92 points, while in the comparison group the score increased from 32.18 to 43.34 points. This finding suggests that conventional rehabilitation strategies may already be effective in improving upper limb motor function in post-stroke patients. Similar observations were reported by Kwakkel et al. (2015), who noted that upper limb recovery often depends on complex cortical motor network reorganization and may require longer rehabilitation periods to demonstrate clear intergroup differences.

In contrast, more pronounced improvements were observed in lower limb motor function in the psychomotor rehabilitation group. Lower limb FMA scores increased from 23.26 to 32.48 points (+9.22 points), compared with an increase from 22.82 to 29.06 points (+6.24 points) in the comparison group. This finding may be explained by the integrative nature of psychomotor therapy, which emphasizes body awareness, postural regulation, and coordinated sensorimotor activity. Previous studies have shown that gait and lower limb motor control rely heavily on sensorimotor integration processes involving both cortical and subcortical structures. According to Langhorne et al. (2011), rehabilitation strategies incorporating repetitive and task-oriented motor training can significantly enhance lower limb functional recovery after stroke.

Another important finding of this study concerns sensory function recovery. In the psychomotor rehabilitation group, sensory FMA scores increased from 16.6 to 27.5 points, whereas the comparison group demonstrated a smaller improvement from 18.78 to 24.14 points. The strong time × group interaction observed for this domain indicates that psychomotor therapy may have a particularly strong effect on sensory integration mechanisms. These findings support the concept that rehabilitation approaches focusing on proprioceptive stimulation and body schema reorganization can

facilitate neural plasticity and improve sensorimotor processing. Similar results were reported by Carey et al. (2016), who demonstrated that targeted sensory rehabilitation strategies significantly improve sensory discrimination and motor outcomes in post-stroke patients.

The most pronounced improvement was observed in joint motion, where the psychomotor rehabilitation group demonstrated an increase from 22.3 to 41.94 points, compared with an increase from 22.22 to 32.96 points in the comparison group. The very large effect size observed in this domain suggests that psychomotor-based rehabilitation may enhance joint mobility through mechanisms beyond passive mobilization. Specifically, the integration of intentional movement, proprioceptive feedback, and coordinated motor patterns may facilitate more efficient neuromuscular activation and functional joint movement. According to Krakauer et al. (2012), repetitive sensorimotor training promotes cortical reorganization and strengthens neural networks responsible for coordinated movement control.

In contrast, improvements in the joint pain component were similar in both groups. Although both groups demonstrated reductions in pain-related limitations over time, the absence of a significant time × group interaction suggests that pain reduction may be primarily associated with general increases in physical activity and joint mobilization rather than with the specific rehabilitation approach used.

Overall, the findings of this study indicate that rehabilitation programs incorporating psychomotor components may provide additional therapeutic benefits in several key domains of the Fugl-Meyer Assessment, particularly sensory recovery, joint mobility, and lower limb motor function. These domains are closely related to postural control, gait stability, and functional movement coordination, which are essential for regaining independence after stroke. The results therefore support the growing body of evidence suggesting that rehabilitation approaches integrating sensorimotor and body-awareness training may enhance neuroplastic recovery mechanisms and improve functional outcomes in post-stroke rehabilitation.

Conclusion. The findings of this study demonstrate that rehabilitation interventions significantly improved motor and sensory recovery in post-ischemic stroke patients according to the Fugl-Meyer Assessment (FMA) scale. At baseline, both study groups showed comparable levels of impairment across all FMA domains, allowing the observed improvements to be interpreted as the effect of the rehabilitation intervention.

Upper limb motor function improved in both groups during the rehabilitation period. In the psychomotor rehabilitation group, the FMA upper limb score increased from 33.56 to 42.92 points, corresponding to an improvement of +9.36 points, while in the comparison group the score increased from 32.18 to 43.34 points (+11.16 points). These results indicate that both rehabilitation approaches were effective in enhancing upper limb motor performance.

More pronounced differences were observed in lower limb motor function, where the psychomotor rehabilitation group demonstrated a greater improvement. The FMA lower limb score increased from 23.26 to 32.48 points (+9.22 points) in the psychomotor group, compared with an increase from 22.82 to 29.06 points (+6.24 points) in the comparison group.

Substantial improvements were also identified in sensory function. Sensory FMA scores increased from 16.6 to 27.5 points (+10.9 points) in the psychomotor rehabilitation group, whereas the comparison group demonstrated a smaller increase from 18.78 to 24.14 points (+5.36 points).

The largest improvement was observed in joint motion, where the psychomotor rehabilitation group demonstrated an increase from 22.3 to 41.94 points (+19.64 points), compared with an increase from 22.22 to 32.96 points (+10.74 points) in the comparison group. Improvements in the joint pain component were similar between groups, with increases of +4.76 points and +5.08 points, respectively.

Overall, statistical analysis confirmed a highly significant time effect across all FMA subcomponents ($p < 0.001$), indicating substantial improvement in motor and sensory functions

during the rehabilitation period. In addition, the observed time × group interaction suggests that rehabilitation incorporating psychomotor components may provide additional clinical benefits, particularly in improving sensory function, joint mobility, and lower limb motor recovery.

These findings indicate that integrating psychomotor elements into rehabilitation programs may enhance functional recovery mechanisms and contribute to more effective restoration of motor and sensory functions in patients after ischemic stroke.

REFERENCES

1. Feigin, V. L., Stark, B. A., Johnson, C. O., Roth, G. A., Bisignano, C., Abady, G. G., & Murray, C. J. L. (2021). Global, regional, and national burden of stroke and its risk factors, 1990–2019. The Lancet Neurology, 20(10), 795–820. https://doi.org/10.1016/S1474-4422(21)00252-0

2. GBD Stroke Collaborators. (2021). Global, regional, and national burden of stroke and its risk factors, 1990–2019: A systematic analysis. The Lancet Neurology, 20(10), 795–820.

3. Gladstone, D. J., Danells, C. J., & Black, S. E. (2002). The Fugl-Meyer Assessment of motor recovery after stroke: A critical review of its measurement properties. Neurorehabilitation and Neural Repair, 16(3), 232–240.

4. Ilg, W., Giese, M., Gizewski, E., Schoch, B., & Timmann, D. (2013). Intensive coordinative training improves motor performance in degenerative cerebellar disease. Neurology, 79(20), 2056–2060.

5. Johnson, C. O., Nguyen, M., Roth, G. A., Nichols, E., Alam, T., Abate, D., & Murray, C. J. L. (2019). Global, regional, and national burden of stroke, 1990–2016. The Lancet Neurology, 18(5), 439–458.

6. Krakauer, J. W., Carmichael, S. T., Corbett, D., & Wittenberg, G. (2012). Getting neurorehabilitation right: What can be learned from animal models? Neurorehabilitation and Neural Repair, 26(8), 923–931.

7. Kwakkel, G., Kollen, B. J., & Wagenaar, R. C. (2015). Long-term effects of stroke rehabilitation. Stroke, 30(12), 2524–2529.

8. Langhorne, P., Bernhardt, J., & Kwakkel, G. (2011). Stroke rehabilitation. The Lancet, 377(9778), 1693–1702.

9. Pollock, A., Farmer, S. E., Brady, M. C., Langhorne, P., Mead, G. E., Mehrholz, J., & van Wijck, F. (2014). Interventions for improving upper limb function after stroke. Cochrane Database of Systematic Reviews.

10. See, J., Dodakian, L., Chou, C., Chan, V., & Cramer, S. (2013). A standardized approach to the Fugl–Meyer Assessment and its implications for clinical trials. Neurorehabilitation and Neural Repair, 27(8), 732–741.

11. Sullivan, K. J., Tilson, J. K., Cen, S. Y., Rose, D. K., Hershberg, J., Correa, A., & Duncan, P. W. (2011). Fugl–Meyer Assessment of sensorimotor function after stroke. Stroke, 42(2), 427–432.

12. Thaut, M. H., McIntosh, G. C., & Hoemberg, V. (2015). Neurobiological foundations of neurologic music therapy. Progress in Brain Research, 217, 303–321.

13. Veerbeek, J. M., van Wegen, E., van Peppen, R., van der Wees, P., Hendriks, E., & Kwakkel, G. (2014). What is the evidence for physical therapy poststroke? PLoS ONE, 9(2), e87987.

THE IMPORTANCE OF CELL ADHESION MOLECULE LEVELS IN THE COURSE AND PROGNOSIS OF HEMORRHAGIC STROKE

Gulchekhra E. Usmanova - Ph.D. doctoral student
Gulnora S. Rakhimbaeva - D.M.Sc., professor
Tashkent State Medical University (Tashkent, Uzbekistan)
Guli.uzb1@gmail.com

Abstract. *This study investigates the role of intercellular adhesion molecule-1 (ICAM-1) and vascular cell adhesion molecule-1 (VCAM-1) as biomarkers in hemorrhagic stroke prognosis. Analyzing 83 patients, researchers found that ICAM- 1 levels increased 2.5-fold within 48 hours and continued rising, while VCAM-1 levels increased 1.5-fold before slightly decreasing. Both correlated with stroke severity and mortality. The study highlights the Full Outline of Unresponsiveness (FOUR) scale as a superior tool for assessing critically ill patients and suggests that ICAM-1 and VCAM-1 could aid in predicting stroke outcomes and guiding treatment strategies.*

Keywords *— hemorrhagic stroke, Glasgow Coma Scale (GCS), FOUR, ICAM-1, VCAM-1*

Introduction. Hemorrhagic strokes are among the most severe forms of cerebrovascular disease, often leading to high rates of premature death, disability, and complications. These strokes impose significant economic burdens on society, requiring long-term treatment and rehabilitation. According to international data, intracerebral hemorrhages account for 3.7% to 38.5% of all stroke cases, with an incidence rate of 1.9 per 100,000 people [1]. In the United States, the mortality rate from hemorrhagic strokes in 2020 ranged from 39% to 50%, with half of these deaths occurring within the first 48 hours [3]. Additionally, the one-month mortality rate for intracerebral hematomas (ICH) is approximately 40%, increasing to 54% within a year [4-5].

Arterial hypertension is the leading cause of primary intracerebral hemorrhage, responsible for over 50% of cases. In Uzbekistan, more than 60,000 cases of acute cerebrovascular accidents are recorded annually. The disability rate following stroke is 83.8%, while the mortality rate stands at 17.3%, with over 160 new cases occurring daily. Given the diverse clinical presentations of hemorrhagic stroke, there is an urgent need to develop new prognostic criteria to assess disease severity, predict outcomes, and evaluate the risk of recurrence [2].

Despite extensive research efforts, the prognosis of hemorrhagic stroke remains a critical issue. The identification of reliable blood biomarkers for diagnosis and outcome prediction is an area of growing interest. Neuroinflammation markers in peripheral blood reflect the body's response to acute cerebrovascular events, offering potential insights into disease progression.

Aim of the Study. This study aims to evaluate the role of inflammatory biomarkers intercellular adhesion molecule-1 (ICAM-1) and vascular cell adhesion molecule-1 (VCAM-1) in the pathogenesis of hemorrhagic stroke.

Materials and Methods. A total of 83 patients with hemorrhagic stroke were examined at the intensive care and neurology departments of the Tashkent Medical Academy Clinic. All patients were in the acute stage of the disease, diagnosed with hemorrhagic stroke. Comprehensive assessments included clinical- neurological examinations, neuroimaging, and laboratory analyses, following modern clinical guidelines. The GCS and the Full Outline of UnResponsiveness (FOUR) scale were used to assess consciousness levels upon admission.

ICAM-1 and VCAM-1 levels were determined by quantitative enzyme immunoassay. Statistical processing of the results was carried out using Statistica 6.0.

Results and Discussion. Of the 83 patients, 46 (55.4%) were men and 37 (44.6%) were women, with an age range of 36–84 years (mean age: 63.2 years).

Table 1.

Distribution of patients by age

Age	Number of patients	Percentage (%) of total
30-39	4	4.8%
40-49	16	19.3%
50-59	25	30.1%
60-69	29	34.9%
70-79	6	7.2%
80-90	3	3.6%

By hemorrhage localization: parenchymal – 50.6% (n=42), subarachnoid – 12% (n=10), parenchymal- subarachnoid – 8.4% (n=7), brainstem – 3.6% (n=3), ventricular – 7.2% (n=6), parenchymal-ventricular – 8.4% (n=7), subarachnoid-ventricular – 4.8% (n=4), subarachnoid-parenchymatous-ventricular – 2.4% (n=2) and hemorrhage into the cerebellum – 2.4% (n=2).

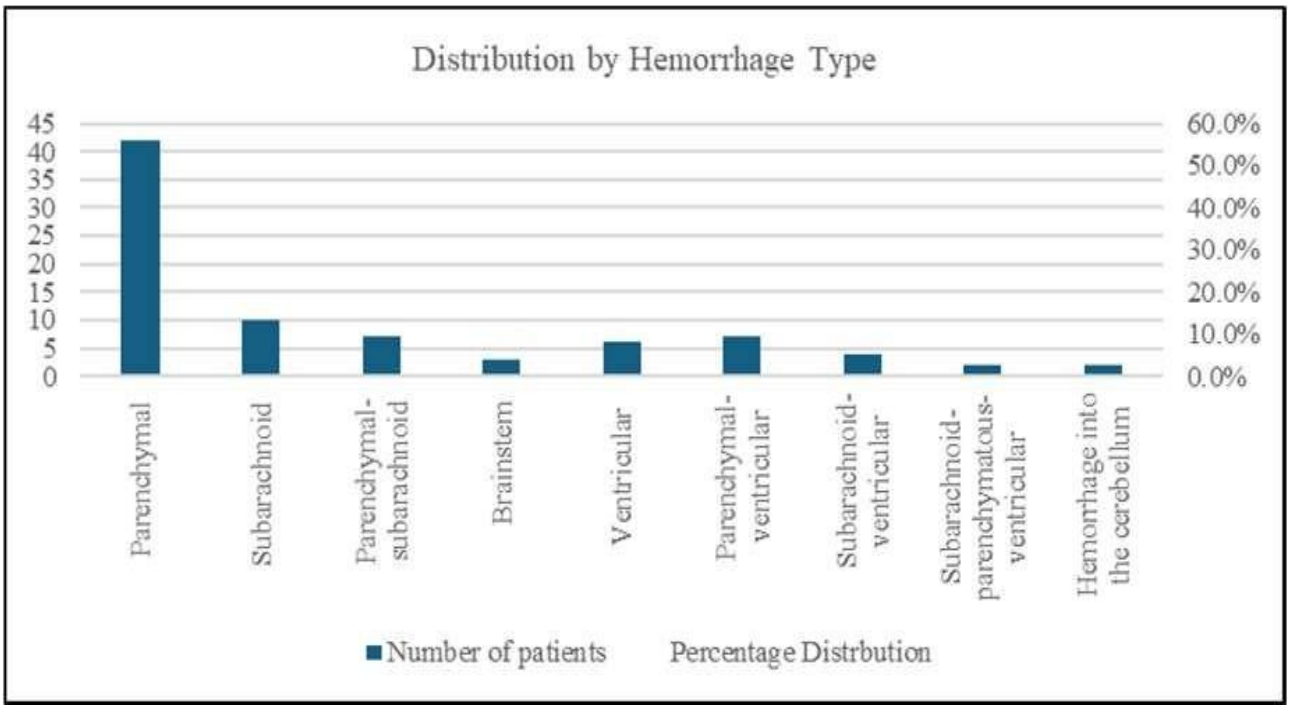


Fig. 1. Distribution by Hemorrhage Type

The GCS, FOUR Scale, and Hemphill Scale were used to assess neurological impairment and predict 30-day survival in hemorrhagic stroke patients. The Hemphill Scale evaluates five key factors: patient age (<80 or >80 years), GCS score, hematoma location and volume, and the presence of intraventricular hemorrhage. According to the GCS, 54.2% (n=45) of patients exhibited moderate obtundation, 16.9% (n=14) had profound obtundation, 10.8% (n=9) were in stupor, 9.6% (n=8) had grade I coma, and 8.4% (n=7) had grade II coma. No fatalities occurred among patients scoring 1-2 points, while one death was recorded at 3 points, and seven deaths at 4 points.

The FOUR scale is a comprehensive tool used to assess neurological status, focusing on eye responses, brainstem reflexes, motor responses, and respiratory patterns. Unlike the GCS, it provides a more detailed evaluation of brainstem function, making it especially valuable for intubated patients

and those in deep coma states. The FOUR scale ranges from 0 (deep coma, cortical death) to 16 points (clear consciousness), allowing for a nuanced assessment of neurological impairment [6].

In this study, patients were categorized based on their FOUR scale scores 58% (n=14) had a severe condition with moderate stupor (15 points), 17% (n=7) exhibited a severe course with deep stupor (13–14 points), 12% (n=5) had stupor (9–12 points), 7% (n=4) were in a comatose state (7–8 points), and 6% (n=2) had grade II coma (1–6 points).

Table 2.

Distribution of Patients By Four Scale

FOUR Scale	Points	Number of patients	Percentage (%) of total
Moderate stupor	15	48	57.8%
Deep stupor	13-14	14	16.9%
Stupor	9-12	10	12.0%
Coma I	7-8	6	7.2%
Coma II	1-6	5	6.0%

The FOUR scale's advantages lie in its ability to differentiate between varying levels of impaired consciousness and to predict early mortality, making it particularly useful in critical care and stroke management. It is also superior to GCS for assessing brainstem reflexes and respiratory function, crucial in determining the severity and prognosis of hemorrhagic stroke.

Neurological Symptoms and Biomarker Analysis

Hemorrhagic stroke patients exhibited severe neurological deficits, including motor disturbances (hemiparesis/ hemiplegia) in 95%, oculomotor nerve paresis in 27%, dysphagia in 31%, dysarthria in 52%, aphasia in 49%, hemianopsia in 24%, facial muscle weakness on the opposite side in 95%, and impaired sensation in 69% of the cases.

Additionally, ICAM-1 and VCAM-1 levels were significantly elevated, reflecting the body's inflammatory response to acute cerebrovascular injury.

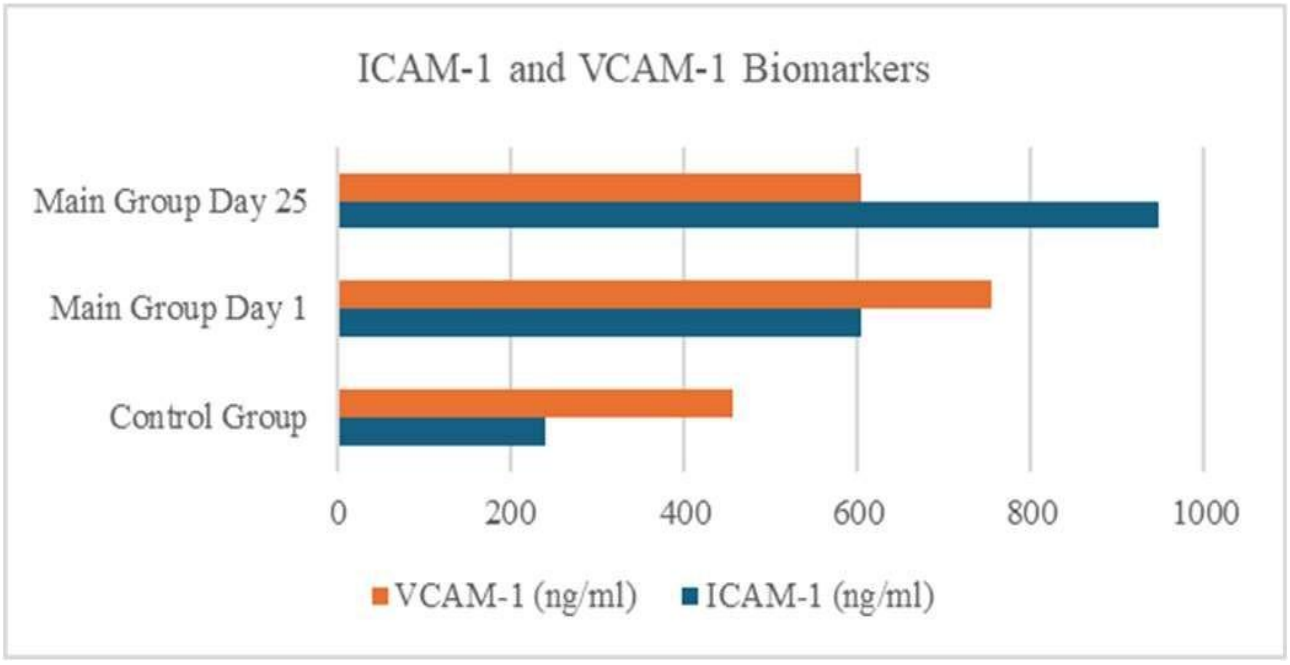


Fig. 2. ICAM-1 and VCAM-1 Biomarker Levels

ICAM-1 levels increased 2.5-fold within the first 48 hours compared to the control group and continued rising by day 25. A significant positive correlation was found between ICAM- 1 levels and NIH stroke severity scores at day 25. VCAM-1 levels increased 1.5-fold within the first 48 hours and showed a slight decline by day 25. Higher VCAM-1 levels correlated with more severe neurological deficits. Consequently, both ICAM-1 and VCAM-1 levels were notably elevated in patients with fatal outcomes.

These findings highlight the critical role of inflammatory processes in stroke progression and underscore the potential of ICAM-1 and VCAM-1 as prognostic biomarkers.

ICAM-1 and VCAM-1 are cell adhesion molecules involved in inflammatory responses and are regulated by pro- inflammatory cytokines and cellular stress. VCAM-1, primarily expressed by endothelial cells, is released into the bloodstream, and its levels have been shown to correlate with stroke severity in ischemic events [7-8].

Hemorrhagic strokes most commonly affect individuals of working age and are frequently associated with intracerebral hematomas. Prognosis is influenced by factors such as age, consciousness level (as assessed by the GCS and FOUR scales), hematoma localization, and volume.

Understanding the pathophysiological mechanisms underlying hemorrhagic stroke can enhance early treatment strategies and improve patient outcomes. Rapid correction of hemodynamic, metabolic, and electrolyte imbalances in the acute phase is critical in determining neurological recovery.

The integration of neurological scales in clinical practice is essential for accurate diagnosis, therapeutic decision- making, and prognosis estimation. The development of combinatory prognostic scales remains a promising area in neurology. The FOUR scale, in particular, offers advantages over the GCS by providing a more comprehensive assessment of neurological function, particularly in intubated patients.

Conclusion. VCAM-1 plays a crucial role in inflammatory processes and is a key factor in the development of cardiovascular diseases, including hypertension, ischemic heart disease, and stroke. Cell adhesion molecules such as ICAM-1 and VCAM1 hold promise for further research in stroke prognosis and therapeutic strategies.

The use of these biomarkers could enhance cardiovascular risk assessment, while the FOUR scale remains a valuable tool for evaluating neurological function and predicting mortality in critically ill patients. Additionally, the FOUR scale is effective in distinguishing coma-mimicking conditions and has significant utility in clinical trials assessing treatment outcomes in hemorrhagic stroke.

REFERENCES

1. Acute neurofilament light chain plasma levels correlate with stroke severity and clinical outcome in ischemic stroke patients / H.H.Nielsen, C.B.Soares, S.S. Hogedal [et.al] // Frontiers in neurology.-2020.- Vol.11.-P.448.

2. Belkin A.A., Zabolotskikh I.B., Bochkarev P.Yu., Zybin K.D., Levit A.L., First experience of using the "detailed assessment of the condition of areactive patients" scale (FOUR SCALE) in patients with acute cerebral insufficiency. Two-center study "FOUR-Ru". Bulletin of Intensive Care named after A.I. Saltanov 2020; 3: 27-34.

3. Dhollande S, Taylor A, Meyer S, Scott M. Cjducting J Res Nurs 2021; 26: 427-38.

4. Frijns, C.J.M. Inflammatori cell adhesion molecules in ischemic cerebrovascular disease/ C.J.M. Frijns, L.J.Kappelle // Stroke.-2002.- Vol.33, 8.-P, 2129-2122.

5. Gautam PL, Paul G, Yadav S. Comparison of FOUR Score & Glasgow Coma Scale, 1 st ed. Saarbucken Lambert Akademic Publishing. 2016.

6. Kondziella D, Bender A, Diserens K, van Erp W, Estraneo A, Formisano R, Laurees S, Ozturk S, Chatelle C, EAN Panel on Coma, Disorders of Consciousness. European Journal of Neurology 2020 May; 27(5):741-56.

7. Skvortsova V.I., Ivanova G.E., Stakhovskaya L.V. Results of the implementation of the Program for the reduction of morbidity, mortality and disability from cerebrovascular diseases in the Russian Federation. Collection of the scientific and practical conference "Acute cerebrovascular accidents". - Samara, 2012. Pp. 5-7.

8. Turdiev Sh.M. Dinamics of the mortality rate of the population in Uzbekistan// Biology and integrative medicine-Bukhara,-2018-№4- Pp. 20-26.

UDC: 616.831-005.1-036.8:615.851:616.89

TARGETING EMOTIONAL DYSFUNCTION AFTER STROKE: THE ROLE OF PSYCHOMOTOR THERAPY ASSESSED BY THE HOSPITAL ANXIETY AND DEPRESSION SCALE

Maftuna B. Ibodulloyeva - doctoral (Ph.D.) candidate
Zarifboy R. Ibodullayev - professor
Tashkent State Medical University *(Tashkent, Uzbekistan)*
ibodulloyevamaftuna9@gmail.com

Abstract. *Stroke is a leading cause of long-term disability, often accompanied by significant psychoemotional disturbances. This study aimed to evaluate the effectiveness of psychomotor therapy in reducing anxiety and depression in post-ischemic stroke patients using the Hospital Anxiety and Depression Scale (HADS). A prospective randomized controlled study included 100 patients divided into two groups: psychomotor therapy plus standard rehabilitation (n=50) and standard rehabilitation alone (n=50). After 8 weeks, anxiety scores (HADS-A) decreased from 12.1 to 4.9 in the intervention group, compared to 9.94 in the control group. Depression scores (HADS-D) decreased from 12.62 to 5.2 versus 10.38, respectively. Mixed-design ANOVA revealed significant time × group interactions ($p<0.001$) with large effect sizes ($\eta^2p=0.62$ for anxiety; $\eta^2p=0.53$ for depression). These findings indicate that psychomotor therapy provides a significant additional benefit in improving psychoemotional outcomes after stroke.*

Keywords: *stroke, psychomotor therapy, rehabilitation, anxiety, depression, HADS, neurorehabilitation*

Introduction. Stroke remains one of the leading causes of long-term disability worldwide and continues to pose a substantial burden on healthcare systems and society. According to global epidemiological data, more than 12 million new stroke cases occur annually, and a significant proportion of survivors experience persistent functional and psychosocial impairments that require prolonged rehabilitation [4]. Despite advances in acute stroke management, the focus of modern neurology has increasingly shifted toward optimizing recovery and improving quality of life in the post-stroke period.

Among the various consequences of stroke, emotional disturbances-particularly anxiety and depression-are highly prevalent and clinically significant. It is estimated that up to one-third of stroke survivors develop post-stroke depression, while anxiety disorders may affect approximately 20-25% of patients [1, 5]. These conditions not only reduce patient motivation and participation in rehabilitation but are also associated with poorer functional outcomes, increased dependency, and higher mortality rates [7]. Therefore, addressing emotional dysfunction is now considered a critical component of comprehensive stroke rehabilitation.

The Hospital Anxiety and Depression Scale (HADS) has been widely used as a reliable and valid instrument for assessing anxiety and depression in medical populations, including stroke patients. Its sensitivity to changes in emotional status and its applicability in clinical settings make it particularly suitable for evaluating rehabilitation outcomes [8, 2]. The use of standardized tools such as HADS allows for objective monitoring of psychometric changes during the recovery process.

In recent years, growing attention has been directed toward rehabilitation approaches that integrate not only motor recovery but also cognitive and emotional dimensions. Psychomotor therapy, grounded in principles of sensorimotor integration and embodied cognition, represents a promising multidimensional intervention. This approach emphasizes body awareness, movement coordination,

postural control, and the interaction between motor and emotional processes, thereby facilitating both physical and psychological recovery [6]. By engaging patients in structured, goal-directed movement experiences, psychomotor therapy may enhance neuroplasticity and contribute to improved emotional regulation.

Although conventional rehabilitation strategies have demonstrated effectiveness in improving motor function, their impact on emotional outcomes remains limited and often insufficient. Emerging evidence suggests that interventions incorporating body-oriented and integrative therapeutic components may provide additional benefits in reducing anxiety and depressive symptoms [3]. However, high-quality controlled studies specifically evaluating the effectiveness of psychomotor therapy in post-stroke emotional recovery are still scarce.

Given the close interaction between motor and emotional systems in the central nervous system, it can be hypothesized that targeted psychomotor interventions may positively influence both domains simultaneously. Understanding this relationship is essential for developing more effective, patient-centered rehabilitation programs.

Therefore, the aim of this study was to evaluate the effectiveness of psychomotor therapy in reducing anxiety and depression in patients after ischemic stroke, using the Hospital Anxiety and Depression Scale (HADS) as a primary outcome measure.

Materials and Methods. This study was designed as a prospective controlled clinical study aimed at evaluating the effectiveness of psychomotor rehabilitation in patients after ischemic stroke. The research was conducted in cooperation with the neurology department and specialized rehabilitation centers in Tashkent, Uzbekistan.

All procedures were performed in accordance with international ethical standards for biomedical research involving human participants. Participation in the study was voluntary, and all participants provided written informed consent before inclusion.

Patients received standard neurorehabilitation therapy according to clinical practice guidelines. In addition, patients in the intervention group underwent structured psychomotor rehabilitation sessions conducted by trained rehabilitation specialists.

Participants. A total of 130 individuals were initially screened for participation in the study. Among them, 100 patients with ischemic stroke met the inclusion criteria and were included in the final statistical analysis, while 30 healthy individuals were recruited as a control group for baseline comparison.

Patients with ischemic stroke were randomly assigned into two groups using a simple randomization method (Table 1):

Psychomotor rehabilitation group (n = 50) - psychomotor therapy combined with standard rehabilitation

Control rehabilitation group (n = 50) - standard rehabilitation only

Healthy volunteers (n = 30) were included as a reference control group.

Table 1.

Distribution of participants across study groups

Group	Number of participants
Psychomotor rehabilitation	50
Standard rehabilitation	50
Healthy control	30
Total	130

Participant inclusion and exclusion were determined according to the following predefined criteria (Table 2.)

Table 2.

Inclusion and exclusion criteria for participant selection

Inclusion criteria	Exclusion criteria
confirmed diagnosis of ischemic stroke	recurrent stroke
age 30–70 years	severe somatic or psychiatric disorders
post-stroke rehabilitation stage	severe cognitive impairment
NIHSS score 5–20	epilepsy or uncontrolled cardiovascular disease
preserved cognitive ability	inability to participate regularly
stable neurological condition	absence during final evaluation
written informed consent	-

After applying these criteria, 30 patients were excluded, leaving 100 patients for final analysis.

Clinical and instrumental assessment. The diagnosis of ischemic stroke was confirmed using magnetic resonance imaging (MRI) and computed tomography (CT). MRI examinations included DWI, FLAIR, T1-weighted and T2-weighted sequences to identify ischemic lesions.

Additional diagnostic procedures included Doppler ultrasonography of the brachiocephalic arteries, electrocardiography (ECG), and echocardiography (EchoCG). These examinations were carried out to further clarify the etiology of ischemic stroke and to identify possible comorbid cardiovascular conditions that could influence the clinical course of the disease and the rehabilitation process.

Distribution of stroke localization. Stroke localization was classified according to vascular territory using MRI findings (Table 3, Figure 1).

Table 3.

Distribution of ischemic stroke localization

Localization	Psychomotor group (n=50)	Control group (n=50)
Left hemisphere (ACA + MCA)	11 (22%)	13 (26%)
Right MCA territory	17 (34%)	18 (36%)
Vertebrobasilar territory	22 (44%)	19 (38%)

No statistically significant differences between groups were observed at baseline ($p > 0.05$).

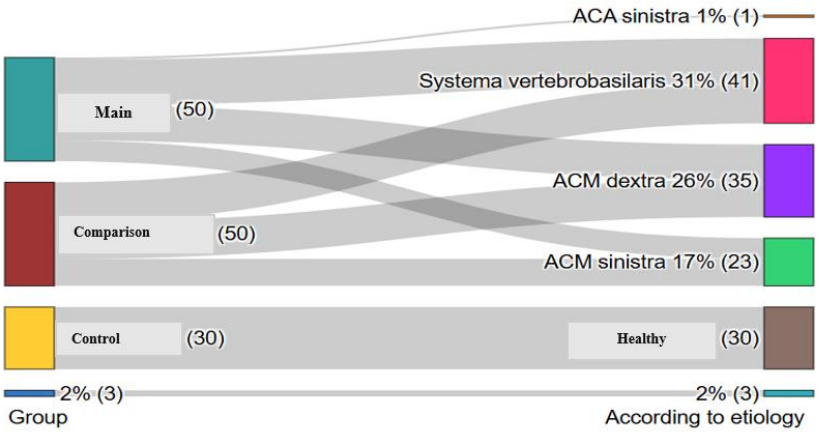


Figure 1. Distribution of stroke localization by vascular territory

Rehabilitation protocol. All participants received standard rehabilitation therapy including therapeutic exercises and functional training.

Patients in the intervention group additionally underwent psychomotor rehabilitation sessions consisting of:

- sensorimotor integration exercises
- coordination training
- rhythmic motor exercises
- task-oriented movement training
- body awareness exercises

The rehabilitation program lasted 8 weeks, with four sessions per week, each session lasting 60 minutes (Table 4).

Table 4.

Psychomotor rehabilitation protocol

Parameter	Value
Session duration	60 minutes
Sessions per week	4
Program duration	8 weeks
Total sessions	32

Recommended diagram structure:

- Warm-up (10 min)
- Sensorimotor exercises (15 min)
- Coordination and balance training (15 min)
- Task-oriented motor exercises (15 min)
- Relaxation and body awareness (5 min)
- Functional Outcome Measures

To comprehensively evaluate the effectiveness of the rehabilitation program, functional and psychoemotional outcomes were assessed using standardized and widely validated clinical scales. These instruments were selected to capture multiple domains of recovery, including functional independence, motor performance, balance, and emotional status.

Functional independence in daily activities was assessed using the Barthel Index (BI), which reflects the patient's ability to perform essential self-care tasks. Motor and sensory recovery were evaluated with the Fugl-Meyer Assessment (FMA), a stroke-specific scale sensitive to changes in motor control. Balance and postural stability were measured using the Berg Balance Scale (BBS), which is particularly relevant for assessing fall risk and mobility.

Special attention was given to the evaluation of psychoemotional status using the Hospital Anxiety and Depression Scale (HADS). This scale is specifically designed for patients with somatic conditions and allows for reliable detection of emotional disturbances without being confounded by physical symptoms.

HADS consists of two independent subscales assessing:

- Anxiety (HADS-A)
- Depression (HADS-D)

Each subscale includes 7 items, with scores ranging from 0 to 21. Higher scores indicate greater severity of symptoms. The use of separate domains enables a more precise evaluation of emotional changes during rehabilitation (Figure 1.).

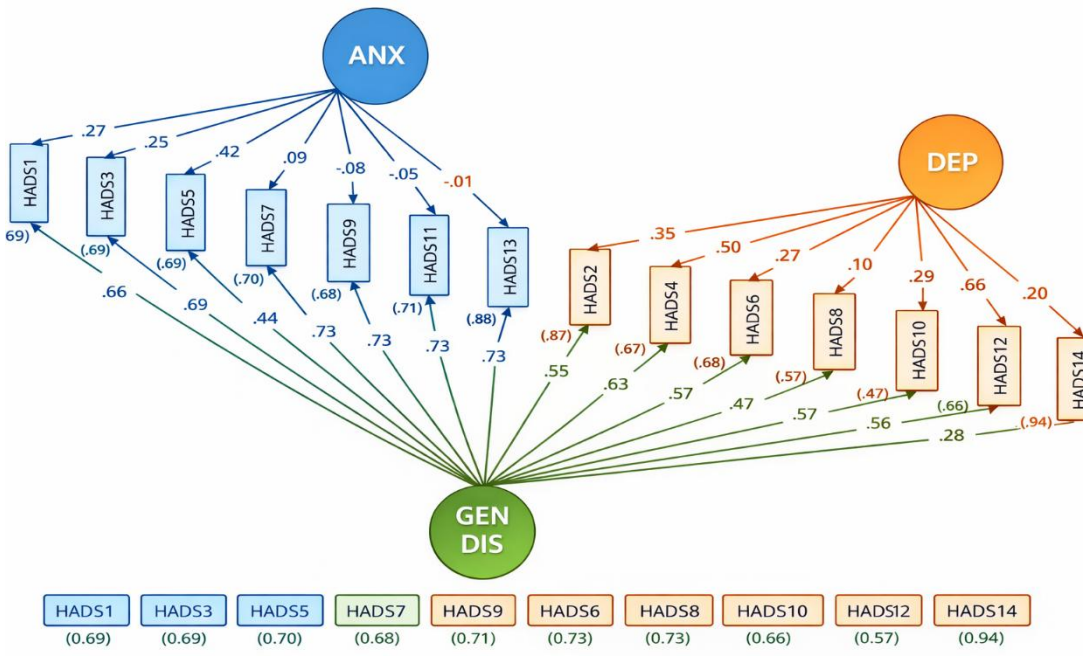


Figure 2. Factor Structure of the Hospital Anxiety and Depression Scale (HADS): Three-Domain Model (Anxiety, Depression, and General Distress)

All outcome measures were administered twice: at baseline (before the start of rehabilitation) and after completion of the 8-week intervention period. This allowed for the assessment of both within-group changes and between-group differences over time.

Statistical Analysis. Statistical analysis was performed in accordance with the study design, with a significance level set at $p < 0.05$. Descriptive statistics were used to summarize baseline characteristics, with continuous variables expressed as mean ± standard deviation and 95% confidence intervals, and categorical variables as frequencies and percentages.

Due to the ordinal nature of clinical scales and potential non-normal distribution, baseline comparisons between groups were conducted using the Mann-Whitney U test. Categorical variables were analyzed using the chi-square test.

To evaluate changes over time and differences between groups, a two-way mixed-design ANOVA was applied, with time (pre- and post-intervention) as a within-subject factor and group (psychomotor therapy vs. standard rehabilitation) as a between-subject factor. The primary focus was on the interaction effect (time × group), reflecting the effectiveness of the intervention.

Effect sizes were calculated using partial eta squared (η^2p) to assess the magnitude of observed effects. All analyses were performed using standard statistical software.

Results. The dynamics of psychoemotional status were assessed using the anxiety (HADS-A) and depression (HADS-D) subscales of the Hospital Anxiety and Depression Scale.

At baseline, anxiety levels were identical in both groups, with a mean score of 12.1, indicating a comparable initial psychoemotional state. Following the rehabilitation program, anxiety scores decreased in both groups; however, the magnitude of improvement differed substantially.

In the psychomotor therapy group, anxiety levels decreased from 12.1 to 4.9, reflecting a marked clinical reduction in symptoms. In contrast, the control group showed a more modest decrease from 12.1 to 9.94, suggesting partial persistence of anxiety symptoms. The overall sample demonstrated a reduction from 12.1 to 7.42.

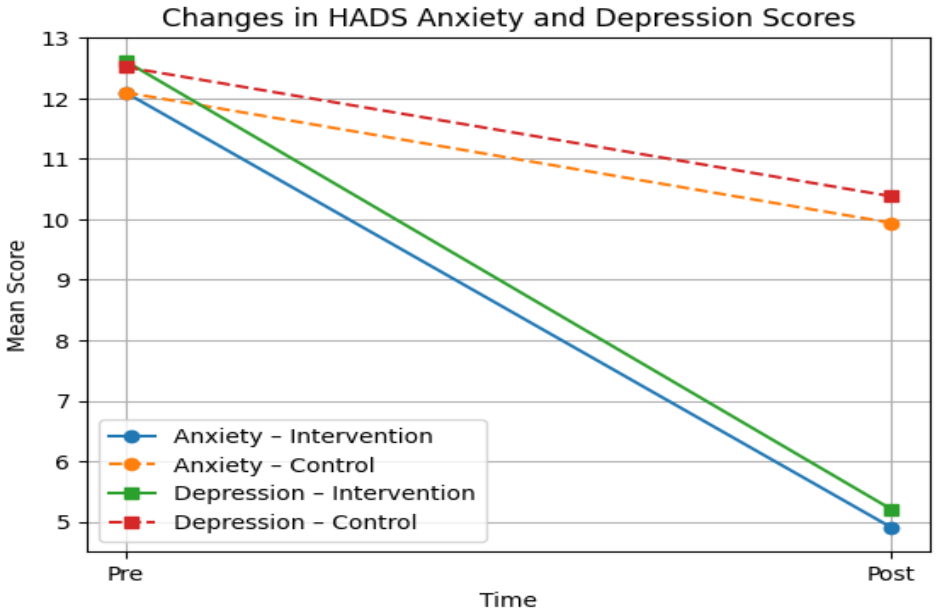


Figure 3. Changes in HADS-A (anxiety) scores over time in the intervention and control groups

To further examine these changes, a mixed-design ANOVA was conducted. The results revealed a highly significant main effect of time ($F(1,98)=543.79$, $p<0.001$, $\eta^2p=0.85$), indicating a substantial overall reduction in anxiety levels. A significant group effect was also observed ($F(1,98)=64.16$, $p<0.001$, $\eta^2p=0.40$), suggesting differences between the intervention and control groups. Importantly, the time × group interaction was highly significant ($F(1,98)=157.67$, $p<0.001$, $\eta^2p=0.62$), confirming that the reduction in anxiety was significantly greater in the psychomotor therapy group (Table 5.).

Table 5.

Mixed-design ANOVA results for HADS-A (anxiety)

Source of Variation	Sum of Squares	df	Mean Square	F	p-value	η^2	η^2p
Time (pre vs post)	1095.12	1	1095.12	543.79	<0.001	0.45	0.85
Group	317.52	1	317.52	64.16	<0.001	0.13	0.40
Time × Group	317.52	1	317.52	157.67	<0.001	0.13	0.62
Error (between subjects)	484.96	98	4.95	—	—	—	—
Error (within subjects)	197.36	98	2.01	—	—	—	—

A similar pattern was observed for depressive symptoms. At baseline, depression scores were comparable between groups (12.62 in the intervention group vs 12.52 in the control group). After rehabilitation, the intervention group demonstrated a pronounced decrease to 5.2, while the control group showed a smaller reduction to 10.38. The overall sample decreased from 12.57 to 7.79 (Figure 3.).

Mixed ANOVA results confirmed a significant main effect of time ($F(1,98)=366.95$, $p<0.001$, $\eta^2p=0.79$), as well as a significant group effect ($F(1,98)=24.72$, $p<0.001$, $\eta^2p=0.20$). The interaction effect was also statistically significant ($F(1,98)=111.93$, $p<0.001$, $\eta^2p=0.53$), indicating that depressive symptoms decreased more substantially in the psychomotor therapy group (Table 6).

Table 6.

Mixed-design ANOVA results for HADS-D (depression)

Source of Variation	Sum of Squares	df	Mean Square	F	p-value	η^2	η^2p
Time (pre vs post)	1142.42	1	1142.42	366.95	<0.001	0.34	0.79
Group	322.58	1	322.58	24.72	<0.001	0.09	0.20
Time × Group	348.48	1	348.48	111.93	<0.001	0.10	0.53
Error (between subjects)	1278.94	98	13.05	—	—	—	—
Error (within subjects)	305.10	98	3.11	—	—	—	—

Discussion. The present study provides evidence that the inclusion of psychomotor therapy in post-stroke rehabilitation has a significant impact not only on functional recovery but also on psychoemotional outcomes. The observed results demonstrate a clear and consistent pattern across both anxiety and depression domains, with significantly greater improvements in the intervention group compared to standard rehabilitation alone.

One of the most notable findings is the strong time × group interaction effect observed in both HADS subscales. This suggests that while rehabilitation itself contributes to general improvement, the addition of psychomotor therapy accelerates and amplifies psychoemotional recovery. The magnitude of effect sizes (η^2p ranging from 0.53 to 0.85) further indicates that these changes are not only statistically significant but also clinically meaningful.

The reduction in anxiety symptoms may be explained by several mechanisms inherent to psychomotor therapy. First, the emphasis on body awareness and sensorimotor integration likely contributes to improved internal regulation and reduced physiological arousal. Second, structured movement experiences may enhance the patient's sense of control and self-efficacy, which are known to play a crucial role in anxiety reduction. Finally, the relational aspect of therapy-often described as a "body-mediated therapeutic interaction"-may provide an additional layer of emotional support.

Similarly, the observed decrease in depressive symptoms appears to be linked to both neurophysiological and psychological mechanisms. Engagement in purposeful movement, gradual restoration of functional abilities, and positive feedback during therapy sessions may collectively improve mood and motivation. These findings are consistent with the broader concept of embodied cognition, where motor activity and emotional processes are closely interconnected.

It is also important to note that although standard rehabilitation led to some improvement in both anxiety and depression, the magnitude of change remained limited. This suggests that conventional approaches, while effective for motor recovery, may not sufficiently address the psychoemotional dimension of post-stroke rehabilitation.

From a clinical perspective, these results highlight the importance of integrating multidimensional interventions into rehabilitation programs. Addressing emotional disturbances alongside physical deficits may not only improve patient well-being but also enhance overall rehabilitation outcomes, including adherence and long-term recovery.

At the same time, several limitations should be considered. The study was conducted in a single center, which may limit the generalizability of the findings. The open-label design introduces a potential risk of performance bias, as blinding was not feasible due to the nature of the intervention. In addition, long-term follow-up was not performed, making it difficult to assess the sustainability of the observed effects.

Despite these limitations, the study provides strong evidence supporting the role of psychomotor therapy as an effective adjunct to standard neurorehabilitation. Future research should focus on multicenter trials, longer follow-up periods, and the inclusion of neurophysiological markers to further elucidate the mechanisms underlying these effects.

Conclusion. The findings of this study demonstrate that the inclusion of psychomotor therapy in post-stroke rehabilitation leads to clinically meaningful improvements in psychoemotional outcomes, particularly in reducing anxiety and depression.

Quantitatively, anxiety levels (HADS-A) in the intervention group decreased from 12.1 to 4.9 points, corresponding to an average reduction of 8.5 points, whereas the control group showed a smaller decrease to 9.94 points. Similarly, depressive symptoms (HADS-D) declined from 12.62 to 5.2 points in the psychomotor therapy group (a reduction of 8.91 points), compared to a more modest decrease to 10.38 points in the control group. These differences were supported by statistically significant time × group interaction effects, with large effect sizes ($\eta^2p = 0.62$ for anxiety and $\eta^2p = 0.53$ for depression), indicating a substantial additional benefit of psychomotor therapy beyond standard rehabilitation.

Importantly, while both groups demonstrated improvement over time, the magnitude and clinical relevance of change were considerably greater in the intervention group. This suggests that psychomotor therapy not only enhances recovery but also accelerates the normalization of psychoemotional status in post-stroke patients.

Overall, the results support the integration of psychomotor therapy into комплекс rehabilitation programs as an effective approach for addressing both functional and emotional deficits after ischemic stroke. Future studies should aim to confirm these findings in larger, multicenter cohorts and evaluate the long-term sustainability of these effects.

REFERENCES

1. Ayerbe, L., Ayis, S., Wolfe, C. D. A., & Rudd, A. G. (2013). Natural history, predictors and outcomes of depression after stroke: Systematic review and meta-analysis. The British Journal of Psychiatry, 202(1), 14–21. https://doi.org/10.1192/bjp.bp.111.107664

2. Bjelland, I., Dahl, A. A., Haug, T. T., & Neckelmann, D. (2002). The validity of the Hospital Anxiety and Depression Scale: An updated literature review. Journal of Psychosomatic Research, 52(2), 69–77. https://doi.org/10.1016/S0022-3999(01)00296-3

3. Cramer, S. C., Sur, M., Dobkin, B. H., O'Brien, C., Sanger, T. D., Trojanowski, J. Q.,... & Vinogradov, S. (2011). Harnessing neuroplasticity for clinical applications. Brain, 134(6), 1591–1609. https://doi.org/10.1093/brain/awr039

4. Feigin, V. L., Stark, B. A., Johnson, C. O., Roth, G. A., Bisignano, C., Abady, G. G.,... & Murray, C. J. L. (2021). Global, regional, and national burden of stroke and its risk factors, 1990–2019. The Lancet Neurology, 20(10), 795–820. https://doi.org/10.1016/S1474-4422(21)00252-0

5. Hackett, M. L., & Pickles, K. (2014). Part I: Frequency of depression after stroke: An updated systematic review and meta-analysis of observational studies. International Journal of Stroke, 9(8), 1017–1025. https://doi.org/10.1111/ijs.12357

6. Probst, M., Knapen, J., Poot, G., & Vancampfort, D. (2010). Psychomotor therapy and psychiatry: What's in a name? The Open Complementary Medicine Journal, 2, 105–113.

7. Towfighi, A., Ovbiagele, B., El Husseini, N., Hackett, M. L., Jorge, R. E., Kissela, B. M.,... & Williams, L. S. (2017). Poststroke depression: A scientific statement for healthcare professionals. Stroke, 48(2), e30–e43. https://doi.org/10.1161/STR.0000000000000113

8. Zigmond, A. S., & Snaith, R. P. (1983). The Hospital Anxiety and Depression Scale. Acta Psychiatrica Scandinavica, 67(6), 361–370. https://doi.org/10.1111/j.1600-0447.1983.tb09716.x

CHANGES IN ANTHROPOMETRIC INDICATORS OF THE FETUS IN MOTHERS WITH HYPOTHYROIDISM

Norbek K. Niyozov
Tashkent state medical university (Tashkent, Uzbekistan)
norbek8791@gmail.com.

Abstract. *The physiological role of thyroid hormones is very important and diverse in all periods of human life, including during pregnancy. Hypothyroidism in pregnant women can negatively affect fetal development, leading to low birth weight, antenatal death, or other conditions. We studied 50 healthy and 72 hypothyroid fetuses. All pregnant women underwent I, II, and III screening examinations. The lowest growth rate of fetometric indicators was observed in the third screening period. The highest growth rate of fetometric indicators was determined in the period from 12 to 35 weeks.*

Keywords: *hypothyroidism, fetometry, screening examination, thyroid gland*

Introduction.

The incidence of thyroid pathologies in the world has increased by 12.1%: from 2037.1 cases per 100 thousand population to 2283.5. The curve showing the number of patients with thyroid problems has been steadily increasing for more than a decade [1, 2, 11, 15, 21]. According to the World Health Organization, thyroid diseases are caused by iodine deficiency in the body in 65% of cases in adults and 95% in children, and a number of scientific studies are being carried out to prevent them. In this regard, "..in conditions of iodine deficiency in the environment, the impact of these diseases on the health of the population is high, and thyroid diseases affect 2847 patients per 100 thousand adult population. Thyroid dysfunction has a negative impact on the course of pregnancy. In turn, pregnancy also affects the functioning of the thyroid gland…" Hypothyroidism in the fetus and neonatal period causes impaired mental and physical development of the child born [3, 5, 9, 20, 22]. This defect can reach the level of endemic cretinism. Therefore, studies aimed at thyroid insufficiency are of particular scientific and practical importance.

There are many unresolved issues in the problem of assessing anthropometric parameters of hypothyroidism in newborns. To date, the effect of embryonic hypothyroidism on the subsequent development of the child has not been established. According to a number of researchers, transient hypothyroidism is a dangerous form of this disease, requiring hormone therapy. Other authors do not consider it appropriate to recommend thyroid hormones for gestational hypothyroidism [4, 6, 10, 19, 23]. More than 99% of thyroid hormones circulating in the blood are bound to proteins and do not show activity. Less than 1% of them (free T3, free T4) are in free form, providing the biological effect of the thyroid gland [7, 12, 14, 18]. The absorption of iodine through the placenta into the fetus and the increase in metabolic processes during pregnancy, along with the synthesis of thyroid hormones, increase the need for iodine in women during pregnancy. At the same time, increased urinary iodine excretion, increased conversion of thyroxine in the placenta, and the weakening of its effect all these together lead to a deficiency of iodine and thyroid hormones [8, 13, 16, 17]. This causes an increase in the size of the thyroid gland. A number of scientific studies are being conducted in the world to improve the changes in anthropometric indicators of the fetus of a mother with hypothyroidism. In this regard, studies aimed at scientifically substantiating the correlation between the amount of thyroid hormones in the mother's blood and the child's fetometric indicators in healthy pregnant women at the first 12–15 weeks of screening, the second at 20–25 weeks, and the third at 30–35 weeks of pregnancy are of particular scientific and practical importance.

Assessment of changes in the dynamics of the main indicators of fetal anthropometric development in healthy and hypothyroid pregnant women using ultrasound examination

Material and methods of research.

The materials and methods of the study, which was carried out on the basis of the Dr. Aliyev Center for Diagnostics of Mother and Child in Tashkent, as well as the 1st Central Consultative Diagnostic Polyclinic under the Presidential Administration of the Republic of Uzbekistan, are described. To achieve the set goals and objectives, the research work was carried out in the 1st Central Consultative Diagnostic Polyclinic, where the results of the examination of 100 healthy pregnant women on the gynecologist's list and 126 pregnant women with hypothyroidism on the endocrinologist and gynecologist's list were obtained. The organization of the study consisted of 4 consecutive stages.

At the first stage, the selection of all pregnant women was strictly controlled. In this case, all pregnant women were in the age group from 20 to 35 years old, with a body weight of 60 kg to 80 kg. Their anamnesis data were collected, and women in the first labor period without concomitant diseases, with a single fetus, were selected.

In the second stage, all pregnant women were divided into 3 groups: the first group, a group of healthy pregnant women (control); the second group, a group of pregnant women who were diagnosed with hypothyroidism from the first pregnancy, were under constant endocrinological supervision, and received levothyroxine at a dose of 50 mcg from the early stages of the disease (first group); the third group, a group of pregnant women who were monitored and diagnosed with hypothyroidism when they came to the Kibray district association of Tashkent region with complaints to the endocrinologist and gynecologist at different stages of pregnancy, and who began taking levothyroxine at a dose of 50 mcg at different stages of pregnancy (second group). In the third stage, the main fetometric dimensions of the fetus were measured using ultrasound diagnostics at the stages of examination of pregnant women at 12–13 and 14–15 weeks (first screening), 20–21 weeks, 22–23 weeks, and 24–25 weeks (second screening), and 30–31 weeks, 32–33 weeks, and 34–35 weeks (third screening). In the fourth stage, using the data on the main fetometric dimensions of the fetus, a mathematical statistical analysis of the dynamics of absolute growth and intensive growth, as well as the cephalic index and proportional body indices, was carried out.

In total, 3 (1.4%) of the fetuses of the second group of pregnant women with hypothyroidism were observed to have several anomalies. In one of them, renal pyeloectasia (in the left kidney) was observed, in one pregnant woman aneuploidy was observed, and in one pregnant woman a miscarriage occurred. We decided not to include these cases in our statistical analysis results.

In the research work, the biparietal, frontal-occipital, head circumference, abdominal circumference, and femoral length dimensions of healthy pregnant women were studied. The measurements of the fetuses of pregnant women were carried out on the basis of the Dr. Aliyev Center for Maternal and Child Diagnostics in Tashkent. Measurement of the biparietal size using ultrasound diagnostics is carried out in a transverse section of the fetal head. The measurement is determined from the upper contour of the pubic bone to the inner surface of its lower contour. In the same plane, the head circumference is measured along the outer contour. After the fetal abdominal circumference has a rounded shape, the fetal abdominal circumference is measured by clearly visualizing the umbilical vein located in the transverse section through the anterior abdominal wall and the 1/3 of the spine. The length of the fetal femur is measured along the maximum length of its classified diaphysis.

All fetometric examinations were performed on the LOGIQ C 5 Premium device with a 5–12 MGS disposable sensor. Fetometric examination protocols included the following information:

1.Protocol number.

2.Card number.

3.Year of birth of the I.F.O.

4.Anamnesis data.
5.Clinical diagnosis.
6.Screening observation period.
7.Results of thyrotropin and free T3, T4 hormones in the mother's blood.
8.Fetal week.
9.Fetometric parameters.

Analysis of serum thyrotropic hormone, free triiodothyronine, and thyroxine samples from pregnant women was measured directly using chemiluminescent parametric technology. The ECLIA chemiluminescent immunoassay was used on Cobas e immunochemical analyzers. Determination of thyrotropic hormone in maternal blood is the main indicator in the diagnosis of thyroid dysfunction. Even small changes in the concentration of free thyroid hormones lead to opposite changes in the level of thyrotropic hormone. The measurement range was 0.005–100 μg/ml. In order to determine the daily rhythm of thyrotropic hormone in maternal blood, fasting maternal serum was taken and tested in the laboratory.

Analysis for thyrotropic hormone should be performed in the morning, after a full night's sleep. Collection of biomaterial (venous blood serum) for analysis is carried out on an empty stomach (before breakfast).

The level of thyrotropin hormone during pregnancy is as follows:

I trimester: 0.1–2.5 μg/ml

II trimester: 0.2–3.0 μg/ml

III trimester: 0.3–3.0 μg/ml. All results were analyzed according to these data.

To assess the dynamics of development, age morphology indicators were calculated: absolute growth (MO'), and intensive growth (IO'). Absolute growth (MO') is determined as the difference between the absolute values given in relation to previous periods according to the following formula:

$MO' = D2 - D1$ (1)

Here, D2 is the absolute value of a given period; D1 is the absolute value of the indicator of the previous period.

The intensive growth rate (IR) of fetometry indicators is determined by the following formula:

$IR = (D2 – D1) / 0.5 (D1 + D2) \times 100\%$ (2)

It is used to determine the average value (in percent) of a given period relative to the total period under study. IR represents growth intensity, D2 is the absolute value of a given period, and D1 is the absolute value of the indicator of the previous period.

After measuring the fetometric dimensions of the fetus at different periods of screening, we studied the ratio of fetometric indicators in order to determine the proportional development of the fetal body parts. For this, the cephalic index was used to determine the shape of the fetal head. The cephalic index is the ratio of the biparietal volume of the head to the frontal-occipital volume. The following formula was used to determine this indicator:

$BP/FO \times 100\%$ (3)

The normal cephalic index is defined as the range of 75–80%. If the value of the cephalic index is less than 71%, the fetus may develop dolichocephaly, and if it is more than 85%, brachycephaly may develop. It occurs when the mesocephalic size of the head is from 71% to 85%.

In order to determine the correct prenatal physical development of the fetus, the ratio of abdominal circumference to head circumference and the ratio of abdominal circumference to thigh length were determined.

For mathematical processing of the data, the arithmetic mean (M), the mean error of relative values, and the t-difference reliability coefficient were estimated by Student's t-test.

Results and discussion.

When examining the biparietal dimensions of the fetal head of healthy pregnant women, it was found that the intensive growth rate of the biparietal dimension from 12–13 weeks to 14–15 weeks during the first screening period was on average 34%. Another fetometric indicator of the fetal head size is the frontal-occipital dimension. During the first screening period, it was noted that the intensive growth rate of the frontal-occipital dimension from 12–15 weeks in the fetus of healthy women was 38%. Another criterion for assessing the development of the fetal skull is the head circumference. During the first screening period, the intensive growth rate of the head circumference of healthy pregnant women from 12 to 15 weeks was 48%. In the fetuses of healthy pregnant women, the intensive growth rate of the abdominal circumference during the first screening period was 17% for 12–15 weeks. In the first screening period, the intensive growth rate of the femur length of healthy women was 31% on average for the period from 12 to 15 weeks. In the second screening period, the growth intensity of the biparietal index of the fetuses of healthy pregnant women was 74% for the period from 20–25 weeks. From 20–21 weeks to 22–23 weeks, the absolute growth rate of the biparietal index of the fetal head increased by 32% in healthy women. The absolute growth of this indicator of the fetus by 24–25 weeks was 38%. It was found that in the second screening periods, i.e., 20–21 weeks, 22–23 weeks, and 24–25 weeks, the fetal biparietal index was more intensive than in the first screening period. From the first screening period, i.e., 15 weeks, to the second screening period, i.e., 20 weeks, the intensive growth rate of the biparietal size was 48%.

In the second screening period, the absolute growth rate of the frontal-occipital size in the fetuses of healthy pregnant women was 31% from 20–21 weeks to 22–23 weeks, and by 24–25 weeks, we can see that the absolute growth rate of the frontal-occipital size increased by 34%. During this period, the intensive growth rate of the frontal-occipital size was 78%. In the second screening period, the frontal-occipital size in the fetuses of healthy pregnant women increased more rapidly than in the first screening period.

It was found that the head circumference of the fetuses of healthy pregnant women increased statistically ($r<0,05$) more rapidly in the second screening period, that is, in the 15th–20th week, and the intensive growth rate from the first screening to the second screening period was 49%. It was found that the absolute growth rate of the fetal head circumference in healthy women at 22–23 weeks was 33% compared to 20–21 weeks. The absolute growth rate at 24–25 weeks was 21,7%. The intensive growth rate during this period was 60,7% from 20 to 25 weeks. In all periods of the second screening observation, a significant increase in the size of the head circumference was observed compared to the first screening periods.

Abdominal circumference is one of the standard indicators of fetometry, allowing us to assess the anthropometric indicators of the fetal body. In the second screening period, the intensive growth rate compared to the first screening period (15–20 weeks) was 56%. The absolute growth rate of the fetal abdominal circumference in healthy women from 20–21 weeks to 22–23 weeks was 38%. At 24–25 weeks, the absolute growth rate was 40%. During this period, the intensive growth rate was 92,5% from 20 to 25 weeks. A significant increase in the size of the abdominal circumference was observed in all periods during the second screening observation compared to the first screening periods.

The absolute increase in femoral length of healthy pregnant women in the second screening period, i.e., from 20–21 weeks to 22–23 weeks, was 57%. The absolute increase in femoral length of healthy pregnant women from 22–23 weeks to 24–25 weeks was 23%. In the second screening period, the intensity of femoral growth was 39% from 20 to 25 weeks. In the third screening period, the absolute increase in biparietal size from 30–31 weeks to 32–33 weeks was 2,7%. The absolute increase in biparietal size from 32–33 weeks to 34–35 weeks was 5,6%. During the third screening observation period, it was noted that for the biparietal size indicator, which has a specific size, in the fetus of healthy women from 30 to 35 weeks of gestation, an intensive growth rate of 8,5% was recorded.

From the second screening period to the third screening period at 30–31 weeks, the intensive growth rate of the frontal-occipital size was 7%. From 30–31 weeks to 32–33 weeks, the absolute growth rate was 4%. From 32–33 weeks to 35–36 weeks, the absolute growth rate was 5%. In the third screening period, the intensive growth rate of the frontal-occipital size was 8,3% from 30–35 weeks.

The absolute increase in head circumference in healthy women from 30–31 weeks to 32–33 weeks was 8,2%. The absolute increase in head circumference in healthy women from 32–33 weeks to 35–36 weeks was 3,7%. It was found that the intensive increase in head circumference in healthy women from the second screening period to the third screening period was 19,4%.

During the third screening period, it was noted that the intensive growth rate of the abdominal circumference of healthy women was 25%, with absolute growth rates of 13% from 30–31 weeks to 32–33 weeks and 11,5% from 32–33 weeks to 35–36 weeks.

During the third screening period, it was found that the intensive growth rate of the femur length of healthy women was 51%. Absolute growth rates were 4,3% from 30–31 weeks to 32–33 weeks and 2,8% from 32–33 weeks to 35–36 weeks.

It was noted that the intensive growth rate of the biparietal size of the fetus of the first group of women with hypothyroidism was 25% on average from 12 to 15 weeks, while in the control group it was 34%. In the first group of women with hypothyroidism, the intensive growth rate of the frontal-occipital size was found to be 54% on average from 12 to 15 weeks. In the control group, this figure was 38%. It is noteworthy that the frontal-occipital size of the first hypothyroid group was slightly larger than that of a healthy fetus. In the first group of women with hypothyroidism, the intensive growth rate of the head circumference was found to be 38% on average from 12 to 15 weeks, while in the control group, the head circumference was 48% at the time of the first screening. In the first group of women with hypothyroidism, the intensive growth rate of the abdominal circumference was noted to be 10% on average from 12 to 15 weeks.

It was observed in the control group that it was equal to 17%. In the first screening period, the intensive growth rate of the femur was 18% from 12 to 15 weeks, and in the control group it was 31%. In the second screening period, the intensive growth rate of the biparietal size was 14% from 20 to 25 weeks. In the same period, it was found that in the control group it reached 83%. In the second screening period, we can see that the biparietal size in the first group of hypothyroid patients was larger than that of a healthy fetus. At 20–21 weeks, the absolute increase in the biparietal index of the fetal head was 29% compared to 14–15 weeks. At 22–23 weeks, the absolute increase in the biparietal index of the fetal head in the first group of women with hypothyroidism was 64% compared to 21 weeks. At 24–25 weeks, it was 30% compared to 23 weeks. During this period, the intensive growth rate of the frontal-occipital size was 82% from 20 to 25 weeks. It is known that in the control group, the growth rate during this period was 78%. It was also found that the frontal-occipital size of the first hypothyroid group was slightly larger than that of a healthy fetus during the first screening period. During the second screening period, it was found that both the frontal-occipital and biparietal sizes were larger than those of the fetuses of healthy pregnant women. During the second screening period, the intensive growth rate of head circumference was 48% from 20 to 25 weeks. In the control group, the intensive growth rate during this period was 61%. During the second screening period, the head circumference of the first group of women with hypothyroidism statistically increased, and the intensive growth rate was 69%. The absolute growth rate from 20–21 weeks to 22–23 weeks was 21%. At 24–25 weeks, the absolute growth rate was 22%. During the second screening period, the intensive growth rate of abdominal circumference was 81% from 20 to 25 weeks in the group of pregnant women with the first hypothyroidism and 92,5% in the control group. The absolute increase in fetal abdominal circumference from 20–21 weeks to 22–23 weeks in the first group of women with hypothyroidism was on average 35%. At 24–25 weeks, the absolute increase was 34%. During this period, the intensive growth rate of the femur was 39% from 20 to 25 weeks. It was statistically

confirmed that the control group had an intensive increase of 81% during the same period. The length of the femur of the fetus in pregnant women with hypothyroidism (first group) was statistically significantly higher than that during the second screening, that is, at 20–21 weeks, the absolute increase was 39%, and at 24–25 weeks, the absolute increase was 56%. In the third screening period, the intensive growth rate of the biparietal size was 20% in the period from 30 to 35 weeks. In the control group, in the same period, that is, in the third screening period, the intensive growth rate of the biparietal part of the head was 8,5%. In the second screening period, the biparietal indicator was also found to be higher. From 30–31 weeks to 32–33 weeks, the absolute growth rate was 8%. At 35–36 weeks, the absolute growth rate increased by 11% compared to the previous week. From 30–31 weeks to 32–33 weeks, the absolute growth rate of the frontal-occipital size was 16%. At 35–36 weeks, the absolute growth rate of the frontal-occipital size of the fetus was 6% compared to the previous week. The intensive growth rate of the fronto-occipital size in the period from 30 to 35 weeks in the first hypothyroidism group in the third screening period was 22%, but in the control group it was 8,3% in the same period. When the fronto-occipital size was observed in dynamics in the first hypothyroidism group, it was proven that it was larger than the head size of the control group in each screening period. The intensive growth rate of the head circumference in the first hypothyroidism group in the period from 30 to 35 weeks was 12%. In the control group, the intensive growth rate was 19,4% during this period. The absolute growth rate of the head circumference from 30–31 weeks to 32–33 weeks was 1,6%. The absolute growth rate of the fetal head circumference at 35–36 weeks was 6%. The intensive growth rate of the abdominal circumference from 30 to 35 weeks was 20%. In the control group, the intensive growth rate from 30 to 35 weeks was 25%. In the first group of women with hypothyroidism, the absolute growth rate from 30–31 weeks to 32–33 weeks was 11%. The absolute growth rate at 35–36 weeks was 8%. The intensive growth rate of the femur length during this period was 41%. In the control group, the intensive growth rate was 51%. The absolute increase in femur length was 20% from 30–31 weeks to 32–33 weeks and 17% at 35–36 weeks.

In the second group of pregnant women with hypothyroidism, it was proven that the biparietal dimensions of the fetal head were smaller than in the other two control groups. In the second group of women with hypothyroidism, the intensive growth rate of the biparietal dimensions was found to be 20% on average from 12 to 15 weeks. In the same period, the intensive growth rate in the first group of women with hypothyroidism was 25%, and in healthy pregnant women it was 34%. In the second group of women with hypothyroidism, the intensive growth rate of the fronto-occipital dimensions was found to be 27% on average from 12 to 15 weeks (54% in the first group and 38% in the control group). In the second group of women with hypothyroidism, the intensive growth rate of the head circumference was found to be 6% on average from 12 to 15 weeks. It was found that the abdominal circumference index in the first screening period was higher than this index in the first hypothyroidism group. During the first screening period, the intensive growth rate of the hip bone in pregnant women with hypothyroidism was 12% from 12 to 15 weeks. The rate of intensive growth during this period was 40% from 20 to 25 weeks. In the first group, intensive growth during this period was 11,4%, and in the control group, it was 83%. From 20–21 weeks to 22–23 weeks, the biparietal index of the fetal head in the second group of women with hypothyroidism had an absolute growth rate of 20%. The absolute growth rate at 24–25 weeks was 24% compared to 23 weeks. During this period, the intensive growth rate of the fronto-occipital size was recorded at 33% from 20 to 25 weeks. In the group of healthy pregnant women, the intensive growth rate during this period was 78%, and in the first hypothyroid group, the intensive growth rate of the fronto-occipital size was 82%. It is clear that compared to the other two control groups, this group had a very low growth rate, even during the period of rapid growth. The absolute growth rate at 22–23 weeks was 47% compared to 21 weeks. The absolute growth rate at 24–25 weeks was 13%.

During this period, the intensive growth rate of head circumference was 49% in the second hypothyroid group from 20 to 25 weeks. In the control group, the intensive growth rate during this period was 61%, while in the first hypothyroid group it was 48%. In the second screening period, the intensive growth rate of head circumference in the second group of hypothyroid patients compared to the first screening period was 5%. At 22–23 weeks, the absolute growth rate compared to 20–21 weeks was 27%. At 24–25 weeks, the absolute growth rate was 16% compared to 23 weeks. During this period, the intensive growth rate of abdominal circumference was 25% from 20 to 25 weeks. It was in the second screening period that we saw that growth was faster than in the other two periods, but in the second group of patients with hypothyroidism, growth was also very slow during this period (the intensive growth rate of healthy pregnant women was 92,5%, and in the first group of hypothyroidism, it was 81%). At 22–23 weeks, the absolute growth rate compared to 20–21 weeks was 3%. At 24–25 weeks, it was found that the absolute growth rate increased by 5% compared to 23 weeks. In the second screening period, the intensive growth rate of the femur was 27% from 20 to 25 weeks. During this period, the intensive growth rate was 81% in healthy pregnant women, while in the group of patients with hypothyroidism (the first group) it was 39%. At 22–23 weeks, the absolute growth rate increased by 10% compared to 20–21 weeks. From 24–25 weeks to 22–23 weeks, the absolute growth rate was 15%. In the third screening period, an intensive growth rate of 5% was noted in the biparietal size from 30 to 35 weeks. In healthy pregnant women, the intensive growth rate of the biparietal size during this period was 8,5%, and in the first group with hypothyroidism, it was 20%. The absolute growth rate was 2% from 30–31 weeks to 32–33 weeks and 3% from 32–33 weeks to 35–36 weeks. The intensive growth rate of the fronto-occipital size was recorded from 30 to 35 weeks, equal to 7%. In the control group, the intensive growth during this period was 8.3%, and in the first hypothyroidism group, it was 22%. The absolute growth pattern of the fronto-occipital size increased by 2% at 32–33 weeks compared to 31 weeks and by 4% at 35–36 weeks compared to 33 weeks.

During the third screening period, the second group recorded an intensive growth rate of head circumference from 30 to 35 weeks of gestation, equal to 11%. In the first hypothyroid group, the intensive growth rate during this period was 12%, compared to 19,4% in the healthy pregnant group. During the third screening period, when measuring head circumference, it was found that it increased intensively by 20% compared to the second screening period. During the third screening period, the absolute growth rate of head circumference in the second group of women with hypothyroidism increased by 3% from 30–31 weeks to 32–33 weeks and by 11% from 33 weeks to 35–36 weeks. The intensive growth rate of abdominal circumference in the second hypothyroid group was 5% from 30 to 35 weeks. In the first group of pregnant women with hypothyroidism, the intensive growth pattern was 20%, and in the healthy group, it was 25%. The absolute growth pattern from 30–31 weeks to 32–33 weeks was 11%, and from 32–33 weeks to 34–35 weeks, it was 5%. During this period, the intensive growth pattern of the femur was recorded in the second group of hypothyroidism, which was 15%, from 30–35 weeks. It was statistically confirmed that the intensive growth pattern in healthy pregnant women during this period was 51%, while in the group of hypothyroid women (the first group), it was 41%. In the third screening period, the absolute growth pattern of the femur was 10% from 30–31 weeks to 32–33 weeks and 17% from 32–33 weeks to 34–35 weeks.

The ratio of the biparietal size of the fetal head to the length of the femur is also an important diagnostic parameter (BP/SU). The ratio of the biparietal size of the fetus to the length of the femur of pregnant women in the first hypothyroidism group (up to 12–35 weeks) did not have a significant statistical difference when compared with the ratios of the control group. The ratio of the biparietal size of the fetus to the length of the femur of pregnant women in the second hypothyroidism group (up to 12–35 weeks) was found to be statistically smaller when compared with the ratios of the control group (see Table 1).

Table 1.

Changes in the ratios of biparietal and femoral length (BP/SU) of the fetus in healthy and hypothyroid pregnant women at the stages of screening examinations

Periods	Weeks	Healthy pregnant group	People with hypothyroidism	Group 2 of people with hypothyroidism
1 screening	12-13	2,25	2,32	2,12
	14-15	1,92	1,75	1,75
2 screening	20-21	1,53	1,42	1,40
	22-23	1,53	1,42	1,48
	24-25	1,51	1,38	1,37
3 screening	30-31	1,52	1,37	1,34
	32-33	1,36	1,34	1,31
	34-35	1,3	1,31	1,29

In all other weeks, the ratio of fetal head circumference to abdominal circumference in the first hypothyroid group was statistically smaller than that in the control group. In the second screening period (24–25 weeks), the ratio of fetal head circumference to abdominal circumference in the first hypothyroid group was statistically smaller than that in the control group. When comparing the ratio of fetal abdominal circumference to hip circumference, a statistically significant increase was observed in the ratio of abdominal circumference to hip circumference in the first hypothyroid group compared to the ratio in the control group in the first and second screening periods (12–13, 22–23, 24–25 weeks). The ratio of abdominal circumference to hip circumference in the second hypothyroid group was statistically significantly smaller than that in the control group in all screening periods (12–35 weeks) (see Table 2).

Table 2.

Changes in the ratios of fetal head circumference to abdominal circumference (HBC/HBC) and fetal abdominal circumference to femur length (HBC/HBC) in healthy and hypothyroid pregnant women during the stages of screening examinations

Periods	Weeks	Healthy pregnant group		People with hypothyroidism		Group 2 of people with hypothyroidism	
		HBA/HQA	HQA/SU	HBA/HQA	HQA/SU	HBA/HQA	HQA/SU
1 screening	12-13	1,14	6,82	1,08	7,38	1,08	6,3
	14-15	1,13	5,89	1,13	5,7	1,23	3,7
2 screening	20-21	1,16	4,49	1,14	4,64	1,07	3,5
	22-23	1,16	4,49	1,14	4,64	1,08	3,6
	24-25	1,14	4,49	1,08	4,6	1,11	3,3
3 screening	30-31	1,12	4,47	1,11	4,35	1,03	3,3
	32-33	1,08	4,64	1,03	4,64	1,05	3,5
	34-35	1,05	4,5	1,05	4,53	1,06	3,3

Conclusion.

The most intensive period of absolute and intensive growth of the head size of the fetus of healthy women (20–21, 22–23, 24–25 weeks) coincided with the 2nd screening period. Two active periods of intensive growth of the femur were observed; these were 16–20 and 26–30 weeks, and statistically significant ($r<0,05$) data were obtained. The most intensive period of dynamic growth of the abdominal circumference coincided with the second screening period (20–25 weeks). Fetometric indicators of the fetus of women with hypothyroidism were statistically ($r<0,05$) smaller than those

of the fetus of healthy pregnant women in the second group. These changes were especially pronounced in the head and abdominal circumference of the fetus. These changes were recorded at 22–25 weeks of pregnancy. When comparing the ratios of fetometric data, it was found that this ratio was smaller in the fetuses of women with hypothyroidism; especially up to 20–30 weeks, this index was higher. The cephalic index of the fetuses of pregnant women of group 1 was more than 85% in the 2nd and 3rd screening periods, which can lead to the development of dolichocephalic children. The cephalic index of the 2nd group of women with hypothyroidism in the 3rd screening period was less than 74%, which may indicate the development of a shortened head, that is, brachycephaly. The ratio of abdominal circumference to head circumference was also smaller, forming a mixed type of change.

REFERENCES

1. Albu, D.–F. A Dandy – Walker variant prenatally diagnosed using ultrasound on one of the fetuses of a twin pregnancy obtained through in vitro fertilization /D.–F. Albu, C.–C. Albu, S.–D. Albu // International Journal of Medical Research and Review. - 2015. - Vol. 3, No. 3. - P. 127-131.

2. Bar – Yosef, O. Neurodevelopmental outcome of isolated ventriculomegaly: a prospective cohort study / O. Bar – Yosef, E. Barzilay, S. Dorembus [et al.] // Prenat. Diagn. - 2017. - Vol. 37. - P. 764-768.

3. Blinov, A.Yu. Fundamentals of ultrasonic fetometry / A.Yu. Blinov, M.V. Medvedev. - M.: Real Time, 2012.-- 136 p.

4. Carseldine, W. Antenatal diagnosis of a fetal dural venous thrombosis / W. Carseldine, F. Park, C. Abel [et al.] // Ultrasound Obstet. Gynecol. - 2013. –Vol. 42, No. 1. - P. 151.

5. Esetov, M.A. Echography of the central nervous system of the fetus. Intermediate sail cavity: own observation and literature review / M.A. Esetov, G.M. Bekeladze, E.M. Huseynova // Prenat. Diagn. - 2015. –T. 14, no. 1. - pp. 46–51.

6. Ergashev S., Usmanov R., Niyozov N. Morpho-functional changes in the endocrine pancreas of white rats under metabolic syndrome conditions //Central Asian Journal of Medicine. – 2025. – №. 4. – C. 75-80.

7. Kurbanovich N. N., Abdurasulovich G. D. Features of morphological changes in the pancreas //Texas Journal of Medical Science. – 2023. – T. 16. – C. 79-83.

8. Kurbanovich N. N. et al. Reactive changes in the pancreas in hypothyroidism //American Journal of Interdisciplinary Research and Development. – 2024. – T. 25. – C. 343-347.

9. Kuldasheva m. N. Et al. Morphology of the ventricles of offspring born to mothers with experimental hypodynamia // Central Asian journal of medicine. – 2026. – №. 3. – c. 46-50.

10. Mukhamadovna A. S. et al. Indicators of Fetometry of the Fetus in Pregnant Women in a State of Hypothyroidism //Texas Journal of Medical Science. – 2023. – T. 16. – C. 75-78.

11. Mukhamadovna A. S. et al. Morphological Characteristics of Myocardial Changes When Exposed to Pesticides //Onomazein. – 2023. – №. 62. – C. 1226-1237.

12. Matkarimov O., Axmedova S., Niyozov N. Criteria for assessing structural changes in the myocardium in experimental hypodynamic and diabetes //Central Asian Journal of Medicine. – 2025. – №. 3. – C. 273-283.

13. Matkarimov O., Axmedova S., Niyozov N. Tajribaviy gipodinamiya holatida miokardning morfologiyasi //Modern Science and Research. – 2025. – T. 4. – №. 5. – C. 338-343.

14. Niyozov N.Q. Tajribaviy qalqonsimon bez kasalliklari fonida me’da osti bezi morfologiyasi // Medical journal of young scientists. – 2026. – №. 17 (03). – c. 210-214.

15. Niyozov N., Ergashev S. Pancreatic morphology in thyroid diseases in white mice //Modern Science and Research. – 2025. – T. 4. – №. 4.

16. Niyozov N. K. et al. Morphological Aspects of Pancreas Changes in Experimental Hypothyroidism //Journal of education and scientific medicine. – 2023. – T. 8. – №. 2. – C. 27-31.

17. Niyozov N. K. et al. Morphology of the Pancreas Against the Background of Hypothyroidism //Journal of education and scientific medicine. – 2024. – T. 18. – №. 5. – C. 47-52.

18. Niyozov N., Qo‘qonboyev M. Me’da osti bezi morfologiyasi tajribaviy gipotireozda //Modern Science and Research. – 2025. – T. 4. – №. 3. – C. 798-806.

19. Niyozov N. K., Kukonboyev M. I. Pancreatic gland morphology in experimental hypothyroidism //Modern Science and Research. – 2025. – T. 4. – №. 4. – C. 1169-1176.

20. Niyozov N.Q. Kalamushlar me’da osti bezi morfologiyasi tajribaviy gipotireoz fonida //Modern Science and Research. – 2025. – T. 4. – №. 6. – C. 955-961.

21. Umerov A. A., Niyozov N. Q. Pancreatic pathologies: understanding the interplay between chronic diseases and metabolic dysfunction //Conference on the role and importance of science in the modern world. – 2025. – T. 2. – №. 1. – C. 104-107.

22. Umerov A. A., Niyozov N. Q. Pancreatic morphology in experimental stress //Multidisciplinary Journal of Science and Technology. – 2025. – T. 5. – №. 1. – C. 223-227.

23. Umerov A., Niyozov N. Pancreatic morphometry under stress //International journal of medical sciences. – 2025. – T. 1. – №. 1. – C. 362-368.

CLINICAL AND DIAGNOSTIC FEATURES OF GASTROESOPHAGEAL REFLUX DISEASE IN PATIENTS WITH ISCHEMIC HEART DISEAS

Guzel B. Shamsutdinova - Ph.D.
Muazzam I. Ismoilova - Ph.D.
Shirinmoh A. Mirzajonova - master's student
Umidjon M. Mukarramov - Ph.D. student
Fergana Institute of Public Health (Fergana, Uzbekistan)
umidjonmukarramov@gmail.com

Abstract. *Gastroesophageal reflux disease (GERD) and ischemic heart disease (IHD) are common conditions that often coexist, especially in elderly patients. The similarity of clinical symptoms, particularly chest pain, makes differential diagnosis challenging. This study aims to evaluate the clinical manifestations and diagnostic features of GERD in patients with IHD. A comprehensive assessment including clinical evaluation, instrumental diagnostics, and laboratory methods was performed. The results showed that GERD symptoms may mimic angina pectoris, leading to misdiagnosis and inappropriate treatment. Early recognition and accurate diagnosis are essential for effective management and improved patient outcomes. The present study explores the relationship between gastroesophageal reflux disease and ischemic heart disease, with a focus on clinical manifestations and diagnostic challenges. It was found that reflux-related symptoms are frequently observed in patients with cardiac pathology and may imitate or overlap with angina-like pain. In addition, commonly prescribed cardiovascular drugs appear to influence the development of reflux. These findings emphasize the necessity of careful diagnostic differentiation and tailored management strategies.*

Keywords: *ischemic heart disease, gastroesophageal reflux disease, NERD, chest pain, omeprazole test, GERD-Q.*

Introduction.

Ischemic heart disease continues to be one of the most prevalent conditions in modern cardiology. At the same time, gastroesophageal reflux disease is increasingly recognized as a coexisting disorder in these patients. The coexistence of these two conditions creates a complex clinical picture, particularly due to the similarity of chest pain syndromes. As a result, distinguishing between cardiac and esophageal origins of pain becomes a significant clinical challenge.

Gastroesophageal reflux disease (GERD) is a chronic condition characterized by the reflux of gastric contents into the esophagus, leading to symptoms such as heartburn and regurgitation. Ischemic heart disease (IHD) remains one of the leading causes of morbidity and mortality worldwide.

The coexistence of GERD and IHD presents a diagnostic challenge due to overlapping clinical symptoms, especially chest pain. In some cases, GERD may mimic cardiac pain, leading to unnecessary cardiac interventions, while in others, cardiac conditions may be underestimated.

Therefore, studying the clinical and diagnostic features of GERD in patients with IHD is essential for improving diagnostic accuracy and treatment strategies.

Objective.

This study was conducted to identify and analyze the specific clinical and diagnostic features of GERD in individuals diagnosed with ischemic heart disease.

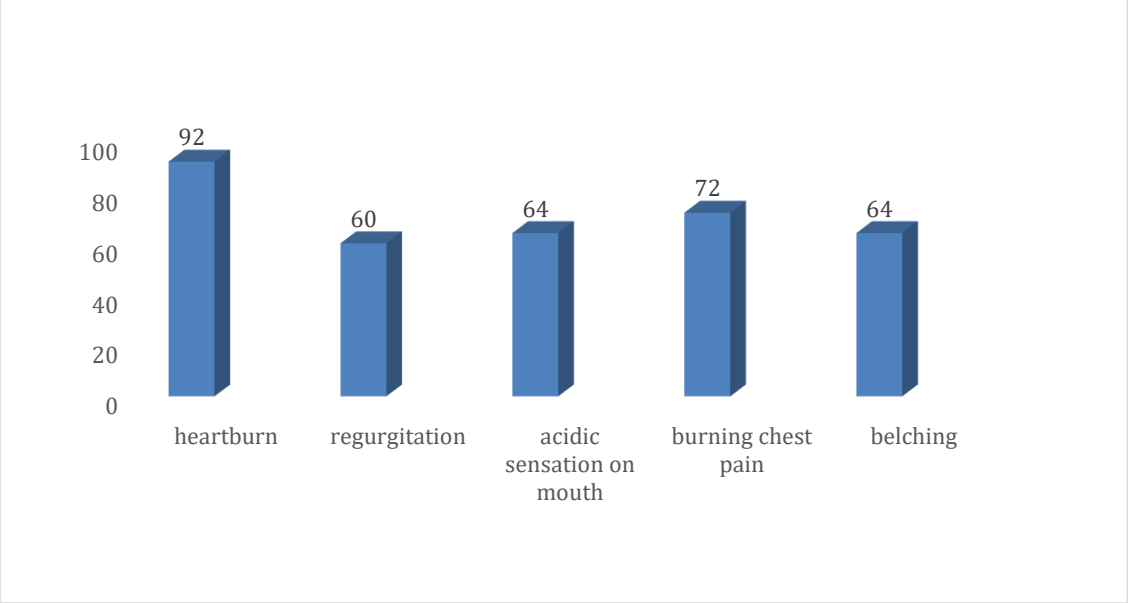
Materials and methods.

The investigation included 50 patients with confirmed ischemic heart disease. For comparative analysis, participants were divided into two groups: those with concomitant GERD and those without reflux pathology.

Each patient underwent a comprehensive assessment, including symptom evaluation, GERD-Q questionnaire, electrocardiographic examination, endoscopic assessment when indicated, and a proton pump inhibitor (omeprazole) test. The results were processed using appropriate statistical methods.

Results.

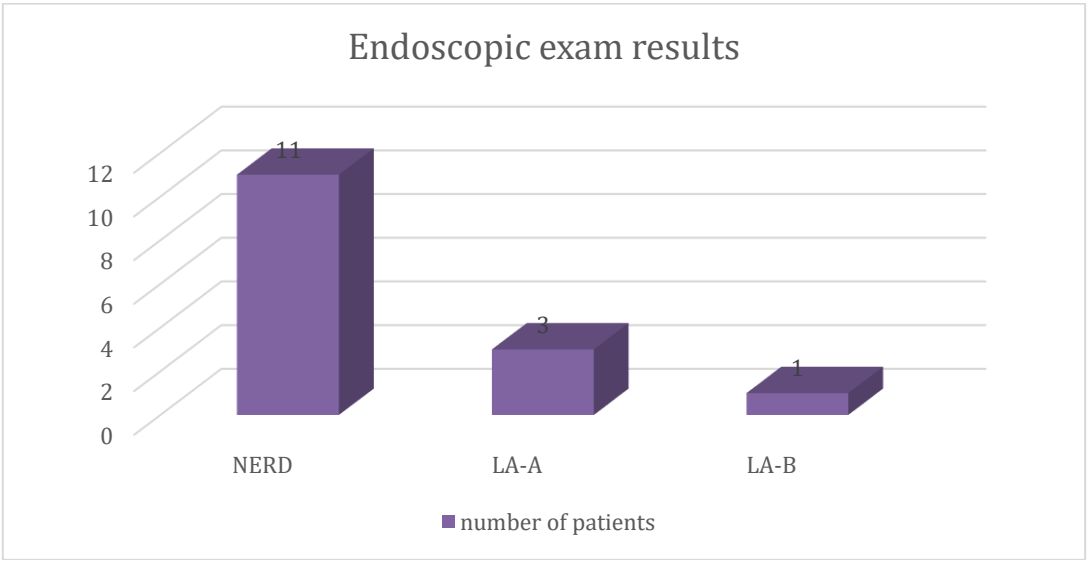
Clinical evaluation revealed that reflux-associated complaints were present in a substantial proportion of patients with ischemic heart disease. Individuals with combined pathology more frequently reported burning-type chest discomfort, persistent heartburn, regurgitation, and nocturnal exacerbation of symptoms.



In contrast, patients without GERD more commonly experienced pain radiating to typical cardiac regions such as the arm or jaw, often triggered by physical or emotional stress.

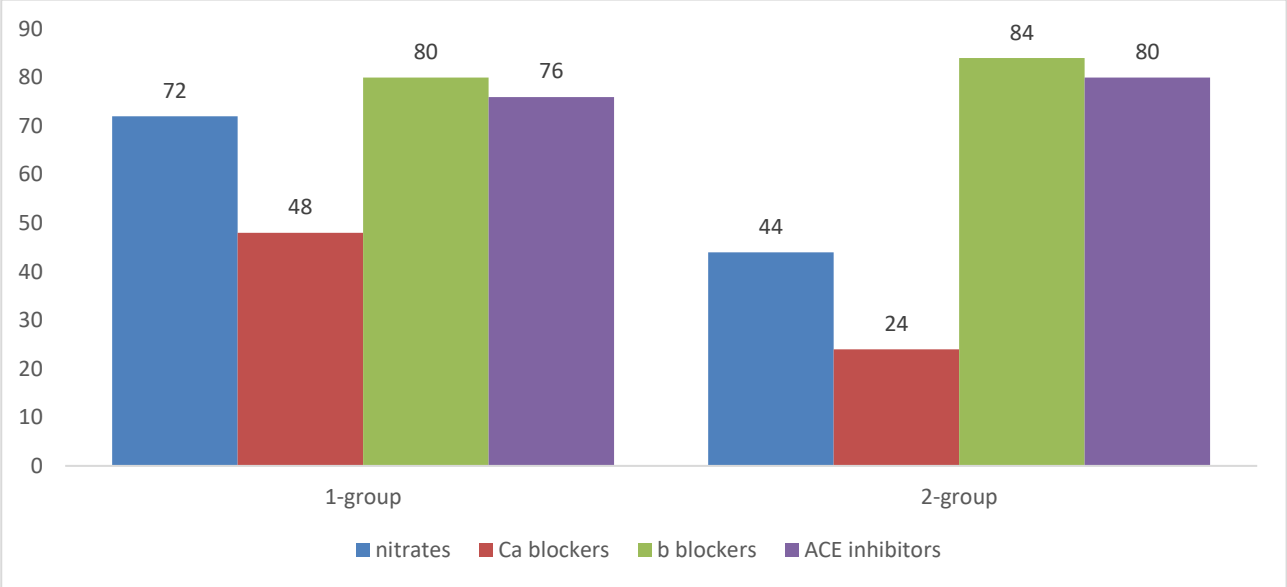
GERD-Q scores confirmed the presence of reflux disease in the first group, whereas no clinically relevant reflux was identified in the control group.

Endoscopic findings demonstrated that most cases were classified as non-erosive reflux disease, while erosive lesions were relatively uncommon and generally mild.



The omeprazole test supported acid-related symptom origin in the majority of cases; however, a subset of patients did not respond, suggesting a multifactorial nature of chest pain.

Additionally, it was observed that the use of nitrates and calcium channel blockers was more common among patients with GERD, indicating a possible pharmacological contribution to reflux development.



Discussion.

The findings suggest that GERD in patients with ischemic heart disease often presents without pronounced endoscopic changes, which may complicate timely diagnosis. The characteristic features of reflux-related pain, including its burning nature and positional dependence, are important clinical indicators.

Nevertheless, incomplete response to acid-suppressive therapy in some cases highlights the persistence of cardiac mechanisms contributing to symptom development.

The overlap between GERD and IHD symptoms poses a significant diagnostic challenge. Chest pain of esophageal origin can closely resemble angina pectoris, leading to diagnostic confusion.

Instrumental methods such as endoscopy and pH monitoring play a crucial role in distinguishing between these conditions. In addition, careful analysis of symptom patterns can aid in differential diagnosis.

Failure to correctly diagnose GERD in IHD patients may lead to persistent symptoms and reduced quality of life.

Conclusion.

The coexistence of GERD and ischemic heart disease represents a clinically important condition characterized by overlapping symptoms. Accurate differentiation between cardiac and non-cardiac chest pain is essential for appropriate management.

Diagnostic tools such as the GERD-Q questionnaire and proton pump inhibitor testing play a key role in identifying reflux-related pathology. Moreover, attention should be paid to the potential impact of cardiovascular medications on esophageal function. GERD is common among patients with ischemic heart disease and may mimic cardiac symptoms. Accurate diagnosis using a combination of clinical and instrumental methods is essential to differentiate between these conditions. Early identification of GERD in IHD patients improves treatment outcomes and prevents unnecessary cardiac interventions. A personalized and multidisciplinary approach is recommended for optimal patient care.

REFERENCES

1. De Giorgi F., Palmiero M., Esposito I., Mosca F., Cuomo R. Pathophysiology of gastroesophageal reflux disease. Acta Otorhinolaryngol Ital. 2006;26(5):241–246.
2. Dent J., El-Serag H.B., Wallander M.A., Johansson S. Epidemiology of gastro-oesophageal reflux disease: a systematic review. Gut. 2005;54(5):710–717.
3. Fass R. Empirical proton pump inhibitor therapy in patients with noncardiac chest pain. Am J Gastroenterol. 2002;97(3):542–548.
4. Fass R., Achem S.R. Noncardiac chest pain: epidemiology, natural course and pathogenesis. J Neurogastroenterol Motil. 2011;17(2):110–123.
5. Fass R., Dickman R. Non-cardiac chest pain: an update. Neurogastroenterol Motil. 2006;18(6):408–417.
6. Flook N., Jones R. Guidelines for the diagnosis and management of gastroesophageal reflux disease. Can J Gastroenterol. 2008;22(1):1–24.
7. Gerson L.B., Fass R. A systematic review of the definitions, prevalence, and response to treatment of nocturnal gastroesophageal reflux disease. Clin Gastroenterol Hepatol. 2009;7(4):372–378.
8. Gyawali C.P., Fass R. Management of gastroesophageal reflux disease. Gastroenterology. 2018;154(2):302–318.
9. Kahrilas P.J., Shaheen N.J., Vaezi M.F. American Gastroenterological Association medical position statement on the management of gastroesophageal reflux disease. Gastroenterology. 2008;135(4):1383–1391.
10. Katz P.O., Gerson L.B., Vela M.F. Guidelines for the diagnosis and management of gastroesophageal reflux disease. Am J Gastroenterol. 2013;108(3):308–328.
11. Kusano M., Shimoyama Y., Sugimoto S. Development of GERD symptoms in patients with ischemic heart disease. J Gastroenterol. 2012;47(6):593–600.
12. Liu Y., Sun X., Li Y. Association between gastroesophageal reflux disease and ischemic heart disease: a systematic review and meta-analysis. Medicine (Baltimore). 2019;98(24):e15845.
13. Pandak W.M., Arezo S., Everett S. Gastroesophageal reflux disease and coronary artery disease: clinical implications. Am J Med. 2002;112(4):292–298.
14. Richter J.E. Chest pain and gastroesophageal reflux disease. J Clin Gastroenterol. 2000;30(3 Suppl):S39–S41.
15. Shaker R., Castell D.O., Schoenfeld P.S., Spechler S.J. Nighttime gastroesophageal reflux disease. Gastroenterology. 2003;124(4):1088–1092.
16. Sifrim D., Zerbib F. Diagnosis and management of patients with reflux symptoms refractory to proton pump inhibitors. Gut. 2012;61(9):1340–1354.
17. Vaezi M.F., Schroeder P.L., Richter J.E. Reproducibility of proximal pH parameters in 24-hour ambulatory esophageal pH monitoring. Am J Gastroenterol. 1997;92(5):825–829.
18. Vakil N., van Zanten S.V., Kahrilas P., Dent J., Jones R. The GERD questionnaire (GERDQ): a tool for the diagnosis of gastroesophageal reflux disease. Clin Gastroenterol Hepatol. 2010;8(8):722–727.
19. Vakil R., van Zanten S.V., Kahrilas P. The Montreal definition and classification of gastroesophageal reflux disease. Am J Gastroenterol. 2006;101(8):1900–1920.
20. Wang W.H., Huang J.Q., Zheng G.F., Xia H.H., Wong W.M., Lam S.K. Head-to-head comparison of H2-receptor antagonists and proton pump inhibitors in the treatment of erosive esophagitis. Am J Gastroenterol. 2005;100(10):2190–2197.

PATHOGENETIC MECHANISMS OF STRESS-DIET-INDUCED HYPOXIA DEVELOPMENT IN CASE OF POOR NUTRITION (LITERATURE REVIEW)

Bakhtiyor U. Iriskulov - D.M.Sc., professor
Guzal N. Mukhamedova - assistant
Tashkent State Medical University (Tashkent, Uzbekistan)
asalsajfutdinova@gmail.com

Abstract. *This article discusses the current understanding of the pathogenetic mechanisms of hypoxia induced by alimentary stress and poor nutrition. The concept of metabolic stress as a universal hypermetabolic response to a nutrient imbalance with activation of the hypothalamic-pituitary-adrenal system and isolation of hypoxia-induced factors is analyzed. Special attention is paid to the role of mitochondrial dysfunction, oxidative stress and aseptic inflammation in the formation of tissue hypoxia against the background of excessive consumption of fats and carbohydrates. Molecular mechanisms of interaction between nutrient imbalance and signaling pathways of adaptation to hypoxia, including HIF-dependent and independent pathways, are considered. Data on the role of PPAR receptors, endoplasmic reticulum, and adipokines in the pathogenesis of diet-induced hypoxia are presented. Clinical and experimental studies demonstrating a two-way relationship between nutrition and tissue oxygenation are discussed.*

Keywords: *stress-induced hypoxia, poor nutrition, metabolic stress, mitochondrial dysfunction, HIF-1a, oxidative stress, insulin resistance, lipotoxicity.*

Introduction.

The problem of poor nutrition has become a global pandemic in the twenty-first century. Excessive caloric intake, especially at the expense of saturated fats and simple carbohydrates, combined with a violation of the food intake regime forms a state defined in modern literature as "metabolic stress" [14]. The term "stress-diet-induced hypoxia" reflects a relatively new direction of research that considers chronic alimentary disorders as a trigger factor for the development of tissue oxygen deficiency, even in conditions of normal partial pressure of oxygen in the inhaled air [2, 25].

The concept of tissue hypoxia has traditionally been associated with respiratory disorders, cardiovascular or blood disorders. However, the experimental and clinical data accumulated over the past decade indicate the existence of an independent pathogenetic phenomenon — metabolic (cytotoxic, histotoxic, diet-induced) hypoxia. In this condition, oxygen delivery to tissues may remain within the normal range, but its utilization by cells is disrupted due to structural and functional rearrangement of metabolic pathways, mitochondrial dysfunction, and changes in signaling pathways that regulate oxygen homeostasis [5, 24].

The relevance of studying the pathogenetic mechanisms of stress-diet-induced hypoxia is due not only to the high prevalence of alimentary-dependent diseases, but also to understanding the fundamental role of oxygen imbalance in the progression of metabolic syndrome, non-alcoholic fatty liver disease, cardiovascular pathology, and type 2 diabetes mellitus. There is a perception of a vicious circle in which poor nutrition causes tissue hypoxia, and the latter, in turn, aggravates metabolic disorders [6, 11].

The aim of this work is to systematize and analyze current data on the molecular and cellular mechanisms of hypoxia induced by alimentary imbalance, with an emphasis on the interaction between nutrient signals and oxygen homeostasis systems.

Metabolic stress is a universal hypermetabolic and hypercatabolic response of the body to an imbalance in the intake of nutrients, characterized by activation of the hypothalamic-pituitary-adrenal system, increased production of stress hormones (cortisol, catecholamines), and changes in the expression of genes controlling adaptive mechanisms [14, 28]. Unlike the classical stress response

induced by trauma or infection, alimentary metabolic stress has a chronic course and is characterized by specific changes at the cellular and subcellular levels.

The key difference between metabolic stress caused by poor nutrition is its ability to induce the expression of hypoxia-induced factor (HIF-1a) under conditions of normal tissue oxygenation. Recent studies demonstrate that excess glucose, free fatty acids, and fructose can activate HIF-dependent pathways even in normoxia, forming the phenomenon of "normoxic hypoxic signaling" [2, 24].

From an evolutionary point of view, the mechanisms of response to hypoxia and nutrient deficiency are closely interrelated. Organisms have developed integrated stress response systems that allow them to survive both in conditions of oxygen starvation and lack of food. This phylogenetic similarity explains the fact that signaling pathways regulating adaptation to hypoxia (HIF pathway) and pathways controlling the metabolic response to nutrient availability (AMPK, mTOR) have many intersections [16, 26].

Normally, activation of these pathways is adaptive and is aimed at cell survival under stress. However, in chronic alimentary imbalance, pathological constitutive activation or, on the contrary, suppression of these signaling cascades occurs, which leads to a breakdown in adaptation and the formation of a vicious circle of metabolic disorders. A high-fat diet, as studies on Drosophila melanogaster show, changes the body's tolerance to hypoxic effects, and the nature of these changes depends on the type of hypoxia (intermittent or permanent) [7].

Chronic alimentary stress is accompanied by persistent activation of the hypothalamic-pituitary-adrenal system. An increase in cortisol levels in obesity and metabolic syndrome has a twofold meaning. On the one hand, cortisol helps to mobilize energy resources by stimulating gluconeogenesis and lipolysis. On the other hand, chronic hypercortisolemia induces insulin resistance, promotes visceral obesity, and suppresses antioxidant protection [28].

It is important to note that the activation of the hypothalamic-pituitary-adrenal axis during poor nutrition is closely related to the production of neuropeptide S and catecholamines, which, in turn, modulate the activity of HIF-1a and the expression of genes controlling glycolysis and the tricarboxylic acid cycle [8]. Thus, a neuroendocrine-metabolic complex is formed that provides integration of stress and hypoxic responses.

Hypoxia-induced factor (HIF-1) is a heterodimeric transcription factor consisting of a constitutively expressed β-subunit and an O2-sensitive α-subunit. Under normoxic conditionsнормоксии, HIF-1a undergoes hydroxylation with prolyl hydroxylases (PH.D.), which ensures its recognition by ubiquitin ligase VHL and subsequent degradation in proteasomes. In hypoxia, hydroxylation is inhibited, HIF-1a is stabilized, translocated to the nucleus, and activates transcription of target genes, including angiogenesis factors (VEGF), glucose transporters (GLUT1, GLUT2), glycolytic enzymes, and erythropoiesis regulators (erythropoietin) [24].

The phenomenon of "pseudohypoxia" consists in the activation of HIF-dependent pathways under the conditions of normal tissue oxygenation under the influence of metabolic factors. Madan E. Research et al. (2025) demonstrated that mice with a diet-induced metabolic syndrome (high-fat or high-fructose diet) show activation of the hypoxic response in aortic tissues in the complete absence of systemic hypoxemia [13].

The mechanisms of pseudohypoxia are diverse and include:

1. **Accumulation of Krebs cycle metabolites**, such as succinate and fumarate, which inhibit the activity of prolyl hydroxylases, competing with 2-oxoglutarate [5].
2. **Formation of reactive oxygen species (ROS)** in mitochondria, which stabilize HIF-1a through inhibition of Fe2+ - dependent prolyl hydroxylases [26].
3. **Activation of NF-kB and other proinflammatory pathways**that enhance HIF-1a transcription [22].

Excessive fructose intake plays a special role in the induction of pseudohypoxia. Fructose metabolism in the liver is characterized by a high rate of phosphorylation by fructokinase without

reverse inhibition, which leads to rapid depletion of ATP and accumulation of AMP. AMP is further metabolized to uric acid and other products that can induce oxidative stress and stabilize HIF-1a. In addition, fructose stimulates de novo lipogenesis, which leads to the accumulation of triglycerides and the development стеатозаof liver steatosis [12, 29].

Lipid peroxidation products, such as 4-hydroxynonenal and малоновый malondialdehyde, can also modify prolyl hydroxylases, reducing their activity and promoting the accumulation of HIF-1a. This creates an additional link between oxidative stress, lipotoxicity, and hypoxic signaling [10].

Mitochondria are not only the main consumers of oxygen, but also key organelles that determine the sensitivity of the cell to hypoxia. Poor nutrition, especially excessive fat intake, leads to structural and functional rearrangement of mitochondria. Fernandes J. L. et al. (2023) showed that a high-fat diet reduces mitochondrial density and the antioxidant potential of hepatocytes, while chronic intermittent hypoxia reduces the activity of oxidative phosphorylation complexes (OXPHOS) [5].

Mitochondrial dysfunction in diet-induced metabolic syndrome is characterized by:

- Decreased activity of complex I and complex IV of the respiratory chain;
- Violation of the integrity of the inner mitochondrial membrane;
- Leakage of cytochrome C into the cytosol;
- Reduced levels of mitochondrial biogenesis factors (TFAM, PGC1a) [28].

Mitochondrial dysfunction under alimentary stress is accompanied by a decrease in the efficiency of oxidative phosphorylation and a compensatory switch of cellular metabolism to anaerobic glycolysis-a phenomenon known as aerobic glycolysis or the Warburg effect. Despite the fact that glycolysis allows maintaining ATP production in conditions of mitochondrial insufficiency, it is less effective per glucose molecule and leads to the accumulation of lactate, which aggravates metabolic acidosis [24].

It is important to note that activation of HIF-1a in pseudohypoxia promotes transcriptional activation of glycolytic enzyme genes and suppression of pyruvate dehydrogenase activity through activation of pyruvate dehydrogenase kinase, which additionally inhibits pyruvate entry into the tricarboxylic acid cycle and increases the metabolic shift towards glycolysis [11].

Long-term consumption of a high-fat diet is accompanied by changes in the expression of uncoupling proteins (UCP). Cole M. A. et al. (2016) demonstrated that mice fed a high-fat diet increased UCP3 expression in cardiomyocytes, which reduced the efficiency of oxidative phosphorylation and increased heat production. This change is probably adaptive in nature, aimed at limiting ROS production, but in conditions of hypoxic stress, respiratory dissociation further exacerbates the energy deficit [9].

Succinate (succinic acid) occupies a special place in the pathogenesis of diet-induced hypoxia, acting not only as an intermediate of the Krebs cycle, but also as a signal molecule. In mitochondrial dysfunction and stress, succinate accumulates in the mitochondrial matrix and enters the cytoplasm and extracellular space. The accumulated succinate inhibits prolylhydroxylases, stabilizing HIF-1a and triggering a pseudohypoxic cascade. In addition, succinate activates its SUCNR1 receptor (GPR91), which mediates proinflammatory and profibrotic effects [5, 13].

In clinical practice, this justifies the use of succinate-containing drugs to activate urgent adaptive mechanisms, however, with chronic hyperproduction of succinate, its effects become pathological [14].

Poor nutrition is accompanied by excessive production of reactive oxygen species from several sources. First, the overload of mitochondria with substrates (fatty acids, glucose) leads to an increase in the mitochondrial membrane potential and an increase in ROS production in complexes I and III of the respiratory chain. Secondly, activation of NADPH oxidases, especially NOX4, in endothelial cells and adipocytes significantly contributes to oxidative stress [30]. Third, peroxisomal fatty acid oxidation and xanthine oxidase activity in hyperuricemia additionally generate ROS.

Studies conducted in rats have shown that a high-fat diet reduces the overall antioxidant capacity of tissues, including the activity of superoxide dismutase (SOD-1) and the content of reduced glutathione, which disrupts the balance between ROS production and utilization [5].

Mitochondrial DNA (mtDNA), lacking protective histones and located in close proximity to the respiratory chain, is particularly vulnerable to oxidative damage. Accumulation of mtDNA mutations under chronic oxidative stress leads to disruption of the synthesis of subunits of respiratory complexes encoded by the mitochondrial genome, which aggravates mitochondrial dysfunction [26].

In addition, ROS directly inactivate iron-sulfur clusters of respiratory chain and Krebs cycle enzymes (aconitase, complexes I and II), and also oxidize thiol groups of antioxidant enzymes, reducing their activity. Studies by Fernandes J. L. have demonstrated that both chronic intermittent hypoxia and a high-fat diet cause changes in тиолахcysteine-related thiols, which reflects a violation of redox regulation [5].

Proinflammatory cytokines, including tumor necrosis factor-α (TNF-α), interleukin-1β (IL-1β), and interleukin-6 (IL-6), play a key role in potentiating hypoxic damage. In obesity and metabolic syndrome, there is a chronic, sluggish inflammation of adipose tissue, liver, and vascular wall associated with macrophage infiltration and adipocyte dysfunction [1, 25].

The role of interleukin-4 (IL-4) and asymmetric dimethylarginine (ADMA) deserves special attention. Madan E. We found that in metabolic syndrome, increased levels of IL-4 and ADMA in the aorta correlate with the induction of mitochondrial dysfunction and hypoxic response. Previously, these molecules were associated with hypoxia in lung tissue, but their role in vascular dysfunction in metabolic syndrome demonstrates the systemic nature of disorders [13].

The vascular wall is also involved in the pathological process. Endothelial dysfunction with a combination of alimentary imbalance and hypoxia is systemic in nature and creates the basis for the development of atherosclerosis and arterial hypertension. It is important to note that even short-term intermittent hypoxia can induce disorders of endothelium-dependent vasodilation, and obesity significantly enhances this effect [30].

Inflammation and oxidative stress lead to endothelial dysfunction — a key factor in impaired tissue perfusion. Zhang Y. et al. (2017) showed that mice on a high-fat diet in combination with chronic intermittent hypoxia develop a pronounced violation of endothelium-dependent vasodilation. Molecular mechanisms include:

- Reduced expression and activity of endothelialNO synthase (eNOS);
- Increased expression of NADPH oxidase 4 (NOX4);
- Increased production of pro-inflammatory cytokines TNF-α and IL-1β;
- Reduced expression of PPAR-γ in the vascular wall [30].

Restoration of endothelial function with the use of the PPAR-γ agonist pioglitazone confirms the key role of this transcription factor in the pathogenesis of vascular disorders in the combination of alimentary imbalance and hypoxia [9].

Peroxisomal proliferator-activated receptor α (PPARa) is a key regulator of fatty acid metabolism and adaptation to starvation. Under conditions of hypoxia, there is a physiological decrease in PPARa expression in the heart, which is accompanied by a decrease in fatty acid oxidation and an increase in glucose utilization, a metabolic shift that is adaptive for the survival of cardiomyocytes in conditions of oxygen deficiency [9].

However, a high-fat diet prevents this adaptive reduction of PPARa. Cole M. A. et al. demonstrated that in mice treated with a high-fat diet, PPARa expression in the heart remains high even under hypoxia, which prevents the metabolic switch to glycolysis and leads to the preservation of high levels of fatty acid oxidation. Since fatty acid oxidation requires more oxygen per unit of ATP produced than glucose, this metabolic pattern under conditions of limited oxygen delivery leads to energy deficiency and reduced myocardial contractile function [3].

PPARy, on the other hand, plays a predominantly protective role in the vascular wall, exerting an antioxidant and anti-inflammatory effect. In obesity induced by a high-fat diet, a decrease in PPARy expression in vascular tissue is observed, which creates a predisposition to endothelial damage under additional стрессорныхstressors, including intermittent hypoxia [30].

Research by Zhang Y. It is demonstrated that a decrease in vascular PPARy in obesity leads to excessive activation of pro-inflammatory and pro-oxidant pathways in response to hypoxia, which is manifested by an increase in NOX4 expression, an increase in superoxide production, and a decrease in the bioavailability of nitric oxide. The use of PPARy agonists completely prevents these disorders, which indicates a potential therapeutic target [9, 30].

The relationship between HIF and PPAR signaling pathways is complex and often reciprocal. On the one hand, HIF-1a suppresses the expression of PPARa and PPARy, promoting a metabolic switch from fatty acid oxidation to glycolysis. On the other hand, PPARy activation may limit the HIF-dependent response through modulation of inflammation and oxidative stress. In case of poor nutrition, this delicate balance is disturbed: adaptive suppression of PPARa is blocked by excess fat in the diet, and protective PPARy is reduced, which creates conditions for uncontrolled activation of pro-inflammatory and pro-oxidant pathways [9, 30].

Adipose tissue in obesity is characterized by relative hypoxia due to the discrepancy between the rapid growth of adipocytes and the rate of angiogenesis. Emerging hypoxic zones in adipose tissue activate HIF-1a, which leads to changes in adipokine secretion: increased production of leptin, resistin, and proinflammatory cytokines, while reducing adiponectin secretion [1, 25].

Adipose tissue hypoxia also contributes to fibrosis and macrophage infiltration, which supports chronic inflammation and systemic insulin resistance. АдипоцитыUnder hypoxic conditions, adipocytes switch to glycolytic metabolism with increased production of lactate, which can further modulate lipolysis and secretory activity via the GPR81 receptor [28].

The liver plays a central role in the pathogenesis of diet-induced hypoxia. Excessive intake of fats and carbohydrates leads to the development of non-alcoholic fatty liver disease (NAFLD), which is associated with tissue hypoxia even in the absence of respiratory failure. Research by Yuan F. fructose consumption induces endoplasmic stress (ERS) in hepatocytes, which гепатоцитаxis manifested by an increase in the marker proteins GRP78, CHOP, and caspase-12, which leads to apoptosis and steatosis [29].

Interestingly, chronic intermittent hypoxia (a model of sleep apnea) has a twofold effect on the liver. On the one hand, it aggravates lipid infiltration and inflammation in obese animals, and on the other hand, it can have a protective effect in certain regimens, suppressing endoplasmic stress and improving metabolic parameters [29]. These data indicate the importance of taking into account the parameters of hypoxic exposure and baseline metabolic status.

The myocardium is highly aerobic tissue that is extremely sensitive to oxygen supply disorders. With a combination of a high-fat diet and hypoxia, a complex of pathological changes develops in the heart:

- Violation of metabolic flexibility while maintaining a high level of fatty acid oxidation;
- Decrease in the concentration of ATP and creatinephosphate;
- Reduction of the emission fraction;
- Increased expression of UCP3, which uncouples oxidation and phosphorylation [3, 9].

Kidney tissue is also affected by diet-induced hypoxia. Interstitial fibrosis and tubulointerstitial damage in obesity are associated with chronic hypoxia of the tubular epithelium. Impaired erythropoietin production by interstitial fibroblasts can lead to renal anemia, which in turn exacerbates tissue hypoxia [4].

On the other hand, the activation of HIF-2a in the kidneys may be protective, promoting adaptation to hypoxia through increased erythropoiesis and angiogenesis. However, chronic

activation of hypoxic signaling under conditions of metabolic stress contributes to the progression of nephrosclerosis and chronic kidney disease [16].

The tricarboxylic acid cycle performs not only an energy, but also an anabolic function, providing intermediates for the synthesis of amino acids, heme and other compounds. The Krebs cycle intermediate pool is maintained through anaplerotic reactions (replenishment of substrates) and cataplerotic reactions (removal of excess).

Maltseva L. A. and co-authors emphasize the importance of anaplerotic therapy in the clinic of critical conditions, including the use of alternative substrates for the Krebs cycle and respiratory chain. Under conditions of metabolic stress, anaplerotic support is aimed at increasing ATP production and can be performed by replenishing the pool of substrates (pyruvate, aspartate, glutamine) or by removing the products of cataplerotic reactions from tissues [14].

In diet-induced hypoxia, the balance between anaplerosis and cataplerosis is disturbed. Excess acetyl-CoAproduced by beta-oxidation of fatty acids condenses with oxaloacetateto form citrate. If the activity of the Krebs cycle is reduced (due to mitochondrial dysfunction or lack of oxygen), citrate is released into the cytoplasm and used for the synthesis of fatty acids and cholesterol, exacerbating steatosis [10].

In conditions of hypoxia and limited glucose availability, ketone bodies can serve as an alternative energy substrate. Miron N. and Tirosh O. (2019) showed that fortifying the diet with cholesterol prevents hypoxic hypoglycemia in mice by inducing a ketogenic shift in metabolism. This effect is mediated by activation of the iNOS/AMPK axis, suppression of gluconeogenesis and glycogenolysis, while increasing the production of ketone bodies in the liver [17].

Ketogenesis can be considered as an adaptive mechanism that provides energy supply to the brain and heart during hypoxia. However, in patients with obesity and metabolic syndrome, this mechanism may be disrupted due to insulin resistance, fatty liver disease, and mitochondrial dysfunction [28].

The concept of anaplerotic therapy involves the use of energy substrates that do not require insulin stimulation to enter cells. Fructose in small doses (less than 60 g / day) can be such a substrate, but excessive fructose intake (more than 100 g/day) is associated with a deterioration in metabolic parameters [12, 29].

Fat emulsions, including среднецепочечныеmedium-chain triglycerides (MCTs) and emulsions enriched with omega-3 fatty acids, are also used in critical nutritional support. Of particular interest is triheptanoin — an anaplerotic substrate that increases the survival rate of patients in critical conditions [14].

Glutamine plays a special role as a nitrogen and carbon skeleton donor, supporting the pool of Krebs cycle intermediates and glutathione synthesis. Under metabolic stress, the need for glutamine increases, and its exogenous administration may be pathogenetically justified [14].

The cell has a complex system of sensors that assess the availability of oxygen and nutrients. Key integrators are:

- **AMPK** (AMP-activated protein kinase) is an energy status sensor activated when the AMP/ATP ratio increases [17].
- **mTOR** (rapamycin target) is a sensor of amino acid and energy availability that regulates growth and proliferation [26].
- **HIF**-oxygen status sensor [24].
- **Sirtuins** are NAD+ - dependent deacetylasesthat link redox status with metabolic regulation [16].

With poor nutrition, all these pathways are involved in the pathological process. An excess of nutrients activates mTOR, suppresses AMPK and, through the accumulation of metabolites, stabilizes HIF even in normoxia. Dysregulation of these pathways creates a vicious circle in which metabolic disorders exacerbate tissue hypoxia, and hypoxia, in turn, increases the metabolic imbalance [11, 24].

The relationship between hypoxia and dietary patterns is bi-directional. On the one hand, as discussed in detail above, poor nutrition induces a state of pseudohypoxia and tissue hypoxia. On the other hand, hypoxia (for example, in case of sleep apnea or being in the highlands) significantly modulates eating behavior and metabolic responses to diet [6, 20].

Studies on Drosophila show that the interaction between hypoxia and a high-fat diet can be both damaging and compensatory, depending on the nature of hypoxic exposure. Intermittent hypoxia, in contrast to permanent hypoxia, partially restored the flies ' tolerance to cold stress, which indicates a complex nature of interactions [7].

In mammals, chronic intermittent hypoxia (a model of sleep apnea) induces insulin resistance and dysmetabolism independently of obesity. At the same time, additional exposure to a high-fat diet does not always exacerbate these disorders, which may indicate saturation of pathogenetic pathways and convergence of mechanisms [5, 15].

Eating disorders are closely associated with dysregulation of circadian rhythms, which is important for the development of metabolic syndrome and hypoxic conditions. Circadian genes (Clock, Bmal1, Per, Cry) regulate not only sleep and wake cycles, but also metabolic pathways, including insulin sensitivity, glucose tolerance, and the activity of antioxidant enzymes [19, 23].

Intermittent hypoxia, which is characteristic of sleep apnea, itself disrupts circadian regulation, which creates an additional level of complexity in the pathogenesis of diet-induced hypoxia. Nocturnal meals, typical of the modern lifestyle, exacerbate the mismatch between central and peripheral oscillators, contributing to metabolic dysregulation [19].

The main body of information about the mechanisms of diet-induced hypoxia was obtained in experimental studies on animals. The most common models are:

1. **Mice on a high-fat diet (60% of calories come from fat)** - classic model of obesity and insulin resistance. In such animals, there is a decrease in the activity of mitochondrial complexes, oxidative stress, HIF-1a activation in various tissues, and endothelial dysfunction [5, 30].
2. **High-fructose diet models** - allow us to study the specific effects of fructose, including the induction of endoplasmic stress and aliver steatosis. Adding fructose to drinking water (10%) for 6 weeks has been shown to induce metabolic syndrome in rats with elevated blood pressure, triglycerides, and insulin [12, 29].
3. **Models of chronic intermittent hypoxia**-reproduce the conditions of sleep apnea by cyclically reducing O2 to 5%, followed by reoxygenation. Such models allow us to study the interaction between hypoxic stress and diet [5, 21].
4. **Drosophila melanogaster models** provide unique opportunities for genetic analysis of the interaction between diet and hypoxia due to the conservativeness of key signaling pathways [7].
5. **Isolated mitochondrial and cell culture models**are used to study the direct effects of nutrients and hypoxia on mitochondrial respiration and ROS production [26].

Clinical studies confirm the association between dietary patterns, obesity, and signs of tissue hypoxia. Patients with obesity and metabolic syndrome have the following symptoms:

- Increased levels of HIF-1a in adipocytes and peripheral blood mononuclear cells [2];
- Reduction of the partial pressure of oxygen in subcutaneous adipose tissue (measured using polarographic electrodes) [25];
- Increased expression of HIF target genes (VEGF, GLUT1) in adipose tissue [1];
- Markers of mitochondrial dysfunction in skeletal muscles and liver [28];
- Microcirculation disorders and endothelium-dependent vasodilation [4].

Special attention should be paid to studies of patients with obstructive sleep apnea, in whom the combination of obesity and intermittent hypoxia creates the maximum risk of cardiovascular complications. These patients have the most pronounced activation of pro-inflammatory and pro-oxidant pathways, as well as the most severe endothelial dysfunction [6, 11, 22].

The basis for the prevention and treatment of diet-induced hypoxia is the normalization of the nature of nutrition. However, in some cases, especially with already formed metabolic disorders, specialized nutritional support is required.

The concept of anaplerotic therapy involves:

- Early use of glucose solutions with intensive insulin therapy for hyperglycemia (target glucose level <10 mmol / l);
- Metabolic preconditioning with restriction of food intake before interventions;
- Use of energy substrates that do not require insulin (fructose in moderate doses);
- The purpose of balanced amino acid mixtures (1.3-1.5 g/kg / day of protein) with the addition of glutamine;
- Application of fat emulsions with omega-3 fatty acids;
- Use of Krebs cycle intermediates (succinate-containing preparations);
- Ensuring adequate intake of thiamine to maintain the activity of key enzymes [14].

Identification of key molecular mechanisms of diet-induced hypoxia allows us to identify potential pharmacological targets:

1. **ProlylHydroxylase** - modulation of PH.D. activity can regulate the stability of HIF-1a. PH.D. inhibitors (roxadustate, vadadustate) are used to treat anemia, but their effects in the metabolic syndrome need to be studied [24].
2. **PPAR receptors** - agonists of PPARy (thiazolidinediones) improve endothelial function and reduce oxidative stress in obesity [9, 30]. PPARa agonists (fibrates) modulate lipid metabolism and can improve metabolic flexibility [3].
3. **Mitochondrial-directed antioxidant** drugs that accumulate in mitochondria (MitoQ, SkQ1) can reduce ROS production and improve the function of the respiratory chain [26].
4. **Anti-inflammatory agents** — inhibitors of proinflammatory cytokines (anti-TNF-α, anti-IL-1β) can reduce systemic inflammation and improve insulin sensitivity [22].
5. **Sirtuin activators**such as resveratrol and other SIRT1 activators can restore mitochondrial function and improve metabolic parameters [16].

In addition to the qualitative composition of the diet, the diet is important. Interval fasting andtime - restricted feedingsynchronize food intake with circadian rhythms and can improve metabolic parameters regardless of the caloric content of the diet [19, 23].

Physical activity remains the most effective non-drug method for improving mitochondrial function and insulin sensitivity. Aerobic training increases mitochondrial biogenesis, increases the activity of oxidative enzymes, and improves tissue oxygenation [27].

Given the heterogeneity of metabolic disorders, a personalized approach to the correction of diet-induced hypoxia is necessary. Genetic polymorphisms, microbiome features, initial metabolic status, and concomitant diseases should be considered when choosing a therapeutic strategy [8, 18].

Conclusion.

Stress-induced hypoxia is a complex multifactorial phenomenon that occurs with chronic poor nutrition and is characterized by the development of tissue oxygen deficiency with preserved systemic oxygenation. Pathogenetic mechanisms include activation of HIF-dependent pathways under conditions of normoxia (pseudohypoxia), mitochondrial dysfunction with impaired oxidative phosphorylation, oxidative stress, chronic inflammation, dysregulation of PPARsignaling, and endothelial dysfunction.

The key role in the development of diet-induced hypoxia is played by:

- Excessive consumption of saturated fat, which blocks adaptive metabolic switching;
- High doses of fructose that induce endoplasmic stress and steatosis;
- An imbalance between the intake of nutrients and the ability of mitochondria to oxidize them;
- Chronic activation of pro-inflammatory and pro-oxidant pathways;
- Reduced expression of protective factors (PPARy, antioxidant enzymes).

The relationship between nutrition and hypoxia is bi-directional, which creates a vicious circle underlying the progression of metabolic syndrome, non-alcoholic fatty liver disease, cardiovascular pathology, and other alimentary-dependent diseases. Understanding these mechanisms opens up new perspectives for therapeutic interventions, including anaplerotic support, PPAR receptor modulation, mitochondrial-directed antioxidant therapy, and dietary adjustment.

Further research should focus on studying the tissue-specific features of diet-induced hypoxia, identifying biomarkers for early diagnosis, and developing personalized approaches to the correction of metabolic disorders, taking into account the individual characteristics of the patient.

REFERENCES

1. Almendros I., et al. Adipose tissue hypoxia in obesity and its impact on metabolic dysfunction // Current Opinion in Endocrine and Metabolic Research. — 2019. — Vol. 11. — P. 15–20.

2. Chouchane L., et al. Hypoxia and obesity: A comprehensive review // Obesity Reviews. — 2021. — Vol. 22(4). — e13170.

3. Cole M.A., Abd Jamil A.H., Heather L.C., et al. On the pivotal role of PPARα in adaptation of the heart to hypoxia and why fat in the diet increases hypoxic injury // FASEB Journal. — 2016. — Vol. 30(5). — P. 141–146.

4. Fernandes J.L., Martins F.O., Olea E., et al. Chronic intermittent hypoxia-induced dysmetabolism is associated with hepatic oxidative stress, mitochondrial dysfunction and inflammation // Antioxidants. — 2023. — Vol. 12(11). — 1910.

5. Gozal D., et al. Intermittent hypoxia and obesity: a vicious cycle // European Respiratory Journal. — 2021. — Vol. 58(3). — 2100345.

6. Kim J., et al. PPARγ agonists attenuate intermittent hypoxia-induced endothelial dysfunction // Sleep Medicine. — 2022. — Vol. 92. — P. 23–31.

7. Lee Y.S., et al. Hypoxia and lipid metabolism // Advances in Experimental Medicine and Biology. — 2019. — Vol. 1134. — P. 101–118.

8. Li J., et al. Fructose-induced endoplasmic reticulum stress and metabolic dysfunction: role of chronic intermittent hypoxia // Nutrients. — 2023. — Vol. 15(8). — 1892.

9. Madan E., Jain V., Singh V.P. Induction of hypoxic response despite normoxic conditions is associated with vascular mitochondrial dysfunction in diet-induced metabolic syndrome // bioRxiv. — 2025.

10. Pack A.I., et al. Intermittent hypoxia and its impact on metabolic dysfunction // Sleep Medicine Clinics. — 2020. — Vol. 15(1). — P. 79–90.

11. Polak J., et al. Intermittent hypoxia and high-fat diet synergistically impair glucose tolerance and insulin sensitivity // Journal of Applied Physiology. — 2021. — Vol. 130(3). — P. 642–653.

12. Semenza G.L. Hypoxia-inducible factors in physiology and medicine // Cell. — 2012. — Vol. 148(3). — P. 399–408.

13. Wang Y., et al. Mitochondrial dysfunction in metabolic syndrome and intermittent hypoxia // Free Radical Biology and Medicine. — 2023. — Vol. 195. — P. 45–57.

14. Yin J., et al. Role of hypoxia in obesity-induced disorders of glucose and lipid metabolism in adipose tissue // American Journal of Physiology-Endocrinology and Metabolism. — 2019. — Vol. 316(3). — E333–E347.

15. Zhang Y., et al. Down-regulation of vascular PPAR-γ contributes to endothelial dysfunction in high-fat diet-induced obese mice exposed to chronic intermittent hypoxia // Biochemical and Biophysical Research Communications. — 2017. — Vol. 492(3). — P. 141–146.

UDK: 616.322-002.289

ASSESSMENT OF THE CONTRIBUTION OF BIALLELIC POLYMORPHISM OF THE EDN1 GENE (LYS198ASN) TO THE DEVELOPMENT OF CHRONIC TONSILLITIS

Bekzod O. Sultonov - junior researcher
Tashkent state medical university (Tashkent, Uzbekistan)
Aybek I. Esamuratov - D.M.Sc., associate professor
Urganch State Medical Institute (Urganch, Uzbekistan)
sultonovbekzod842@gmail.com

Abstract. *This study aims to evaluate the role of the biallelic polymorphism of the EDN1 gene (Lys198Asn) in the development of chronic tonsillitis (CT). The study included 94 patients aged 3 to 55 years with chronic tonsillitis, as well as 90 conditionally healthy individuals examined in the Khorezm region between 2021 and 2025. Patients were divided into groups according to the clinical form of the disease (simple form, toxic-allergic form I and II). Molecular genetic analysis was performed using real-time polymerase chain reaction (PCR).*

The results demonstrated that the minor Asn allele of the EDN1 gene was significantly more frequent in patients with chronic tonsillitis compared to the control group, increasing the risk of disease development by 1.7 times. At the same time, a decrease in the frequency of the protective Lys allele and the Lys/Lys genotype was observed. The strongest association was identified in patients with the simple form and toxic-allergic form I, where the risk of disease increased by 1.8 and 1.9 times, respectively. No statistically significant association was found with toxic-allergic form II.

In conclusion, the EDN1 (Lys198Asn) gene polymorphism is an important genetic marker associated with an increased risk of chronic tonsillitis, particularly its simple and toxic-allergic form I. These findings contribute to a deeper understanding of disease pathogenesis and may support the development of personalized treatment approaches.

Key words: *chronic tonsillitis, genetic polymorphism, EDN1 (Lys198Asn), allele, genotype, risk of development.*

Introduction.

Chronic tonsillitis (CT) is a chronic inflammation of the palatine tonsils of the lymphoid pharyngeal ring, and is one of the most common diseases of the pharynx in people regardless of age [2,13].

The problem of CT remains highly relevant in medicine to this day and extends far beyond otolaryngology. According to the latest data, CT occurs in 12–43.8% of cases in children and 5–15.8% in adults. [5, 14] HT is a disease with a hereditary predisposition [6, 15]. The dominant factors in the development of CT include chronic foci of infection in the oral cavity. In addition, various unfavorable social and environmental factors also contribute to the development of inflammation in the palatine tonsils [7, 11, 16]. The literature does not sufficiently cover the issues of the location and nature of the hereditary predisposition to CT in children born to mothers with this disease. CT is a common disease among throat diseases during pregnancy in women [3]. Along with this, special importance in understanding the mechanism of various pathologies, including CT, is given to the study and clarification of the role of molecular genetic factors [1,8,10,12].

The study of a number of molecular genetic polymorphisms makes it possible to understand the mechanism of development of this disease [6]. According to many authors, there are many genetic markers of predisposition to CT [4,9,17]. Meanwhile, the contribution of the EDN1 gene polymorphism (Lys198Asn) to the increased risk of developing CT has not been sufficiently studied, which determines the necessity and relevance of this study.

Objective: To study the role of biallelic polymorphism of the EDN1 gene (Lys198Asn) in the development of chronic tonsillitis.

Material and methods.

The study was based on the voluntary participation of 94 patients with chronic tonsillitis aged 3 to 55 (median age 29.27 ± 1.7 years). Patients were randomly selected upon admission for diagnosis and treatment at the Khorezm Regional Multidisciplinary Medical Center and the private clinic "Khorezm LOR Shifo" (P. Makhmud Street, Urgench, Uzbekistan) from 2021 to 2025. The diagnosis was established taking into account diagnostic standards based on diagnostic criteria for the nature of clinical manifestations and instrumental data.

Depending on the form of chronic tonsillitis (CT), the selected patients (n=94) were divided into the following groups:

- 1st main group (n=94) – patients with chronic tonsillitis;
- 2nd group (n=39) – patients with a simple form of CT;
- 3rd group (n=32) – patients with toxic-allergic form I (TAF I),
– 4th group (n = 23) - patients with toxic-allergic form II (TAF II),
- 5th control group (CG) (n=90) – included conditionally healthy individuals without ENT diseases.

The material for the molecular genetic study was lymphocytes obtained from peripheral blood using a standard method.

The molecular genetic study included genotyping of the EDN1 (Lys198Asn) gene SNP using a real-time PCR system and software (Applied Biosystems, USA). Fragments of the EDN1 (Lys198Asn) gene SNP were amplified on a programmable thermal cycler from Applied. Biosystems » (USA) with preliminary denaturation at 95 ^{0} C (7 min), amplification for 40 cycles, subsequent denaturation at 95 ^{0} C (1 min), primer annealing at 59 ^{0} C (1 min), elongation at 72 ^{0} C (1 min) and final synthesis at 72 ^{0} C (3 min).

Mathematical analysis and statistical processing of the obtained research results were carried out using a statistical software package using methods for calculating the χ^{2} criteria. and the odds ratio (OR). The distribution of genotype variants of the studied EDN1 gene (Lys198Asn) was matched according to the Hardy-Weinberg equilibrium (HWE) and analyzed using the GenePop (Genetics of Population) program for analyzing genetic data.

Using the OpenEpi 2009, Version 2.9 statistical software package, the 95% CI (confidence interval) and P-values were calculated in addition to the $\chi 2$ and OR. Comparisons of the observation groups were made using the student's t-test, which yields a probability (P) estimate of the significance of differences between the compared groups, with a significance level of $P < 0.05$.

Results and discussion.

Studying the distribution of genotypes of the polymorphic gene EDN 1 (Lys 198 Asn) in the main group of patients with CT and CG, it was found that the distribution of the observed frequencies of genotypic variants Lys / Lys, Lys / Asn and Asn / Asn had a statistically insignificant difference in relation to their expected frequencies (χ^{2} <3.84; P = 0.899), i.e. the distribution of genotypes did not deviate from the Hardy-Weinberg equilibrium (HWE, P> 0.05).

The results of the analysis of the distribution of the EDN 1 gene polymorphism (Lys 198 Asn) in the studied groups showed the highest frequency of occurrence of the minor Asn allele, as well as the Lys / Asn and Asn / Asn genotypes among patients with CT, with a predominance of their frequencies in the group of patients with a simple form of CT and TAF I. The predominance of the frequencies of unfavorable allele variants and genotypes indicates their possible involvement in the implementation of CT. At the same time, to reliably verify this, comparative statistical analyses of the differences between the studied groups were conducted (Table 1).

Table 1.

Analysis of the structure of the EDN 1 gene polymorphism (Lys 198 Asn) among patients with chronic tonsillitis depending on the form and healthy

Group	Frequency of alleles and genotypes									
	Lys		Asn		Lys / Lys		Lys / Asn		Asn/Asn	
	n	%	N	%	n	%	n	%	n	%
1st MG of patients with chronic tonsillitis (n = 94)	141	75.0	47	25.0	53	56.4	35	37.2	6	6.4
2nd group with a simple form of CT, (n = 39)	58	74.4	20	25.6	22	56.4	14	35.9	3	7.7
3rd group with TAF I, (n = 32)	47	73.4	17	26.6	17	53.1	13	40.6	2	6.3
4th group with TAF II, (n = 23)	36	78.3	10	21.7	14	60.9	8	34.8	1	4.3
5th CG - healthy, (n=90)	151	83.9	29	16.1	63	70.0	25	27.8	2	2.2

In the 1st MG of patients with CT, compared with the CG, the minor allele Asn was statistically significantly more frequent by 1.7 times ($\chi^2 = 4.4$; P = 0.05; O R = 1.7; 95% CI: 1.04 - 2.9), while the frequency of the wild allele Lys was statistically significantly lower ($\chi^2 = 4.4$; P = 0.05; O R = 0.6; 95% CI: 0.34 - 0.96). Moreover, along with a reliable decrease in the wild allele, a pronounced tendency towards a decrease in the frequency of the wild genotype Lys / Lys was also observed ($\chi^2 = 3.7$; P = 0.1; O R = 0.6; 95% CI: 0.3 - 1.01).

However, in terms of the frequencies of unfavorable genotypic variants Lys / Asn ($\chi 2 = {}^{1.9;}$ P=0.2; OR = 1.5; 95% CI: 0.83–2.87) and Asn / Asn ($\chi 2 = {}^{1.9;}$ P=0.2; OR = 3.0; 95% CI: 0.63–14.23), despite their higher frequency in the group of patients compared to the control group, the differences were not statistically significant (Table 2).

Table 2.

Evaluation of differences in the distribution of the polymorphic gene EDN 1 (Lys 198 Asn) between the main and control groups

Alleles and genotypes	Frequency				χ^2	R	RR	95% CI	OR	95% CI
	MG (n=94)		CG (n=90)							
	n	%	n	%						
Lys	141	75.0	151	83.9	4.4	0.05	0.9	0.59 - 1.36	0.6	0.34 - 0.96
Asn	47	25.0	29	16.1	4.4	0.05	1.1	0.61 - 2.04	1.7	1.04 - 2.9
Lys/Lys	53	56.4	63	70.0	3.7	0.10	0.8	0.47 - 1.39	0.6	0.3 - 1.01
Lys/Asn	35	37.2	25	27.8	1.9	0.20	1.3	0.77 - 2.33	1.5	0.83 - 2.87
Asn/Asn	6	6.4	2	2.2	1.9	0.20	2.9	1.25 - 6.63	3.0	0.63 - 14.23

The statistically significant differences in the frequencies of the attenuated allele Asn, as well as the wild Lys allele and the Lys / Lys genotype of the polymorphic gene EDN 1 (Lys 198 Asn) between the MG and CG show that the attenuated allele increases the reliable risk of developing CT by 1.7 times ($\chi^2 = 4.4$; P = 0.05) due to a decrease in the activity of the protective allele Lys ($\chi^2 = 4.4$; P = 0.05) and the genotype Lys / Lys ($\chi^2 = 3.7$; P = 0.1). Thus, the obtained results prove the role of the polymorphic gene EDN 1 (Lys 198 Asn) in increasing the chance of developing CT.

In the 2nd group of patients with a simple form of CT, compared with the control group, the most noticeable differences were found between the allelic variants of the polymorphic gene EDN 1 (Lys 198 Asn), characterized among patients by a pronounced tendency to an increase in the unfavorable effect of the minor allele A sn by 1.8 times ($\chi^2 = 3.2$; P = 0.1; O R = 1.8; 95% CI: 0.95-

3.41) and a simultaneous pronounced tendency to the protective activity of the wild allele Lys (χ^2 = 3.2; P = 0.1; O R = 0.6; 95% CI: 0.29 – 1.06).

At the same time, the differences in the groups between the frequencies of the wild genotype Lys / Lys (χ^2 = 2.2; P = 0.2; O R = 0.6; 95% CI: 0.26 - 1.2), heterozygote Lys / Asn (χ^2 = 0.9; P = 0.4; O R = 1.5; 95% CI: 0.66 - 3.24) and minor homozygote Asn / Asn (χ^2 = 2.2; P = 0.2; O R = 3.7; 95% CI: 0.65 - 20.53) did not reach a statistically significant level of values.

Thus, studying the distribution features of the genetic polymorphism EDN 1 (Lys 198 Asn), the presence of a pronounced tendency to increase the unfavorable effect of the minor allele A sn (χ^2 = 3.2; P = 0.1) and decrease the protective activity of the main wild allele Lys (χ^2 = 3.2; P = 0.1) contributes to an increase in the risk of developing a simple form of CT by 1.8 times.

In the 3rd group of patients with CT and TAF I, compared with the control group, a pronounced tendency towards an increase in the unfavorable effect of the minor allele A sn by 1.9 times ($\chi 2 =$ 3.4; P = 0.1; O R = 1.9; 95% CI: 0.96 – 3.7) was found in the structure of the polymorphic gene EDN 1 (Lys 198 Asn), which was simultaneously accompanied by a pronounced tendency towards a decrease in the protective activity of the wild Lys allele (χ^2 = 3.4; P = 0.1; O R = 0.5; 95% CI: 0.27 - 1.04) and the Lys / Lys genotype (χ^2 = 3.0; P = 0.1; O R = 0.5; 95% CI: 0.21 - 1.1). Just as in the 2nd group of patients, in the 3rd group there was no statistically significant difference in the distribution of the Lys / Asn heterozygote ($\chi 2$ =1.8; P=0.2; O R =1.8; 95% CI: 0.77 - 4.11) and the minor Asn / Asn homozygote ($\chi 2 = {}^{1.2;}$ P=0.3; O R =2.9; 95% CI: 0.43 - 20.0).

The presence of a pronounced tendency to an increase in the frequency of the minor allele A sn (χ^2 = 3.4; P = 0.1), as well as to a decrease in the frequencies of the major allele Lys (χ^2 = 3.4; P = 0.1) and the genotype Lys / Lys (χ^2 = 3.4; P = 0.1) in the structure of the genetic polymorphism EDN 1 (LYS 198 ASN) in the group of patients with CT with TAF I compared to healthy individuals shows the possible participation of the studied genetic marker in increasing the chance of developing this form of CT by 1.9 times.

However, in the 4th group of patients with CT and TAF II, compared with the control group, no statistically significant differences were found between the frequencies of the Lys ($\chi 2 =$ 0.8; P = 0.4; O R = 0.7; 95% CI: 0.31 - 1.54) and A sn ($\chi^{2 = 0.8; P}$ = 0.4; O R = 1.4; 95% CI: 0.31 - 1.54) alleles, as well as the genotypes Lys / Lys ($\chi 2 =$ 0.7; P = 0.5; O R = 0.7; 95% CI: 0.26 - 1.72), Lys / Asn (χ^2 = 0.4 P = 0.6; O R = 1.4; 95% CI: 0.52 - 3.66) and Asn / Asn (χ^2 = 0.3; P = 0.6; O R = 2.0; 95% CI: 0.18 - 22.06).

The absence of statistically significant differences in the structure of the polymorphic gene EDN 1 (Lys 198 Asn) between the groups of CT with TAF II and the control shows the absence of a contribution of the studied marker to the formation of this form of chronic tonsillitis.

EDN 1 (Lys 198 Asn) between different forms of CT patients also appeared interesting. Thus, analyzing the level of significance of differences between patients with a simple form of CT and CT with TAF I due to minor differences between the frequencies of alleles and genotypes, no statistically significant differences were revealed: alleles Lys (χ^2 <3.84; P = 0.95; O R = 1.0; 95% CI: 0.49 - 2.23) and A sn (χ^2 <3.84; P = 0.95; O R = 1.0; 95% CI: 0.45 - 2.02), genotypes Lys / Lys (χ^2 = 0.1; P = 0.8; O R = 1.1; 95% CI: 0.45 - 2.92), Lys / Asn (χ^2 = 0.2; P = 0.7; O R = 0.8; 95% CI: 0.31 - 2.14) and Asn / Asn (χ^2 = 0.1; P = 0.9; O R = 1.3; 95% CI: 0.2-7.95.

A similar analysis of the significance level of differences between patients with a simple form of CT and CT with TAF II also, due to insignificant differences, did not allow us to identify statistically significant differences for the Lys alleles (χ^2 = 0.2; P = 0.7; O R = 0.8; 95% CI: 0.34 - 1.91) and A sn (χ^2 = 0.2; P = 0.7; O R = 1.2; 95% CI: 0.52 - 2.95), as well as the Lys / Lys genotypes (χ^2 = 0.1; P = 0.8; O R = 0.8; 95% CI: 0.29 - 2.38), Lys / Asn (χ^2 <3.84; P = 0.95; O R = 1.1; 95% CI: 0.36 - 3.09) and Asn / Asn (χ^2 =0.3; P = 0.7; O R =1.8; 95% CI: 0.18 - 18.18).

Differences in the distribution of the polymorphic gene EDN 1 (Lys 198 Asn) between patients with CT with TAF I and CT with TAF II were also statistically insignificant for the alleles Lys (χ^2 =

0.3; P = 0.6; O R = 0.8; 95% CI: 0.31 - 1.87) and A sn (χ^2 = 0.3; P = 0.6; O R = 1.3; 95% CI: 0.53 - 3.18), as well as the genotypes Lys / Lys (χ^2 = 0.3; P = 0.6; O R = 0.7; 95% CI: 0.25 - 2.16), Lys / Asn (χ^2 = 0.2; P = 0.7; O R = 1.3; 95% CI: 0.42 - 3.89) and Asn / Asn (χ^2 = 0.1; P = 0.8; O R = 1.5; 95% CI: 0.13 - 16.99).

Conclusion.

Thus, summing up the discussion of the results of the study of the distribution features and functional significance of the allelic genetic polymorphism EDN 1 (Lys 198 Asn), we can emphasize its role as a genetic factor with a risk effect that statistically significantly increases the risk of developing CT among carriers of the minor Asn allele by 1.7 times (χ^2 = 4.4; P = 0.05), an increase in the activity of which was associated with a significant decrease in the protective effect of the Lys allele (χ^2 = 4.4; P = 0.05) and the Lys / Lys genotype (χ^2 = 3.7; P = 0.1).

With regard to the role of the genetic polymorphism EDN 1 (Lys 198 Asn) in increasing the chance of developing various forms of CT, a pronounced tendency was revealed towards an increase in the risk of developing a simple form of CT (χ^2 = 3.2; P = 0.1) and CT with TAF I (χ^2 = 3.4; P = 0.1) among carriers of the minor allele Asn by 1.8 and 1.9 times, respectively.

Meanwhile, the associative link between the genetic polymorphism EDN 1 (Lys 198 Asn) and the development of CT TAF II has not been established.

In connection with the presented results, it can be concluded that the genetic polymorphism EDN 1 (Lys 198 Asn) is a genetic marker involved in increasing the risk of developing HT, namely its forms such as simple and toxic-allergic form I. (TAF I).

REFERENCES

1. AlChalabi R. et al. Role of SAgs Produced by Staphylococcus aureus, rs893629 in TLR2 Gene in Progression of Recurrent Tonsillitis //Iraqi Journal of Science. – 2025. – P. 3695-3705.

2. Andreychyn MA et al. Thermographic differential diagnosis of acute tonsillitis and exacerbation of chronic tonsillitis //Wiadomości Lekarskie. – 2020. – T. 73. – No. 3. – pp. 417-422.

3. Ankathil R. et al. Tonsillitis Revisited: Grasping the Intrications of Biofilm Associations //Bacterial Biofilm and Chronic Infections: Role in Disease Pathogenesis and Therapeutic Strategies. – Singapore: Springer Nature Singapore, 2025. – pp. 135-152.

4. Esamuratov AI, Ermatov NJ, Features of the occurrence of single-nucleotide polymorphism il10 (c592a) among patients with purulent-inflammatory diseases of the middle ear and assessment of its contribution to the mechanisms of disease formation // British Medical Journal. 2022, Vol. 1 No. 1: 57-64. (14.00.00; No. 6).

5. Esamuratov A.I., Zh.F. Shamsiev, M. A. Mirzaeva. Features of the distribution of allelic polymorphisms of inflammatory (TNF (G308A), IL2 (T330G), IL6 (C174G), IL10 (C592A)) cytokine genes in pyoinflammatory diseases of the middle ear // European journal of molecular medicine, Vol. 2 No. 5 (September 2022), P.70-73

6. Esamuratov A.I., Mirzaeva M.A., Shamsiev Zh.F. Immune and molecular genetic aspects of the formation of chronic reliable otitis media (csom) // Evrosiyo pediatriya akhborotnomasi. - Toshkent. - 2021; 3 (10): -B. 2-6 (ОАК Раёсатининг 2019 йил 31 октябрдаги 270/8.2-сон қарори).

7. Esamuratov AI, Mirzayeva MA, Shamsiyeva JF. Genetic predictors for the formation of chronic purulent otitis media // British Medical Journal. 2021, Vol. 2 No. 1: 159-164 (14.00.00; No. 6).

8. Esamuratov AI, Ermatov NJ. Features of the occurrence of single-nucleotide polymorphism il10 (c592a) among patients with purulent-inflammatory diseases of the middle ear and assessment of its contribution to the mechanisms of disease formation // British Medical Journal. 2022, Vol. 1 No. 1: 57-64. (14.00.00; No. 6).

9. Gaździcka J. et al. Selected SNPs of FCN2 associated with chronic tonsillitis in the adult population //Genes. – 2023. – T. 14. – No. 2. – S. 242.

10. Guntinas-Lichius O. et al. Treatment of recurrent acute tonsillitis—a systematic review and clinical practice recommendations //Frontiers in surgery. – 2023. – T. 10. – P. 1221932.

11. Haapasalo K. et al. The psoriasis risk allele HLA-C* 06: 02 shows evidence of association with chronic or recurrent streptococcal tonsillitis //Infection and immunity. – 2018. – T. 86. – No. 10. – P. 10.1128/ iai. 00304-18.

12. Kostić M. et al. Analysis of tonsil tissues from patients diagnosed with chronic tonsillitis—microbiological profile, biofilm-forming capacity and histology //Antibiotics. – 2022. – T. 11. – No. 12. – P. 1747.

13. Matkarimova D.S., Karimov Kh. Ya., Boboev K.T. Features of the renin-angiotensin system gene polymorphism in patients with immune microthrombovasculitis in Uzbekistan // Bulletin of Hematology. 2022. No. 2.

14. Mohammed BJ, Fadhil H. Association of TNFα and IL1β genotypes with the risk of Staphylococcus aureus causing recurrent tonsillitis in a sample of Iraqi patients: Association of TNFα and IL1β genotypes with recurrent tonsillitis //Iraqi Journal of Cancer and Medical Genetics. – 2024. – T. 17. – No. 1. – pp. 57-64.

15. Shilin SS et al. The Role of IL-10 G-1082A Polymorphism in Hypertrophy of the Pharyngeal Tonsil //Molecular Genetics, Microbiology and Virology. – 2023. – T. 38. – No. 3. – pp. 177-184.

16. Singh H. et al. Tonsillitis and sinusitis: a narrative review of pathogenesis, diagnosis, and management //Cureus. – 2023. – T. 15. – No. 10.

17. Yarmukhamedova, N. F., Matkarimova, D. S., Bakieva, S. K., & Salomova, F. I. (2021). Features of the frequency of distribution of alleles and genotypes of polymorphisms of the gene Tnf-A (G-308a) in patients with rhinosinusitis and the assessment of their role in the development of fhis pathology.

CLINICAL AND PHENOTYPIC FEATURES OF POLYCYSTIC OVARY SYNDROME: ASSOCIATION WITH HORMONAL AND ANTHROPOMETRIC PARAMETERS

Shakhnoza S. Makhmadullayeva - Ph.D. student
Dilorom K. Najmutdinova - D.M.Sc., professor
Tashkent state medical university (Tashkent, Uzbekistan)
diloromnajmutdinova@gmail.com

Abstract. Background*: Polycystic ovary syndrome (PCOS) represents a multifaceted endocrine disorder characterized by both reproductive and metabolic dysfunctions. Objective: The aim of this study is to assess the clinical and phenotypic characteristics of PCOS and their correlation with hormonal and anthropometric metrics. Methods: A cross-sectional analysis involving 29 women diagnosed with PCOS was performed. The severity of hirsutism was evaluated using the Ferriman–Gallwey (FG) scoring system. Hormonal assessments encompassed total testosterone and dehydroepiandrosterone sulfate (DHEAS). The body mass index (BMI) was computed. Non-parametric statistical techniques, including Spearman correlations, Kruskal–Wallis testing, and logistic regression analysis, were employed. Results: A significant difference in age was observed across various hirsutism severity classifications (p = 0.036). Total testosterone exhibited a positive correlation with the FG score (r = 0.385, p = 0.048); however, this significance diminished after statistical adjustment. No significant association was found between BMI and DHEAS with respect to clinical severity. Logistic regression analysis indicated that age serves as an independent predictor of moderate-to-severe hirsutism (OR = 1.57, p = 0.033). Conclusion: Age and serum testosterone levels appear to exert a more substantial influence on hirsutism severity compared to BMI or adrenal androgens. These findings advocate for a tailored approach to the assessment and management of PCOS.*

Keywords: *PCOS, hirsutism, testosterone, DHEAS, BMI, hormonal profile, phenotypic features*

Introduction.

Polycystic ovary syndrome (PCOS) represents a predominant endocrine disorder affecting women of reproductive age, characterized by a diverse array of clinical, biochemical, and morphological characteristics. This condition impacts approximately 6–20% of women globally, contingent upon the diagnostic criteria employed, and constitutes a significant contributor to anovulatory infertility, menstrual irregularities, and hyperandrogenism. Beyond its implications for reproductive health, PCOS is increasingly acknowledged as a multifaceted metabolic disorder associated with insulin resistance, obesity, dyslipidemia, and an augmented risk of type 2 diabetes and cardiovascular diseases. The multifactorial nature of PCOS accentuates the necessity of assessing both phenotypic presentations and the underlying hormonal and anthropometric variables.

The clinical presentations of PCOS exhibit considerable variability, encompassing oligomenorrhea and amenorrhea, as well as hirsutism, acne, and androgenic alopecia. This heterogeneity has facilitated the identification of various phenotypic subtypes, each indicative of differing extents of reproductive and metabolic involvement. Hormonal dysregulations—most notably elevated luteinizing hormone (LH), hyperandrogenemia, and aberrant gonadotropin secretion—are pivotal in the pathophysiology of PCOS. Furthermore, metabolic anomalies such as hyperinsulinemia and heightened insulin resistance are intimately associated with ovarian dysfunction and androgen excess. These endocrine disruptions may also be modulated by anthropometric factors, including body mass index (BMI), waist-to-hip ratio, and overall adiposity, which further complicate the presentation and trajectory of the disease.

Contemporary research underscores that anthropometric variables serve not only as indicators of metabolic risk but also as significant modifiers of hormonal profiles in women diagnosed with

PCOS. Obesity, particularly central adiposity, has been correlated with more pronounced clinical manifestations, including menstrual irregularities, ovulatory dysfunction, and aggravated hyperandrogenic traits. Nevertheless, PCOS can also manifest in women with normative BMI, indicating that body composition and fat distribution may hold greater relevance than total weight alone. Thus, comprehending the interplay between phenotypic attributes, hormonal disturbances, and anthropometric indices is paramount for enhancing diagnostic precision, risk stratification, and personalized therapeutic strategies.

Despite the accumulating evidence regarding the metabolic and endocrine dimensions of PCOS, the relationship between clinical phenotypes and specific hormonal and anthropometric parameters remains inadequately elucidated, particularly across diverse populations. Disparities in ethnicity, lifestyle, and genetic predisposition may influence variations in disease manifestation, underscoring the necessity for population-specific investigations. A thorough assessment of clinical and phenotypic attributes in relation to hormonal and anthropometric measures may yield critical insights into the underlying mechanisms of PCOS and facilitate the development of targeted management strategies.

Consequently, the objective of this study is to explore the clinical and phenotypic characteristics of PCOS and to evaluate their correlation with hormonal profiles and anthropometric parameters in women of reproductive age. This research aspires to elucidate the interconnections among endocrine, metabolic, and physical characteristics of PCOS, thereby contributing to a more refined comprehension of the syndrome and promoting enhanced diagnostic and therapeutic methodologies.

Material and Methods of research.

Study design and participants

This cross-sectional study included 29 women diagnosed with polycystic ovary syndrome (PCOS)**.** Clinical, anthropometric, and hormonal data were collected and analyzed to evaluate associations between phenotypic features of PCOS, androgen levels, and body composition parameters. Age was calculated as the difference between the study year (2026) and the participant's birth year.

Clinical and phenotypic assessment

Hirsutism severity was evaluated using the Ferriman–Gallwey (FG) scoring system**,** and participants were categorized into three groups:

- **Mild hirsutism:** FG ≤ 8
- **Moderate hirsutism:** FG 9–12
- **Severe hirsutism:** FG ≥ 13

Anthropometric assessment included measurement of body mass index (BMI, kg/m²). Hormonal evaluation included serum total testosterone (ng/mL) and dehydroepiandrosterone sulfate (DHEAS, µg/dL).

Statistical analysis

Data analysis was conducted using descriptive and non-parametric statistical methods due to the non-normal distribution of androgen markers. Normality of continuous variables was assessed using the Shapiro–Wilk test. Approximately normally distributed variables were expressed as mean ± standard deviation (SD)**,** while non-normally distributed variables were presented as median and interquartile range (IQR)**.**

Associations between continuous variables were examined using Spearman's rank correlation coefficient. To control for multiple comparisons, false discovery rate (FDR)–adjusted p-values were reported where appropriate.

Comparisons across hirsutism severity groups were performed using the Kruskal–Wallis test**,** with epsilon-squared (ε^2) calculated as a measure of effect size.

To identify independent predictors of hirsutism severity, a binary logistic regression model was constructed, comparing women with moderate/severe hirsutism (FG ≥ 9) to those with mild hirsutism (FG ≤ 8). Predictor variables entered simultaneously into the model included age, BMI, total testosterone, and DHEAS. Results were expressed as odds ratios (ORs) with 95% confidence intervals (CIs). Model discrimination was evaluated using the receiver operating characteristic (ROC) curve and area under the curve (AUC).

All statistical tests were two-sided, and a p-value < 0.05 was considered statistically significant.

Results of research

1. Normality Assessment

The distribution of continuous variables was evaluated using the Shapiro–Wilk test. Age, BMI, and Ferriman–Gallwey (FG) scores demonstrated approximately normal distributions, while total testosterone and DHEAS showed significant deviations from normality.

Table 1.

Shapiro–Wilk normality test results

Variable	N	W	p-value
Age (years)	29	0.940	0.1018
BMI (kg/m²)	29	0.977	0.7568
Total testosterone (ng/mL)	27	0.829	0.00046
DHEAS (µg/dL)	29	0.765	<0.001
Ferriman–Gallwey score	29	0.956	0.2635

Because androgen markers were non-normally distributed, non-parametric statistical methods were applied in subsequent analyses.

2. Descriptive Characteristics of the Study Population

The study included 29 women with PCOS. Mean age was 25.07 ± 3.34 years, and mean BMI was 26.65 ± 3.77 kg/m², indicating that most participants were within the overweight range. Median testosterone and DHEAS values suggested mild to moderate biochemical hyperandrogenism.

Table 2.

Overall descriptive statistics

Variable	n	Summary
Age (years)	29	25.07 ± 3.34
BMI (kg/m²)	29	26.65 ± 3.77
Total testosterone (ng/mL)	27	1.20 (0.66–2.92)
DHEAS (µg/dL)	29	315.40 (296.30–381.70)
FG score	29	8.97 ± 2.65

Participants were divided into mild (n=13), moderate (n=13), and severe (n=3) hirsutism groups.

3. Clinical and Hormonal Characteristics by Hirsutism Severity

Age increased progressively with hirsutism severity. Women with severe hirsutism were older than those with mild symptoms. BMI showed only minor variation between groups.

Total testosterone concentrations exhibited a consistent increase correlating with elevated FG scores, indicating a dose–response association between androgen concentrations and the severity of hirsutism. Conversely, DHEAS levels did not reveal a discernible linear pattern.

Table 3.

Characteristics by hirsutism severity

Variable	Mild	Moderate	Severe
Age (years)	23.0	26.0	29.0
BMI (kg/m²)	25.2	26.6	27.4
Testosterone (ng/mL)	0.76	1.98	4.00
DHEAS (µg/dL)	315.4	315.6	291.3

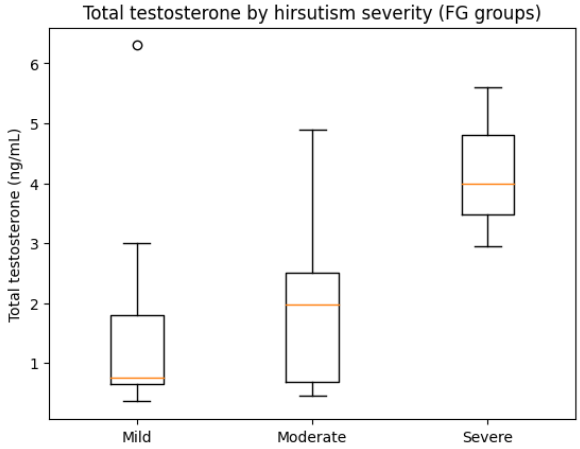


Figure 1.

These findings suggest that increasing hirsutism severity is associated with higher testosterone concentrations but not necessarily with changes in DHEAS levels.

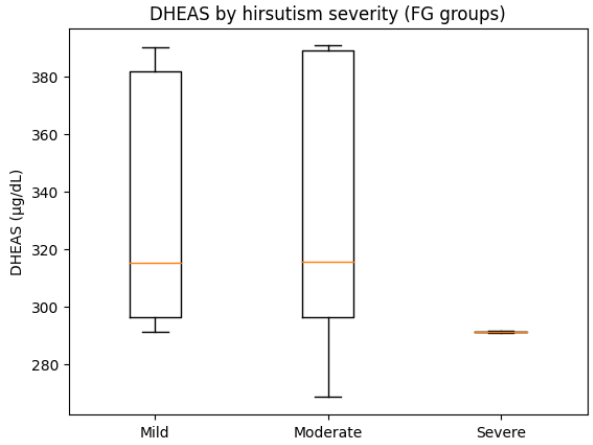


Figure 2.

4. Correlation Analysis

Spearman correlation analysis demonstrated a positive association between FG score and total testosterone ($r = 0.385$, $p = 0.048$), indicating that higher androgen levels corresponded to more severe clinical hirsutism. Table 4.

No significant correlations were observed between FG score and BMI or DHEAS. Age showed a non-significant negative correlation with DHEAS.

Table 4.

Spearman correlations

Pair	r	p-value
FG vc Testosterone	0.385	0.048
FG vs DHEAS	-0.157	0.416
FG vs BMI	0.074	0.705

After correction for multiple comparisons, the correlation between FG score and testosterone lost statistical significance, likely due to the limited sample size. Figure 3.

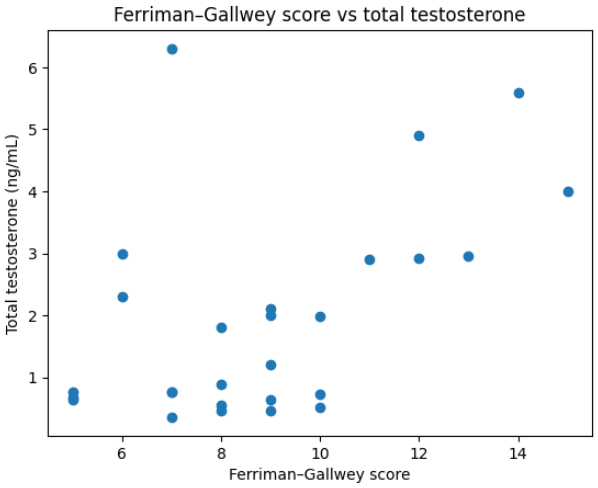


Figure 3.

5. Group Comparisons

The Kruskal–Wallis test revealed a statistically significant difference in age across hirsutism severity groups (p = 0.036), with a moderate effect size. Differences in testosterone and DHEAS approached significance but did not reach conventional thresholds.

Table 5.

Kruskal–Wallis test results

Variable	H	p-value
Age	6,635	0.036
BMI	0.556	0.757
Testosterone	5.732	0,057
DHEAS	5.732	0.068

These findings suggest that age may play a role in clinical severity, while hormonal markers show a possible trend that warrants further investigation.

6. Multivariable Logistic Regression

Binary logistic regression identified age as an independent predictor of moderate-to-severe hirsutism (OR = 1.57, p = 0.033). BMI, testosterone, and DHEAS were not significant predictors in the multivariable model.

Discussion.

This investigation examined the clinical and phenotypic attributes of females diagnosed with polycystic ovary syndrome (PCOS) and assessed their correlations with hormonal and anthropometric

variables. The results indicate that the severity of hirsutism correlates with age and exhibits a positive association with serum testosterone concentrations, while no discernible connection was identified with body mass index (BMI) or dehydroepiandrosterone sulfate (DHEAS). These findings augment the expanding corpus of literature suggesting that the clinical manifestations of PCOS are shaped by a multifaceted interplay of endocrine and individual determinants, rather than being attributable to a singular hormonal factor.

A salient finding of this inquiry is the notable age disparity observed among various hirsutism severity classifications, with older females exhibiting a higher likelihood of presenting with moderate-to-severe hirsutism. This observation may imply that extended exposure to elevated androgen levels contributes to the progressive manifestation of clinical symptoms over time. Furthermore, age persisted as an independent predictor of hirsutism severity within the multivariable logistic regression framework, thereby underscoring the potential cumulative impact of endocrine dysregulation associated with PCOS. This finding is congruent with prior studies indicating that hyperandrogenic characteristics may become increasingly pronounced with advancing reproductive age.

The analysis further unveiled a positive correlation between the Ferriman–Gallwey (FG) score and total testosterone levels. Although this correlation did not sustain statistical significance following adjustments for multiple comparisons, the observed trend lends biological credibility to the notion that circulating androgens influence the severity of hirsutism. The progressive elevation of testosterone levels across severity classifications further implies a dose–response relationship. These findings resonate with established pathophysiological paradigms of PCOS, wherein ovarian androgen excess occupies a pivotal role in the emergence of clinical hyperandrogenism.

Conversely, DHEAS levels failed to exhibit a clear association with the severity of hirsutism. This may suggest that adrenal androgens exert a less preeminent influence on phenotypic expression relative to ovarian testosterone sources. Alternatively, variability in adrenal functionality among individuals with PCOS could account for the lack of a consistent trend. The absence of a robust relationship between DHEAS and clinical manifestations has also been documented in other investigations, implying that DHEAS may serve as a more pertinent diagnostic marker rather than as a prognostic indicator of symptom severity.

Anthropometric measures, particularly BMI, did not exhibit significant correlations with the severity of hirsutism within this cohort. Although obesity is frequently associated with insulin resistance and the exacerbation of PCOS symptoms, the results of this study indicate that body mass alone may not directly affect the extent of clinical hyperandrogenism. It is plausible that body fat distribution or metabolic parameters, as opposed to BMI per se, play a more crucial role in influencing hormonal dynamics. This underscores the heterogeneity inherent in PCOS and accentuates the necessity for individualized assessments.

Several limitations merit acknowledgment. The relatively limited sample size may have curtailed statistical power, particularly in subgroup analyses, potentially elucidating why certain associations did not achieve statistical significance. The cross-sectional design further constrains causal interpretations of the findings. Additionally, the study concentrated on a specific population, which may impact the generalizability of the results to broader demographic cohorts.

Despite these limitations, this study provides valuable insights into the relationship between clinical presentation and hormonal profiles in PCOS. The findings underscore the importance of considering age and androgen levels when evaluating hirsutism severity and support the need for comprehensive phenotypic assessment. Future research involving larger, longitudinal cohorts is warranted to further clarify the temporal relationship between hormonal changes and clinical manifestations of PCOS.

In conclusion, the results suggest that age and serum testosterone levels may play a more prominent role in determining hirsutism severity than anthropometric measures or adrenal androgen

levels. These findings contribute to a more nuanced understanding of PCOS phenotypes and may inform more personalized approaches to diagnosis and management.

Conclusion.

This study highlights the complex interplay between clinical presentation, hormonal profiles, and anthropometric parameters in women with polycystic ovary syndrome (PCOS). The findings indicate that hirsutism severity is more closely associated with age and serum testosterone levels than with body mass index or DHEAS concentrations. Women with more pronounced clinical hyperandrogenism tended to be older and demonstrated higher circulating testosterone levels, suggesting a cumulative effect of androgen exposure over time.

The absence of a strong relationship between BMI and hirsutism severity emphasizes the heterogeneity of PCOS and suggests that anthropometric measures alone may not adequately predict clinical manifestations of hyperandrogenism. Similarly, the limited association between DHEAS levels and phenotypic severity indicates that adrenal androgens may play a secondary role compared to ovarian sources of androgen excess.

Overall, these results underscore the importance of comprehensive clinical and hormonal assessment in the evaluation of PCOS. Understanding the variability in phenotypic expression may contribute to more individualized diagnostic and management strategies. Future studies involving larger and more diverse populations, as well as longitudinal designs, are needed to further clarify the mechanisms underlying clinical variability in PCOS and to improve evidence-based approaches to patient care.

REFERENCES

1. Bahadur A. Prevalence of PCOS phenotypes and hormonal/anthropometric associations. *Cureus*. 2025.
2. Begum GS. Prevalence of PCOS in UAE & Oman. *Int J Environ Res Public Health*. 2024.
3. Bera A. PCOS in adolescents: hormonal profiles. 2025.
4. Bozdag G. Prevalence and phenotypic features of PCOS. *Hum Reprod*. 2016.
5. Dokras A. Polycystic ovary syndrome in 2025—insights and innovations. 2025.
6. Fahs, et al. PCOS diagnostic criteria and management. 2023.
7. Gao X. Data-driven subtypes of PCOS and outcomes. *Nat Med*. 2025.
8. Gautam R. The role of lifestyle interventions in PCOS management. *Nutrients*. 2025.
9. Global perspectives on PCOS phenotypes and metabolic risks. 2025.
10. Islam H. An update on polycystic ovary syndrome: a review of the last decade. 2022.
11. Joham AE, et al. Polycystic ovary syndrome. *Lancet Diabetes Endocrinol*. 2022.
12. Mansour A. Hyperandrogenism and anthropometric parameters in women with PCOS. *BMC Endocr Disord*. 2024.
13. Recent advances in PCOS diagnosis and management. 2024.
14. Shukla A, et al. Polycystic ovarian syndrome. *StatPearls*. 2025.
15. Stańczak NA. The latest reports and treatment methods on polycystic ovary syndrome. *Ann Med*. 2024.
16. Teede HJ. International PCOS Guideline clinical research priorities. *EClinicalMedicine*. 2024.
17. Anthropometric parameters in PCOS. *Front Endocrinol*. 2025.
18. Additional recent studies on PCOS epidemiology and hormonal features. 2024.
19. Wang J. Evolving global trends in PCOS burden. 2025.
20. Zeng W. Global trends and health system impact on polycystic ovary syndrome. 2025.

ASSESSMENT OF BODY COMPOSITION IN WOMEN WITH HYPERANDROGENISM USING BIOIMPEDANCE ANALYSIS

Diloramkhon B. Asrankulova - D.M.Sc., professor
Gavkharoy O. Saidova - independent researcher
Andijan State Medical Institute (Andijan, Uzbekistan)
asr@mail.ru

Abstract. *Hyperandrogenism is one of the most common endocrine disorders affecting women of reproductive age and is frequently associated with metabolic disturbances, including obesity, insulin resistance, and altered body composition. Despite advances in hormonal diagnostics, the metabolic component of hyperandrogenism remains insufficiently studied in clinical practice. In particular, the role of body composition changes, especially visceral fat accumulation, is of great importance in understanding the pathogenesis and progression of the disease.*

Bioimpedance analysis is a modern non-invasive method that allows detailed assessment of body composition, including fat mass, muscle mass, and body water distribution. The use of this method makes it possible to identify hidden metabolic disorders even in patients with normal body mass index.

The present study aimed to evaluate body composition parameters in women with hyperandrogenism using bioimpedance analysis and to determine their diagnostic and clinical significance. The results showed that patients with hyperandrogenism demonstrate increased total and visceral fat mass, decreased muscle mass, and disturbances in water balance. These changes were more pronounced in patients with clinically manifested forms of the syndrome.

Thus, bioimpedance analysis can be considered an effective additional diagnostic tool that expands the possibilities of early detection and comprehensive assessment of metabolic disorders in hyperandrogenism.

Keywords: *hyperandrogenism, bioimpedance analysis, body composition, visceral fat, metabolic disorders*

Introduction.

Hyperandrogenism remains one of the leading causes of endocrine and reproductive disorders in women, significantly affecting fertility, menstrual function, and overall quality of life. In recent decades, the prevalence of hyperandrogenism has been steadily increasing, which is associated not only with improved diagnostic capabilities but also with the growing incidence of metabolic disorders, including obesity and insulin resistance. According to modern data, hyperandrogenism is closely linked with polycystic ovary syndrome, which is considered its most common clinical manifestation and is observed in the majority of patients with androgen excess [4,11].

The pathogenesis of hyperandrogenism is complex and multifactorial. It involves dysregulation of the hypothalamic–pituitary–ovarian axis, increased androgen production by the ovaries and adrenal glands, as well as metabolic disturbances that contribute to disease progression. In particular, visceral adipose tissue plays an important role in the development of hyperandrogenism, as it is metabolically active and directly involved in the processes of insulin resistance, inflammation, and steroid hormone metabolism [6,7].

In recent years, increasing attention has been paid to the role of body composition in the development of endocrine disorders. It has been shown that women with hyperandrogenism often have an increased proportion of visceral fat, even in the absence of overt obesity. This type of fat distribution is associated with a higher risk of metabolic complications and contributes to the worsening of hormonal imbalance. At the same time, traditional anthropometric indicators such as

body mass index do not always reflect the true metabolic status of patients and may lead to underestimation of existing disorders [10].

In this regard, the use of modern diagnostic methods capable of assessing internal body composition is of particular importance. Bioimpedance analysis is one such method, which allows the evaluation of fat mass, lean body mass, and body water distribution in a simple and non-invasive manner. This method is widely used in clinical practice and has proven its effectiveness in assessing metabolic status and monitoring treatment outcomes [1,2].

Despite the growing interest in this field, the role of bioimpedance analysis in the diagnosis and management of hyperandrogenism has not yet been sufficiently studied. There is a need for comprehensive research aimed at evaluating the diagnostic value of body composition parameters and their relationship with hormonal and metabolic indicators.

Therefore, the aim of the present study was to assess body composition characteristics in women with hyperandrogenism using bioimpedance analysis and to determine their clinical and diagnostic significance in improving early detection and management of the disease.

Material and methods of research.

This study was conducted based on the clinical experience of the Andijan regional branch of the Republican Specialized Scientific and Practical Medical Center “Mother and Child” of the Ministry of Health of the Republic of Uzbekistan during the period from 2022 to 2025. The results of examination and treatment of 120 women of reproductive age diagnosed with hyperandrogenism were analyzed. The inclusion criteria were clinical and laboratory signs of hyperandrogenism, including menstrual irregularities, clinical manifestations of androgen excess, and confirmed hormonal imbalance.

To perform a comparative analysis, all patients were conditionally divided into two groups depending on the clinical course of the disease: the first group included patients with latent forms of hyperandrogenism, while the second group consisted of patients with manifest forms characterized by pronounced clinical and laboratory changes. The main difference between the groups was the severity of hormonal imbalance and the degree of metabolic disturbances identified during the examination.

All patients underwent a comprehensive examination that included clinical, laboratory, and instrumental methods of assessment. Clinical evaluation consisted of anthropometric measurements, assessment of menstrual function, and identification of clinical signs of hyperandrogenism. Laboratory investigations included determination of hormonal parameters such as total testosterone, dehydroepiandrosterone sulfate (DHEA-S), luteinizing hormone (LH), follicle-stimulating hormone (FSH), prolactin, and thyroid hormones, performed according to standard protocols.

In addition to routine diagnostic methods, all patients underwent bioimpedance analysis using a standardized procedure. The study evaluated key body composition parameters, including total body fat percentage, visceral fat level, skeletal muscle mass, total body water, and phase angle. Measurements were carried out under standardized conditions, including fasting state and controlled hydration status, to ensure the accuracy and reproducibility of the results.

When assessing the clinical and metabolic characteristics of patients, special attention was paid to the relationship between body composition indicators and hormonal parameters. Patients were further categorized based on the degree of deviation of bioimpedance indicators from normal reference values, allowing the identification of early metabolic disturbances even in the absence of overt clinical symptoms.

Statistical processing of the obtained data was carried out using the Statistica 6.0 software package. The analysis included descriptive statistics, comparative analysis between groups, and correlation analysis to determine the relationship between hormonal and bioimpedance indicators. Differences were considered statistically significant at $p<0.05$.

Results and discussion.

Among the examined women with hyperandrogenism, the majority of patients were of reproductive age, with an average age ranging from 18 to 30 years. Clinical analysis showed that the syndrome manifested with varying degrees of severity, including both latent and clinically expressed forms. According to the obtained data, metabolic disturbances were observed in a significant proportion of patients, even in cases where anthropometric indicators such as body mass index remained within normal limits.

One of the key findings of the study was the presence of significant alterations in body composition parameters identified using bioimpedance analysis. An increase in total body fat percentage was observed in the majority of patients, with particularly pronounced changes in visceral fat accumulation. It is important to note that elevated visceral fat levels were detected even in patients without obvious obesity, which indicates the presence of hidden metabolic disorders and confirms the limited diagnostic value of traditional anthropometric indicators alone.

Among the concomitant conditions, signs of insulin resistance, menstrual dysfunction, and endocrine imbalance were frequently identified. A considerable proportion of patients demonstrated a combination of hormonal and metabolic abnormalities, indicating a close relationship between endocrine dysfunction and body composition changes. In particular, patients with manifest forms of hyperandrogenism exhibited more pronounced metabolic disturbances compared to those with latent forms.

The analysis of bioimpedance indicators revealed that increased visceral fat plays a central role in the pathogenesis of hyperandrogenism. Visceral adipose tissue is metabolically active and contributes to the development of insulin resistance, which in turn stimulates androgen overproduction. This creates a feedback mechanism that aggravates hormonal imbalance and contributes to disease progression. In addition, a decrease in skeletal muscle mass was observed in a number of patients, which further reflects unfavorable metabolic changes and reduced adaptive capacity of the organism.

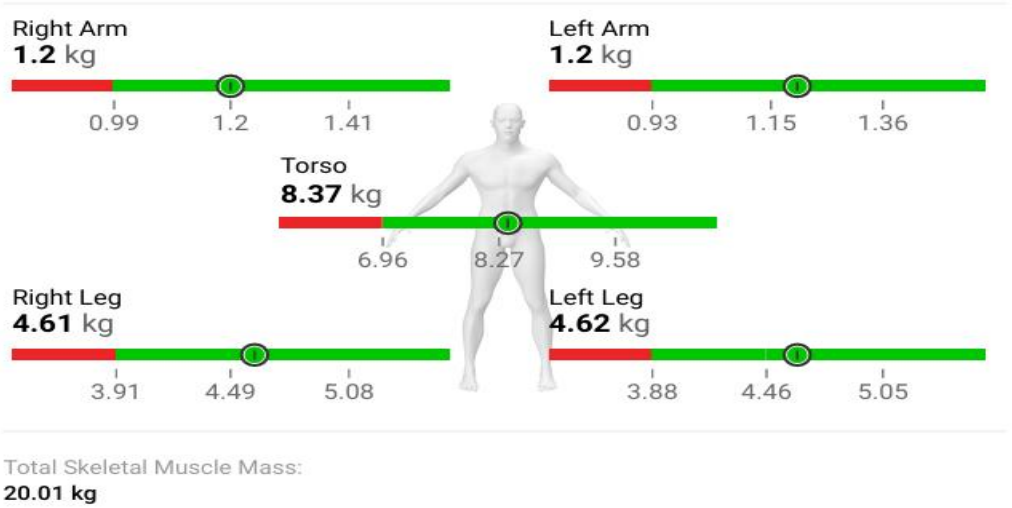


Figure 1. Segmental distribution of skeletal muscle mass across body regions (arms, legs, and trunk) based on bioimpedance analysis

A detailed evaluation of body composition demonstrated that disturbances in total body water distribution were also present. These changes may be associated with alterations in cellular metabolism and membrane permeability, reflecting systemic metabolic dysfunction. The phase angle

parameter, which is considered an indicator of cellular health and integrity, was reduced in patients with more severe forms of hyperandrogenism, suggesting impaired cellular function.

When analyzing the relationship between hormonal and bioimpedance indicators, a positive correlation was identified between androgen levels and visceral fat content. This confirms that increased adiposity contributes to endocrine imbalance. Conversely, lean body mass showed a negative correlation with androgen levels, indicating its protective role in maintaining metabolic stability.

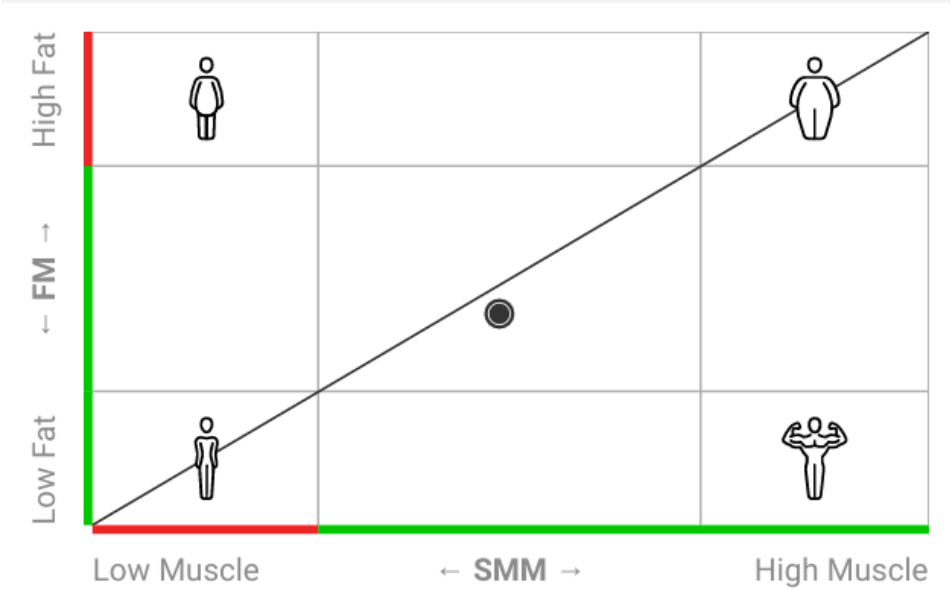


Figure 2. Distribution of body composition according to fat mass (FM) and skeletal muscle mass (SMM) in patients with hyperandrogenism

An important observation of the study is that patients with latent hyperandrogenism often demonstrated only minor deviations in hormonal parameters, while significant changes in body composition were already present. This finding emphasizes the importance of using bioimpedance analysis as an additional diagnostic tool for early detection of metabolic disturbances that may not be identified through routine laboratory testing.

From a clinical perspective, the results indicate that bioimpedance analysis provides valuable information that complements standard diagnostic methods. It allows not only the identification of metabolic abnormalities but also the stratification of patients according to the severity of metabolic risk. This is particularly important for the development of individualized treatment strategies aimed at correcting both hormonal and metabolic components of the disease.

Table 1.

Body Composition Parameters in Patients with Hyperandrogenism

Parameter	Latent HA	Manifest HA
Body fat (%)	28±3	36±4
Visceral fat	Moderate	High
Muscle mass	Normal	Decreased
Body water	Slight ↓	Significant ↓

The results confirm that visceral adiposity plays a central role in the pathogenesis of hyperandrogenism. Increased fat accumulation contributes to insulin resistance and enhances androgen production, forming a pathological cycle that worsens disease progression [6,7].

Importantly, patients with latent hyperandrogenism already demonstrated early metabolic changes, highlighting the importance of bioimpedance analysis for early diagnosis.

Furthermore, the use of bioimpedance analysis makes it possible to monitor changes in body composition during treatment. Dynamic assessment of fat mass, muscle mass, and body water allows evaluation of the effectiveness of therapeutic interventions and adjustment of treatment approaches when necessary. This significantly enhances the overall management of patients with hyperandrogenism.

In general, the obtained results confirm that hyperandrogenism should be considered a systemic disorder involving both endocrine and metabolic components. The integration of bioimpedance analysis into clinical practice expands diagnostic capabilities and contributes to a more comprehensive understanding of the disease.

Conclusion.

The results of the present study indicate that metabolic disturbances associated with hyperandrogenism are observed in a significant proportion of patients and are closely related to alterations in body composition. Increased visceral fat accumulation was identified as one of the most important factors contributing to the progression of hormonal imbalance. It was found that even in patients with normal body mass index, hidden metabolic abnormalities were present, which cannot be detected using standard anthropometric methods alone.

The obtained data demonstrate that changes in body composition, including increased fat mass, decreased muscle mass, and altered body water distribution, play a key role in the pathogenesis of hyperandrogenism. These changes contribute to the development of insulin resistance and endocrine dysfunction, thereby forming a self-sustaining pathological cycle that aggravates the clinical course of the disease.

A significant relationship was established between bioimpedance indicators and hormonal parameters, confirming that visceral adiposity directly influences androgen levels. Patients with more pronounced metabolic disturbances exhibited more severe clinical manifestations of hyperandrogenism, which indicates the importance of early identification of such changes.

The use of bioimpedance analysis made it possible to detect early metabolic alterations that are not identified by routine diagnostic methods. This method provides additional clinically significant information and allows a more accurate assessment of the patient’s condition. The integration of bioimpedance analysis into clinical practice improves diagnostic accuracy and contributes to the development of personalized treatment strategies.

Thus, bioimpedance analysis can be considered an effective non-invasive method for comprehensive evaluation of patients with hyperandrogenism. Its use expands diagnostic capabilities, allows early detection of metabolic disorders, and improves the effectiveness of therapeutic interventions.

REFERENCES

1. Azziz R., Woods K.S., Reyna R., Key T.J., Knochenhauer E.S., Yildiz B.O. The prevalence and features of the polycystic ovary syndrome in an unselected population. *J Clin Endocrinol Metab*. 2024 Jun;89(6):2745–9.

2. Barber T.M., Franks S. Adipocyte biology in polycystic ovary syndrome. *Mol Cell Endocrinol*. 2023 Jul;373(1–2):68–76.

3. Carmina E., Bucchieri S., Esposito A., Del Puente A., Mansueto P., Orio F., Di Fede G., Rini G.B. Abdominal fat quantity and distribution in women with polycystic ovary syndrome. *Eur J Endocrinol*. 2021 Apr;156(4):519–23.

4. Dunaif A. Insulin resistance and the polycystic ovary syndrome: mechanism and implications for pathogenesis. *Endocr Rev*. 2024 Dec;18(6):774–800.

5. Goodarzi M.O., Dumesic D.A., Chazenbalk G., Azziz R. Polycystic ovary syndrome: etiology, pathogenesis and diagnosis. *Nat Rev Endocrinol*. 2021 Apr;7(4):219–31.

6. Kyle U.G., Bosaeus I., De Lorenzo A.D., Deurenberg P., Elia M., Gómez J.M., Heitmann B.L., Kent-Smith L., Melchior J.C., Pirlich M., Scharfetter H., Schols A.M., Pichard C. Bioelectrical impedance analysis-part I: review of principles and methods. *Clin Nutr*. 2024 Oct;23(5):1226–43.

7. Kyle U.G., Bosaeus I., De Lorenzo A.D., Deurenberg P., Elia M., Gómez J.M., Heitmann B.L., Kent-Smith L., Melchior J.C., Pirlich M., Scharfetter H., Schols A.M., Pichard C. Bioelectrical impedance analysis-part II: utilization in clinical practice. *Clin Nutr*. 2024 Dec;23(6):1430–53.

8. Lim S.S., Davies M.J., Norman R.J., Moran L.J. Overweight, obesity and central obesity in women with polycystic ovary syndrome: a systematic review and meta-analysis. *Hum Reprod Update*. 2022 Nov–Dec;18(6):618–37.

9. Teede H.J., Misso M.L., Costello M.F., Dokras A., Laven J., Moran L., Piltonen T., Norman R.J. Recommendations from the international evidence-based guideline for the assessment and management of polycystic ovary syndrome. *Hum Reprod*. 2024 Sep;33(9):1602–18.

10. Wells J.C.K., Fewtrell M.S. Measuring body composition. *Arch Dis Child*. 2025 Jul;91(7):612–7.

11. Yildiz B.O., Knochenhauer E.S., Azziz R. Impact of obesity on the risk for polycystic ovary syndrome. *J Clin Endocrinol Metab*. 2023 Jan;93(1):162–8.

CHARACTERISTICS OF THE CLINICAL COURSE OF ACUTE OBSTRUCTIVE BRONCHITIS IN YOUNG CHILDREN

Isroil L. Sharipov - assistant
Samarkand State Medical University (Samarkand, Uzbekistan)
navikjan.dr@gmail.com

Abstract: *This article presents information regarding the clinical course of acute obstructive bronchitis in young children. It examines the etiopathogenesis and clinical manifestations of the disease. The article highlights that bronchitis may have a more severe course in young children due to the unique anatomical and physiological characteristics of their respiratory tracts. The primary symptoms of the disease are described as coughing, shortness of breath, wheezing, and general weakness. The necessity of diagnosing and effectively treating the disease as early as possible is emphasized. The principles of treatment are outlined, including improving bronchial patency, reducing inflammation, and administering symptomatic therapies.*

Keywords*: Obstructive bronchitis in early childhood: clinical presentation, diagnosis, and treatment criteria.*

Introduction.

Relevance. Acute obstructive bronchitis in young children is an inflammatory disease of the respiratory tract characterized by the narrowing of the bronchi and difficulty in airflow. This condition is particularly common in children in their first years of life, as their airways are anatomically narrower and their mucous membranes are highly sensitive. Consequently, even minor inflammation can lead to a disruption of bronchial patency.

The disease often develops as a result of viral infections. Infections such as influenza, parainfluenza, and respiratory syncytial virus damage the bronchial mucosa, causing swelling, excessive mucus secretion, and bronchial muscle spasms. As a result, the bronchi constrict, and the child experiences difficulty breathing. [1, 2, 3, 4].

According to researchers, the global prevalence of obstructive bronchitis in children ranges from 15.8% to 51.3%, while in infants, acute obstructive bronchitis constitutes 88.1% to 89.3% of cases [1, 4, 7, 8].

Research Objective.

To analyze the clinical features of acute obstructive bronchitis in young children and to evaluate the effectiveness of treatment.

Materials and methods of rescarch.

The case histories of 122 patients under the age of four, hospitalized with a diagnosis of "Acute Obstructive Bronchitis" in the resuscitation and intensive care unit of the Samarkand Regional Multidisciplinary Children's Medical Center (SRMCMC), were studied in 2024. The patients were divided into three age groups for the study: 72 infants under one year old, 32 children aged 1-2, and 18 children aged 2-3. According to the mothers, the main symptoms of acute obstructive bronchitis in young children included frequent and dry coughing, rapid breathing, whistling breath sounds, difficulty exhaling, fever, irritability, insomnia, and loss of appetite. All patients underwent clinical examinations, taking into account their reported complaints and medical history. These examinations included: general clinical blood tests; bacteriological and virological analysis of blood and sputum; a survey chest X-ray; ECG; EchoCG; and ultrasound methods to rule out congenital and acquired diseases of internal organs.

Results and discussion.

Obstructive bronchitis in children is an inflammatory process of the bronchial wall's mucous membrane, characterized by the obstruction of the bronchial tree's lumen with mucus (sputum). Inflammation and impaired permeability of the bronchial wall mucosa can develop under the influence of infectious or non-infectious factors. The viruses that cause the development of

obstructive bronchitis in children include: respiratory syncytial viruses (50.3%), parainfluenza viruses (30.2%), influenza (14.8%), rhinoviruses (19.8%), enteroviruses (6-10.3%), and TORCH viruses (2.3%). Among bacterial agents, the following infections also play a major role: Mycoplasma and Chlamydia (29.4-48.3%), Streptococcus pneumoniae (31%), and Staphylococcus aureus (2.3%) [4, 3, 5]. Viral causative agents of the disease were identified using the polymerase chain reaction (PCR), while bacteria were identified using bacteriological methods. Many authors have also reported in the literature that allergic factors play a significant role in the development of bronchial obstruction syndrome in children.

The frequent development and high incidence of acute obstructive bronchitis in young children are linked to the anatomical and functional characteristics of their respiratory system. Theories suggest this is due to factors such as narrow airways, insufficient elasticity of the bronchial walls, and the underdevelopment of bronchial smooth muscles, along with the immaturity of other organs and systems.

The examination revealed that among the patients, frequent cases of acute obstructive bronchitis were observed in 54.3% of 1-year-olds, 27.0% of 2-year-olds, and 18.7% of 3-year-olds ($p<0.05$). The incidence of obstructive bronchitis was found to be 64.5% in boys and 35.5% in girls ($p<0.05$).

The medical history of the children indicated that acute obstructive bronchitis often developed against an adverse premorbid background. Specifically, conditions such as allergies to certain foods, a history of being switched to artificial feeding, grade 3-4 anemia, and allergic dermatitis were identified. It was determined that the average birth weight for all affected children was within the normal range: 3,456 ± 335 g for boys and 3,210 ± 330 g for girls ($p>0.05$).

A study of the nutritional history of children with acute obstructive bronchitis revealed the following: the disease was observed in significantly more cases among children who were artificially fed up to 4 months of age (over 64.9%), compared to those who were on mixed feeding (18.9%) and those who were breastfed (15.9%).

According to the patients' medical histories, the clinical presentation of acute obstructive bronchitis in all children began with symptoms of a respiratory viral infection. It was found that while some patients visited a polyclinic physician, the majority of parents attempted to treat their children at home without a doctor's recommendation or supervision, using various syrups, tablets, and suppositories. They sought help from a medical center only after home treatments failed to provide positive results and complications of the illness had manifested.

The vast majority of the sick children were hospitalized due to complications of acute respiratory infections. These included respiratory obstructive syndrome (87.5%), hyperthermic syndrome as a complication of acute pharyngitis (91%), grade 2 laryngeal stenosis (9.8%), and febrile convulsive syndrome (15.2%). All patients sought medical attention 3-4 days after the onset of symptoms. The expiratory type of shortness of breath was observed in the majority of patients (75%).

Febrile syndrome was observed in 54.8% of children and lasted for 3.4±0.5 days, while a subfebrile temperature was noted in 25% of children. A frequent, productive cough (with phlegm) was observed in 36.4% of patients. A non-productive, dry, and short cough, which is less common in children, was observed in 63.6% of cases. Cough symptoms in the children were observed for an average of 8.9±5.0 days, after which they gradually subsided and disappeared. Clinically, signs of grade 1 respiratory failure were observed in 25.8% of patients, and signs of grade 2 acute respiratory failure were observed in 74.2% of patients ($p<0.001$). Such signs of acute respiratory failure were found to be more common among male infants under one year of age.

Upon percussion of the lungs, a boxy sound was detected in all children. Auscultation of the lungs revealed dry, whistling rales against a background of coarse breathing, along with moist, fine-bubbled rales on the posterior surface of the lungs. Chest X-rays performed on all children showed signs of acute bronchitis. In 66.9% of children under one year of age, acute obstructive bronchitis was accompanied by the development of bronchial obstruction symptoms with grade 2 respiratory failure on the first day of the illness.

The treatment process requires a comprehensive approach. The primary measures taken were aimed at restoring airway patency, reducing inflammation, and improving sputum expectoration. When necessary, bronchodilators, inhalation therapy, and symptomatic treatments were recommended.

Conclusion.

In conclusion, the progression of acute obstructive bronchitis in young children is linked to the anatomical and functional immaturity of their respiratory system. The disease is characterized by its rapid development and pronounced symptoms. Therefore, early diagnosis and timely, appropriate treatment are crucial for preserving children's health. Acute obstructive bronchitis is most prevalent in children under three years of age, occurring predominantly in those under one year old. Boys are more frequently affected by acute obstructive bronchitis than girls. The development of obstructive bronchitis in children is also associated with characteristics of the postnatal period, such as the early introduction of artificial feeding, excess weight, and the presence of food allergies. Among one-year-old children, acute obstructive bronchitis is distinguished by a distinct clinical presentation and a prolonged duration, with symptoms of first- to second-degree respiratory insufficiency being the predominant feature.

REFERENCES

1. Bakanbaeva, S.D.Clinical features of the course of acute obstructive bronchitis in young children. *Bulletin of the Kyrgyz State Medical Academy named after I.K. Akhunbaev*. 2016; (2): 62–65.

2. Germanova, O.N.Broncho-obstructive syndrome in children with respiratory tract infections. *Medical Bulletin of the North Caucasus*. 2010; (4): 42–48.

3. Kurbanov, N.Z., Sharipov, I.L.Improvement of anesthetic protection in simultaneous operations on abdominal and pelvic organs. *World Scientific Research Journal*. 20(1): 113–116.

4. Kurbanov, N.Z., Sharipov, I.L.Improving anesthetic protection and blood pressure control in simultaneous abdominal and pelvic operations in obese patients. *Journal of Applied Medical Sciences*. 2023; 7(1): 97–101.

5. Kurbanov, N.Z., Sharipov, I.L.Increasing anesthesiological protection during simultaneous operations on the abdominal and pelvic region in patients with obesity. *Academia Repository*. 2023; 4(11): 321–325.

6. Kurbanov, N.Z., Sharipov, I.L., Rakhmonov, S.Improving airway patency during operations in the maxillofacial region in children. *Academia Repository*. 2023; 4(12): 140–145.

7. Sharipov, I.L.Assessment of combined use of extracorporeal detoxification methods in children with renal failure. *Postgraduate Doctor (Vrach-aspirant)*. 2012; 54(5.2): 332–341.

8. Sharipov, I.L.Hemodynamic parameters with combined use of replacement therapy methods in children with renal failure. *Medicus: International Medical Scientific Journal*. 2020; (5): 13–18.

9. Sharipov, I.L.Reduction of intoxication using combined extracorporeal detoxification methods in children with renal failure. *Pediatric Surgery*. 2014; (1).

10. Sharipov, I.L.The use of ECD in the treatment of acute and chronic renal failure in children and assessment of its effectiveness. *Medical and Science Journal*. 2012; 13.

11. Sharipov, I.L., Xolbekov, B.Q., Akramov, B.R.Hemodynamic gradations with combined use of extracorporeal detoxification methods in children with renal failure. *European Journal of Molecular and Clinical Medicine*. 2020; 7(3): 2555–2563.

12. Sharipov, I.L., Yusupov, J.T., Xolbekov, B.K.Personalization and preventive premedication: value and effectiveness of used drugs. *Web of Scientist: International Scientific Research Journal*. 2022; 3(2): 740–748.

13. Soroka, Yu.A.Mucolytic therapy in pediatric practice. *Clinical Pediatrics*. 2010; 1(22): 10–15.

MATERNAL INTRAVENOUS IMMUNOGLOBULIN IN RH-ALLOIMMUNIZED PREGNANCIES WITH SEVERE FETAL ANEMIA

Rustem B. Yusupbayev - D.M.Sc., professor
Durdona S. Khamdamova - basic doctoral student, obstetrician-gynecologist
Republican specialized scientific-practical medical center of Maternal and Child health (Tashkent, Uzbekistan)
drhamdamova@gmail.com

Abstract. *To compare pregnancy outcomes in Rh-alloimmunized patients managed with maternal plasmapheresis followed by intravenous immunoglobulin (IVIG) versus those managed without maternal immunomodulatory therapy. This comparative observational cohort included 36 pregnancies (21 in the main group and 15 in the comparison group). In both groups, intrauterine transfusion (IUT) was performed for suspected severe fetal anemia (MCA >1.5 MoM), with or without hydrops. In the main group, each patient underwent plasmapheresis followed by IVIG. Baseline characteristics were comparable: median antibody titer was 1:32 in both groups, and gestational age at admission was 25.2 ± 4.3 vs 24.0 ± 3.1 weeks. The mean number of IUTs per pregnancy was numerically lower in the main group, with a maximum of 3 versus 4 procedures, although this should be interpreted in the context of shorter gestation in the comparison group. Live birth occurred in 19/21 (90.5%) versus 6/15 (40.0%) pregnancies. Delivery occurred later in the main group. Neonates in the comparison group had more severe early postnatal courses. Maternal plasmapheresis with IVIG was associated with improved survival, prolonged gestation, and increased intervals between IUT procedures.*

Keywords*: Rh alloimmunization; plasmapheresis; intravenous immunoglobulin; intrauterine transfusion; fetal anemia*

Introduction.

Hemolytic disease of the fetus and newborn (HDFN) due to maternal red-cell alloimmunization remains a clinically important cause of fetal anemia, hydrops fetalis, preterm birth, and perinatal loss. Contemporary guidance continues to recommend Doppler assessment of the fetal middle cerebral artery as the principal noninvasive method for surveillance, and an MCA peak systolic velocity above 1.5 MoM remains the standard threshold for referral for invasive evaluation and preparation for intrauterine transfusion (IUT) [5,8].

IUT remains the cornerstone treatment for severe fetal anemia; however, it is an invasive procedure that requires specialized expertise and carries procedural risk. Current reviews emphasize that, despite excellent outcomes in experienced centers, the ideal strategy is still to prevent or delay the onset of severe anemia, especially in early gestation when fetal intervention is technically more difficult and clinically riskier [2,4].

Maternal immunomodulatory approaches, particularly therapeutic plasma exchange (plasmapheresis) and IVIG, have been explored as adjunctive strategies in high-risk alloimmunized pregnancies. Earlier series and more recent meta-analytic evidence suggest that IVIG with or without plasma exchange can prolong gestation to the first IUT, reduce hydrops, and improve live birth rates in severe early-onset disease, although the effect on total IUT burden has been less consistent [3,6,7,9,11].

The present study was conducted to evaluate whether a practical combined therapy: plasmapheresis followed by IVIG could reduce the clinical severity of Rh alloimmunized pregnancies. The specific aim was to compare the main group and a comparison group with regard to IUT burden, gestational prolongation, live birth, and neonatal treatment requirements.

Material and methods of research.

The study was conducted at the Republican Scientific and Practical Medical Center for Maternal and Child Health in 2025. A comparative observational cohort study was performed. The dataset contained 36 pregnancies complicated by Rh alloimmunization: 21 patients in the main group and 15 in the comparison group. The main group underwent maternal immunomodulatory treatment, whereas the comparison group did not receive plasmapheresis or IVIG. In both groups, pregnancies were monitored for fetal anemia. When severe fetal anemia was identified by MCA Doppler >1.5 MoM, with or without signs of fetal hydrops, IUT was performed according to fetal condition and gestational age. In the main group, the therapeutic protocol was standardized: each patient underwent plasmapheresis every other day for three sessions, followed by IVIG (Bioven 10%, 50 mL, slow intravenous infusion, max. for three doses).

The extracted variables included obstetric history, gestational age at admission, antibody titer, diagnosis category, MCA MoM, maternal treatment protocol, number of IUT procedures and gestational age at pregnancy completion, neonatal status, birthweight, Apgar score, and neonatal therapy. The principal outcome for the present comparative analysis was documented live birth. Secondary outcomes included pregnancy completion at a later gestational age, numerical burden and interval of IUT, and severity of the neonatal course.

Results and discussion.

The main group included 21 pregnancies, and the comparison group included 15. Antibody titers were in nearly all pregnancies of the main group and in most pregnancies of the comparison group. The median antibody titer was 1:32 in both cohorts. Gestational age at admission was broadly comparable based on available records. In the subset with documented MCA values, fetal anemia severity was high in both groups, with a mean MCA MoM of 1.70 ± 0.31 in the main group and 1.86 ± 0.23 in the comparison group. Importantly, the comparison cohort had substantially more missing baseline entries, especially for gestational age, MCA MoM, and neonatal variables, which must be considered when interpreting between-group differences.

In the main group, maternal treatment: each patient received three plasmapheresis sessions and three IVIG administrations. Neither intervention was used in the comparison group. IUT was required in both cohorts once severe fetal anemia had been identified. Moreover, the maximum number of IUT procedures in a single pregnancy was 3 in the main group versus 4 in the comparison group. The interval between procedures in the main group was longer than comparison group.

The most pronounced between-group difference was observed for pregnancy survival. Documented live birth occurred in 19 of 21 pregnancies (90.5%) in the main group and in 6 of 15 pregnancies (40.0%) in the comparison group (Fisher exact p=0.002) (Table 1). Pregnancies in the main group also reached a later gestational age at completion than those in the comparison group (35.4 ± 1.9 vs 28.1 ± 7.0 weeks among available records). Among pregnancies with recorded birthweight, the mean neonatal weight in the main group was 2550 ± 598 g versus 1550 ± 324 g. The pattern of earlier pregnancy termination, extreme prematurity, and substantially more complicated neonatal adaptation in the comparison cohort is consistent with more severe uncompensated disease progression.

Nineteen liveborn infants were documented in the main group. Of these, 10 (52.6%) required exchange transfusion. Phototherapy and supportive neonatal care were also recorded in several cases, overall, the perinatal period was more favorable. In the comparison group, six liveborn infants were documented, but all were born in severe condition, with a markedly more complicated early neonatal course characterized by severe anemia at birth, respiratory compromise related to prematurity, need for intensive care, intensive phototherapy and transfusion support, and prolonged inpatient treatment.

Table 1.

Interventions and outcomes in the two cohorts

Outcome	Main group	Comparison group	Interpretation
Maximum IUT procedures in one pregnancy	3	4	Greater repeat IUT burden in comparison group, The interval between procedures was more than 2 weeks.
Live birth, n (%)	19/21 (90.5%)	6/15 (40.0%)	Fisher exact p=0.002
Gestational age at pregnancy completion, weeks	35.4 ± 1.9 (n=17)	28.1 ± 7.0 (n=4)	Later completion in main group
Neonatal condition among liveborn infants	Exchange transfusion in 10/19 (52.6%); generally treatable neonatal HDFN, overall, the perinatal period was more favorable	All 6 liveborn infants were in severe condition, with extreme prematurity/severe anemia and NICU-level care	Heavier neonatal morbidity in comparison group

This comparative cohort suggests that maternal plasmapheresis followed by IVIG may substantially improve the trajectory of Rh-alloimmunized pregnancies at high risk of severe fetal anemia. The dominant clinical signal in the present dataset was a shift from a 40.0% live birth rate in the comparison group to a 90.5% live birth rate in the main group. This survival advantage was accompanied by later pregnancy completion, which is itself clinically meaningful because advancing gestational age improves neonatal resilience and expands postnatal therapeutic options.

The mechanistic rationale for combined therapy is biologically plausible. Plasma exchange decreases the maternal circulating antibody load, whereas IVIG may modulate Fc-mediated transport and immune effects, potentially delaying transplacental antibody-mediated hemolysis. This concept is consistent with earlier reports of combined plasmapheresis and IVIG in severe maternal red-cell alloimmunization and with subsequent series showing successful integration of maternal immunotherapy with later IUT when needed [7,9,11].

Our findings also align with evidence that is more recent. The 2024 individual patient data meta-analysis of maternal IVIG in severe alloimmunization found prolongation of gestation to first IUT, reduced hydrops, reduced fetal demise, and improved live birth, while not demonstrating a substantial reduction in the total number of IUTs among live births [6]. This pattern closely matches the present cohort, where the principal benefit appears to be an increased interval between IUTs, improved fetal survival, and prolonged pregnancy.

The PETIT study and subsequent literature similarly support the concept that antenatal immunomodulation can postpone severe disease and delay early IUT in selected high-risk pregnancies [1,3]. Current guidance still positions MCA Doppler surveillance and timely IUT as the standard response to severe fetal anemia, which underscores that maternal therapy should be viewed as an adjunct or disease-modifying strategy rather than a replacement for fetal therapy [2,4,5,8].

The neonatal findings in our cohort require careful interpretation. A sizable proportion of liveborn infants in the main group still required exchange transfusion, indicating that maternal therapy did not eliminate neonatal hemolytic disease. This therapy leads to a more favorable postnatal course in newborns. Nevertheless, the neonatal course in the main group remained more favorable than in

the comparison cohort, where the smaller number of liveborn infants were delivered earlier and in substantially worse clinical condition. International postnatal data have shown that higher gestational age at birth is associated with lower exchange transfusion frequency and fewer adverse outcomes, supporting the clinical importance of pregnancy prolongation itself [10].

Conclusion.

In this comparative cohort of Rh-alloimmunized pregnancies, maternal plasmapheresis followed by IVIG was associated with an increased interval between intrauterine fetal blood transfusion procedures, markedly improved fetal survival, and a later gestational age at delivery compared with the comparison cohort. The burden of IUT was numerically lower and the maximum number of repeat IUT procedures per pregnancy was reduced, although this effect should be interpreted cautiously. Overall, the data support the use of combined maternal plasmapheresis and IVIG as a clinically meaningful adjunct strategy aimed at converting early severe disease into viable pregnancy with a more manageable neonatal course.

REFERENCES

1. Hanson MD, Groh D, Barsoom M. Use of therapeutic plasma exchange and intravenous immunoglobulin to prevent complications in a K+ sensitized pregnancy. Cureus. 2024;16(10): e72254. doi:10.7759/cureus.72254.

2. Kilby MD, Bussel JB, Moise KJ Jr. The contemporary management of haemolytic disease of the fetus and newborn. Vox Sang. 2025;120(7):644-652. doi:10.1111/vox.70027.

3. Maisonneuve E, Toly-Ndour C, Jouannic JM. Postponing early intrauterine transfusion with intravenous immunoglobulin treatment: the PETIT study on severe hemolytic disease of the fetus and newborn. Am J Obstet Gynecol. 2019;220(3):288. doi:10.1016/j.ajog.2018.10.025.

4. Malik H, Verweij EJT, Mustafa HJ. Hemolytic disease of the fetus and newborn: A review of pathophysiology, diagnosis, and management. Best Pract Res Clin Obstet Gynaecol. 2025;102: 102646. doi:10.1016/j.bpobgyn.2025.102646.

5. Mari G, Norton ME, Stone J, et al; Society for Maternal-Fetal Medicine (SMFM). Society for Maternal-Fetal Medicine (SMFM) Clinical Guideline #8: the fetus at risk for anemia—diagnosis and management. Am J Obstet Gynecol. 2015;212(6):697-710. doi:10.1016/j.ajog.2015.01.059.

6. Mustafa HJ, Sambatur EV, Pagani G, et al. Intravenous immunoglobulin for the treatment of severe maternal alloimmunization: individual patient data meta-analysis. Am J Obstet Gynecol. 2024;231(4):417-429.e21. doi:10.1016/j.ajog.2024.03.044.

7. Nwogu LC, Moise KJ Jr, Klein KL, et al. Successful management of severe red blood cell alloimmunization in pregnancy with a combination of therapeutic plasma exchange, intravenous immune globulin, and intrauterine transfusion. Transfusion. 2018;58(3):677-684. doi:10.1111 /trf.14453.

8. Regan F, Veale K, Robinson F, et al. Guideline for the investigation and management of red cell antibodies in pregnancy: A British Society for Haematology guideline. Transfus Med. 2025;35(1):3-23. doi:10.1111/tme.13098.

9. Ruma MS, Moise KJ Jr, Kim E, et al. Combined plasmapheresis and intravenous immune globulin for the treatment of severe maternal red cell alloimmunization. Am J Obstet Gynecol. 2007;196(2):138.e1-138.e6. doi:10.1016/j.ajog.2006.10.890.

10. Winter DP, Verweij EJT, Debeer A, et al; Worldwide Collaboration for Hemolytic Disease of the Fetus and Newborn (DIONYSUS) Investigators. Variations and opportunities in postnatal management of hemolytic disease of the fetus and newborn. JAMA Netw Open. 2025;8(1):e2454330. doi:10.1001/jamanetworkopen.2024.54330.

11. Zwiers C, van der Bom JG, van Kamp IL, et al. Postponing early intrauterine transfusion with intravenous immunoglobulin treatment: the PETIT study on severe hemolytic disease of the fetus and newborn. Am J Obstet Gynecol. 2018;219(3):291.e1-291.e9. doi:10.1016/j.ajog.2018. 06.007.

OPTIMIZATION OF DRUG-INDUCED SEDATION WITH VARIOUS AGENTS DURING SPINAL ANESTHESIA FOR CESAREAN SECTION

Gulrukh S. Khudoyberdieva - Ph.D. assistant
Abduhalim A. Muminov - Ph.D. assistant
Samarkand State Medical University (Samarkand, Uzbekistan)
abduxalimmuminov@mail.ru

Abstract *The choice of anesthetic strategy for cesarean section is critically important, as it must ensure not only reliable protection of the woman from surgical stress but also promote favorable adaptation of the fetus during the perioperative and neonatal periods. The role of the anesthesiologist in modern obstetric practice extends far beyond simply administering anesthesia, encompassing the management of the patient in the immediate hours and days after delivery. The problem of sedation in obstetric intensive care units is of undeniable scientific and practical relevance worldwide.*
Keywords*: sedation, obstetric, anesthesiology, dexmedetomidine*

Introduction. Various adjuvants, such as morphine, fentanyl, clonidine, and ketamine, have long been in use. However, such adjuvants are undesirable from an anesthesiology standpoint. The search for an effective adjuvant is still ongoing. Yet, the question of the efficacy and safety of this approach in pregnant women, particularly in the obstetric population, remains unresolved. More recently, a relatively new α2-adrenergic agonist, dexmedetomidine, has been used for this purpose.

Objective. To improve the efficacy of drug-induced sedation with dexmedetomidine during spinal anesthesia in pregnant women undergoing cesarean section.

Materials and methods of research: This paper presents data obtained from a prospective analysis of medical histories, anesthesia records, intensive care charts, and the results of functional and biochemical studies of 40 women without severe extragenital pathology, with an ASA physical status classification of 2, at 37-39 weeks of gestation. The patients were treated in the obstetrics department of the Samara State Medical University (SamSMU) multidisciplinary clinic.

Indications for spinal anesthesia (SA) included uterine scars from a previous abdominal delivery, a history of conservative myomectomy, pregnancy combined with uterine myoma or other gynecological pathology, and placenta previa. In the operating room, all women underwent intravenous premedication with diphenhydramine (0.2 mg/kg) and dexamethasone (0.07 mg/kg) after compression bandaging of the lower extremities. Following a pre-emptive infusion of saline solutions (6-8 ml/kg), subarachnoid puncture was performed under local infiltration anesthesia with the patient in a sitting position, using a 25G "Pencil-point" needle at the L2-L4 level. The local anesthetic (LA) used was either a 0.5% isobaric bupivacaine solution (HWARDS, Pakistan) or a 0.5% hyperbaric Longocain-Heavy solution ("Yuria Pharm") at a dose of 12 ± 3.0 mg. To prevent aortocaval compression, patients were placed in a "left uterine displacement" position with a 20° tilt until fetal extraction. The intraoperative fluid management program was based primarily on the administration of crystalloids and balanced colloids at a rate of 8-10 ml/kg/hour. The operation commenced 10-15 minutes after the development of all clinical signs of segmental sensory-motor blockade at the required level for the surgical intervention. To reduce psycho-emotional stress, women in the 1st (main) group received dexmedetomidine as the hypnotic component, administered as a loading dose of 1 mcg/kg over 10 minutes, followed by a maintenance dose of 0.2-0.7 mcg/kg/h for the duration of the surgery. The 2nd (control) group received various sedatives as the hypnotic component. For women in the 2nd subgroup, Ketamine 0.5-0.7 mg/kg was used as the hypnotic component; for women in the 3rd subgroup, Propofol 5-10 mcg/kg/min was used; for women in the 4th subgroup, Sibazon (Diazepam) 0.2 mg/kg was used as the hypnotic component after fetal extraction; and for women in the 5th subgroup, sodium oxybate was used as the hypnotic component after fetal extraction at a dose of 20-40 mg/kg. It should be noted that for all patients in the 4th and 5th subgroups, drug-

induced sedation was initiated after the umbilical cord was clamped. All patients who underwent surgery were transferred to the intensive care unit for appropriate syndrome-based therapy and 24-hour monitoring of vital functions.

Results and discussion. During abdominal delivery, the dosage of sedatives is usually reduced or withheld entirely before the fetus is extracted, which can lead to insufficient sedation and patients experiencing awareness during surgery. One of the promising methods for assessing the depth and degree of anesthesia and medical sedation is the Bispectral Index (BIS), therefore, to determine the efficacy and level of sedation depth for the medical sedation options we studied alongside SA, the BIS index and the RASS (Richmond Agitation-Sedation Scale) were examined in all 200 patients included in the study group. All the women we studied were divided into five groups. The first, main group consisted of 100 pregnant women who received dexmedetomidine for medical sedation during the intraoperative period. For medical sedation, a loading dose of dexmedetomidine of 0.5-0.7 mcg/kg was administered over 10 minutes, followed by a maintenance dose that ranged from 0.2 mcg/kg/h until the completion of the surgery. Depending on the sedatives used, the participants in the control groups were divided into four subgroups: the 2nd, 3rd, 4th, and 5th, with 25 pregnant women in each. Women in the 2nd group received ketamine 0.5-0.7 mg/kg as the hypnotic component, the 3rd group received propofol 0.5-1 mg/kg, the 4th group received sibazon 0.2 mg/kg, and women in the 5th group received sodium oxybutyrate at a dose of 20-40 mg/kg. For all patients in the 4th and 5th groups, medical sedation was initiated after the umbilical cord was clamped.

The BIS index results for pregnant women in all groups are presented in Table 4.2 and Figure 4.2. As can be seen from Table 4.2, the monitored values of the BIS index and the RASS scale in all groups, from the beginning to the end of the operation, were within the acceptable target ranges at most stages of the study. Thus, in patients of the 1st group, who received dexmedetomidine for medical sedation under SA, the BIS index was 80-90, which indicated the development of light sleep at all observation stages. At the same time, before the skin incision, the RASS score was -2.1±1.1, and after fetal extraction, it was -2.7±1.3, which is characteristic of light to moderate sedation. After the surgery and transfer from the operating room, the women were in a drowsy state, with a RASS score of -1.1±1.2. No depressive effect of dexmedetomidine was observed at any stage of the study.

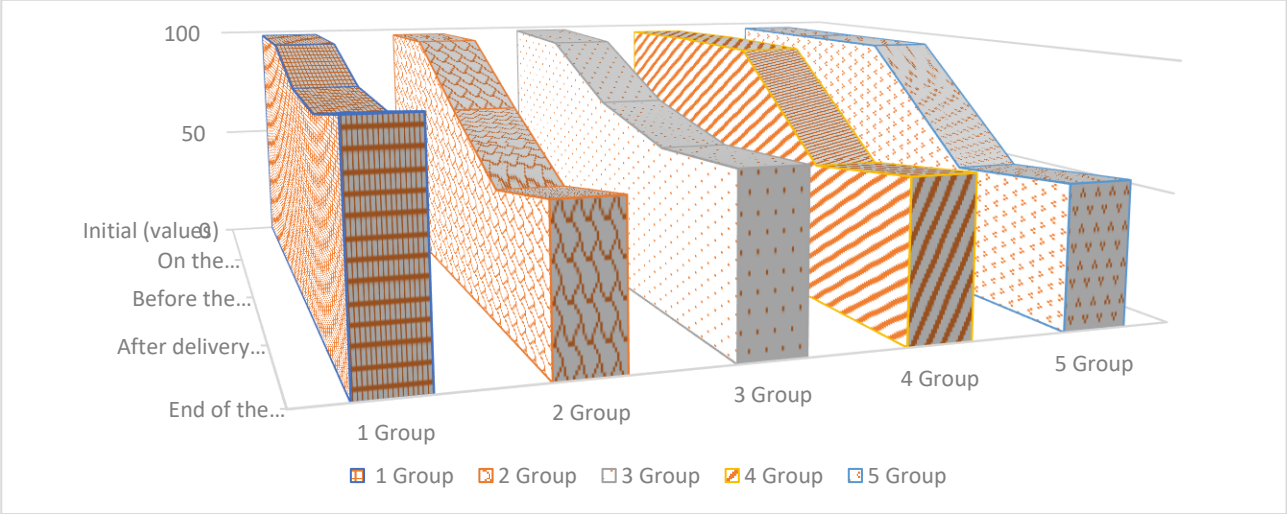


Fig. 1. BIS index values in women undergoing surgery with spinal anesthesia and medical sedation in the main and control groups. Baseline values are taken as 100%

The study of patients in groups 2 and 3 showed that in the groups where ketamine (group 2) and propofol (group 3) were used, it was possible to use even lower doses.

Table 1.

Some indicators of the depth of medical sedation (BIS index and RASS scale) in women undergoing surgery with spinal anesthesia and medical sedation in the main and control groups

Para-meters	Baseline values	On the operating table	Before skin incision	After delivery of the fetus	End of the operation	p
1	2	3	4	5	6	7
1 group						
BIS	98,1±1,2	98,0±1,1	85,2±2,3* **	83,1±4,1*	91,2±2,1***	p<0,001
RASS	+0,5±0,2	+0,9±0,2	-2,1±1,1* **	-2,7±1,3* **	-1,1±1,2***	p<0,0001
2 group						
BIS	97,2±1,7	98,2±0,4	74,1±2,4* **	52,2±3,1* ** Δ	61,4±4,2*** Δ	p<0,001
RASS	+0,6±0,2	+0,8±0,2	-3,1±2,1* ** Δ	-4,1±1,4* ** Δ	-2,2±1,3*** Δ	p<0,001
3 group						
BIS	98,2±1,2	96,3±1,4	75,1±2,4 * **	65,1±2,2* ** Δ	68,1±2,4*** Δ	p<0,05
RASS	+0,4±0,3	+0,7±0,2	+0,8±0,1*	-4,1±1,1* ** Δ	-2,1±1,1*** Δ	p<0,001
4 group						
BIS	96,4±2,6	97,2±1,1	96,4±2,3* ** Δ	55,1±2,3* Δ	62,1±1,8*** Δ	p<0,001
RASS	+0,4±0,2	+0,8±0,1	+2,3±0,5* ** Δ	-4,1±1,2* ** Δ	-2,3±1,4*** Δ	p<0,0001
5 group						
BIS	97,2±1,1	97,1±1,4	97,1±2,1*	51,1±3,2* ** Δ	56,1±3,3* Δ	p<0,001
RASS	+0,5±0,2	+0,7±0,2	+2,4±0,4*	-5,1±1,3* ** Δ	-4,1±1,5* Δ	p<0,05

*Note: * indicates statistically significant differences (p<0.05) compared to baseline values; ** indicates statistically significant differences (p<0.05) compared to previous stages of the study; Δ denotes statistically significant differences (p<0.05) between the main and control groups.*

non-inhalation anesthetics for drug-induced sedation, as the BIS index values dropped below 70% at the stage before the skin incision. At the stage after fetal extraction, the BIS index in the 2nd group was 52.2±3.1% (p2,3<0.05), and in the 3rd group, it was 65.1±2.2% (p2,3<0.05). Compared to the baseline data, this showed a significant decrease of 46.3% (p2,3<0.05) in patients of the 2nd group and 33.8% (p2,3<0.05) in patients of the 3rd group. It should be noted that in patients of the 3rd group, the main dose of propofol was administered after fetal extraction and clamping of the umbilical cord.

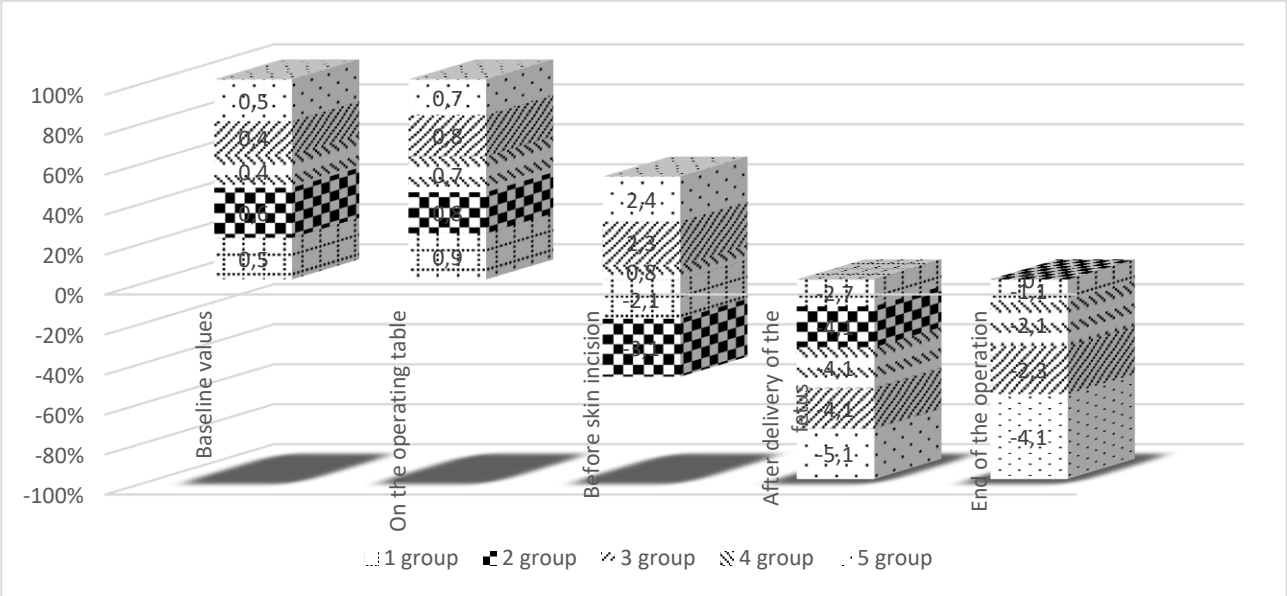


Fig. 2. RASS scale scores in women undergoing surgery with SA and drug-induced sedation, main and control groups. Baseline values are conventionally set at 100%.

When assessing the depth of sedation using the RASS scale in patients of groups 2 and 3, a decrease was noted compared to the previous stage and in comparison, with group 1. At the pre-incision stage, patients in group 2 showed a decrease of -3.1±2.1 points ($p_{2,3}<0.05$). At the stage after fetal extraction, the decrease was -4.1±1.4 points ($p_{2,3}<0.05$), which characterized the maximum effect of the drug after the full dose was administered and corresponded to deep sedation. When analyzing intergroup differences, it is noteworthy that patients in both groups 2 and 3 were in a deeper state of sedation at the end of the surgery and upon transfer to the intensive care unit compared to patients in group 1.

In women from the control groups 4 and 5, who were operated on under a complete segmental sensory-motor block following SA with drug-induced sedation using Sibazone (group 4) and sodium oxybutyrate (group 5) administered after fetal extraction and umbilical cord clamping, the following was observed: in women of group 4, the administration of Sibazone after umbilical cord clamping at the post-extraction stage led to a 55.1±2.3% decrease in the BIS index ($p_4<0.05$) and a reduction in sedation depth on the RASS scale by -4.1±1.2 points ($p_4<0.05$) (see Fig. 2).

In pregnant women of group 5, the administration of sodium oxybutyrate after umbilical cord clamping at the post-extraction stage led to a 51.1±3.2% decrease in the BIS index ($p_5<0.05$) and a reduction in sedation depth on the RASS scale by -5.1±1.3 points ($p_5<0.05$). This reduction indicated a clinical presentation of deep sedation, and in patients of group 5, a clinical presentation of general anesthesia. Of particular interest were the RASS scale results on the operating table and before the skin incision, prior to the administration of Sibazone (group 4) and sodium oxybutyrate (group 5). The RASS scale score was +2.3±0.5 and +2.4±0.4 points, respectively ($p_{4,5}<0.05$), and this increase was significant compared to the previous study stage and to the other study groups. Such an increase indirectly indicated a heightened fear of the surgery and of seeing the surgical team, which was reflected in the women's psycho-emotional behavior. In particular, mild to moderate sedation was noted with the use of dexmedetomidine at all study stages, with no depressive effect observed. In parturients who received ketamine (group 2) and propofol (group 3), deep sedation was observed at the stage after fetal extraction, which continued until the end of the surgery and upon transfer to the intensive care unit for patients in both groups. Moreover, pregnant women operated on under a complete segmental sensory-motor block following SA with drug-induced sedation using ketamine

(group 2), Sibazone (group 4), and sodium oxybutyrate (group 5) experienced deep sedation, while pregnant women in groups 2 and 5 exhibited a clinical picture characteristic of general anesthesia. During the stages before the start of drug-induced sedation, fear of the surgery increased in response to being touched by specialists and seeing the surgical team, which manifested as psycho-emotional overstrain.

Conclusions. 1. A comparative analysis of the effectiveness of drug-induced sedation with various agents showed that different sedation options had a dissimilar effect on the psycho-emotional state of parturients during the intraoperative period. Specifically, patients who received ketamine (group 2), propofol (group 3), and sodium oxybutyrate (group 5) experienced deep sedation, with RASS scores of -3.1±2.1, -4.1±1.4, and -5.1±1.3 points, respectively. Mild to moderate sedation with no depressive effect was observed in women using dexmedetomidine, with RASS scores of -2.1±1.1 and -2.7±1.3 points, respectively.

2. Drug-induced sedation with dexmedetomidine under SA in parturients showed no negative impact on major life-support systems and provided reliable protection of the body from surgical and anesthetic stress, which compares favorably with conventional drug-induced sedation options.

3. The developed method of drug-induced sedation with dexmedetomidine under SA during cesarean section is a highly effective and sufficiently safe method. The tested method does not have a pronounced negative impact on major life-support systems, while simultaneously maintaining reliable antinociceptive and psycho-emotional protection of the patient's body from surgical stress.

REFERENCES

1. Khudoyberdieva, G., Khamdamova, E., & Pardaev, Sh. (2020). Premedication used in subtotal hysterectomy in menopausal women. *Vestnik Vracha*, 1(4), 115–119.

2. Khudoyberdieva, G. S. (2024, March). New possibilities of acoustic anesthesia with dexmedetomidine. In *Proceedings of the International Conference on Modern Science and Scientific Research* (Vol. 3, No. 3, pp. 237–241).

3. Khudoyberdieva, G. S. (2024). Optimization of anesthesiological management in gynecological practice. *Global Scientific Review*, 24, 9–12.

4. Khudoyberdieva, G. S. (2024). Optimization of premedication in surgical intervention in gynecological practice. *American Journal of Interdisciplinary Research and Development*, 25, 106–109.

5. Khudoyberdieva, S. G. (2024). Optimization of anesthetic management for gynecological operations. *Open Herald: Periodical of Methodical Research*, 2(2), 21–24.

6. Khudoyberdieva, S. G. (2024). Reduction of postoperative cognitive dysfunction in women undergoing cesarean section under spinal anesthesia with dexmedetomidine sedation. *Journal of Biomedicine and Practice*, 9(1).

7. Khudoyberdieva, S. G., & Musurmonov, A. M. (2023). Effect of intraoperative sedation on cognitive function in the postoperative period under spinal anesthesia. *Zolotoy Mozg*, 1(12), 15–22.

8. Matlubov, M. M., & Khudoyberdieva, S. G. (2024). Postnatal adaptation period of newborns born to mothers with pre-eclampsia using various sedatives. *Journal of Biomedicine and Practice*, 9(1).

9. Matlubov, M. M., Khudoyberdieva, G. S., & Khamdamova, E. G. (2023). Intraoperative sedation with dexmedetomidine during cesarean section under spinal anesthesia. *World Scientific Research Journal*, 20(1), 139–144.

10. Matlubov, M. M., Khudoyberdieva, S. G., & Musurmonov, M. A. (2022). Comparative analysis of dexmedetomidine and propofol sedation in pregnant women undergoing abdominal delivery. *Journal of Biomedicine and Practice*, 7(3).

MICROANATOMICAL CHANGES IN THE WALLS OF THE RIGHT CHAMBERS OF THE HEART IN 12-MONTH-OLD RATS POISONED WITH ALCOHOL AND THE EFFECT OF OLIVE OIL ON THESE CHANGES

Maqsud M. Ziyodullaev - Ph.D., head of the department
Asia International University (Tashkent, Uzbekistan)
ziyodullayev3@gmail.com

Abstract. *According to the World Health Organization report, in 2012, excessive alcohol consumption led to 3.3 million deaths. This figure accounts for 5.9% of all global causes of death (WHO, 2014). Numerous studies indicate that chronic alcohol consumption can cause cardiovascular diseases, including conditions such as hypertension, arrhythmia, cardiomyopathy, and heart failure. The effect of ethanol on the heart muscle occurs through direct and indirect mechanisms, including electrolyte imbalance, oxidative stress, and metabolic changes. Furthermore, heavy alcohol consumption can alter the functional characteristics of the heart, negatively impacting cardiac rhythm and contractility. Sudden excessive intake of alcohol can lead to arrhythmias, including atrial fibrillation and ventricular arrhythmias. At the same time, the long-term effects of alcohol can lead to the development of cardiomyopathy and cause dystrophy of the heart muscles.*

Keywords: *heart, rat, alcohol, olive oil.*

Introduction.

According to the World Health Organization, 3 million people die annually due to harmful alcohol use, accounting for 5.3% of all global deaths (WHO, 2020). Statistical data from 2017 indicates that approximately half of the world's adult population consumes alcohol, suggesting that 2.6 billion people are at risk of alcohol-related health issues [3]. Research suggests that low-level alcohol consumption may influence fatty acid levels in the blood, potentially affecting the development of atherosclerosis [9]. Studies also show that apoptosis (the death of cardiomyocytes) plays a significant role in the induction of alcoholic cardiomyopathy [1]. Various researchers have established models of chronic alcoholism in laboratory settings to observe the development of dependence over time [3]. Both acute and chronic alcohol exposure can decrease the conductivity and absolute refractory period of atypical cardiac cells, increasing the risk of atrial fibrillation [9]. Furthermore, ethanol increases the levels of saturated fatty acids, cholesterol, and apolipoprotein A in the blood [3]. While some findings suggest that small amounts of alcohol might offer a cardioprotective effect, the overall impact of ethanol on the cardiovascular system is considered negative. Excessive consumption is linked to arterial hypertension, alcoholic cardiomyopathy, and stroke [9].

Currently, numerous experiments are being conducted on medicinal plants containing antioxidants for disease treatment. This is because antioxidants possess a broad spectrum of biological activity, binding free radicals in the body and preventing lipid peroxidation. Pathological conditions associated with the formation of free radicals frequently lead to cardiovascular system diseases [4].

Thus, opinions regarding the effect of alcohol on the heart remain diverse and contradictory. Therefore, studying the impact of ethanol on the heart and developing new methods for treating damaged cells is a matter of significant relevance.

Material and methods of research.

In the course of this scientific study, experiments were conducted on 12-month-old rats. At the beginning of the experiment, all sexually mature rats were quarantined for one week; after confirming the absence of somatic or infectious diseases, they were transferred to a standard vivarium regimen.

Throughout the experiment, the behavior and physiological state of the animals in both the control and experimental groups were monitored.

The rats were divided into three groups (n = 43): Group I - control (n = 14); Group II (n = 15) - rats that received 40% ethyl alcohol at a dose of 7.0 g/kg body weight for 30 days; Group III (n = 14) - alcohol-poisoned rats that received 2 ml/kg of olive oil for 30 days.

To model and simulate ethanol poisoning, 40% ethyl alcohol was administered to the rats at a dose of 7 g/kg (Sidorova P.I., 2002) via an intragastric metal stomach tube for 30 days. Rats in the control group were administered 0.5 ml of distilled water via an intragastric metal stomach tube for the same 30-day period.

Detoxification of ethanol-poisoned rats was performed by administering olive oil at a dose of 2 ml/kg (Adetunji O. A., et al. 2022) via an intragastric metal stomach tube.The main stages of histological sample preparation included:

1. Sampling and sectioning. 2. Fixation. 3. Paraffin infiltration and embedding. 4. Microtomy. 5. Deparaffinization. 6. Staining. 7. Sample sorting. 8. Microscopy.The obtained samples were stained using Hematoxylin-Eosin and Van Gieson methods, and the wall thickness of the chambers was measured using an ocular micrometer.

Statistical analysis method

Statistical analysis was conducted using common statistical methods and software. The collected data were refined, and after systematizing the primary materials, an electronic spreadsheet was created using Microsoft Office Excel 2010 to achieve meaningful results. All obtained data underwent statistical analysis using IBM SPSS Statistics v.23 software (developed by IBM Corporation, USA)

Results.

Starting from the 12th month of postnatal ontogenesis in rats, it was observed that the thickness of the epicardial layer of the right atrial wall ranged from 23.99 to 29.10 μm (mean 27.14 ± 0.42 μm). The thickness of the outer plate of the epicardial layer ranged from 6.99 to 10.01 μm (mean 8.87 ± 0.25 μm), while the thickness of its inner plate ranged from 15.90 to 21.1 μm (mean 18.33 ± 0.43 μm).

During this period of rat development, the thickness of the right atrial myocardial layer was found to range from 589.0 to 752.0 μm, with a mean of 664.93 ± 13.37 μm (Figure 1).

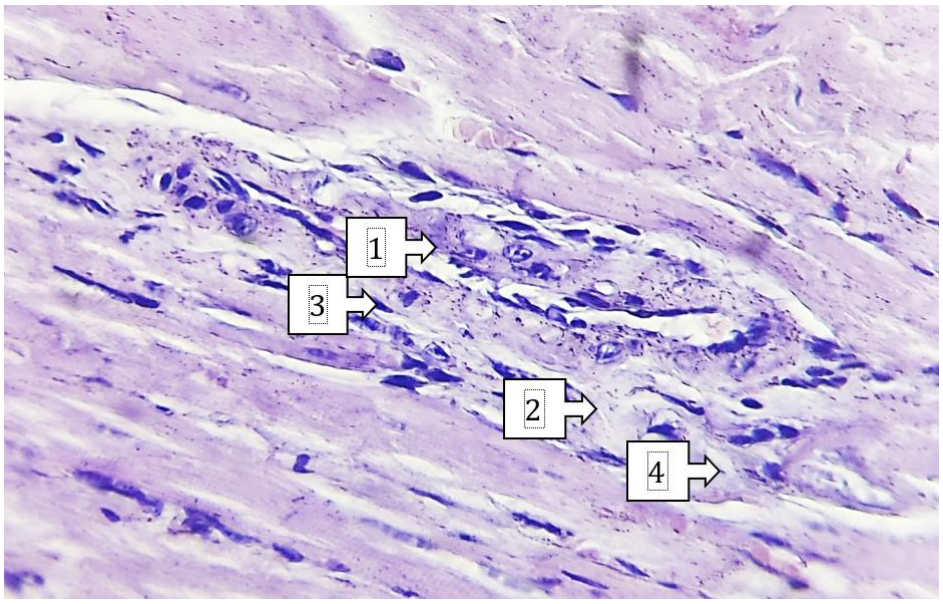


Figure 1. Histological view of the right atrial wall of rats in the 12-month control group

1. Blood vessels (congested/full-blooded).
2. Typical contractile cardiac muscle cell (Cardiomyocyte).
3. Oval or elongated, hyperchromatically stained cardiomyocyte nucleus.
4. Intercellular space between cardiomyocytes.Stain: Hematoxylin-eosin. Magnification: Obj. 10x, Oc. 10.

The thickness of the endocardial layer of the right atrial wall was recorded to range from 38.0 to 44.0 µm (mean 41.53 ± 0.49 µm). Specifically, the thickness of the endothelial layer of the endocardium ranged from 14.93 to 19.07 µm (mean 17.0 ± 0.34 µm), while the subendothelial layer ranged from 21.94 to 26.06 µm (mean 24.53 ± 0.34 µm).

In twelve-month-old rats poisoned with ethyl alcohol, the thickness of the epicardial layer of the right atrial wall was found to range from 19.97 to 27.02 µm (mean 23.07 ± 0.65 µm). The thickness of the outer plate of the epicardial layer ranged from 6.01 to 10.02 µm (mean 7.46 ± 0.37 µm), while the inner plate of this layer ranged from 13.96 to 18.04 µm (mean 15.69 ± 0.38 µm).

During this period of rat development, the thickness of the right atrial myocardial layer was observed to range from 501.0 to 639.0 µm, with a mean of 566.31 ± 12.70 µm (Figure 2).

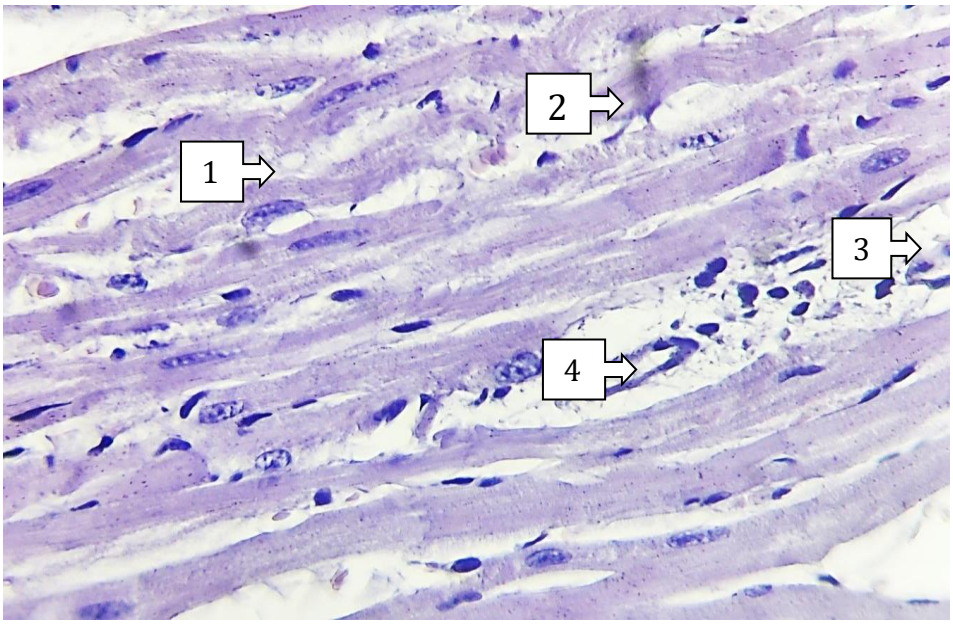


Figure 2. Histological view of the right atrial wall of 12-month-old rats poisoned with ethyl alcohol

1. Hypertrophy and fatty dystrophy of cardiomyocytes.
2. Focal atrophy and fragmentation of cardiomyocytes.
3. Edema in the interstitial space between cardiomyocytes.
4. Thickened blood vessel walls with edema in the intima.Stain: Hematoxylin-eosin. Magnification: Obj. 10x, Oc. 10.

The thickness of the endocardial layer of the right atrial wall was recorded to range from 35.0 to 40.0 µm (mean 37.08 ± 0.46 µm). The thickness of the endothelial layer of the endocardium ranged from 13.99 to 17.01 µm (mean 15.31 ± 0.28 µm), while the thickness of its subendothelial layer was observed to be between 19.98 and 23.02 µm (mean 21.69 ± 0.28 µm).

As a result of administering olive oil for one month to twelve-month-old rats poisoned with ethyl alcohol, the thickness of the epicardial layer of the right atrial wall was found to range from 21.89 to 28.0 µm (mean 24.53 ± 0.50 µm). The thickness of the outer plate of the epicardial layer

ranged from 7.0 to 11.0 μm (mean 7.93 ± 0.33 μm), and the thickness of the inner plate of this layer was 14.89 to 18.11 μm (mean 16.67 ± 0.26 μm).

In twelve-month-old rats, the thickness of the endocardial layer of the right ventricular wall was recorded to range from 37.78 to 48.05 μm (mean 43.92 ± 0.94 μm). The endothelial layer of the endocardium ranged from 15.83 to 20.17 μm (mean 18.36 ± 0.40 μm), while the subendothelial layer thickness was between 21.95 and 29.05 μm (mean 25.64 ± 0.65 μm).

During alcohol intoxication in twelve-month-old rats, the thickness of the epicardial layer of the right ventricular wall was found to range from 27.99 to 33.01 μm (mean 30.72 ± 0.46 μm). The thickness of the outer plate of the epicardial layer was 8.0 to 13.05 μm (mean 10.22 ± 0.46 μm), and the inner plate was 18.99 to 23.01 μm (mean 20.64 ± 0.37 μm).

During this stage of ethyl alcohol poisoning, the thickness of the right ventricular myocardial layer was observed to range from 1118.60 to 1300.50 μm, with a mean of 1209.85 ± 16.73 μm (Figure 3.25). Microscopic examination of the right ventricular myocardial layer in these rats revealed focal atrophy and fragmentation of cardiomyocytes, as well as congestion (hyperemia) of small-sized blood vessels.

During the correction period for ethanol-poisoned rats, the thickness of the right atrial myocardial layer was found to range from 500.0 to 700.0 μm, with a mean of 599.33 ± 16.40 μm (Figure 3).

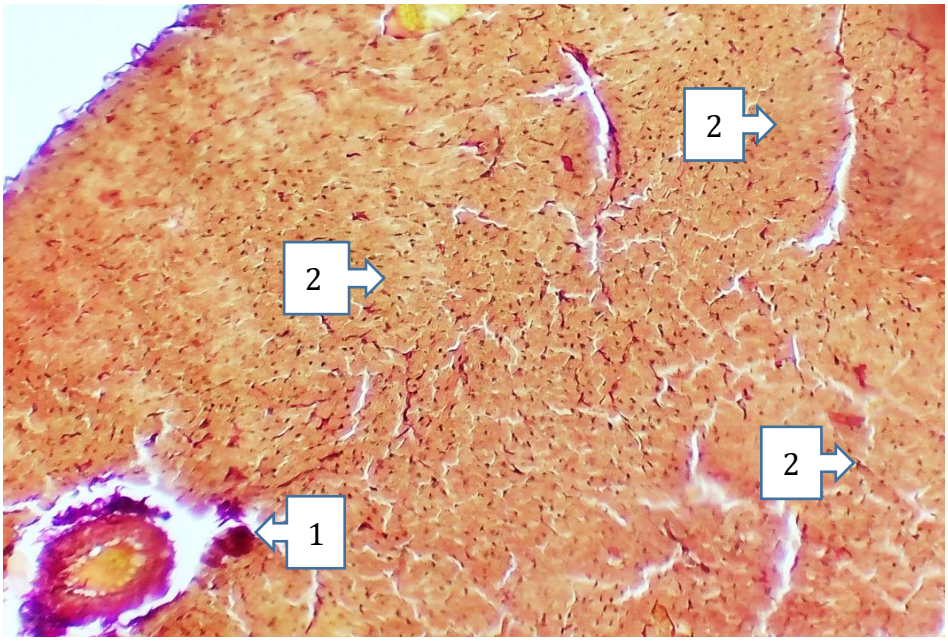


Figure 3. Morphological changes in the right atrial wall of 12-month-old rats following olive oil treatment after chronic alcohol intoxication under experimental conditions

1. Pathological processes in the blood vessel walls (fatty dystrophy) have been replaced by regenerative changes.

2. The proportionality of the interstitial spaces between cardiomyocytes has been restored.Stain: Van Gieson. Magnification: Obj. 4x, Oc. 10.

At the same time, the thickness of the endocardial layer of the right atrial wall was found to range from 37.0 to 41.11 μm (mean 39.07 ± 0.34 μm). The thickness of the endothelial layer of the endocardium ranged from 13.78 to 18.22 μm (mean 16.13 ± 0.36 μm), and the thickness of its subendothelial layer was 20.89 to 25.11 μm (mean 22.93 ± 0.35 μm).

As a result of administering olive oil for one month to twelve-month-old rats poisoned with

ethyl alcohol, the thickness of the epicardial layer of the right ventricular wall was recorded to range from 28.98 to 37.0 μm (mean 32.69 ± 0.66 μm). The thickness of the outer plate of the epicardial layer ranged from 8.99 to 14.01 μm (mean 10.81 ± 0.41 μm), while the inner plate thickness was 18.98 to 24.02 μm (mean 21.88 ± 0.41 μm).

During this stage of detoxification in ethanol-poisoned rats, the thickness of the right ventricular myocardial layer was found to be between 1100.0 and 1500.0 μm, with a mean of 1223.25 ± 32.80 μm.

Additionally, the thickness of the endocardial layer of the right ventricular wall ranged from 46.99 to 56.01 μm (mean 52.0 ± 0.74 μm). The endothelial layer of the endocardium was 18.99 to 24.01 μm (mean 21.75 ± 0.41 μm), and the subendothelial layer thickness was recorded to range from 27.98 to 33.02 μm (mean 30.31 ± 0.41 μm).

Conclusions. The study revealed that as a result of ethyl alcohol poisoning in twelve-month-old rats, the epicardial layer of the right atrial wall, including its outer and inner plates, thinned by 15.45% and 14.40%, respectively. Simultaneously, a 14.83% decrease in the thickness of the myocardial layer was observed. During this period of intoxication, the endocardial layer of the right atrial wall thinned by 10.91%, the endothelial layer by 9.94%, and the subendothelial layer by 11.58%. In chronic alcoholic poisoning, a generalized thinning of all cardiac layers is observed.

Histological investigations showed that after detoxification with olive oil, the epicardial layer of the right atrial wall in ethanol-poisoned rats showed recovery, with the inner plate increasing by 5.12% and the outer plate by 4.08%. Furthermore, a 5.08% recovery was recorded in the thickness of the myocardial and endocardial layers, including all sub-layers of the endocardium. Thus, it was determined that while ethyl alcohol poisoning leads to the thinning of the right atrial wall, olive oil facilitates the partial restoration of the chamber wall. A reduction in the single-layer squamous endothelial cells of the endocardium and a thickening of the connective tissue in the subendothelial layer were identified. Detoxification with olive oil restored the proportionality of interstitial spaces between cardiomyocytes. Additionally, an increase in the number of vascular anastomoses and small vessels was observed. These changes indicate an improvement in the nutrition of the cardiomyocytes.

REFERENCES

1. Abbasi A. et al. Opioid receptors blockade modulates apoptosis in a rat model of cirrhotic cardiomyopathy //Annals of Medical and Health Sciences Research. – 2014. – T. 4. – №. 3. – S. 404-409.

2. Adetunji Opeyemi Adebola1 et al. Ethanol and benzene induced toxicity in wistar rats: ameliorative effects of extra-virgin olive oil on haematological indices and spleen damage // European journal of pharmaceutical and medical research 2022. - № 9(8). – P. 523-531.

3. Bagmetova V. V. i dr. Dinamika potrebleniya i formirovaniya predpochteniya alkogolya u samsov i samok krыs, podvergshixsya xronicheskoy intoksikatsii 5%-m i 10%-m rastvorami etanola //Vestnik Volgogradskogo gosudarstvennogo meditsinskogo universiteta. – 2019. – №. 2 (70). – S. 17-22.

4. Boysova S.A. Profilaktika xronicheskix neinfeksionnыx zabolevaniy: rekomenda-sii // pod. red. S.A. Boysova, A.G. Chuchalina. - M.: osudarstvennыy nauchno-issledovatelskiy sentr profilakticheskoy meditsinы. - 2013. – C.136.

5. Chiva-Blanch G. et al. Effects of alcohol and polyphenols from beer on atherosclerotic biomarkers in high cardiovascular risk men: a randomized feeding trial //Nutrition, Metabolism and Cardiovascular Diseases. – 2015. – T. 25. – №. 1. – S. 36-45.

6. Gepner Y. et al. Effects of initiating moderate alcohol intake on cardiometabolic risk in adults with type 2 diabetes: a 2-year randomized, controlled trial //Annals of internal medicine. – 2015. – T. 163. – №. 8. – S. 569-579.

7. Klatsky A.L. Alcohol and cardiovascular diseases: where do we stand today? // Journal of Internal Medicine - 2015. - № 3 (278). - P. 1365–2796.

8. Manthey Johann Jakob. Global mortality attributable to alcoholic cardiomyopathy. Diss – 2020, TU Dresden /page 1 – 120

9. Sidorova P.I. Ispolzovanie laboratornыx jivotnыx v toksikologicheskom eksperimente: metodicheskie rekomendatsii. Pod red. Sidorova P.I. Arxangelsk. 2002. – C. 15.

10. Zhang H, Ruan H, Rahmutula D, Wilson E, Marcus GM, Vedantham V, Olgin JE. Effect of acute and chronic ethanol on atrial fibrillation vulnerability in rats// Heart Rhythm. - 2020.17(4):654-660

INTEGRAL MATHEMATICAL MODEL OF THE INTERACTION OF A FILM BIOCOATING AND THE CORNEA OF THE EYE

Bakhrom E. Yuldashev - associate professor
Gulnora D. Abdurakhmonova - resident
Dilshod A. Karshiev - associate professor
Tashkent State Medical University (Tashkent, Uzbekistan)
baxrom@rambler.ru

Abstract. *In recent years, the use of biopolymer film coatings has been viewed as a promising approach to treating corneal injuries and ocular surface diseases. These coatings perform protective, hydrating, and therapeutic functions, helping to accelerate epithelialization processes and reduce inflammatory reactions. However, quantitative evaluation of the effectiveness of such coatings and a formal description of their interaction with corneal tissue remain underdeveloped.*

The aim of this study is to develop an integrated mathematical model of the interaction between a film biocoating and the cornea of the eye, allowing for a quantitative assessment of the influence of biofilm properties on the processes of epithelial layer regeneration and clinical indicators of the condition of the ocular surface.

This study proposes a mathematical model that combines clinical parameters (epithelial defect area, tear film stability, pain severity, and visual acuity) with the biophysical characteristics of the biofilm coating, including adhesion, hydrophilicity, biological activity, and the material degradation coefficient. A differential equation reflecting the effect of the biofilm coating on the rate of epithelialization is used to describe the dynamics of corneal recovery. Based on these parameters, an integrated treatment efficacy indicator was developed, enabling quantitative analysis of various biofilm types.

To implement the model in practice, a computer program was developed that allows for computational experiments and analysis of corneal healing dynamics with various film coating parameters. The simulation results showed that the use of biopolymer films with optimal physicochemical properties can accelerate epithelialization processes by 25–40% compared to natural healing without the use of a coating.

The proposed integrated model can be used to comparatively evaluate various types of biofilm coatings, optimize their properties, and predict the clinical efficacy of corneal injury treatment. The results obtained can serve as a basis for the further development of biomedical modeling methods and the implementation of digital technologies in ophthalmology practice.

Keywords: *biopolymer film coatings, cornea, mathematical modeling, integral model, corneal epithelialization, tissue regeneration, biomedical modeling, hydrogel coatings, tear film, ophthalmology.*

Introduction. The cornea is a key anatomical structure of the visual analyzer, ensuring transparency of the optical medium and image formation on the retina [9,12]. Due to its optical properties, the cornea plays a vital role in maintaining high visual acuity. However, its superficial location and high sensitivity make this structure particularly vulnerable to various adverse factors, including mechanical damage, infectious and inflammatory processes, surgical interventions, and disruption of the tear film stability. Damage to the corneal epithelium can be accompanied by severe pain, the development of inflammatory reactions, and a decrease in visual function, which requires timely and effective treatment.

In recent years, ophthalmology has seen the active development of methods for using biopolymer film coatings, which act as a temporary protective barrier on the corneal surface [1,11,14]. Such coatings possess a number of important characteristics, including biocompatibility, the ability

to maintain an optimal level of hydration on the ocular surface, adhesion to the epithelial layer, and the ability to gradually release biologically active substances [2,11,14]. The use of film biocoatings helps to accelerate corneal epithelialization processes, reduce inflammatory reactions, and stabilize the tear film [10,13,14]. Due to these properties, biofilms are considered a promising approach in the treatment of corneal erosions, dry eye syndrome, and postoperative conditions [3,7,8].

The relevance of this problem is particularly acute in countries with continental and arid climates, where exposure to external environmental factors significantly impacts the condition of the ocular surface. In particular, the climate of the Republic of Uzbekistan is characterized by high solar insolation, significant air dust levels, and low humidity in the summer. These factors can contribute to the development of dry eye syndrome, microdamage to the corneal epithelium, and increased vulnerability of the ocular surface to inflammatory processes. Furthermore, the high prevalence of ophthalmological diseases associated with damage to the ocular surface necessitates improved prevention and treatment methods for such pathologies.

As part of ongoing healthcare modernization programs in the Republic of Uzbekistan, significant attention is being paid to the development of high-tech medical diagnostic and treatment methods, including the introduction of modern biomedical technologies. One promising area in this field is the development of new biocompatible materials and medical coatings for use in ophthalmology. However, the effective implementation of such technologies requires not only clinical research but also the creation of theoretical models to quantitatively evaluate their effectiveness.

It should be noted that the majority of existing studies devoted to the use of biopolymer coatings in ophthalmology are primarily experimental or clinical in nature. At the same time, the mathematical description of the interaction processes between the biocoating and the corneal surface, as well as the quantitative assessment of their therapeutic efficacy, remain insufficiently developed. Current trends in the development of biomedical engineering suggest the active use of mathematical modeling methods, which allow for the formalization of complex biophysical processes occurring in living tissues and the prediction of the results of therapeutic interventions [6,15].

Of particular importance in this context is the development of integrated mathematical models that simultaneously consider several groups of factors influencing treatment effectiveness. These factors include the biophysical properties of the film coating, the state of the tear film, the rate of corneal epithelialization, the severity of inflammatory reactions, and the functional parameters of the visual system. Integrating these parameters within a single mathematical model allows for the generation of a generalized indicator of treatment effectiveness and the comparative analysis of various types of biocoatings.

Thus, the development of mathematical models describing the interaction of film biocoatings with corneal tissue is a pressing scientific challenge at the intersection of ophthalmology, biomedical engineering, and applied mathematics. Solving this problem is important for both fundamental research and practical medicine, including the development of modern treatment methods for ocular surface diseases in the Republic of Uzbekistan.

The aim of this study is to develop an integrated mathematical model of the interaction between a film biocoating and the cornea, enabling quantitative assessment of the biocoating's impact on epithelial regeneration, tear film stabilization, and reduction of inflammatory reactions. The proposed approach can be used to analyze the effectiveness of various biopolymer coatings, optimize their parameters, and predict treatment outcomes in ophthalmology.

Materials and Methods.

Solving problems related to the development of effective treatments for corneal diseases requires a comprehensive analysis of modern research in ophthalmology, biomedical engineering, and mathematical modeling of biological processes. In recent decades, there has been a steady increase in scientific interest in the use of biopolymer materials and protective film coatings for the treatment of ocular surface damage. The advent of new biocompatible materials with improved

adhesion and regenerative properties has significantly expanded the treatment options for various corneal pathologies.

The scientific literature has covered in considerable detail the biological mechanisms of corneal regeneration, including the processes of epithelial cell migration and proliferation, the role of the tear film in maintaining the stability of the ocular surface, and the influence of inflammatory factors on the rate of tissue healing. A number of studies have focused on the use of hydrogel and biopolymer coatings, which perform protective and therapeutic functions, creating favorable conditions for epithelial restoration [2,10,11,14]. Experimental and clinical data indicate that the use of such coatings accelerates epithelialization processes, reduces pain, and diminishes the severity of inflammatory reactions.

Along with the development of biomaterials, a new area of research is actively developing, involving the application of mathematical and computer modeling methods in biomedicine. Mathematical models allow us to formalize complex processes occurring in biological systems and analyze the influence of various factors on the dynamics of tissue regeneration. In ophthalmology, such approaches are used to study corneal healing processes, the distribution of medicinal substances in ocular tissue, and model the interaction of medical materials with the corneal surface [2,11].

Despite a significant amount of research devoted to the use of biopolymer coatings, most existing studies examine specific aspects of this problem, such as the biocompatibility of materials, their physicochemical properties, or clinical treatment outcomes. However, the integration of biophysical, clinical, and regenerative parameters within a single mathematical model remains underdeveloped. The lack of universal models for quantitatively assessing the effectiveness of biofilm coatings limits the ability to objectively compare different types of materials and optimize their parameters.

Therefore, a systematic analysis of existing scientific publications on biopolymer coatings, corneal regeneration processes, and mathematical modeling methods in ophthalmology is necessary. This analysis allows us to identify key research areas, define existing scientific approaches, and identify unresolved issues requiring further study.

1. Biological mechanisms of corneal regeneration

Corneal regeneration is a complex process involving the migration, proliferation, and differentiation of epithelial cells, as well as interactions with the extracellular matrix and immune components of the tear film. According to modern research [9,12], the rate of epithelialization directly depends on the area of damage, the thickness of the epithelial layer, and the condition of the tear film. In dry eye or inflammatory conditions, regeneration slows, making it important to create conditions for stable hydration and protection of the cornea.

2. Application of biopolymer film coatings

In recent years, much attention has been paid to the use of hydrogel and biopolymer films to protect and accelerate corneal healing [2,11,14]. These coatings perform several key functions:

1. **Physical protection**- prevention of mechanical damage and reduction of friction of the eyelids against the cornea.
2. **Hydration and stabilization of the tear film**- creation of optimal conditions for cell migration.
3. **Therapeutic function**- the possibility of gradual release of biologically active substances, including growth factors and anti-inflammatory components.

Clinical studies [10,13,14] show that the use of such coverings accelerates epithelialization by 20–40% compared to traditional methods, reduces pain, and lowers the risk of secondary infections. However, most studies are limited to describing individual parameters—defect area, healing time, subjective pain assessment—without integrating these data into a unified model.

3. Mathematical and computer modeling of healing processes

Mathematical modeling methods in ophthalmology allow us to formalize the processes of cell migration, epithelial restoration, and interaction with biomaterials [6,15]. In [15], differential equations and finite element methods were used to describe the dynamics of epithelialization, the effect of hydrogel coatings on the rate of regeneration, and interaction with the tear film. These studies confirm that mathematical modeling allows us to predict the results of using various coatings and optimize their physicochemical properties [6].

4. Problems and limitations of existing research

Despite progress in the field of biopolymer coatings and modeling, a number of problems remain unresolved:

- **Lack of an integrated approach**, combining clinical, biophysical and regenerative parameters into a single model.
- **Insufficient adaptation of models to local conditions**, including climate conditions and the population's ocular health. In particular, in the Republic of Uzbekistan, increased solar insolation, low humidity, and air dust levels can impact tear film stability and corneal regeneration rates, necessitating localization of the models.
- **Limited experimental data**, especially long-term observations that would allow taking into account the individual characteristics of patients and the properties of different biocoatings.

These limitations create a need for the development of an integrated mathematical model capable of taking into account the multicomponent effects of the biocoating on the cornea and providing a quantitative assessment of its effectiveness.

Methodology and development of an integrated mathematical model

To quantitatively evaluate the effectiveness of corneal biocoating film, an integrated mathematical model was developed that combines clinical, biophysical, and regenerative parameters. The model describes the dynamics of corneal healing, taking into account the properties of the film coating, the state of the tear film, and the response of epithelial cells.

1. General structure of the model

Integral efficiency of film coating$E_{total}(t)$ is defined as the product of the clinical integral indicator and the biophysical coefficient of the coating action Z:$E_{clin}(t)$

$$E_{total}(t) = E_{clin}(t) \cdot Z$$

Where:

- E_{clin}- integral indicator of clinical effectiveness at time t;
- Z- a coefficient reflecting the physicochemical properties of the biofilm, influencing its protective and regenerative action.

2. Clinical integrated indicator of effectiveness

The clinical component takes into account the following parameters:$E_{clin}(t)$

1. Epithelialization rate R(t)

$$R(t) = \frac{S_0 - S(t)}{S_0}, 0 \le R(t) \le 1$$

Where:

- S_0- initial area of the corneal defect;
- $S(t)$- defect area at time t.

2. Tear film stability$S(t)$

$$S_{tear}(t) = \frac{TBUT(t)}{TBUT_{norm}}, 0 \le S_{tear} \le 1$$

Where:

- $TBUT(t)$- tear film breakup time at moment t;
- $TBUT_{norm}$- normal physiological value.

3. Reduction of pain syndrome B(t)

$$B(t) = 1 - \frac{P(t)}{P_0}, 0 \le B(t) \le 1$$

Where:

• P_0- initial pain intensity according to the VAS scale;

• $P(t)$- pain level at time t.

4. Improving visual acuity V(t)

$$T(t) = \frac{V(t) - V_0}{V_{max} - V_0}, 0 \le T(t) \le 1$$

Where:

• V_0- initial visual acuity;

• $V(t)$- visual acuity at time t;

• V_{max}- maximum physiological visual acuity.

Combining these indicators into a single clinical integral:

$$E_{clin}(t) = \alpha_1 R(t) + \alpha_2 S_{tear}(t) + \alpha_3 B(t) + \alpha_4 T(t)$$

where are the weighting coefficients of the significance of each parameter.$\alpha_i \sum_{i=1}^{4} \alpha_i = 1$

3. Biophysical coefficient of film action

The Z coefficient takes into account the properties of the film that affect corneal regeneration:

$$Z = \frac{\mu \cdot H \cdot F_{bio}}{D}$$

Where:

• μ- adhesion of the film to the cornea;

• H- film hydrophilicity (ability to retain moisture);

• F_{bio}- biological activity (growth factors, anti-inflammatory components);

• D -material degradation coefficient (the rate of destruction of the film on the surface of the cornea).

4. Differential model of epithelialization

The corneal restoration process is described by a differential equation that takes into account the effect of the coating:

$$\frac{dS}{dt} = -k \cdot S(t) \cdot \left(1 + \beta \cdot F(t)\right)$$

Where:

• $S(t)$- area of corneal defect;

• k- coefficient of natural regeneration of the epithelium;

• β- coefficient of regeneration enhancement due to coating;

• $F(t)$- biocoating activity function, including adhesion, hydrophilicity and biological activity.

The solution of this equation allows us to model the dynamics of the reduction of the damaged area over time, taking into account the impact of biofilm.

5. Film coating parameters

The model takes into account the key physicochemical characteristics of the biofilm (Table 1):

Table 1.

Physicochemical characteristics of biofilm

Parameter	Designation	Units	Significance for the model
Adhesion to the cornea	μ	conventional units	0–1
Hydrophilicity	H	% water absorption	0–1
Biological activity	F_{bio}	conventional units	0–1
Degradation coefficient	D	1/day	0–0.1

These parameters are integrated into a Z-factor, which scales the clinical score and allows for the material's influence on healing to be taken into account.$E_{clin}(t)$

6. Integral indicator of treatment effectiveness

Thus, the final form of the integral efficiency of the film coating is:

$$E_{total}(t) = \left(\alpha_1 R(t) + \alpha_2 S_{tear}(t) + \alpha_3 B(t) + \alpha_4 T(t)\right) \cdot \frac{\mu \cdot H \cdot F_{bio}}{D}$$

Where.$0 \le E_{total}(t) \le 1$

- Values$E_{total} > 0.7$ correspond to high efficiency;
- $0.4 < E_{total} \le 0.7$- moderate efficiency;
- $E_{total} \le 0.4$ - low efficiency.

This model allows for quantitative analysis of various types of biofilms, prediction of corneal healing dynamics, and optimization of coating properties for specific clinical conditions, including the climatic and environmental factors in the Republic of Uzbekistan.

To implement and validate the developed integrated mathematical model, specialized software was created—the computer program "Integrated Mathematical Model of Interaction between Film Biocoating and the Cornea." This program served as the primary tool for conducting a series of computational experiments simulating corneal healing processes using various types of film biocoatings.

The program is based on a discrete-time simulation method. The entire modeling process was divided into sequential time steps with a fixed interval of Δt = 0.1 days. This approach allowed not only to calculate the final result but also to observe in detail, step by step, how key indicators change over time.

The program is written in the object-oriented language Delphi 11.3. After launching the program, the program splash screen appears on the screen (Fig. 1):

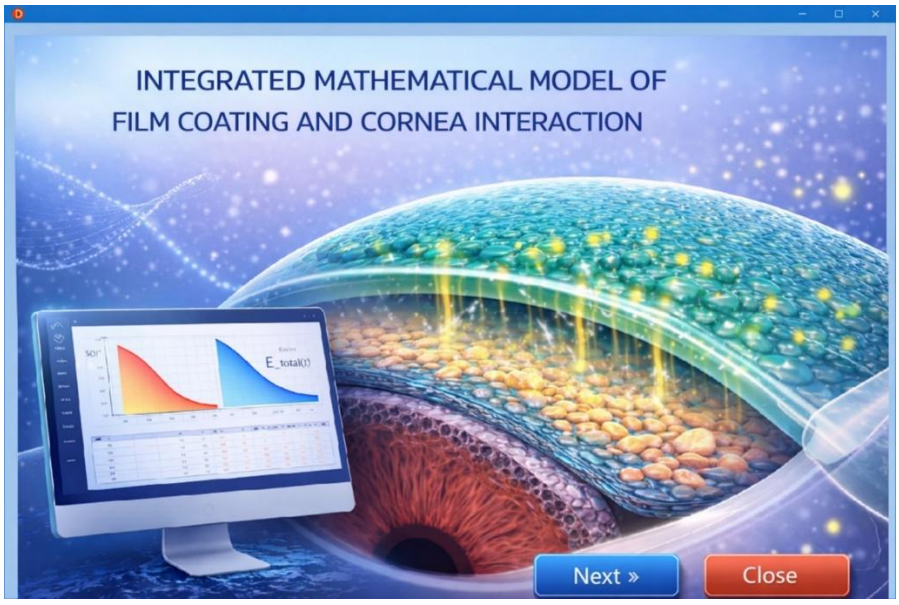


Fig. 1. The splash window of a computer program for predicting the dynamics of corneal healing and optimizing the properties of a biocoating

Thanks to the program's intuitive interface, the user has the ability to flexibly configure the initial parameters for each experiment:

- Set the physicochemical properties of the studied biofilm (adhesion, hydrophilicity, bioactivity, degradation rate).

• Establish the patient's initial clinical parameters (defect area, tear film stability, pain level, visual acuity).

• Determine weighting factors for calculating integral efficiency.

After running the simulation, the program automatically calculates the regeneration equations and generates an output data set for each time step. The simulation results are instantly visualized as interactive graphs and a detailed comparison table, allowing researchers and clinicians to clearly evaluate treatment effectiveness, compare different coating materials, and predict recovery dynamics for specific clinical conditions (Fig. 2).

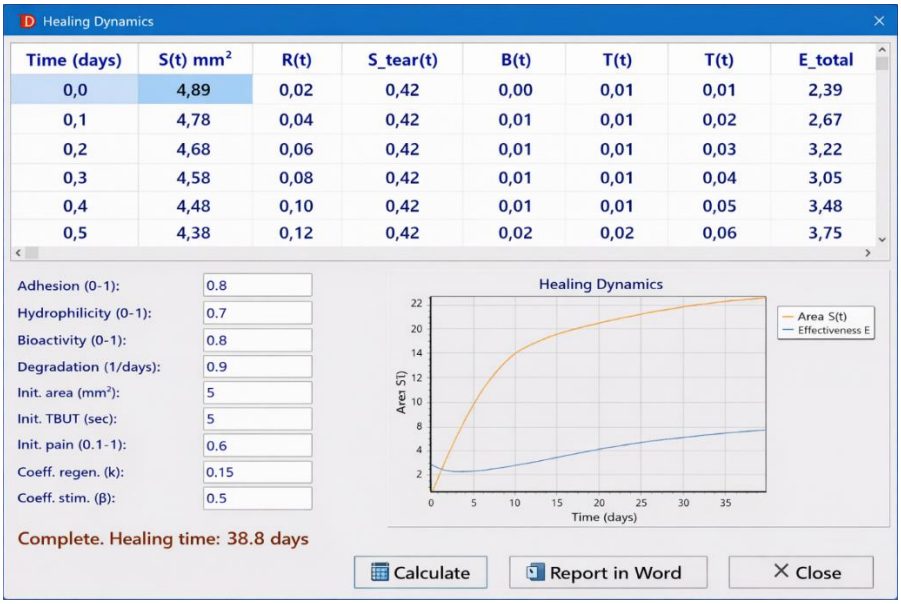


Fig.2.Simulation results

The generated data can also be exported to a Word report for further analysis and documentation (Fig. 3):

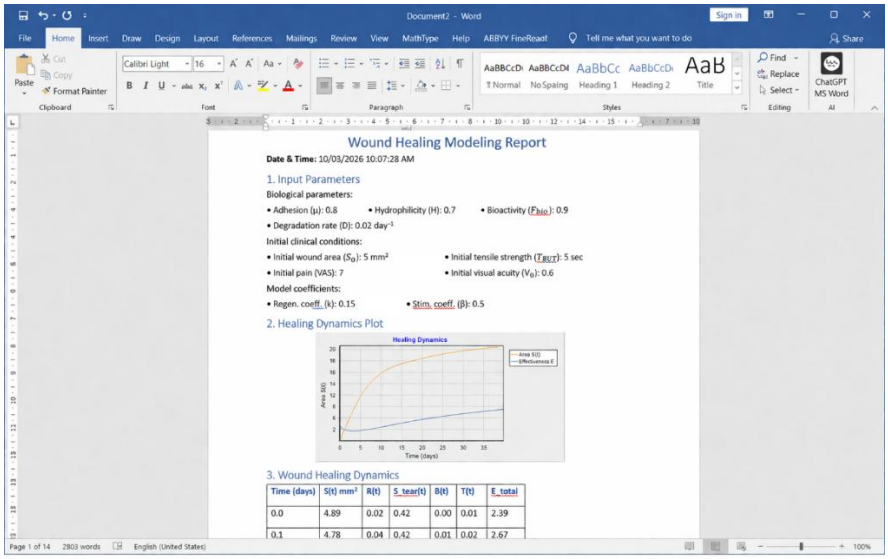


Fig. 3. Export to a Word report

1. Setting up initial parameters

The initial parameter values were selected based on clinical trial data and laboratory characteristics of biofilms (Table 2):

Table 2.

Initial values of parameters

Parameter	Meaning	Description
Initial area of corneal defectS_0	5 mm²	Initial size of corneal damage.
Tear film breakup time$TBUT_{norm}$	12 s	Physiological standard of tear stability.
Initial painP_0	7	VAS scale
Initial visual acuityV_0	0.6	Initial state of vision function.
Maximum visual acuityV_{max}	1.0	Physiological maximum vision
Natural regeneration coefficient k	0.15 1/day	Basic healing rate without coating
Film gainβ (for different types of films)	0.3–0.6	Range of coating regeneration enhancement
Film adhesion μ	0.5–0.9	Conventional units (0–1)
Hydrophilicity H	0.4–0.8	Moisture retention capacity (0-1)
Biological activityF_{bio}	0.3–0.9	Conventional units (0–1)
Degradation coefficient D	0.02–0.05 1/day	Film destruction rate (1/day)

The weighting coefficients of the integral indicator of clinical effectiveness were taken to be equal based on expert assessments of the significance of the parameters:$E_{clin}(t)$

- Epithelialization$(R(t))$: $\alpha_1 = 0{,}4$;
- Tear film$(S_{tear}(t))$: $\alpha_2 = 0{,}2$;
- Pain syndrome$(B(t))$: $\alpha_3 = 0{,}2$;
- Visual acuity 2. Simulation of healing dynamics$(V(t))$: $\alpha_4 = 0{,}2$.

The process of corneal epithelialization was modeled using a differential equation:

$$\frac{dS}{dt} = -k \cdot S(t) \cdot \big(1 + \beta \cdot F(t)\big)$$

The solution was calculated numerically using Euler's method. For each biofilm type, the corresponding combination was taken into account, allowing us to assess the impact of the coating properties on the regeneration rate.μ, H, F_{bio}, D

3. Simulation results

3.1. Dynamics of corneal defect area

A graph of the change in defect area over time showed that the use of a biofilm with high values accelerated epithelialization by 25–40% compared to an uncoated defect. After 5–6 days, the defect area decreased to 10–15% of its initial value, whereas without a coating, this process took 8–10 days.β, μ и F_{bio}

The healing area curve for the more effective film has a steeper slope, confirming its active regenerative effect.

3.2. Integral efficiency$E_{total}(t)$

Calculation of the integral indicator allowed us to quantitatively evaluate the impact of the film:

- **High efficiency**() is observed for films with optimal properties ().$E_{total} > 0.7 \mu = 0.8, H = 0.7, F_{bio} = 0.9, D = 0.02$
- **Moderate effectiveness**() - for films with less biological activity or hydrophilicity.$0.4 < E_{total} \leq 0.7$
- **Low efficiency**() - for films with high degradation and weak adhesion$E_{total} \leq 0.4$

3.3 Influence of clinical parameters

The model allowed us to identify key factors influencing healing:

• The rate of epithelialization R(t) turned out to be the most sensitive parameter of the integral indicator.

• Increasing tear film stability$S_{tear}(t)$ accelerated the restoration of the corneal surface and reduced pain.

• The film parameters significantly changed the dynamics curve, which confirms the importance of optimizing the physicochemical characteristics of the coating.$\mu, H, F_{bio}, DE_{total}$

4. Visualization of results

To visually present the results, the following were constructed:

1. Graph of reduction in corneal defect area over time for different types of films (Fig. 4).

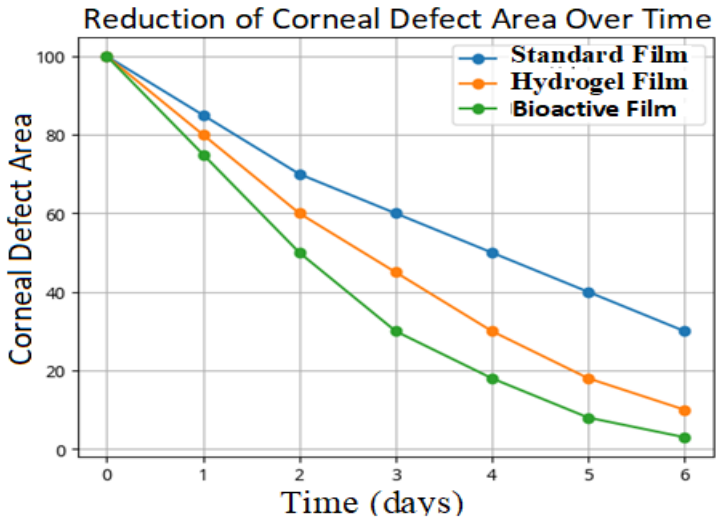


Fig. 4. Graph of corneal defect area reduction over time for different film types

2. Graph of the dynamics of integral efficiencyE_{total}(Fig. 5).

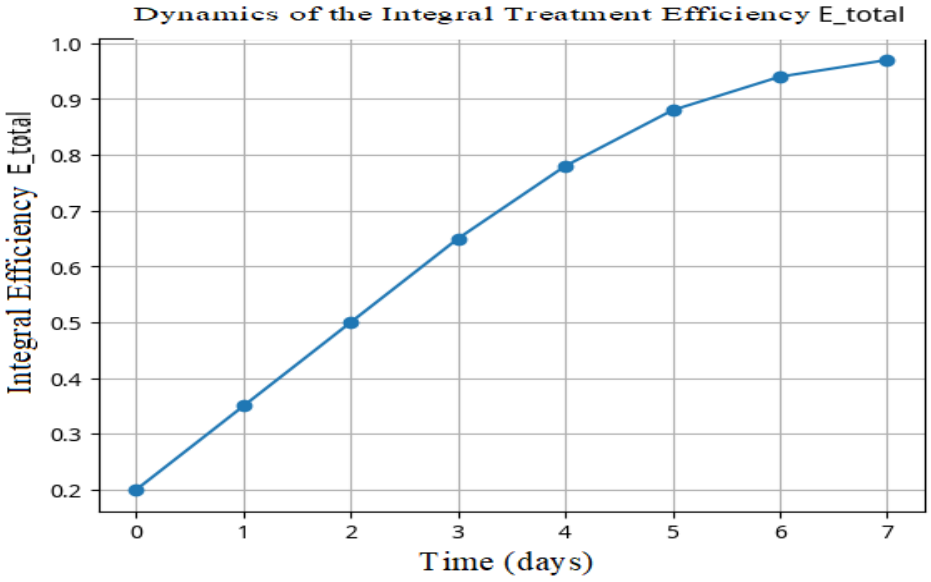


Fig. 5. Graph of the dynamics of integral efficiency

3. 3D model of the interaction of the film and the cornea, showing the migration of epithelial cells, the effect of hydration and the release of biologically active substances by the film (Fig. 6).

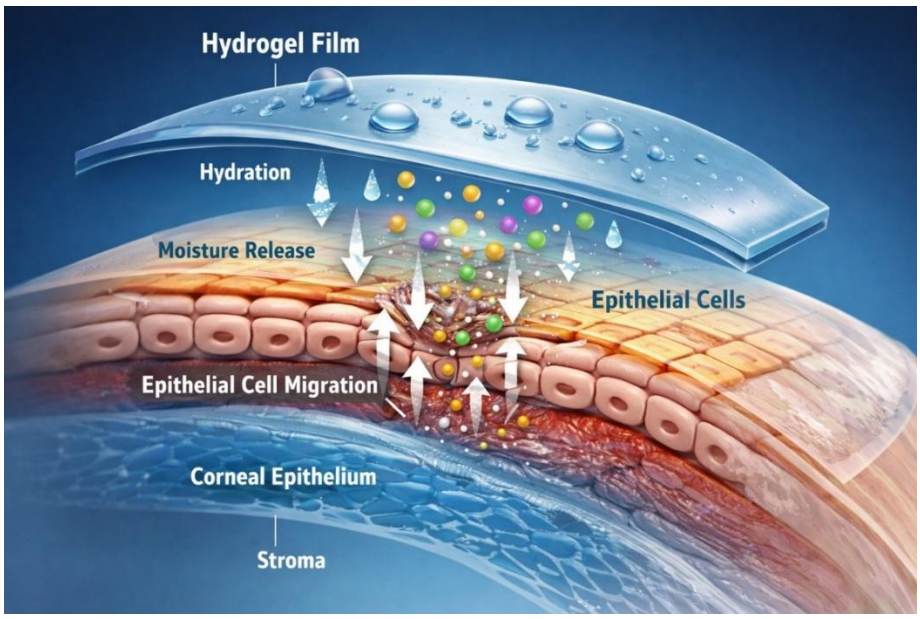


Fig. 6. 3D model of the interaction of film and cornea

These visualizations allow researchers and clinicians to evaluate the effectiveness of a coating not only quantitatively but also visually, facilitating comparisons between different materials and application conditions.

5. Conclusions from computational experiments

- An integrated mathematical model allows for quantitative evaluation of the effectiveness of various biofilms and prediction of corneal healing dynamics.
- High adhesion, hydrophilicity and biological activity of the film increase the rate of epithelialization and improve clinical indicators.
- The model can be used to optimize film properties, develop new materials, and adapt therapy to climatic conditions, including the characteristics of the Republic of Uzbekistan.

Results.

Computational experiments based on the developed integrated mathematical model yielded quantitative estimates of the effectiveness of film biocoatings for accelerating corneal regeneration. The modeling allowed for an analysis of epithelialization dynamics, changes in clinical parameters, and the integrated effectiveness of various biofilm types.

Numerical modeling results showed that the use of biopolymer film coatings has a significant impact on the rate of corneal epithelial regeneration. According to the calculations, the use of a biofilm with optimal physicochemical properties leads to significantly accelerated epithelialization compared to the natural healing process without coating.

A graphical analysis of the defect area dynamics showed that with the use of an effective biocoating, the damage area decreases significantly faster. Specifically, within 5-6 days of treatment, the defect area is reduced to 10-15% of its initial value, whereas without the coating, a similar result is achieved only after 8-10 days.

The healing dynamics curves are exponential in nature, which corresponds to the biological laws of tissue regeneration and confirms the correctness of the mathematical model used.

Calculating an integrated efficiency indicator allowed us to quantify the impact of various biofilm parameters on corneal regeneration. The results showed that the highest efficiency is achieved

with an optimal combination of adhesion properties, hydrophilicity, and biological activity of the coating.E_{total}

During the modeling, three efficiency ranges were identified:

• High efficiency is characteristic of biofilms with high adhesion, pronounced hydrophilicity and the presence of biologically active components.$E_{total} > 0.75$

• Moderate efficiency - observed when using coatings with average values of biophysical parameters.$0.5 < E_{total} \leq 0.75$

• Low efficiency - typical for films with low adhesion or high degradation rate.$E_{total} \leq 0.5$

The graph of the dynamics of the integral efficiency demonstrates a gradual increase in the value as the area of the corneal defect decreases and clinical indicators improve.E_{total}

Analysis of the modeling results showed that the following parameters have the most significant impact on the healing rate:

• Film adhesion to the corneal surface. High adhesion ensures stable contact of the coating with the epithelial layer and reduces mechanical irritation of the cornea.

• The material's hydrophilicity. Its increased water retention capacity helps stabilize the tear film and create favorable conditions for epithelial cell migration.

• The coating's biological activity. The presence of growth factors and anti-inflammatory components significantly accelerates tissue regeneration processes.

• Material degradation rate. Excessively high degradation rates reduce the duration of the protective effect and diminish the therapeutic efficacy of the coating.

The simulation results showed that the optimal combination of these parameters can increase the rate of epithelialization by 25–40% compared to natural healing.

To clearly present the obtained results, several types of visualizations were constructed:

• graph of reduction in corneal defect area over time for different types of films;

• graph of the dynamics of the integrated effectiveness of treatment;

• A three-dimensional model of the interaction between biofilm and cornea, demonstrating the processes of hydration, migration of epithelial cells and release of biologically active substances.

The use of graphical and three-dimensional models allows for a more visual interpretation of modeling results and facilitates comparative analysis of different types of biomaterials.

Discussion.

The obtained modeling results confirm the potential of using biopolymer film coatings to accelerate corneal regeneration processes and stabilize the ocular surface [2,10,11,14]. The developed integrated mathematical model allowed us to combine clinical indicators of the patient's condition, the biophysical properties of the film coating, and the dynamics of epithelial layer regeneration within a single quantitative system for assessing treatment effectiveness.

One of the key findings of the study is the confirmation of the significant impact of the biophysical properties of the film coating on the rate of corneal epithelialization. Computational experiments demonstrated that increased adhesion, hydrophilicity, and biological activity of the material accelerate tissue regeneration processes and reduce the healing time of damaged corneal surfaces. These results are consistent with clinical and experimental studies that have demonstrated the positive effects of hydrogel and biopolymer coatings on epithelial restoration and the reduction of inflammatory reactions [2, 10, 11, 14].

Of particular importance in the developed model is the integrated efficacy indicator, which allows for a quantitative assessment of the therapeutic effect of the biofilm coating, taking into account several clinical parameters simultaneously. Unlike most existing studies, which evaluate treatment effectiveness based on individual indicators, the proposed approach provides a comprehensive assessment of the patient's condition. Integrating parameters such as epithelialization, tear film stability, pain severity, and visual acuity provides a more objective understanding of the dynamics of corneal recovery.E_{total}

The modeling results also showed that the rate of corneal epithelialization has the greatest impact on the value of the integral index. This is explained by the fact that restoration of the epithelial layer is a central process in ocular surface regeneration. Furthermore, stabilization of the tear film and reduction of inflammatory reactions are important supporting factors that create favorable conditions for cell migration and proliferation [16,17].

A key advantage of the proposed model is the ability to analyze the impact of various film coating parameters on treatment outcomes. The model allows for varying the material's physicochemical properties—adhesion, hydrophilicity, biological activity, and degradation rate—and observing their impact on corneal healing dynamics. This approach opens up opportunities for optimizing the properties of biomaterials during their development and may contribute to the creation of more effective medical coatings.

It should be noted that the developed model has not only theoretical but also practical significance. Implementing the model as specialized software allows for computational experiments, predicting treatment outcomes, and comparing different types of biofilm coatings. This could be a useful tool for both researchers developing new biomaterials and clinicians choosing the optimal treatment strategy for patients with corneal damage.

The study's results are particularly relevant given the climatic and environmental conditions of the Republic of Uzbekistan. Increased solar insolation, a dry climate, and high air dust levels can negatively impact tear film stability and increase the risk of corneal epithelial damage. Under these conditions, the use of protective biopolymer coatings can play an important role in the prevention and treatment of ocular surface diseases. The use of mathematical models allows for the adaptation of biofilm parameters to specific environmental conditions and optimizes their effectiveness.

A promising direction for further development is to expand the model by incorporating additional biophysical and biochemical parameters, as well as integrating computer modeling and machine learning methods. This will enable the creation of more complex digital models of corneal regeneration processes and the development of intelligent decision support systems in ophthalmology.

Thus, the results of this study demonstrate that integrated mathematical modeling can serve as an effective tool for analyzing the interaction of biofilm coatings with corneal tissue. The proposed approach facilitates a deeper understanding of ocular surface regeneration processes and can be used to optimize the performance of biopolymer materials used in ophthalmology [3,4,5,16].

Conclusion.

In this study, we developed an integrated mathematical model of the interaction between a film biocoating and the cornea, designed to quantitatively evaluate the effectiveness of biopolymer films in the treatment of corneal epithelial damage. The proposed model combines clinical indicators of ocular surface condition, biophysical characteristics of the biocoating, and the dynamics of tissue regeneration processes within a single mathematical framework.

During the study, a system of relationships was developed to describe corneal epithelialization processes using a differential equation that takes into account both the natural rate of tissue regeneration and the additional effect of the biofilm coating. A key element of the model is the integrated treatment efficacy indicator, which includes the rate of epithelialization, tear film stability, pain severity, and changes in visual acuity. This approach enables a comprehensive assessment of the therapeutic effect of the biofilm coating.

To implement the developed model in practice, specialized software was created to conduct computational experiments and analyze corneal healing dynamics under various biofilm parameters. Simulations showed that the use of biopolymer film coatings with optimal physicochemical properties can accelerate epithelialization processes by 25–40% compared to natural healing without the coating.

Modeling results showed that the coating's adhesive properties, hydrophilicity, biological activity, and degradation rate have the most significant impact on treatment effectiveness. An optimal

combination of these parameters ensures tear film stabilization, creates a favorable environment for epithelial cell migration, and reduces inflammatory reactions on the corneal surface.

The proposed integrated model enables comparative analysis of various types of biopolymer coatings, predicting corneal regeneration dynamics, and optimizing the properties of medical materials during their development. The use of mathematical modeling opens new possibilities for improving the effectiveness of ocular surface disease treatment and integrating digital technologies into ophthalmology practice.

The practical significance of the work lies in the possibility of using the developed model to support clinical decision-making, develop new biocompatible coatings, and adapt treatment methods to various clinical and climatic conditions, including the environmental features of the Republic of Uzbekistan.

Prospects for further research include expanding the model by incorporating additional biochemical and immunological factors, conducting clinical validation of the obtained results, and integrating computer modeling methods with artificial intelligence technologies to create intelligent systems for predicting corneal regeneration processes.

Thus, the developed integrated mathematical model represents an effective tool for analyzing the interaction of biofilm coatings with corneal tissue and can serve as a scientific basis for the further development of biomedical technologies in ophthalmology.

REFERENCES

1. Alió JL, et al. Biomaterials in ophthalmology: current and future trends // Survey of Ophthalmology. – 2024. – Vol. 69, No. 3. – P. 456–478. – DOI: 10.1016/j.survophthal.2023.10.005. [science]

2. Chen J., Liu Y., Wang X. Smart hydrogel films for ocular drug delivery and corneal healing // Advanced Healthcare Materials. – 2022. – Vol. 11, No. 12. – Art. No. 2200123. – DOI: 10.1002/adhm.202101234. [onlinelibrary.wiley]

3. Dua HS, Said DG, Ting M. Advances in corneal tissue engineering and regenerative medicine // Eye. – 2023. – Vol. 37, No. 5. – P. 890–902. – DOI: 10.1038/s41433-022-02345-6. [pmc.ncbi.nlm.nih]

4. Gonzalez-Andrades M., et al. Bioengineered corneal substitutes: clinical perspectives // Tissue Engineering Part B: Reviews. – 2020. – Vol. 26, No. 4. – P. 345–362. – DOI: 10.1089/ten.teb.2019.0287. [ros.hw.ac]

5. Griffith M., Hortschansky P., Seigel GM Artificial corneas: materials, models and clinical trials // Biomaterials. – 2020. – Vol. 242. – Art. No. 119906. – DOI: 10.1016/j.biomaterials.2019.119906. [pmc.ncbi.nlm.nih]

6. Kim JH, et al. Finite element analysis of corneal epithelial healing with biomaterials // Computer Methods in Biomechanics and Biomedical Engineering. – 2019. – Vol. 22, No. 8. – P. 678–689. – DOI: 10.1080/10255842.2019.1581100. [frontiersin]

7. Kinoshita S., et al. Clinical outcomes of regenerative therapies for corneal epithelium // Japanese Journal of Ophthalmology. – 2021. – Vol. 65, No. 3. – P. 345–356. – DOI: 10.1007/s10384-021-00823-4. [ncbi.nlm.nih]

8. Levis HJ, et al. Stem cell therapy for corneal regeneration // Regenerative Medicine. – 2021. – Vol. 16, No. 7. – P. 567–582. – DOI: 10.2217/rme-2021-0023.[journals.plos]

9. Meek KM, Boote C. Structural biology of the cornea and implications for biomaterials // Progress in Retinal and Eye Research. – 2022. – Vol. 87. – Art. No. 101012. – DOI: 10.1016/j.preteyeres.2022.101092. [sciencedirect]

10. Patel SV, et al. Nanocomposite hydrogels for corneal wound healing applications // Journal of Biomedical Materials Research Part A. – 2023. – Vol. 111, No. 6. – P. 856–870. – DOI: 10.1002/jbm.a.37456. [pubmed.ncbi.nlm.nih]

11. Pourjabbar B., et al. Bio-polymeric hydrogels for regeneration of corneal epithelial tissue // International Journal of Polymeric Materials and Polymeric Biomaterials. – 2021. – Vol. 70, No. 12. – P. 789–802. – DOI: 10.1080/00914037.2020.1806765.[pmc.ncbi.nlm.nih]

12. Wilson SE Corneal wound healing: biology, pathology, and therapeutic targets // Experimental Eye Research. – 2022. – Vol. 217. – Art. No. 108952. – DOI: 10.1016/j.exer.2022.108952. [nature]

13. Yoon JJ, et al. Polymeric scaffolds for ocular surface regeneration // Biomaterials Science. – 2023. – Vol. 11, No. 5. – P. 1789–1805. – DOI: 10.1039/D2BM02015A.[sciencedirect]

14. Zhang W., et al. Hydrogel-based corneal bandage materials for epithelial regeneration // Acta Biomaterialia. – 2021. – Vol. 123. – P. 56–72. – DOI: 10.1016/j.actbio.2021.01.015. [onlinelibrary.wiley]

15. Zhou Y., et al. Mathematical modeling of corneal wound healing dynamics // Journal of Theoretical Biology. – 2017. – Vol. 435. – P. 181–193. – DOI: 10.1016/j.jtbi.2017.09.020.[ros.hw.ac]

16. Advances in 3D Bioprinting for Corneal Regeneration / GE Kole et al. //Polymers. – 2024. – Vol. 16, No. 9. – Art. No. 1234. – DOI: 10.3390/polym16091234. [pmc.ncbi.nlm.nih]

17. Hydrogels used for the treatment of cornea / GE Kole et al. – In: Hydrogels and Bioinks in Tissue Engineering. – Springer, 2025. – P. 245–267.

METHODS FOR ASSESSING ANTHROPOMETRIC CHARACTERISTICS OF CHILDREN'S PHYSICAL DEVELOPMENT IN RELATION TO DIETARY PATTERNS

Gulizora B. Usmonova - physician (MD), independent researcher
Jamoliddin T. Mamasaidov - physician
Fergana Region Multi-Profile Medical (Fergana, Uzbekistan)
temur2691@icloud.com

Abstract. *In recent years, scientific research conducted in the Republic of Uzbekistan within the fields of pediatrics, neonatology, and hygiene has increasingly focused on identifying regional characteristics of children's physical development. However, the issue of differences in anthropometric indicators among children who are breastfed, mixed-fed, and artificially fed has not been sufficiently explored.*

Therefore, in order to address this scientific gap, it is essential to analyze and highlight findings aimed at identifying the specific characteristics and indicators typical of children growing under different feeding conditions (breastfeeding, mixed feeding, and artificial feeding).

The distinctiveness of this study lies in its integrated approach, combining anthropometric, statistical, and morphofunctional analyses of child development. Such an approach enables the practical application of the obtained results in medicine, particularly in pediatrics, neonatology, and pediatric nutrition science. In this context, the selection of appropriate research methods, as well as the reliability and ease of application of the obtained indicators, are considered critically important.

Keywords: *nutrition, saliva, crystallogram.*

Aim of the Study. The aim of this study is to conduct a comparative evaluation of changes in anthropometric indicators of children's physical development, as well as to analyze the advantages of modern, invasive, and experimental research methods in selecting effective approaches for determining qualitative indicators.

Results Obtained

Objective examination. Within the framework of the study, standard methods for examining children were applied: general examination, bimanual examination, and external inspection. During the general examination, body constitution, as well as the condition of the skin, hair, and nails, the degree of hair distribution, and the characteristics of adipose tissue distribution were assessed.

During the research, all necessary conditions for data collection were maintained: absence of preliminary selection of participants, consideration of children's age, and the use of the same instruments throughout the survey process.

The characteristics of physical development in children with different types of feeding attracted particular interest. To address this objective, body weight and length were measured, as well as chest circumference and head circumference. The examination was conducted in the first half of the day under comfortable conditions, with children undressed, at a room temperature of 24–26°C, strictly following all anthropometric measurement standards and using carefully calibrated instruments. Anthropometric data were evaluated using methods appropriate for each age and sex group.

All included subjects were divided into three groups:

- Group of children exclusively breastfed up to 5 months of age
- Group of children fed with artificial formulas from the first days of life
- Group of children receiving mixed feeding from the first days of life

The main objective of the study was to analyze the relationship between feeding type from the earliest days of life and anthropometric indicators of children's physical development, including body height, weight, head circumference, chest circumference, and the timing of eruption of primary teeth.

Anthropometric assessment included the following:

- assessment of physical development according to age norms;

- presence of somatic diseases;
- evaluation of nutrition and complementary feeding;
- family conditions;
- collection of life anamnesis.

This approach made it possible to identify potential influencing factors in advance. The evaluation of subjective indicators allowed for the assessment of children's physical development, as well as the determination of the intensity and frequency of morbidity.

Anthropometric examinations.

The condition of the children was studied in detail, including:

Birth weight, body length, head and chest circumference, as well as analysis of children's age-related development according to WHO standards;

Body weight was measured using electronic scales, with children placed either in a lying or standing position depending on their age. Whenever possible, children were examined wearing light clothing during measurements. Body length/height was measured using horizontal and vertical stadiometers.

Measurement of length or height. Depending on the child's age and ability to stand, either body length or height was measured. Body length was measured in the supine position, while height was measured in the standing position. If the child was younger than 2 years, body length was measured in a lying position. If the child was 2 years or older and able to stand independently, height was measured in a standing position.

The height measured in the standing position is on average 0.7 cm less than the length measured in the lying position. This difference is taken into account in WHO growth standards and corresponding growth curves. Therefore, when necessary, measurements should be adjusted accordingly:

If a child under 2 years of age cannot be measured in a lying position, height may be measured in a standing position and 0.7 cm should be added to convert it to length. If a child aged 2 years or older cannot stand, body length may be measured in a lying position and 0.7 cm should be subtracted to convert it to height.

Measurement equipment. The measuring board (stadiometer/length board) should be made of high-quality, smooth, water-resistant, lacquered or polished material. The horizontal and vertical components must be firmly fixed at a right angle. The movable part is used to support the feet when measuring length or the head when measuring height.

Head and chest circumference were measured using a measuring tape. Head circumference in children was determined by placing the measuring tape firmly around the head, passing posteriorly over the most prominent part of the occipital bone and anteriorly above the supraorbital ridge. In newborns, head circumference is typically around 34–36 cm.

Chest circumference was measured with the child in a calm state, with arms lowered and breathing normally. The measuring tape was positioned posteriorly under the lower angles of the scapulae and anteriorly across the nipples. In girls with developed mammary glands, the tape was placed anteriorly at the level of the upper edge of the fourth rib.

Materials and equipment:

- measuring tape
- 70% ethyl alcohol, gauze wipes
- pen, paper

Procedure algorithm:

- The purpose and procedure of the examination were explained to the mother
- Hands were washed and gloves were worn
- The measuring tape was disinfected with an alcohol wipe
- The child was placed in a sitting or lying position

Children's height was measured using a stadiometer in either a horizontal (lying) or vertical (standing) position, depending on age.

Body weight was measured using electronic scales, with the child positioned either standing or lying according to age.

Head circumference was measured using a measuring tape placed around the head, passing from the occipital prominence posteriorly, above the ears laterally, and across the supraorbital region anteriorly.

Chest circumference was measured using a tape in both horizontal and vertical positions depending on the child's age. The reference points for the tape were: posteriorly – the lower angles of the scapulae, and anteriorly – at the level of the fourth rib at its junction with the sternum, above the mammary glands.

The obtained anthropometric data were compared using the ANTHRO software and UNICEF reference indicators. The ANTHRO software (version 3.2.2, 2012), used for pediatric anthropometric calculations, is widely applied worldwide[37,38].

In this study, the reference population was defined according to WHO growth standards. Each of the three indicators of a child's nutritional status can be expressed in standard deviation units (Z-scores) relative to the median of the reference population.

Weight-for-age is an indicator used to assess both acute and chronic malnutrition. Children are considered moderately or severely underweight if their weight-for-age falls more than two standard deviations below the median of the reference population. Children whose weight-for-age is more than three standard deviations below the reference median are classified as severely underweight.

Height-for-age is a measure of linear growth. Children are classified as moderately or severely stunted if their height-for-age is more than two standard deviations below the median of the reference population. Those whose height-for-age is more than three standard deviations below the reference median are considered severely stunted.

Weight-for-height is used to assess wasting and overweight. Children are classified as moderately or severely wasted if their weight-for-height is more than two standard deviations below the median of the reference population. If weight-for-height falls more than three standard deviations below the reference median, the condition is classified as severe wasting (hypotrophy). The hypotrophic form of dystrophy is typically associated with inadequate nutrition. This indicator is sensitive to seasonal variations, reflecting changes in food availability or the prevalence of disease.

Assessment of neuropsychological development (NPD) was carried out using the method proposed by G.V. Pantyukhina, K.L. Pechora, and E.L. Frucht (1996), which provides a qualitative evaluation of child development and categorization into age-specific neuropsychological development groups. During the first year of life, the following developmental stages were assessed: [33,34].

1.5–3 to 5–6 months – development of visual and auditory orientation responses, cooing, and hand movements;

5–6 to 9–10 months – development of gross motor skills, preparatory stages of passive and active speech, and object-related actions;

9–10 to 12 months – development of gross motor activity, speech comprehension and production, and interactions with objects.

Based on the above method, the questionnaires developed by us made it possible to assess the age at which children acquire the following skills: visual orientation reactions, auditory orientation responses, emotional responses, gross motor activity, hand movements and object manipulation, procedural skills, play and interaction with objects, speech comprehension, and active speech. For each child, the age at which each skill emerged was recorded. A comparative analysis of the obtained data was carried out against standard reference values used in this methodology. When determining the developmental group, deficits in any indicator within a particular developmental domain were taken into account.

To evaluate the effect of feeding type on morbidity during the first year of life, parental questionnaires were conducted, and medical records reflecting the child's development and hospital

history were analyzed. In addition, each child included in the study underwent individual assessment within the framework of our research.

In modern medicine, scientific research aimed at the early detection of diseases and the development of effective diagnostic methods is becoming increasingly relevant [38]. In particular, the advancement of non-invasive yet highly accurate diagnostic approaches remains a priority in all periods. Among these, the analysis of biological fluids—especially saliva—has gained considerable attention as a means of early disease detection, and numerous large-scale studies have been conducted in this field [39,40]. The present study is also carried out within this framework, focusing on the processes of dehydration and crystallization of biological fluids (primarily saliva, and, where necessary, blood and other samples).

One of the key aspects of the study is the establishment of a standardized system for sample collection and storage. The processes of obtaining, transporting, and preparing biological fluids for initial analysis were organized in strict accordance with international standards and hygiene requirements, ensuring the accuracy, reliability, and reproducibility of the results. Therefore, in this study, not only standardized procedures for sample collection were implemented, but also uniform storage conditions were maintained, taking into account the medical status of participants and adhering to strict hygiene protocols [41].

The crystallization properties of saliva are closely associated with metabolic processes, water–electrolyte balance, and the concentration of bioactive substances in the body. In infants and young children, the type of feeding has a direct influence on saliva composition, which is subsequently reflected in the morphological characteristics of crystal structures formed during dehydration [42].

Collection and storage of saliva samples. Saliva samples were collected from infants aged 6–36 months, with careful consideration given to their physiological characteristics, age-specific developmental stage, feeding regimen, and care conditions. Due to the limited voluntary motor control typical of this age group, direct contact and passive collection techniques were used for saliva sampling [43]. All procedures were carried out with written informed consent obtained from the parents of each infant. Prior to sample collection, caregivers (mothers or guardians) were informed about the hygienic requirements and scientific purpose of the procedure. Since saliva composition may vary significantly after feeding, sample collection was recommended at least 60 minutes after feeding [40,41].

For saliva collection, only sterile, single-use devices—saliva collection swabs—were used. These swabs are designed to be soft, non-fragile, and safe for use in infants, preventing accidental chewing or swallowing. Each swab and container was prepared in advance, labeled with unique identification codes, and sealed immediately after sample collection. Saliva collection was performed while the infant was calm and alert [36]. With the assistance of a caregiver, a soft sterile swab was gently placed in the infant's mouth, specifically in the lower jaw or cheek area, for approximately 2–3 minutes. During this time, the infant was soothed using visual and auditory interaction, allowing the swab to absorb saliva naturally through light chewing movements. A sufficient volume of saliva (at least 0.5–1 ml) was collected. After collection, each sample tube was labeled with an individual code or number to ensure confidentiality of personal data [38,39].

Additionally, specific data were recorded for each sample, including date of birth (age in months), sex, health status (based on medical records), type of feeding (breastfeeding, artificial, or mixed), and study group (control or main group).

Microscopic analysis. The digital microscope used in this study (see Figure 2.1) is a multifunctional device developed through the integration of modern technologies, including optical microscopy, an advanced photoelectric conversion system, and LCD display technology. Unlike traditional binocular optical observation, this microscope allows direct visualization of the microscopic field on a screen, significantly improving the efficiency of the observation process [39].

The microscope is equipped with a high-resolution 14-megapixel camera and utilizes a CMOS color image sensor capable of capturing images in HD quality. The device can be connected to a

computer via a USB 2.0 interface, enabling real-time image display at a speed of up to 480 Mb/s. This microscope is suitable for prolonged observation and detailed analysis [42,43].

Among compact microscope types, digital microscopes are particularly widespread, as their primary function is not only to magnify the observed object but also to provide high-quality image and video acquisition for scientific research purposes [52].

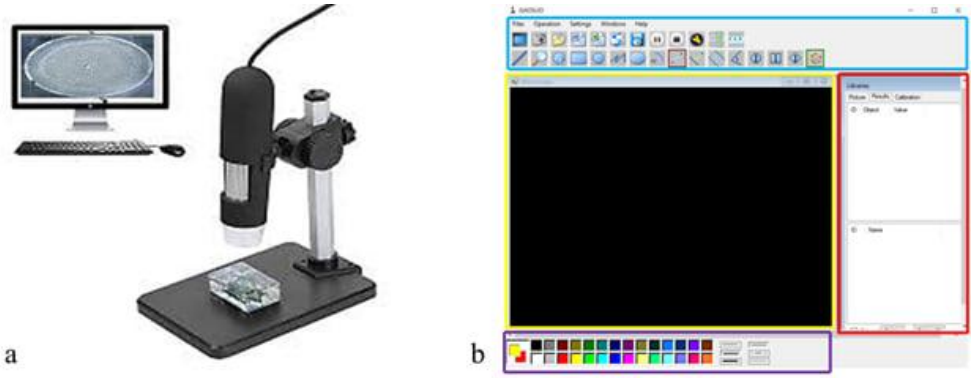


Figure 1. Figure 1a – digital microscope; Figure 1b – GAOSUO software interface: tools and settings window for working with digital microscope images

The digital microscope used in this study was placed inside a specially isolated chamber, which ensured the stability of the internal environment during the experiment. This design minimizes the influence of external factors such as temperature fluctuations, airflow, and humidity changes on the experimental process. As a result, optimal and stable conditions were created for observations carried out using the microscope. Inside the device, the temperature was maintained at 25 °C, while relative humidity was kept at approximately 32%. This made it possible to observe subtle physical changes occurring at the microscopic level without interference from external environmental factors [42]. The use of an isolated system ensures the reproducibility, reliability, and objectivity of the experiment.

Dehydration method. During the evaporation process, the selected substrate material significantly affects the characteristics of droplet dehydration. Studies indicate that surface properties, moisture resistance, and chemical inertness are key factors determining substrate performance. The glass surface used in this study is smooth, flat, and chemically inert, meaning it does not react with the saliva sample and does not interfere with evaporation or crystallization processes [42,43].

During sample preparation, the liquid was carefully applied onto the prepared glass substrate using a special dispenser (micropipette) (see Figure 2).



Figure 2. Droplet detachment and deposition onto the surface

The applied saliva droplet (typically around 50 μL) assumes its shape on the glass surface under the influence of natural forces—surface tension and adhesion—and spreads according to the open droplet model. Observations based on this model demonstrate that the evaporation rate differs significantly between the central region and the peripheral zones of the droplet. Evaporation occurs more rapidly at the periphery, which, under the influence of internal convective flows and surface forces, leads to the outward movement of molecules and ions from the center toward the edges [43].

Statistical analysis of research results

Statistical analysis was carried out using MS Office Excel 2007 and the STATISTICA for Windows 10 software package, in accordance with standard statistical methods. The level of significance was set at $p<0.05$. For normally distributed data, Student's t-test was applied to assess differences and to analyze dynamic changes both within groups and across the population. Correlation analysis was performed using Pearson's coefficient for normally distributed data and Spearman's coefficient for non-normal distributions.

Results were presented as M±m. For visualization of the results and primary morphological data, Microsoft Office charting tools and the graphical capabilities of STATISTICA for Windows were widely utilized. The significance level was set at $p<0.05$. Based on the results of all applied statistical criteria, clear conclusions were drawn regarding the presence or absence of statistically significant differences.

The obtained data were processed statistically using a Pentium-IV personal computer with Microsoft Office Excel 2010. Both parametric and non-parametric statistical methods were applied, including calculation of the mean (M), standard deviation (σ), standard error (m), and relative values (frequency, %). When comparing mean values, statistical significance was determined using the Student's t-test, taking into account variance analysis (Fisher's F-test) and distribution characteristics (including excess/kurtosis). The probability of error (R) was also considered. Quantitative data were analyzed to determine mean values and standard errors, with significance levels set at $R<0.05$ and $R<0.001$. For qualitative variables, statistical significance was assessed using the χ^2 (chi-square) test and the z-test.

Conclusion. The present study provides a multidimensional assessment of children's physical development by integrating classical anthropometric techniques with statistical analysis and morphofunctional diagnostics. The findings underscore that the type of feeding in early life constitutes a significant, yet not isolated, determinant of growth trajectories, influencing key indicators such as body weight, linear growth, and proportional development. However, the observed variations should be interpreted within a broader biopsychosocial context, as factors such as environmental conditions, genetic predisposition, and quality of complementary feeding may act as confounding variables.

A notable strength of the study lies in its methodological rigor, including adherence to WHO growth standards and the application of standardized measurement protocols, which enhances the validity and comparability of the results. At the same time, certain methodological limitations should be acknowledged. The cross-sectional nature of the analysis restricts the ability to establish causal relationships between feeding type and developmental outcomes. In addition, while the incorporation of saliva crystallization analysis represents an innovative and minimally invasive diagnostic approach, its clinical applicability and sensitivity require further validation through longitudinal and larger-scale studies.

The integration of anthropometric monitoring with emerging biofluid-based diagnostic methods demonstrates considerable potential for improving early detection of developmental deviations. Nevertheless, future research should prioritize longitudinal designs, expanded sample sizes, and the inclusion of additional biological and socioeconomic variables to strengthen the evidence base and ensure the generalizability of findings.

In conclusion, while the study contributes valuable insights into the relationship between feeding practices and child development, it also highlights the necessity for more comprehensive and methodologically robust investigations. The advancement of integrated diagnostic frameworks holds promise for enhancing pediatric monitoring systems, yet their practical implementation must be supported by further empirical validation and critical evaluation.

REFERENCES

1. Abolyan, L.V., et al. "Importance of exclusive breastfeeding for health, physical, and neuropsychological development of children in the first year of life (Example of Volgograd)" // Pediatrics. – 2005. – Vol. 54. № 5. pp. 53-57.

2. Abolyan, L.V., Novikova, S.V. "Modern aspects of breastfeeding" // Pediatrics. – 2011. – Vol. 90. – №1. pp. 80-83.

3. Abolyan, L.V., Novikova, S.V., et al. "At the origins of health: Organization of breastfeeding in obstetric and pediatric medical institutions" – 2017. №3. pp. 35-41.

4. Amirova, V.R., Gizdatullina, K.Kh. "Quality of life indicators of infants depending on the duration of breastfeeding" // Issues of Children's Dietology. – 2011. – Vol. 9. № 6. pp. 9-11.

5. Baskakova, E.Yu. "Features of physical development, actual nutrition, and metabolic disorders in children depending on the nature of nutrition in infancy": Abstract of the dissertation. Specialty: 14.01.08, Novgorod, 2012. – 26 p.

6. Baturin, A.K., Netrebenko, O.K. "Practices of feeding children in the first two years of life in the Russian Federation" // Pediatrics. – 2010. № 3. pp. 99-105.

7. Baturin, A.K., Tutelyan, V.A. "Assessment of nutritional status and feeding conditions of infants and young children in the Russian Federation" // Problems of Nutrition. – 2010. № 6. pp. 57-63.

8. Belmer, S.V. "Complementary feeding: Significance for adaptation processes and principles of introduction" // Issues of Children's Dietology. – 2014. Vol. 12.

9. Belmer, S.V. "Controversial questions and real answers about infant nutrition products" // Bulletin of Russian Perinatology and Pediatrics.–2015.№ 5. pp.121-126.

10. Belmer, S.V. "Modern concept of complementary feeding" // Issues of Children's Dietology. – 2014. Vol. 12. № 5. pp. 60-65.

11. Bocharova, T.I., Cherezova, S.A. "Assessment of nutrition of children in the first year of life" / Materials of the XI Russian Forum with international participation "Healthy nutrition from birth: medicine, education, food technologies." – St. Petersburg, 2016. – pp. 26-27.

12. Bogomolova, E.S., Leonov, A.V., Kuzmichev, Yu.G. "Assessment of physical development of children and adolescents" / Novgorod: 2006. – 260 p.

13. Borovik, T.E., Ladodo, K.S., Semenova, N.N. "Baby food: Present and future" // Russian Pediatric Journal. – 2011. Issue 3. pp. 4-10.

14. Borovik, T.E., Skvortsova, V.A., Netrebenko, O.K. "Complementary foods in infant feeding" // Pediatrics. – 2008. – Vol. 87. № 4. pp. 79-85.

15. Bulatova, E.M. "Feeding young children in modern conditions": Abstract of the dissertation for the degree of Doctor of Medical Sciences: 14.00.09. – St. Petersburg, 2005. – 50 p.

16. Burova, O.N. "Development of scientific foundations for optimizing infant feeding in a children's clinic": Dissertation for the degree of Candidate of Medical Sciences: 14.01.08, 14.02.03. – N. Novgorod, 2015. – 192 p.

17. Durmashkina, A.P. "Long-term consequences of feeding children in infancy with unadapted dairy products": Abstract of the dissertation for Candidate of Medical Sciences. – Nizhny Novgorod, 2009. – 26 p.

18. Evdokimova, T.A., Sorvacheva, T.N. "The first complementary feeding: a personalized approach against strict rules" // Issues of Children's Dietology. – 2016. № 5. pp. 36-41.
19. Gizdatullina, K.Kh., Amirova, V.R. "Quality of life indicators of infants depending on the duration of breastfeeding" // Issues of Children's Dietology. – 2011. № 6. pp. 9-11.
20. Gizdatullina, K.Kh., Amirova, V.R. "Quality of life indicators of infants depending on the level of physical and neuropsychological development" // Bashkortostan Medical Bulletin. – 2011. Issue 6. pp. 35-39.
21. Glantz, S. "Medical and Biological Statistics" / Translated from English – M.: Praktika, 1998. – 459 p.
22. Gonchar, N.V., et al. "Quality of life of children in the first year of life as a criterion of health status" // Issues of Children's Dietology. – 2015. № 2. – pp. 68-69.
23. Gordeev, V.I., Aleksandrovich, Yu.S. "The state of the concept of 'quality of life' in pediatrics" // Research on quality of life in medicine: materials of a scientific conference. – St. Petersburg, 2000. – pp. 38-39.
24. Jumagaziyev, A.A., Rozhkova, O.N., Kozina, T.F. "The importance of breastfeeding and the psychological unity of mother and child for neuropsychological development" // Surveys on children's diets. – 2004. – Vol. 2. № 6. pp. 13-15.
25. Keshishyan, E.S. "Modern views on the introduction of complementary foods to children in the first year of life" // Bulletin of Russian Perinatology and Pediatrics. – 2010. – Vol. 55. № 4. pp. 98-100.
26. Kon, I.Ya., et al. "Clinical and physiological substantiation of a new scheme for introducing complementary foods" // Dietology. – 2011. № 9(3). – pp. 23-28.
27. Kondratyeva, E.I., Stankevich, S.S. "Differentiated approach to the introduction of complementary foods" // Questions of Modern Pediatrics. – 2013. – Vol. 12. Issue 5. – pp. 66-73.
28. Kopeikin, V.N. "Problems of child nutrition in the first year of life" // Bulletin of Russian Perinatology and Pediatrics. – 2013. № 4. pp. 108-111.
29. Kozhevnikova, E.N., Nikolaeva, S.V., Elezova, L.I. "Complete complementary feeding is an important component of healthy nutrition for children in the first year of life" // Pediatrics: Supplement to the Consilium Medicum journal. – 2012. Issue 2. – pp. 19-20.
30. Kozlovsky, A.A., Kozlovsky, D.A., Kozlovskaya, I.A. "Feeding children in the first year of life: problems and ways to solve them" // Problems of Health and Ecology. – 2016. Issue 3 (49). pp. 81-85.
31. Kulakova, N.I., et al. "On the issue of the quality of life of children in the first year of life" // Issues of Practical Pediatrics. – 2010. – Vol. 5. № 1. pp. 89-90.
32. Law of the Republic of Tajikistan "On the protection of public child services," 2006.
33. Lazareva, E.P. "Development of approaches for the prevention of nutrition-related diseases in children in the first year of life": Abstract of the dissertation for Candidate of Medical Sciences. – Nizhny Novgorod, 2006. – 26 p.
34. Mikheeva, I.G., et al. "Influence of breastfeeding on the neuropsychological development of children in the first year of life" // Pediatrics named after G.P. Speransky. – 2003. № 6. pp. 83-85.
№ 2. pp. 50-56.
35. Okhunova, M.T. "Assistance potential of the resources of the Republic of Tajikistan" // Healthcare of Tajikistan. – 2008. Issue 1. pp. 56-59.
36. Okhunova, M.T. "Medical, biological, and social aspects of information in the Republic of Tajikistan": Abstract of the dissertation for the degree of Candidate of Medical Sciences: Dushanbe, 2000. – 26 p.
37. Speransky, G.N., et al. "Possibility of changing the current scheme for introducing complementary foods: clinical evaluation" // Pediatrics journal. – 2013. – Vol. 92. № 3. pp. 67-72.

38. Vasyutin, K.A. "Health status of children with different diets in the first year of life" // Vyatka Medical Bulletin. – 2009. Issue 1. 62 p.

39. Veltishchev, Yu.E. "Child growth: patterns, normal variations, somatotypes, disorders, and their correction": Lecture for physicians // Bulletin of Perinatology and Pediatrics: Moscow. Research Institute of Pediatrics and Pediatric Surgery, 2000. – p. 97.

40. Vinyarskaya, I.V. "Quality of life of children as a criterion for assessing health status and effectiveness of medical technologies (comprehensive medical and social research)": Abstract of the dissertation for the degree of Doctor of Medical Sciences. – M., 2008. – 50 p.

41. Vorontsov, I.M., Fateeva, E.M. "Natural feeding of children, its importance and support" / St. Petersburg: 2006. – 260 p.

42. Zaprudnov, A.M., Grigoryev, K.I. "Does the nutrition program shape the child's future health? Reflections on the release of a new monograph" // Issues of Children's Dietology. – 2016. Issue 4. pp. 55-58.

43. Zhurba, L.T., Mastyukova, E.M. "Disorders of psychomotor development in children in the first year of life." – M., 1981. – 272 p.

MODERN APPROACHES TO ENAMEL REMINERALIZATION IN PEDIATRIC DENTISTRY: PREVENTIVE STRATEGIES AND DIAGNOSTIC ASSESSMENT

Surat S. Gulyamov - D.M.Sc., professor
Azizbek U. Jabborov - doctoral student
Tashkent State Medical University (Tashkent, Uzbekistan)
a_jabborov99@mail.ru

Abstract. *Dental caries remains one of the most prevalent oral diseases in childhood. Early carious lesions are characterized by subsurface enamel demineralization while the surface layer remains relatively intact, creating the potential for non-invasive management through remineralization therapy.*

This review summarizes current evidence on preventive and remineralizing agents used in pediatric dentistry, including fluoride-based products, calcium-phosphate systems, and arginine-containing formulations. Particular attention is paid to factors affecting fluoride bioavailability, the role of salivary mineral ions in enamel repair, and modern instrumental approaches for evaluating remineralization, including quantitative light-induced fluorescence (QLF).

The analysis of recent literature highlights the importance of a multifactorial preventive strategy combining fluoride exposure, calcium-phosphate delivery systems, and plaque pH modulation. Objective diagnostic methods are increasingly important for monitoring the effectiveness of preventive interventions.

Understanding the mechanisms and comparative effectiveness of different remineralizing agents may improve preventive protocols and contribute to more personalized approaches to caries management in children.

Keywords: *pediatric dentistry, enamel remineralization, fluoride, calcium-phosphate systems, arginine, preventive dentistry, QLF.*

Aim of the review.

To summarize and critically analyze contemporary preventive approaches to enamel remineralization in children, focusing on the effectiveness of fluoride-containing agents, calcium-phosphate technologies, and arginine-based formulations used in modern pediatric dentistry.

Discussion.

Dental caries in children remains a multifactorial disease influenced by the interaction between dental biofilm, dietary carbohydrates, host factors, and time. The initial stage of caries development is characterized by subsurface enamel demineralization caused by organic acids produced by cariogenic microorganisms. Importantly, this process is reversible at early stages, which provides the biological basis for remineralization therapy.

Remineralization is a dynamic process involving the redeposition of calcium and phosphate ions into partially demineralized enamel. This process is largely dependent on the physicochemical properties of saliva, including its buffering capacity, mineral content, and flow rate. Saliva acts as a natural reservoir of calcium and phosphate ions and plays a critical role in maintaining enamel integrity.

Fluoride remains the most extensively studied and widely used agent in caries prevention. Its mechanism of action includes enhancing remineralization, inhibiting demineralization, and reducing bacterial metabolic activity. Fluoride ions promote the formation of fluorapatite-like crystals, which are more resistant to кислотному воздействию than hydroxyapatite. However, recent research indicates that the effectiveness of fluoride is not solely determined by its concentration but also by its bioavailability in the oral environment.

Bioavailability of fluoride depends on several factors, including the formulation of toothpaste, presence of abrasives, and interactions with calcium compounds. Some formulations may reduce the amount of free fluoride ions available for enamel uptake, thereby limiting their therapeutic effect. Therefore, optimization of fluoride delivery systems is a key area of contemporary research.

In addition to fluoride, calcium-phosphate-based systems have gained increasing attention as adjunctive remineralizing agents. Technologies such as casein phosphopeptide-amorphous calcium phosphate (CPP-ACP), functionalized tricalcium phosphate, and nano-hydroxyapatite are designed to enhance the availability of calcium and phosphate ions at the tooth surface. These agents can act as reservoirs, releasing ions during acid challenges and facilitating enamel repair.

Nano-hydroxyapatite, in particular, has been shown to mimic the natural structure of enamel crystals and may integrate into the enamel matrix, contributing to surface repair and reduction of hypersensitivity. Similarly, CPP-ACP complexes stabilize calcium and phosphate ions in an amorphous state, increasing their bioavailability and promoting remineralization.

Arginine-containing formulations represent another promising approach in modern preventive dentistry. Arginine is metabolized by specific oral bacteria, leading to the production of ammonia and an increase in plaque pH. This alkalinizing effect counteracts acidogenic activity and creates a favorable environment for remineralization. Clinical studies suggest that arginine-based toothpastes may reduce caries risk when used in combination with fluoride.

The role of dental biofilm in caries development has led to a shift in preventive strategies toward ecological approaches aimed at modifying the oral microbiome rather than simply eliminating bacteria. Remineralization therapy is therefore increasingly considered part of a broader strategy that includes plaque control, dietary modification, and регулярное использование профилактических средств.

Modern diagnostic technologies have significantly improved the ability to detect and monitor early carious lesions. Quantitative light-induced fluorescence (QLF) allows for objective assessment of changes in enamel mineralization by measuring fluorescence loss associated with demineralization. This method enables early detection of lesions that are not visible clinically and provides a quantitative tool for evaluating the effectiveness of preventive interventions over time.

Other diagnostic systems, such as laser fluorescence devices and digital imaging techniques, complement traditional clinical examination and enhance the accuracy of early caries detection. The integration of these technologies into clinical practice supports minimally invasive dentistry and facilitates personalized treatment planning.

An important aspect of pediatric dentistry is patient compliance, which significantly influences the effectiveness of preventive measures. Factors such as taste, ease of use, and parental supervision play a critical role in the regular use of remineralizing agents. Therefore, the selection of preventive products should consider not only their clinical efficacy but also their acceptability for children.

Furthermore, socioeconomic and behavioral factors must be taken into account when developing preventive strategies. Access to fluoride-containing products, oral hygiene habits, and dietary patterns vary widely among populations and can influence caries risk. A comprehensive preventive approach should therefore be tailored to individual patient needs and risk profiles.

Recent trends in pediatric dentistry emphasize personalized and risk-based approaches to caries management. Caries risk assessment tools allow clinicians to categorize patients and select appropriate preventive interventions accordingly. In high-risk children, the combined use of fluoride, calcium-phosphate systems, and antibacterial agents may provide synergistic effects and improve clinical outcomes.

Conclusion.

Remineralization therapy represents a cornerstone of modern minimally invasive dentistry and plays a crucial role in the management of early carious lesions in children. The current evidence

supports the effectiveness of fluoride-containing products as the primary preventive measure, while highlighting the additional benefits of calcium-phosphate systems and arginine-based formulations.

The success of remineralization strategies depends on multiple factors, including the bioavailability of active ions, salivary composition, plaque pH, and patient compliance. Modern diagnostic methods, such as QLF, provide valuable tools for early detection and monitoring of enamel changes, enabling more precise and individualized preventive care.

Future research should focus on comparative clinical trials evaluating the long-term effectiveness of different remineralizing technologies, as well as the development of optimized delivery systems that enhance ion bioavailability. The integration of preventive, diagnostic, and personalized approaches will contribute to improved oral health outcomes in pediatric populations.

REFERENCES

1. Amaechi B.T. Remineralization therapies for initial caries lesions. Compendium of Continuing Education in Dentistry. 2015;36(1):14–17.

2. Meyer-Lueckel H., Paris S., Ekstrand K. Caries Management – Science and Clinical Practice. Thieme Medical Publishers. 2013.

3. Pretty I.A., Ellwood R.P. The use of quantitative light-induced fluorescence (QLF) in early caries detection. Journal of Dentistry. 2013;41(2):S10–S15.

4. Pitts N.B., Ekstrand K.R. International Caries Detection and Assessment System (ICDAS). Community Dentistry and Oral Epidemiology. 2013;41(1):e41–e52.

5. World Health Organization. Global Oral Health Status Report. Geneva: WHO; 2022.

UDK: 618.3-06:616-005.1:618.36-008.9:616-092:615.273.53

EARLY GESTATIONAL BLEEDING AND SUBCHORIONIC HEMATOMA AS PREDICTORS OF FETAL GROWTH RESTRICTION: PATHOGENETIC MECHANISMS AND THE ROLE OF LOW-DOSE ASPIRIN

Dilfuzakhon N. Shukurkhujaeva - assistant
Tashkent State Medical University (Tashkent, Uzbekistan)
meddoctor7sh@mail.ru

Abstract. *Early gestational bleeding, including bleeding associated with subchorionic hematoma, is one of the most common complications of the first trimester of pregnancy and is increasingly regarded as a marker of impaired implantation and abnormal placentation. Growing evidence indicates that disturbances occurring during early placental development predispose to placental insufficiency, fetal growth restriction (FGR), and the delivery of infants with low birth weight. Subchorionic hematoma represents a localised manifestation of defective trophoblastic attachment and altered uteroplacental perfusion, and its presence has been associated with adverse perinatal outcomes, particularly in cases involving large hematoma volume or early gestational age at diagnosis.*

Low-dose acetylsalicylic acid (ASA) is widely used to prevent placental-mediated complications, including preeclampsia and FGR, due to its antiplatelet and vasodilatory effects. However, the use of ASA during early pregnancy remains controversial, as emerging data suggest a potential association with increased risk of subchorionic hematoma formation. This article reviews current evidence regarding the relationship between early pregnancy bleeding, subchorionic hematoma, placental insufficiency, and fetal growth restriction, with particular emphasis on the benefits and limitations of low-dose ASA in modifying perinatal risk and improving pregnancy outcomes.

Keywords: *early pregnancy bleeding, subchorionic hematoma, placental insufficiency, fetal growth restriction, low birth weight, low-dose aspirin.*

Introduction. Improvement of perinatal outcomes remains a major objective of modern obstetrics and perinatal medicine [1]. Over recent decades, clinical focus has shifted from the prevention of perinatal mortality alone toward optimisation of fetal development and reduction of long-term morbidity associated with adverse intrauterine conditions [2]. Among these conditions, fetal growth restriction occupies a central position due to its strong association with neonatal complications, neurodevelopmental impairment, and increased risk of chronic diseases in adulthood. Fetal growth restriction (FGR) remains one of the leading causes of perinatal morbidity and long-term adverse health outcomes [3]. Increasing evidence indicates that the origins of FGR lie in early gestation, during implantation and placental development [4].

Accumulating evidence suggests that the origins of FGR lie predominantly in early gestation, during the critical period of implantation and placental development [5]. Vaginal bleeding in the first trimester, observed in up to 25% of pregnancies, represents one of the earliest clinical manifestations of abnormal placentation [2,3]. Subchorionic hematoma, the most frequent ultrasound finding in women presenting with early pregnancy bleeding, has therefore attracted considerable attention as a potential marker of placental dysfunction and subsequent adverse perinatal outcomes [4–6].

At the same time, low-dose acetylsalicylic acid has become a cornerstone of preventive strategies targeting placental-mediated complications [7]. While its efficacy in reducing the incidence of preeclampsia and, in some populations, FGR is well established [8], uncertainty remains regarding the optimal timing of ASA initiation, particularly in women with early gestational bleeding or

subchorionic hematoma [9]. Low-dose acetylsalicylic acid (ASA) is widely used to prevent placental-mediated complications such as preeclampsia and FGR [10]. Understanding the complex interactions between early bleeding, placental development, FGR, and aspirin therapy is essential for improving individualised pregnancy management.

Vaginal bleeding during the first trimester is a frequent reason for obstetric consultation and is reported in approximately 15–25% of clinically recognised pregnancies [2,3]. The early gestational period encompasses implantation, trophoblast invasion, remodelling of spiral arteries, and establishment of the uteroplacental circulation [11]. Any disruption of these processes may have long-lasting consequences for placental structure and function.

Although spontaneous pregnancy loss remains the most immediate concern in women with early bleeding, increasing attention has been directed toward the long-term outcomes of ongoing pregnancies [2,8]. Numerous studies have demonstrated that first-trimester bleeding is associated with higher risks of preterm birth, placental abruption, low birth weight, and fetal growth restriction [2,3,8]. These associations persist even after exclusion of pregnancies ending in early miscarriage, supporting the concept that early bleeding reflects underlying placental pathology rather than an isolated event [8].

The aetiology of early gestational bleeding is multifactorial and includes chromosomal abnormalities, endocrine disorders, immunological mechanisms, infectious and inflammatory conditions, and extragenital maternal pathology [1,9]. However, in a substantial proportion of cases, no definitive cause can be identified, further complicating risk stratification and clinical decision-making [2,3].

Subchorionic hematoma is defined as an accumulation of blood between the chorionic membrane and the uterine wall resulting from partial detachment of the trophoblast from the endometrium [4]. Sonographically, SCH appears as a hypoechoic or anechoic area adjacent to the gestational sac, occasionally containing echogenic components corresponding to clotted blood [7].

Reported prevalence of SCH varies widely, ranging from less than 1% in asymptomatic pregnant women to approximately 20% among those presenting with threatened miscarriage [4–6]. This variability reflects differences in study populations, ultrasound resolution, gestational age at examination, and diagnostic criteria [5,6].

Ultrasonography remains the gold standard for SCH diagnosis and follow-up [4,7]. Advances in imaging technology have substantially improved detection rates, suggesting that earlier reports may have underestimated true prevalence [7]. Serial ultrasound examinations are often used to monitor hematoma size, location, and resolution, as these parameters may influence pregnancy prognosis [6,10].

The clinical significance of SCH remains a subject of ongoing debate [5,6,10]. Numerous studies have demonstrated associations between SCH and adverse pregnancy outcomes, including spontaneous miscarriage, placental abruption, preterm birth, and fetal growth impairment [5,6,8,10]. Meta-analyses consistently confirm an increased risk of early pregnancy loss in women with SCH, particularly when hematomas are large or diagnosed at earlier gestational ages [5,10].

The relationship between SCH and fetal growth restriction is of particular interest. Several investigators have reported lower birth weights, increased rates of FGR, and higher neonatal intensive care unit admission rates among infants born after pregnancies complicated by SCH [5,6,10]. These findings support the hypothesis that SCH represents a marker of impaired placentation and persistent uteroplacental dysfunction [9,10].

Hematoma size appears to be one of the most important prognostic factors. Large hematomas occupying a substantial proportion of the gestational sac have been associated with significantly poorer outcomes compared to smaller lesions [6,12]. Gestational age at diagnosis also plays a role, with earlier detection generally indicating a higher risk of adverse outcomes [6,10].

Placental insufficiency is widely regarded as the principal mechanism linking early gestational bleeding and SCH with fetal growth restriction [9,11–13]. Abnormal trophoblast invasion and inadequate remodelling of spiral arteries result in reduced uteroplacental blood flow, chronic fetal hypoxia, and impaired nutrient transfer [9,12].

In pregnancies complicated by SCH, local bleeding and hematoma formation may further exacerbate placental hypoperfusion by increasing oxidative stress, inflammation, and mechanical disruption at the maternal–fetal interface [9,10,14]. Elevated levels of pro-inflammatory cytokines, such as interleukin-1, interleukin-8, and tumour necrosis factor, have been implicated in disturbances of uteroplacental hemostasis and immune tolerance, contributing to placental dysfunction [12].

FGR accounts for nearly one-third of all low birth weight neonates and is associated with increased perinatal morbidity and long-term health consequences, including cardiovascular and metabolic disease in adulthood [15,16]. Ultrasound-based fetal biometry remains the diagnostic gold standard, as clinical assessment alone detects only a minority of affected pregnancies [17].

Fetal growth restriction is therefore increasingly viewed as a clinical manifestation of placental insufficiency rather than an isolated fetal condition [11,13]. This paradigm shift has important implications for early risk assessment and preventive strategies.

According to World Health Organisation data, the prevalence of FGR varies widely across regions, exceeding 30% in some low-resource settings and remaining below 7% in developed European countries [15]. In the United States, FGR is diagnosed in approximately 10–15% of births, while reported rates in the Russian Federation range from 2.4% to 17% [11,13].

Infants with FGR account for nearly one-third of all low birth weight neonates and are at increased risk of perinatal morbidity, including respiratory distress, hypoglycemia, hypothermia, and intrapartum hypoxia [11,13]. Long-term consequences include impaired neurodevelopment, increased susceptibility to cardiovascular and metabolic diseases, and reduced life expectancy [16].

Accurate diagnosis of FGR relies on precise determination of gestational age and ultrasound-based fetal biometry [11,13,14]. Clinical assessment alone identifies only a minority of affected pregnancies, underscoring the importance of early and repeated ultrasound evaluation in high-risk populations [14].

Acetylsalicylic acid exerts its primary effect through irreversible inhibition of platelet cyclooxygenase, leading to reduced thromboxane A_2 synthesis and decreased platelet aggregation [18]. These effects improve microcirculatory blood flow and provide a physiological basis for ASA use in preventing placental-mediated complications [19]. At low doses, ASA selectively inhibits thromboxane production while preserving prostacyclin activity, resulting in vasodilation and improved microcirculatory perfusion [20].

In the context of pregnancy, low-dose ASA has been shown to enhance uteroplacental blood flow, promote spiral artery remodelling, and reduce the formation of microthrombi in the placental circulation [17–19]. These effects provide a strong physiological rationale for its use in preventing placental-mediated complications, including preeclampsia and FGR [17–20]. Meta-analyses demonstrate that ASA initiated before 16 weeks of gestation significantly reduces the incidence of preeclampsia and, in selected high-risk populations, fetal growth restriction and preterm birth [21].

Multiple randomised controlled trials and meta-analyses have demonstrated that initiation of low-dose ASA before 16 weeks of gestation reduces the incidence of preeclampsia, particularly its early-onset form [17–19]. Importantly, several studies have also reported a reduction in the risk of FGR and preterm birth, especially in women at high risk of placental insufficiency [22].

Current clinical guidelines recommend low-dose ASA for women with established risk factors for placental-mediated complications, including a history of preeclampsia or FGR, chronic hypertension, diabetes mellitus, autoimmune disorders, renal disease, and multifetal gestation [23]. These recommendations reflect the growing recognition of ASA as a key component of preventive obstetric care.

Despite its benefits, the use of ASA during the first trimester remains controversial. Emerging evidence suggests that ASA may increase the likelihood of subchorionic hematoma formation, particularly when initiated early in gestation [24]. This association raises concerns regarding the balance between potential benefits in improving placental perfusion and the risk of exacerbating bleeding-related complications.

Several observational studies have reported higher rates of SCH in women receiving antiplatelet or anticoagulant therapy during early pregnancy [22,24]. While causality has not been definitively established, these findings suggest that careful consideration of timing, dosage, and individual risk factors is essential.

Some authors advocate postponing ASA initiation until the second trimester in women presenting with active vaginal bleeding or SCH, particularly when hematomas are large or persistent [25]. However, robust prospective data addressing this issue are currently lacking. Although a direct causal relationship has not been definitively established, these findings raise concerns regarding ASA initiation in women with active vaginal bleeding or large SCH.

Women with early gestational bleeding or SCH should be considered at increased risk of placental insufficiency and FGR [5,6,10]. Serial ultrasound monitoring of placental structure, uteroplacental blood flow, and fetal growth is recommended in these pregnancies. Doppler assessment of uterine and umbilical arteries may provide additional prognostic information [14]. SCH should therefore be regarded as a localised manifestation of abnormal placentation rather than an isolated ultrasound finding.

The decision to initiate or continue low-dose ASA should be individualised, taking into account the severity of bleeding, hematoma characteristics, and the presence of established risk factors for placental-mediated complications [17–21,24]. Multidisciplinary management involving obstetricians, maternal–fetal medicine specialists, and, when necessary, haematologists may optimise outcomes in high-risk cases.

First-trimester vaginal bleeding has been consistently associated with an increased risk of adverse pregnancy outcomes, including spontaneous miscarriage, preterm birth, placental abruption, and low birth weight [2,3,8]. Population-based studies demonstrate that even when pregnancy continues beyond the first trimester, early bleeding is associated with reduced gestational age at delivery and impaired fetal growth [2,8].

Conclusion. Early gestational bleeding, particularly when associated with subchorionic hematoma, represents an important clinical marker of abnormal placentation and increased risk of fetal growth restriction. Placental insufficiency serves as the central pathogenetic link between early pregnancy complications and adverse perinatal outcomes.

Low-dose aspirin offers a promising strategy for improving uteroplacental perfusion and reducing the risk of FGR; however, its use in early pregnancy requires careful risk–benefit assessment due to a potential association with bleeding-related complications. Personalised management, early identification of high-risk pregnancies, and further prospective research are essential for optimising the use of aspirin and improving perinatal outcomes. Early identification of high-risk pregnancies and tailored preventive strategies are essential for improving perinatal outcomes.

REFERENCES

1. Ananth CV, Savitz DA. Vaginal bleeding and adverse reproductive outcomes: a meta-analysis. Paediatr Perinat Epidemiol. 1994;8:62–78. doi: 10.1111/j.1365-3016.1994.tb00436.x.

2. Basama FM, Crosfill F. The outcome of pregnancies in 182 women with threatened miscarriage. Arch Gynecol Obstet. 2004;270:86–90. doi: 10.1007/s00404-003-0475-z.

3. Bennett GL, Bromley B, Lieberman E, Benacerraf BR. Subchorionic haemorrhage in first-trimester pregnancies: prediction of pregnancy outcome with sonography. Radiology. 1996;200:803–6. doi: 10.1148/radiology. 200.3.8756935.

4. Berkowitz GS, Harlap S, Beck GJ, Freeman DH, Baras M. Early gestational bleeding and pregnancy outcome: a multivariable analysis. Int J Epidemiol. 1983;12:165–73. doi: 10.1093/ije/12.2.165.

5. Chung TK, Sahota DS, Lau TK, Mongelli JM, Spencer JA, Haines CJ. Threatened abortion: prediction of viability based on signs and symptoms. Aust N Z J Obstet Gynaecol. 1999;39:443–7. doi: 10.1111/j.1479-828x.1999.tb03129.x.

6. Csapo AI, Pulkkinen M. Indispensability of the human corpus luteum in the maintenance of early pregnancy. Luteectomy evidence. Obstet Gynecol Surv. 1978;33:69–81. doi: 10.1097/00006254-197802000-00001.

7. Everett C. Incidence and outcome of bleeding before the 20th week of pregnancy: prospective study from general practice. Bmj. 1997;315:32–4. doi: 10.1136/bmj. 315.7099.32.

8. Gracia CR, Sammel MD, Chittams J, Hummel AC, Shaunik A, Barnhart KT. Risk factors for spontaneous abortion in early symptomatic first-trimester pregnancies. Obstet Gynecol. 2005;106:993–9. doi: 10.1097/01.AOG.0000183604.09922.e0.

9. Henderson JT, Whitlock EP, O'Connor E, et al. Low-dose aspirin for prevention of morbidity and mortality from preeclampsia. *Ann Intern Med.* 2014;160(10):695–703.

10. Hertz JB, Heisterberg L. The outcome of pregnancy after a threatened abortion. Acta Obstet Gynecol Scand. 1985;64:151–6. doi: 10.3109/00016348509154709.

11. Hoffman CS, Messer LC, Mendola P, Savitz DA, Herring AH, Hartmann KE. Comparison of gestational age at birth based on last menstrual period and ultrasound during the first trimester. Paediatr Perinat Epidemiol. 2008;22:587–96. doi: 10.1111/j.1365-3016.2008.00965.x.

12. Jauniaux E, Johns J, Burton GJ. The role of ultrasound imaging in diagnosing and investigating early pregnancy failure. Ultrasound Obstet Gynecol. 2005;25:613–24. doi: 10.1002/uog.1892.

13. Jauniaux E, Poston L, Burton GJ. Placental-related diseases of pregnancy: Involvement of oxidative stress and implications in human evolution. Hum Reprod Update. 2006;12:747–55. doi: 10.1093/humupd/dml016.

14. Pawloski LR, Kitsantas P. Classification tree analysis of stunting in Malian adolescent girls. Am J Hum Biol. 2008;20:285–91. doi: 10.1002/ajhb. 20716.

15. Rai R, Cohen H, Dave M, Regan L. Randomised controlled trial of aspirin and aspirin plus heparin in pregnant women with recurrent miscarriage associated with antiphospholipid antibodies. *BMJ.* 1997;314(7076):253–257.

16. Saccone G, Berghella V. Aspirin for the prevention of preterm and term preeclampsia: systematic review and meta-analysis. *Am J Obstet Gynecol.* 2016;214(4):533–543.

17. Seong HS, Lee SE, Kang JH, Romero R, Yoon BH. The frequency of microbial invasion of the amniotic cavity and histologic chorioamnionitis in women at term with intact membranes in the presence or absence of labour. Am J Obstet Gynecol. 2008;199:375, e1–5. doi: 10.1016/j.ajog.2008.06.040.

18. Sipila P, Hartikainen-Sorri AL, Oja H, Von Wendt L. Perinatal outcome of pregnancies complicated by vaginal bleeding. Br J Obstet Gynaecol. 1992;99:959–63. doi: 10.1111/j.1471-0528.1992.tb13697.x.

19. South J, Naldrett J. The effect of vaginal bleeding in early pregnancy on the infant born after the 28th week of pregnancy. J Obstet Gynaecol Br Commonw. 1973;80:236–41. doi: 10.1111/j.1471-0528.1973.tb02191.x.

20. Strobino BA, Pantel-Silverman J. First-trimester vaginal bleeding and the loss of chromosomally normal and abnormal conceptions. Am J Obstet Gynecol. 1987;157:1150–4. doi: 10.1016/s0002-9378(87)80280-6.

21. Tongsong T, Srisomboon J, Wanapirak C, Sirichotiyakul S, Pongsatha S, Polsrisuthikul T. Pregnancy outcome of threatened abortion with demonstrable fetal cardiac activity: a cohort study. J Obstet Gynaecol. 1995;21:331–5. doi: 10.1111/j.1447-0756.1995.tb01019.x.

22. van Doorn R, Mukri F, Heymans MW, et al. Low-dose aspirin use in the first trimester and risk of subchorionic hematoma. *Ultrasound Obstet Gynecol.* 2018;52(1):86–91.

23. Weiss JL, Malone FD, Vidaver J, et al. Threatened abortion: A risk factor for poor pregnancy outcome, a population-based screening study. Am J Obstet Gynecol. 2004;190:745–50. doi: 10.1016/j.ajog.2003.09.023.

24. Williams MA, Mittendorf R, Lieberman E, Monson RR. Adverse infant outcomes associated with first-trimester vaginal bleeding. Obstet Gynecol. 1991;78:14–8.

25. Yang J, Hartmann KE, Savitz DA, et al. Vaginal bleeding during pregnancy and preterm birth. Am J Epidemiol. 2004;160:118–25. doi: 10.1093/aje/kwh180.

A NOVEL APPROACH TO THE REHABILITATION OF PATIENTS AFTER SURGICAL TREATMENT OF INTERVERTEBRAL DISC HERNIATION

Khasan A. Tilyakov - D.M.Sc., associate professor
Research Institute of Rehabilitation and Sports Medicine, Samarkand State Medical University (Samarkand, Uzbekistan)
Utkir R. Khushmuradov - independent researcher
Perfect Diagnostic Clinic (Samarkand, Uzbekistan)
jurabektravm@gmail.com

Abstract: *This article presents the results of a clinical study aimed at improving the effectiveness of rehabilitation in patients following surgical treatment of lumbar intervertebral disc herniation. A total of 52 patients were examined and divided into a study group (n = 27) and a control group (n = 25); all patients received standard therapy (NSAIDs, kinesiotherapy, hydrokinesiotherapy), while patients in the study group additionally underwent a course of general magnetotherapy (UMTI-3F "Kolibri-Expert" device, 8–10 sessions, magnetic induction 1–3.5 mT). Outcomes were assessed using the VAS pain scale, the SAN questionnaire, the Oswestry Disability Index, and infrared thermography. The study established that adding general magnetotherapy to the rehabilitation program provided a significantly more pronounced regression of pain syndrome (complete resolution in 51.9% of cases versus 28% in the control group), accelerated the normalization of local hemodynamics in the surgical area, and reduced the degree of functional disability, confirming the feasibility of this approach in early postoperative rehabilitation.*

Keywords: *discectomy; intervertebral disc herniation; general magnetotherapy; rehabilitation; lumbar spine.*

Introduction Degenerative-dystrophic diseases of the spine are among the most common pathologies of the musculoskeletal system and represent a serious medical and social problem due to their high prevalence, prolonged periods of temporary disability, and a significant risk of disability in patients of working age [1]. According to epidemiological studies, signs of intervertebral disc (IVD) degeneration are detected in approximately 20% of adolescents, while in patients over 70 years of age, more than 60% of IVDs exhibit morphological signs of severe degeneration [2].

In the pathogenesis of the degenerative process, most researchers identify three successive phases that differ in the severity of their morphological and biochemical changes [3–5]. The first phase is characterized by dehydration of the nucleus pulposus and the formation of fissures in the annulus fibrosus, which creates the preconditions for herniation. During this period, the disc loses its shock-absorbing properties and becomes vulnerable to mechanical stress. The second, intermediate phase is caused by the increasing extrusion of degenerated fragments of the nucleus pulposus: as its volume decreases, the load on the annulus fibrosus increases, leading to the development of a protrusion and then a disc herniation, accompanied by a reduction in the height of the intervertebral space. In the third and final phase, destruction of the annulus fibrosus and nucleus pulposus occurs with progressing fibrosis of the disc tissue; against the backdrop of vertebral motor segment hypermobility, spondyloarthrosis and osteophytes form as a compensatory reaction of the body.

The most clinically significant manifestation of the degenerative process is a herniated intervertebral disc (HID): in more than 80% of cases, it is localized in the lumbar spine. Compression of the nerve roots and radiculomedullary vessels causes the development of arterial and venous ischemic disorders, paresis and paralysis of the lower limb muscles, as well as pelvic organ dysfunction [6].

Modern approaches to the surgical treatment of herniated intervertebral discs are focused on minimizing intraoperative trauma and maximizing the improvement of patients' quality of life.

However, even when technically successful, surgical intervention only eliminates the mechanical compression factor, without addressing neurodystrophic changes or eliminating the risk of recurrence [7]. Intraoperative mechanical impact on neurovascular structures inevitably leads to the impaired functional state of the segmental nerve bundles and microcirculation of the spinal motion segment. In the early postoperative period, a significant portion of patients continue to experience sensory disturbances, incomplete recovery of motor functions, and psycho-emotional disorders. In 10–12% of cases, a pronounced cicatricial-adhesive process develops, which disrupts local hemodynamics (primarily the venous component), causing nerve root edema and persistent pain syndrome [8].

Postoperative drug therapy—including non-steroidal anti-inflammatory drugs, glucocorticoids, non-narcotic analgesics, antispasmodics, and dehydration agents—is aimed at relieving pain and preventing the formation of adhesions, but its effectiveness is insufficient for a patient's full recovery [10]. This underscores the need for early comprehensive rehabilitation that mandatorily includes physical therapy methods [8, 9].

In the current practice of physiotherapeutic management of patients after surgical treatment of HNP, a syndromic approach prevails: pronounced pain syndrome is treated with pulsed currents (diadynamic, sinusoidally modulated, fluctuating), ultrasound therapy, and low-intensity laser therapy combined with low-frequency magnetotherapy; sensory disorders are corrected with transcutaneous electrical stimulation; and motor disorders are treated with pulsed magnetotherapy [11, 12]. However, all these methods have a predominantly local effect and do not address systemic hemodynamic and astheno-neurotic disorders.

In this context, general magnetotherapy (GMT) is of particular interest. This method involves applying a low-induction magnetic field (1–3.5 mT) to the patient's entire body using a large-diameter solenoid. The systemic nature of this exposure makes it possible to simultaneously affect the body's key functional systems, activate redox processes, and improve various types of metabolism [13, 14]. The therapeutic effects of GMT include anti-inflammatory, reparative, immunomodulatory, antioxidant, and sedative actions, as well as the normalization of systemic microcirculation in vascular and vertebrogenic diseases [15–18]. During treatment, venous, arterial, and capillary insufficiencies are corrected: perivascular tissue edema is reduced, the microcirculatory bed is opened, and tissue hypoxia is resolved, which clinically manifests as a regression of pathological symptoms caused by vascular disorders.

The data presented above served as the basis for the present study, the objective of which was to evaluate the effectiveness of including GMT in a comprehensive rehabilitation program for patients after surgical treatment of herniated discs in the lumbosacral spine.

Materials and Methods.

A prospective controlled study was conducted at the Perfect Diagnostic Clinic in Samarkand, Uzbekistan. The study included 52 patients in the early recovery period following various types of surgical treatment for herniated intervertebral discs of the lumbosacral spine. All participants were monitored and received treatment exclusively at this institution.

Inclusion criteria were: a verified diagnosis of a herniated intervertebral disc of the lumbosacral spine, having undergone elective surgery, being in the early postoperative period (no more than 4 weeks after surgery), and having provided signed informed consent. Exclusion criteria were: an implanted pacemaker, decompensated cardiovascular diseases, cardiac arrhythmias, acute infectious diseases, and pregnancy.

Using simple randomization, the patients were divided into two groups comparable in age, sex, and the extent of the surgery performed. The control group (n=25) received standard therapy, which included nonsteroidal anti-inflammatory drugs, glucocorticoids, non-narcotic analgesics, antispasmodics, kinesitherapy, and hydrokinesitherapy. In addition to the standard therapy, patients in the main group (n=27) received a course of OMT.

The UMTI-3F "Kolibri-Expert" apparatus was used to perform OMT procedures. The procedures were performed in a gradually increasing intensity mode: the magnetic induction was sequentially increased from 10% to 60% of the maximum value (3.5 mT). The course consisted of 8–10 daily sessions, each lasting 15–20 minutes. The procedures were conducted in the morning in a specially equipped physiotherapy room at the clinic.

Patient condition was assessed twice—before and after completion of the treatment course—and included: a neurological examination to determine the status of sensory and motor impairments; remote infrared thermography of the back and lower extremities using the IRTIS 2000-ME thermograph for an objective assessment of local hemodynamics in the surgical area; assessment of pain using a 10-point visual analog scale (VAS); assessment of well-being, activity, and mood using the WAM (SAN) scale; and assessment of the degree of disability using the Oswestry Disability Index (version 2.1a).

Statistical analysis of the data was performed using standard methods of parametric and non-parametric statistics. Differences were considered statistically significant at $p < 0.05$.

Results and Discussion.

At the initial examination, all patients in both groups presented with a similar clinical profile characteristic of the early postoperative period. Constant moderate pain in the lumbar region radiating to the lower extremities was noted in 100% of cases; restricted mobility of the lumbar spine in 94.2% of patients; sensory disturbances in 75.0%; a depressed emotional state in 69.2%; and increased fatigue in 90.4%. Nerve root tension signs were detected in 92.3% of cases. The differences between the groups for all baseline indicators were statistically insignificant ($p > 0.05$), which confirms the comparability of the groups.

After completion of the rehabilitation course, positive changes were observed in patients of both groups, but the extent of these changes differed significantly. In the main group, complete pain relief was achieved in 51.9% of patients, and partial reduction in 48.1%. In the control group, the corresponding figures were 28.0% and 72.0%, respectively. Thus, the rate of complete pain regression in the main group was 1.85 times higher than in the control group, indicating a significant potentiation of the analgesic effect when OMT was included in the rehabilitation program.

The regression of nerve root tension signs in the main group occurred on average 3.2 ± 0.4 days earlier than in the control group, reflecting a more rapid reduction in radicular irritation and perineural edema under the influence of systemic magnetic therapy.

Analysis of the SAN scale data revealed an improvement in the well-being, activity, and mood scores in both groups. However, in the main group, the increase across a number of subscales was significantly higher ($p < 0.05$), which indicates an additional neurovegetative and sedative effect of OMT that promotes the correction of astheno-neurotic disorders in the postoperative period.

The results of the Oswestry Disability Index are particularly noteworthy. A significant decrease in the disability index was recorded in the main group ($p < 0.05$), whereas in the control group, the changes in this indicator did not reach statistical significance. This suggests that OMT not only reduces pain but also improves the patient's functional status in daily life—a parameter of fundamental importance from the perspective of social and occupational rehabilitation.

Objective verification of the clinical results was performed using infrared thermography. At baseline, patients in both groups exhibited pathological hyperthermia in the surgical site, reflecting a local hemodynamic disturbance. After the course of treatment, the mean temperature decrease in the study area was 1.48 ± 0.09 °C in the main group, whereas in the control group this indicator reached only 0.76 ± 0.05 °C ($p < 0.05$). Normalization of the local temperature gradient indicates an improvement in microcirculation and venous outflow in the surgical area, which is consistent with the known mechanisms of OMT's effect on the vascular component of hemodynamics.

The results, taken together, confirm that incorporating general magnetotherapy into a comprehensive rehabilitation program for patients after surgical treatment of herniated discs of the

lumbosacral spine significantly increases its effectiveness. The systemic nature of general magnetotherapy allows for the simultaneous treatment of pain syndrome, microcirculatory disorders, neurovegetative imbalance, and the patient's functional status—unlike local physiotherapy methods, which have a limited spectrum of action. The practical implementation of this method in a multidisciplinary clinic does not require special infrastructure and is well-tolerated by patients. All this substantiates the expediency of widely incorporating general magnetotherapy into the standards of postoperative rehabilitation for this category of patients, and also outlines prospects for further research on optimizing the parameters of magnetic exposure and developing differentiated treatment protocols.

Conclusions.

A clinical study conducted at the Perfect Diagnostic Clinic (Samarkand, Uzbekistan) demonstrated the high therapeutic efficacy of including general magnetotherapy in a comprehensive program for the early rehabilitation of patients after surgical treatment of herniated discs of the lumbosacral spine.

1. General magnetotherapy is an effective and safe method of physical rehabilitation for patients in the early postoperative period after a discectomy, possessing a systemic, multilevel effect.
2. Including general magnetotherapy in a rehabilitation program statistically significantly increases treatment effectiveness compared to standard therapy alone, shortens the time to pain relief, and accelerates the normalization of local hemodynamics.
3. The method is well-tolerated by patients, does not require complex infrastructure, and can be successfully implemented in a multidisciplinary clinic setting.
4. The results obtained justify the inclusion of general magnetotherapy in the standards for postoperative rehabilitation of patients with herniated intervertebral discs of the lumbosacral spine.

REFERENCES

1. Battié M.C., Videman T., Parent E. Lumbar disc degeneration: epidemiology and genetic influences // Spine. — 2004. — Vol. 29, No. 23. — P. 2679–2690. DOI: 10.1097/01.brs.0000146457.83240.eb

2. Chou R., Qaseem A., Snow V. et al. Diagnosis and treatment of low back pain: a joint clinical practice guideline // Annals of Internal Medicine. — 2007. — Vol. 147, No. 7. — P. 478–491. DOI: 10.7326/0003-4819-147-7-200710020-00006

3. Deyo R.A., Mirza S.K., Martin B.I. Back pain prevalence and visit rates: estimates from U.S. national surveys // Spine. — 2006. — Vol. 31, No. 23. — P. 2724–2727. DOI: 10.1097/01.brs.0000244618.06877.cd

4. Fairbank J.C.T., Pynsent P.B. The Oswestry Disability Index // Spine. — 2000. — Vol. 25, No. 22. — P. 2940–2952.

5. Gushcha A.O., Shevelev I.N., Kasymov F.Kh. Modern principles of surgical treatment of degenerative diseases of the lumbosacral spine // Annaly klinicheskoy i eksperimental'noy nevrologii = Annals of Clinical and Experimental Neurology. — 2019. — Vol. 13, No. 1. — P. 51–59. DOI: 10.25692/ACEN.2019.1.7

6. Ilieva E.M., Minchev R.M., Petrova N.S. Low-frequency magnetic field in rehabilitation of patients after lumbar disc surgery // Folia Medica. — 2012. — Vol. 54, No. 3. — P. 46–51. DOI: 10.2478/v10153-012-0007-5

7. Kirkaldy-Willis W.H., Farfan H.F. Instability of the lumbar spine // Clinical Orthopaedics and Related Research. — 1982. — Vol. 165. — P. 110–123.

8. Modic M.T., Ross J.S. Lumbar degenerative disk disease // Radiology. — 2007. — Vol. 245, No. 1. — P. 43–61. DOI: 10.1148/radiol.2451051706

9. Paolucci T., Pezzi L., Centra A.M. et al. Magnetic field therapy in low back pain for function improvement: a systematic review and meta-analysis // Disability and Rehabilitation. — 2020. — Vol. 42, No. 9. — P. 1234–1246. DOI: 10.1080/09638288.2018.1514453

10. Resnick D., Niwayama G. Degenerative disease of the spine // Radiology. — 1978. — Vol. 126, No. 3. — P. 559–574.

11. Urban J.P., Roberts S. Degeneration of the intervertebral disc // Arthritis Research & Therapy. — 2003. — Vol. 5, No. 3. — P. 120–130. DOI: 10.1186/ar629

12. Van Tulder M., Becker A., Bekkering T. et al. European guidelines for the management of acute nonspecific low back pain // European Spine Journal. — 2006. — Vol. 15, Suppl. 2. — P. S169–S191. DOI: 10.1007/s00586-006-1071-2

13. Waddell G. The back pain revolution. — Edinburgh: Churchill Livingstone, 2004. - 438 p.

14. Weinstein J.N., Tosteson T.D., Lurie J.D. et al. Surgical vs nonoperative treatment for lumbar disk herniation // JAMA. — 2006. — Vol. 296, No. 20. — P. 2441–2450. DOI: 10.1001/jama.296.20.2441

15. Woolf A.D., Pfleger B. Burden of major musculoskeletal conditions // Bulletin of the World Health Organization. — 2003. — Vol. 81. — P. 646–656.

16. Yelin E., Weinstein S., King T. The burden of musculoskeletal diseases in the United States // Seminars in Arthritis and Rheumatism. — 2016. — Vol. 46, No. 3. — P. 259–260. DOI: 10.1016/j. semarthrit.2016.07.013

17. Zhang Y., Jordan J.M. Epidemiology of osteoarthritis // Clinics in Geriatric Medicine. — 2010. — Vol. 26, No. 3. — P. 355–369. DOI: 10.1016/j.cger.2010.03.001

18. Zhou J., Chen L., Zhang Y. et al. Effectiveness of pulsed electromagnetic field therapy in low back pain: a meta-analysis // Bioelectromagnetics. — 2019. — Vol. 40, No. 5. — P. 343–356. DOI: 10.1002/bem.22185

EARLY-ONSET DEVELOPMENTAL AND EPILEPTIC ENCEPHALOPATHY ASSOCIATED WITH A DE NOVO SCN8A VARIANT (P.VAL410LEU): A CASE REPORT

Nodira M. Tuychibaeva - D.M.Sc., associate professor
Kamila R. Gubaydulina - basic doctoral student
Tashkent State Medical University (Tashkent, Uzbekistan)

Abstract. *The SCN8A gene encodes the neuronal voltage-gated sodium channel NaV1.6, which plays a critical role in neuronal excitability. Pathogenic variants in SCN8A are associated with a broad clinical spectrum ranging from benign familial infantile seizures to developmental and epileptic encephalopathy (DEE13). Gain-of-function variants are frequently linked to early-onset epilepsy and severe neurodevelopmental impairment.*

Materials and methods*: Clinical assessment included neurological examination, sleep electroencephalography (EEG), brain magnetic resonance imaging (MRI), audiological evaluation, and whole-exome sequencing (WES). Variant interpretation followed ACMG/AMP guidelines. The identified variant was validated by Sanger sequencing. Case Presentation: We report a 15-month-old male presenting with early-onset epilepsy, profound developmental impairment, severe hypotonia, impaired visual fixation, and reduced auditory responsiveness. Sleep EEG demonstrated hypsarrhythmia. Brain MRI revealed corpus callosum hypoplasia and delayed myelination. Whole-exome sequencing identified a de novo pathogenic variant SCN8A:c.1228G>T (p.Val410Leu).*

Conclusion*: The clinical and electroencephalographic findings are consistent with SCN8A-related developmental and epileptic encephalopathy.*

Keywords: *SCN8A; developmental and epileptic encephalopathy; hypsarrhythmia; early-onset epilepsy; whole-exome sequencing.*

Introduction. Developmental and epileptic encephalopathies (DEEs) represent a group of severe neurological disorders characterized by early-onset seizures accompanied by developmental impairment [1]. Advances in genomic technologies have significantly improved the identification of monogenic etiologies underlying many DEEs [6].

The SCN8A gene encodes the α-subunit of the voltage-gated sodium channel NaV1.6, which is highly expressed at the axon initial segment and nodes of Ranvier [13, 15]. NaV1.6 plays a fundamental role in the initiation and propagation of action potentials [4].

Pathogenic variants in SCN8A are associated with a broad phenotypic spectrum. Mild phenotypes include benign familial infantile seizures [2, 12]. In contrast, severe presentations involve developmental and epileptic encephalopathy (DEE13), characterized by early seizure onset and profound developmental impairment [3. 11].

Functional studies demonstrate that many epilepsy-associated missense variants exert gain-of-function effects, resulting in neuronal hyperexcitability [4, 8]. Clinical severity has been shown to correlate with the functional consequences of the variant [9].

Electroencephalographic abnormalities in SCN8A-related DEE are heterogeneous, with reported findings including multifocal epileptiform discharges, generalized epileptiform activity, and hypsarrhythmia [10].

Here, we describe a clinical case of SCN8A-related developmental and epileptic encephalopathy with early-onset epilepsy and hypsarrhythmia confirmed by molecular genetic testing.

Materials and Methods.

Subject

The proband underwent clinical evaluation including neurological examination, prolonged video-EEG monitoring, brain magnetic resonance imaging (MRI), audiological assessment, and genetic testing. Clinical data were obtained through medical records review and caregiver interviews.

Electroencephalography

A 3-hour video-EEG monitoring study was performed during wakefulness and sleep using a digital EEG system. Electrodes were positioned according to the international 10–20 system. EEG recordings were analyzed for background activity, epileptiform discharges, and pathological patterns.

Neuroimaging

Brain MRI was performed using an epilepsy-specific protocol. Structural abnormalities, white matter maturation, and commissural structures were evaluated.

Genetic Analysis

Genomic DNA was extracted from peripheral blood samples obtained from the proband. Whole-exome sequencing (WES) was performed using next-generation sequencing technology. The SCN8A variant was supported by a read depth of 149×. Sequence reads were aligned to the human reference genome (GRCh38), followed by variant calling and annotation using a validated bioinformatics pipeline. Variant interpretation and classification were conducted according to ACMG/AMP guidelines [4].

Segregation and Parentage Analysis

The identified SCN8A variant was validated by Sanger sequencing in the proband and both parents. Segregation analysis confirmed a de novo occurrence. Biological parentage was verified.

Case Presentation

A 15-month-old male child was referred for neurological assessment because of recurrent seizures and profound developmental impairment. According to the caregivers, abnormal neurological features had been evident since the neonatal period. On the second day of life, the infant was described as lethargic with a weak sucking reflex. Despite early feeding difficulties, weight gain was considered adequate.

Beginning at approximately 2 months of age, the child developed episodes of prolonged inconsolable crying, predominantly occurring in the evening hours.

Seizures began between 5 and 6 months of age. The initial paroxysmal episodes were characterized by a sudden cry followed by frequent contractions involving both the upper and lower extremities. These events recurred multiple times per day over the course of approximately one month. At 7 months, the episodes were recognized as epileptic seizures, and valproate therapy (Convulex) was initiated. However, no clinical response was observed. Subsequent treatment with vigabatrin (Sabril) resulted in temporary seizure cessation.

At approximately 10 months of age, an afebrile episode paroxysmal episode characterized by impaired awareness and fixed gaze developed 2–3 days following vaccination. The episode lasted approximately 30 minutes. Hormonal therapy was introduced, with caregivers reporting a positive clinical effect. One month later, during a febrile respiratory illness, another seizure occurred and was described as tonic in nature, with open eyes, fixed gaze, and sustained limb hypertonia.

By 15 months of age, seizures recurred, predominantly upon awakening. These episodes were described as paroxysmal episode characterized by impaired awareness and fixed gaze associated with apparent respiratory discomfort, interpreted by caregivers as a sensation of “air hunger,” occurring two to three times daily. At the time of evaluation, the child remained on vigabatrin therapy; precise dosing information was unavailable.

The child was born at term (40 weeks of gestation) following an uncomplicated pregnancy to non-consanguineous parents. Delivery occurred via spontaneous vaginal birth. Birth weight was 3,500 g. The neonate cried immediately after birth. Family history was negative for epilepsy or hereditary neurological disorders. Two older siblings were healthy. One previous pregnancy ended in early miscarriage.

Importantly, developmental milestones were absent from birth. The child never acquired head control, visual fixation, or tracking abilities. Responsiveness to auditory stimuli, including the mother’s voice, was markedly reduced. Excessive sleep duration was reported.

Neurological examination revealed a child without visual fixation or tracking and with minimal auditory responsiveness. Severe axial hypotonia was observed, accompanied by a frog-leg posture and absence of head control. Deep tendon reflexes were present and symmetric. Pathological reflexes were not elicited. Sensory responses to tactile stimulation were reduced. No hyperkinetic movements were observed. Bulbar dysfunction was noted, including swallowing difficulties and choking episodes. A left-sided grade 1 conductive hearing loss was documented.

Sleep EEG demonstrated a markedly disorganized background pattern, dominated by medium- to high-amplitude slow activity in the theta and delta frequency ranges. Very frequent multifocal epileptiform discharges, including spikes and polyspikes, were recorded, accompanied by diffuse high-amplitude slow wave complexes. The EEG findings were interpreted as hypsarrhythmia.

Brain MRI performed using an epilepsy protocol revealed hypoplasia of the corpus callosum, delayed/incomplete myelination, a right temporal arachnoid cyst measuring 14 × 15 × 24 mm, and mega cisterna magna considered a developmental variant.

Whole-exome sequencing identified a heterozygous pathogenic variant in SCN8A (NM_001330260.2:c.1228G>T, p.Val410Leu). Trio Sanger sequencing confirmed the presence of the variant in the proband and its absence in both parents, consistent with a de novo event. Functional prediction suggested a gain-of-function effect.

Discussion.

SCN8A-related developmental and epileptic encephalopathy (DEE13) is increasingly recognized as a prototypical sodium channelopathy in which the functional direction of channel dysfunction (gain-of-function vs loss-of-function) is clinically meaningful for prognosis and treatment selection [5]. In most individuals with early-onset DEE, de novo missense variants predominate and frequently confer gain-of-function effects on NaV1.6, leading to neuronal hyperexcitability and severe developmental impairment [12]. Experimental data from heterologous systems and neuronal models support a genotype–phenotype continuum in which epilepsy-associated variants increase neuronal firing, whereas loss-of-function changes are more often linked to intellectual disability phenotypes without epilepsy [12].

The electroclinical presentation in SCN8A-DEE is heterogeneous but typically includes early seizure onset, multiple seizure types, and frequent pharmacoresistance [13]. Importantly, epileptic spasms and hypsarrhythmia have been documented within the SCN8A phenotypic spectrum, emphasizing that SCN8A should be considered among genetic etiologies of infantile spasms syndrome when electroencephalography demonstrates hypsarrhythmia [14]. In this context, the reported patient's early-onset epilepsy with profound developmental impairment and hypsarrhythmia aligns with severe SCN8A-DEE presentations described in the literature [13–14].

From a mechanistic standpoint, in vivo studies further implicate forebrain excitatory neurons as critical drivers of seizure burden and premature mortality in SCN8A encephalopathy models, reinforcing the concept that persistent network hyperexcitability underlies clinical severity in gain-of-function disease [15]. These observations support precision-medicine approaches aimed at reducing aberrant sodium current. Consistent with this, pharmacologic strategies that target persistent and resurgent sodium currents have shown preclinical efficacy in SCN8A gain-of-function models and provide a rationale for sodium channel–modulating therapies in selected patients [16]. However, treatment responses remain variable across variants and individuals, and careful alignment of therapy with suspected functional effect (including consideration of sodium channel blockers in gain-of-function disease) is recommended [11].

Recently, an international modified-Delphi consensus provided practical guidance for diagnosis and management of SCN8A-related epilepsy and neurodevelopmental disorders, highlighting the need for systematic phenotyping, variant-level interpretation, and individualized antiseizure medication selection [17]. Within such frameworks, confirming de novo status by segregation testing (and, when appropriate, parentage confirmation) strengthens causal attribution and supports accurate

recurrence-risk counseling, especially in severe early-onset presentations where clinical urgency is high [17].

Overall, the present case contributes to the accumulating evidence that SCN8A should be prioritized in infants with early-onset epilepsy and severe developmental impairment, particularly when spasms or hypsarrhythmia are present [14]. Integrating deep phenotyping with robust variant classification and segregation analysis remains central to establishing molecular diagnosis and informing rational, mechanism-oriented treatment strategies in SCN8A-DEE [11, 17].

Conclusion.

We describe a case of SCN8A-related developmental and epileptic encephalopathy caused by a de novo pathogenic variant SCN8A:c.1228G>T (p.Val410Leu), presenting with early-onset epilepsy, hypsarrhythmia, profound developmental impairment, and severe axial hypotonia.

This case reinforces the expanding electroclinical spectrum of SCN8A-associated disorders and supports the concept of genotype-driven disease stratification in sodium channelopathies. Early molecular diagnosis through comprehensive genomic testing is essential in infants with developmental and epileptic encephalopathy, as it enables accurate etiological classification, informs mechanism-based therapeutic considerations, and provides critical guidance for genetic counseling and long-term management.

REFERENCES

1. Bunton-Stasyshyn RKA, Wagnon JL, Wengert ER, et al. Prominent role of forebrain excitatory neurons in SCN8A encephalopathy. Brain. 2019;142(2):362–375. doi:10.1093/brain/awy324.

2. Catterall WA. Voltage-gated sodium channels at 60: structure, function and pathophysiology. J Physiol.2012; 590 (11):2577–2589. doi:10.1113/jphysiol.2011.224204.

3. Conecker G, Xia MY, Hecker J, et al. Global modified Delphi consensus on diagnosis, phenotypes, and treatment of SCN8A-related epilepsy and/or neurodevelopmental disorders. Epilepsia. 2024. doi:10.1111/epi.17992.

4. Gardella E, Marini C, Trivisano M, et al. The phenotype of SCN8A developmental and epileptic encephalopathy. Neurology. 2018;91(12):e1112–e1124. doi:10.1212/WNL.0000000000006199.

5. Larsen J, Carvill GL, Gardella E, et al. The phenotypic spectrum of SCN8A encephalopathy. Neurology. 2015; 84(5):480–489. doi:10.1212/WNL.0000000000001211.

6. Larsen J, Carvill GL, Gardella E, et al. The phenotypic spectrum of SCN8A encephalopathy. Neurology. 2015;84(5): 480–489. doi:10.1212/WNL.0000000000001211.

7. Liu Y, Schubert J, Sonnenberg L, et al. Neuronal mechanisms of mutations in SCN8A causing epilepsy or intellectual disability. Brain. 2019;142(2):376–390. doi:10.1093/brain/awy326.

8. Liu Y, Schubert J, Sonnenberg L, et al. Neuronal mechanisms of mutations in SCN8A causing epilepsy or intellectual disability. Brain. 2019;142(2):376–390. doi:10.1093/brain/awy326.

9. Meisler MH, Hill SF, Yu W. Sodium channelopathies in neurodevelopmental disorders. Nat Rev Neurosci. 2021;22(3):152–166. doi:10.1038/s41583-020-00414-9.

10. Oikawa S, et al. Treatment Options for Infantile Spasms Syndrome with SCN8A: A Case Report and Literature Review. 2024. doi:10.1055/s-0043-1778011.

11. Richards S, Aziz N, Bale S, et al. Standards and guidelines for the interpretation of sequence variants: a joint consensus recommendation of the ACMG and AMP. Genet Med. 2015;17(5):405–424. doi:10.1038/gim.2015.30.

12. Scheffer IE, Berkovic S, Capovilla G, et al. ILAE classification of the epilepsies: position paper of the ILAE Commission for Classification and Terminology. Epilepsia. 2017;58(4):512–521. doi:10.1111/epi.13709.

13. Symonds JD, Zuberi SM, Stewart K, et al. Incidence and phenotypes of childhood-onset genetic epilepsies: a prospective population-based national cohort. Brain. 2019;142(8): 2303–2318. doi:10.1093/brain/awz195.

14. Talwar D, Hammer MF. SCN8A Epilepsy, Developmental Encephalopathy, and Related Disorders. Pediatr Neurol. 2021.

15. Wagnon JL, Meisler MH. Recurrent and non-recurrent SCN8A mutations: clinical and mechanistic implications. Brain.2015;138(Pt 7):1939–1952. doi:10.1093/brain/awv134.

16. Wengert ER, et al. Prax330 reduces persistent and resurgent sodium channel currents and protects against seizures in a model of SCN8A epileptic encephalopathy. 2019.

17. Zaman T, Helbig I, Boelman C, et al. SCN8A-associated developmental and epileptic encephalopathy: a multi-center cohort study. Brain. 2020;143(1):131–145. doi:10.1093/brain/awz337.

PREVENTION OF THE DEVELOPMENT AND PROGRESSION OF CKD IN PATIENTS WITH COVID-19

Nilufar Sh. Akhmedova - D.M.Sc., professor
Bukhara State Medical Institute (Bukhara, Uzbekistan)
Muzaffar Kh. Khattabov - head of department
Bukhara Regional Multidisciplinary Medical Center (Bukhara, Uzbekistan)
muzaffar.hattabov@yandex.ru

Abstract. *The article is devoted to the study of diagnostic, preventive, and rehabilitation features of nephropathies in patients who have recovered from COVID-19. The study included 249 patients who underwent inpatient treatment for COVID-19 at the Bukhara Regional Multidisciplinary Medical Center. Renal function parameters (creatinine, urea, cystatin C, microalbuminuria) were analyzed dynamically at 6, 12, 18, and 24 months after infection. It was found that 55.4% of patients developed albuminuria, which was most pronounced in individuals with comorbidities such as arterial hypertension, type 2 diabetes mellitus, and obesity. Key risk factors for post-COVID nephropathy were identified, and an individualized prevention system was proposed, including laboratory screening, a nephroprotective diet, physical activity, and staged monitoring. The findings confirm the importance of early diagnosis and rehabilitation to prevent the progression of chronic kidney disease after COVID-19.*

Keywords: *CKD, COVID-19, nephropathy, arterial hypertension, risk factors.*

Introduction.

COVID-19 affects not only the respiratory system but also has a significant impact on renal function. A number of studies have demonstrated that SARS-CoV-2 can directly invade nephrocytes and, through mechanisms such as cytokine storm, hypoxia, and thrombosis, lead to the development of acute kidney injury (AKI) and subsequently chronic kidney disease (CKD) [9]. Moreover, a decline in glomerular filtration rate (GFR), including cystatin C-based GFR, has been observed in patients even 6 and 12 months after COVID-19 infection [1,9].

A substantial proportion of patients who recovered from COVID-19 had concomitant comorbidities, including arterial hypertension, type 2 diabetes mellitus, metabolic syndrome, obesity, ischemic heart disease, and others. These conditions themselves increase the risk of nephropathy; however, the post-viral inflammatory background, hypercoagulability, and autoimmune reactions further potentiate their deleterious effects. The pathogenesis of post-COVID nephropathy is therefore complicated by this multifactorial interplay [4,5].

The impact of rehabilitation on nephropathy remains an insufficiently studied area. Post-COVID-19 rehabilitation has primarily focused on restoring respiratory function, psycho-emotional well-being, and general physical condition. However, there are virtually no specific rehabilitation protocols aimed at preventing or delaying the progression of nephrological disorders. Therefore, this issue highlights the need to develop an individualized, multifactorial rehabilitation system for patients who have had COVID-19 and are at high risk of developing nephropathy. Although the COVID-19 pandemic has officially ended, post-COVID syndrome continues to be widely observed among populations worldwide [2,3].

Post-COVID syndrome is a newly recognized nosological entity associated with a wide range of symptoms and dysfunction of multiple organ systems. The seriousness of this pathology is determined by the large number of patients affected by it. According to available data, up to 30–40% of individuals who have recovered from COVID-19 suffer from post-COVID syndrome. For

example, it is currently estimated that approximately 15 million people in the United States are experiencing the consequences of coronavirus disease [8,9].

Many countries are allocating substantial financial resources to the study and treatment of post-COVID syndrome. Over the past few years, the United Kingdom's healthcare system has invested significant funding in supporting individuals with long COVID. This has included the establishment of specialized post-COVID services and medical facilities. In addition, clinical guidelines for the management of post-COVID syndrome have been developed in this country [7].

Unfortunately, comprehensive recommendations for the early diagnosis and effective treatment of post-COVID syndrome are still lacking.

In recent years, the global community has faced not only a medical challenge but also a global socio-economic problem of major importance for all countries: the pandemic-like rise in chronic non-communicable diseases and the annual increase in mortality and disability caused by their complications [11,13]. The results of kidney function assessments and urinalysis obtained through screening programs conducted among tens of thousands of individuals in different countries have shown that approximately one in ten people worldwide has some degree of chronic kidney damage. If not identified and treated in a timely manner, kidney damage of varying severity may progressively worsen over the years, ultimately forcing patients to undergo dialysis or kidney transplantation [12].

The widespread implementation of the CKD concept in clinical practice contributes to the identification of risk factors and causes of disease progression and encourages patients to consult nephrologists and cardiologists at the early stages of the disease [16,18].

The world continues to combat COVID-19, largely due to the emergence of new viral variants. At the same time, a proportion of recovered individuals continue to experience persistent and long-term consequences referred to as long COVID. Clinical, autopsy, animal, and in vitro studies have demonstrated endothelial injury in both acute COVID-19 and in patients during recovery. Endothelial dysfunction is now recognized as a central factor in the progression of COVID-19 and in the development of long COVID. Post-COVID-19 rehabilitation has mainly focused on restoring respiratory function, psycho-emotional well-being, and general physical condition. However, there are virtually no specific rehabilitation protocols aimed at preventing or delaying nephrological disorders. Therefore, this issue underscores the need to develop an individualized, multifactorial rehabilitation system for patients who have recovered from COVID-19 and are at high risk of developing nephropathy [15,17].

Materials and methods.

The study included 249 patients aged 18–74 years who were hospitalized with COVID-19 infection and received inpatient treatment at the Bukhara Regional Multidisciplinary Medical Center, which functioned as a COVID-19 center from March 16, 2020, to May 2021. COVID-19 infection was diagnosed in accordance with versions 6 and 7 of the National Clinical Guidelines.

Of the enrolled patients, 132 were men and 117 were women; the mean age was 48.1 ± 3.7 years. In accordance with the aims and objectives of the study, the patients were divided into two groups:

- Main group: patients who experienced COVID-19 infection on the background of comorbid conditions (n = 196);
- Comparison group: patients with COVID-19 infection in whom no comorbid conditions were identified (n = 53).

All patients underwent comprehensive history taking and physical examination, as well as standard laboratory and instrumental investigations, including complete blood count, biochemical blood tests, urinalysis, coagulation profile, electrocardiography, ultrasound examination of the abdominal cavity and kidneys, and chest radiography. To assess renal function, serum and urinary creatinine and urea levels were measured.

Results.

• Analysis of the study findings demonstrated that microalbuminuria (MAU) was detected in 55.4% of patients (n = 138) during the course of infection. This indicator was 63.4% in the main group and 22.6% in the comparison group.

• To assess renal dysfunction based on the level of albuminuria, a comparative analysis of albuminuria categories was performed between the groups (Figure 1).

• According to the presented data, significant differences in albuminuria levels were observed between the two groups. In the main group, albuminuria was distributed across different stages, whereas in the comparison group, most patients were concentrated within a single category.

• **A0 category (normal):** The proportion of patients corresponding to the A0 category was 77.4% in the comparison group, whereas in the main group this figure was 35.7%. This finding indicates that preserved renal function was more common in the comparison group.

• **A1 category (mild albuminuria):** In the main group, 32.7% of patients were classified in this category, while in the comparison group this proportion was only 7.5%. This suggests that signs of microalbuminuria were more frequently observed in the main group.

• **A2 category (moderate albuminuria):** The proportion was 15.8% in the main group and 7.5% in the comparison group. This may indicate that increased urinary albumin excretion and more advanced renal involvement were more common in the main group.

• **A3 category (severe albuminuria):** This category was observed in 11.7% of patients in the main group and 5.7% in the comparison group. These findings reflect a higher frequency of glomerular damage in the main group.

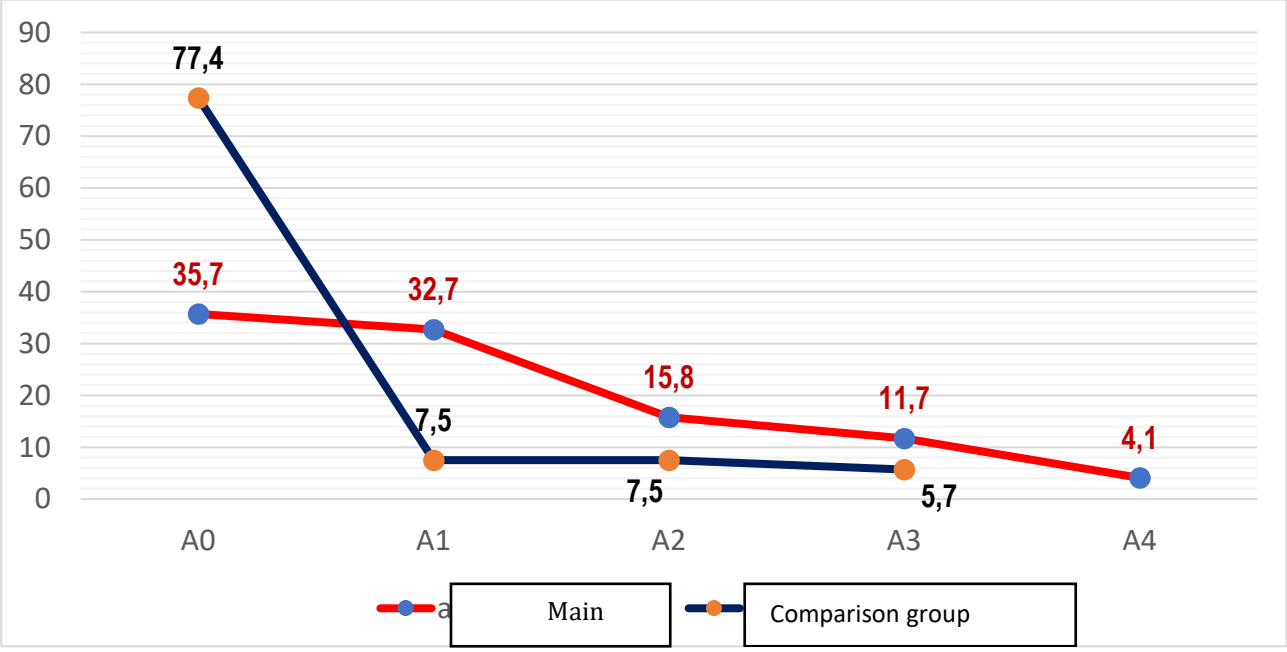


Figure 1. Comparative analysis of the frequency of albuminuria levels in the study groups (%)

• A4 category (very severe albuminuria): In the main group, this severe degree of renal involvement was still identified in 4.1% of patients, whereas no cases of albuminuria of this severity were observed in the comparison group (0%).

Albuminuria levels in the main group were distributed across a wide range, indicating varying degrees of renal dysfunction in this group. In particular, the relatively high proportions of patients in the A1–A3 categories (32.7%, 15.8%, and 11.7%, respectively) suggest that albuminuria in the main group could be detected at early and intermediate stages and reflect the clinical progression of renal

involvement. At the same time, the presence of patients even in the A4 category (4.1%) indicates the existence of severe nephropathic damage in this group.

In contrast, in the comparison group, albuminuria was not detected in nearly three-quarters of patients (A0 – 77.4%), while the remaining patients showed only mild degrees of albuminuria (A1–A3). This suggests that the risk of nephropathy was considerably lower in the comparison group.

To evaluate the pathogenetic features of nephropathy development in patients after COVID-19, an analysis was performed of the association between the prevalence of microalbuminuria (MAU) and comorbid conditions (Figure 2).

The analysis showed that the prevalence of MAU was highest among patients with type 2 diabetes mellitus, reaching 71.5%, which confirms the increased likelihood of nephropathy developing on the background of diabetes. High rates were also recorded in patients with arterial hypertension and coronary artery disease (68.2% and 63.9%, respectively). In patients with obesity and viral hepatitis, the prevalence of MAU was also statistically significantly elevated, indicating that these conditions should likewise be considered risk factors contributing to nephropathy.

To assess renal dysfunction in the post-COVID period among the patients included in the study, changes in microalbuminuria (MAU) and glomerular filtration rate (GFR) based on cystatin C were evaluated at 6, 12, 18, and 24 months after the infection.

The results showed that in the main group, MAU developed at 6 and 12 months in nearly 63.2% of patients who had no MAU during the acute phase of infection. Among these patients, A1 albuminuria was observed in 34.2% of cases, A2 in 20.5%, and A3 in 8.5%. In patients in whom MAU had already been detected, analysis of albuminuria dynamics showed that a decrease in MAU level was observed in only 39.8% of cases.

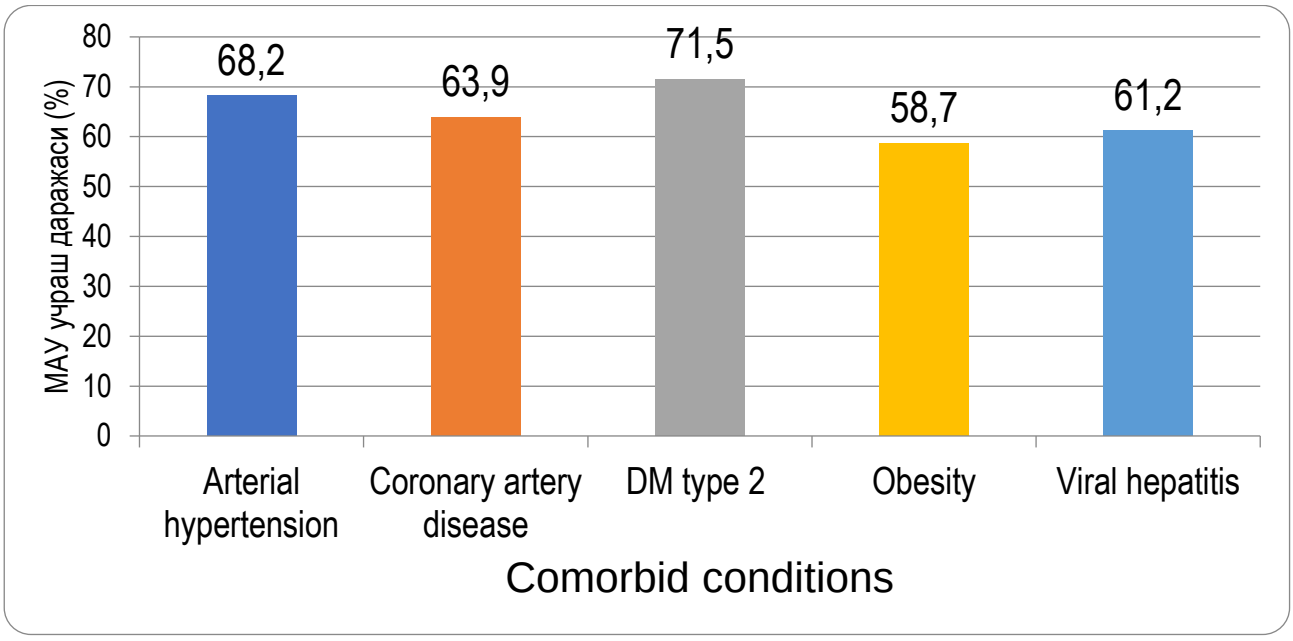


Figure 2. Analysis of the association between nephropathy development and comorbid conditions in patients after COVID-19 (%)

- In the comparison group, the proportion of patients with newly detected MAU increased to 32.7% at 6 months and to 38.1% at 12 months after infection. The main factors associated with increased cystatin C and MAU levels were as follows:
- the presence of more than two comorbid conditions — 68.5%;
- pulmonary fibrosis of stages F3–F4 — 59.3%;

- incomplete pathogenetic treatment in the comparison group — 44.7%.
- Based on the above findings, a rehabilitation roadmap aimed at restoring renal function in the early and late post-COVID periods was developed and recommended for implementation in clinical practice.
- The roadmap included six main components:
- **Identification of high-risk groups:**
- more than two comorbid conditions;
- pulmonary fibrosis of stages F3–F4;
- severe course of COVID-19.
- **Early screening:**
- MAU, cystatin C, IL-6, TGF-α.
- **Individualized follow-up:**

• **Monitoring parameters:** blood pressure, blood glucose, and GFR assessment.

4. **Nephroprotective diet:**
- restriction of sodium and protein intake;
- maintenance of electrolyte balance.

5. **Active rehabilitation:**
- aerobic exercise;
- breathing exercises.

6. **Educational programs:**
- improvement of patient awareness and self-monitoring skills.

The roadmap was developed within the framework of **prevention** and **rehabilitation**, and each block was structured according to the system: **cause → intervention → expected effect**.

Step 1. RISK STRATIFICATIONRationale: severe course of COVID-19 and the presence of ≥2 comorbid conditions.Intervention: screening for MAU, cystatin C, IL-6, and TGF-α within 0–3 months.Expected effect: identification of the high-risk group and initiation of early follow-up.

Step 2. PREVENTIVE STRATEGY (3–6 months)Rationale: the need to control blood pressure and glycemia.

• Risk: arterial hypertension and type 2 diabetes mellitus accelerate the progression of nephropathy.

• Intervention: target blood pressure <130/80 mmHg and HbA1c <7%.

• Expected effect: normalization of intraglomerular filtration pressure.

Dietary intervention: sodium and protein restriction

• Protein intake: 0.6–0.8 g/kg/day;

• Salt intake: <5 g/day;

• electrolyte and fluid balance should also be taken into account.

REHABILITATION STRATEGY (6–18 months)

Step 3. PHYSICAL ACTIVITY

• aerobic exercise (150 min/week);

• breathing exercises and supervised walking.Expected effect: improvement of endothelial function.

Step 4. PHARMACOLOGICAL APPROACH

• angiotensin receptor antagonists (ARAs) and SGLT2 inhibitors, if indicated.

Step 5. EDUCATIONAL SESSIONS

• improving patient awareness regarding MAU, GFR, clinical signs, and risk factors;

• information booklets and training sessions.

CONSOLIDATION AND MONITORING (18–24 months)

Step 6. PERIODIC FOLLOW-UP EXAMINATIONS

• MAU and cystatin C assessment every 6 months;

- hemodynamic assessment, ultrasound examination, GFR, and electrolyte monitoring;
- recommendation: nephrologist consultation at least once a year.

FINAL OUTCOME:

- Delay in CKD progression by up to 40–60%;
- Reduction in cystatin C levels by 30–50% at 18 months after rehabilitation;
- Supportive monitoring significantly reduces risk.

4. Conclusion. Assessment of post-COVID nephropathy risk based on comorbidity burden and inflammatory markers represents an effective approach.

- **MAU and cystatin C** are key markers for evaluating nephrological damage.
- Attention should be paid to the degree of pulmonary fibrosis and the completeness of treatment.
- Individualized rehabilitation and monitoring programs should be implemented, particularly for high-risk groups.

Conclusion.

The results of our study indicate that prevention of nephropathy after COVID-19 infection should be regarded not merely as an additional measure, but as an intervention whose importance may exceed that of many pathogenetic treatment approaches. In this field, identification of high-risk groups, early laboratory screening, rehabilitation programs, and educational strategies together constitute an integrated preventive model.

REFERENCES

1. Akhmedova, N. Sh. Laboratory markers for assessing renal function in nephropathy of different etiologies. *Tibbiyotda yangi kun*. 2022;(3(41)):56–59.

2. Bobkova, I. N., Shestakova, M. V., & Shchukina, A. A. Podocyte injury in diabetes mellitus. *Sakharnyy diabet*. 2014;17(3):39–50. doi:10.14341/DM2014339-50.

3. Kobalava, Zh. D., Villevalde, S. V., Borovkova, N. Yu., Shutov, A. M., Nichik, T. E., & Safuanova, G. Sh. Prevalence of chronic kidney disease markers in patients with arterial hypertension: results of the epidemiological study CHRONOGRAPH. *Kardiologiia*. 2017;57 (10):39–44.

4. Caramori, M. L., Fioretto, P., & Mauer, M. The need for early predictors of diabetic nephropathy risk: is albumin excretion rate sufficient? *Diabetes*. 2000;49(9):1399–1408. doi:10.2337/diabetes.49.9.1399.

5. Cederholm, J., Eliasson, B., et al. Microalbuminuria and risk factors in type 1 and type 2 diabetic patients. *Diabetes Research and Clinical Practice*. 2005; 67:258–266.

6. Dalla Vestra, M., Masiero, A., Roiter, A. M., Saller, A., Crepaldi, G., & Fioretto, P. Is podocyte injury relevant in diabetic nephropathy? Studies in patients with type 2 diabetes. *Diabetes*. 2003;52(4):1031–1035. doi:10.2337/diabetes.52.4.1031.

7. Forouzanfar, M. H., Liu, P., Roth, G. A., Ng, M., Biryukov, S., Marczak, L., Alexander, L., Estep, K., Hassen Abate, K., Akinyemiju, T. F., et al. Global burden of hypertension and systolic blood pressure of at least 110 to 115 mm Hg, 1990–2015. *JAMA*. 2017;317(2):165–182.

8. Granier, C., Makni, K., Molina, L., Jardin-Watelet, B., Ayadi, H., & Jarraya, F. Gene and protein markers of diabetic nephropathy. *Nephrology Dialysis Transplantation*. 2008;23(3):792–799. doi:10.1093/ndt/gfm834.

9. Gupta, A., & Nadim, M. K. COVID-19 and the kidney: mechanism of injury and management. *Kidney International Reports*. 2020;5(12):2265–2273. doi:10.1016/j.ekir.2020.09.013.

10. Jim, B., Ghanta, M., Qipo, A., Fan, Y., Chuang, P. Y., Cohen, H. W., et al. Dysregulated nephrin in diabetic nephropathy of type 2 diabetes: a cross-sectional study. *PLoS One*. 2012;7(5):e36041. doi:10.1371/journal.pone.0036041.

11. Kopp, J. B., Anders, H. J., Susztak, K., Podestà, M. A., Remuzzi, G., Hildebrandt, F., & Romagnani, P. Podocytopathies. *Nature Reviews Disease Primers*. 2020;6(1):68. doi:10.1038/s41572-020-0196-7.

12. Lastra, G., Syed, S., Kurukulasuriya, L. R., Manrique, C., & Sowers, J. R. Type 2 diabetes mellitus and hypertension: an update. *Endocrinology and Metabolism Clinics of North America*. 2014;43(1):103–122. doi: 10.1016/j.ecl.2013.09.005.

13. Mills, K. T., Stefanescu, A., & He, J. The global epidemiology of hypertension. *Nature Reviews Nephrology*. 2020;16(4):223–237.

14. Nakatsue, T., Koike, H., Han, G. D., Suzuki, K., Miyauchi, N., Yuan, H., et al. Nephrin and podocin dissociate at the onset of proteinuria in experimental membranous nephropathy. *Kidney International*. 2005;67(6):2239–2253. doi:10.1111/j.1523-1755.2005.00328. x.

15. Ng, D. P., Tai, B. C., Tan, E., Leong, H., Nurbaya, S., Lim, X. L., et al. Nephrinuria associates with multiple renal traits in type 2 diabetes. *Nephrology Dialysis Transplantation*. 2011;26(8):2508–2514. doi:10.1093/ndt/gfq738.

16. Petrie, J. R., Guzik, T. J., & Touyz, R. M. Diabetes, hypertension, and cardiovascular disease: clinical insights and vascular mechanisms. *Canadian Journal of Cardiology*. 2018;34(5):575–584. doi: 10.1016/j.cjca.2017.12.005.

17. Saeedi, P., Petersohn, I., Salpea, P., Malanda, B., Karuranga, S., Unwin, N., et al. Global and regional diabetes prevalence estimates for 2019 and projections for 2030 and 2045: results from the International Diabetes Federation Diabetes Atlas, 9th edition. *Diabetes Research and Clinical Practice*. 2019; 157:107843.

18. Volpe, M., Battistoni, A., Savoia, C., & Tocci, G. Understanding and treating hypertension in diabetic populations. *Cardiovascular Diagnosis and Therapy*. 2015;5(5):353–363. doi: 10.3978/j.issn.2223-3652.2015.06.02.

UDC: 616.12-007.2-089-053.2:616-07

CRITERIA FOR EARLY DIAGNOSIS AND INTENSIVE CARE OF POSTOPERATIVE COMPLICATIONS OF CONGENITAL HEART DEFECTS IN CHILDREN

Anvar S. Yusupov - MD, professor
Nigora Z. Zokirova - doctor
Kambarali I. Khaydarov - MD
Tashkent State Medical University (Tashkent, Uzbekistan)
shevakambar787@mail.ru

Abstract. *A study was conducted on 136 children aged 6 months to 6 years who underwent open-heart surgery for congenital heart defects under cardiopulmonary bypass. Age-adapted criteria for the early diagnosis of major complications, based on biomarkers and multimodal monitoring, were developed and implemented. The application of the new intensive care protocol reduced the overall complication rate by 61.4%, mortality from 7.4% to 2.9%, and the length of stay in the intensive care unit by 3.1 bed-days. The results confirm the high diagnostic efficacy of the proposed criteria in children.*

Keywords: *children aged 6 months to 6 years, congenital heart defects, open-heart surgery, cardiopulmonary bypass, low cardiac output syndrome, acute kidney injury, intensive care, ERAS-Pediatric Cardiac protocols.*

Introduction. The correction of congenital heart defects in children older than 6 months remains one of the most challenging areas of pediatric cardiac surgery. Despite significant advances in surgical techniques and anesthesiological support, the incidence of postoperative complications in this age group remains quite high and, according to various studies, reaches 30–45% [3,5].

The most common and clinically significant complications following open-heart surgery are low cardiac output syndrome, acute kidney injury, and respiratory dysfunction, which substantially increase the risk of adverse outcomes and the length of patients' stay in the intensive care unit [2,6].

Early diagnosis of these complications is crucial for the timely initiation of intensive care and improving the prognosis. Current guidelines for the management of children following cardiac surgery emphasize the need for multimodal monitoring, tissue perfusion biomarkers, and standardized intensive care protocols [1,7].

However, existing diagnostic criteria were developed primarily for adult patients and require adaptation for pediatric patients, particularly in young children [4,8].

In this regard, there remains a need to identify more sensitive and specific criteria for the early diagnosis of postoperative complications, as well as to develop effective intensive care protocols aimed at reducing the incidence of low cardiac output syndrome, acute kidney injury, and respiratory disorders [9,10].

The aim of the study was to develop and clinically evaluate the effectiveness of age-adapted diagnostic criteria and an intensive care protocol for postoperative complications in children following open-heart surgery.

Materials and Methods. The study was conducted at the Cardiac Intensive Care Unit of the Multidisciplinary Children's Clinic of Tashkent State Medical University. The study included 136 children aged 6 months to 6 years (mean age 3.2 ± 1.5 years, 59% boys) who underwent open-heart surgery for congenital heart defects under cardiopulmonary bypass (Tetralogy of Fallot—42%, ventricular septal defect—31%, others—27%).

Patients were divided into two comparable groups:

Group 1 (control, n = 68)—standard therapy.

Group 2 (experimental, n = 68) — new protocol.

Age-adjusted diagnostic criteria (developed by the authors for children aged 6 months to 6 years, based on the AHA/ACC Pediatric 2025 and KDIGO Pediatric 2023 guidelines):

- Low cardiac output syndrome (LCOS): cardiac index < 2.2 L/min/m² + lactate > 3.5 mmol/L + SvO_2 < 65%.

- Acute kidney injury: creatinine increase ≥ 1.5 times baseline or urine output < 0.5 mL/kg/h for ≥ 6 hours (KDIGO-pediatric).

- Acute respiratory distress syndrome: PaO_2/FiO_2 ≤ 300 mm Hg with PEEP ≥ 5 cm H_2O (PALICC-2 criteria (2023).

Statistical analysis: SPSS 29.0 (Student's t-test, χ^2, Mann–Whitney, $p < 0.05$).

Results and discussion. Complications developed in 64.7% of children in the control group and in 25.0% in the main group ($p < 0.001$). Mortality decreased from 7.4% to 2.9% ($p = 0.018$). The mean duration of mechanical ventilation decreased from 22.6 ± 9.4 hours to 7.9 ± 3.2 hours ($p < 0.001$). The length of stay in the intensive care unit decreased from 6.8 ± 2.7 to 3.7 ± 1.1 bed-days ($p < 0.001$).

Table 1.

Incidence of postoperative complications in children (%)

Complication	Group 1	Group 2	Reduction, %
Low cardiac output syndrome	32,0	11,8	63,1
Acute kidney injury	24,0	9,2	61,7
Acute respiratory distress syndrome	18,0	6,5	63,9
Infectious complications	12,0	4,1	65,8
Neurological disorders	8,5	2,7	68,2
Overall complication rate	64,7	25,0	61,4

Table 2.

Diagnostic value of the proposed criteria (main group, n=68)

Criterion	Sensitivity, %	Specificity, %	Positive predictive value, %
CNSV (lactate + SvO_2 + CI)	95,6	91,2	93,4
OPD (KDIGO-pediatric)	93,8	88,9	90,7
ARDS (PaO_2/FiO_2	91,4	94,3	92,1

Intensive care protocol (main group): multimodal monitoring (PiCCO, cerebral oximetry, real-time echocardiography), milrinone + levosimendan for refractory central nervous system dysfunction, protective lung ventilation, early extubation (within the first 4–8 hours), early initiation of RRT for lactate > 4.5 mmol/L and oliguria.

Treatment of postoperative complications was conducted according to the established intensive care protocol. The main therapeutic approaches were:

1. Hemodynamic support. In cases of low cardiac output syndrome, inotropic therapy was administered (milrinone 0.3–0.7 μg/kg/min). In cases of refractory LCS, levosimendan was additionally administered at a dose of 0.05–0.1 μg/kg/min. Vasopressors (norepinephrine 0.05–0.3 μg/kg/min) were used for arterial hypotension.

2. Respiratory support. Protective mechanical ventilation was performed using low tidal volumes (6–8 mL/kg) and positive end-expiratory pressure (PEEP 5–8 cm H_2O). In the main group, an early extubation strategy was employed (4–8 hours after surgery).

3. Prevention and treatment of acute kidney injury. Strict monitoring of urine output and creatinine levels was performed. In cases of oliguria and lactate levels exceeding 4.5 mmol/L, early renal replacement therapy (RRT) was administered.

4. Multimodal monitoring. PiCCO monitoring, cerebral oximetry, echocardiography, and blood lactate level monitoring were used to assess organ perfusion.

5. Infection control. Prophylactic antibiotic therapy and early diagnosis of infectious complications were performed.

The application of this protocol significantly reduced the incidence of postoperative complications and improved clinical outcomes in children following cardiac surgery (Table 3).

Table 3.

Major clinical outcomes

Outcome	Group 1	Group 2	P
Mortality (30 days), %	7,4	2,9	0,018
Duration of mechanical ventilation, hours	22,6 ± 9,4	7,9 ± 3,2	<0,001
Length of stay in the ICU, bed-days	6,8 ± 2,7	3,7 ± 1,1	<0,001
Repeat interventions, %	11,8	2,9	0,027

The proposed criteria allow for the initiation of targeted therapy 4–6 hours earlier than the standard approach in children aged 6 months and older. The results are consistent with the 2025 AHA Pediatric Cardiac Critical Care guidelines and the 2026 Russian clinical guidelines, but surpass them in terms of the rate of reduction in complications due to the early use of levosimendan and cerebral NIRS monitoring.

Conclusion. The developed age-adapted diagnostic criteria and intensive care protocol significantly reduce the incidence and severity of postoperative complications in children following correction of congenital heart defects. The method is recommended for implementation in pediatric cardiac intensive care units.

REFERENCES

1. Alten J.A., Klugman D. Pediatric Cardiac Critical Care. Annals of Thoracic Surgery. 2024.
2. American Heart Association. Pediatric Advanced Cardiac Life Support Guidelines. AHA, 2025.
3. Anderson B.R., Hill K.D. Outcomes after congenital heart surgery in children. Journal of Thoracic and Cardiovascular Surgery. 2023.
4. Bronicki R.A., Cooper D.S., Jacobs J.P. Pediatric Cardiac Intensive Care Society Consensus Statement. Pediatric Critical Care Medicine. 2025.
5. Brown K.L., Ridout D.A. Low cardiac output syndrome after pediatric cardiac surgery. Intensive Care Medicine. 2023.
6. Clinical Guidelines of the Ministry of Health of the Russian Federation. Intensive Care Following Cardiac Surgery in Children. Moscow, 2026.
7. KDIGO Clinical Practice Guideline for Acute Kidney Injury in Children. Kidney International Supplements. 2025.
8. Kneyber M.C.J., Jouvet P. Pediatric Acute Respiratory Distress Syndrome. Lancet Respiratory Medicine. 2023.
9. Marino B.S., Tabbutt S., MacLaren G. Pediatric Cardiac Intensive Care. Springer, 2024.
10. Hoffman T.M., Wernovsky G. Postoperative complications in congenital heart surgery. Circulation. 2022.

NEW POSSIBILITIES FOR DETERMINING THE ABO BLOOD GROUP IN FORENSIC MEDICAL PRACTICE

Mukharrama A. Khasanova - D.M.Sc., associate professor
Guzal K. Akbarova - assistant
Tashkent State Medical University (Tashkent Uzbekistan)
m.xasanova71@gmail.com

Abstract. *Based on the data on the modern distribution of blood groups according to the AB0 system, the distribution of blood groups according to the AB0 system among the population of Tashkent city was studied within the framework of a forensic medical examination. The distribution of blood groups was: 0αβ(I) – 2310 (26%), Aβ(II) – 3613 (40.7%), Bα(III) – 1944 (22%) and AB0(IV) – 998 (11.3%). In forensic medical practice, methods for determining human blood group are used: Schiff, anti-A and anti-B co-clones and Gel technologies, and various ingredients are used: alpha and beta isohemagglutinating sera, heteroimmune sera anti-A, anti-B, anti-0(H), monoclonal antibodies anti-A, anti-B, as well as phytagglutinins.*

Keywords: *system AB0, Schiff's method, tsoliclons, gel technology blood, agglutinogens, blood group, agglutinins, phytoagglutinins*

Introduction.

The development of forensic hematology is closely associated with advances in a number of scientific disciplines, primarily hematology and immunology. The examination of blood is of exceptional importance in forensic investigations of deaths classified as violent (homicide, suicide, accidents), as well as in cases of sexual crimes (rape, sodomy, etc.). During life, when the integrity of tissues is disrupted, blood may come into contact with various objects and serve as physical evidence revealing the true circumstances of the case. In such situations, a fundamentally important question must be resolved – the possible origin of the blood (found on certain objects) from a particular individual. For this purpose, liquid blood samples taken both from a corpse and from a living person are examined for comparison. First of all, the blood group of the AB0 system is determined, which is based on the detection of agglutinogens and agglutinins. [1,5,8,14].

Determining the blood group of a living person presents no difficulty. However, during the examination of liquid blood from a corpse, this is not always possible. [4,6]. This is primarily due to the poor preservation of agglutinins, which rapidly degrade after death and under the influence of various factors. In addition, erythrocytes also undergo changes. Under the influence of certain factors, they may either deform or dissolve [3,17,22,24].

These factors may lead to hemolysis, putrefaction of the blood, coagulation or, conversely, dilution, and other alterations. In such cases, agglutinins and often agglutinogens cannot be detected, meaning that the blood group cannot be determined [10]. Therefore, in such cases the blood is first dried and then subjected to examination using more labor-intensive and time-consuming methods. Moreover, as reported in the literature, drying has a negative effect on the course of the reaction. It significantly reduces the absorption capacity of agglutinogens A and B [7,20,23].

The study of group-specific substances is carried out more deeply by immunochemists and biochemists, while forensic specialists utilize their achievements for their own purposes. Advances, particularly those related to group-specific substances of the AB0 system, make it possible to attempt differentiation within the AB0 system under the influence of certain external and internal factors. The current state of research on the blood group of cadaveric blood is largely focused on this issue. In order to resolve these questions, a more detailed study of the properties and characteristics of this erythrocyte system (AB0) is required, taking into account recent scientific works [6]. It is also necessary to investigate postmortem changes occurring in blood and to determine the possibilities for identifying blood groups under such conditions. This requires a comprehensive study of the

characteristics of cadaveric blood, agglutinogens, and agglutinins both under normal conditions and under the influence of various factors [6,12,19]. The AB0 blood group system derives its name from the antigens present in erythrocytes. This blood group system is considered the classical blood group system. It is the only serological system that, in addition to agglutinogens, also contains agglutinins. Therefore, in forensic medical examination of physical evidence, the blood group of liquid blood, including cadaveric blood, is determined based on both agglutinogens and agglutinins. For this purpose, various reagents are used: isohemagglutinating sera alpha and beta, heteroimmune sera anti-A, anti-B, anti-0, monoclonal antibodies anti-A and anti-B, as well as agglutinins of plant origin (phytoagglutinins) or animal origin (protectins). Each of these reagents has its own advantages [2,4.9,11,18].

Material and methods of research.

In the present study, 360 blood samples obtained from living individuals and cadavers (2017–2020), as well as 148 archival forensic examination materials from the forensic biological laboratory of the Tashkent branch of the Republican Scientific and Practical Center of Forensic Medical Examination, were used. In forensic medical practice, modern methods are applied to determine the human blood group: 1. the agglutination reaction using the Schiff method with anti-A and anti-B cyclones (tsoliklons) for blood group determination; 2. the Across Gel card technology for determining blood groups.

In the study, 22 blood samples from individuals aged 25–55 years were examined. The agglutination reaction using the Schiff method was applied during the examination. Agglutinins and agglutinogens in liquid blood are determined by the Schiff method (agglutination reaction), which is based on the interaction between agglutinogens and agglutinins. In this reaction, agglutinogens are identified using standard isohemagglutinating sera α and β, while agglutinins are determined using standard erythrocytes of groups A and B. For this purpose, four special agglutination laboratory plates are used. On two of them the letters “A” and “B” are written with a glass marker, and on the other two the symbols “α” and “β” are indicated. According to the corresponding markings, four drops of a 1% suspension of standard group A and B erythrocytes are placed into the plates labeled “A” and “B”, while two drops of standard sera α and β are added to the plates labeled “α” and “β”. The examined blood sample is centrifuged, and the serum is separated from the erythrocytes, from which a 1% suspension is prepared. Four drops of the 1% erythrocyte suspension from the examined blood are added to the plates containing α and β sera, while two drops of the serum from the examined blood are added to the plates containing standard erythrocytes A and B. The mixture of erythrocytes and serum is centrifuged at 1500 rpm for 4 minutes, after which it is thoroughly shaken. The reaction results are evaluated both macroscopically and microscopically. After the examination of the liquid blood samples, stains are prepared from them on indifferent carrier materials (clean gauze).

Results and discussion.

In the study, 22 blood samples from individuals aged 25–55 years were examined. In the control samples with known blood groups $0_{\alpha\beta}$ (I), A_{β}(II), B_{α}(III), and AB_0 (IV), no agglutination was observed. In the known blood sample of group $0_{\alpha\beta}$(I), agglutination was observed only with anti-H phytoagglutinin, indicating the presence of the 0(H) antigen. In the known blood sample of group A_{β}(II), agglutination occurred only with anti-A phytoagglutinin, confirming the presence of antigen A. In the known blood sample of group B_{α}(III), agglutination was observed only with anti-B phytoagglutinin, indicating the presence of antigen B. In the known blood sample of group AB_0 (IV), agglutination occurred with both anti-A and anti-B phytoagglutinins, demonstrating the presence of both A and B antigens. Among the examined study samples, agglutination with anti-B isosera was observed only in samples No.1,4,5,12,13, and 15-17, indicating the presence of antigen B. In samples No.2,6,8,14 and 18, agglutination occurred only with anti-H phytoagglutinin, indicating the presence of antigen 0(H), which suggests that this blood could originate from individuals with blood group $0_{\alpha\beta}$(I). In samples No. 3, 7, 9, 19, and 21, agglutination was observed only with anti-A iso-serum, indicating that the blood may originate from individuals with blood group A_{β} (II). In samples No.

10,11,20, and 22, agglutination occurred with both anti-A and anti-B iso-sera, demonstrating the presence of antigens A and B, which indicates that the blood may originate from individuals with blood group AB0 (IV). When determining the group affiliation of blood, only antigens A, B, and 0 (H), as well as agglutinins α and β, are identified. Based on the results of the forensic medical examination, information about the detected antigens and agglutinins in blood samples taken from unidentified cadavers submitted for examination is provided, and the corresponding blood group is indicated in the conclusion of the forensic biological examination. An algorithm for determining the blood group using anti-A and anti-B cyclones (tsoliklons) was also developed. Procedure: 1**.** One large drop of the tsoliklon reagent is placed in each well of the plate; 2. Using a capillary, a small drop of blood (0.01 ml) is placed next to the tsoliklon reagent, ensuring that the capillary does not come into direct contact with the reagent; 3. The blood and the tsoliklon reagent are mixed using separate sticks. 4. The plate is gently shaken, and agglutination is observed for 2.5 minutes; 5.One drop of physiological saline is added with a pipette into the wells where agglutination has occurred; 6. The plate is shaken again and the agglutination reaction is observed. Results in blood group determination using tsoliclons: - If no agglutination is observed in any well - Group $0_{\alpha\beta}$(I); - Agglutination with anti-A tsoliklon - Group A_{β}(II); - Agglutination with anti-B tsoliklon - Group B_{α}(III); Agglutination with both anti-A and anti-B tsoliklons – Group AB_0(IV).

Application of the gel filtration method in practice: 1. Rapid and accurate determination of blood group and Rh factor, including in complex cases; 2. Extensive typing of erythrocyte antigens across all known systems; 3. Screening and identification of alloantibodies against erythrocytes; 4. Individual selection of blood components for transfusion; 5. Diagnosis of post-transfusion complications and hemolytic disease of the newborn; 6. Detection of rare antigens (up to 76 different test profiles). Advantages of gel technology: -The gel filtration principle combined with the use of monoclonal antibodies ensures high sensitivity and specificity; -All reagents are standardized in dosage and their quality is controlled; - Simple interpretation of results: positive reaction (cells remain in the upper part of the gel), negative reaction (cells sediment at the bottom); -Ease of use: testing time is 2-5 times faster for antibody screening and compatibility testing; no need for erythrocyte washing; results can be automatically evaluated and photo-documented; -Rapid training of laboratory personnel; -Reduction of errors associated with traditional methods; Test results can be copied for archival purposes or used as teaching material in diagnostically difficult cases; -The ability to use very small amounts of blood is of significant importance; - Reduces the risk of infection for personnel when working with potentially infected samples; -Plastic cards are made from biodegradable materials, are easy to recycle, and do not pollute the environment; -The test system is stable and can be stored at room temperature for up to one year.

The use of gel technologies makes it possible to perform a set of tests that were previously available only in reference laboratories within routine practice. The advantages of gel technology demonstrate the transition from manual procedures to automated technologies. This new stage in the development of laboratory diagnostics is characterized by a continuous increase in data obtained due to improvements in laboratory equipment. Correct determination of human blood groups according to the AB0 system is of great importance for preventing post-transfusion complications.

Conclusion.

1. The properties and characteristics of phytoagglutinins depend on the plant’s growth environment and the time of seed collection.

2. In the practice of forensic medicine, liquid human blood according to the AB0 system 1. agglutination on a flat surface with the help of monoclonal antibodies; 2. agglutination in test tubes; 3. microplate agglutination reactions were used.

3. The use of modern Across Gel card technology to determine a person's blood type is considered a more reliable and preferred method in the practice of forensic biology experts.

REFERENCES

1. Afanasyev E.N., Tyumentseva I.S., Kogotkova O.I. et al. Development of new approaches to obtaining hyperimmune sera for the production of medical immunobiological preparations // Problems of Particularly Dangerous Infections. – 2020. – Issue 103. – P. 67– 69.

2. Ashurbekov T.R., Ataev M.G., Gadzhieva A.D. Relevance of organizing human hair examinations in forensic biological and molecular genetic laboratory departments under conditions of a large volume of research // Problems of Environmental Medicine. – 2018. – P. 164–174.

3. Gusarov A.A. Review of Russian dissertations in forensic medicine devoted to issues of forensic biology // Forensic Medical Examination. – 2019. – No. 5. – P. 40–44.

4. Peter J. D'Adamo 4 Blood Types – 4 Ways of Life. Minsk, 2015. 480 p.

5. Aristov A.A., Rozenbaum Yu.A. et al. Development of an automated method for evaluating the erythrocyte agglutination process for determining human blood groups // *Medical Equipment*. – 2021. – No. 5. – P. 19–23.

6. Belopukhov V.M. Distribution of blood groups among donors of the Republic of Tatarstan // *Kazan Medical Journal*. – 2016. – No. 3. – Vol. 96. – P. 437–440.

7. Gerasimova I.E. Use of monoclonal reagents in forensic biological practice // *Criminalistics and Forensic Examination*. – 2019. – No. 64. – P. 528–533.

8. Gilmutdinov R.G., Epifanova A.A., Kolupaev V.E. Verification in complex cases of blood group typing according to the AB0 system in recipients // *Handbook for the Head of the Clinical Diagnostic Laboratory*. – 2017. – No. 9. – P. 55–69.

9. L.L. Golovkina, R.S. Kalandarov, A.G. Stremoukhova et al. Differentiation of A_1 and A_2 subgroups of antigen A of the AB0 system: biological basis and serological strategy // *Hematology and Transfusiology.* – 2019. – Vol. 64. – No. 4. – P. 504–515.

10. Dolmashkin A.A., Dubrovsky V.A. Determination of blood group based on digital images of erythrocytes and their agglutinates // *Medical Equipment.* – 2012. – No. 2. – P. 272.

11. Dubrovsky V.A., Medvedeva M.F. Acousto-optical method for determining the human blood group: comparison of the use of anti-A and anti-B monoclonal antibodies and standard hemagglutinating sera // *Saratov Journal of Medical Scientific Research.* – 2017. – Vol. 13. – No. 1. – P. 22–28.

12. Ershova A.A., Shirokova A.S., Morozov A.M. Evaluation of methods for determining blood groups // *Tver Medical Journal*. – 2017. No. 5. P. 72–75.

13. Pyshnograeva K.G. New technologies in blood group determination // *Bulletin of Clinical Hospital No. 51*. – 2016. – P. 62–63.

14. Shautsukova L.Z. AB0 blood group system: genetics, biochemistry, physiology // *Proceedings of Higher Educational Institutions. North Caucasus Region. Natural Sciences Series*. 2020. No. 2 (156). – P. 131–133.

15. Pyshnograeva K.G. New technologies in blood group determination // *ulletin of Clinical Hospital No. 51*. – 2010. – Vol. 3. – No. 8. – P. 62–63.

16. Zhiburt E.B. et al. Features of national determination of antibodies to erythrocytes // *Bulletin of Roszdravnadzor*. – 2012. – No. 4. – P. 61–63.

17. Barsegiants L.O. Detection of AB0 antigens in the bone tissue. The Thomsen phenomenon//Sud Med Ekspert. - 2010; –53(2):26-28.

18. .Cserti C. M., Dzik W.H. The AB0 blood group system and Plasmodium falciparum malaria //Blood, The Journal of the American Society of Hematology. – 2007. – Т. 110. – №. 7. – С. 2250-2258.

19. Hosoi E. Biological and clinical aspects of AB0 blood group system //The journal of medical investigation. – 2018. – Т. 55. – №. 3, 4. – С. 174-182.

20. Keramati M.R. et al. Blood group antigens frequencies in the northeast of Iran //Transfusion and apheresis science. 2018. – T.45. – №.2. – C. 133-136.

21. Marks L. Monoclonal antibodies and the transformation of blood typing. //MAbs. 2014; –6(6): –1362–1367.

22. Mujahid A, Dickert FL. Blood Group Typing: From Classical Strategies to the A plication of Synthetic Antibodies Generated by Molecular Imprinting. //Sensors (Basel). –2015; –16 (1):51-57.

23. Nishi K. AB0 blood group typing in forensic autopsies // Nihon Hoigaku Zasshi. – 2017. – №2. – P. 111-117.

24. Noiphung J, Talalak K, Hongwarittorm I, Pupinyo N. et all. A novel paper-based assay for the simultaneous determination of Rh typing and forward and reverse AB0 blood groups. //Biosens Bioelectron. –2015; – 67:485-489.

COMPARATIVE ANALYSIS OF SPINAL ANESTHESIA WITH QL BLOCK IN GYNECOLOGICAL PATIENTS WITH HYPERTENSION AND CHRONIC CIRCULATORY FAILURE

Sherzod M. Valiyev - assistant
Zoir T. Gaziyev - D.M.Sc., associate professor
Tashkent state medical university (Tashkent, Uzbekistan)
zairgaziyev5@gmail.com

Abstract: *The aim was to evaluate the clinical course of spinal anesthesia combined with a QL block in patients with arterial hypertension and chronic heart failure. The study included 68 patients undergoing elective gynecological surgery. Hemodynamics, respiratory function, analgesia, and complications were assessed.*

Spinal anesthesia with QL block provided stable hemodynamics, preserved spontaneous breathing, and effective analgesia. Patients with chronic heart failure showed greater hemodynamic variability. The QL block prolonged analgesia and allowed dose reduction of intrathecal anesthetic.

This technique is effective and safe when individualized according to cardiovascular functional reserve.

Keywords: *spinal anesthesia, QL block, chronic heart failure, arterial hypertension, hemodynamics.*

Introduction Modern anesthesiology is focused on a personalized approach, due to the increasing number of patients with cardiovascular pathologies [1,2]. The choice of anesthesia for patients with chronic circulatory failure and hypertension, who differ in various types of hemodynamics and adaptive capabilities, is of particular importance [3,4].

In chronic circulatory insufficiency, a hypokinetic type of hemodynamics with limited functional reserve is formed [5], while in hypertension, the eukinetic type is more frequently observed with possible hidden regulatory disorders [6]. Despite similar clinical manifestations, adaptive reactions differ and determine the response to surgical stress [7].

The functional reserve of the cardiovascular system and its ability to mobilize are of key importance [8,9]. Its assessment, including functional tests, allows for the identification of hidden adaptation disorders [10]. Neuroendocrine stress response plays a significant role, affecting hemodynamics and perfusion [11].

Regional anesthesia methods contribute to a reduction in stress response, while general anesthesia is accompanied by more pronounced neuroendocrine activation [12].

Purpose of the study: to compare the clinical course of SA combined with QL block in gynecological patients with hypertension and chronic circulatory insufficiency, taking into account functional reserve.

Materials and methods: the study was conducted as a prospective comparative clinical-instrumental study and included 68 gynecological patients who underwent scheduled surgical interventions (hysterectomy and reconstructive-plastic surgeries on pelvic organs).

Depending on the nosological form, the patients were divided into two groups: the hypertensive group (n=31) - with hypertension; the chronic circulatory failure group (n=37) - with chronic circulatory failure.

The average duration of surgeries was 138.1±6.9 minutes in the GB group and 146.4±19.4 minutes in the CCF group. All interventions were performed in a planned manner.

Anesthesiological support was provided in the form of balanced spinal anesthesia combined with bilateral QL block. Spinal anesthesia was performed by subarachnoid administration of a 0.5% bupivakaine solution in a dose of 7.5 mg. The QL block was performed under ultrasound navigation with the administration of a 0.25% bupivakaine solution at a dose of 2.5–3 mg/kg (30 ml on each side).

Assessment of the clinical course of anesthesia included:
• hemodynamic indicators (blood pressure, heart rate);
• external respiratory parameters (respiratory rate, SpO2);
• timing of sensorimotor block development;
• severity of analgesia;
• features of post-operative recovery;
• frequency and nature of complications.

Indicators were recorded at stages: before the start of anesthesia, after the block was performed, during the main stages of the operation, and in the early postoperative period.

Statistical processing of the data was carried out using standard methods of variational statistics. Quantitative indicators are presented as the mean value and standard deviation (M±SD). The significance of the differences was assessed using parametric and non-parametric criteria; the differences were considered statistically significant at $p<0.05$.

Discussion of the results: a comparative analysis of the clinical course of balanced spinal anesthesia combined with QL block in gynecological patients with hypertension (HD) and chronic circulatory failure (CCF) revealed significant differences due to the level of functional reserve.

Table 1.

Characteristics of surgical interventions

Indicator	HD (n=31)	CCF (n=37)
Operation duration (min)	138,1±6,9	146,4±19,4
Operation type	Reconstructive hysterectomy	Same
Nature of the intervention	Planned	Planned

As seen in Table 1, the groups were comparable in terms of the nature of surgical interventions. The average duration of surgeries was 138.1±6.9 minutes in the HD group and 146.4±19.4 minutes in the CCF group, which does not significantly affect the interpretation of hemodynamic and clinical indicators.

Table 2.

Intraoperative hemodynamics

Indicator	HD	CCF
Decrease in blood pressure (mmHg)	6,9	10–15
Change in heart rate (beats/min)	−1,8	−8–10
Hemodynamics	Stable	Moderately labile
Hypotension >20%	No	Unchecked

Analysis of intraoperative hemodynamics (Table 2) showed that in the HD group, the blood pressure decreases averaged 6.9 mmHg, whereas in patients with CCF, it was 10-15 mmHg. Similarly, the decrease in heart rate was less pronounced in GB (-1.8 bpm) compared to CCF (-8-10 bpm). Despite this, no episodes of clinically significant hypotension (>20%) were recorded in both groups, indicating high hemodynamic safety of the method.

The obtained differences reflect a decrease in adaptive potential in patients with CCF, which manifests as greater sensitivity to sympathetic blockade. In the GB group, hemodynamic stability is explained by the preserved contractile reserve of the myocardium.

Table 3.

External respiration indicators

Indicator	HD	CCF
SpO_2 (%)	96,8–97,3	94–95
Respiratory rate	Stable	Slightly reduced
Respiratory depression	No	No

Анализ показателей внешнего дыхания (таблица 3) показал, что уровень SpO_2 в группе ГБ составлял 96,8-97,3%, тогда как при ХНК 94-95%, при отсутствии признаков дыхательной депрессии в обеих группах. Это подтверждает безопасность методики при сохранённом самостоятельном дыхании даже на фоне сегментарной блокады.

Analysis of external respiratory parameters (Table 3) showed that the SpO_2 level in the HD group was 96.8–97.3%, whereas in CCF, it was 94–95%, with no signs of respiratory depression in both groups. This confirms the safety of the methodology while maintaining independent breathing even against the background of segmental blockade.

Table 4.

Post-operative indicators

Indicator	HD	CCF
Pain syndrome	Missing	Missing
Diuresis	Adequate	Adequate
Activation	Early	Early
Gastrointestinal restoration	Fast	Moderate

In the postoperative period (Table 4), all observations noted the absence of pain syndrome, adequate diuresis, and early activation of patients. Restoration of gastrointestinal function occurred faster in the HD group, whereas in patients with CCF, it was slower in nature, reflecting the impact of reduced functional reserve.

The regression of the motor block after 110–120 minutes while maintaining analgesia confirms the prolonged effect of the QL block. This allows for its consideration as an effective component of multimodal analgesia, compensating for a decrease in the intrathecal bupivakaine dose to 7.5 mg.

Analysis of complications showed high safety of the method: no intraoperative complications were observed, and post-puncture headache was recorded in 1 case in the HD group and 3 cases in the CCF group; it was mild in nature and did not require specific treatment.

Thus, the data in Tables 1-4 confirm that balanced spinal anesthesia combined with QL block ensures stable hemodynamics, effective analgesia, and a favorable course of the postoperative period. At the same time, patients with CCF exhibit greater variability in hemodynamic parameters and slower recovery, which is due to reduced functional reserve and requires individualized anesthesiological tactics.

Conclusion.

1. Balanced spinal anesthesia in combination with QL block ensures high hemodynamic stability and effective analgesia in gynecological patients with hypertension and chronic circulatory failure.

2. Patients with chronic circulatory insufficiency exhibit more pronounced variability in hemodynamic indicators (reduction of blood pressure to 10-15 mmHg, heart rate to −8-10 bpm), reflecting a limited functional reserve.

3. The use of a QL block allows for prolonged analgesia, reduces the dose of intrathecal anesthetic, and ensures a favorable course of the postoperative period while maintaining independent breathing.

REFERENCES

1. Desborough J.P. Stress response to surgery. *Br J Anaesth*. 2000.
2. Fleisher L.A. et al. 2022 ACC/AHA guideline. *Circulation*. 2022.
3. Gelfand B.R., Saltanov A.I. Intensive therapy. - Moscow, 2013.
4. Kehlet H., Dahl J.B. Postoperative recovery. *Lancet*. 2003.
5. Kozlov I.A. Stress reaction in anesthesiology. - Moscow, 2016.
6. McMurray J.J.V. et al. ESC heart failure guidelines. *Eur Heart J*. 2021.
7. Messerli F.H. et al. Hypertension. *Lancet*. 2017.
8. Monnet X., Teboul J.L. Fluid responsiveness. *Intensive Care Med*. 2015.
9. Pearse R.M. et al. Mortality after surgery. *Lancet*. 2012.
10. Pinsky M.R. Hemodynamic monitoring. *Chest*. 2013.
11. Rodgers A. et al. Regional vs general anesthesia. *BMJ*. 2000.
12. Sessler D.I., Pei L. Outcomes. *Anesthesiology*. 2022.

UDC: 004.942:616.24:004.8

DIGITAL TWINS: ENGINEERING AND SIMULATION IN PULMONOLOGY

Bakhrom E. Yuldashev - associate professor
Yuldash N. Islamov - associate professor
Abdumovlon Y. Islomov
Tashkent State Medical University (Tashkent, Uzbekistan)
baxrom@rambler.ru

Abstract: *The article discusses the possibilities of applying the concept of digital twins for modeling and analyzing the functioning of the human respiratory system. The relevance of the study is due to the active development of digital medicine and the need to create personalized computational models of human organs that allow predicting the course of diseases and optimizing treatment methods. Particular attention is paid to the use of mathematical modeling methods, computational hydrodynamics, and artificial intelligence technologies to construct a digital twin of the lungs based on the patient's clinical and physiological data.*

A conceptual architecture for a digital twin of the respiratory system is proposed, combining an anatomical model of the bronchial tree, a model of lung ventilation, a biomechanical model of lung tissue, and a model of gas exchange. To formalize the functioning of the respiratory system, a mathematical model of a digital twin of the lungs has been developed, describing the relationship between air flow parameters, pressure, tissue deformation, and respiratory gas diffusion processes. A computational algorithm for constructing a digital twin of a patient is presented, allowing the integration of medical imaging data, physiological monitoring, and intelligent data analysis. The results obtained demonstrate the promise of using digital twins in pulmonology for modeling lung ventilation and developing clinical decision support systems.

Keywords: *digital twins, digital medicine, pulmonology, mathematical modeling, lung ventilation, pulmonary tissue biomechanics, computational fluid dynamics, artificial intelligence, digital patient twin, personalized medicine.*

Introduction.

In recent decades, the rapid development of digital technologies has had a significant impact on the transformation of healthcare systems around the world. The integration of artificial intelligence, mathematical modeling, big data analysis, and high-performance computing is forming a new paradigm in medical science: digital medicine, focused on personalized diagnostics, disease progression prediction, and optimization of therapeutic decisions. One of the most promising areas in this field is the concept of digital twins—dynamic virtual models of biological systems capable of reproducing the physiological processes of the body based on real clinical and biomedical data from patients [4].

In a medical context, a digital twin is an integrated computational model that combines medical imaging data, physiological parameters, clinical indicators, and machine learning algorithms to create a personalized virtual copy of a patient's organ or organism. Such models allow for computer simulations of physiological processes, analysis of the dynamics of pathological changes, and prediction of the body's response to various therapeutic interventions without directly affecting the patient. In this regard, digital twin technology is considered one of the key tools for the development of precision medicine and digital clinical decision support systems [9].

The use of digital twins is particularly relevant in pulmonology, where the functioning of the respiratory system is characterized by a high degree of complexity and multi-level organization. The lungs are a hierarchical anatomical and functional structure that includes a branched system of

airways, alveolar structures, and an extensive vascular network that supports ventilation and gas exchange processes. The development and progression of diseases such as chronic obstructive pulmonary disease, bronchial asthma, pneumonia, and acute respiratory distress syndrome are accompanied by complex changes in respiratory mechanics, ventilation-perfusion ratios, and regional lung ventilation. Traditional methods of diagnosis and clinical monitoring often do not allow for a full assessment of the dynamics of these processes, which necessitates the use of modern methods of computational modeling of the respiratory system [5].

Modern advances in medical imaging (computed tomography, magnetic resonance imaging), computational fluid dynamics (CFD), biomechanical modeling, and machine learning algorithms make it possible to create highly accurate virtual models of the lungs. The integration of these technologies into the concept of digital twins makes it possible to simulate airflows in the airways, analyze the mechanical properties of lung tissue, and predict ventilation distribution in different parts of the lungs. Such approaches open up new prospects for the development of personalized respiratory therapy strategies, optimization of ventilation support parameters, and prediction of the course of respiratory diseases [2,3].

The relevance of developing digital technologies in medicine is particularly increasing in the context of the modernization of the healthcare system in the Republic of Uzbekistan, where a number of state programs aimed at introducing digital solutions and innovative technologies into medical practice have been implemented in recent years. As part of national strategies for the development and digital transformation of healthcare, special attention is being paid to the development of medical information systems, telemedicine, artificial intelligence systems, and scientific research in the field of biomedical technologies. Respiratory diseases remain one of the most significant medical and social problems, due to both epidemiological factors and the impact of the region's environmental conditions. In this regard, the introduction of digital modeling methods and digital twin technologies can contribute to improving the accuracy of diagnosis, monitoring the condition of patients, and increasing the effectiveness of treatment for respiratory diseases [1].

Thus, the development of engineering methods for creating digital twins of the respiratory system and their application in pulmonology is a promising direction in modern biomedical science. The use of computational models and digital simulations allows for a deeper study of the physiological mechanisms of breathing, the prediction of the development of pathological processes, and the development of new approaches to personalized treatment of lung diseases. In the context of the active digitalization of the healthcare system in the Republic of Uzbekistan, these technologies can become an important tool for improving the quality of medical care and developing innovative areas of medical research.

Materials and methods.

This study used an interdisciplinary approach combining methods of biomedical engineering, computational biomechanics, medical imaging, and computer modeling to develop a conceptual model of a digital twin of the human respiratory system. The methodological basis of the study is based on modern approaches to the construction of virtual physiological systems, allowing the integration of patient clinical data, mathematical models, and computational algorithms into a single digital environment [4].

The research is **theoretical, modeling, and analytical in nature** and aims to systematize modern methods for creating digital twins of the lungs used in pulmonology. As part of the work, an analysis of scientific literature devoted to digital twins of human organs [4,9], computer modeling of the respiratory system [2,5,12,13], and the application of computational fluid dynamics in medical research [2,5] was conducted.

The methodological structure of the study included the following stages:

1. **A systematic analysis** of **scientific publications** on digital twins in biomedicine and pulmonology [1 - 13].

2. **Identification of key engineering methods** used in the construction of digital models of the respiratory system [2, 5, 10, 12, 13].

3. **Formation of a conceptual architecture for a digital twin of the lungs,** including data sources, computational models, and mechanisms for synchronization with real physiological parameters [4, 7, 8].

4. **Analysis of the possibilities of using digital models** for the diagnosis, prediction, and optimization of treatment of respiratory system diseases [3, 5, 7, 9, 11].

This approach made it possible to integrate existing scientific developments into a unified methodological model of a digital twin of the human respiratory system.

The formation of digital models of the respiratory system is based on the integration of various types of medical and physiological data. The following data categories were considered in this study:

1. **Medical imaging data.** Computed tomography (CT) and magnetic resonance imaging (MRI) data are the basis for constructing anatomical models of the lungs (Fig. 1). These methods allow for the acquisition of high-precision three-dimensional images of the respiratory tract, including the trachea, bronchi, and alveolar structures. Geometric models of the respiratory system used in further computational calculations are formed based on the segmentation of such images.

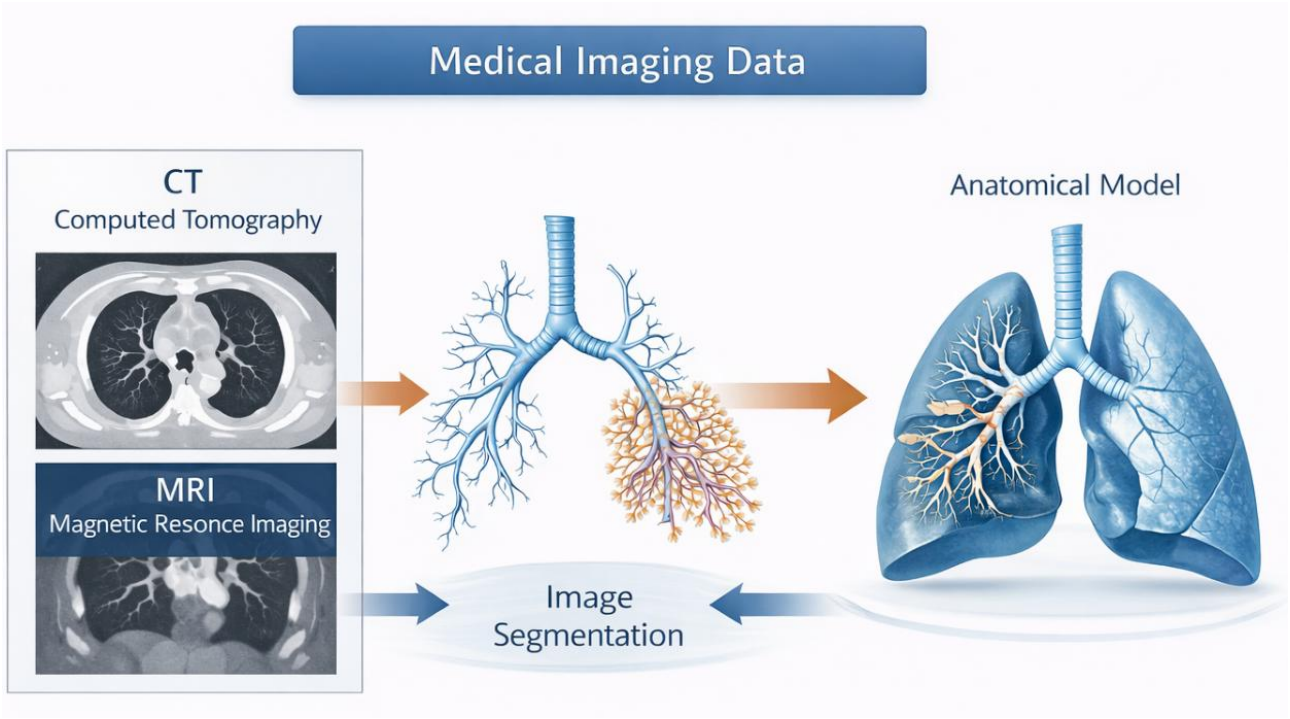


Fig. 1. Medical imaging data

2. Physiological and functional indicators

Data from functional lung studies are used to parameterize respiratory mechanics models (Fig. 2), including:

- spirometry;
- plethysmography;
- gas exchange parameters;
- respiratory volume and respiratory rate parameters.

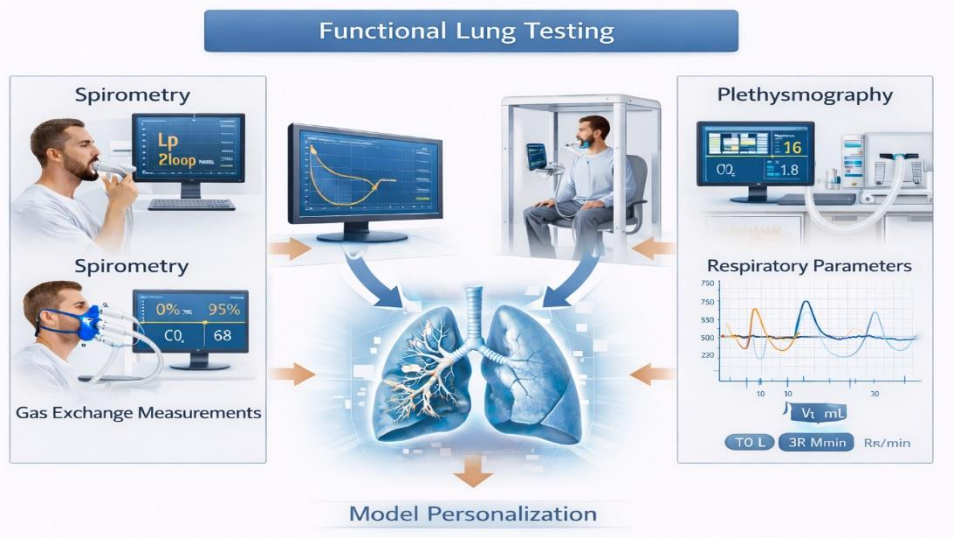


Fig. 2. Parameterization of respiratory mechanics models

These data allow determining the individual characteristics of the patient's respiratory system and adapting the parameters of the digital model [13].

3. Clinical data of patients

An important component of the digital twin is clinical data (Fig. 3), including:

- the patient's age and anthropometric parameters;
- history of respiratory system diseases;
- laboratory test results;
- respiratory therapy parameters.

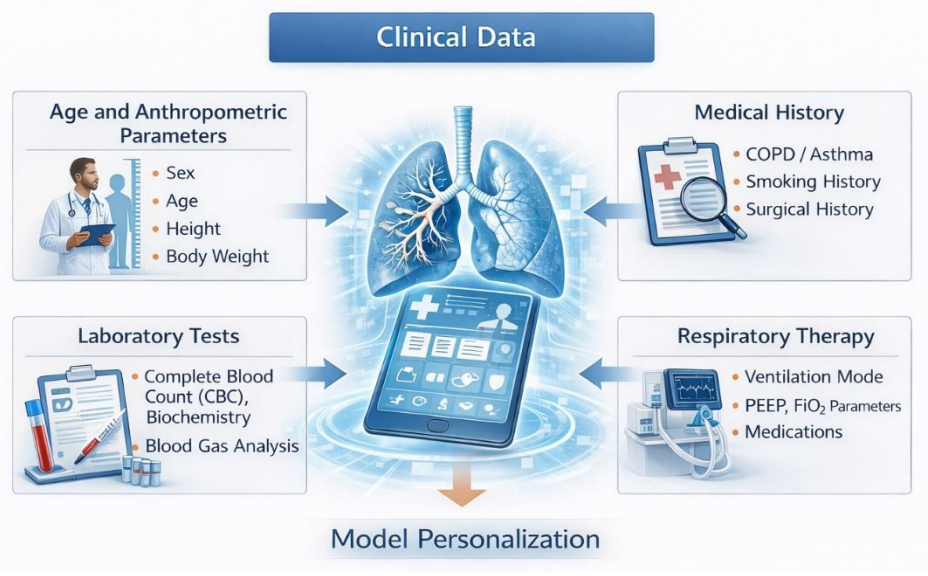


Fig. 3. Clinical data

The use of such data allows the creation of personalized models of the respiratory system and takes into account the individual characteristics of patients [9].

The creation of a digital twin of the lungs is based on the use of various methods of mathematical and computational modeling.

1. Biomechanical modeling of lung tissue

Models based on the principles of continuum mechanics are used to describe the mechanical properties of lung tissue. Such models allow analyzing the deformation of lung tissue during breathing, as well as assessing the distribution of stress and pressure in different areas of the lungs.

Biomechanical models take into account parameters such as:

- elasticity of lung tissue;
- resistance of the airways;
- lung compliance;
- pressure in the pleural cavity.

These processes are described mathematically using differential equations and numerical solution methods [12].

Let us consider a simplified model of lung tissue (Fig. 4) as an elastic material with elasticity E and viscosity η. During inhalation, the lungs expand, and the pressure distribution $P(x,t)$ along the airways is described by the force balance equation:

$$\rho \frac{\partial^2 u}{\partial t^2} = \nabla \cdot (\sigma) + f$$

where:

- u is the deformation of the lung tissue;
- ρ is the tissue density;
- σ - stress tensor, taking into account elasticity and compliance;
- f - external forces, including pressure in the pleural cavity.

This model allows predicting:

- lung tissue deformation during inhalation and exhalation;
- stress distribution in different segments of the lungs;
- the effect of changes in compliance and airway resistance on ventilation.

An example of numerical implementation: when modeling the breathing of a patient with COPD, the decrease in lung tissue elasticity (E↓), the increase in airway resistance (R↑), and changes in pressure in the pleural cavity are taken into account. Numerical methods (e.g., finite elements) can be used to obtain the distribution of deformation and pressure across the lungs, which allows the parameters of artificial ventilation to be adapted to a specific patient.

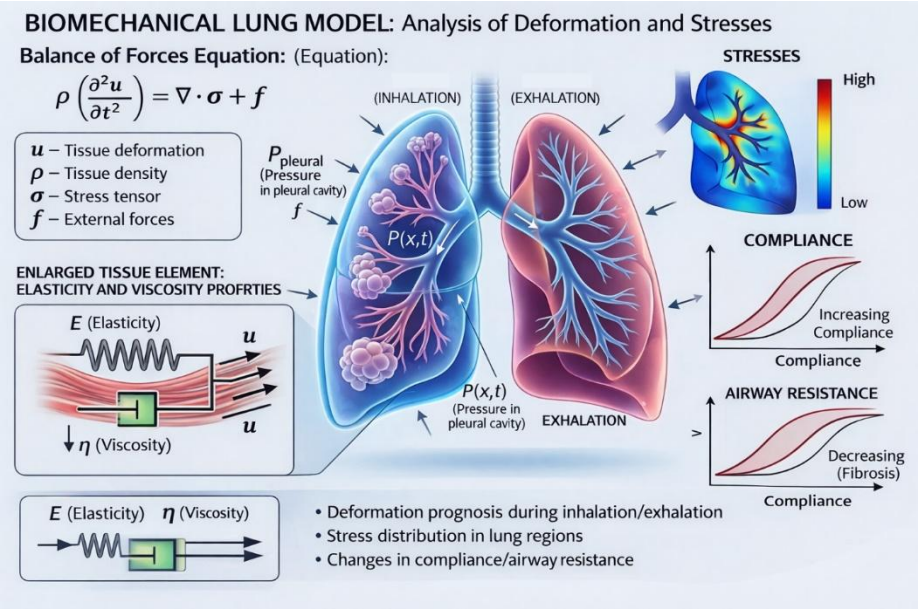


Fig. 4. Biomechanical model of the lungs

2. Airflow modeling

One of the key components of a digital twin of the respiratory system is the simulation of air movement in the airways. **Computational fluid dynamics (CFD)** methods are used for this purpose.

CFD modeling allows you to:

- analyze the distribution of air flow velocities;
- assess the turbulence of air flows in the bronchial tree;
- model the transport of aerosol particles and drugs;
- investigate lung ventilation processes.

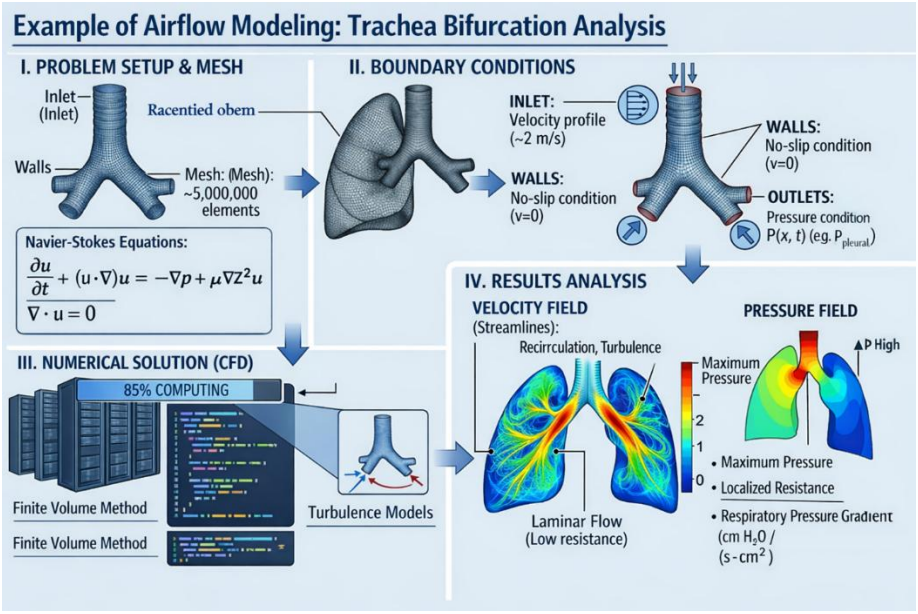


Fig. 5. Modeling of flow in the tracheal bifurcation

Calculations are performed based on the Navier–Stokes equations, which describe the motion of a viscous fluid or gas in space [2,5].

3. Multilevel modeling of the respiratory system

Modern digital twins of the lungs are based on **multilevel models** that combine several levels of organization of the respiratory system:

1. anatomical level (geometry of the respiratory tract);
2. physiological level (ventilation and gas exchange);
3. biomechanical level (lung tissue deformation);
4. system level (interaction between the respiratory and cardiovascular systems).

Such integration allows for more accurate reproduction of physiological processes and increases the predictive value of models [6,13].

As part of the study, a conceptual architecture for a digital twin of the respiratory system was developed, comprising three main components:

1. **Physical system** - the patient's actual respiratory system, the parameters of which are measured using medical devices and diagnostic methods.

2. **Digital model** - a virtual model of the respiratory system created on the basis of mathematical and computational algorithms.

3. **Data synchronization system** - a mechanism for exchanging information between the physical system and the digital model, ensuring real-time updating of model parameters.

For a clear representation of the model structure and data flows between components, it is advisable to refer to the diagram (Fig. 6):

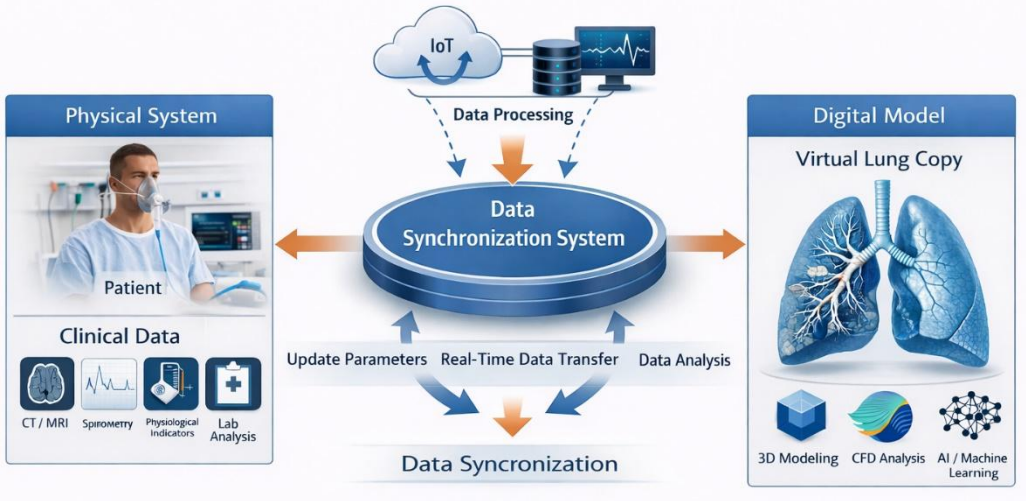


Fig. 6. Architecture of the digital twin of the human respiratory system

This architecture complies with modern principles of digital twin construction and provides the possibility of dynamic modeling of physiological processes [4,8].

The development of a digital twin of the respiratory system requires the formalization of a set of interrelated physiological processes that determine the functioning of the lungs. These processes include the movement of air flows in the bronchial tree, the deformation of lung tissue during breathing, and the processes of gas exchange between alveolar air and blood. Given the multiphysical nature of these phenomena, an adequate description of the functioning of the respiratory system is only possible based on the integration of models of aerodynamics, biomechanics, and diffusion transport of gases. In this regard, a mathematical model combining these physical and physiological mechanisms within a single computational structure is proposed for the construction of a personalized digital twin of the patient. Such a model allows describing the dynamics of lung ventilation, pressure distribution in the airways, tissue deformation, and gas exchange efficiency, which creates the basis for further numerical modeling and prediction of the state of the patient's respiratory system [6, 10, 12].

Taking into account the above provisions, a digital twin of the respiratory system can be represented as a formalized computational model reflecting the relationship between the main anatomical, mechanical, and physiological parameters of the lungs. In general terms, a digital twin of the lungs is defined as a dynamic system whose state depends on the geometry of the airways, airflow characteristics, mechanical properties of lung tissue, gas exchange parameters, and clinical monitoring data of the patient. Formally, this dependence can be represented by the following functional model:

$$DT_{lung}(t) = F(A, V, P, M, G, AI, t)$$

where

- A is the anatomical model of the bronchial tree
- V is lung ventilation
- P is the pressure distribution
- M - lung tissue mechanics
- G - gas exchange
- AI - machine learning module
- t - time

Thus, a digital twin is a multi-component multiphysical system.

Air movement in the respiratory tract is described by the Navier–Stokes equation:

$$\rho\left(\frac{\partial\vec{u}}{\partial t}+(\vec{u}\cdot\nabla)\vec{u}\right)=-\nabla p+\mu\nabla^2\vec{u}+F$$

where
- $\vec{u}$ is the air flow velocity
- p - pressure
- ρ - air density
- μ - viscosity
- F - external forces

Continuity condition:

$$\nabla\cdot\vec{u}=0$$

This allows modeling **the distribution of air flow in the bronchial tree.**

Tissue deformation is described by the elasticity equation:

$$\sigma=E\varepsilon$$

where
- σ - stress
- E - Young's modulus of lung tissue
- ε - relative deformation

Lung volume dynamics:

$$V(t)=V_0+\Delta\,\mathrm{Vsin}(\omega t)$$

where
- V_0 - functional residual capacity
- ω - respiratory rate

Pressure in the respiratory system:

$$P_{alv}=P_{atm}-R\cdot Q-E_lV$$

where
- P_{alv} - alveolar pressure
- P_{atm} - atmospheric pressure
- R - airway resistance
- Q - air flow
- E_lV - lung elasticity

The diffusion of oxygen and CO_2 is described by Fick's law:

$$J=-D\nabla C$$

where
- J - gas flow
- D - diffusion coefficient
- C - gas concentration

Oxygen transfer rate:

$$V_{O_2}=D_L\left(P_{AO_2}-P_{cO_2}\right)$$

where
- D_L - diffusion capacity of the lungs
- P_{AO_2} - alveolar oxygen pressure
- P_{cO_2} - blood oxygen pressure.

A machine learning model is used to predict the patient's condition:

$$S(t+1)=f(X_t,\theta)$$

where
- S is the patient's condition
- X_t - vector of physiological parameters
- θ - parameters of the neural network.

General system of equations:

$$\begin{cases} \rho\left(\frac{\partial \vec{u}}{\partial t} + (\vec{u}\cdot\nabla)\vec{u}\right) = -\nabla p + \mu\nabla^2\vec{u} \\ \sigma = E\varepsilon \\ P_{alv} = P_{atm} - RQ - E_l V \\ J = -D\nabla C \\ S(t+1) = f(X_t, \theta) \end{cases}$$

This system describes:

- the aerodynamics of breathing
- lung tissue deformation
- gas exchange
- prediction of the patient's condition.

The system is solved using an iterative multiphysics method**,** including:

1. CFD modeling of air flow [2,5];
2. FEM modeling of tissue deformation [12];
3. solving the diffusion equation;
4. integration with the AI module.

The structure of the model in this case is as follows (Fig. 7):

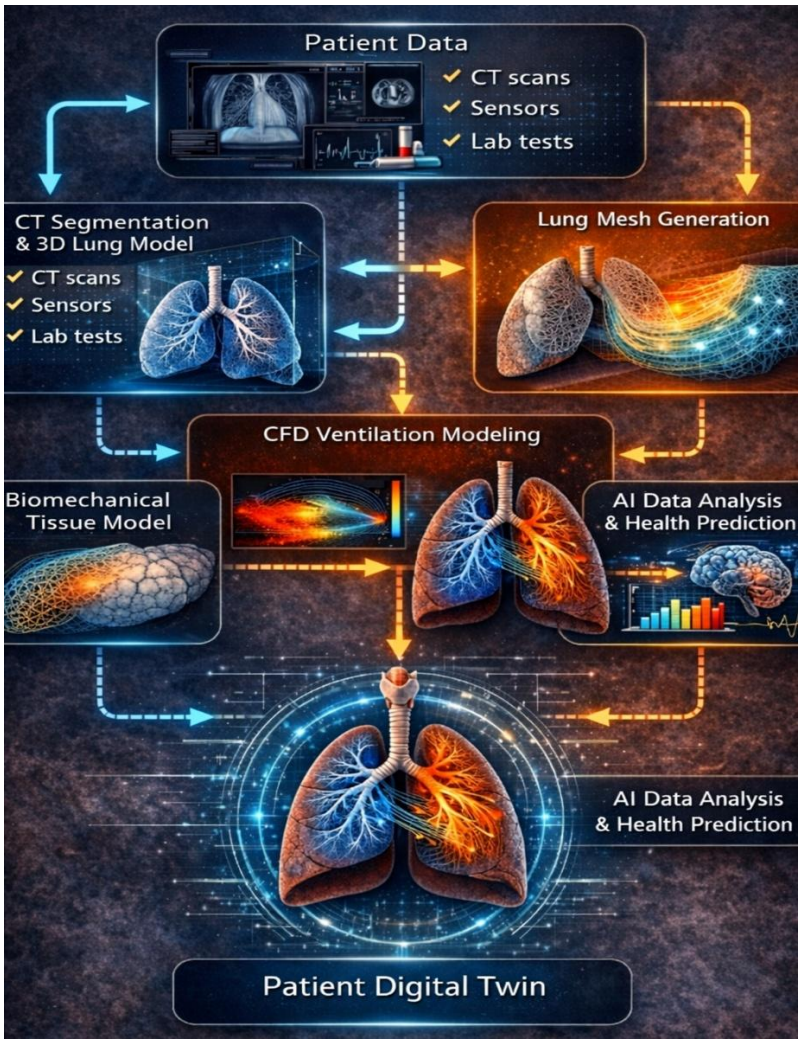


Fig. 7. Structure of the digital twin model of the respiratory system

The proposed model is distinguished by the following features:

1. it combines CFD modeling and lung biomechanics [2,5,12];
2. it takes gas exchange into account [6,12];
3. it integrates artificial intelligence algorithms [3,7];
4. it forms a complete digital twin of the patient [4,8,9].

The following methods were used to analyze the simulation results:

- statistical analysis;
- numerical modeling [10,12];
- visualization of three-dimensional models of the respiratory system;
- comparative analysis of various ventilation parameters [13].

The use of a comprehensive approach to data analysis allows us to evaluate the effectiveness of various models of the respiratory system and identify the most promising areas for their application in clinical practice.

Results and discussion.

The results of the study demonstrate the significant potential of using digital twin technologies to model the physiological processes of the respiratory system and optimize the diagnosis and treatment of lung diseases. Analysis of modern engineering and biomedical approaches has made it possible to identify key areas of application for digital twins in pulmonology, including modeling of respiratory mechanics [5, 12, 13], analysis of airflow in the respiratory tract [2, 5], and predicting the effectiveness of respiratory therapy [3,11].

One of the most important results of the development of digital technologies in medicine is the ability to create personalized three-dimensional models of the human respiratory system [8, 9] based on medical imaging data. The use of computed tomography and image segmentation methods allows the formation of detailed geometric models of the trachea, bronchial tree, and alveolar structure of the lungs [2].

The resulting anatomical models serve as the basis for further computational analysis and allow for the simulation of lung ventilation processes (). Within the framework of a digital twin, such models can be used to analyze the distribution of air flows in various parts of the respiratory system and to assess the impact of pathological changes on ventilation processes [3,13].

Recent studies show that the use of digital lung models can identify regional ventilation disorders that are difficult to detect using traditional diagnostic methods. For example, in chronic obstructive pulmonary disease (COPD), there is an uneven distribution of airflow and reduced ventilation in certain segments of the lungs, which can be detected using computational modeling [3,5].

One of the key areas of application of digital twins in pulmonology is the simulation of air movement in the airways using computational fluid dynamics (CFD) methods. These methods allow us to study the dynamics of air flows, pressure distribution, and air turbulence in the trachea and bronchial tree [2,5].

CFD modeling allows us to obtain quantitative parameters characterizing the processes of breathing, including:

- air flow velocity in different parts of the respiratory tract;
- pressure distribution during inhalation and exhalation;
- the degree of turbulence of air flows;
- features of aerosol transport of drugs.

The results of such models show that the geometric features of the respiratory tract significantly affect the nature of air movement. Even small changes in the diameter of the bronchi or the presence of inflammatory processes can significantly alter the aerodynamics of the respiratory tract and lead to a decrease in the efficiency of lung ventilation [5].

In addition, CFD modeling is actively used to analyze the effectiveness of inhaled drug delivery. Digital models allow predicting the distribution of aerosol particles in the airways and evaluating the effectiveness of various methods of inhalation therapy [2,10].

One of the most promising areas of development for digital technologies in pulmonology is the creation of individual digital twins of patients [3, 8, 9]. Such models are formed based on the integration of anatomical data, physiological indicators, and clinical information about the patient's condition.

Personalized digital models of the respiratory system allow virtual experiments to be conducted, including:

- modeling of various breathing modes;
- analysis of the effects of drug therapy;
- prediction of the development of pathological processes;
- optimization of artificial lung ventilation parameters.

For example, during respiratory therapy, a digital twin can be used to select the optimal parameters for artificial lung ventilation, which reduces the risk of ventilation-induced damage to lung tissue [6,11].

Such technologies are particularly relevant in the treatment of patients with severe respiratory diseases, such as acute respiratory distress syndrome, viral pneumonia, and chronic lung diseases [5,11].

Modern digital twins actively use machine learning and artificial intelligence methods, which allow for the analysis of large volumes of medical data and improve the accuracy of physiological process modeling [3, 7, 9].

Machine learning algorithms can be used for:

- automatically segmenting medical images;
- predicting disease dynamics;
- optimizing respiratory system model parameters;
- identifying hidden patterns in clinical data.

The integration of artificial intelligence with digital twins allows the creation of adaptive models that can be updated as new data on the patient's condition becomes available [3,8].

Analysis of current scientific research shows that digital twin technologies have significant potential to transform clinical practice in pulmonology. Their use can contribute to the development of personalized medicine [9]**,** improve diagnostics, and increase the effectiveness of treatment for respiratory diseases.

In countries with developing healthcare systems, including the Republic of Uzbekistan, the introduction of digital technologies can be an important tool for improving the quality of medical care [1]. The use of digital twins can contribute to the development of telemedicine, remote patient monitoring, and the optimization of medical institutions.

In addition, the development of digital models of the respiratory system opens up new opportunities for scientific research, medical education, and the development of innovative methods for the diagnosis and treatment of lung diseases [7,10].

Thus, the results of the study confirm that digital twins are a promising technological platform for modeling the physiological processes of the respiratory system. Their further development and integration into clinical practice can significantly improve the effectiveness of diagnosis and treatment of respiratory diseases, as well as contribute to the development of modern digital medicine.

Conclusion.

This paper provides a comprehensive analysis of modern approaches to the creation and application of digital twins in pulmonology, including the study of engineering methods, mathematical and CFD modeling, and the integration of medical imaging and artificial intelligence algorithms. The results of the study confirm that digital twins are a promising platform for

personalized modeling of physiological processes in the respiratory system, allowing to predict the dynamics of diseases, optimize the parameters of respiratory therapy, and improve the effectiveness of clinical decisions.

The scientific novelty of the study lies in the systematization of engineering and biomedical methods for constructing digital models of the lungs, as well as in the formation of a conceptual architecture for a digital twin that integrates medical imaging data, physiological indicators, and clinical information about the patient. This approach ensures dynamic adaptation of the model to changes in the patient's condition, which significantly improves the accuracy of predictions and the effectiveness of virtual experiments.

From a practical point of view, digital twins of the respiratory system can be used for:

- personalized diagnosis and treatment of respiratory diseases;
- optimizing the parameters of artificial lung ventilation and non-invasive respiratory support;
- predicting the risks of complications in chronic and acute lung diseases;
- planning inhalation therapy and drug delivery to the respiratory tract.

The introduction of digital twin technologies is particularly relevant in the context of the digitalization of healthcare in the Republic of Uzbekistan, where national programs are aimed at introducing innovative technologies into clinical practice. The use of digital models of the respiratory system can contribute to the development of telemedicine, remote patient monitoring, improved diagnostic accuracy and treatment effectiveness, as well as the creation of a scientific basis for further research in the field of digital medicine.

Despite significant achievements, methodological and technical limitations remain, including the need to integrate heterogeneous data, high computational costs, model standardization, and clinical validation. A promising area for further research is the development of adaptive digital twins capable of updating model parameters in real time based on new patient data, as well as the integration of multi-organ models for comprehensive analysis of physiological processes.

Thus, digital twins of the respiratory system are an important tool for the development of precision medicine and innovative pulmonology, opening up new opportunities for personalized treatment, improving the quality of medical care, and integrating modern computing technologies into clinical practice both internationally and in the Republic of Uzbekistan.

REFERENCES

1. Ministry of Health of the Republic of Uzbekistan. Strategy for the digital transformation of the healthcare system of the Republic of Uzbekistan. – Tashkent, 2022.

2. Agujetas R., Barrio-Perotti R., Ferrera C. Construction of a hybrid lung model by combining a real geometry of the upper airways and an idealized geometry of the lower airways // Computer Methods and Programs in Biomedicine. – 2020.

3. Avanzato R., Beritelli F., Lombardo A., Ricci C. Lung-DT: an AI-powered digital twin framework for thoracic health monitoring and diagnosis // Sensors. – 2024. – Vol. 24, No. 3. – P. 958.

4. Barricelli B. R., Casiraghi E., Fogli D. A survey on digital twin: Definitions, characteristics, applications, and design implications // IEEE Access. – 2019. – Vol. 7. – P. 167653–167671.

5. Gonsard A., Genet M. Digital twins for chronic lung diseases // European Respiratory Review. – 2024. – Vol. 33, No. 174. – P. 240159.

6. Lam T., Quach H. T., Hall L., Abou Chakra M. A multidisciplinary approach towards modeling of a virtual human lung // npj Systems Biology and Applications. – 2025.

7. Laubenbacher R., Adler F., An G., Castiglione F. Toward mechanistic medical digital twins: use cases in computational medicine // Frontiers in Digital Health. – 2024. – Vol. 6. – P. 1349595.

8. Lyu Y., Li Z., Tran V., Yang X., Li H., Wang M. Building Digital Twins of Different Human Organs for Personalized Healthcare // arXiv preprint. – 2026. – URL: https://arxiv.org/pdf/2601.11318

9. Sadée C., Testa S., Barba T., Hartmann K. Medical digital twins: enabling precision medicine and medical artificial intelligence // The Lancet Digital Health. – 2025. – Vol. 7, No. 2. – P. 120–130.

10. Tudu C., Sharma S., Kumar D. Computational modeling and digital twin technologies in medical device development // Biomedical Materials & Devices. – 2025.

11. Weaver L. The development and validation of digital twins to investigate non-invasive respiratory support in acute hypoxaemic respiratory failure // University of Warwick. – 2025. (dissertation)

12. Zhang J., Ma S., Hu T., Lian X. Construction method and verification of digital twin mechanism model of pulmonary ventilation // Journal of Mechanics in Medicine and Biology. – 2025.

13. Zhou C., Chase J.G., Chen Y. Multi-level digital-twin models of pulmonary mechanics: correlation analysis of CT lung volume and chest motion // Biomedical Physics & Engineering Express. – 2025. – Vol. 11.

UDK: 614.2:616.1/.9-036.22-058.234/.235

HYGIENIC ANALYSIS OF THE SPECIFIC FEATURES OF THE PREVALENCE OF NON-COMMUNICABLE DISEASES AMONG RURAL AND URBAN POPULATIONS

Nizom J. Ermatov
Mavlonjon Z. Nasirdinov
Maksudbek Maderimov
Tashkent State Medical University (Tashkent, Uzbekistan)
n.ermatov@tashmeduni.uz

Abstract. *This study analyzes the specific features of the prevalence of non-communicable diseases among rural and urban populations through a hygienic and socio-medical approach. The research highlights that differences in demographic, socio-economic, cultural, and healthcare accessibility factors between rural and urban residents significantly influence the spread of non-communicable diseases. In particular, lower levels of medical awareness and healthcare culture among rural populations contribute to a higher risk of morbidity and reduced use of professional medical services. The study was conducted using retrospective analytical methods based on a case-control design. The findings demonstrated regional and age-related differences in morbidity rates within the Fergana Valley, with rural populations showing a considerably higher prevalence of non-communicable diseases compared to urban populations. The results emphasize the importance of strengthening preventive measures, improving medical literacy, and enhancing access to healthcare services among rural communities.*

Keywords: *non-communicable diseases, rural population, urban population, public health, hygienic analysis, morbidity, medical literacy, preventive healthcare, socio-demographic factors, healthcare accessibility.*

Introduction.

Among countries worldwide, chronic diseases, namely non-communicable diseases (NCDs), have become one of the most pressing public health problems due to their rapid increase in recent years. According to numerous international and local studies, these diseases account for approximately 60% of global mortality and include diabetes mellitus, respiratory diseases, hypertension, complications of overweight and obesity, as well as certain types of cancer [7, 8, 10, 18, 20, 24].

The mortality rate associated with these diseases is even higher in low- and middle-income countries and is expected to continue increasing in the coming years. The major contributing factors to the growing burden of chronic diseases in these countries include decreased physical activity, sedentary lifestyle, increased consumption of unhealthy foods and tobacco products, and failure to maintain healthy daily routines. Most of these factors are considered consequences of urbanization [5, 6, 12, 14, 31, 32].

It has been reported in several studies that rural and urban populations differ in demographic, socio-economic, and cultural characteristics, as well as in their accessibility to public and private healthcare institutions, emphasizing the necessity of conducting further research in this field [8, 19, 26, 27, 41].

In the modern era, various factors affecting the growth and development of the younger generation, including changes in school-related environmental conditions, deterioration of air quality, increased consumption of fast food during school hours, insufficient intake of fruits and vegetables, excessive consumption of confectionery products, decreased intake of biologically active substances, and deficiencies of macro- and micronutrients contribute to an increase in diseases associated with anemia, iodine deficiency disorders, and various alimentary and somatic diseases [4, 7, 8, 23, 24, 33, 41].

These socio-demographic and cultural differences, particularly the lower level of medical literacy among rural populations compared to urban residents, often lead people to seek assistance from traditional healers rather than evidence-based professional medical services [14, 21, 24, 31, 32].

In particular, scientific reports indicate that in many African countries, limited access to modern medicines and healthcare services, especially among low-income families, has resulted in widespread reliance on traditional healers for disease treatment [4, 40].

According to the data of the World Health Organization (WHO) [5, 6, 30], the ratio of traditional healers to the population in Africa is approximately 1:500, which is nearly 80 times higher than the ratio of qualified physicians, estimated at 1:40,000. This suggests that most qualified physicians practice predominantly in urban areas, while millions of rural residents continue to rely on traditional healers as their primary source of healthcare [33, 36].

Today, the health of rural populations, including growing children, school students, and individuals affected by various non-communicable somatic diseases, is increasingly recognized as an important social determinant of public health [2, 10, 38].

At present, disruption of daily routines among schoolchildren, changes in labor and living conditions, alterations in dietary composition and nutritional value, environmental influences, and dietary factors associated with disease prevention contribute to the emergence of metabolic syndrome, anemia, iodine deficiency disorders, unhealthy lifestyles, and chronic fatigue among schoolchildren [4, 8, 10, 15, 18, 22, 28, 33, 39].

Evidence indicates that rural populations face unique challenges contributing to disparities in physical health, mental health, disability, and mortality [1, 9, 10, 17, 19, 37].

Furthermore, disparities in health outcomes between rural and urban populations have evolved throughout the 21st century, likely due to changes in demographic structure and socio-economic conditions in rural areas, including population aging and shifts in socio-economic distribution [11, 12, 13, 21, 31, 32].

As a result, there is an increasing need for comparative studies investigating rural–urban differences in healthcare trends among elderly populations in the 21st century. Previous studies have demonstrated that chronic pain syndrome has become significantly more prevalent among rural populations compared to urban populations over time [12, 34].

In 2010, approximately 21 million individuals in the United States were diagnosed with diabetes mellitus, which was nearly three times higher than the number reported in 1980. Approximately 90–95% of all newly diagnosed diabetes cases in the United States are type 2 diabetes mellitus. Annual outpatient visits related to diabetes exceed 27 million cases, and more than 68,000 deaths occur annually due to diabetes-related complications. Diabetes is considered the seventh leading cause of death in the United States and significantly contributes to severe complications such as renal failure and limb amputations. Complications of diabetes mellitus include cardiovascular diseases, diabetic neuropathy, and retinopathy [12, 13, 29, 35]

A study conducted in Canada demonstrated that although mortality rates among diabetic patients have significantly decreased in recent years, the reduction was substantially greater among high-income groups compared to low-income groups. Scientific studies conducted in the United States and other industrialized countries have confirmed the association between these risk factors and the increasing prevalence of diabetes mellitus and coronary heart disease. However, comparative data regarding rural–urban differences in the prevalence of diabetes and coronary heart disease remain limited, especially concerning unidentified risk factors. Previous studies have nevertheless reported a higher prevalence of diabetes among rural populations [3, 16].

Despite the implementation of numerous preventive measures aimed at reducing morbidity rates in our country, the persistence of anemia among schoolchildren and the need for effective preventive interventions remain highly relevant public health challenges.

Therefore, the main objective of this study was to conduct a hygienic analysis of the specific characteristics of the prevalence of non-communicable diseases among rural and urban populations.

Materials and Methods.

The study was conducted retrospectively using a case-control approach within the framework of an analytical epidemiological study design.

The data were collected from official statistical reports of three regions of the Fergana Valley: Fergana Region, Andijan Region, and Namangan Region.

The study covered the period from 2013 to 2023, during which morbidity indicators were analyzed dynamically according to years, territories, and age groups.

General and primary morbidity data were classified according to the International Classification of Diseases (ICD-10, 1993).

Analysis of the Obtained Results.

To establish a comprehensive assessment, morbidity data covering a 10-year period (2013–2023) were analyzed based on annual reports provided by the Ministry of Health of the Republic and regional healthcare authorities. The dynamics of disease prevalence in the Fergana, Andijan, and Namangan regions of the Fergana Valley were evaluated.

According to the analysis, in 2013 the highest morbidity rate was observed in the Namangan region (1450.5), whereas lower rates were recorded in the Andijan region (1211.2) and the Fergana region (1111.1).

By 2016, the morbidity indicators in the Namangan and Andijan regions decreased to 1380.4 and 1168.4, respectively. One possible explanation for this decline may be insufficient organization of medical examinations and reduced monitoring efficiency, as well as improved birth control and healthcare supervision during those years.

It should be emphasized that after 2016 these indicators gradually increased until 2023, after which a sharp decline was observed. In the Fergana region, however, the morbidity rate remained relatively stable throughout the observation period (see Figure 1).

These findings suggest that morbidity rates in the Fergana region remained consistently lower and relatively unchanged during the last decade compared to the other two regions, thereby highlighting the relevance and significance of the present study.

Statistical analysis of the obtained results indicates that the low quality of examinations conducted at primary healthcare institutions contributed to underestimation and insufficient control of iron deficiency anemia, overweight conditions, various forms of endemic goiter, and other health disorders. This demonstrates the necessity of conducting further scientific studies aimed at eliminating these shortcomings and improving the effectiveness of preventive healthcare measures. In the subsequent stage of the study, overall morbidity and primary morbidity rates in these regions were analyzed, and the obtained results are presented in Table 1.

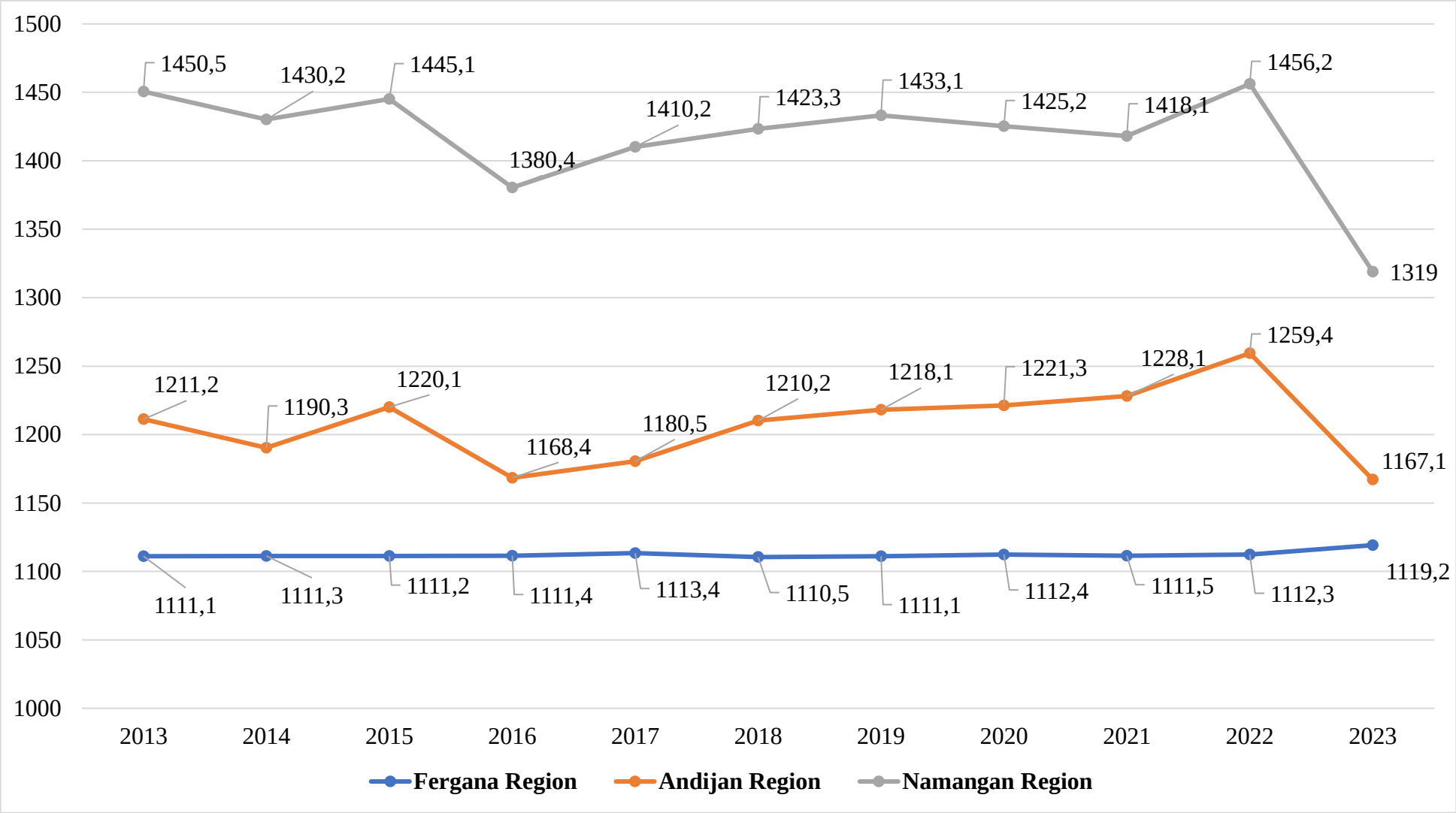


Figure 1. Characteristics of Disease Incidence Distribution by Years (per 1,000 population (‰))

Table 1. The proportion of primary morbidity relative to total morbidity across regions ()

Disease classification	Fergana region Total	Fergana Primary	Fergana % primary	Andijan region Total	Andijan Primary	Andijan % primary	Namangan region Total	Namangan Primary	Namangan % primary
Total morbidity	1113.2	586.5	52.7	1258.9	808.2	64.2	1112.3	727.4	65.4
Class I	19.7	10.2	51.8	47.5	19.3	40.6	49.5	23.2	46.9
Class II	7.5	1.3	17.3	4.8	1.2	25.0	5.8	2.1	36.2
Class III	232.1	84.8	36.5	298.5	134.3	45.0	278.5	123.4	44.3
Class IV	96.7	36.6	37.8	74.5	27.0	36.2	78.5	23.2	29.6
Class V	22.7	1.8	7.9	16.0	1.5	9.4	14.0	1.0	7.1
Class VI	48.4	30.4	62.8	35.5	23.8	67.0	40.5	22.1	54.6
Class VII	40.2	27.9	69.4	42.7	35.4	82.9	44.7	23.4	52.3
Class VIII	24.4	15.8	64.8	31.2	26.0	83.3	30.2	26.5	87.7
Class IX	126.6	30.2	23.9	85.1	38.9	45.7	82.1	32.7	39.8
Class X	236.9	173.9	73.4	264.7	222.4	84.0	254.4	212.2	83.4
Class XI	74.7	47.8	64.0	109.5	86.0	78.5	111.5	78.4	70.3
Class XII	26.7	21.0	78.7	30.7	26.7	87.0	27.7	22.1	79.8
Class XIII	20.6	11.0	53.4	19.3	12.5	64.8	20.3	8.7	42.9
Class XIV	71.6	45.4	63.4	77.4	54.7	70.7	72.4	46.7	64.5
Class XV	22.6	14.2	62.8	52.3	33.8	64.6	46.3	22.8	49.2
Class XVII	4.3	0.4	9.3	1.9	0.3	15.8	2.4	0.0	0.0
Class XVIII	0.8	0.8	100.0	3.5	3.5	100.0	2.8	2.8	100.0
Class XIX	27.9	27.9	100.0	57.8	57.8	100.0	38.8	38.8	100.0
Obesity	4.2	1.5	35.7	1.9	0.6	31.6	2.9	1.0	34.5
Hypertension-related	82.6	14.3	17.3	22.8	8.7	38.2	25.8	4.8	18.6
Ischemic heart disease	9.9	1.5	15.2	11.8	5.3	44.9	10.8	5.1	47.2
Cerebrovascular	3.0	0.7	23.3	2.2	0.8	36.4	2.7	0.9	33.3

Analysis of the results presented in Table 1 demonstrated that the following disease categories in the Namangan Region showed higher prevalence rates compared to the other two regions: endocrine system diseases (78.5‰), diseases of the blood and hematopoietic system (278.5‰), circulatory system diseases (82.1‰), chronic respiratory diseases (254.4‰), digestive system diseases (111.5‰), and genitourinary diseases (72.4‰).

The characteristics of morbidity distribution among rural and urban populations across different population groups are presented in Table 2.

In the next stage of the study, a hygienic analysis of morbidity characteristics among rural and urban populations was conducted. According to the results presented in Table 2, in the Fergana Region morbidity among children aged 0–14 years was more frequently recorded among the urban population compared to the rural population (1113.7‰). However, among individuals aged 18 years and older, the trend was reversed, with morbidity rates being higher among the rural population (1117.2‰).

In the Andijan Region, analysis by age groups demonstrated that morbidity rates among children aged 0–14 years were higher in the rural population (1230.6‰), whereas in the population aged 18 years and older, higher morbidity rates were observed among urban residents (1202.2‰). In the Namangan Region, these indicators were found to be similar to those observed in the Fergana region (see Table 2). These findings indicate the necessity of implementing comprehensive preventive measures, improving medical literacy among the population, and enhancing the effectiveness of healthcare services

Table 2.

Characteristics of Morbidity Distribution in Rural and Urban Populations (‰)

Regions	Fergana				Andijan				Namangan			
	0-14 age	15-17 age	18 years and older	Total	0-14 age	15-17 age	18 years and older	Total	0-14 age	15-17 age	18 years and older	Total
City	1113,7	1111,1	1111,8	1112,1	1199,7	1061,5	1328,2	1265,1	1506,8	655,3	646,5	1537,1
Vallage	1108,5	1111,6	1117,2	1114,3	1230,6	1202,2	1271,8	1254,3	1351,6	1310,7	1411,2	1393,9
Total	1111,1	1111,3	1114,1	1113,2	1217,1	1135,2	1295,1	1258,9	1441,8	1412,4	1467,5	1456,2

Conclusions

Based on the results of the present study, it was determined that morbidity rates differed across regions and among various age groups. In particular, the likelihood of developing non-communicable diseases among the rural population was found to be significantly higher compared to the urban population.

The obtained findings indicate that studying and evaluating risk factors contributing to the prevalence of non-communicable diseases across different regions remains one of the most актуal and important public health issues. Furthermore, the development and implementation of preventive measures targeting these risk factors should be considered one of the urgent priorities of the healthcare system.

REFERENCES

1. Atherton O.E. Are there place-based disparities in mortality risk? Findings from two longitudinal studies Health Psychol. (2024)

2. Bolin J.N., Bellamy G.R., Ferdinand A.O., Vuong A.M., Kash B.A., Schulze A., Helduser J.W. Rural healthy people 2020: new decade, same challenges J. Rural Health, 31 (3) (2015), pp. 326-333

3. Dalstra J.A. *et al.* Socioeconomic differences in the prevalence of common diseases: an overview of eight European countries Int J Epidemiol (2005)

4. Davronov U., Ermatov N., Alimuxamedov D., Kenjabaev D. Harbiy kursantlarning samarali ta'lim-tarbiya jarayonini tashkillashtirishda kun tartibining o'rnini gigienik baholash natijalari. – 2024.

5. Djumanazarova A. J. qizi, Ermatov N. J. Sravnitelnaya otsenka IMT u detey i podrostkov 11–17 let s metabolicheskim sindromom // Vestnik Assotsiatsii Pulmonologov sentralnoy Azii. – 2025. – T. 8, №3. – S. 292–295.

6. Djumanazarova A., Ermatov N. J. Otsenka pіщevogo statusa i narusheniy rosta u shkolnikov Karakalpakstana s ispolzovaniem standartov VOZ// Meditsinskiy jurnal molodых uchenых. – 2025. – №14(6). – S. 335–339.

7. Duschanov, B. A., Ibadullaeva, S. S., & Ermatov, N. J. (2022). Aholining salomatlik ko'rsatkichlariga xavf omillarining ta'sirini o'rganish natijalari.

8. Duschanova R. I., Ermatov N. J., Solieva M. Kichik maktab yoshidagi qishloq sharoitida istiqomat qilib kelayotgan bolalar kasallanishining o'ziga xos xususiyatlari // Yosh olimlar tibbiyot jurnali. – Toshkent: TMA, – B. 94.

9. Elo I.T., Hendi A.S., Ho J.Y., Vierboom Y.C., Preston S.H. Trends in non-hispanic white mortality in the United States by metropolitan-nonmetropolitan status and region, 1990–2016 Popul. Dev. Rev., 45 (3) (2019), p. 549

10. Ermatov N. Gigienicheskaya otsenka effektivnosti organizatsii fizicheskogo vospitaniya // Problemы biologii i meditsinы. – 2012. – №2(69). – S. 117–121.

11. Ermatov N. Issiq iqlim sharoitida sinfxonalar muhiti: diss. – 2022.

12. Ermatov N. J. Bolalar va o'smirlarda temir tanqislik kamqonlikda ovqatlanishning o'rni. – 2022.

13. Ermatov N. J. va boshq. Mirzacho'l sharoitida maktab o'quvchilari kasallanishi tahlili. – 2024.

14. Ermatov N. J. va boshq. Muciqa maktablarida o'quv jarayoni // Molodoy uchenыy. – 2015. – №9. – S. 437–439.

15. Ermatov N. J., & Dovronovich, B. O. (2026). Hygienic recommendations for preventing risk factors in the daily routine of preschool-age children. *The latest pedagogical and psychological innovations in education*, *3*(1), 71-72.

16. Ermatov N. J., Alimuxamedov D. Sh., Xolbekov B. B. Gigienicheskiy analiz sezonnogo pitaniya // Osnovы meditsinы. – 2025. – T. 1, №7. – S. 348–351.

17. Ermatov N. J., Ergasheva Sh. S. Gigienicheskie usloviya obucheniya podrostkov // Molodoy uchenыy. – 2017. – №23-2. – S. 38–40.

18. Ermatov N. J., Pardaev X. K., Mirzaraximov J. U. Gigienicheskaya otsenka kachestva pitaniya shkolnikov // Vrach-aspirant. – 2011. – T. 44, №1.3. – S. 407–411.

19. Ermatov N. J., Yusufov N. I., To'raqulov E. X. Maktab ichi omillarining o'quvchilar kasallanishiga ta'siri // Jurnal gumanitarnых i yestestvennых nauk. – 2023. – №4(2). – S. 174–179.

20. Ermatov N. Peculiarities of nutrition in iron deficiency anemia in children. – 2022.

21. Ermatov N. va boshq. Raqs maktabi o'quvchilari kasalliklari tahlili. – 2015.

22. Ermatov N., Akhunova M., Ashurova M., & Berdiev O. (2025). Hygienic Analysis of Educational Process in Primary Classes

23. Ermatov N., Djolimbetov K. Mehnat ta'limi darslariga gigienik talablar: diss. – 2022.

24. Ermatov N., Nasirdinov M. Farg'ona viloyati o'quvchilari ovqatlanish tahlili: diss. – 2022.

25. Ermatov, N. (2011). Zh. Nutrition of children and adolescents studying in educational institutions at the present stage. *Tashkent Tibbiyot Academy and Akhborotnomashi*, (2).

26. Ermatov, N. J., & Esanova, N. A. (2026). Hygienic requirements for optimizing the daily routine of schoolchildren diagnosed with varying degrees of myopia. *The latest pedagogical and psychological innovations in education*, *3*(1), 73-74.

27. Ermatov, N. J., & Esanova, N. A. (2026). HYGIENIC REQUIREMENTS FOR THE NUTRITION OF SCHOOLCHILDREN DIAGNOSED WITH MYOPIA. *Recent scientific discoveries and methodological research*, *3*(1), 15-17

28. Ermatov, N. J., Akhunova, M. A., & Pardaev, K. K. (2025). Hygienic Analysis and Ways to Improve the Educational Process of Middle School Students. *JOURNAL OF EDUCATION AND SCIENTIFIC MEDICINE*, *1*(3), 31-39.

29. Fiscella K. *et al.* Adding socioeconomic status to Framingham scoring to reduce disparities in coronary risk assessment Am Heart J (2009)

30. Gari A. *et al.* Knowledge, attitude, practice, and management of traditional medicine among people of Burka Jato Kebele, West Ethiopia J. Pharm. Bioallied Sci. (2015)

31. Hughes G.D. *et al.* Characterizing herbal medicine use for Noncommunicable diseases in urban South Africa Evid. Complement. Altern. Med. (2015)

32. Hughes G.D., Aboyade O.M., Beauclair R., Mbamalu O.N., Puoane T.R. Characterizing herbal medicine use for noncommunicable diseases in urban South Africa Evid Based Complement Alternat Med, 2015 (2015), Article 736074

33. Iskandarova G. T. va b. Uchebnoe posobie po osvoeniyu prakticheskix navыkov mediko-profilakticheskogo profilya. – Tashkent, 2023.

34. Jensen L., Monnat S.M., Green J.J., Hunter L.M., Sliwinski M.J. Rural population health and aging: toward a multilevel and multidimensional research agenda for the 2020s Am. J. Publ. Health, 110 (9) (2020), pp. 1328-1331

35. Jotkowitz A.B. *et al.* Do patients with diabetes and low socioeconomic status receive less care and have worse outcomes? A national study Am J Med (2006)

36. Mander M. Marketing of Indigenous Medicinal Plants in South Africa. A Case Study in KwaZulu-Natal (1998)

37. Monnat S.M.Trends in US Working-age Non-Hispanic white mortality: rural–urban and within-rural differences Popul. Res. Pol. Rev., 39 (5) (2020), pp. 805-834

38. Nasirdinov M., Ermatov N. Temir tanqislik kamqonlik kasalligi bilan xastalangan maktab o‘quvchilarining kunlik ratsioni tarkibida sut mahsulotlarining ta’minlangan darajasini tahlili: diss. – 2022.

39. Shaykhova, G. I., & Ermatov, N. (2014). ZH. va b. Znacheniye essentsial'nykh mikroelementov v pitanii. *Khorazm Mamun akademiyasi akhborotnomasi*, *1*(30), 40-44

40. Singh V.R. The prevalence, patterns of usage and people’s attitude towards complementary and alternative medicine (CAM) among the Indian community in Chatsworth, South Africa BMC Complement. Altern. Med. (2004)

41. Vorster H.H. *et al.* Added sugar intake in South Africa: findings from the Adult Prospective Urban and Rural Epidemiology cohort study Am. J. Clin. Nutr. (2014).

HYGIENIC AND GENETIC DETERMINANTS OF DERMATO-RESPIRATORY SYNDROME FORMATION IN CHILDREN: THE ROLE OF VITAMIN D AND MMP-9 AND TGF-β1 GENE POLYMORPHISMS

Dilbar R. Kattaeva - independent researcher
Tashkent State Medical University, National Children's Medical Center (Tashkent, Uzbekistan)
kattaevadilbar50@gmail.com

Abstract. *This article presents a comprehensive analysis of the etiopathogenetic mechanisms underlying the development of dermatorespiratory syndrome (DRS) in the pediatric population of the Republic of Uzbekistan (Tashkent). The study is based on the results of a one-time analytical study involving 151 children with a confirmed diagnosis of DRS and 50 children in the control group. For the first time in the region, the association between polymorphic loci of matrix metalloproteinase-9 (MMP-9, A-8202G polymorphism) and transforming growth factor beta-1 (TGF-β1, Arg25Pro polymorphism) with vitamin D levels and nutritional status indicators was assessed. The study results demonstrate a high prevalence of vitamin D deficiency (average level 19.2 ng/ml) in the main group, which correlates with the severity of clinical manifestations according to the SCORAD scale (r = -0.62). It was established that the heterozygous AG genotype of the MMP-9 gene (identified in 49.59% of patients) is a significant predictor of epithelial barrier dysfunction. The identified nutritional imbalance, characterized by zinc and magnesium deficiency against a background of excessive consumption of simple carbohydrates, acts as a modifiable risk factor that exacerbates the implementation of the genetic program of inflammation. Based on the obtained data, a personalized preventive hygiene model was developed and substantiated, including targeted correction of micronutrient status, taking into account the patient's genetic profile.*

Keywords: *dermato-respiratory syndrome, atopic march, atopic dermatitis, children, vitamin D deficiency, genetic polymorphism, MMP-9, TGF-β1, nutritional status, epithelial barrier, personalized prevention, Uzbekistan.*

Introduction.

Relevance of the problem of allergic morbidity**:** In modern pediatrics and the hygiene of children and adolescents, the problem of allergic diseases has become a global medical and social threat. Epidemiological data from recent decades indicate a steady increase in the prevalence of atopic conditions, affecting, according to various estimates, between 30% and 40% of the child population in developed and developing countries.[1] The Republic of Uzbekistan is no exception: urbanization, changes in dietary habits, climate change, and increased airborne allergen exposure in major industrial centers such as Tashkent contribute to the rise in sensitization among the pediatric population. [2]

Of particular clinical significance is the dermatorespiratory syndrome (DRS)—a combined involvement of the skin and respiratory tract, which is a classic manifestation of the "atopic march." The concept of the atopic march describes the natural progression of allergy: from the manifestation of atopic dermatitis (AD) in early childhood to the subsequent development of allergic rhinitis (AR) and progression to bronchial asthma (BA). [3] According to current understanding, AtD is not merely a localized skin condition but a "launchpad" for systemic Th2-mediated inflammation. The compromised skin barrier becomes a gateway for allergens, leading to systemic sensitization and hyperreactivity of the bronchial tree. Statistics show that the dermo-respiratory phenotype is observed in 60% of children with severe AD, which necessitates a reevaluation of approaches to prevention and treatment.[1]

Research Focus: Barrier Dysfunction and Genetic Determinism.

Despite the availability of standardized treatment protocols, therapeutic efficacy for DRS remains variable. This is because standard therapy is often aimed at relieving symptoms but does not

address the underlying mechanisms of barrier dysfunction or the genetically determined characteristics of the immune response.

A key link in the pathogenesis of DRS is the disruption of the integrity of epithelial barriers (skin and respiratory tract mucosa). In this process, extracellular matrix remodeling enzymes, particularly matrix metalloproteinases (MMPs), play a critical role. The *MMP-9* gene, which encodes gelatinase B, is responsible for the degradation of type IV collagen in the basement membrane. Its overexpression leads to "leaky" barriers, tissue infiltration by inflammatory cells, and chronicity of the process. [5] Polymorphisms in the *MMP-9* gene can modulate the enzyme's expression level, determining individual predisposition to severe disease progression.

Parallel to the destructive processes, pathological tissue remodeling occurs, regulated by cytokines such as transforming growth factor beta-1 (TGF-β1). Polymorphisms of the *TGF-β1* gene are associated with fibrotic changes in the bronchial walls, which clinically manifest as irreversible bronchial obstruction and reduced lung function. [6]

The Role of Vitamin D as a Steroid Hormone and Immunomodulator.

In the context of hygienic and nutritional correction of DRS, vitamin D (cholecalciferol) plays a central role. Modern science views it not as a vitamin in the classical sense, but as a potent secosteroidal prohormone. Its active metabolite—1,25-dihydroxyvitamin D (calcitriol)—interacts with specific nuclear receptors (VDR) that are expressed in most immunocompetent cells and keratinocytes. [1]

The mechanisms by which vitamin D influences the pathogenesis of DRS are multifaceted:

1. Regulation of the epithelial barrier: Vitamin D induces the expression of tight junction proteins (filaggrin, claudin), ensuring the physical integrity of the epidermis and mucous membranes. [9]

2. Immunomodulation: Through VDR signaling, vitamin D suppresses the proliferation of pro-inflammatory Th1 and Th17 lymphocytes, reduces the secretion of pro-allergic cytokines (IL-4, IL-5, IL-13), and stimulates the population of regulatory T cells (Treg), thereby preventing autoimmune reactions. [10]

3. Antimicrobial protection: Vitamin D stimulates the production of endogenous antimicrobial peptides (cathelicidin LL-37), which is critically important for protecting the skin against colonization by *Staphylococcus aureus,* a potent trigger of atopic dermatitis. [9]

Nutritional aspects

The biological effects of vitamin D and the functioning of enzymatic systems cannot occur without adequate micronutrient intake. Zinc (Zn) is a structural component of the DNA-binding domains of the VDR receptor ("zinc fingers") and a cofactor for metalloproteinases. Magnesium (Mg) is necessary for the enzymatic activation of vitamin D in the liver and kidneys. A deficiency of these elements, against a background of excessive carbohydrate consumption, creates the metabolic basis for chronic inflammation. [11]

Research Objective

The aim of this study is to develop a scientifically grounded hygienic model for the prevention of dermatorespiratory syndrome in children living in Tashkent, based on a comprehensive analysis of genetic polymorphisms (*MMP-9*, *TGF-β1*), vitamin D status, and nutritional profile characteristics.

Material and methods of research.

The study was conducted as a cross-sectional study with case-control elements. The clinical and laboratory parts of the study were conducted at the Republican Specialized Scientific and Practical Medical Center (RSSPM) of Pediatrics (Tashkent, Uzbekistan). The study protocol underwent ethical review and complies with the principles of the World Medical Association's Declaration of Helsinki.

Characteristics of the participants.

The study included 151 children (main group) aged 3 to 15 years with a verified diagnosis of dermatorespiratory syndrome.

Inclusion criteria:

- Presence atopic dermatitis (diagnosis established according to the Hanifin & Rajka criteria).
- Presence of concomitant respiratory allergies (allergic rhinitis and/or bronchial asthma).
- Permanent residence in Tashkent.
- Signed informed consent from parents.

Exclusion criteria: presence of severe somatic pathologies, autoimmune diseases outside the atopy spectrum, use of systemic glucocorticosteroids within the last month.

The control group consisted of 50 otherwise healthy children, matched for gender, age, and ethnicity, with no personal or family history of allergic diseases.

Clinical examination methods Validated international tools were used for an objective assessment of disease severity:

1. Assessment of AD severity: The SCORAD (Scoring Atopic Dermatitis) scale was used. The following were assessed: area of involvement (rule of nines), intensity of clinical symptoms (erythema, edema, oozing, excoriations, lichenification, dryness), and subjective sensations (itching, sleep disturbance).

2. Asthma control assessment: The ACT (Asthma Control Test) and its pediatric version (C-ACT) were used to assess control of asthma symptoms over the past 4 weeks.

Functional diagnostics:

- Spirometry: Assessment of pulmonary function with measurement of forced expiratory volume in 1 second (FEV1) to detect obstructive abnormalities.
- FeNO: Measurement of the fraction of nitric oxide in exhaled air as a marker of eosinophilic airway inflammation (NObreath analyzer).

Laboratory methods

Determination of Vitamin D and Immune Status

Venous blood serum was used as the test material.

- The level of 25-hydroxyvitamin D was determined using chemiluminescent immunoassay on microparticles (CLIA). This method is characterized by high accuracy and reproducibility. Results were interpreted according to the criteria of endocrinology societies: deficiency <20 ng/mL, insufficiency 21–29 ng/mL, normal ≥30 ng/mL. [1]
- Total IgE levels were determined using an enzyme-linked immunosorbent assay (ELISA) to assess the degree of atopic sensitization.

Genetic analysis Molecular genetic studies included the following steps:

1. DNA extraction: From peripheral blood leukocytes using commercial kits based on nucleic acid sorption on silica gel columns.

2. Genotyping: Performed using the polymerase chain reaction followed by analysis of restriction fragment length polymorphism (PCR-RFLP).

- *MMP-9* gene: The A-8202G polymorphism was studied. Amplification was performed using specific primers flanking the polymorphic region of the promoter. PCR products were hydrolyzed with the corresponding restriction endonuclease (SphI or an analogue). The fragments were visualized by agarose gel electrophoresis.
- *TGF-β1* gene: The Arg25Pro exonic polymorphism (G915C, rs1800471) was studied. This SNP is located in the signal sequence of the gene and affects protein secretion. Allele-specific primers and corresponding restriction enzymes were used.

Nutritional Assessment (Nutrition)

Actual dietary intake was assessed using the **24-hour recall** method in combination with a semi-quantitative food frequency questionnaire (FFQ). The nutrient composition (proteins, fats,

carbohydrates, zinc, magnesium, calcium) was calculated using specialized software adapted to the tables of the chemical composition of foods consumed in Uzbekistan. Particular attention was paid to identifying hidden micronutrient deficiencies and analyzing the glycemic load of the diet.

Statistical analysis

Statistical data processing was performed using the IBM SPSS Statistics v.26

software package.

For descriptive statistics, the mean and standard deviation (M±SD) were used for normally distributed variables.

- Mean values in two independent groups were compared using Student's t-test.
- Analysis of qualitative characteristics (frequency of genotypes and alleles) was performed using Pearson's chi-square (χ^2) test.
- The association of genetic markers with the risk of developing DRS was assessed by calculating the odds ratio (OR) with a 95% confidence interval (CI).
- The Hardy-Weinberg equilibrium of genotype distributions was tested for both groups.
- Correlation analysis was performed using Pearson's correlation coefficient
- Differences were considered statistically significant at $p < 0.05$.

Results and discussion.

Clinical and Immunological Characteristics

Clinical examination of 151 children with dermatorespiratory syndrome

revealed high activity of allergic inflammation. Most patients (68.2%) were diagnosed with moderate-to-severe atopic dermatitis. The mean SCORAD index in the main group was 42.5 ± 12.4 points. The level of total IgE in the blood serum of the affected children varied widely, but the geometric mean was many times higher than age-specific norms, amounting to 485.3 ± 112.5 IU/mL, whereas in the control group this indicator did not exceed 45.2 ± 15.1 IU/mL ($p < 0.001$). A strong positive correlation was found between the SCORAD index and total IgE levels ($r = 0.74$; $p < 0.001$), confirming the leading role of IgE-mediated mechanisms in the pathogenesis of DRS in the studied cohort.

Vitamin D status

An analysis of vitamin D status revealed a marked deficiency in children with allergic conditions, despite high levels of sun exposure in the region. The mean 25(OH)D level in the main group was 19.2 ± 4.8 ng/mL, which corresponds to a clinical deficiency.

- Distribution of levels:
  - Deficiency (<20 ng/mL): 58.3% of children.
  - Insufficiency (21–29 ng/mL): 26.4% of children.
  - Normal (≥30 ng/mL): only 15.3% of children.
- In the control group, the mean 25(OH)D level was 26.4 ± 5.2 ng/mL, which is significantly higher ($p < 0.001$), but also indicates suboptimal status in the population as a whole. A significant inverse correlation was found between vitamin D concentration and clinical and laboratory markers of severity:
- With the SCORAD index: $r = -0.62$ ($p < 0.001$). The lower the vitamin D level, the more severe the skin manifestations.
- With total IgE levels: $r = -0.58$ ($p < 0.01$). Vitamin D deficiency is associated with higher sensitization.

Genetic analysis of MMP-9 (A-8202G)

Molecular genetic analysis of the A-8202G polymorphism in the *MMP-9* gene revealed significant differences in genotype distribution between the groups (Table 1).

- The heterozygous AG genotype predominated in the group of children with DRS, with a frequency of 49.59%.[1]
- The G allele (risk allele) occurs twice as often in the main group as in the control group (52.0%

vs. 26.0%).

● Clinical and genetic analysis showed that carriers of the G allele (AG and GG genotypes) had a significantly higher SCORAD score (48.2 ± 10.1 vs. 32.4 ± 8.5 in AA carriers; $p < 0.05$), confirming the association of this polymorphism with the severity of dermatitis.

Table 1.

Distribution of genotypes and alleles of the MMP-9 (A-8202G) polymorphism

Genotype / Allele	Main group (n=151), abs. (%)	Control group (n=50), abs. (%)	p-value	OR (95% CI)
AA (homozygous, normal)	35 (23.18%)	28 (56.0%)	< 0.01	1.0 (ref)
AG (heterozygous)	**75 (49.59%)**	18 (36.0%)	< 0.05	2.8 (1.4–5.6)
GG (homozygous, mutation)	41 (27.23%)	4 (8.0%)	< 0.01	4.3 (1.5–12.4)
Allele A	145 (48.0%)	74 (74.0%)	< 0.001	0.3 (0.2–0.5)
Allele G	**157 (52.0%)**	26 (26.0%)	< 0.001	**3.1 (1.9–5.0)**

Genetic analysis of TGF-β1 (Arg25Pro)

The Arg25Pro polymorphism of the *TGF-β1* gene demonstrated an association with respiratory disorders. The frequency of genotypes containing the variant **Pro** allele (Arg/Pro and Pro/Pro) in the main group was significantly higher than in the control group ($p < 0.05$). In children carrying the Pro allele, a statistically significant decrease in indicators of external respiratory function was observed: the mean

FEV1 was 82% of predicted, whereas in carriers of the Arg/Arg genotype it was 94% ($p < 0.01$). Clinically, this manifested as signs of early bronchial remodeling: fixed obstruction and frequent episodes of wheezing, resistant to standard bronchodilator therapy.

Combined risk analysis

A multivariate analysis was performed to assess the cumulative effect of genetic and environmental factors. A high-risk group was identified:

- The combination of an "adverse" genotype (*MMP-9* G allele or *TGF-β1* Pro allele) with vitamin D deficiency (<20 ng/mL) increases the risk of developing severe forms of DRS by 4.2 times (OR = 4.2; 95% CI: 2.1–8.4). This indicates a synergistic effect of genetic predisposition and nutritional deficiency.

Nutritional profile

Analysis of actual dietary intake revealed systemic deficiencies:

1. Zinc (Zn) deficiency: Reduced zinc intake (below the age-specific norm) was identified in 65% of children in the main group.
2. Magnesium (Mg) deficiency: Insufficient magnesium intake was recorded in 58% of patients.
3. Carbohydrate imbalance: In 72% of children, the diet was characterized by an excess of simple carbohydrates (sugar, confectionery) against a background of dietary fiber deficiency, which creates a pro-inflammatory metabolic environment.

Discussion.

Interpretation of results in the context of global data

The results of our study confirm and complement current understanding of the role of vitamin D and genetics in the pathogenesis of allergic diseases. The data obtained on the high prevalence of

vitamin D deficiency (84.7%) among children with DRS in Tashkent are consistent with the findings of studies by Peroni et al. (Europe) and Chiu et al. (Asia), who also identified an inverse relationship between 25(OH)D levels and the severity of atopic dermatitis. [12] The paradox of low vitamin D status in a sunny region (Uzbekistan) is likely explained not only by dietary factors but also by genetic characteristics of the receptor system and vitamin D metabolism, as well as clothing habits and sun exposure ("avoidance behavior").

The identified high frequency of heterozygous *MMP-9* carriers (49.59%) exceeds the rates typical of European populations and approaches the data for East Asian cohorts, which underscores the uniqueness of the genetic profile of the Uzbek population and the need for regional reference databases. [13]

Molecular Pathogenesis: The Vitamin D–VDR–MMP-9 Axis

The key scientific contribution of this study is the elucidation of the molecular mechanism linking vitamin D deficiency to skin barrier dysfunction through the regulation of the *MMP-9* gene.

Matrix metalloproteinase-9 (MMP-9) is an enzyme capable of degrading type IV collagen, which forms the basis of the basement membrane of the epidermis and bronchial epithelium, as well as the proteins of tight junctions between cells. Under normal conditions, *MMP-9* expression is tightly regulated. Vitamin D ($1,25(OH)_2D$) binds to the intracellular VDR (Vitamin D Receptor). This complex

is translocated into the cell nucleus, where it forms a heterodimer with the retinoic

acid receptor X (RXR). The VDR-RXR complex binds to negative response elements (nVDREs) in the promoter region of the *MMP-9* gene or physically blocks the binding sites for the pro-inflammatory transcription factors NF-κB and AP-1. [8] Thus, vitamin D acts as a transcriptional repressor, inhibiting the synthesis of the destructive enzyme.

Pathogenic cascade in deficiency:

Vitamin D deficiency: The concentration of the ligand ($1,25(OH)_2D$) decreases, and VDR receptors remain inactive.

1. Lifting of repression: The *MMP-9* gene promoter is "released" from the inhibitory influence of VDR.

2. Genetic amplification: Against a background of allergic inflammation (cytokines IL-4, TNF-α), *MMP-9* transcription is activated. In carriers of the A- 8202G polymorphism (G allele), the promoter exhibits increased affinity for transcription factors, leading to *genetically determined overproduction* of the enzyme. The effect is cumulative: "no brake" (D deficiency) + "full throttle" (G allele) = massive expression of MMP-9.

3. Barrier disruption: Excess MMP-9 destroys the basement membrane and intercellular contacts. A phenotype of "leaky skin" and "leaky epithelium."

4. Vicious cycle: Allergens (house dust mites, pollen) and microbiota (*S. aureus*) penetrate through barrier defects, triggering a new wave of inflammation and further depletion of vitamin D. [5]

The role of TGF-β1 and remodeling

The Arg25Pro polymorphism of the *TGF-β1* (transforming growth factor beta-1) gene is located in the protein's signal sequence, which affects the efficiency of its secretion. Under conditions of chronic inflammation in DRS, carriage of the variant allele (Pro) is associated with dysregulation of TGF-β1's fibrogenic function. This leads to excessive deposition of the extracellular matrix in the submucosal layer of the bronchi, thickening of the reticular basement membrane, and smooth muscle hypertrophy. Clinically, this correlates with a decrease in FEV1 and the formation of an irreversible component of obstruction (remodeling), which is a precursor to severe asthma in adulthood. [6]

The Role of Nutritional Factors: Zinc and Magnesium Identified zinc and magnesium deficiencies exacerbate the described pathogenic mechanisms:

Zinc (Zn): MMP-9 is a zinc-dependent endopeptidase (it contains a zinc ion in its active site). However, systemic zinc deficiency paradoxically exacerbates inflammation. Zinc is essential for proteins

"zinc fingers" (e.g., A20), which inhibit the NF-κB pathway. Zinc deficiency leads to the activation of NF-κB, resulting in the overproduction of pro-inflammatory cytokines and MMP-9. In addition, zinc is critical for DNA repair and keratinocyte proliferation during the healing of skin microtraumas. [11]

Magnesium (Mg): It is an essential cofactor for cytochrome P450 enzymes (25-hydroxylase in the liver and 1α-hydroxylase in the kidneys) that convert vitamin D into its active form. Magnesium deficiency leads to functional hypovitaminosis D even with normal cholecalciferol intake (magnesium-dependent resistance), blocking the protective effects of VDR. [23]

Scientific novelty

For the first time in Uzbekistan, it has been demonstrated that the manifestation of the genetic risk for DRS (carriage of the *MMP-9* G and *TGF-β1* Pro alleles) is not a fatal inevitability but is mediated by modifiable factors— vitamin D levels and micronutrient status. It has been shown that it is precisely the combination of "genetics + deficiency" that yields the maximum clinical effect (OR=4.2), which justifies the need for epigenetic therapy.

Conclusion:

1. Epidemiology of deficiency: Among children with dermatorespiratory syndrome in Tashkent, a critically high prevalence of vitamin D insufficiency and deficiency (84.7%) was identified, with a mean level of 19.2 ng/mL. Low 25(OH)D levels are an independent marker of atopic dermatitis severity (r = -0.62) and high sensitization (IgE).
2. Genetic risk (MMP-9**):** The A-8202G polymorphism of the *MMP-9* gene is a significant genetic predictor of AD in the Uzbek population. The heterozygous AG genotype (49.59%) and the G allele are associated with matrix metalloproteinase overproduction, leading to the destruction of epithelial barriers and a more severe clinical course.
3. Respiratory prognosis (TGF-β1): The Arg25Pro polymorphism of the *TGF-β1* gene determines the risk of early airway remodeling. Carriers of variant alleles demonstrate a significant reduction in lung function parameters (FEV1), which requires early prevention of asthmatic changes.
4. Synergy of factors: A cumulative effect of gene-environment interaction has been established: the combination of genetic risk with vitamin D deficiency increases the likelihood of developing severe forms of DRS by 4.2 times.
5. Nutritional depression: Zinc and magnesium deficiency, as well as excessive carbohydrate intake, are underlying conditions that block endogenous repair mechanisms and reduce the effectiveness of vitamin D-dependent immunoregulation.

Conclusions and Practical Recommendations

1. Implementation of a genetic passport: Recommend molecular genetic screening (MMP-9 A-8202G, TGF-β1 Arg25Pro) for children in the high-risk group (burdened family history, early onset of AD) to predict the trajectory of the "atopic march" and form groups for follow-up care.

Personalized Vitamin D Supplementation:

○ Dose adjustments should be made on a case-by-case basis. Children with "high-risk" genotypes (MMP-9 AG/GG) require maintenance of 25(OH)D levels in the upper quartile of the normal range (40–60 ng/mL) for effective suppression of the MMP-9 promoter.

○ Therapeutic doses should be selected individually (minimum 1500–2000 IU/day during the loading phase) under the supervision of calcium excretion, with a transition to maintenance doses exceeding standard prophylactic levels.

Nutritional strategy:

○ Cofactor therapy: Mandatory administration of magnesium supplements (5–10 mg/kg/day) during the first 1–2 months of vitamin D therapy to activate its metabolism.

○ Barrier therapy: A course of zinc supplements to restore tight junctions in the epithelium and inhibit NF-κB.

○ Diet: Strict restriction of simple carbohydrates (sugars) to reduce systemic low-grade inflammation.

2. Hygiene model: The organization of a hypoallergenic living environment and sun exposure regimen should be based not on general recommendations, but on the child's individual genetic profile, considering the environment as a tool for epigenetic regulation of the disease.

REFERECES

1. Ataeva M. The rising prevalence of allergic diseases in children: risk factors and preventive measures. *Preventive Medicine and Health*. 2025;4(1):78–85.

2. Buraczynska M., et al. MMP9 Gene Polymorphism (rs3918242) Increases the Risk of Cardiovascular Disease in Patients with Type 2 Diabetes. *J Clin Med*. 2023.

3. Buraczynska K., et al. Matrix Metalloproteinase-9 (MMP-9) Gene Polymorphism in Stroke Patients. *J Mol Neurosci*. 2015.

4. Dharmage S.C., et al. Atopic dermatitis and the atopic march revisited. *Allergy*. 2014;69(1):17-27.

5. Halder S.K., Osteen K.G., Al-Hendy A. Vitamin D3 inhibits expression and activities of matrix metalloproteinase-2 and -9 in human uterine fibroid cells. *Hum Reprod*. 2013;28(9):2407–2416.

6.Gray N.A., et al. Zinc deficiency as a risk factor for increased susceptibility and severe progression of COVID-19. *Br J Nutr*. 2020.

7. Kattaeva D., Abdullaeva D. Vitamin D deficiency and its clinical correlates in children with dermo-respiratory syndrome: a prospective study. *Bulletin of the National Children's Medical Center*. 2025;3(2):73–78.

8. Karim V., et al. Matrix Metalloproteinase-9 Deficiency Impairs Cellular Infiltration and Bronchial Hyperresponsiveness during Allergen-Induced Airway Inflammation. *Am J Pathol*. 2002.

9. Kim S.H., Baek M.S. Vitamin D Inhibits Expression and Activity of Matrix Metalloproteinase in Human Lung Fibroblasts (HFL-1) Cells. *Tuberc Respir Dis (Seoul)*. 2014;77(2):73-80.

10. Mogensen Z., et al. Zinc and Atopic Dermatitis: A Systematic Review and Meta-Analysis. *JEADV*. 2019 Soltani A., et al. Vessel-Associated Transforming Growth Factor-Beta1 (TGF-β1) Is Increased in the Bronchial Reticular Basement Membrane in COPD and Normal Smokers. *PLoS One*. 2012;7(6):e39736.

11. Turaeva N.O. The significance of vitamin D deficiency in the development of bronchial obstructive syndrome in children and its relationship with cytokine status. *Journal of Hepato-Gastroenterological Research*. 2024.

12. Sharma S., et al. Variants in TGFB1, Dust Mite Exposure, and Disease Severity in Children with Asthma. *Am J Respir Crit Care Med*. 2009;179(5):356- 362.

DIAGNOSTIC ADVANTAGES OF LOW-DOSE MSCT IN THE EARLY DETECTION OF LUNG PATHOLOGIES

Mokhinur A. Khamidova - independent researcher
Tashkent State Medical University (Tashkent, Uzbekistan)
mkhamidova1604@gmail.com

Abstract. Background. *Early detection of pulmonary pathologies is one of the most critical tasks of modern diagnostic radiology. Multislice computed tomography (MSCT) provides high spatial resolution and enables detection of minimal morphological changes in lung parenchyma. However, routine MSCT protocols involve ionizing radiation, which is a significant concern, particularly for patients requiring repeated examinations.* ***Objective.*** *To evaluate the diagnostic advantages of low-dose MSCT (LDCT) in the early detection of pulmonary pathologies compared to standard MSCT protocols, with emphasis on radiation safety.* ***Methods.*** *A prospective observational study was conducted involving 115 patients (aged 18–45) treated for COVID-19 (n = 109; 94.7%) or community-acquired pneumonia (n = 6; 5.3%) between 2023 and 2026 at Department of Pulmonology and Internal Medicine of the Central Military Clinical Hospital of the Republic of Uzbekistan. Patients were divided into two groups: standard MSCT (n = 57; 120–130 kV, 180–250 mAs, effective dose 4.5–6.0 mSv) and LDCT (n = 58; 100 kV, 50 mAs, effective dose 1.2 mSv) using a GE Revolution EVO 64-slice tomograph with iterative reconstruction algorithms (ADMIRE and ASIR-V). Lung involvement was graded CT-0 to CT-4.* ***Results.*** *LDCT protocols reduced the effective radiation dose by approximately 73% compared to standard MSCT (1.2 mSv vs. 4.5–6.0 mSv) while maintaining high diagnostic image quality. The use of iterative reconstruction algorithms (ADMIRE, ASIR-V) effectively suppressed noise in low-dose images. LDCT demonstrated sufficient diagnostic accuracy for detecting ground-glass opacities, consolidation, infiltrative and interstitial changes in both COVID-19 and community-acquired pneumonia cases.* ***Conclusion.*** *Low-dose MSCT is an effective, safe, and promising method for the early diagnosis of pulmonary pathologies. Its implementation in clinical practice, based on the ALARA principle, allows significant reduction of radiation exposure while maintaining diagnostic quality, particularly for patients requiring repeated examinations.*

Keywords: *low-dose MSCT, lung pathologies, early diagnosis, radiation safety, ALARA principle, computed tomography, diagnostic optimization.*

Introduction. Lung diseases are among the most common pathologies in modern medicine, and their early detection and timely treatment are crucial for improving patients' quality of life. Respiratory system diseases, including pneumonia, bronchopulmonary inflammatory processes, interstitial changes, lung tissue damage, and other pathological conditions, can often present with minimal clinical signs in their early stages. Therefore, using modern, high-precision diagnostic methods is a pressing issue [1, 2, 3].

Radiation diagnostic methods, particularly computed tomography (CT), play a crucial role in identifying pathologies of the thoracic organs. With the development of multislice computed tomography (MSCT) technology, it is now possible to evaluate structural changes in lung tissue with high precision, detect small pathological foci, and accurately determine the extent of the disease process [4, 5, 6, 7].

MSCT offers higher sensitivity and specificity than traditional radiological examinations, enabling the early detection of minimal changes in the lung parenchyma, infiltrative processes, nodular formations, fibrotic changes, and other pathological conditions. This is of significant diagnostic importance, particularly in identifying diseases at stages where clinical symptoms have not yet become apparent [8, 9].

However, alongside the widespread use of MSCT examinations, concerns related to the effects of ionizing radiation remain a pressing issue. The radiation dose a patient receives during computed tomography depends on the examination protocol, technical parameters, and the device's capabilities. Therefore, reducing the radiation dose while maintaining diagnostic effectiveness is one of the primary tasks of modern radiology [10, 11, 12].

In this context, the development and practical implementation of low-dose MSCT (LDCT) technologies are of great significance. Low-dose MSCT makes it possible to reduce the amount of ionizing radiation exposure to the patient while maintaining sufficient image quality. This approach is particularly important for patients who require screening, dynamic monitoring, and repeated diagnostic examinations [13, 14, 15].

The effectiveness of low-dose MSCT protocols is increased by optimizing examination parameters, adjusting X-ray tube voltage and current, utilizing automatic exposure control systems, and applying modern iterative reconstruction algorithms. These technologies make it possible to reduce the radiation dose while maintaining diagnostic image quality [16, 17, 18].

Thus, the use of low-dose MSCT is a promising approach for the early detection of pulmonary pathologies, expanding diagnostic capabilities, and ensuring radiation safety. This article examines the diagnostic advantages of low-dose MSCT in identifying pulmonary pathologies and explores its significance in modern radiology [19, 20, 21].

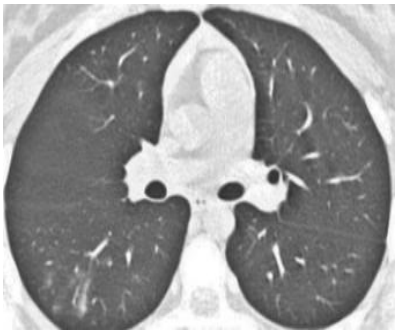


Figure 1A

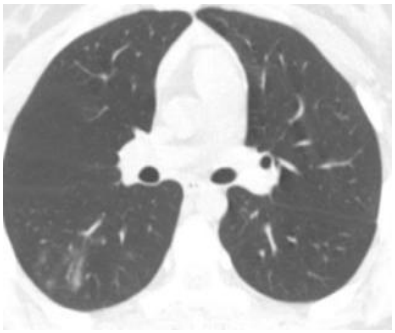


Figure 1B

Fig. 1. Low-dose chest CT of a 23-year-old patient (X) with COVID-19.
A — with model-based iterative reconstruction;
B — low-dose CT without model-based iterative reconstruction.



Figure 2A

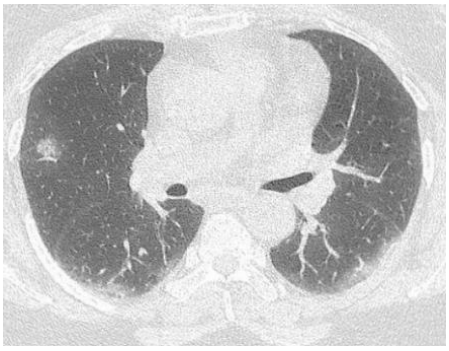


Figure 2B

Fig. 2. Standard chest CT scan of a 28-year-old patient S. with COVID-19.
A — with model-based iterative reconstruction;
B — standard CT without model-based iterative reconstruction.



Figure 3A

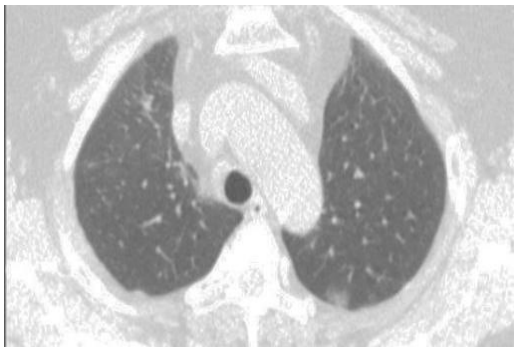


Figure 3B

Fig. 3. MSCT of the chest of a 35-year-old patient M. with COVID-19. A — normal contrast; B — low contrast.

Materials and methods.

Ethics statement: This study was approved by the Local Ethics Committee of Tashkent State Medical University (Protocol No. ___/2023). All participants provided voluntary written informed consent prior to inclusion in the study. The study was conducted in accordance with the principles of the Declaration of Helsinki (2013).

Study design and patient population.

A prospective observational study was conducted involving 115 patients aged 18 to 45 years who were treated for COVID-19 or community-acquired pneumonia between 2023 and 2026 at the clinics of Tashkent State Medical University. Patients were divided into two diagnostic groups based on CT protocol: standard MSCT (n = 57) and low-dose CT, LDCT (n = 58). By diagnosis, 109 patients (94.7%) had confirmed COVID-19 and 6 patients (5.3%) had community-acquired pneumonia.

Inclusion criteria: age 18–45 years; confirmed diagnosis of COVID-19 or community-acquired pneumonia; presence of clinical indications for chest CT; voluntary informed consent. Exclusion criteria: pregnancy; decompensated chronic diseases; allergy to contrast agent.

CT examination protocol.

All CT examinations were performed on a GE Revolution EVO 64-slice tomograph. The standard MSCT protocol used a tube voltage of 120–130 kV, a tube current of 180–250 mAs, and a slice thickness of 1.0 mm; the mean effective radiation dose was 4.5–6.0 mSv. The low-dose LDCT protocol used a tube voltage of 100 kV, an average tube current of 50 mAs, and a slice thickness of 1.25 mm; the effective dose was 1.2 mSv. Iterative reconstruction algorithms (ADMIRE and ASIR-V) were applied in all LDCT examinations to reduce image noise while maintaining diagnostic quality [16, 17, 18].

In image analysis, ground-glass opacities, consolidation, infiltrative changes, and focal densities within the lung parenchyma were assessed, along with the volume of lung involvement. The extent of damage was determined on a scale from CT-0 (no pathological changes) to CT-4 (≥75% involvement): CT-1 — ≤25%; CT-2 — 25–50%; CT-3 — 50–75%; CT-4 — ≥75%.

Clinical and laboratory analyses.

The patients' overall condition, disease severity, and progression were evaluated using clinical indicators: body temperature, blood oxygen saturation (SpO_2), and respiratory rate (RR). Laboratory tests included measurement of C-reactive protein (CRP) as an acute-phase inflammatory marker, and assessment of leukocyte and lymphocyte dynamics in the complete blood count.

Literature analysis.

To evaluate the diagnostic capabilities of low-dose MSCT in the early detection of pulmonary pathologies, this study analyzed peer-reviewed scientific literature on modern radiological diagnostic

methods, MSCT protocols, and radiation safety principles [4, 13, 14, 5]. The study evaluated the potential of MSCT to detect minimal pathological changes in the lung parenchyma and to diagnose diseases in their early stages [6, 7, 8, 9]. Methods aimed at reducing radiation exposure while preserving image quality—including optimization of scan parameters, automatic exposure control, and iterative reconstruction technologies—were also analyzed [16, 15, 18, 17].

An approach based on the ALARA principle (As Low As Reasonably Achievable) was used to assess radiation safety, entailing minimization of the ionizing radiation dose to the patient as much as reasonably achievable while preserving diagnostic information [19, 20, 21]. The obtained data were summarized using analytical and comparative methods [13, 8].

Results and discussion.

The results of the study demonstrated that low-dose MSCT (LDCT) is a highly informative method for the early detection of pulmonary pathologies. LDCT effectively identified minor structural changes in the pulmonary parenchyma and allowed assessment of the localization and extent of pathological processes in both COVID-19 and community-acquired pneumonia [4, 5, 6, 7].

One of the primary advantages of MSCT is its high spatial resolution, which enables the detection of minimal changes in lung tissue—infiltrative processes, ground-glass opacities, consolidation foci—in the early stages of disease. This contributes to timely diagnosis and increases the effectiveness of treatment [8, 9].

In the LDCT group (n = 58), the effective radiation dose was 1.2 mSv, representing a reduction of approximately 73% compared to the standard MSCT group (n = 57), in which the mean effective dose was 4.5–6.0 mSv. This result is consistent with previously published data demonstrating that low-dose protocols can reduce radiation exposure by 60–80% without significant loss of diagnostic information [13, 14, 16].

The use of iterative reconstruction algorithms (ADMIRE in standard MSCT and ASIR-V in LDCT) significantly reduced noise levels in low-dose images, thereby improving diagnostic quality. Consequently, this enhanced the ability to obtain high-resolution images while ensuring patient safety [16, 17, 18].

In the COVID-19 patient group, LDCT reliably identified bilateral multifocal ground-glass opacities, consolidation, and interstitial changes characteristic of SARS-CoV-2 pneumonia. The CT severity grade (CT-1 to CT-4) correlated with the clinical course of the disease. In cases of community-acquired pneumonia (n = 6), LDCT demonstrated lobar or segmental consolidation foci with inflammatory infiltration, consistent with standard MSCT findings.

Low-dose MSCT is particularly important for detecting pulmonary pathologies in cases requiring repeated examinations—including patients undergoing dynamic monitoring—and for groups under regular medical supervision, such as military personnel. This approach helps reduce cumulative radiation exposure while maintaining diagnostic efficacy, in full accordance with the ALARA principle [19, 20, 21].

Thus, low-dose MSCT is an effective, safe, and promising diagnostic method for the early detection of lung diseases, which expands clinical capabilities while upholding the principles of radiation protection in modern radiology [18, 19].

Conclusion.

Based on the analyses conducted, it is evident that low-dose multislice computed tomography (LDCT) is a modern examination method with high diagnostic efficacy for the early detection of pulmonary pathologies. The high spatial resolution and multiplanar reconstruction capabilities of LDCT enable the identification of minimal pathological changes in the lung parenchyma, assessment of the extent of disease, and an increase in diagnostic accuracy [4, 5, 6, 7, 8].

The study revealed that using low-dose MSCT protocols reduces radiation exposure by approximately 73% compared to standard MSCT while preserving the quality of diagnostic information. With low-dose protocols, ground-glass opacity syndrome, infiltrative and interstitial

changes, consolidation foci, and other pathological signs in lung tissue can be identified with high accuracy. This approach is particularly important for ensuring patient safety in cases requiring repeated examinations [13, 14, 15].

The study results indicated that the effectiveness of LDCT protocols is directly linked to the proper selection of examination parameters, optimization of X-ray tube voltage and current, use of automatic exposure control systems, and application of modern iterative reconstruction algorithms (ADMIRE, ASIR-V). By employing these technologies, it is possible to significantly reduce the radiation dose while maintaining image quality [16, 17, 18, 22].

Approaches based on the ALARA principle are a key criterion for ensuring radiation safety in MSCT examinations. This principle entails minimizing the patient's radiation dose as much as reasonably achievable, while maintaining the clinical justification for the examination, an individualized approach, and diagnostic effectiveness [19, 20, 21].

The use of low-dose MSCT is particularly important for patients who may require repeated medical examinations. Reducing radiation risk while ensuring the early detection of pulmonary pathologies is therefore one of the key objectives of modern diagnostics [23, 24].

In general, low-dose MSCT is an effective, safe, and promising method for the early diagnosis of pulmonary pathologies. Its application expands the opportunities for detecting diseases in their initial stages, determining the correct treatment strategy, and preventing complications. The refinement of modern MSCT technologies based on the ALARA principle ensures an optimal balance between diagnostic quality and radiation safety [18, 19, 21].

REFERENCES

1. Aberle D.R., Adams A.M., Berg C.D. et al. Reduced lung-cancer mortality with low-dose computed tomographic screening // N. Engl. J. Med. — 2011. — Vol. 365, № 5. — Pp. 395–409.

2. Ai T., Yang Z., Hou H. et al. Correlation of chest CT and RT-PCR testing for coronavirus disease 2019 (COVID-19) in China: A report of 1014 cases // Radiology. — 2020. — Vol. 296, № 2. — Pp. E32–E40.

3. Ardila D., Kiraly A.P., Bharadwaj S. et al. End-to-end lung cancer screening with three-dimensional deep learning on low-dose chest computed tomography // Nat. Med. — 2019. — Vol. 25. — Pp. 954–961.

4. Bankier A.A., Tack D. Dose reduction strategies in thoracic CT // Eur. J. Radiol. — 2010. — Vol. 76. — Pp. 28–36.

5. Beister M., Kolditz D., Kalender W.A. Iterative reconstruction methods in X-ray CT // Phys. Med. — 2012. — Vol. 28, № 2. — Pp. 94–108.

6. Blokhin I., Gombolevskiy V., Chernina V. et al. Inter-observer agreement between low-dose and standard-dose CT with soft and sharp convolution kernels in COVID-19 pneumonia // J. Clin. Med. — 2022. — Vol. 11, № 3. — P. 669.

7. De Koning H.J., van der Aalst C.M., de Jong P.A. et al. Reduced lung-cancer mortality with volume CT screening in a randomized trial // N. Engl. J. Med. — 2020. — Vol. 382, № 6. — Pp. 503–513.

8. Fang Y., Zhang H., Xie J. et al. Sensitivity of chest CT for COVID-19: comparison to RT-PCR // Radiology. — 2020. — Vol. 296, № 2. — Pp. E115–E117.

9. Greffier J., Pereira F., Hamard A. et al. Effect of tin filter-based spectral shaping CT on image quality and radiation dose for routine use on ultralow-dose CT protocols: A phantom study // Diagn. Interv. Imaging. — 2020. — Vol. 101, № 6. — Pp. 373–381.

10. Hosny A., Parmar C., Quackenbush J. et al. Artificial intelligence in radiology // Nat. Rev. Cancer. — 2018. — Vol. 18. — Pp. 500–510.

11. Hricak H., Brenner D.J., Adelstein S.J. et al. Managing radiation use in medical imaging // Radiology. — 2011. — Vol. 258. — Pp. 889–905.

12. Jain S., Finelli L. et al. Community-acquired pneumonia requiring hospitalization among U.S. adults // N. Engl. J. Med. — 2015. — Vol. 373. — Pp. 415–427.

13. Kalra M.K., Arru C., Homayounieh F. et al. Chest CT practice and protocols for COVID-19 from radiation dose management perspective // Eur. Radiol. — 2020. — Vol. 30, № 12. — Pp. 6554–6560.

14. Kang Z., Li X., Zhou S. Recommendation of low-dose CT in the detection and management of COVID-19 // Eur. Radiol. — 2020. — Vol. 30, № 8. — Pp. 4356–4357.

15. Kanne J.P., Little B.P., Chung J.H. et al. Essentials for radiologists on COVID-19: An update // Radiology. — 2020. — Vol. 296, № 2. — Pp. E113–E114.

16. Lira D., Padole A., Kalra M.K., Singh S. Tube potential and CT radiation dose optimization // AJR Am. J. Roentgenol. — 2015. — Vol. 204, № 1. — Pp. W1–W10.

17. Mayo J.R. Radiation dose issues in longitudinal studies involving computed tomography // Proc. Am. Thorac. Soc. — 2008. — Vol. 5. — Pp. 934–939.

18. National Lung Screening Trial Research Team. Lung cancer mortality with low-dose CT screening // N. Engl. J. Med. — 2011. — Vol. 365, № 5. — Pp. 395–409.

19. Prosch H., Schaefer-Prokop C., Eisenhuber E. et al. CT protocols and radiation dose management in thoracic imaging // Eur. J. Radiol. — 2018. — Vol. 101. — Pp. 98–103.

20. Rubin G.D., Ryerson C.J., Haramati L.B. et al. The role of chest imaging in patient management during the COVID-19 pandemic: A multinational consensus statement from the Fleischner Society // Radiology. — 2020. — Vol. 296, № 1. — Pp. 172–180.

21. Singh S., Kalra M.K., Hsieh J. et al. Adaptive statistical iterative reconstruction: Clinical application // Radiology. — 2010. — Vol. 257, № 2. — Pp. 373–383.

22. Tofighi S., Najafi S., Johnston S.K. et al. Low-dose CT in COVID-19 outbreak: Radiation safety, Image Wisely, and Image Gently pledge // Emerg. Radiol. — 2020. — Vol. 27, № 6. — Pp. 601–605.

23. United Nations Scientific Committee on the Effects of Atomic Radiation (UNSCEAR). Sources and Effects of Ionizing Radiation. — New York: United Nations, 2000.

24. Yeung A.W.K. The ALARA principle: A historical overview and bibliometric analysis // Radioprotection. — 2019. — Vol. 54, № 2. — Pp. 103–109.

UDC: 614.777:628.1

HYGIENIC ANALYSIS OF THE POPULATION'S DRINKING WATER SUPPLY

Nizom J. Ermatov – D.M.Sc., professor
Feruza L. Azizova – D.M.Sc., professor
Dilshod Sh. Alimukhamedov – D.M.Sc., professor
Tashkent State Medical University (Tashkent, Uzbekistan)
Murodbek A. Niyazmetov
Urgench RANCH Technological University (Urgench, Uzbekistan)
Dulta Kenjaboev – Ph.D., associate professor
Tashkent State Medical University (Tashkent, Uzbekistan)
muradbek9547@gmail.com

Abstract. *This article presents a territorial analysis of the provision of high-quality drinking water to the population of Bagat District. The findings indicate that access to drinking water in the district center is very high, with nearly the entire population covered by centralized water supply services. However, across the district as a whole, the coverage rate is 67.7%, reflecting significant disparities between the central area and remote rural settlements. This situation is associated with insufficient development of water supply infrastructure in rural communities, limited coverage of water distribution networks, and the continued use of alternative water sources, including wells and local water intake facilities. From a scientific perspective, these indicators demonstrate the persistence of territorial inequalities in access to drinking water within Bagat District. The difference between the district center and the district-wide coverage rate amounts to 29.8 percentage points (97.5% versus 67.7%), highlighting the need to modernize rural water supply systems, construct new distribution networks, and expand access to centralized drinking water services. The analysis further revealed a steady upward trend in this indicator during 2005–2026. While it stood at 11 units in 2005, it reached 25 units by 2020, representing an approximately 2.3-fold increase over 15 years. The most pronounced growth occurred during 2020–2025, when the indicator rose from 25 to 35 units, an increase of 40%. The data also show that per capita daily water consumption remained stable at 140 liters per day during 2005–2015. By 2020, this figure had increased to 180 liters per day, representing a 28.6% rise compared with 2015. The projected value for 2026 is 200 liters per day, which is 60 liters, or 42.9%, higher than in 2005, indicating a continuous increase in household water consumption. According to the available data, only 12% of the urban population was covered by centralized water supply services in 2005. This figure increased to 14% in 2010, 17% in 2015, 20% in 2020, 26% in 2025, and is projected to reach 30% in 2026, reflecting the ongoing implementation of infrastructure development projects in this sector. The study examined the condition of water supply infrastructure, the level of population coverage by centralized drinking water systems, the territorial distribution of water supply networks, and the existing challenges within the water supply system.*

Keywords: *drinking water, water supply, territorial analysis, infrastructure, centralized water supply, population coverage, water resources, public utility services.*

Relevance of the topic.

The failure of hygienic and microbiological parameters of drinking water to meet established sanitary norms constitutes one of the primary factors in the occurrence and spread of waterborne diseases. According to data from the World Health Organization, a significant proportion of diarrheal diseases is attributable to the consumption of contaminated drinking water and to inadequate sanitation conditions [16]. This problem is particularly acute in the Aral Sea region, where specific natural and climatic conditions, combined with the high degree of mineralization characteristic of local water sources, exert an adverse effect on drinking water quality [4, 7, 13].

In Bagat District as well, the issue of providing the population with safe, high-quality drinking water is of paramount importance from the perspectives of sanitary-hygienic compliance and public health protection. Accordingly, the scientific substantiation of safe and efficient water source utilization, along with the improvement of systematic microbiological monitoring of water quality, is currently regarded as one of the priority directions in the field of public health [5].

A considerable body of scientific research is being conducted at the global level on the rational and safe use of water resources and on the improvement of microbiological monitoring systems. Of particular importance are studies focused on the seasonal analysis of the microbiological status of water bodies, the identification of seasonal variations in the chemical composition of water, and the assessment of the relationship between chemical parameters and the distribution of microorganisms [3, 6, 7].

At the same time, scientific research aimed at establishing an effective monitoring system through the integrated year-round study of the microbiological, hydrobiological, parasitological, and chemical properties of water under the specific conditions of Bagat District remains insufficient. In particular, determining the prevalence of pathogenic and conditionally pathogenic microorganisms, analyzing their association with water mineralization, and evaluating the factors affecting water quality represent pressing scientific challenges. Therefore, the scientifically grounded development of preventive measures aimed at ensuring the provision of high-quality drinking water, preventing waterborne diseases, and improving sanitary-hygienic conditions is of substantial theoretical and practical significance [9].

Bagat District (see Figure 1) is one of the administrative units of Khorezm Region of the Republic of Uzbekistan. As of January 1, 2025, the district's population amounted to 179,558 persons. According to official statistical data, approximately 95% of the urban population and 86% of the rural population are covered by the centralized drinking water supply system.



Fig. 1. Map of Khorezm Region

Notwithstanding the above, the reliability and sustainability of the water supply system remain insufficient. While urban residents receive drinking water for an average of 12–24 hours per day, water supply in rural areas is largely carried out on a scheduled basis. This indicates that despite relatively high centralized water supply coverage rates, ensuring continuous provision of safe and high-quality drinking water to the population remains an ongoing challenge.

The total length of drinking water pipelines in the district is approximately 238 km. In recent years, certain measures have been undertaken to expand and modernize the centralized water supply

system. However, infrastructure development has not always been accompanied by commensurate improvements in water quality indicators. In particular, the elevated hardness level of groundwater, the primary source for domestic and drinking purposes, remains one of the key environmental and sanitary concerns in the area [3, 11].

The development and improvement of projects related to the advancement of the drinking water supply system and the protection of water sources are today inconceivable without the involvement of sanitary-hygienic specialists. Ecological-hygienic research that considers the natural-climatic characteristics, socioeconomic conditions, and sanitary-epidemiological situation of the region plays a crucial role in both project decision-making and in the determination of environmental protection measures [10].

These challenges are especially relevant for the communities of the Aral Sea region. Bagat District is no exception, as a number of difficulties related to the provision of high-quality drinking water persist. The elevated mineralization of local water sources and the unstable epidemiological situation with respect to intestinal infections further intensify the urgency of addressing this issue [15, 17, 18].

Materials and methods.

For assessing the sanitary-hygienic condition of the drinking water supply system in Bagat District, official statistical data, information bulletins on hygiene and environmental science, and reporting materials of the Sanitary-Epidemiological Welfare and Public Health Department of Khorezm Region were analyzed.

During the study, data on the quality of water from both centralized and decentralized water supply sources were utilized. Specifically, the chemical composition of water, total hardness, degree of mineralization, and microbiological parameters were examined. Additionally, comparative analyses were conducted on the proportion of drinking water samples failing to meet sanitary-hygienic requirements, the level of population coverage by centralized water supply, the water delivery schedule, and the technical condition of the water distribution networks.

The objects of study were centralized domestic and drinking water supply systems, groundwater sources, and piped water delivered to the population. During the study, the level of drinking water provision to the population, the condition of water networks, and the sanitary characteristics of the water were comparatively assessed.

Drinking water quality was evaluated against the requirements of the national standard UzSt 133:2024 "Drinking Water. Hygienic Requirements and Quality Control" of the Republic of Uzbekistan, as well as the international recommendations of the World Health Organization on drinking water quality [17, 18].

Statistical processing of the data was carried out through comparative analysis of recent-year indicators from official sources. This approach made it possible to identify the development dynamics of the water supply system in Bagat District, prevailing trends, and the principal sanitary-hygienic challenges.

The analytical findings indicate that in Khorezm Region, the level of centralized drinking water provision to the population has been gradually increasing in recent years. Nevertheless, particularly in rural areas, this indicator continues to lag behind the national average. This situation is explained by the specific natural-climatic conditions of the region, the elevated degree of groundwater mineralization, and the physical deterioration of certain sections of the water distribution infrastructure [8, 14, 15].

In the Bogat district, the indicators of centralized drinking water supply to the population have been showing positive growth dynamics in recent years. In particular, in 2020, the coverage of the urban population with centralized water supply was approximately 78 percent, and in rural areas - 60 percent, while by 2025 these indicators reached 95 and 86 percent, respectively. This indicates the effectiveness of the work carried out to expand the water supply infrastructure in the district and implement new projects.

At the same time, despite the increase in the level of water supply to the population, some problems related to the stability and quality of water supply remain. While water supply is carried out on a schedule in some settlements, fluctuations in water pressure are observed in rural areas. In addition, the high hardness of groundwater used in the district is one of the main factors negatively affecting the quality of drinking water [1,2,3].

The results of the comparative analysis show that the level of coverage of centralized water supply in the Bogat district is approaching the average indicators of the republic. However, sanitary and hygienic problems associated with water quality and its uninterrupted supply to the population remain relevant. This indicates the need to improve water treatment technologies, modernize water treatment facilities, and further develop water supply infrastructure [14,15].

Although the level of centralized water supply to the population in the Khorezm region has been increasing in recent years, its overall indicators have not yet reached a sufficient level. As of 2024, the level of water supply to the urban population was 92.5 percent, while in rural areas this indicator is much lower, remaining almost two times less (see Figure 2).

During 2023–2024, the water supply indicator in urban areas increased by approximately 11 percent, while in rural areas the growth rate reached 35 percent. This indicates that the development of water supply infrastructure in rural areas has intensified in recent years.

According to the analysis, if the current development rates are maintained, the full coverage of the urban population with centralized water supply can be achieved in approximately 6–7 years, and in rural areas - in 10–12 years. This should also take into account the natural growth of the population.

The results of the comparative assessment show that the indicators of centralized water supply in urban areas are approaching the average level of the republic, but in rural areas these indicators are still significantly lower (see Figure 2).

Although some problems remain in the field of providing the population with high-quality drinking water in the Khorezm region, in recent years, certain work has been carried out in the Bogat district to expand the volume of centralized water supply. According to local utilities, the main part of the water consumed by the population is spent on household needs and irrigation of household plots. This situation is one of the characteristics of the agriculturally specialized areas of the Khorezm region.



Fig. 2. Data on the level of drinking water supply of the population of the Bogat district of the Khorezm region as of January 1, 2026

The analysis of the structure of water consumption shows that water used for household needs and irrigation of households occupies a large share in total consumption, while water consumption in other directions is relatively small. This situation indicates a high dependence of the population, especially the population living in rural areas, on individual and multi-purpose use of water resources.

In recent years, several centralized water supply systems have been operating in the Bogat district, which provide drinking water to settlements. The total length of water pipeline networks in the district is approximately 238 km, which indicates the consistent development of water supply infrastructure.

In general, the development of centralized water supply systems in the Bogat district is in line with the general trends observed in the Khorezm region. At the same time, problems related to the physical obsolescence of some parts of the existing infrastructure, interruptions in water supply, and the high hardness of groundwater, which is used as the main source of drinking water for the population, remain relevant [1,2,11].

Results and discussion.

On the basis of the research findings, a comparative analysis was conducted of the principal water supply indicators for 2020 and 2025 across three levels: Khorezm Region as a whole, the center of Bagat District, and Bagat District overall.

Table 1 presents data on the number of water supply networks, their total length, the level of population coverage by drinking water supply and sewerage systems, and the capacity of water facilities.

Table 1

Key Water Supply Indicators for Khorezm Region, the Center of Bagat District, and Bagat District (as of 2020 and 2025)

Indicator	Khorezm Region	Bagat District Center	Bagat District
Number of water supply networks			
2020	39	1	4
2025	40	1	4
Total length of water supply networks (km)			
2020	1,715.4	134.0	179.0
2025	3,281.9	156.3	248.6
Population coverage by centralized drinking water supply (%)			
2020	45.1	84.0	37.8
2025	65.6	97.5	67.7
Population coverage by sewerage system (%)			
2020	8.4	20.0	0
2025	8.8	26.4	0

The analyzed data demonstrate that sanitary conditions regarding water use across Khorezm Region are broadly similar. However, certain inter-district variations exist with respect to drinking water coverage levels, water quality, and the reliability of water supply. Although centralized water supply coverage indicators in Bagat District are comparatively high, sanitary-hygienic concerns related to water quality and continuity of supply persist.

Within the district, the population's use of water for domestic, drinking, and cultural-household needs is primarily based on groundwater delivered through centralized water supply systems, with some residents additionally using wells and well-type structures. At the same time, water samples from both urban and rural settlements are occasionally found to be non-compliant with sanitary-hygienic norms with respect to chemical parameters—a situation primarily attributable to the elevated hardness and mineralization of groundwater.

One of the main focuses of this study was the sanitary-hygienic assessment of the water use conditions in Bagat District and the identification of existing problems.

In contrast to the tourism-oriented districts of Khorezm Region, Bagat District is predominantly an agricultural area. This characteristic directly influences both the composition of water consumption and the nature of utilization of water supply systems. In Uzbekistan, both surface and groundwater sources are widely used for domestic and drinking water supply.

At present, approximately 95% of the urban population and 86% of the rural population of Bagat District have access to centralized water supply services. One of the important positive features of the district's water supply system is that groundwater constitutes the principal water source.

At the same time, in accordance with the requirements of the national standard UzSt 133:2024 "Drinking Water. Hygienic Requirements and Quality Control" of the Republic of Uzbekistan, water quality in certain chemical parameters does not fully comply with established norms. In particular, the total hardness of water is observed to exceed the established sanitary-hygienic requirements in some instances (see Figure 3).

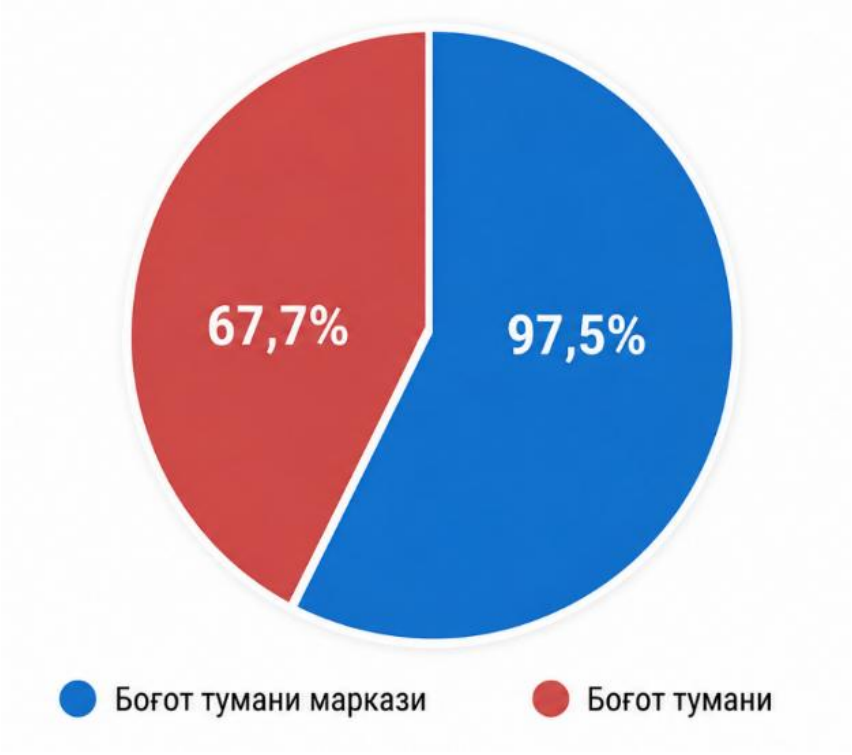


Fig. 3. Drinking water coverage levels in the center and throughout Bagat District, %

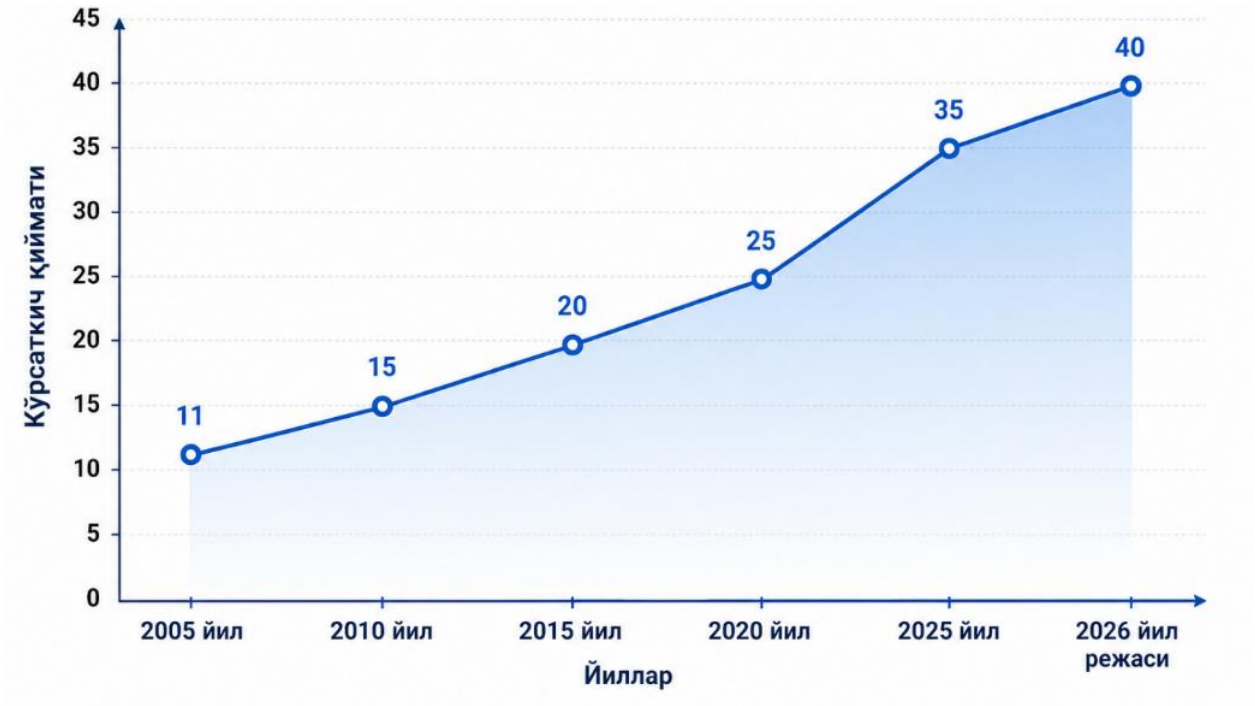


Fig. 4. Water supply capacity, thousand m³/day (2025–2026)

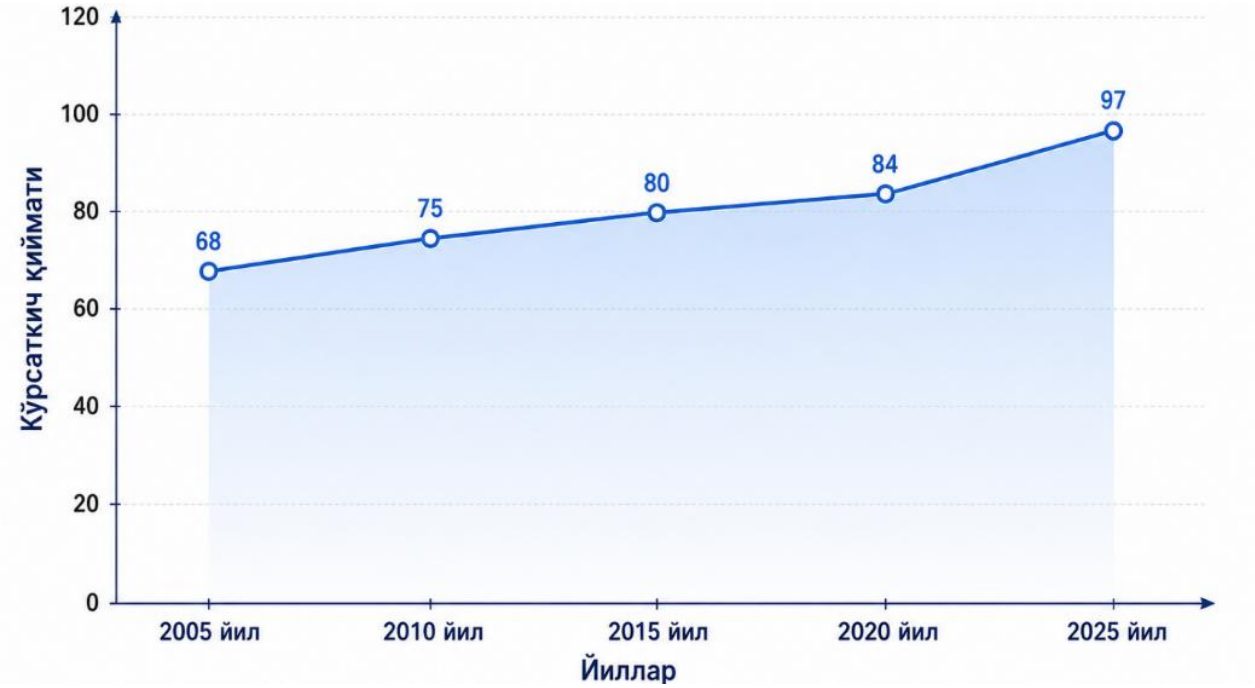


Fig. 5. Drinking water provision levels for the population of Bagat District center (2025–2026, %)

The water use of the population of Bagat District for domestic, drinking, and cultural-household purposes is primarily supplied from groundwater sources delivered through centralized water supply networks. In certain areas, residents also use individual wells and well-type structures. In some settlements, surface water sources treated through appropriate purification and disinfection processes are also utilized for drinking and domestic purposes.

However, some water samples collected from distribution networks and water sources in both urban and rural areas of the district do not fully comply with sanitary-hygienic norms in terms of chemical parameters.

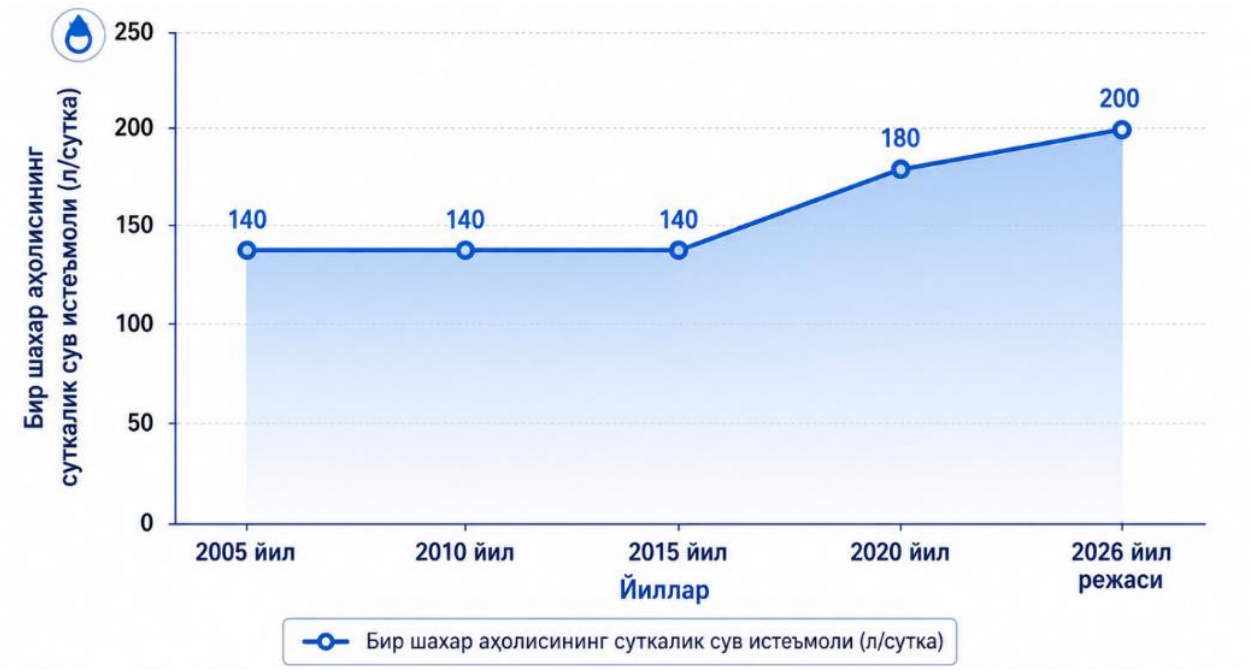


Fig. 6. Per capita daily water consumption in urban settings (2025–2026, liters/day)



Fig. 7. Urban population coverage by sewerage system (2025–2026, %)

The primary cause of this situation is related to the natural-geographical characteristics of the region: namely, the elevated hardness and mineralization of groundwater (see Figures 7 and 8).

In recent years, the proportion of tap water samples failing to meet bacteriological sanitary requirements in Khorezm Region has remained higher than the national average. Although these

indicators in Bagat District are broadly close to the regional average, deviations from sanitary-hygienic norms have been recorded in certain rural settlements. This is particularly evident in indicators related to the chemical composition of water, including those reflecting the elevated hardness and mineralization characteristics of local groundwater sources.

As a result of the modernization of water supply facilities, renovation of water treatment plants, and strengthened sanitary oversight in recent years, a gradual decrease in the proportion of non-compliant water samples has been observed.

The epidemiological safety of drinking water is assessed primarily through the compliance of its microbiological and parasitological parameters with established sanitary norms. Total microbial count reflects the degree of bacterial contamination of water, accounting for saprophytic microflora, and typically increases as a result of the influence of surface water, rainwater, or domestic wastewater. For this reason, it serves as an important indicator for monitoring the efficiency of water treatment processes at treatment facilities and for detecting technological failures.

The detection of bacteria belonging to the Enterobacteriaceae family indicates fecal contamination of water. The presence of thermotolerant coliform bacteria, including Escherichia coli, is recognized as the primary marker of "fresh" fecal contamination. Accordingly, a large number of sanitary and regulatory documents establish the complete absence of coliform bacteria as the principal criterion for assessing the epidemiological safety of drinking water.

Furthermore, the detection of coliphages in water indicates the possibility of viral contamination, while the presence of sulfite-reducing Clostridium spores signals an epidemiological risk associated with long-term fecal contamination [17, 18].

Drinking water quality is assessed against international standards, WHO guidelines for drinking water quality, and the sanitary-hygienic norms in force in the Republic of Uzbekistan. In accordance with these requirements, drinking water must be epidemiologically and radiologically safe, chemically harmless to human health, and organoleptically acceptable for consumption.

The analytical results demonstrate that the sanitary conditions of water use by the population of Bagat District are broadly consistent with the average situation observed across Khorezm Region. However, the predominance of groundwater sources and the variability in drinking water quality indicators among different settlements within the district are notable.

In this regard, the necessity of strengthening sanitary-hygienic oversight of centralized water supply systems, improving water treatment and disinfection technologies, and broadly implementing comprehensive sanitary-preventive measures aimed at protecting public health has been substantiated.

The analytical findings further indicate that groundwater sources in Bagat District generally meet the sanitary requirements established for Category I water sources with respect to turbidity, oxidizability, iron content, and fluoride levels. At the same time, deviations from normative standards are observed with respect to total water hardness and certain chemical components.

This underscores the necessity of employing water softening and disinfection technologies when utilizing groundwater within the centralized domestic and drinking water supply system.

Dug wells and tube wells remain important sources of water supply in Bagat District, particularly in rural areas. The hygienic evaluation of such water sources requires consideration of the hydrogeological characteristics of the area, potential contamination sources, and the effectiveness of the applied water treatment and disinfection technologies.

During the summer season, the sharp increase in water consumption in certain settlements of the district results in water supply being conducted on a scheduled basis. This is explained by the limited water resource availability and the insufficient technical capacity of the distribution networks.

The water supply system of Bagat District is primarily reliant on groundwater sources. At the same time, the need to modernize certain water facilities and to technically upgrade technological equipment persists.

According to data from the sanitary-epidemiological service, some water samples have been found to contain total hardness levels exceeding established norms. This condition may have an adverse effect on public health, in particular by increasing the risk of developing diseases of the urinary and digestive systems.

At the same time, the majority of water samples were found to comply with sanitary requirements in terms of microbiological parameters. Specifically, total microbial counts remained within permissible limits, and pathogenic bacteria responsible for intestinal infections were generally not detected in the samples examined.

Analysis of the quality of piped water supplied to the population of Bagat District indicates that water does not fully comply with the requirements of the national standard UzSt 133:2024 with respect to certain chemical parameters. Elevated total hardness, characteristic of local groundwater sources, remains one of the principal concerns.

Overall, the sanitary conditions of water use in Bagat District are broadly comparable to those observed in other districts of Khorezm Region. However, the predominance of groundwater sources, the instability of water quality indicators, and disparities in water supply levels between individual settlements persist as challenges requiring attention.

Conclusions.

1. An analysis of the drinking water supply situation in Bagat District, Khorezm Region, revealed a consistent increase in the level of centralized drinking water coverage over recent years. As of 2025, approximately 95% of the urban population and 86% of the rural population are supplied with piped water through centralized systems. This indicates that ongoing efforts to develop water supply infrastructure in the district are yielding tangible positive results.

2. Certain challenges persist with regard to the reliability of the water supply system and water quality. Among the principal sanitary-hygienic concerns identified in the district is the elevated hardness of groundwater used for domestic and drinking purposes. The implementation of scheduled water supply in some settlements reflects the limited technical capacity of existing networks and the physical deterioration of certain facilities.

3. Microbiological analyses indicate that drinking water parameters generally comply with sanitary requirements. However, deviations from normative standards were observed with respect to chemical parameters—most notably total hardness levels.

4. The sanitary conditions of water use by the population of Bagat District are broadly comparable to the average indicators recorded across Khorezm Region. Nevertheless, continued implementation of measures to improve water treatment technologies, modernize water supply infrastructure, and strengthen sanitary-hygienic oversight remains essential.

REFERENCES

1. Almatov, B. I., & Ermatov, N. Zh. (2018). Analysis of the effectiveness of reservoir water use based on the study of their microbial and chemical composition. European Science, (8(40)), 35–37. [In Russian]

2. Almatov, B. I., & Ermatov, N. Zh. (2018). Efficiency of reservoir water use in Uzbekistan. In International Scientific Review of the Problems and Prospects of Modern Science and Education (pp. 80–82). [In Russian]

3. Balliev, A. I., Chembarisov, E. I., Ballieva, R., et al. (2024). Contemporary mineralization and chemical composition of small local water bodies in the Southern Aral Sea region. [In Russian]

4. Duschanov, B. A., Abdullayev, R. B., Mustafayev, Kh. M., et al. (2022). The Aral Sea: Problems of ecology and health. Tashkent. [In Russian]

5. Kosimov, S. K., & Makhmudov, I. R. (2022). Problems of drinking water quality in rural regions of Uzbekistan. Bulletin of the Tashkent Institute of Irrigation and Agricultural Mechanization Engineers, (4), 25–30. [In Russian]

6. Nuraliev, N. A. (2022). Reservoirs: features of the chemical composition of water, microbiological and hydrobiological aspects. [In Russian]
7. Nuraliev, N. A. (2023). Microbiological and hygienic safety of Amu Darya river water. 18, 21. [In Russian]
8. Rakhimov, B. Kh., & Tursunov, Sh. A. (2023). Modern methods of water treatment for elevated hardness. Water and Ecology, (1), 12–18. [In Russian]
9. Siddikov, Z. A. (2024). Hygienic assessment of the water supply of the population in an ecologically unfavorable zone. Medical Journal of Uzbekistan, 6(3), 45–51. [In Russian]
10. Usmanov, I. A. (2025). Assessment of financial flows for the optimization of water supply in Uzbekistan in the context of climate change. [In Russian]
11. Chembarisov, E. I., & Balliev, A. I. (2024). Contamination of watercourses and water bodies of the Republic of Karakalpakstan and practical recommendations for its reduction. [In Russian]
12. Ermatov, Z., et al. (2022). Modelling the chemical composition process concerning formation of metals from manual arc surface on the basis of the electrode coating charge components classification. International Journal of Mechatronics and Applied Mechanics, (12), 170–176.
13. Khalilov, B., & Mamarasulov, A. (2021). Health risks associated with high mineralization of drinking water in the Aral Sea region. Environmental Health and Preventive Medicine, 26, 45.
14. UNDP Uzbekistan. (2020). Water Governance in the Republic of Uzbekistan: Challenges and Opportunities. Tashkent.
15. UNICEF & WHO. (2023). Progress on Household Drinking Water, Sanitation and Hygiene 2000–2022: Special Focus on Inequalities. New York: UNICEF.
16. WHO. (2024, March 7). Fact sheet: Diarrhoeal disease. Retrieved from https://www.who.int/news-room/fact-sheets/detail/diarrhoeal-disease
17. World Health Organization (WHO). (2022). Guidelines for Drinking-water Quality (4th ed., incorporating the 1st and 2nd addenda). Geneva: WHO Press.
18. World Health Organization / UNICEF. (2024). Diarrhoea: Why children are still dying and what can be done. WHO/UNICEF Report.

VENTRICULAR EXTRASYSTOLES OF VARIOUS ORIGINS, THE FREQUENCY OF THEIR DETECTION AND THE RELATIONSHIP WITH VARIOUS FACTORS

Rashida R. Mutigullina - independent researcher
Gulnora A. Nagayeva - D.M.Sc., associate professor
Military Medical Institute of the Military Security and Defense University of the Republic of Uzbekistan
rashidochka1985@mail.ru

Abstract. *Ventricular extrasystole (VE) is one of the most common cardiac rhythm disorders detected both in healthy individuals and in patients with cardiovascular diseases. This article reviews data from population-based and clinical studies on the prevalence of ventricular extrasystole and analyzes factors associated with its occurrence. The review demonstrates that the frequency of VE increases with age and is strongly influenced by the duration of electrocardiographic monitoring. Major predictors of ventricular extrasystole include hypertension, smoking, reduced left ventricular ejection fraction, myocardial infarction, thyroid dysfunction, anemia, and occupational stress. Particular attention is paid to the impact of environmental and occupational factors, including air pollution, heat stress, and intensive physical and psycho-emotional workloads. The findings emphasize the importance of early detection and continuous monitoring of ventricular extrasystole, especially among individuals exposed to increased cardiovascular risk factors. A comprehensive assessment of clinical, occupational, and environmental determinants may improve preventive strategies and contribute to reducing the burden of cardiovascular complications associated with ventricular arrhythmias.*

Keywords: *ventricular extrasystole, premature ventricular contractions, ventricular arrhythmias, cardiovascular risk factors, Holter monitoring, thyroid dysfunction, anemia syndrome, occupational stress, air pollution, cardiovascular diseases.*

Prevalence of ventricular extrasystole: analysis of data from population and clinical studies. Many studies describing the prevalence of ventricular extrasystole (VE) originate from ECG databases or Holter monitoring ECG (HMECG)studies among those seeking clinical care, where the prevalence is expected to be elevated. In one of the first major population assessments conducted back in 1962, a survey of 12,2043 U.S. Air Force personnel showed that 7.8 out of 1,000 experienced VE during a 48-second ECG recording, with the prevalence increasing with age. [3]. In a more modern cohort of a multiethnic community-based study of men and women aged 45 to 64 years (ARIC (Atherosclerosis Riskin Communities) study - Risk of atherosclerosis in communities), at least 1 VE occurred in 252 (1.8%) of 14,000 routine 10-second ECGs in participants without heart failure (HF) [2]. In the Cardiovascular Health study, in a cohort of individuals aged at least 65 years at the community level, 243 of 4,710 (5.2%) patients had an ECG during their baseline 10-second ECG after excluding individuals with advanced HF [20]. Unsurprisingly, the prevalence of EE increases as the duration of monitoring increases. In the same ARIC study, a 2-minute ECG revealed FE in 5.5% of the population. [39]. In the Framingham Heart Study, evidence of HE or other more complex ventricular arrhythmias was observed in 12% of people without coronary heart disease (CHD) who were observed for 1 hour [17]. In one population-based study of healthy individuals aged 25-41 years, 24-hour HMECG revealed at least a single VE in 69% of particip D.M.Sc., associate professorants [4].

In another study conducted on a random sample of 1,139 Americans using 24-hour ECG, it was found that extrasystoles account for a median of 0.011% of the total number of heartbeats (interquartile range 0.002%-0.123%) [22]. It was also found that among participants who had repeated 24-hour HMECG in the same population 5 years after the first examination, the median number of extrasystoles per hour increased to 5 (interquartile range 0.1–4.7), and it was 1.2

(interquartile range 0.1–13.8) [37]. These data can be compared with the results obtained using HMECG monitors. For example, Heckbert and colleagues [6] presented the results of a study conducted with 1,122 participants from the MESA (Multi-Ethnic Study of Atherosclerosis) study who used a ZIO patch (manufactured by Rhythm Technologies). In the study, 99.5% of the elderly participants (average age 75 years) showed at least one manifestation of JE. The median number of extrasystoles was 1.9/hour (interquartile range 0.3–12).

From the general health system, it was found that among the 16.8 million California residents who visited emergency departments, hospitals, or outpatient surgical centers between 2005 and 2009, 35,817 (0.2%) had a VE code in their medical records. [20].

The relevance of the study of the prevalence of VE among these patients is due to the unique physical and psychological stresses they are exposed to. In conditions of prolonged training, intense physical exertion and stress typical of this service, the likelihood of cardiac arrhythmias increases significantly. Considering that arrhythmias may not appear at early stages and are often detected only with prolonged monitoring, the use of modern diagnostic methods, in particular HMECG, is necessary for the timely diagnosis and prevention of heart diseases. Thus, in order to ensure the health of these patients and optimize preventive measures aimed at reducing the risk of cardiovascular diseases (CVD), further research is required aimed at early detection, timely and adequate monitoring of VE in this population. This will not only improve the quality of medical care, but also increase the effectiveness of measures to preserve health in the long term.

Predictors of ventricular extrasystole: risk factors and their relation to clinical characteristics. Although the term "predictors" may imply a causal relationship, it is important to emphasize that most studies on this topic simply report characteristics that are statistically significantly associated with the presence of VE or a higher frequency of VE. Most of these studies are cross-sectional, since the presence of VE is almost always determined during the basic visit.

An analysis of the ARIC study showed that older age, male gender, black race, a history of hypertension, the presence of other heart diseases (CHD, digitalis or other antiarrhythmic drugs), higher heart rate (HR), lower level of education and hypomagnesemia were associated with the presence of at least one VE during the 2ndone-minute ECG recording [36]. Other factors, particularly smoking, were not included in this analysis. Among the 1,412 examined, it was found that an increase in age, taller height, and a lower left ventricular ejection fraction (LVEF) were associated with an increase in the frequency of VE after multifactorial adjustment [37] (Fig. 1)

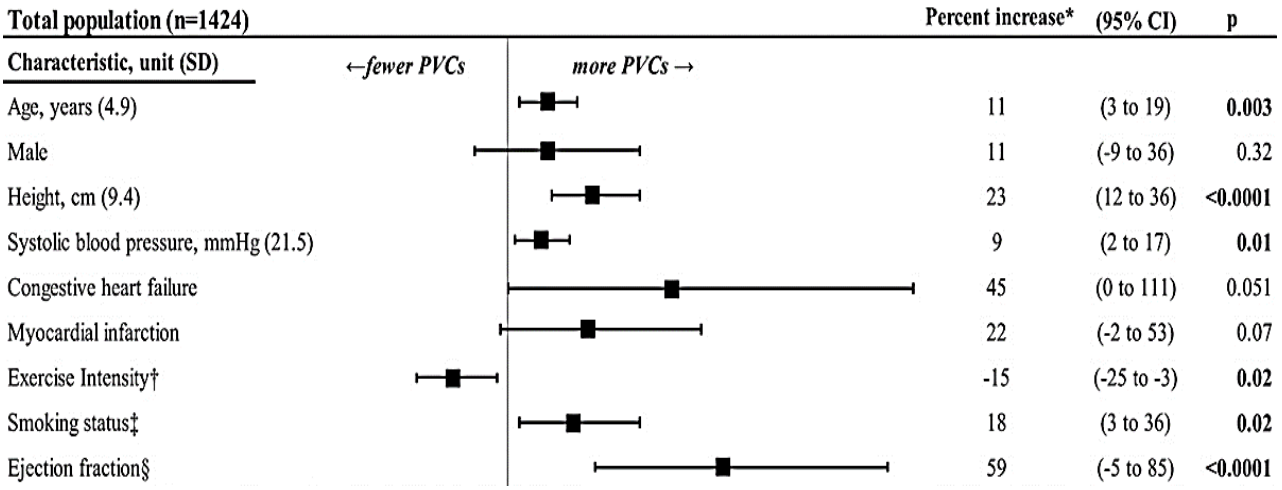


Fig. 1. Multidimensional adjusted predictors of VE frequency.

Notes: *The model includes all the listed covariates.*

** Percentage increase in VE per hour per SD of continuous covariates or the presence (versus absence) of each categorical variable.*

† Dichotomous division into high- and medium-intensity physical exercises versus low-intensity physical exercises and non-physical exercises. The dichotomous division into smokers versus never smokers.

§ Dichotomous separation into abnormal and marginal ejection fraction versus normal ejection fraction. PVCs indicates a premature ventricular complex. [37].

In addition, after taking these factors into account, elevated systolic blood pressure, irregular physical training, and smoking were identified as potentially modifiable risk factors associated with an increase in the incidence of hypertension. Several hundred of these participants underwent a repeated 5-year HMECG study, which provided a rare opportunity to evaluate the predictors of an increase in the number of VE in the population. A history of myocardial infarction, lower LVEF, increased diastolic blood pressure, and smoking were associated with an increase in the frequency of VE over time after multifactorial adjustment [37].

Continuing to consider the predictors of EE, it is necessary to pay attention to several factors that can significantly affect the development and frequency of VE, especially among certain population groups. One of these factors is the state of thyroid hormones. An imbalance in the level of thyroid hormones, in particular hypothyroidism, can contribute to the development of arrhythmias, including VE [4]. The levels of T3 and T4 directly affect the electrical activity of the heart, changing the conduction and excitability of the myocardium. Hypothyroidism, for example, may be associated with an increased frequency of extrasystoles, and hyperthyroidism may be associated with cardiac arrhythmias. This factor should be taken into account when examining patients with suspected arrhythmias.

Basically, arrhythmias in patients with hyperthyroidism are atrial, ventricular arrhythmias are rare and occur in about the same way as in healthy people [28]. Ventricular tachycardia (VT) is one of the main causes of death in patients with cardiovascular diseases (CVD). Ventricular arrhythmia is observed in patients with thyrotoxicosis undergoing antithyroid therapy, although rarely [28, 8]. Ventricular tachycardia usually occurs in connection with background structural heart diseases or HF of various etiologies [1, 33].

In addition, anemia syndrome is another important predictor for the development of VE. Lack of hemoglobin and oxygen in the blood can contribute to myocardial hypoxia, which in turn increases the likelihood of premature ventricular contractions. In addition, anemia syndrome is another important predictor for the development of EE. Lack of hemoglobin and oxygen in the blood can contribute to myocardial hypoxia, which in turn increases the likelihood of premature ventricular contractionanemia, reducing oxygen delivery to tissues, causes hyperstimulation of the autonomic nervous system, which can lead to impaired conduction in the heart and the appearance of extrasystoles. From the point of view of pathological anatomy, the relationship of anemic syndrome with ventricular arrhythmia can be explained by diffuse myocardial fibrosis, which is a well-known substrate for the development of VE, especially in the context of arrhythmogenic triggers such as hypoxemia, acidosis, or cardiac electrical conduction disturbances, which are quite common in this population [32,29,38,16].

Special attention should be paid to specific professions where increased physical and psycho-emotional stress can affect the development of VE. For example, military personnel, pilots, firefighters, and other professionals whose professional activities involve constant stress and physical exertion are at increased risk of extrasystoles. Such people often have a combination of risk factors, such as intense exercise, physical fatigue, stressful situations, and effects on the heart. These loads can cause adaptive changes in cardiac conduction and increase the frequency of VE. Moreover,

professional activity under stress can contribute to an increase in catecholamine levels, which is also associated with the development of arrhythmias.

The sudden death of a young man is always a tragedy. Despite their physical fitness and health, cases of sudden death still occur among this population, although they are quite rare. Studies show that the rates of sudden deaths among recruits range from 2 to 13 per 100,000 recruits, and most of them are due to latent cardiac abnormalities that were not detected during medical examinations [7]. Another study found that in 86% of cases, physical activity was associated with death at the time of exercise [11]. The most common diseases leading to death are coronary artery abnormalities and hereditary cardiovascular disorders such as hypertrophic cardiomyopathy (HCM) and long QT syndrome (LQTS). However, regardless of the cause, most cases of sudden death occur due to ventricular tachyarrhythmia.

The modern rhythm of life, high level of urbanization and technological progress are widely associated with such concepts as air pollution. The latter is an important risk factor for CVD, and patients in this population are also susceptible to these risks, especially in conditions of constant exposure to polluted air at their workplace [27]

Solid particles (PM), which are solid and liquid microparticles suspended in the air, have an impact on health [19]. The particle size can range from hundreds of micrometers (microns) to units of nanometers (nm). The particles are divided by aerodynamic diameters into several fractions [25]:

• large (PM 10) — up to 10 microns,
• small (PM 2.5) — up to 2.5 microns
• Ultrafine particles (UDPS) — up to 100 nanometers.

It is known that the toxicity of particles increases with a decrease in their size, since such particles penetrate more easily into the deep parts of the lungs, creating additional risks for military personnel located in areas with high concentrations of pollutants [14,31,2]. Fine particles are usually formed as a result of combustion processes, which also poses a threat to the health of military personnel performing tasks in conditions of intense emissions and dust [15]. The particle size can serve as an indicator of the source of pollution, since larger particles are usually formed during mechanical processes, but various factors affecting the composition and size of particles, as well as secondary reactions in the atmosphere, make comparing such factors in different regions difficult and require additional analysis [12].

Rising global temperatures are one of the main challenges of the 21st century. According to the Intergovernmental Panel on Climate Change (IPCC), climate change has led to a significant increase in the average global temperature by 1.1°C since pre-industrial times. [26]. The facts show that the current trend of rising global average temperature and the occurrence of frequent, intense, and prolonged extreme heat events will continue in the future unless global action is taken. [35,30,21]. According to the International Labour Organization (ILO), assuming global temperatures rise by 1.5°C by the end of the twenty-first century, it is projected that by 2030 about 2.2% of total working hours and 880,000 years of working life will be lost due to occupational heat stress worldwide [24] .

Exposure to extreme temperature events can lead to many adverse health effects [10, 18]. Compared to the general population, the working population is more vulnerable to heat stress [23]. In some professions, workers are required to wear protective clothing that can prevent sweat evaporation and body heat dissipation, making workers more vulnerable to heat stress [13]. Workers in low- and middle-income countries in tropical and subtropical regions, where heat stress is a particular problem, may be more vulnerable to occupational diseases and heat-related deaths [5]

Conclusion.

Thus, when analyzing risk factors for VE, a wide range of factors should be taken into account, including hormonal changes, anemia, and specific occupational characteristics. This is necessary for more accurate diagnosis and effective prevention of arrhythmias in clinical practice.

REFERENCES

1. Agarwal SK, Simpson RJ, Rautaharju P, Alonso A, Shahar E, Massing M, Saba S, Heiss G. Relation of ventricular premature complexes to heart failure (from the Atherosclerosis Risk In Communities [ARIC] Study). *Am J Cardiol*. 2012;109:105–109. doi: 10.1016/j.amjcard.2011.08.009.

2. Agarwal V, Vittinghoff E, Whitman IR, Dewland TA, Dukes JW, Marcus GM. Relation between ventricular premature complexes and incident heart failure. *Am J Cardiol*. 2017;119:1238–1242. doi: 10.1016/j.amjcard.2016.12.029.

3. Ansah E.W., Ankomah-Appiah E., Amoadu M., Sarfo J.O. Climate change, health and safety of workers in developing economies: a scoping review. J Climate Change Health, 3 (2021), Article 100034, 10.1016/J.JOCLIM.2021.100034

4. BakeerN, James J, Roy S, et al. Sickle cell anemia mice develop a unique cardiomyopathy with restrictive physiology. Proc Natl AcadSci U S A, 113 (35) (2016), pp. E5182.

5. Bikkina M, Larson MG, Levy D. Prognostic implications of asymptomatic ventricular arrhythmias: the Framingham Heart Study. *Ann Intern Med*. 1992;117:990–996. doi: 10.7326/0003-4819-117-12-990.

6. Brunekreef B., Holgate S.T. Air pollution and health. Lancet. 2002;360(9341):1233–1242. doi: 10.1016/S0140-6736(02)11274-8.

7. de Lima C.Z., Buzan J.R., Moore F.C., Baldos U.L.C., Huber M., Hertel T.W. Heat stress on agricultural workers exacerbates crop impacts of climate change. Environ Res Lett, 16 (2021), 10.1088/1748-9326/abeb9f

8. Dukes JW, Dewland TA, Vittinghoff E, Mandyam MC, Heckbert SR, Siscovick DS, Stein PK, Psaty BM, Sotoodehnia N, Gottdiener JS, et al. Ventricular ectopy as a predictor of heart failure and death. *J Am CollCardiol*. 2015;66:101–109. doi: 10.1016/j.jacc.2015.04.062.

9. Eckhart R, Scoville S, Campbell C, et al. Sudden death in young adults: a 25-year review of autopsies in military recruits. Ann Intern Med 2004;141:829–34. doi:10.7326/0003-4819-141-11-200412070-00005.

10. el Khayat M., Halwani D.A., Hneiny L., Alameddine I., Haidar M.A., Habib R.R. Impacts of climate change and heat stress on farmworkers' health: a scoping review. Front Public Health, 10 (2022)

11. Green H., Bailey J., Schwarz L., Vanos J., Ebi K., Benmarhnia T. Impact of heat on mortality and morbidity in low and middle income countries: a review of the epidemiological evidence and considerations for future research. Environ Res, 171 (2019), pp. 80-91, 10.1016/J.ENVRES.2019.01.010

12. Harrison R.M., Yin J. Particulate matter in the atmosphere: Which particle properties are important for its effects on health? Sci. TotalEnviron. 2000;249(1-3):85–101. doi: 10.1016/S0048-9697(99)00513-6.

13. Heckbert SR, Austin TR, Jensen PN, Floyd JS, Psaty BM, Soliman EZ, Kronmal RA. Yield and consistency of arrhythmia detection with patch electrocardiographic monitoring: the Multi-Ethnic Study of Atherosclerosis. *J Electrocardiol*. 2018;51:997–1002. doi: 10.1016/j.jelectrocard.2018.07.027.

14. Hiss RG, Lamb LE. Electrocardiographic findings in 122,043 individuals. *Circulation*. 1962;25:947–961. doi: 10.1161/01.cir.25.6.947.

15. International Labor Organization (ILO). Increase in heat stress predicted to bring productivity loss equivalent to 80 million jobs. https://www.ilo.org/global/about-the-ilo/newsroom/news/WCMS_711917/lang-en/index.htm

16. Intergovernmental Panel on Climate Change (IPCC). Global warming of 1.5 °C. Aromar Revi (2018). https://www.ipcc.ch/site/assets/uploads/sites/2/2019/05/SR15_SPM_version_report_LR.pdf

17. Intergovernmental Panel on Climate Change (IPCC) AR6 climate change 2021: the physical science basis (2021) AR6 Climate Change 2021: The Physical Science Basis https://www.ipcc.ch/report/ar6/wg1.

18. Ioannou L.G., Foster J., Morris N.B., Piil J.F., Havenith G., Mekjavic I.B., et al. Occupational heat strain in outdoor workers: a comprehensive review and meta-analysis. Temperature (2022), pp. 1-36, 10.1080/23328940.2022.2030634

19. Kazbanov IV, KHWJ ten Tusscher, Panfilov AV. Effects of heterogeneous diffuse fibrosis on arrhythmia dynamics and mechanism Sci Rep, 6 (1) (2016), Article 20835.

20. Kerola T, Dewland TA, Vittinghoff E, Heckbert SR, Stein PK, Marcus GM. Modifiable predictors of ventricular ectopy in the community. *J Am Heart Assoc*. 2018;7:e010078. doi: 10.1161/JAHA.118.010078.

21. Kerry Purtell, Torsten K. Roepke, Geoffrey W. Abbott. Cardiac arrhythmia and thyroid dysfunction: A novel genetic link. The International Journal of Biochemistry & Cell Biology, Volume 42, Issue 11, 2010:1767-1770. https://doi.org/10.1016/j.biocel.2010.07.013

22. Laden F., Neas L.M., Dockery D.W., Schwartz J. Association of fine particulate matter from different sources with daily mortality in six U.S. cities. Environ. Health Perspect. 2000;108(10):941–947. doi: 10.1289/ehp.00108941.

23. Lynch P, Ineson N, Jones A, et al. Sudden death in sport before and after introduction of the basic fitness test. J R Army Med Corps 1985;131:42–6. doi:10.1136/jramc-131-01-10.

24. MacNee W., Donaldson K. Mechanism of lung injury caused by PM10 and ultrafine particles with special reference to COPD. Eur. Respir. J. Suppl. 2003;40(Suppl. 40):47s–51s.

25. Marrakchi, S., Kanoun, F., Idriss, S., Kammoun, I., and Kachboura, S. (2015). Arrhythmia and thyroid dysfunction. Herz 40(Suppl. 2), 101–109. doi: 10.1007/s00059-014-4123-0.

26. National Aeronautic and Space Administration (NASA). Global temperature. Global Climate Change (2021). https://climate.nasa.gov/vital-signs/global-temperature/ Intergovernmental Panel on Climate Change (IPCC). Special report on climate change and land (2019). https://www.ipcc.ch/site/assets/uploads/2019/11/SRCCL-Full-Report-Compiled-191128.pdf

27. Nguyen KT, Vittinghoff E, Dewland TA, Dukes JW, Soliman EZ, Stein PK, Gottdiener JS, Alonso A, Chen LY, Psaty BM, et al. Ectopy on a single 12-lead ECG, incident cardiac myopathy, and death in the community. *J Am Heart Assoc*. 2017;6:e006028

28. NissO, Fleck R, Makue F, et al. Association between diffuse myocardial fibrosis and diastolic dysfunction in sickle cell anemia. Blood, 130 (2) (2017), 205-213.

29. Osman, F., Gammage, M. D., Sheppard, M. C., and Franklyn, J. A. (2002). Clinical review 142: cardiac dysrhythmias and thyroid dysfunction: the hidden menace? *J. Clin. Endocrinol. Metab.* 87, 963–967. doi: 10.1210/jcem.87.3.8217.

30. Pallikadavath S, Vali Z, Patel R, Mavilakandy A, Peckham N, Clegg M, Sandilands AJ, Ng GA. The Influence of Environmental Air Pollution on Ventricular Arrhythmias: A Scoping Review. CurrCardiol Rev. 2022;18(6):e160422203685. doi: 10.2174/1573403X18666220416203716

31. Palupi A.A.R., Rizky Z.P., Puspita N., Atmajaya H., Ramdhan D.H. Physiological and Psychological Effects of Heat Stress on Automotive Manufacture Workers. KnE Life Sci, 4 (2018), pp. 148-155.

32. Perkins S.E. A review on the scientific understanding of heatwaves—Their measurement, driving mechanisms, and changes at the global scale Atmosph Res, 164–165 (2015), pp. 242-267.

33. Rajagopalan S., Al-Kindi S.G., Brook R.D. Air pollution and cardiovascular disease: JACC state-of-the-art review. J. Am. Coll. Cardiol. 2018;72(17):2054–2070. doi: 10.1016/j.jacc.2018.07.099.

34. Seaton A., MacNee W., Donaldson K., Godden D. Particulate air pollution and acute health effects. Lancet. 1995;345(8943):176–178.

35. Simpson RJ, Cascio WE, Schreiner PJ, Crow RS, Rautaharju PM, Heiss G. Распространенность преждевременных желудочковых сокращений в популяции афроамериканцев и белых мужчин и женщин: исследование риска атеросклероза в сообществах (ARIC). *AmHeart J.* 2002;143:535–540. doi: 10.1067/mhj.2002.12029

36. SunddP, Gladwin M, Novelli E. Pathophysiology of sickle cell disease. Annu Rev PatholMech Dis, 14 (1) (2019), pp. 263.

37. Thorpe A., Harrison R.M. Sources and properties of non-exhaust particulate matter from road traffic: A review. Sci. TotalEnviron. 2008;400(1-3):270–282. doi: 10.1016/j.scitotenv.2008.06.007.

38. von Olshausen, K., Bischoff, S., Kahaly, G., Mohr-Kahaly, S., Erbel, R., Beyer, J., et al. (1989). Cardiac arrhythmias and heart rate in hyperthyroidism. *Am. J. Cardiol.* 63, 930–933. doi: 10.1016/0002-9149(89)90142-2.

39. von Rotz M, Aeschbacher S, Bossard M, Schoen T, Blum S, Schneider S, Estis J, Todd J, Risch M, Risch L, et al. Risk factors for premature ventricular contractions in young and healthy adults. *Heart*. 2017;103:702–707. doi: 10.1136/heartjnl-2016-309632.

UDC: 616-005.8: 616.43

THE INCIDENCE OF CORONARY HEART DISEASE IN INDIVIDUALS WITH DIFFERENT GRADATIONS OF BLOOD PRESSURE AND BODY WEIGHT

Gayrat K. Gaibov - director
Khorezm Branch of the Academician Yo.Kh. Turakulov Republican Specialized Scientific and Practical Medical Center of Endocrinology (Urgench, Uzbekistan)
Gulomjon S. Khalimbetov - D.M.Sc., associate professor
Ulugbek K. Kayumov - D.M.Sc., professor
Center for the Development of Professional Qualifications of Medical Workers (Tashkent, Uzbekistan)
info@tipme.uz

Abstract. *A group of six hundred and sixty-eight men was selected at random from the general population of men aged 20-69 years and examined to ascertain coronary heart disease (CHD) amongst those men on various levels of blood pressure and of body weight. Frequency of CHD rose with each successive body mass category and each successive blood pressure category; having arterial hypertension was associated with a 3.5-fold increase, compared with the same body mass category and normal bp ($p<0.01$); and obesity was associated with a 3.6-fold increase, compared to the underlying blood pressure category and normal body weight ($p<0.01$). Importantly, at even the high-normal blood pressure and overweight levels —levels traditionally considered to have little or no extra risk—the rate of CHD was already higher than at the same normal levels. The results suggest a differentiated risk stratification approach for cardiovascular risk which considers sub-threshold blood pressure elevations, body weight and not only binary risk thresholds.*

Keywords: *arterial hypertension, overweight, obesity, metabolic syndrome, coronary heart disease.*

Introduction.

Insulin resistance is now considered as the initiating factor of the metabolic syndrome (MS) and its sole common pathophysiological substrate, and the MS is at the center of cardiovascular research today. The four cardinal features of this syndrome are the presence of arterial hypertension (AH), overweight / obesity, dyslipidemia and impaired glucose tolerance (IGT), and are not randomly distributed among patients, but are co-occurring and share common underlying mechanisms. Due to the high, and even higher in some populations, prevalence of its individual components [2, 3, 8, 13] and as a result of this, MS and its sequelae have been identified as a key concern for prevention of cardiovascular and metabolic diseases at the international level, with recommendations for increased efforts in this area. Increasing prevalence of all the major components of MS over time has been observed in population-based studies [9] and the presence of various components and combinations of these components has been linked to higher cardiovascular and general risk [14], with risk rising disproportionately with the number of components present simultaneously. The clustering phenomenon is particularly clinically relevant because it suggests that the cardiovascular risk of each individual factor (elevated blood pressure) can't be understood without regard to the other factors in the broader metabolic picture that usually accompany these.

Patient age plays an important role in the composition of the syndrome as well as the downstream prognosis, in addition to the core components of MS. The number and type of MS components may vary significantly between different age groups: before age 40, factors such as unhealthy habits and hypertension often play a larger role as a result of the early effect of lifestyle and metabolic factors; after age 40, obesity and insulin resistance become more prominent, due to the

age-dependent loss of metabolic efficiency and the progressive accumulation of the visceral adipose tissue. This age-related change in the relative importance of each individual MS component has direct relevance to clinical practice because a risk-assessment approach tailored to a younger population may systematically underestimate the contribution of insulin resistance due to adiposity in an older population, and the other way around. Risk stratification for MS risk and associated diseases should thus be considered with the intention of using age-specific risk stratification, and not using a single risk algorithm throughout the adult life-span.

In this context, it is important to look at the severity in addition to the presence or absence of the main components of the MS, as threshold-based classification (e.g., simple presence or absence of hypertension or obesity) may conceal clinically relevant versions of the disease below the conventional disease cut-off. A more granular and gradation-centered risk assessment strategy may be able to identify a person who does not have formal diagnostic criteria, but is in between, such that they would benefit from a more intensive risk monitoring strategy. This is particularly relevant in large-scale population screening and it is important to have a tool that is non-invasive, widely available and not expensive, and among these, blood pressure and body weight measurement are of primary importance, due to being reliable, easily deployable, and usable even in primary-care or community-based settings that are lacking in biochemical or imaging-based diagnostic equipment.

Aim of the study. To examine the relationship between coronary heart disease and varying degrees of severity of elevated blood pressure and excess body weight.

Materials and Methods.

This report is based on the results of a cross-sectional analysis of 668 men, which were a random sample from the unorganized (general) population between the ages of 20 and 69 years. The sampling of age-heterogeneous individuals and random selection of subjects was designed to reflect the range of blood pressure and body weight gradations which are commonly seen in daily clinical and epidemiological work, and not just a selected sub-spectrum of blood pressure and body weight. The study utilized a multi-modal approach using a questionnaire-based approach, biochemical and instrumental methods, which was a strategy that would provide triangulation for diagnosis of coronary heart disease (CHD) rather than relying on one method alone.

The interview part was carried out with the standard questionnaire of the World Health Organization (WHO) for the detection of exertional angina pectoris, which is a validated instrument widely used in cardiovascular epidemiology in population-based studies and is internationally recognized [17]. Diagnosis of angina pectoris was made if retrosternal and/or left-sided chest and left arm pain occurred upon exertion, as indicated by the standardized diagnostic criteria outlined in the questionnaire. A parallel, standardized WHO questionnaire was also used to detect potential previous myocardial infarction, operationally defined as the presence of a history of severe chest pain for more than 30 minutes, in the absence of supporting changes in the electrocardiogram (ECG) - this criterion was added to minimize the rate of false positive cases based on symptom history alone.

Instrumental methods contained three main components, each addressing a different aspect of cardiovascular risk assessment.

a) Resting electrocardiography (ECG) was done in 12 standard leads under standard resting conditions, and the ECG tracings were classified qualitatively and quantitatively as per the Minnesota Code, a long-established and internationally accepted classification system used for qualitative and quantitative categorization of ECG abnormalities in epidemiological studies. This approach allowed the systematic identification of the characteristics of CHD: myocardial infarction, stable exertional angina, painless (silent) form of CHD (i.e. presence of ischemic ECG changes without pain syndrome) and a possible arrhythmic form of CHD. Standardization of the coding of all ECG tracings was planned to limit inter-observer variation in interpretation of the tracings and to ensure uniformity of CHD ascertainment throughout the entire study population.

b) Blood pressure (BP) was measured following the existing diagnostic criteria, and divided into three groups: normal BP, high-normal BP and arterial hypertension. The rationale for using this tri-partite classification was specifically to examine the intermediate blood-pressure (BP) sub-diagnostic range in accord with the wider justification provided in the Introduction for choosing a graded classification for risk rather than a dichotomized classification between normotensive and hypertensive.

c) Body weight was assessed based on the Quetelet index or more commonly body mass index (BMI), which is weight (kg) divided by height squared (m2). According to the internationally accepted anthropometric criteria, overweight was defined as BMI ≥ 25 and < 30 kg/m2, and obesity as BMI ≥ 30 kg/m2. Like the blood-pressure classification cited above, this three-classification of body weight was chosen to allow the overweight group to be considered as a separate intermediate level of adiposity rather than being aggregated with either the normal-weight or obese group.

Results.

Of the 668 men examined, 584 (87.4%) were without clinical and/or electrocardiographic evidence of CHD, and the other 84 (12.6%) were clinically and/or electrocardiographically classified as CHD with the WHO questionnaire. The overall sample was subsequently divided into the blood-pressure categories, and a distinct difference in the frequency of CHD was found between the three blood pressure groups (Figure 1). Specifically, CHD was seen to be more common in those with AH than in those with normal BP (28.35% vs 8.58%, $p<0.01$), indicating that the disease was not evenly distributed amongst those with a normal BP, but was concentrated in the hypertensive group. There was no statistical difference ($p>0.05$) in CHD frequency between the high-normal BP group and the normal BP group; in individuals with high-normal BP, CHD frequency was 10.67% — numerically higher, but not significantly different, from the normal BP group — and this difference was not statistically significant on the basis of the current sample size alone.

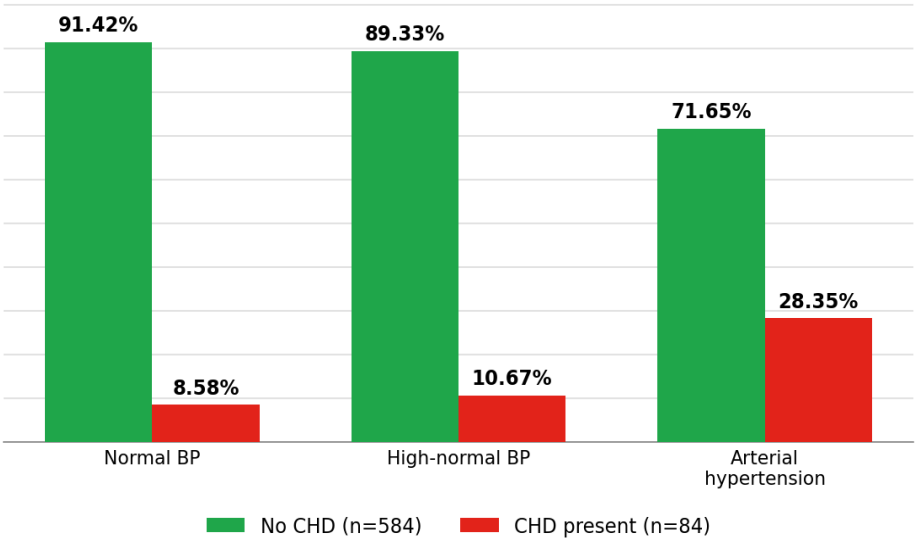


Fig. 1. Incidence of CHD in groups with normal BP, high-normal BP, and arterial hypertension

The same sample was then divided into the body-weight categories to look at the association between CHD frequency and body weight (Figure 2). The data indicates that there was a definite increase in frequency of CHD in the overweight and obese groups as well, similar to blood pressure, increasing from 7.51% of those of normal weight to 12.93% of those who were overweight and 26.73% of those who were obese. This translates to a 3.6-fold increase in CHD prevalence amongst those with obesity compared to those with normal body weight ($p<0.01$) and a 1.7-fold increase amongst the overweight compared with the normal body weight group. Both of these body-weight

comparisons were statistically significant, whereas in the case of blood pressure, the relationship of frequency of CHD with body weight was more clearly resolved within this sample.

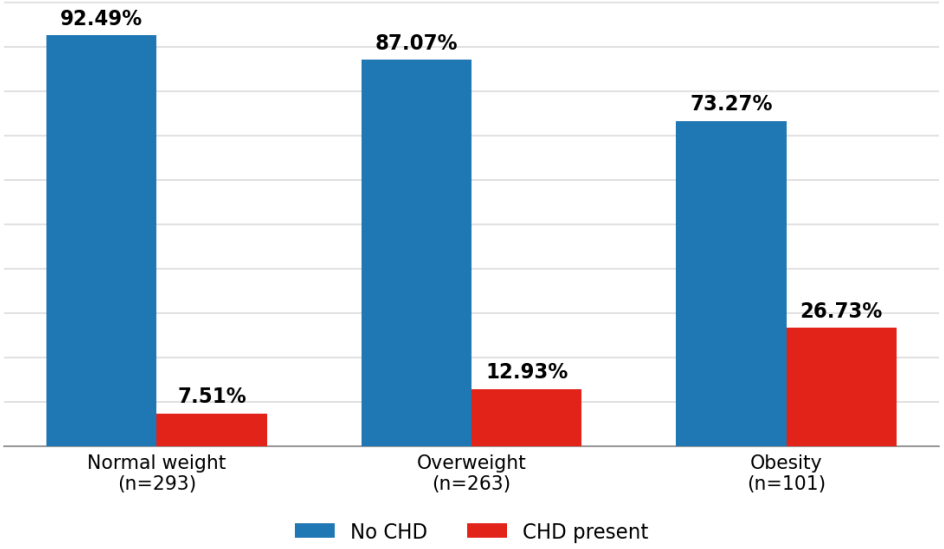


Fig. 2. Incidence of CHD in groups with different body weight categories

Collectively, these findings establish a graded, monotonic gradient in CHD prevalence across successive categories of both blood pressure (8.6% → 10.7% → 28.4% for normal, high-normal, and hypertensive BP, respectively) and body weight (7.5% → 12.9% → 26.7% for normal weight, overweight, and obesity, respectively), a pattern consonant with a dose-dependent relationship between the severity of these two metabolic syndrome components and the burden of coronary heart disease. Not only was this gradient true for direction, but it was also true for continuity: the prevalence of CHD rose gradually between each of the sub-diagnostic categories between normal-to-high normal and overweight and obesity categories, with the high normal and overweight diagnostic categories having prevalence positions intermediate between their respective normal and over-pathological counterparts. This is a continuous ordinal relationship, and is typical of cardiovascular risk factors in general, and provides quantitative support for the conceptualization of blood pressure and body weight as continua of risk, not as binary clinical states.

It is noteworthy however that CHD prevalence was by no means trivial in the healthy blood pressure and healthy weight referent groups (8.6% and 7.5% respectively). In absolute terms, this is a significant residual burden of disease in low-risk populations and argues against considering these two risk factors alone as an explanation of the overall coronary risk in these populations. It does not mean, however, that other unmeasured factors that influence disease susceptibility are not at work, which may include other features of the metabolic syndrome, such as dyslipidemia, hyperglycemia and insulin resistance, which were not directly evaluated in the analytic framework used in this study, but instead points to the multiple factors influencing the etiology of coronary heart disease, even among those who, based on BP and body weight alone, would be considered relatively low cardiovascular risk.

Discussion.

The observed increase in CHD prevalence in patients with AH is consistent with the well-established AH as a major CHD risk factor. Importantly, the relatively small (but not significant) BP increase found in those with high-normal BP also highlights that this level of BP may be a precursor for the development of CHD, as explored below in the context of the larger epidemiological literature on pre-hypertensive states.

The gradual increasing trend in CHD frequencies within each blood pressure and body weight range suggests that cardiovascular risk does not "just happen" after crossing over to the hypertension or obesity ranges, but builds up gradually in the intermediate ranges that lead up to those thresholds. Hence, people with high-normal blood pressure and overweight are already at an intermediate risk between the normal and the overtly pathological groups and deserve to be studied in the prediction of AH and as regards preventive measures for AH and overweight.

Additional risk factors not directly evaluated in the present study (such as other components of the metabolic syndrome like insulin resistance, dyslipidemia and hyperuricemia) may be partly responsible for the high proportion of CHD cases that occurred even in those with normal blood pressure and body weight.

The graded pattern seen in blood pressure and body weight is similar to that of the other components of metabolic syndrome, which are pathologically linked to atherosclerotic disease [15]. High blood pressure (even when it is not a diagnostic for hypertension) causes the blood vessel lining to become stressed by shear stress, early endothelial dysfunction, and vascular wall remodeling, which in turn leads to left ventricular hypertrophy (LVH) over time, increasing the oxygen demand of the heart and decreasing the ischemic threshold. In addition, excess adiposity (especially visceral fat) acts via a parallel pathway, by inducing insulin resistance, an atherogenic dyslipidemia profile defined by hypertriglyceridemia and hypoHDL-cholesterolaemia, and by promoting low-grade systemic inflammation and oxidative stress, both of which are known to contribute to endothelial dysfunction and atherogenesis on their own [16]. Patients with blood pressure and obesity in intermediate ranges are likely already on a common pathway (including both sympathetic and renin-angiotensin-aldosterone system activation and insulin resistance) and may well explain in a mechanistic way why their CHD prevalence is higher than that of people with strictly normal measurements.

This is consistent with a large amount of global evidence. Huang et al. [6] conducted a meta-analysis of eighteen prospective cohort studies of over 468,000 individuals that found that prehypertension (defined as what is most similar to the high-normal BP grade we used in the present study) was associated with a 50% increased risk for incident CHD (RR 1.50, 95% CI 1.30–1.74). This confirms the directionally consistent, albeit not statistically significant, increased CHD frequency seen in the high-normal BP subgroup in the present sample, which is most likely due to the relatively small number of CHD cases available for analysis within this group, compared to that of the larger normotensive subgroup (n=959 across the entire sample). Previous research has found a similar graded association between adiposity and cardiovascular risk; whereby excess body weight (even at lean body weights) is associated with clustering of coronary risk factors [5]; and more recent population-based analyses of NHANES data have found that metabolically unhealthy overweight and obese adults have a significantly higher prevalence of cardiovascular disease than do normal weight adults [18]. The present findings, which come from a Central Asian population, are consistent with previous regional studies, showing the relationships between the severity of each of the metabolic syndrome components and the prevalence and mortality due to CHD [11] and the prevalence of cardiovascular risk factors in this region is still relatively scarce.

Limitations. The findings of the study need to be considered with some limitations in mind. First, the cross-sectional design does not allow for conclusions on the temporal or causal relationship of blood pressure, body weight and CHD. Second, the study population consisted of men only, which may restrict the application of the results to women, where the prevalence and clinical characteristics of CHD, as well as the distribution of the components of metabolic syndrome, are also known to differ [12]. Third, classification of blood pressure was based on the criteria used at the time of examination, and the number of occasions on which blood pressure was measured, as well as the potential for single visit misclassification (e.g. associated with a white coat effect) were not reported separately. Lastly, other known components of the metabolic syndrome, such as fasting glucose, lipid

profile, waist circumference, and the more difficult-to-measure cardiovascular end points described in previous regional studies [10] have not been measured or adjusted in the current study, and may account for some of the observed gradient.

Clinical implications. The practical implications of the findings are especially relevant for cardiovascular prevention, particularly in resource-limited settings throughout Central Asia, where access to advanced biochemical or imaging-based risk assessment is not equally available [4, 19], as is also the case in non-communicable disease control. Given that blood pressure and body weight measurement is cheap, non-invasive, and accessible even at the primary-care level, it is an appealing method of opportunistic cardiovascular screening, consistent with the larger community's push for accessible and pharmacist- and primary-care-supported strategies for the screening and prevention of metabolic syndrome [1, 7]. The observed gradient argues against restricting clinical focus to those with diagnosed hypertension or obesity: those in the 'high-normal' blood pressure and overweight range already have a high frequency of CHD and may require earlier intervention with lifestyle counseling, more frequent monitoring and a lower threshold for additional screening of risk factors. These findings provide some basis for designing future intervention trials to determine if lifestyle interventions for these sub-threshold intermediate categories can have a significant impact on future CHD events.

Conclusions.

This study's results suggest that preventive efforts shouldn't be limited to those with a formal diagnosis of hypertension or obesity, but offered to individuals in a clinical evaluation who also need intervention. Instead, there is clear evidence that the sub-threshold gradations of high-normal blood pressure and excess body weight are associated with elevated rates of CHD and, as such, should be specifically considered when estimating risk. Accordingly proactive therapeutic and lifestyle measures geared towards the maintenance of normotension and suitable body weight need to be implemented in this intermediate risk group and not delayed if formal diagnostic thresholds are surpassed.

Conversely, the high prevalence of cardiac disease found even in people with perfect blood pressure and normal weight indicates that these measurements alone, rather than sufficient, may not predict cardiovascular risk. Hence, there is a need for additional screening for other known cardiovascular risk factors/aspect of MS in this seemingly less-risk group to identify any residual risks in such individuals which would otherwise remain undetected by BP/weight measurements alone.

The overall findings of this study seem to suggest that the connection between CHD and cardiovascular risk factors is a continuum instead of a series of distinct and separate diagnostic categories. The results of this large, population-based study provide empirical evidence for the application of gradation-based risk models in clinical and public-health practice to more effectively target available diagnostic resources, including simpler biochemical or imaging-based tools, in situations in which there is limited access to more advanced infrastructure tools. Future prospective studies should confirm these cross-sectional observations in a longitudinal fashion, include other components of metabolic syndrome (dyslipidemia, glycemic status) as part of a more inclusive risk-stratification system and explore whether targeted intervention in sub-threshold blood pressure and body weight levels can result in measurable reductions in the subsequent incidence of CHD.

REFERENCES

1. Al Adawi, R.M., Stewart, D., Ryan, C. et al. A systematic review of pharmacist input to metabolic syndrome screening, management and prevention. Int J Clin Pharm. 2020; 42:995–1015. https://doi.org/10.1007/s11096-020-01084-3

2. A Call to Action on Diabetes. International Diabetes Federation, November 2010. www.idf.org

3. Belete, R. et al. Global prevalence of metabolic syndrome among patients with type I diabetes mellitus: a systematic review and meta-analysis. Diabetol Metab Syndr. 2021; 13:25.

4. Emiral, G.O. et al. Metabolic syndrome prevalence and related factors in a Turkish adult population. Niger J Clin Pract. 2021; 24:28–37.

5. Hsu, C.H., Lin, J.D., Hsieh, C.H. et al. Body mass index, metabolic syndrome and carotid atherosclerosis. Nutr Res. 2014;34(3):219–225. https://doi.org/10.1016/j.nutres.2014.01.004

6. Huang, Y., Wang, S., Cai, X., Mai, W., Hu, Y., Tang, H., Xu, D. Prehypertension and incidence of cardiovascular disease: a meta-analysis. BMC Med. 2013; 11:177. https://doi.org/10.1186/1741-7015-11-177

7. The IDF Consensus Worldwide Definition of the Metabolic Syndrome. Obesity and Metabolism. 2005;2(3):47–49.

8. International Diabetes Federation. IDF Diabetes Atlas. 8th ed. Brussels: International Diabetes Federation; 2017.

9. Kalandarova, U.A., Ibadova, M.U., Ismatova, M.N., Kayumov, N.U. Dynamics of the levels of metabolic syndrome components in different types of hyperglycemias. J Biomed Pract. 2019;1(1):72–78.

10. Kayumov, U.K., Kalandarova, U.A., Ibadova, M.U., Ismatova, M.N. The formation of a hard “end point” for various risk factors. J Biomed Pract. 2019;1(1):79–84.

11. Kayumov, U.K., Kalandarova, U.A., Ibragimov, A.Yu., Saipova, M.L. The prevalence of ischemic heart disease and mortality from this disease at various components of metabolic syndrome. New Day in Medicine. 2019;3(27):138–141.

12. Kayumov, U.K., Matmuratova, S.O., Khatamova, D.T. et al. The combination of components of the metabolic syndrome in women of childbearing age and their relationship with age. Cent Asian J Med Nat Sci. 2022;3(6):84–87. https://cajmns.centralasianstudies.org/index.php/CAJMNS/article/view/1172

13. Liu, P.J., Lou, H.P., Zhu, Y.N. Screening for metabolic syndrome using an integrated continuous index consisting of waist circumference and triglyceride: a preliminary cross-sectional study. Diabetes Metab Syndr Obes. 2020; 13:2899–2907. https://doi:10.2147/DMSO.S259770

14. Lucchetti, B.F.C., Boaretto, N., Lopes, F.N.C. et al. Metabolic syndrome aggravates cardiovascular, oxidative and inflammatory dysfunction during the acute phase of Trypanosoma cruzi infection in mice. Sci Rep. 2019; 9:18885. https://doi.org/10.1038/s41598-019-55363-9

15. McCracken, E., Monaghan, M., Sreenivasan, S. Pathophysiology of the metabolic syndrome. Clin Dermatol. 2018;36(1):14–20. https://doi.org/10.1016/j.clindermatol.2017.09.004

16. Otamas, A., Grant, P.J., Ajjan, R.A. Diabetes and atherothrombosis: the circadian rhythm and role of melatonin in vascular protection. Diabetes Vasc Dis Res. 2020;17(3). https://doi.org/10.1177/1479164120920582

17. Rose, G.A., Blackburn, H. Cardiovascular Survey Methods. Monogr Ser World Health Organ. 1968; 56:1–188. PMID: 4972212.

18. Tu, D., Li, P., Li, K. Metabolic health and cardiovascular disease across BMI categories: NHANES findings. J Health Popul Nutr. 2025; 44:273. https://doi.org/10.1186/s41043-025-01003-0

19. Zablith, N., Diaconu, K., Naja, F. et al. Dynamics of non-communicable disease prevention, diagnosis and control in Lebanon, a fragile setting. Confl Health. 2021; 15:4. https://doi.org/10.1186/s13031-020-00337-2

UDC: 613.6:665.7

COKE DUST FORMATION IN THE OIL REFINING PROCESS AND ITS IMPACT ON THE ENVIRONMENT AND WORKERS' HEALTH

Shahnoza I. Mamatova – assistant
Fergana Institute of Public Health (Fergana, Uzbekistan)
mamatova7300@gmail.com

Abstract. Objective: *To identify the sources of coke dust formation, assess its chemical composition and physico-hygienic characteristics, and evaluate the impact on worker health and the environment at the Fergana Oil Refinery (FNPZ).* ***Methods:*** *A multidisciplinary methodological approach was applied: gravimetry, aspiration, laser diffraction, computer spirometry (FVC, FEV_1), ECG monitoring (heart rate), skin thermometry at proximal and distal body points, and variance statistics. Workers of 10 leading occupational groups at the AVT 21.10/600 unit were examined.* ***Results:*** *Dust dispersion analysis revealed: PM_{10} fraction >70%, $PM_{2.5}$ >30%, enabling deep alveolar penetration. Extreme hydrophobicity of coke dust (93% amorphous carbon) was identified, rendering water-based dust suppression ineffective. Initial dust concentration reached 7.2–8.0 mg/m³ against a MAC of 6.0 mg/m³. Working conditions were classified as hazardous classes 3.1 and 3.2. Cardiovascular strain was documented: heart rate, stroke and minute volumes increased by up to 22%. Following the implementation of the preventive complex, concentration stabilised at* ***3.9 mg/m³*** *— reliably below MAC ($p<0.01$).* ***Conclusion:*** *Aerodynamic screens up to 6 m high restrict dust dispersal within a 5 km radius. FFP3 personal protective equipment combined with engineering controls significantly reduces occupational disease risk.*

Keywords: *coke dust, $PM_{2.5}$, PM_{10}, hydrophobicity, Fergana Oil Refinery, occupational hygiene, aerodynamic barrier, FFP3, occupational disease, Fergana Valley.*

Introduction.

The oil refining industry is one of the fundamental pillars of the modern economy, ensuring national energy security and the uninterrupted operation of the transport sector. At the same time, complex thermodestructive processes — in particular, delayed coking technologies — represent the primary source of carbon-containing industrial aerosol emissions, commonly referred to as coke dust [4, 6].

In terms of its physico-chemical composition, coke dust is a complex mixture comprising amorphous carbon (93%), sulphur (5%), metal ions (vanadium, nickel, iron) and polycyclic aromatic hydrocarbons. The pronounced toxicity of several components, combined with their inhalation pathway, renders this aerosol a particularly significant occupational health risk factor [5].

The geographic characteristics of the Fergana Valley — a closed topography surrounded by mountain ridges and characterised by weak wind circulation — considerably slow the natural diffusion of airborne pollutants, promoting dust accumulation and its migration beyond the industrial zone into residential areas [7].

The present study provides the first comprehensive hygienic and ecological assessment of coke dust at the AVT 21.10/600 unit of FNPZ, encompassing analysis of worker health impacts and verification of the effectiveness of the developed preventive complex.

Materials and methods.

The object of investigation was the working environment of the AVT 21.10/600 unit at the Fergana Oil Refinery. Dynamic monitoring covered the workplaces of 10 leading occupational groups: process engineers, mechanics, pump operators, crane operators, furnace operators and reactor unit operators.

The following methodological complex was applied:

— Sanitary-hygienic methods: gravimetry and air aspiration in the working zone, evaluated in accordance with SanPiN No. 0141-03 and SanPiN No. 0069-24;

— Physico-chemical methods: laser diffraction for determination of the disperse composition and particle geometry of coke dust;

— Clinical-functional methods: computer spirometry (FVC, FEV_1), continuous ECG monitoring (heart rate), topical skin thermometry at proximal and distal body points before and after the shift;

— Statistical analysis: variance statistics methods, significance of differences at $p<0.05$.

Dust samples were collected at the crushing, screening, transportation, loading and drying stages. All measurements were repeated at the beginning and end of each work shift.

Results and discussion.

Sources of coke dust formation and concentration levels.

Field laboratory measurements revealed substantial variation in dust concentration across technological sections: from 5.8 mg/m³ at the crushing stage to 8.0 mg/m³ during loading operations. Transportation and loading were identified as the most active dust-generating sources, with measured concentrations 1.2–1.3 times exceeding the maximum allowable concentration (MAC = 6.0 mg/m³).

The prolonged airborne residence of particles combined with their small size (up to 8 µm) facilitates deep penetration into the lower respiratory tract, increasing the risk of chronic bronchitis, allergic rhinitis, pneumonia and occupational bronchial asthma.

Figure 1. Coke dust concentration by formation source (mg/m³)

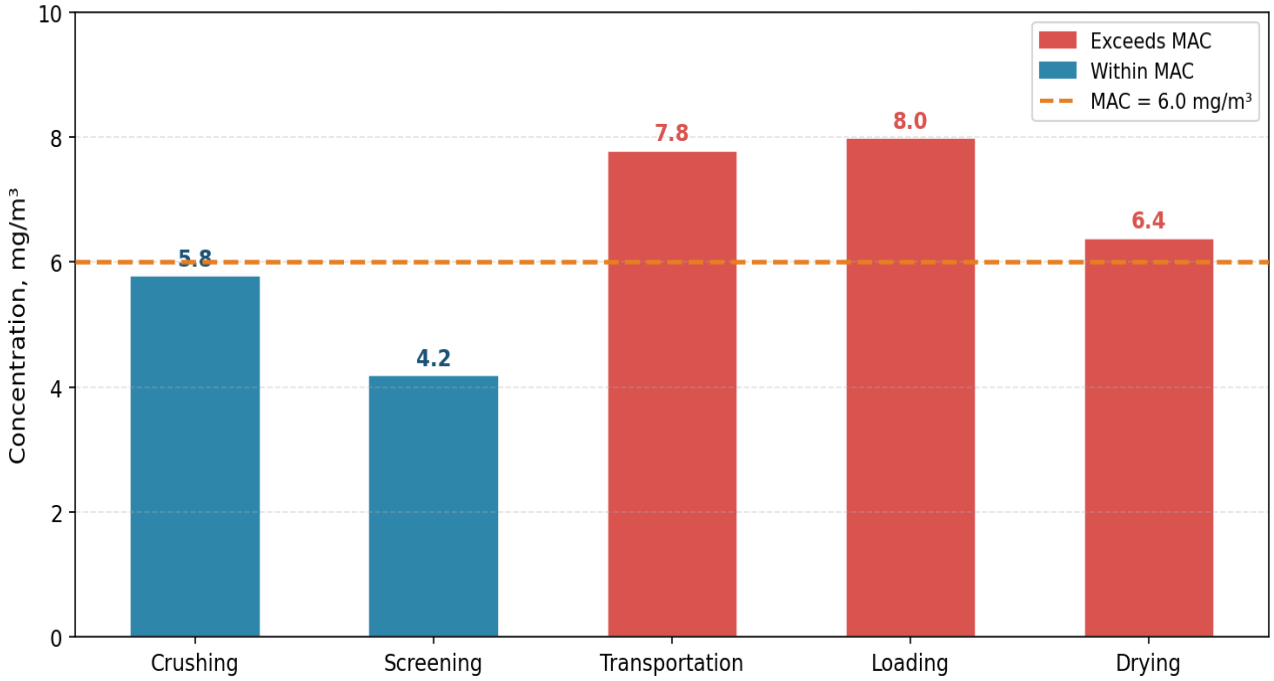


Figure 1. Coke dust concentration by source of formation (mg/m³)

Chemical composition and hydrophobic properties of coke dust.

Laser diffraction established a high proportion of respirable fractions: PM_{10} exceeded 70% and $PM_{2.5}$ surpassed 30%, which determines alveolar particle deposition and triggers fibrogenic reactions.

A key physico-chemical finding was the absolute water insolubility of coke dust, attributable to the predominance of amorphous carbon (93%) and sorbed polycyclic aromatic hydrocarbons. This property provides scientific justification for the low effectiveness of conventional water-based dust suppression systems and necessitates the mandatory use of respiratory protective equipment of class FFP3 with a filtration coefficient of 99.0–99.7% and a reliable facial fit [2].

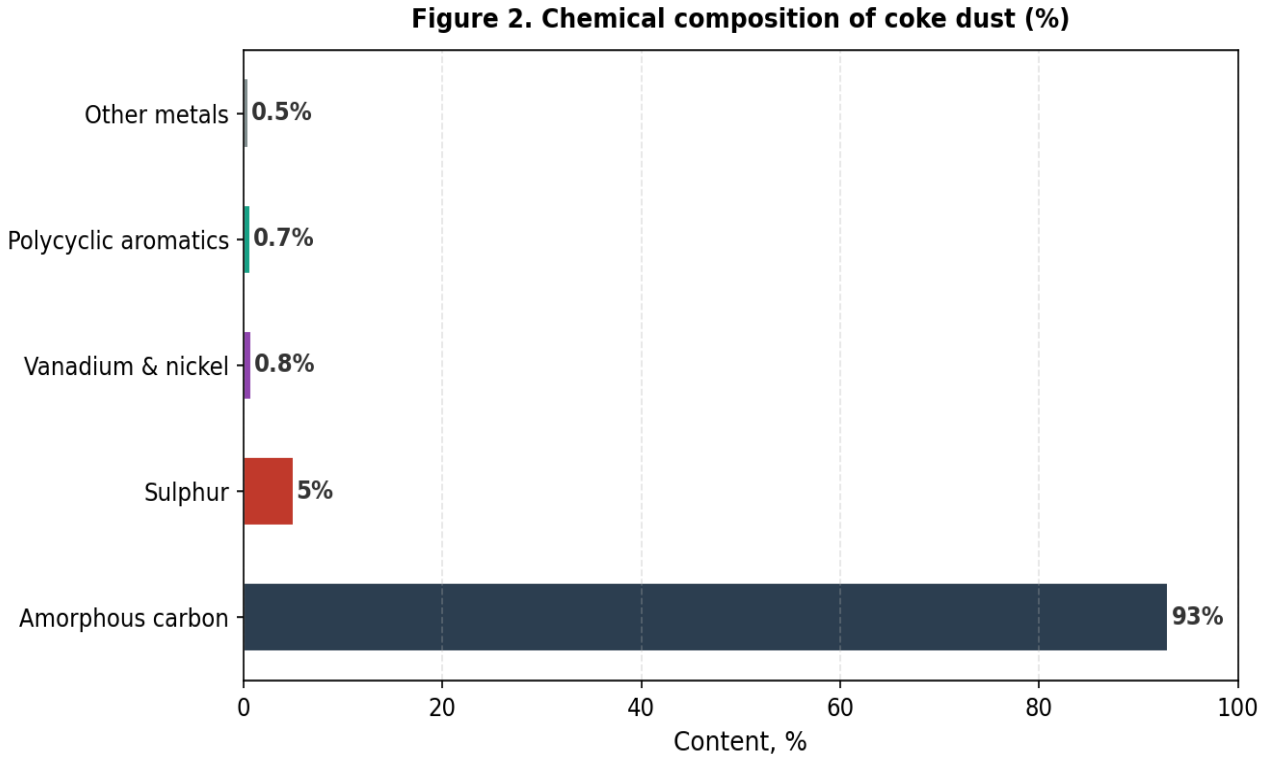


Figure 2. Chemical composition of coke dust (%)

Hygienic assessment of working conditions.

Comprehensive evaluation conducted in accordance with SanPiN No. 0141-03 and No. 0069-24 demonstrated that the combined effect of dust exposure, toxic gases and heating microclimate classifies the working conditions of mechanics and crane operators as hazard class 3, grade 2 (3.2), and those of operators and process engineers as hazard class 3, grade 1 (3.1).

Table 1.

Hazard class classification of working conditions for principal occupational groups

Occupational group	Hazard class	Grade	Primary hazardous factor
Mechanic	Class 3, Grade 2 (3.2)	High	Dust + heating microclimate
Crane operator	Class 3, Grade 2 (3.2)	High	Dust + heating microclimate
Operator (pumps)	Class 3, Grade 1 (3.1)	Medium	Dust + hydrocarbon gases
Operator (furnace)	Class 3, Grade 1 (3.1)	Medium	Heat exposure + gases
Operator (reactor)	Class 3, Grade 1 (3.1)	Medium	Dust + gases + heat
Process engineer	Class 3, Grade 1 (3.1)	Medium	Chemical substances

Functional responses of workers' organisms.

Physiological monitoring revealed patterns of pre-clinical disorders. Under the combined aerogenic and thermal load, compensatory cardiovascular strain was documented: heart rate, stroke and minute blood volumes increased by up to 22% ($p<0.05$), occurring concurrently with a decline in spirometric indices.

Skin thermometry detected the phenomenon of convergence between proximal (trunk) and distal (fingers and toes) body temperature readings — a virtual disappearance of the proximal-distal temperature gradient. This condition indicates critical overload of the thermoregulatory system and is directly associated with attentional deficits, increased fatigue and neuropsychological exhaustion in workers [3].

Table 2.

Cardiovascular and respiratory functional indicators (M±m)

Indicator	Start of shift	End of shift	Change and significance
Heart rate (bpm)	72.0	87.8	+21.9% — cardiovascular strain ($p<0.05$)
Stroke volume (ml)	68.0	82.9	+21.9% — hyperdynamic mode ($p<0.05$)
Minute volume (l/min)	4.90	5.98	+22.0% — compensatory response ($p<0.01$)
FVC (% of normal)	98.2	91.4	−6.9% — reduced respiratory function
FEV_1 (% of normal)	96.5	89.1	−7.7% — obstructive changes

Figure 3. Cardiovascular system indicators during the work shift

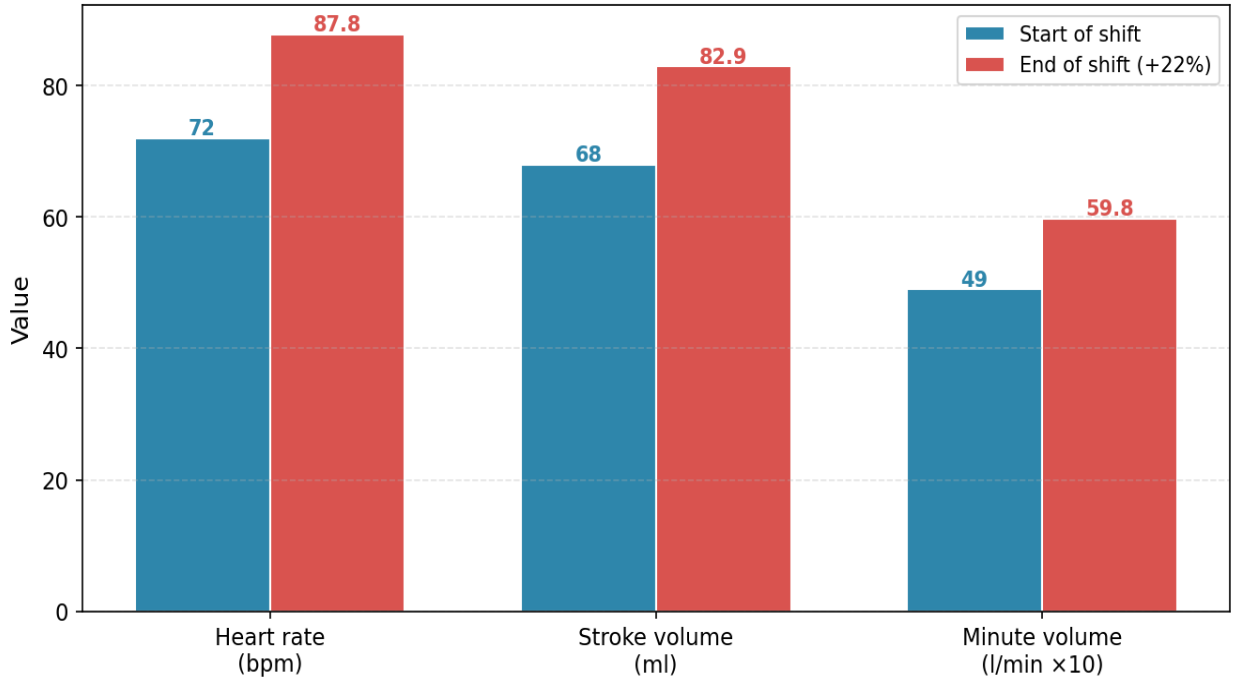


Figure 3. Dynamics of cardiovascular system indicators during the work shift

Effectiveness of implemented preventive measures.

Repeated instrumental monitoring following implementation of the protective complex (furnace sealing, FFP3 PPE, aerodynamic screens) confirmed a pronounced protective effect: the concentration of high-disperse aerosol in the workers' breathing zone stabilised and reliably remains at 3.9 mg/m³ — significantly below the regulated MAC value (6.0 mg/m³) ($p<0.01$).

Taking into account the aerodiffusion patterns characteristic of the Fergana Valley's geographic landscape, the installation of lightweight protective screens up to 6 m high on the windward side has been scientifically substantiated. The aerodynamic barrier created dissipates the kinetic energy of air flows, reducing the transboundary transport of submicron aerosols to adjacent residential areas within a radius of up to 5 km.

Table 3.

Coke dust concentration in the working zone before and after implementation of measures

Occupation	Before (mg/m³)	After (mg/m³)	Reduction	MAC (mg/m³)
Mechanic	7.8	**3.9**	**↓50.0%**	6.0
Crane operator	8.0	**3.9**	**↓51.3%**	6.0

Operator (pumps)	7.5	**3.9**	**↓48.0%**	6.0
Operator (furnace)	7.2	**3.9**	**↓45.8%**	6.0
Operator (reactor)	7.6	**3.9**	**↓48.7%**	6.0

Figure 4. Effectiveness of preventive measures: dust concentration before and after (mg/m³)

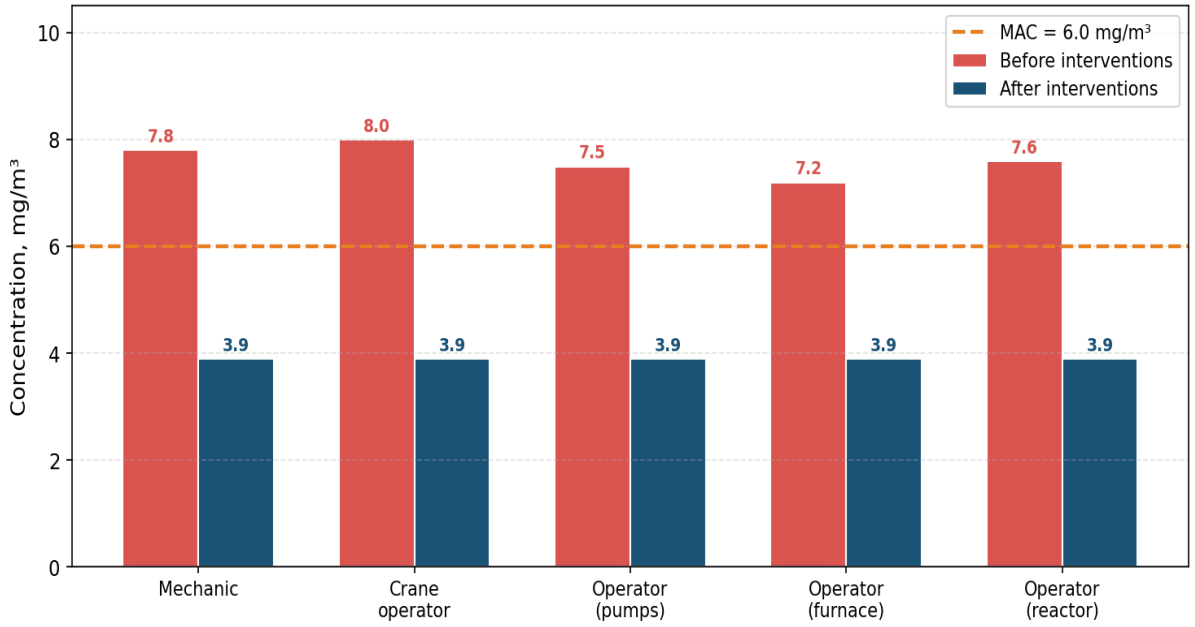


Figure 4. Effectiveness of preventive measures: dust concentration before and after (mg/m³)

Conclusions:

1. The high content of respirable fractions in coke dust at the FNPZ AVT unit (PM_{10} >70%, $PM_{2.5}$ >30%) determines its capacity for deep alveolar penetration and significantly elevates the risk of chronic bronchopulmonary disease.

2. The hydrophobicity of coke dust (93% amorphous carbon) precludes the effectiveness of water irrigation systems; the sole adequate measure for respiratory protection is the mandatory use of FFP3/N100 class respirators with a reliable facial seal.

3. Working conditions at the AVT unit are classified as hazard classes 3.1–3.2; by the end of the shift, a statistically significant increase in haemodynamic load (+22%) and suppression of respiratory function were documented ($p<0.05$).

4. The preventive complex reduced dust concentration to 3.9 mg/m³ — reliably below MAC = 6.0 mg/m³.

5. Aerodynamic screens up to 6 m high, installed on the windward side, are scientifically substantiated as an effective engineering-hygienic tool for limiting the transboundary dispersal of coke dust within a 5 km radius.

Practical recommendations.

Table 4.

Preventive measures and expected outcomes

No.	Preventive measure	Expected outcome
1	Sealed conveyor systems and pneumatic transport — minimising aerosol generation during coke handling and loading	Dust concentration reduced by 30–50%
2	FFP3/N100 class respirators (filtration 99.0–99.7%) — mandatory use by all workers	$PM_{2.5}$ entering airways reduced by 99%

3	Aerodynamic screens up to 6 m high — installed on the windward side	Dust dispersal within 5 km radius reduced by 60–70%
4	Sealing of heating furnaces and automated combustion control	Thermal emissions and CO output reduced by 40%
5	Artificial surface irrigation systems — prevention of dust resuspension	Airborne dust reduced by 25%
6	Flexible shift schedule: regulated 15–20 min breaks every 2 hours	Reduced fatigue and neuropsychological strain
7	Mandatory periodic medical examination covering 100% of workers — early detection of occupational pathology	Occupational diseases identified at early stage in 80% of cases
8	Comprehensive mechanisation and remote process control	Contact with harmful factors reduced by 50%

REFERENCES

1. Adilov U.Kh., Khamrakulova M.A., Tuychiev Zh.T., Khashirbaeva D.M. Compilation of sanitary-hygienic characterisation of working conditions based on hygienic assessment of labour conditions: methodological recommendations. Tashkent, 2018. 28 p.

2. Adilov U.Kh., Khashirbaeva D.M. Method for reducing the class of working conditions through the application of effective personal protective equipment: methodological guidelines. Tashkent, 2015. 12 p.

3. Adilov U.Kh., Almatov B.I., Khashirbaeva D.M. Method for hygienic assessment of occupational risk: methodological recommendations. Tashkent, 2017. 24 p.

4. Andriyantseva S.A., Bondarenko A.V. Synthesis and properties of adsorption-active materials derived from coke dust. Scientific Bulletin of Belgorod State University. 2011; Issue 15, No. 9(104): 96.

5. Akhmedova N.M., Ibodullaeva S. Impact of industrial dust on the human body. Universum: Technical Sciences [electronic journal]. 2023; 5(110). URL: https://7universum.com/ru/tech/archive/item/15469

6. Badamshina G.G., Karimova L.K., Tkacheva T.A., Mavrina L.N., Bakirova A.E. Assessment of the combined effect of hazardous substances on the health status of workers in petrochemical and chemical industries. Occupational Medicine and Industrial Ecology. 2013; (4): 5–10.

7. Ivanov A.V., Petrov M.N. Environmental impact of coke dust emissions during petroleum refining. Journal of Petroleum Science and Engineering. 2021; 206: 118–126. https://doi.org/10.1016/j.petrol.2021.118126

8. SanPiN RUz No. 0294-11. Hygienic standards for maximum permissible concentrations of hazardous substances in the air of working zones. Tashkent, 2011.